Copyright is owned by the Author of the thesis. Permission is given for a copy to be downloaded by an individual for the purpose of research and private study only. The thesis may not be reproduced elsewhere without the permission of the Author.

Small-volume volcanism associated with polygenetic volcanoes, Taupo Volcanic Zone, New Zealand

A thesis presented in partial fulfilment of the
requirements for the degree of

Doctor of Philosophy

in

Earth Science

at Massey University, Palmerston North, New Zealand

VOLCANIC
RISK SOLUTIONS

MASSEY
UNIVERSITY
TE KUNENGA KI PŪREHUROA
UNIVERSITY OF NEW ZEALAND

Szabolcs Kósik

2018

Panoramic view of the west shore of Lake Taupo with three lava domes from the Motuoapa Peninsula

"Each volcano is an independent machine—nay, each vent and monticule is for the time being engaged in its own peculiar business, cooking as it were its special dish, which in due time is to be separately served. We have instances of vents within hailing distance of each other pouring out totally different kinds of lava, neither sympathizing with the other in any discernible manner nor influencing other in any appreciable degree."

Clarence Edward Dutton

Abstract

In the past 350 ky, the Taupo Volcanic Zone (TVZ) has been the most productive silicic volcanic region in the world, with 12 silicic large-volume (35-2200 km^3 DRE) caldera-forming eruptions and hundreds of predominantly silicic smaller-volume eruptions. These spatially and temporally scattered small-volume events are characterised by relatively short-lasting single eruptive episodes that may have been strongly influenced by location-specific environmental factors. The aim of this study is to evaluate the volcanic hazards associated with the activity of these small-volume volcanoes using two different approaches. At the local scale, possible eruption scenarios were defined through three example localities (Ohakune, Motuoapa, Puketerata) that are characterised by different chemical compositions, eruption styles, as well as distinct environmental conditions representative of the entire TVZ. At the field scale, evaluation of small-volume activity was focused on the spatio-temporal and volumetric distribution of vents and their relationship to the structural elements of the TVZ. The most common small-volume eruptions form lava domes that were originally thought to be rarely associated with explosive activity. In contrast, this study shows that dome emplacement is often accompanied by explosive activity. However, the associated pyroclastic deposits are characterised by a low preservation potential. The most likely scenario for future eruptions is a rhyolitic eruption with an initial phreatomagmatic phase followed by the effusive emplacement of lava with or without associated explosive activity. Based on the average eruptive volumes (0.2-0.3 km^3) of single TVZ events and typical eruption rates of dome-forming activity (2-5 m^3/s), future eruptions are expected to last for several months to a few years. TVZ-scale spatio-temporal analysis of eruptive vents indicates that small-volume volcanism is not entirely limited to active calderas. Instead, frequent fissural activity indicates a strong linkage to the fault system of the TVZ. The temporal and volumetric pattern of small-volume volcanism displays a sudden increase of activity at 45 ka, producing at least 130 km^3 of volcanic material to date. The random occurrence, great variability of eruption styles, small but significant volumes, prolonged duration and relatively high frequency of small-volume volcanism pose a significant threat within the entire TVZ, which New Zealand will have to face in the near future.

Acknowledgements

This thesis is the result of 3.5 years-long research at Massey University, New Zealand that I started in April 2014. I am grateful to many people who have worked with or assisted me throughout the maze of the PhD to complete this thesis.

First of all, I am thankful to my chief supervisor, Károly Németh, for our scientific discussions as well as guidance and support in the world of research and beyond. I am also thankful for the contributions and support of my co-supervisors, Jonathan Procter, Georg Zellmer and Shane Cronin. Many thanks to Kate Arentsen for administrative, organizational, and proof reading support. I would like to acknowledge my co-authors, Gábor Kereszturi, Mark Bebbington, Robert Stewart (Massey University), Nobuo Geshi (Geological Survey of Japan), and Jaroslav Lexa (Earth Science Institute, Slovak Academy of Sciences) for their support and contributions to manuscripts or presentations. I also acknowledge the field assistance of many colleagues and friends, such as Braden Walsh, Ermanno Brosch, István Hajdu, Boglarka Németh (Massey University) and Takeshi Hasegawa (Ibaraki University, Japan). I acknowledge Anja Moebis and the staff of the Manawatu Microscopy and Imaging Centre (Matthew Savoian, Niki Minards, and Jordan Taylor) for their priceless technical support. Special thanks go to staff, former and present PhD students of Volcanic Risk Solutions for discussions in various research and non-research-related topics that make university life colourful, Javier Agustin-Flores, Maricar Arpa, Eric Breard, Magret Damaschke, Martha Gabriela Gómez-Vasconcelos (aka Gaby Gómez), Charline Lormand, Gert Lube, Stuart Mead, Adam Neather, Andrea Todde, Rafael Torres-Orozco, Manuela Tost, Marija Voloschina, and Aliz Zemeny and others already mentioned.

I would like to express my gratitude to the Institute of Agriculture and Environment, Massey University for the financial support. I also acknowledge the support of Massey Foundation and Massey University Doctoral Completion Grants for the last months of my studentship. Many thanks to the IAVCEI Commission on Collapse Calderas and Geological Society of New Zealand for their support helping me attend conferences during my study.

LiDAR data in this thesis was provided by Waikato Regional Council, Hamilton and Horizons Regional Council, Palmerston North; the National Institute of Water and Atmospheric Research (NIWA) supplied bathymetry maps of New Zealand lakes.

This is an excellent opportunity to acknowledge the people who helped me to get this far. I would like to thank my two mentors, Róbert Győri (Eötvös Loránd University, Hungary) and István János Kovács (Geological and Geophysical Institute of Hungary) for encouraging me to start a research career at the beginning of my university studies in Hungary. A special recognition goes to my former supervisor, Dávid Karátson (Eötvös Loránd University, Hungary), who endeared me to volcanology and did the most for my research career before coming to New Zealand.

I wish to thank my parents for their help in achieving my life goals and efforts to make me an open minded competent person.

Last but not least I would like to express the greatest thanks to my family. Without the unconditional love and support of my fiancée Zsuzsa it would not have been easy to get so far, while our newborn son, Titusz, inspires me to continue this journey and look for new challenges. This thesis is dedicated to the two of you!

Table of contents

Abstract .... **i**

Acknowledgement .... **iii**

Table of contents .... **vii**

List of figures .... **xv**

List of tables .... **xxvii**

Chapter 1 – Introduction **1**

1.1 Small-volume volcanism of silicic caldera systems *2*

1.2 Problem statement *3*

1.3 Aims and objectives *4*

1.4 Thesis outline and structure *6*

Chapter 2 – Geological setting **9**

2.1 Structural settings and evolution of the TVZ *10*

2.2 Volcanic architecture of the young TVZ *18*

2.2.1 Northern TVZ *19*

2.2.2 Southern TVZ *20*

2.2.3 Central TVZ *23*

Chapter 3 – Review of silicic monogenetic volcanism and a new classification for domes **33**

3.1 Eruptive styles and processes *36*

3.2 Volcanic products and landforms relating to silicic explosive volcanism *39*

3.3 Lava domes and coulees *46*

3.3.1 Factors determining the shape and volcanic hazard of lava domes *47*

3.3.2 Surface and internal structures of lava domes *50*

3.3.3 Appearance at different volcanotectonic environments and relationship with polygenetic volcanoes *54*

3.3.4 Existing morphometric classifications of lava domes *58*

3.4 New lava dome classification based on macro-morphometry of dome surfaces *62*

Chapter 4 – Methodology **75**

4.1 Laboratory techniques *76*

4.1.1 Grain size distribution 76

4.1.2 Componentry and glass morphometry analyses 77

4.1.3 Density measurements 77

4.1.4 Vesicularity and rock/clast microtexture analysis 78

4.1.5 Electron Probe Micro-Analysis (EPMA) 79

4.1.6 X-ray fluorescence spectrometry (XRF) 80

4.2 Digital terrain analysis 81

4.2.1 Introduction 81

4.2.2 Sources of digital elevation data used for terrain analysis 82

4.2.3 Defining topographic/terrain attributes 84

Chapter 5 – Eruption mechanisms and evolution of the Ohakune Volcanic Complex 87

5.1 Introduction 88

5.2 Regional setting 91

5.3 Materials and methods 92

5.3.1 Field observations and sampling 92

5.3.2 Sample preparation and analytical techniques 93

5.4 Architecture of Ohakune Volcanic Complex 94

5.5 Stratigraphy and sedimentology 97

5.5.1 Ash beds (Ab) 98

5.5.1.1 Description 98

5.5.1.2 Emplacement interpretation 98

5.5.2 Ash beds with coarse fragments (Ab_C) 100

5.5.2.1 Description 100

5.5.2.2 Emplacement interpretation 100

5.5.3 Bomb beds with ash (Bb_A) 102

5.5.3.1 Description 102

5.5.3.2 Emplacement interpretation 103

5.5.4 Spatter-scoria bomb beds (Bb) 104

5.5.4.1 Description 104

5.5.4.2 Emplacement interpretation 104

5.6 Density and vesicle microtexture analysis 104

5.6.1 Interpretation of observed density and vesicle microtextures features 106

109

5.7 Petrology, geochemistry and thermobarometry …………………………….. *108*
5.7.1 Evaluation of the results of petrology, geochemistry and thermobarometry ……………………………………………………………………… *112*
5.8 Eruptive volume calculations ……………………………………………………………….. *113*
5.9 Discussion …………………………………………………………………………………….. *115*
5.9.1 Fragmentation and eruptive styles ……………………………………………………. *115*
5.9.2 Eruption history ……………………………………………………………………………… *116*
5.9.3 Volcanic hazard assessment ……………………………………………………. *118*
5.10 Conclusion ……………………………………………………………………………………… *120*

Chapter 6 – Maar-diatreme volcanism relating to the Te Hukui Basalt ……… ***121***
Preamble ………………………………………………………………………………………………. *122*
6.1 Introduction ………………………………………………………………………………………. *124*
6.2 Geological background ………………………………………………………………. *125*
6.3 Stratigraphy and sedimentology ……………………………………………………. *126*
6.4 Petrography and geochemistry of the Te Hukui Basalt …………………………… *130*
6.5 Discussion and conclusions ………………………………………………………………. *133*

Chapter 7 – Understanding the evolution of the Puketerata Volcanic Complex ……………………………………………………………… ***137***
7.1 Introduction ………………………………………………………………………………………. *138*
7.2 Geological setting ………………………………………………………………………………. *140*
7.3 Methods ………………………………………………………………………………………….. *143*
7.4 Architecture of the Puketerata Volcanic Complex …………………………… *144*
7.4.1 Maars ………………………………………………………………………………………….. *144*
7.4.2 Ejecta ring ………………………………………………………………………………………. *144*
7.4.3 Lava domes ………………………………………………………………………………………. *148*
7.5 Stratigraphy and sedimentology ……………………………………………………. *150*
7.5.1 General features ………………………………………………………………………………. *150*
7.5.2 Proximal sequences ……………………………………………………………………………. *151*
7.5.2.1 Eastern outer slopes of tuff ring ……………………………………………………. *152*
7.5.2.2 Moat successions ……………………………………………………………………………. *152*
7.5.2.3 Elevated localities on the eastern rim of the tuff ring and the summit of the larger lava dome ………………………………………………………………. *154*
7.5.3 Medial sequences ……………………………………………………………………………. *154*

7.5.4 Density, vesicularity and volume calculations ………………………… 156
7.6 Petrology and thermobarometry ……………………………………………… 158
7.6.1 Puketerata rhyolites ……………………………………………………… 158
7.6.2 Intensive parameters ……………………………………………………… 160
7.7 Discussion ……………………………………………………………………… 163
7.7.1 Eruption conditions and the role of phreatomagmatism ……………… 163
7.7.2 Emplacement of lava domes in relation with associated ejecta rings ……… 165
7.7.3 Evolution of Puketerata Volcanic Complex ………………………………… 169
7.8 Conclusion ……………………………………………………………………… 172

Chapter 8 – Volcanism of Motuoapa Peninsula and its neighbourhood ……… 173
8.1 Introduction …………………………………………………………………… 174
8.2 Geological setting ……………………………………………………………… 175
8.3 Methodology …………………………………………………………………… 176
8.3.1 Field work ……………………………………………………………………… 176
8.3.2 Laboratory work ……………………………………………………………… 177
8.4 Results …………………………………………………………………………… 178
8.4.1 Geomorphology ……………………………………………………………… 178
8.4.1.1 Motuoapa Peninsula …………………………………………………… 178
8.4.1.2 Korohe dome and Echo Cliffs ………………………………………… 179
8.4.2 Stratigraphy and facies architecture of the Motuoapa Peninsula ……… 180
8.4.2.1 Stratigraphy …………………………………………………………… 180
8.4.2.2 Pyroclast characteristics ……………………………………………… 182
8.4.2.3 Lithofacies relating to explosive activity …………………………… 183
8.4.2.4 Effusive lithofacies (Motuoapa Peninsula) …………………………… 187
8.4.3 Erupted volume calculations ……………………………………………… 189
8.4.4 Petrology and geochemistry ……………………………………………… 191
8.4.4.1 Rhyolites ………………………………………………………………… 193
8.4.4.2 Dacites …………………………………………………………………… 196
8.5 Discussion ……………………………………………………………………… 198
8.5.1 Origin of magmas …………………………………………………………… 198
8.5.2 Eruption and depositional processes …………………………………… 199
8.5.3 Evaluation of paleoenvironmental characteristics and volcanic
architecture of the Motuoapa Peninsula and its neighbourhood ……… 202

8.5.4 Implications for the evolution of the Lake Taupo area in the past 2 ky …… 203
8.5.4 Summary of the geological evolution of the SE margin of Lake Taupo ……. 204
8.5.6 Hazard implications …… 205
8.6 Conclusions …… 205

Chapter 9 – Spatial, temporal and volumetric distribution of vents of small-volume eruptions within the TVZ …… 207
9.1 Introduction …… 207
9.2 Spatial and temporal distribution of eruptive vents …… 210
9.2.1 Mafic eruptions within the central TVZ …… 213
9.2.2 Silicic eruptions within the central TVZ …… 214
9.2.3 Relationship between vent locations and the structural elements of the TVZ …… 215
9.2.4 Temporal distribution of small-volume volcanism and its spatial Implications …… 219
9.3 Eruptive volume distribution in space and time …… 222

Chapter 10 – Discussion and conclusions …… 227
10.1 Synthesis of the volcanism of the studied localities …… 228
10.1.1 Origin, chemical and petrological characteristics of erupted magmas of studied volcanoes …… 229
10.1.2 Local environmental settings …… 231
10.1.3 Eruption styles, type of deposits and morphology of the volcanic structures …… 232
10.1.3.1 Mafic to intermediate eruptions …… 233
10.1.3.2 Silicic eruptions …… 234
10.2 Factors that controlled the eruption styles and courses of eruptions ………. 237
10.2.1 Physical properties of magma and eruption rates …… 237
10.2.2 Local substrate properties and availability of external water ……… 239
10.3 Relationship between small-volume and caldera-forming eruptions within the TVZ …… 240
10.3.1 Spatial correlations …… 241
10.3.2 Temporal correlations …… 243
10.3.3 Magma generation and petrological and geochemical aspects ……… 245
10.4 Hazard implications …… 246

10.4.1 Vent architecture and eruptive styles …… 247

10.4.1.1 Possible eruptive styles of magmas with low to intermediate silica content …… 247

10.4.1.2 Possible eruptive styles of high-silica magmas …… 249

10.4.2 Volume, eruption rates and duration of small-volume eruptions …… 251

10.4.3 Towards forecasting volcanic hazard …… 253

10.4.3.1 Probability model for eruption location prediction …… 253

10.4.3.2 Susceptibility mapping for hydrovolcanic activity of the central TVZ …. 256

10.5 Conclusions …… 258

10.5.1 Main findings in relation to the research objectives …… 258

10.5.1.1 Volcanic architecture and evolution of the volcanoes of example localities …… 258

10.5.1.2 Spatio-temporal and eruptive style pattern of small-volume volcanism of the central TVZ …… 260

10.5.1.3 Globally relevant general findings …… 260

10.5.2 Future directions of research …… 261

10.5.3 Epilogue – personal view …… 262

References …… 264

Appendices …… 302

Appendix A – Supplementary materials for published papers and papers in preparation …… 302

Appendix B – Grain size distribution and envelope density analyses …… 302

Appendix C – Raster and vector datasets used for the evaluation of the spatial, temporal and volumetric distribution of vents of small-volume eruptions of the Taupo Volcanic Zone …… 303

Appendix D – Statement of contribution …… 304

List of figures

Figure 1.1 Locations of the examined case study volcanoes. The boundary (orange dashed lines) of the TVZ (sheded area) after Wilson et al. (1995). The inset map indicates the position of the area of interest within the central North Island of New Zealand. Main roads are indicated by black lines and red polygons represent important townships. ………………………………………… 8

Figure 2.1 Topographic and tectonic settings of the broader environment of New Zealand (Zealandia), with respect to the position of the TVZ. Topographic information was derived from 250 m resolution gridded bathymetric data, National Institute of Water and Atmospheric Research (NIWA) (New Zealand Regional Bathymetry 2016). Tectonic and structural information from Mortimer et al. (2017). Au – Auckland Islands; An – Antipodes Islands; Bo – Bounty Islands; Ca – Campbell Island; Ch – Chatham Islands; Cu – Curtis Island; Lo – Lord Howe Island; Ma – Macauley Island; Mq – Macquaire Island; No – Norfolk Island; Ra – Raoul Island; St – Stewart Island. ……………………………………………………………………………………………………. 12

Figure 2.2 Map of the upper North Island of New Zealand indicating the margin and main volcanic structures (calderas: Ma – Mangakino; Ka – Kapenga; Wh – Whakamaru; Oh – Ohakuri; Ro – Rotorua; Rp – Reporoa; Ok – Okataina; Tp – Taupo; and andesitic composite cones: Mta – Maungatautari; Tit – Titiraupenga; Pur – Pureora; Hah – Hauhungaroa; Hau – Hauhungatahi; Mau – Maungakatote; Kak – Kakaramea; Pih - Pihanga) of the old and young TVZ in relation to the CVZ, Kermadec arc, Havre Trough and other Neogene volcanic fields of the North Island; WG – Waitakere Group; AVF – Auckland Volcanic Field; SAVF – South Auckland Volcanic Field; NVF – Ngatatura Volcanic Field; KVG – Kiwitahi Volcanic Group; AVG – Alexandra Volcanic Group; Kai – Kaimai Volcanic Centre (CVZ). Map modified from Briggs et al. (2005) and Rowland et al. (2010), complemented with data from the GNS 1:250000 map series (Edbrooke, 2001; Edbrooke, 2005; Townsend et al., 2008; Leonard et al., 2010; Lee et al., 2011). Offshore Bay of Plenty structures after Wright (1992), TVZ delineation after Wilson et al. (1995). …… 14

Figure 2.3 Schematic SE-NW trending cross-section of the central North Island, with the main structural elements of the crust and upper mantle as determined by seismology modified after Cole and Spinks (2009). ……………………………………………………………………………………………… 15

Figure 2.4 Topography of the southern TVZ/Tongariro Volcanic Centre as displayed on a shaded slope map derived from an 8 m DEM (LINZ - Land Information New Zealand, 2012). The inset map shows its geographic position and extent within the TVZ, coordinates are in NZTM2000. The vent locations mentioned in the text are labelled: Hau – Hauhungatahi; Mak – Maungaku; Mkt – Maungakatote; 1 – Rangataua Craters; 2 – OVC; 3 – inferred source vent of Rangataua lava flow; 4 – Saddle Cone and Tama Lakes; 5 – Pukeonake; 6 – Waimarino; 7 – vents in the Rotopounamu Graben (from the south: Puketopo, Pukemohono, Lake Rotopounamu and Onepoto); 8 – Te Pohanga. ……………………………………………………………………………………… 23

Figure 2.5 Topography of the Taupo Volcanic Centre as displayed on a shaded slope map derived from an 8 m DEM (LINZ – Land Information New Zealand, 2012). The inset map shows its geographic position and extent within the TVZ, coordinates are in NZTM2000. The vent locations mentioned in the text are labelled: 9 – Motuopuhi Island; 10 – Kuharua; 11 – Motuoapa Peninsula; 12 – inferred post-Oruanui vents related to a NNE-SSW trending lineament; 13 – Ouaha Hills; 14 – Acacia Bay dome; 15 – Kinloch Basalt; 16 – Lake Rotokawa; 17 – PVC and Te Hukui Basalt. …………………………………………………………………………………… 26

Figure 2.6 *Topography of the Whakamaru (Wh) and the Ohakuri (Oh) Volcanic Centres as displayed on a shaded slope map derived from an 8 m DEM (LINZ – Land Information New Zealand, 2012). The inset map shows its geographic position and extent within the TVZ. The vent locations mentioned in the text are labelled: WDC – Western Dome Complex; NWDC – Northwestern Dome Complex; MWC – Maroa West Complex; MEC – Maroa East Complex; 16 – Lake Rotokawa; 17 – PVC and Te Hukui maars; 18 – Whakaahu Dome Belt; 19 – Pukeahua Dome Complex; 20 – Whakamaru Domes and Coulees (part of NWDC).* ……………………… ***27***

Figure 2.7 Topography of the *Kapenga (Ka)-Reporoa (Rp)-Rotorua (Ro)- and Okataina (Ok) Volcanic Centres as displayed on a shaded slope map derived from an 8 m DEM (LINZ – Land Information New Zealand, 2012). The inset map shows its geographic position and extent within the TVZ. The vent locations mentioned in the text are labelled: NWDC – Northwestern Dome Complex; MWC – Maroa West Complex; MEC – Maroa East Complex; 21 – Horohoro Cliffs; 22 – Maungaongaonga and Maungakakaramea/Rainbow Mountain; 23 – Puhipuhi lava dome complex 24 – Earthquake Flat volcano; 25 – Mokoia Island; 26 – Rotokawau-Rotoatua fissure vents; 27 – Terrace Road Basalt.* …………………………………………………………………… ***29***

Figure 3.1 *Potential relationship of small-volume volcanism (typical erupted volume <1 km^3 DRE) based on their spatial and magma plumbing system relationships to polygenetic central vent volcanism.* ……………………………………………………………………………………………………… ***36***

Figure 3.2 *Surface textural features of lava domes. A – explosion pits on the surface of the 2011 dome of Volcán de Colima (photo courtesy: J. Farquharson/CIIV, Universidad de Colima), Mexico; B – Crease structure on the Little Glass Mountain flow, Medicine Lake volcano, USA; C – Crease structure on the Medicine Lake Glass Flow, Medicine Lake volcano, USA; D – Ogives/flow ridges of the Little Glass Mountain flow, Medicine Lake volcano, USA. Light-coloured areas represent finely vesicular pumice (FVP) texture, whereas darker areas comprise obsidian and coarsely vesicular pumice (CVP) textures.* ………………………………………………… ***51***

Figure 3.3 *Figure 3.3 Schematic cross section of a rhyolitic obsidian flow based on drill core observations from Obsidian Dome in the Inyo dome chain, Long Valley caldera, USA, figure modified after Fink and Manley (1987).* ……………………………………………………………………. ***53***

Figure 3.4 *Potential relationship of small-volume volcanoes (erupted volume <~2-3 km^3 DRE) based on their spatial and magma plumbing system characters to caldera volcanoes. Examples: 1 – Kuharua, SW from Lake Taupo; 2 – Western Dome Complex, Whakamaru; 3 – Rangitukua, SW shore of Lake Taupo; 4 – Puketerata, central Whakamaru; 5 – Motuoapa Peninsula, SE shore of Lake Taupo; 6 cryptodome of Edgecumbe (NE lower flank of the main cone); 7 – Showashinzan, Mt Usu, Japan (there is no New Zealand example); 8 – Tauhara; 9 – Saddle Cone, Ruapehu.* ……………………………………………………………………………………………………… ***56***

Figure 3.5 *Classification of lava domes by dome height (H) versus radius (R) ratio (Blake, 1990). H/R calculations of Peléan domes were based on nine historically erupted domes of composite volcanoes/lava dome complexes, whereas low lava dome values were achieved from 16 domes of La Primavera (Mexico), eight domes of the Coso Volcanic Field (USA) and five unidentifiable domes of the Maroa Volcanic Centre (New Zealand). *For low lava domes the average H/R value was recalculated from the graphics of Fig. 13. of Blake's paper (1990), as it was expressed differently than for the values of the Peléan domes, figure modified after Blake (1990).* ……………………………………………………………………………………………………….. ***57***

Figure 3.6 *The classification of lava domes by morphology and surface textures of lava domes corresponds to the decrease of ΨB from spiny to axisymmetric domes (Fink and Griffiths, 1998).* …… ***59***

Figure 3.7 *Examples for rockfall-dominated spiny domes with characteristic conical shape summits. A – Ceboruco 1870, Mexico (photo courtesy: J. Méndez Harper); B – Mt. Redoubt 1990, Alaska (photo courtesy: Alaska Volcano Observatory); C – Mt. St. Helens 2005, USA (photo courtesy: Cascade Volcano Observatory); D – Sinabung 2016, Indonesia (photo courtesy: Z. Ginting); E – Devil Hill domes ~2 ka, South Sister, USA; F – Kelut 2007, Indonesia (photo courtesy: Smithsonian Institution); G – Bezymianny 1956, Russia (photo courtesy: G.S. Gorshkov); H – Paluweh 2012, Indonesia (photo courtesy: R. Roscoe/Stocktrek Images); I – Soufriere Hills 2010, Montserrat (photo courtesy: photovolcanica.com).* …… ***64***

Figure 3.8 *Flat-topped spiny domes with characteristic flat tops that change without transition to the steep-sided slopes. A – Volcan de Colima 2010, Mexico (photo courtesy: CIIV, Universidad de Colima); B – Soufriere ~3 ka, Gaudeloupe (photo courtesy: Smithsonian Institution); C – Mt. Pelee 1902, Martinique (photo courtesy: Smithsonian Institution); D – Augustine 1986, Alaska (photo courtesy: Alaska Volcano Observatory); E – Novarupta 1912, Alaska (photo courtesy: Alaska Volcano Observatory); F – Tarumai 1909, Japan (photo courtesy: panoramio.com); G – Puy de Dome ~10 ka, Auvergne, France (photo courtesy: gettyimages); H – Um Raqubah, Saudi Arabia (photo courtesy: K. Németh); I – Wahanga ~1314, Okataina, New Zealand (photo courtesy: teara.govt.nz).* …… ***66***

Figure 3.9 *Lobate domes with characteristic zigzag-shaped outlines in the early phases. A – Awu 1931, Indonesia (photo courtesy: Smithsonian Institution); B – Soufriere 1972, St. Vincent (photo courtesy: The University of West Indies, Seismic Research Unit); C – Augustine 2011, Alaska (photo courtesy: Alaska Volcano Observatory); D – Puketerata ~16 ka, New Zealand; E – Mt. St. Helens 1986, USA (photo courtesy: Cascade Volcano Observatory); F – Soufriere 1971, St. Vincent (photo courtesy: Smithsonian Institution).* …… ***67***

Figure 3.10 *Platy domes with characteristic convex summit and increasing slope gradient moving away from the vent. A – Sinabung 2014, Indonesia (photo courtesy: M. Szlegat); B – Galunggung 1918, Indonesia (photo courtesy: Smithsonian Institution); C – Taranaki ~1785, New Zealand (photo courtesy: Platz et al., 2012); D – Merapi 2012, Indonesia (photo courtesy: AP Images); E – Mt. Redoubt 2009, Alaska (photo courtesy: Alaska Volcano Observatory); F – Soufriere 1979, St. Vincent (photo courtesy: D. Pyle); G – Mt. St. Helens 1980, USA (photo courtesy: Smithsonian Institution); H – Awu 2004, Indonesia (photo courtesy: flickr.com); I – El Ombligo, Nevado de Toluca ~1350, Mexico (photo courtesy: hiveminer.com); J – Pukekaikiore, Taupo, New Zealand.* …… ***68***

Figure 3.11 *Axisymmetric domes with characteristic low aspect ratio and flat tops aside from crease structures, pressure ridges and diapirs. A – Kei Besi/Makian 1988, Indonesia (photo courtesy: W. Piecha); B – Chillahuita ~400 ka Chile (photo courtesy: volcano.oregonstate.edu); C – Te Horoa ~5 ka, Okataina, New Zealand (Google Earth image); D – Rangitukua (lower part) ~130 ka, New Zealand; E – Little Glass Mountain, Medicine Lake volcano ~1ka, USA; F – Big Obsidian Flow, Newberry volcano ~1 ka, USA.* …… ***69***

Figure 3.12 *Examples of coulees. A – Cerro Chao ~400 ka, Chile (photo courtesy: volcano.oregonstate.edu); B – Big Obsidian Flow, Newberry volcano ~1 ka, USA (photo courtesy: R. A. Jensen); C – Mt. Elden, San Francisco Volcanic Field, USA (photo courtesy: mountainproject.com); D – Satellite image of Cerro Chao, Chile (Google Earth image); E – 1 m* *resolution LiDAR DEM of Big Obsidian Flow, Newberry volcano, USA; F – 1 m resolution LiDAR DEM of Newberry Flow, South Sister, USA.* ………………………………………………………………… **70**

Figure 3.13 *Examples of lava dome complexes. A – Black Butte, ~10 ka, Mt. Shasta, USA; B – Ciomadul/Csomád ~28 ka, Romania (photo courtesy: D. Karátson); C – Chaitén 2010, Chile (photo courtesy: D. Schneider); D – Santiaguito 2012, Guatemala (photo courtesy: photovolcanica.com); E – Tauhara, ~190 ka, New Zealand (photo courtesy: greatlaketaupo.com); F – Tarawera Volcanic Complex, 1886, New Zealand, G – Edgecumbe/Putauaki ~2.5 ka, New Zealand (photo courtesy: wikipedia.org).* …………….. **71**

Figure 3.14 *Comparison of shape of lava dome complexes with other conical-shaped volcanic structures (lava dome and composite volcanoes) with examples from New Zealand. Cross-sections were derived from an 8 m NZ DEM (LINZ - Land Information New Zealand, 2012).* ……………………………………………………………………………………………………… **73**

Figure 4.1 *Comparison of methods in the recognition of vesicles using 2D imagery. Experimental results are indicated. A – ImageJ-based measurement considers all the area of the image, however the incomplete vesicle shapes have to be excluded from the result of shape analyses; B – This hypothetic method includes all the vesicle area in total, but the incomplete vesicles have been excluded from the area of the vesicles; C – FOAMS-based measurements exclude all the incomplete vesicles, thus the measured total vesicularity of the sample will be lower than the actual vesicularity.* ……………………………………………………………………….. **79**

Figure 4.2 *The most common types of elevation data networks (Moore et al., 1991). A – Raster-based grid; B – Vector-based TIN; C – Vector-based contours (polylines).* …………………….. **82**

Figure 5.1 *Topography of the southern, dominantly andesitic part of the TVZ as shown on shaded slope map derived from a 8 m DEM (LINZ - Land Information New Zealand, 2012). Inset map shows its geographic position within New Zealand.* ……………………………………………. **92**

Figure 5.2 *Aerial photograph of OVC with its proposed architecture. The main edifices are labelled; West ejecta ring (WER), East ejecta ring (EER), Central scoria cone (CSC), South scoria cone (SSC), North scoria cone (NSC).* ……………………………………………………………………… **95**

Figure 5.3 *Morphological features of OVC. A: View from the rim of WER to its crater floor. On the right edge the foot of the CSC partly fill in the crater. B: The quarried section of the coalesced EER and the rim of CSC. C: View from the highest part of the CSC to its crater floor (grassland) and its quarried interior of alternating welded and unwelded Strombolian (or Hawaiian) units. The railway line is also cut through the scoria cone and EER on the left and WER on the right.* ………………………………………………………………………………………….. **96**

Figure 5.4 *Stratigraphic sequence of the proximal part of EER at the northwest corner of the quarry. This is one of the locations exhibits the opening of a new vent. Note the oxidation pattern of right hand side of the fault.* ……………………………………………………………………… **99**

Figure 5.5 *SEM images of juvenile ash fragments characterised by high to low vesicularities (A–E) and a typical aggregate (F). Type a with spherical vesicles is extremely rare at OVC would represent Strombolian fragmentation (Heiken and Wohletz, 1985), type b with microlites is the most vesicular of the common fragments and might related to eruptions with minor influence by water/magma interaction, while c–e types might have more phreatomagmatic origin. By comparison, a block was smashed by hammer and the bits were similar to type-c fragments.* ……………………………………………………………………………………………………….. **101**

Figure 5.6 *a – Cumulative grain size distribution of distinct units from the proximal sequence of EER. Bb unit distributions are only represent estimations based on field observations. b – Density variations of bomb/block and lapilli (−3 phi) sized juvenile fragments from EER proximal sequence.* **105**

Figure 5.7 *SEM images of bombs/blocks (A–D, G, H) from OVC and SEM images of scoria fragments from Mt. Roskill (E) and Rangitoto (F), Auckland Volcanic Field (AVF) for comparison. The two samples from AVF exhibit a Hawaiian and Strombolian (or Violent Strombolian)-style eruptions (Kereszturi, unpublished data) as the vesicles show mostly spherical or subspherical shapes (Lautze and Houghton, 2007; Moitra et al., 2013). The textures of samples from OVC are completely different from textures forming during these mild types of eruptions, however similar to basaltic Plinian eruptions of Etna 122 BCE and Tarawera 1886 (Moitra et al., 2013).* **105**

Figure 5.8 *A – Vesicle size distributions (VSD) are ln(n) as a function of L plots,with ln(n) the log of the vesicle number densities per size class, and L is the equivalent diameter in mm. The left part of the segment mostly reflects multiple stages of bubble nucleation and growth. The lower part of the VSD slopes often exhibit coalescence (e.g. J4, T3) which may have occurred at multiple stages. B – Cumulative vesicle size distributions (CVSD) are log(NV > L) as a function of log(L) plots, where NV is the total vesicle number density. Vesicle density measurements were used based on the objects per cubic mm greater than L. CVSD trends also suggest multiple stage of nucleation and growth with coalescence and bubble collapse events in most of the cases (e.g. A1, D3, J4, T3, X2) (Shea et al., 2010).* **107**

Figure 5.9 *Range of OVC bubble number density (NV) values measured on blocks and bombs from Bb and BbA type units in comparison with selected eruptions exhibiting different eruption styles; (A) Stovall et al. (2011);(B) Lautze and Houghton (2007); (C) Mattsson (2010); (D) Murtagh et al. (2011); (E) Sable et al. (2006).* **108**

Figure 5.10 *SEM images of phenocrysts (antecrysts) from Bb and BbA type units showing the hyalopilitic textures and growth relationship between olivine, orthopyroxene and clinopyroxene. Element mapping was executed by EDAX.* **109**

Figure 5.11 *Harker diagrams for selected major element oxides normalised to water-free compositions. Red circles represent ash fragments, blue squares represent groundmass glass compositions of blocks and bombs.* **110**

Figure 5.12 *AFM diagram shows glass compositions measured on ash fragments (red circles) and groundmass glass of blocks and bombs (blue squares) in comparison with whole rock compositions of Ruapehu volcano (grey field) (Price et al., 2012, e-appendix 10).* **111**

Figure 5.13 *Compositional variations of SiO_2, K_2O and MgO of ash (yellow fields) and blocks and bombs through the sequence.* **112**

Figure 5.14 *Delineation of distinct edifices of OVC. The obtained area and thickness values were applied for bulk volume calculations. Pie charts represent the DRE correction scheme applied for volume estimation from the different parts of the volcanic complex (Kereszturi et al., 2013). As the first step of the DRE corrections, the bigger pie charts imply the proportion of juvenile, non-juvenile and interparticle void space. Secondly, the smaller pie charts show the remaining juvenile content was corrected with the available vesicularities.* **114**

Figure 5.15 *Cartoon showing the evolution of facies architecture and eruptive mechanism during the OVC formation (see text for explanation).* **118**

Figure 6.P.1 *A – Locations and exposures of the Te Hukui sequence (yellow lines). See Fig. 6.1 for the location in its broader environment. Orange arrow indicates the viewpoint of B. B – Overview of the type locality of the Te Hukui sequence on the left bank of Te Hukui stream. C – Roadcut exposure of the Te Hukui sequence on the right bank of the Te Hukui stream (full size panoramic image along with further supporing pictures are in Appendix A.6.1).* …………. **123**

Figure 6.1 *Spatial distribution of the basaltic vents within the Whakamaru-Taupo area as displayed on a shaded slope map derived from an 8 m DEM (LINZ - Land Information New Zealand, 2012). Shaded areas represent the edifices of silicic lava domes. Basaltic vents: 1 – Te Hukui, 2 – Tatua, 3 – Kakuki, 4 – Akatarewa Stream, 5 – Mangamingi Road, 6 – Ongaroto, 7 – Trig 8543/Matapan, 8 – Acacia Bay, 9 – Pekanui, 10 – Kaiapo, 11 – K-Trig, 12 – Punatekahi, 13 – Kinloch, 14 – Otaketake Stream, 15 – Marotiri, 16 – Poihipi/Ben Lomond. Caldera margins with black dashed line after Houghton et al. (1995a). Inset maps: (a) shows the geographic position of TVZ; (b) red triangles indicate the location of Te Hukui basalt exposures in relation with the architecture of the Puketerata Volcanic Complex (shaded structures are lava domes of Puketerata, yellow and white dashed lines show the rim of ejecta ring and maar craters, red dashed line represents the Orakeikorako Fault) (Kósik et al., 2016a).* ……………………………. **126**

Figure 6.2 *Lower (a) and upper (b) section of Te Hukui Basalt at the E side of the Te Hukui Stream; (c) indicates unit A and its contact with the basement Orakonui ignimbrite; (d. massive polymict breccia of unit B; (b) and (e) show the topmost part of the sequence with variously inclined units of moderately to well-sorted coarse ash and poorly-sorted fine ash layers (unit F).* ……………………………………………………………………………………………………… **128**

Figure 6.3 *Stratigraphic log of the eastern outcrop of Te Hukui sequence (a) with images of accidental lithic fragments of unit B (scales represent 1 cm), and characteristic sections from the western outcrop (b-d); (b) shows a ~50 cm ignimbrite block from unit B, (d) indicates the uppermost part of western outcrop comprising of reworked deposits accumulated near the bottom of the Te Hukui crater, intersected by a listric normal fault.* …………………………… **129**

Figure 6.4 *Grain morphology and petrographic characteristics of the Te Hukui Basalt; (a) slightly cemented lapilli tuff of unit C; (b) grain morphology of -2.5 - -3.5 phi size scoriaceous juvenile fragments from unit F; (c) grain morphology of bulk 2 phi fragments from unit F, (SEM image); (d) typical morphology of 3 phi size basaltic juvenile and accidental rhyolitic fragments, (SEM image); (e) vesicle textures of lithic clast with two types of vesicularity; (f) crystal nodule with plagioclase (pl) and olivine (ol) crystals; (g-h) groundmass textures, vesicle shapes with predominantly lath shaped plagioclase crystals, cross polarised light; (i) SEM image of clinopyroxene (cpx) and plagioclase crystal with resorbed Na-rich core; (j) SEM image of plagioclase crystal with Na-rich spongy cellular core; (k-l) Na and Ca element map of zoned plagioclase crystal captured by field emission SEM (Hokkaido University).* ……………………. **131**

Figure 6.5 *TAS classification of Te Hukui basalt (L.A. lithic A; L.B. lithic B; S.1. – scoria; S.2. – scoria) and other basalts of the Taupo-Whakamaru area (Ben. – Ben Lomond; Kak. – Kakuki; Kin. – Kinloch; K-Tr. – K-Trig; Ong. – Ongaroto; Tat. – Tatua) (Brown et al., 1994; Hiess et al., 2007; Matheson, 2010).* ……………………………………………………………………………………… **133**

Figure 6.6 *Possible topographic relationships between the craters of the Te Hukui Basalt and Puketerata subject to the exposure of the Te Hukui sequence, not to scale; (a) Te Hukui sequence represents intra-crater deposits; (b) exposed Te Hukui sequence represents the remnant of ejecta ring. In both cases, the Te Hukui outcrops were exposed by the latter Puketerata activity.* …………………………………………………………………………………………………. **134**

Figure 6.7 Conceptual model for possible rock types of erupting magma due to the interaction between variable sized basaltic magma intrusions (BI) and rhyolitic melt lenses (ML) in case of a melt-dominated or crystal mush-dominated silicic magma reservoir. Basaltic eruptions are expected only in case of minor interaction with melt lenses (E), while other cases basaltic magma may trigger rhyolitic eruption (A and B) or mixing with rhyolitic magma without eruption (C and D). Magma reservoir model modified after Cashman and Giordano (2014). …………………………………………………………………………………………… **136**

Figure 7.1 Regional map showing the geographic location of the Taupo Volcanic Zone (TVZ) and the site of study (PVC) within the North Island and its relative position to the subduction of the Pacific Plate beneath the Australian Plate (inset map). The border (bold red dashed lines) between the Old TVZ and the Young TVZ and the present-day compositional divisions (red dotted lines) between the more andesitic Southern and Northern TVZ and the rhyolitic Central TVZ are from Wilson et al. (1995). Outlines of rhyolitic calderas (black dashed lines) located within the Young TVZ are from Houghton et al.(1995b) Ka – Kapenga; Ro – Rotorua; Rp - Reporoa; Tp – Taupo; Wh – Whakamaru; Ok – Okataina; Oh – Ohakuri. Vent locations of domes, dome complexes and coulees were mapped from 8 m NZ DEM (LINZ - Land Information New Zealand, 2012) using geological maps of Rotorua area (Leonard et al., 2010) and Okataina Volcanic Centre (Nairn, 2002). ………………………………………………………………………… **142**

Figure 7.2 Location of the PVC (red dashed square) within the Maroa Volcanic Complex with the nearby lava domes (shaded areas), calderas (dashed lines) and mentioned lava domes/flows; 1 Ngangiho, 2 Hipaua, 3 Ben Lomond (inset map) and architecture of the PVC with the active faults (Langridge et al., 2016) and the important exposures of the Puketerata sequence Coordinates are given in New Zealand Transverse Mercator 2000 (NZTM2000) projection. Letters A and B indicate the viewpoints for Fig. 7.3. ………………………………… **145**

Figure 7.3 Panoramic views of the structures of the Puketerata Volcanic Complex. A: The larger dome and the surrounding ejecta ring from the top of the fault carp of the Orakeikorako Fault. B: View from the summit of the smaller dome to chain of the maar craters (locations of viewpoints are shown at Fig. 7.2). ……………………………………………………………………… **146**

Figure 7.4 Cross sections from the prominent parts of the volcanic complex used 2x vertical exaggeration. The paths of the cross sections are shown at Fig.7.2. …………………………… **147**

Figure 7.5 Slope map of the dome and surrounded ejecta ring using a 5 m resolution shaded relief DEM layer as a background indicates the main morphologic features of the volcanic edifice. ……………………………………………………………………………………………………… **149**

Figure 7.6 Key outcrops at proximal locations. Green dashed lines indicate internal disconformities, yellow dashed lines indicate the boundary between Puketerata and the subsequent Taupo Pumice deposits. Fall beds (F) are delimited by red dashed lines. BS: bomb sags. For accurate geographic positions of the outcrops see Fig. 7.2. …………………………… **153**

Figure 7.7 Main outcrops at the road cut of State Highway 1. Major fall beds (F1 to F8) are delimited by red dashed line, block-and-ash flow units (BAF) delimited by black dashed line within yellow background. BS: bomb sags. Yellow dashed lines indicate the boundary between the basement, Puketerata and the subsequent Taupo Pumice deposits. Blue dashed and dotted lines indicate faults and related displacements (5-15). For precise locations of the outcrops see Fig.7.2. ……………………………………………………………………………………………………… **155**

Figure 7.8 Detailed stratigraphic log of the medial deposits of PVC. The lower 2 m (red) observed at locality 5-15, (Figs. 7.2 and 7.7) while the upper part (blue) incorporates the upper sequence from locality 2-09 (Figs. 7.2 and 7.7). The most dominant lithofacies is indicated for each unit using abbreviations of lithofacies. **156**

Figure 7.9 Density distribution of essential clast from selected major fallout beds. (F2, F4, F6 represents single fall beds sampled from 2-09 (Fig. 7.7), the other two layers marked by asterisks at 4-21 and 3-26 (Fig. 7.6). **157**

Figure 7.10 Photomicrographs and BSE images of Puketerata rhyolite. A: Most frequent phenocrysts; plagioclase (pl), biotite (bt) quartz (qz) in glassy fractured groundmass (sample 3-02), B: network of fractures in dense glass (sample 3-02), C: variability of textures of vesicularity (sample 3-03) , D: BSE image of C showing fracturing of glass among vesicles (sample 3-03), E: Deformed flow banding, dark bands are rich in microlites (sample 3-21), F: detail from E showing two types (t1 and t2) of vesicularity in fluidal glassy groundmass (sample 3-21). **161**

Figure 7.11 Example for ejecta ring (tuff ring) - lava dome complexes with different evolution. Rims of ejecta rings are marked by white dashed lines, dome margins are marked by yellow dashed lines. Source of data: Kaleni (Druitt et al., 1995); Panum Crater (Sieh and Bursik, 1986; Kelleher and Cameron, 1990); Cerro Pinto (Zimmer et al., 2010).(*Possible dome volume of Cerro Pinto derived from the volume of BAF deposits). **168**

Figure 7.12 NE-SW trending profiles along the eruptive vents are showing the evolution of the PVC and pre-eruptive volcanic structures (A) at the vicinity of Puketerata (not to scale). Initial phase (B) was characterised by deep to shallow-seated phreatomagmatic activity along the fissure vents. Main stage (C) was dominated by extrusive emplacement of lava domes with associated shallow-seated phreatomagmatic activity and destruction of the larger dome. Excavation of the dome margins created a moat between the dome and the ejecta ring. The late stage of activity was characterised by dome growth with minor explosive activity (D). **171**

Figure 8.1 Geological settings of the Motuoapa Peninsula and its neighbourhood based on a geological map of the Rotorua area (Leonard et al., 2010). The background slope map was derived from an 8 m NZ DEM (LINZ - Land Information New Zealand, 2012) with the coordinate system of New Zealand Transverse Mercator (NZTM2000). See Fig. 2 for the slope map key. The regional map (inset map A) shows the geographic position of Lake Taupo and the TVZ within the North Island and its relative position to the subduction zone. Inset map B indicates the location of the study area relative to Lake Taupo, with the highest localities of lacustrine sediments at Kaiapo (x) and Rangitukua (y). **176**

Figure 8.2 Geomorphology of the Motuoapa Peninsula as indicated by a slope map with a shaded relief DEM layer as a background. Cross section displays the lake terraces formed after the Lake Taupo post-1.8 ka high stand. Data source was a 1 m resolution LiDAR DEM (Waikato Regional Council and NZ Aerial Mapping Ltd., 2006). Inset map (a) shows the morphology of Korohe dome and lake terraces (north of Korohe). **179**

Figure 8.3 Aerial image of the Motuoapa Peninsula with the sampling locations, main geological units and inferred faults (Waikato Regional Aerial Photography Service - WRAPS, 2012): a. pyroclastic sequence relating to the eruption of rhyolite magma; b. brecciated or coherent rhyolitic lava; and c. coherent dacitic lava. **181**

Figure 8.4 *SEM images of variably vesicular ash particles (A-C) with quenching cracks (C, yellow arrow) and a mosaic of microscopic images of well-cemented lapilli tuff with fragments, with highly vesicular cores and non-vesicular chilled rinds (D, red arrows).* …………………. ***182***

Figure 8.5 *Representative pyroclastic sequences of the Motuoapa Penisula. A – Chaotic arrangement of breccia and stratified lapilli tuff (loc. P3, Fig. 8.3); B – Stratified lapilli tuff alternating with matrix-supported diffusively-stratified tuff breccia; C – Non-graded, clast-supported diffusively-stratified tuff breccia; D – Reversely-graded, poorly-sorted, clast-supported tuff breccia (loc. 2-02, Fig. 8.3); E – Normal-graded, poorly-sorted, clast-supported breccia enclosed by non-graded, matrix-supported lapilli tuff (loc. 2-02, Fig. 8.3); F – Matrix-supported diffusively-stratified tuff breccia (loc. P6, Fig. 8.3); G – ~100 m thick alternating sequence of cross-stratified tuff and matrix to clast-supported lapilli tuff (loc. P5, Fig. 8.3); H – Poorly-sorted, diffusively-stratified lapilli tuff from locality 2-05 (Fig. 8.3) with grain size distribution indicated (MD mean diameter; σ=sorting, Folk and Ward, 1957); I-J – Cross-stratified tuff and matrix to clast-supported lapilli tuff (loc. 3-09, Fig. 8.3); K-L – Cross-stratified tuff and matrix to clast-supported lapilli tuff (loc. P5, Fig. 8.3).* …………………………… ***186-187***

Figure 8.6 *Representative outcrops of effusively emplaced lithofacies of Motuoapa Peninsula. A – Columnar-jointed coherent rhyolite lava (loc. P4, Fig. 8.3); B – Flow-banded, flow-foliated coherent rhyolite lava (loc. P2, Fig. 8.3); C-F – Lava breccia with different degrees of fragmentation (loc. P1, Fig. 8.3).* ……………………………………………………………………………….. ***189***

Figure 8.7 *TAS classification of XRF bulk-rock and EPMA matrix glass chemical results of the extrusive rocks located around the Motuoapa Peninsula. Matrix glass compositions of dacite are at least as evolved as the rhyolite. The outlier bulk-rock low alkali content of rhyolite (sample 3-01) is interpreted by sodium loss during hydration (e.g. Fig. 8.8C).* ……………… ***193***

Figure 8.8 *Characteristic macroscopic and microscopic textures of the two rock types of Motuoapa Peninsula. A – Hydrated and fractured glassy rhyolite from locality 3-01 (Fig. 8.3); B – Less hydrated rhyolite lava variety from the pyroclastic sequence located at 2-05 (Fig. 8.3); C – Perlitic texture of rhyolite lava from locality 3-01 (Fig. 8.3); D – Spherulitic rhyolite from locality 2-06 (Fig. 8.3) with black-coloured spherulites (sp), plagioclases (pl) and a crystal of fayalitic olivine (ol); E – Macroscopic appearance of relatively fresh dacite from locality 3-05 (Fig. 8.3); F – Photomicrograph of dacite with plagioclase (pl), amphibole (am) and pyroxene (px) phenocrysts from locality 2-04 (Fig. 8.3).* ……………………………………………………………. ***194***

Figure 8.9 *Plagioclase and pyroxene compositions of the two rock types of the Motuoapa Peninsula. Classification is after Morimoto (1988). Pink squares represent groundmass plagioclase/pyroxene of rhyolite; green triangles represent plagioclase/pyroxene of dacite.* ……………………………………………………………………………………………………….. ***195***

Figure 8.10 *Amphibole classifications of Motuoapa rocks based on Leake et al. (1997). The amphiboles of rhyolites and dacites are well separated by their different characteristic magnesium numbers and the combined Na and K contents at the cation position A. Calculations were performed using a programmed excel sheet of Locock (2014). Pink squares represent amphiboles of rhyolite; green triangles represent amphiboles of dacite.* ………. ***196***

Figure 8.11 *Harker diagrams for selected major element oxides normalised to water-free compositions. Pink squares represent groundmass glass of rhyolite; green triangles represent groundmass glass of dacite.* ………………………………………………………………………………………. ***197***

Figure 8.12 *Stratigraphy of pyroclastic sequences and structure of the Motuoapa Peninsula indicated on a 1 m LiDAR DEM. The cliff's height near the vent is about 100 m.* ***201***

Figure 9.1 *Vent locations of the eruptions of the young TVZ that produced up to 7.5 km3 DRE volcanic material (Appendix A.9.1). Chemical compositions of the erupted magmas associated with distinct vents are indicated (Nairn, 2002; Leonard et al., 2010). Dashed lines indicate the caldera margins proposed by Wilson et al. (1995). Base map topography was derived from the contour lines of the New Zealand Topo50 map series and the lake bathymetries of the Rotoaira, Taupo, Rotomahana, Tarawera, Okataina, Rotorua, Rotoiti and Rotoma lakes.* ***211***

Figure 9.2 *Locations of hydrothermal/phreatic eruption craters that have not been associated directly to the activity of polygenetic volcanoes, such as Ruapehu, Tongariro and White Island; 1 – Kairua Park and Te Puia, Rotorua; 2 – Tikitere – Hellsgate Geothermal Park; 3 – Kawerau Geothermal Field; 4 – Rerewhakaaitu fissures; 5 Waimangu-Waiotapu; 6 – Orakeikorako; 7 – Rotokawa; 8 – Craters of the Moon. Geothermal fields are after Rowland and Sibson (2004), calderas margins (black dashed lines) are after Wilson et al. (1995).* ***212***

Figure 9.3 *Example for the varied awareness of fault locations between relatively old surfaces (area of Kapenga) and areas covered by young volcanic deposits (Okataina) or lakes (Lake Rotorua) based on GNS Active Fault Database. 1 – Okareka embayment; 2 – Puhipuhi basin; 3 – Rotoma caldera. Traces of fault from the 1:250000 active faults database of New Zealand (Langridge et al., 2016), caldera margins are after Wilson et al. (1995). Coordinates are given in NZTM2000 projection.* ***215***

Figure 9.4 *Spatial relationships (distance and azimuth) between vents and the nearest structural/volcanic features of the TVZ. A – Vents versus faults; B – Vents versus caldera margins; C – Vents versus vents.* ***216***

Figure 9.5 *Temporal characterisation of the small-volume volcanism of the TVZ. A – Number of vents within a 25 ky intervals. B – Age as a function of distance from the southernmost silicic event (Motuopuhi Island, Lake Rotoaira) to NE along the extensional axis of the TVZ. The NE and SW limits of calderas were indicated by the same way as vent locations.* ***220***

Figure 9.6 *Spatial distribution of post-Rotoiti basaltic and silicic vents of the central, predominantly silicic part of TVZ. Caldera margins (dashed lines) are indicated after Wilson et al. (1995).* ***222***

Figure 9.7 *Spatial distribution of silicic lava domes and coulees (light red shaded areas) and erupted volumes in DRE of effusive and explosive eruptions of TVZ within the past 350 ky. Dashed lines indicate the caldera margins proposed by Wilson et al. (1995). Inset Figure (A) indicates the volume size distribution of distinct volcanic events in the past 350 ky.* ***223***

Figure 9.8 *DRE volumes as a function of distance from the southernmost silicic event (Motuopuhi Island, Lake Rotoaira) to NE along the extensional axis of TVZ. A indicates erupted volumes under 10 km3, B is zooming to events under 1 km3 erupted volumes.* ***224***

Figure 9.9 *Cumulative DRE volumes as a function of time for the central TVZ's 337 small-volume eruptions within the past 350 ka. For comparison, the caldera-forming eruptions' temporal distribution and erupted DRE volumes are indicated after Wilson et al. (2009), Danišík et al. (2012) and Gravley et al. (2016);. Wh – Whakamaru, Pa – Paeroa Subgroup, Mat – Matahina, Ch – Chimpanzee, Po – Pokai, Mam – Mamaku Plateau, Oh – Ohakuri, Ka – Kaingaroa, Mo – Mokai, Ro – Rotoiti, Or – Oruanui, Tp – Taupo.* ***225***

Figure 10.1 First approach eruption prediction map for small-volume eruptions of the central TVZ prepared by a combined overlay of the 10 km kernel density map of post-Whakamaru eruptions (Inset A) and structural alignments (faults and calderas) of the TVZ from Langridge et al. (2016) and Wilson et al., (1995). Post-Rotoiti eruptions are indicated by white triangles, letters in yellow square indicate the location of major townships (T: Taupo and R: Rotorua). …….. **255**

Figure 10.2 Preliminary susceptibility map for hydrovolcanic eruptions within the central TVZ prepared by a combined overlay of spatially-identified environmental factors may contribute to inducing hydrovolcanic activity. Caldera margins after Wilson et al. (1995), letters in yellow square indicate the location of major townships (T: Taupo and R: Rotorua). ……………… **257**

List of tables

Table 2.1 Stratigraphic relationship, source and estimated volumes of large-volume, caldera-forming eruptions of the TVZ. DRE volume estimates for most deposits are based on known mapped extents and recorded thicknesses that are converted, assuming that bulk volumes are equivalent to magma volumes when erosion and co-eruptive fall deposits now missing are taken into account (Wilson et al. 2009). The age of eruptions was compiled from: 1 – Wilson et al. (2009); 2 – Leonard et al. (2010); 3 – Deering et al. (2010); 4 – Danišík et al. (2012); 5 – Downs et al. (2014b); 6 – Gravley et al. (2016). ………………………………………………………… **17**

Table 3.1 Effusion rates of well-documented lava dome extrusions from the 20th and 21st centuries (Newhall and Melson, 1983; Yokoyama, 2005; Pallister et al., 2013; Tuffen et al., 2013). …… **47**

Table 3.2 Summary of the characteristic morphometric features of domes distinguished in the new classification proposed (preliminary results). ……………………………………… **63**

Table 5.1 Bubble volume (BV), bubble number density (NV) and typical sizes (equivalent diameter: EqDi) and shapes of vesicles (Regularity, Shape factor) for distinct units and clasts from the proximal sequence of EER. ……………………………………………………………… **106**

Table 5.2 Results of geothermobarometry calculations utilizing Putirka's (2008) two-pyroxene calculations on phenocrysts of bombs and blocks. Earlier calculations (Deering et al., 2011) indicate deeper source region for the erupted magma. ………………………………………… **111**

Table 5.3 Results of DRE volume estimations for the OVC based on bulk edifice volume calculated from DTM of Ohakune and DRE correction schemes presented at Fig. 5.14. …. **115**

Table 6.1 Whole rock major and trace element geochemistry of the Te Hukui Basalt and compositions of Tatua and Ben Lomond Basalts (Hiess et al., 2007). The scoriaceous fragments for S.1 and S.2 samples were collected from the outcrop on the eastern side of Te Hukui Stream from unit F as indicated in Fig. 2b by asterisks. Compositions of scoriaceous fragments indicate some contamination with country rocks. Analyses are by XRF at University of Waikato, New Zealand. ……………………………………………………………………………………………… **132**

Table 7.1 Morphometrical characteristics of selected basaltic (B) and rhyolitic (RH) ejecta rings of tuff rings and maars from the Acigöl Complex, Central Anatolia; Lunar Crater Volcanic Field (LCVF) and Mono Craters (MC), California; Serdán-Oriental (S-O), Trans-Mexican Volcanic Belt and Auckland Volcanic Field (AVF) and Taupo Volcanic Zone (TVZ), New Zealand). *Cerro Pinto ejecta ring most likely sits on the top of block-and-ash flow fans, which extra height difference is included in the 210 m (Zimmer et al., 2010). ………………………………………………………… **148**

Table 7.2 Volume calculation's results of distinct structures of PVC (excluding diatremes) using different resolution DEMs and basement elevations have been identified from cross sections (Fig. 7.4) and field observations. DRE indexes were defined by density measurements of fragments collected from fall beds (Fig. 7.9) and the observed vesicularity of dome rocks. …………………………………………………………………………………………………… **158**

Table 7.3 Compositional range of groundmass glass based on 29 measurements on samples from 3-02, 3-03, 3-04 and 3-21 (Fig. 7.2). ………………………………………………………… **160**

Table 7.4 *Thermometry results based on feldspar-liquid and two-feldspar thermometers of Putirka (2008). For groundmass glass and plagioclase major element compositions see Appendix A.7.1.* …… ***162***

Table 8.1 *Summary of the characteristics of volcanic lithofacies of the Motuoapa Peninsula.* …… ***185***

Table 8.2 *Volume calculations of erupted DRE volume from vents near Motuoapa Peninsula.* …… ***191***

Table 8.3 *Whole rock major and trace element results of XRF measurements. Sample names refer to the sampling points indicated at Fig.8.3.* …… ***192***

Table 10.1 *Summary of general eruption-related, petrologic, morphometric, sedimentary and pyroclastic characteristics of studied volcanoes.* …… ***229***

Table 10.2 *Typical eruption rates and eruption durations of TVZ volcanism derived from eruptive volumes of distinct volcanic events. (1) (Harris et al., 2003), (2) (Lyman et al., 2004).* …… ***253***

Chapter 1

Chapter 1 introduces the aims, objectives and the scientific background of this research, as well as the basic concepts of small-volume/monogenetic volcanism with a linkage to the volcanic activity of the Taupo Volcanic Zone.

Chapter 1 – Introduction

1.1 Small-volume volcanism of silicic caldera systems

Small-volume or monogenetic volcanism refers to the volcanic activity characterised by one single eruption episode with a short duration (hours to years or rarely decades) fed through a newly-established magma plumbing system (e.g. Németh, 2010; White and Ross, 2011; Smith and Németh, 2017). These volcanoes are generally, but not exclusively, characterised by erupted volumes less than 1 km^3 as a part of spatially and temporally dispersed eruptions that often form volcanic fields (Connor et al., 2000; Németh, 2010; Németh and Kereszturi, 2015). Large volcanic fields may encompass many different host rock lithologies and local structural conditions along with the time-variant ground water configurations and hydrographical conditions, which, regardless of the lack of the variability of magmatic internal properties, facilitate the heterogeneity of eruption styles and volcanic structures in time and space (Valentine and Gregg, 2008; Németh, 2010; Kereszturi and Németh, 2012; Kereszturi et al., 2014b; Smith and Németh, 2017). Volcanic fields are common in various tectonic environments and most frequently involve magmas of mafic chemical compositions (e.g. Valentine and Gregg, 2008; Smith and Németh, 2017). The occurrence of polygenetic activity and eruptions of more evolved magmas in volcanic fields are considered to be the result of increasing magma flux (Németh, 2010; Smith and Németh, 2017). From this perspective, caldera systems represent the opposite setting with a very high magma flux and output rate, such as the central part of the Taupo Volcanic Zone (TVZ) in New Zealand (Houghton et al., 1995b; Wilson et al., 1995).

The volcanic activity of the TVZ is dominated by 12 substantial eruptions associated with caldera formation that produced ~3300 km^3 of volcanic material in the past 350 ky (Wilson et al., 2009; Gravley et al., 2016). Nevertheless, the focus of this study is on the small-volume eruptions occurring at least 30 times more frequently, as indicated by the more than 300 volcanic structures and/or related deposits appearing as mappable lithological units cropping out and scattered along the entire TVZ (Nairn, 2002; Townsend et al., 2008; Leonard et al., 2010; Lee et al., 2011). The frequency and the calculated ~250 km^3 erupted volume relating to small-volume eruptions may be far larger, if we consider the possible volume of buried and eroded structures and deposits (Downs et al., 2014a; Cattell, 2015). Without the contribution of caldera-forming eruptions, the magma output rate of the TVZ is still 10 to 100 times larger than the usual values of volcanic fields (Kuntz et al., 1986; Connor and Conway, 2000; Valentine and Perry, 2006; Kereszturi et al., 2013; Le Corvec et al., 2013), which highlights the significant hazard posed by these small-volume eruptions. In spite of the high magma flux, veritable polygenetic volcanoes are only located at the southern and northern parts of the TVZ (e.g. Ruapehu; Hackett and Houghton, 1989; Conway et al., 2016), whereas its central part is characterised by short-lived eruptions with newly-forming vents, including erupted volumes of the two extremes (e.g. Gravley et al., 2016; Kósik et al., 2017b). The majority of documented small-volume eruptions of the TVZ are characterised by the involvement of rhyolitic magma in accordance with the high rate of heat flow (Smith and Németh, 2017), but other eruptions with markedly lower incidence indicate mostly basaltic or dacitic compositions (Leonard et al., 2010). In the silicic realm, small-volume eruptions most frequently create lava domes or coulees often associated with initial explosive activity (Heiken and Wohletz, 1987), however, decreasing magma volumes that are potentially associated with lower magma flux may allow environmental factors to influence or dominate the course of the activity (Kereszturi et al., 2014b; Kósik et al., 2016b; Kósik et al., 2017a; Smith and Németh, 2017).

1.2 Problem statement

In respect of silicic caldera volcanism, the main focus is often on the climactic super-eruptions producing hundreds to thousands of km^3 volume of volcanic material during the evacuation of the magma reservoir, which coincides with the formation of a morphological depression (caldera) due to the subsidence or collapse of the ground surface (e.g. Cole et al., 2005). The hazards and consequences of such large-volume eruptions overshadow the more frequent smaller events, which with random occurrence, great variability of eruption styles, the usual notable volume, and prolonged eruption duration imply serious impacts at local or sometimes regional scales. The TVZ includes more than 300 known small-volume eruptions in the past 350 ka, however only a few of these volcanoes have been evaluated previously regarding their physical volcanology and eruption history (e.g. eruption styles, duration of activity) (Lewis, 1968; Houghton and Hackett, 1984; Brooker et al., 1993; Brown, et al 1994). Small-volume eruptions of the TVZ are sporadically distributed and their appearance is not only influenced by and limited to the structures of latterly collapsed calderas. These eruptions most likely hold the key to understanding the trigger mechanisms of small to large eruptions (e.g. mafic magma injections, as per Nairn and Cole, 1981; Nairn, 1992; Leonard et al., 2002; Nairn et al., 2004; Shane et al., 2007), and processes of melt propagation from source to surface. In addition, they can be fairly energetic eruption events, and thus may pose an immediate hazard to the population and economy of the North Island of New Zealand. Shifting from a single vent or event scale out to the field-scale, the temporal, spatial and volumetric patterns of these smaller events may indicate the evolutionary trends of the overall magmatic system including melt extraction from stalled silicic crystal mush and interaction between crystal mush and ascending less evolved magmas (Smith et al., 2005; Kilgour and Smith, 2008; Bégué et al., 2014).

1.3 Aims and objectives

This study aims to contribute to the understanding of hazards posed by small-volume eruptions within the TVZ through exploring the characteristics of the volcanic activity of small-volume volcanoes. This was approached through two different scales, where it was aimed:

(1) To provide eruption scenarios for small-volume eruptions of the TVZ by investigating selected eruption sites that represent the best possible geologically-validated set of information regarding expected similar-sized eruptions taking place in the future;

(2) To investigate the spatial, temporal, volumetric and eruption-style patterns of small-volume volcanism in relation to caldera-forming and polygenetic volcanism on the scale of the TVZ using Geographic Information System (GIS) techniques.

The main part of the research comprises the detailed investigation of three carefully selected study sites by physical volcanology and GIS in order to determine the volcanological processes and evolution of small-volume eruptions at the local scale. The study sites (Ohakune, Motuoapa and Puketerata, Fig. 1.1) represent different environmental settings, with contrasting basement geological and hydrogeological conditions suspected to play an important role in influencing the volcanic eruption styles (hence the resulting volcanic edifice and its associated effusive and pyroclastic lithofacies). The examined volcanoes are characterised by various eruption styles and chemical conditions (basaltic to rhyolitic) and a complex evolution. The geological information gathered from the specific sites can be used as a proxy for other similar-sized eruptions when shifting to the field-scale of the TVZ. To unfold the relationship between small-volume eruptions and the large-volume volcanism of calderas requires broader-scale investigation of the entire TVZ. In order to reach this goal, the spatial, temporal and volumetric distributions of small-volume eruptions were determined, in order to be able to explore their significance and geological patterns in a broader context. As a part of this research the following objectives were planned to be executed:

(a) Elucidate the volcanic evolution of the parasitic Ohakune tuff ring-scoria cone complex and describe its andesitic explosive activity;
(b) Understand the evolution of the silicic fissure eruption of Puketerata and its explosive activity, as well as determine the factors which control the formation of maars and lava domes along an eruptive fissure;
(c) Elucidate the volcanic processes of a silicic eruption initiated in a subaqueous environment (Motuoapa, Lake Taupo);
(d) Define the hazards and risk of both silicic and mafic small-volume eruptions in the TVZ based on study sites and information gathered from Digital Elevation Model (DEM)-based terrain analysis of the TVZ;
(e) Define the conditions which control the syn-volcanic and the post-volcanic shape of the lava domes within the TVZ by GIS-based morphometrical analyses in the context of global perspectives;
(f) Understand the spatial and temporal relationship between the eruptions of small-volume volcanoes and their neighbouring central volcanoes.

1.4 Thesis outline and structure

This thesis consists of 10 chapters, which can be grouped into four parts. The first four chapters after the introduction (Chapter 1) include a literature review of the geological setting and volcanism of the TVZ (Chapter 2), and a review of silicic small-volume/monogenetic volcanism with a specific focus on lava dome volcanism (Chapter 3). The end of Chapter 3 includes a proposed new classification of lava domes based on the macro-morphology of their structures. The first part of thesis is finished by Chapter 4, which presents the applied field and laboratory techniques.

The main body of the thesis consists of one submitted and three published manuscripts; hence there is some repetition between chapters, particularly about the geology of the TVZ. These manuscripts act as case studies to provide a comprehensive overview of the eruption scenarios of most common-sized small-volume eruptions of the TVZ. Chapter 5 reports on the alternating phreatomagmatic and Strombolian activity of the andesitic Ohakune Volcanic Complex (OVC) located on the distal southern ring plain of the Ruapehu volcano (Fig. 1.1). Chapter 6 introduces the previously unknown Te Hukui basaltic maar, which was fortuitously discovered underneath the deposits of the younger silicic eruption of Puketerata. The deep excavation during the Te Hukui eruption is proved by the varieties of accidental clasts that comprise extrusive rocks with no surface exposures. Chapter 7 explores the volcanic evolution and morphology of the silicic Puketerata Volcanic Complex (PVC), with implications for eruption triggering and conduit processes. The third study site encompasses the volcanic activity of Motuoapa Peninsula and neighbouring areas (Chapter 8), which consists of the products of two temporally separate eruptions. The earlier activity is an example of a silicic activity initiated in subaqueous environment with emergent final phases, whereas the later dacitic eruptions represent some of the youngest silicic events in the southernmost part of the central TVZ. As an offspring, LiDAR-based terrain analysis of the peninsula contributes to a better understanding of the post-1.8 ka lake level changes of Lake Taupo.

As a separate entity, Chapter 9 summarises the first results of the spatio-temporal and volumetric analyses of small-volume volcanism on the scale of the TVZ. This chapter is considered as a good starting reference for further research on this topic.

The final section of the thesis (Chapter 10) provides a discussion on the small-volume volcanism of TVZ, including the subjects of the source of erupting magmas, characteristics of eruption styles, and internal and external factors influencing volcanic activity, as well as expected durations of distinct volcanic events. In essence, the chapter defines the main factors contributing to the hazard of small-volume eruptions, with two conceptual models developed for exploring the spatial likelihood of forthcoming eruptions and the susceptibility to hydrovolcanic activity within the central TVZ. Ultimately, the conclusion summarises the realisation of the research objectives and provides directions for further research on the small-volume volcanism of TVZ.

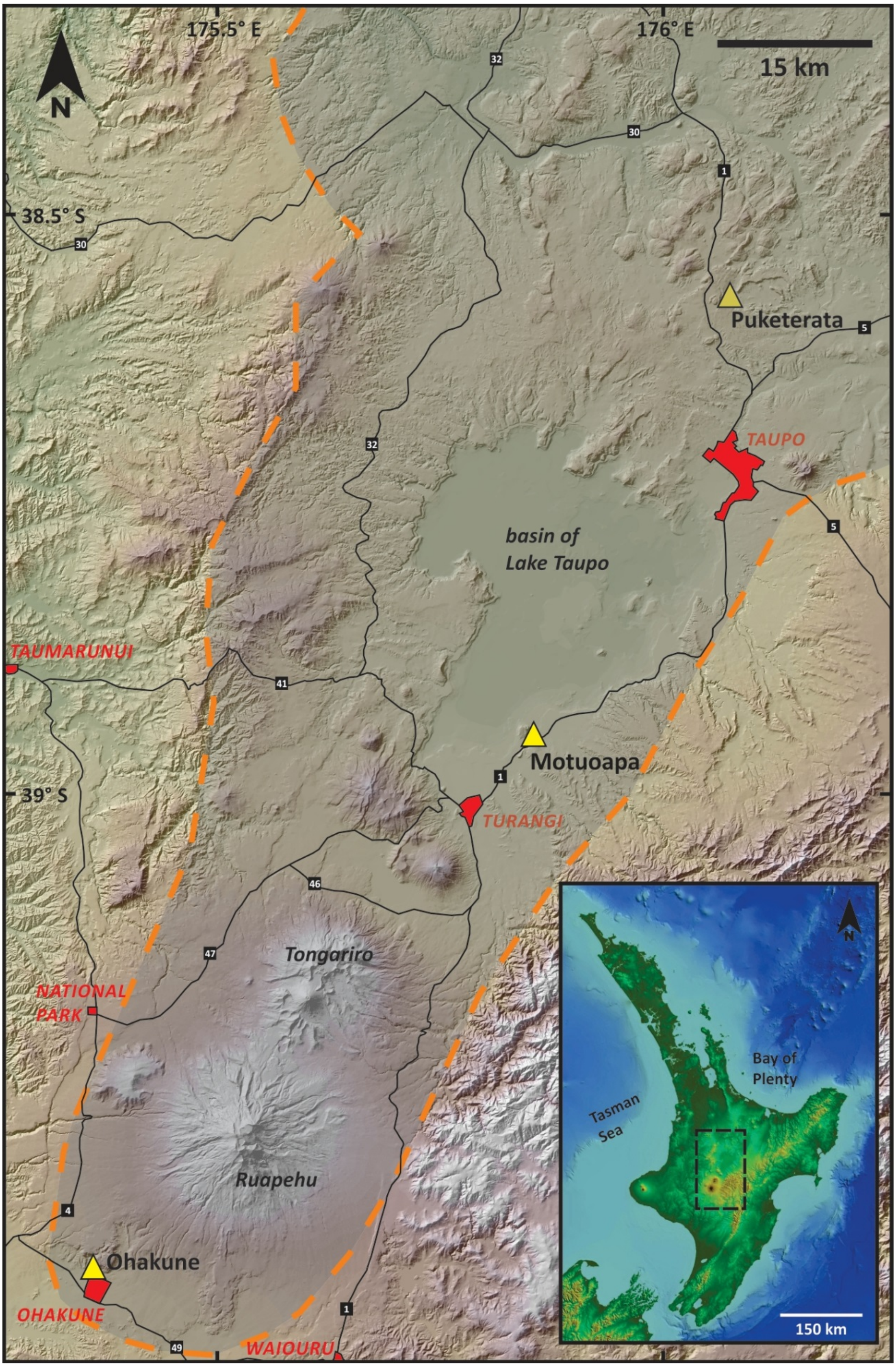
N
175.5° E
176° E
15 km
38.5° S
39° S
32
30
1
5
41
46
47
4
49
Puketerata
TAUPO
basin of
Lake Taupo
TAUMARUNUI
Motuoapa
TURANGI
Tongariro
NATIONAL
PARK
Ruapehu
Ohakune
OHAKUNE
WAIOURU
Bay of
Plenty
Tasman
Sea
150 km

Figure 1.1 Locations of the examined case study volcanoes. The boundary (orange dashed lines) of the TVZ (sheded area) after Wilson et al. (1995). The inset map indicates the position of the area of interest within the central North Island of New Zealand. Main roads are indicated by black lines and red polygons represent important townships.

Chapter

2

Chapter 2 presents the geological settings and evolution of the broader area of North Island of New Zealand, as well as the volcanic architecture of the young Taupo Volcanic Zone.

Chapter 2 – Geological setting

2.1 Structural settings and evolution of the TVZ

The TVZ is the southernmost section of the 2800 km long Tonga-Kermadec arc-back-arc system established at the convergent plate boundary between the Pacific and Australian plates at 2 Ma. From the early Miocene the tectonic regime and volcanic activity of the broader area of North Island were strongly linked to and influenced by complex subductional settings. The first subduction related to a SE-NW trending volcanic arc was established along the Three Kings Ridge southwards to Northland in the Early Miocene (23-18 Ma) (Fig. 2.1) (Herzer, 1995; Mortimer et al., 2010), comprising small to medium-sized basaltic to andesitic shield and cone structures (Smith et al., 1989). From 17 Ma, subduction ceased in at Northland and began along the ENE trending Colville-Lau volcanic arc associated with the convergent plate boundary between the Australian and Pacific plates. The associated Middle Miocene to Early Pleistocene (~18-2 Ma) andesitic to rhyolitic products are mostly preserved onshore in the Coromandel Peninsula and nearby islands, referred to as as the Coromandel Volcanic Zone (CVZ) (Figs. 2.1 and 2.2) (Mortimer et al., 2010; Booden et al., 2012). As a result of the rifting of the Colville-Lau arc from ~5.5 Ma due to the changes of pole rotation of the Pacific Plate, the arc was transferred to the east, forming the Kermadec Arc and opening the Havre Trough back-arc basin in between (Fig. 2.1) (Herzer, 1995; Ballance et al., 1999; King, 2000; Mortimer et al., 2007; Mortimer et al., 2010).

The current configuration is determined by the westward subduction of a 15-25 km thick oceanic crust segment called the Hikurangi Plateau located offshore of the east coast of the North Island (Ballance, 1976; Cole and Lewis, 1981; Mortimer et al., 2010; Reyners, 2013; Timm et al., 2014) (Fig. 2.1). The Hikurangi Plateau is a piece of the Ontong Java Nui Large Igneous Province (LIP), formed as a result of mantle plume magmatism at 125-117 Ma (Timm et al., 2014; Zhang and Li, 2016; Hochmuth and Gohl, 2017). The difference in thickness between the Hikurangi Plateau and the 4-6 km thick crust underneath the Pacific Ocean to the north, as well as the altered and buoyant nature of the LIP-related crust, must have a strong effect on tectonic erosion and the local plate stress regime, as well as being a contributor of volatile components to the overlying mantle (Timm et al., 2014). As a result, the convergence along the Hikurangi Trench is characterised by a shallow-angle oblique (~20°) subduction with a rate of motion of 47-55 mm/yr in the north and 38 mm/yr in the south (Figs. 2.1 and 2.3) (Henrys et al., 2003; Reyners, 2013). As a consequence, the fore-arc is either characterised by extensive shortening due to the reverse faulting of the accretionary prism and dextral strike-slip movements, which are mostly restricted to the eastern margin of the Axial Ranges, or is being induced rotation-like in a clockwise direction as several discrete blocks in the east coast of the North Island (Figs. 2.2 and 2.3) (Davey et al., 1986; Cashman et al., 1992; Barnes and Lépinay, 1997; Beanland and Haines, 1998; Reyners, 1998; Wallace et al., 2004).

The basement of the central North Island consists of Late Paleozoic to Early Mesozoic weakly metamorphosed sandstones and mudstones (greywacke), which are exposed as the thrust-faulted Axial Ranges. Within the fore-arc basins the greywacke is overlain by Early Cretaceous to Late Pliocene calcareous marine sediments (Mortimer, 1994; Lee et al., 2011). The volcanic arc is located about 250 km west of the Hikurangi Trench and coincides with a back-arc rifting, which is accommodated on a highly-thinned crust up to 15-20 km (Bibby et al., 1995; Harrison and White, 2004; Stratford and Stern, 2006; Reyners et al., 2007; Davey, 2010) and a dense system of predominantly NNE-SSW trending, steeply-dipping normal faults of the Taupo rift (Fig. 2.3) (Rowland and Sibson, 2001; Villamor and Berryman, 2001). The fault slip data of the TVZ indicates that rates of rifting increase from 3mm/yr in the SW to 15mm in the NE (Villamor and Berryman, 2001; Wallace et al., 2004), together with a dextral shear of 2.6 mm/yr (Acocella et al., 2003).

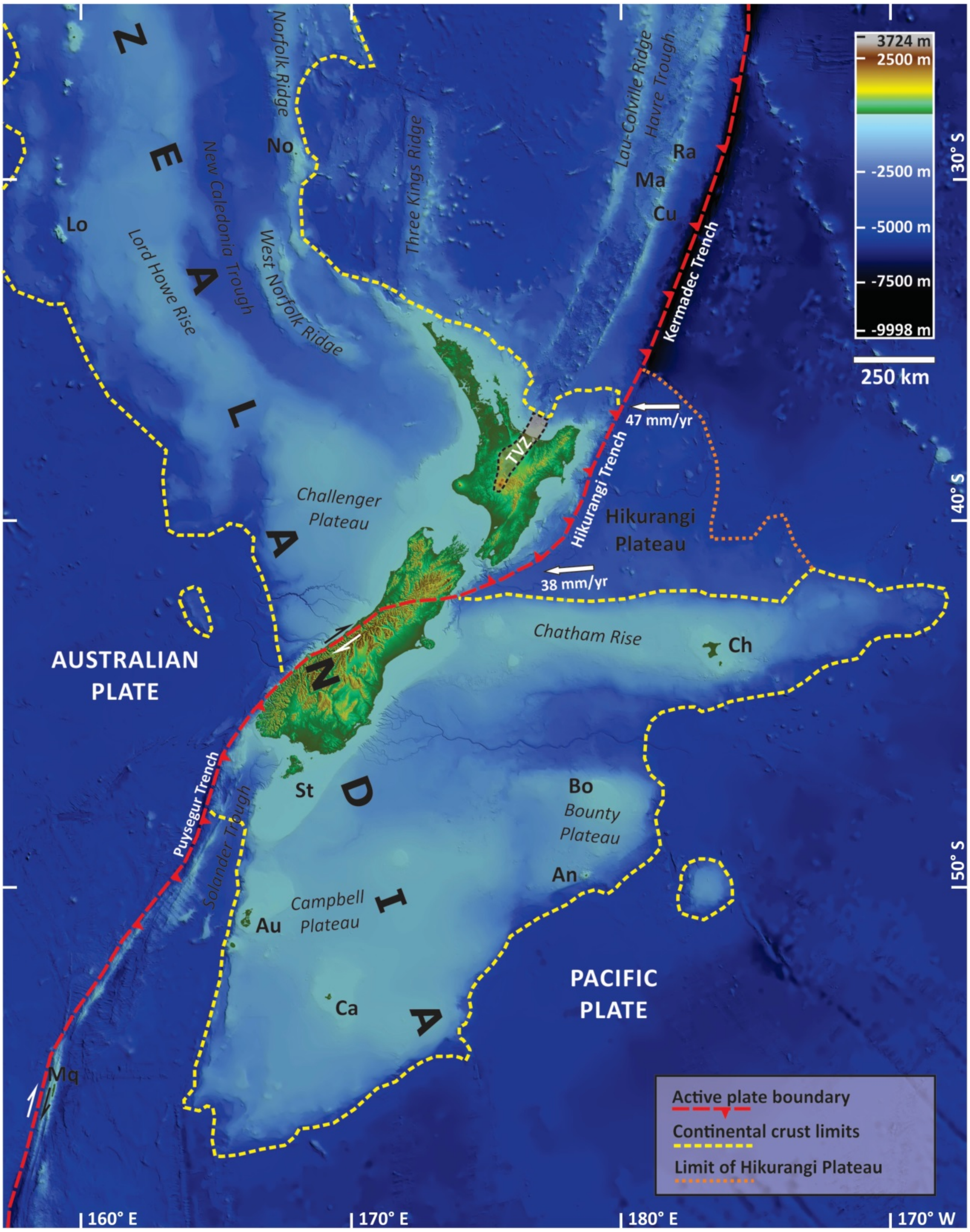
Z
E
A
L
A
N
D
I
A
Norfolk Ridge
No
New Caledonia Trough
Lo
Lord Howe Rise
West Norfolk Ridge
Three Kings Ridge
Lau-Colville Ridge
Havre Trough
Ra
Ma
Cu
Kermadec Trench
3724 m
2500 m
-2500 m
-5000 m
-7500 m
-9998 m
250 km
30° S
40° S
50° S
47 mm/yr
TVZ
Hikurangi Trench
Hikurangi Plateau
38 mm/yr
Challenger Plateau
Chatham Rise
Ch
AUSTRALIAN PLATE
St
Puysegur Trench
Solander Trough
Bo
Bounty Plateau
An
Campbell Plateau
Au
Ca
PACIFIC PLATE
Mq
Active plate boundary
Continental crust limits
Limit of Hikurangi Plateau
160° E
170° E
180° E
170° W

Figure 2.1 Topographic and tectonic settings of the broader environment of New Zealand (Zealandia), with respect to the position of the TVZ. Topographic information was derived from 250 m resolution gridded bathymetric data, National Institute of Water and Atmospheric Research (NIWA) (New Zealand Regional Bathymetry 2016). Tectonic and structural information from Mortimer et al. (2017). Au – Auckland Islands; An – Antipodes Islands; Bo – Bounty Islands; Ca – Campbell Island; Ch – Chatham Islands; Cu – Curtis Island; Lo – Lord Howe Island; Ma – Macauley Island; Mq – Macquaire Island; No – Norfolk Island; Ra – Raoul Island; St – Stewart Island.

The fluids originating from the metasomatised subducting slab induce partial melting in the mantle wedge that is overlapped by decompression-driven melting due to an active back-arc extension, which together provides a vast magma source for calc-alkaline volcanism in the North Island of New Zealand (Price et al., 1992; Gamble et al., 1993b). The generation of most primitive erupted magmas is related to a low degree of partial melting (<10%) of the mantle peridotite, which also indicates chemical enrichment due to the likely contribution of slab components and the further effects of lithospheric contributions (Gamble et al., 1993a; Graham et al., 1995; Hiess et al., 2007). Most commonly, mafic magma is fractionating and assimilating the greywacke basement while migrating through the crust (Harrison and White, 2004; Charlier et al., 2008) or interacting with melt-dominated plutonic bodies (Blake et al., 1992; Leonard et al., 2002; Shane et al., 2007; Kósik et al., 2017b). Rarely, mafic magma may reach the surface via dykes (Nairn and Cole, 1981), demonstrated by the few dozen basaltic occurrences spread over the TVZ (Houghton et al., 1987; Hiess et al., 2007) (the locations of basaltic eruptions are discussed in Chapter 9). Evolved melts have an upper crustal origin as a result of a combination of fractionation from mafic mantle-derived magmas and crustal anatexis (Graham et al., 1995; Charlier et al., 2004). Evolved magmas may also go through multiple mixing events of different magmas prior to their eruption (Blake et al., 1992; Graham et al., 1995; Leonard et al., 2002; Charlier et al., 2004).

The TVZ volcanic activity began around 2 Ma with predominantly andesitic activity, which marks the start of the transition of the volcanic activity from the CVZ to the TVZ (Wilson et al., 1995; Briggs et al., 2005; Gravley et al., 2016). The transition between the two arcs is considered to be completed by the first large silicic eruption of the modern arc (Ngaroma ignimbrite, dense rock equivalent (DRE) volume: ~100 km^3), indicating a substantial shift in back-arc rifting and associated caldera volcanism at 1.55 Ma (Briggs et al., 2005; Wilson et al., 2009).

The volcanism of the TVZ is divided into two time periods representing different vent localisations and the geochemistry of the erupted magmas. From 2 Ma to 0.7 Ma activity was characterised by andesite-dominated volcanism, whereas the second period from 0.7 to the present is dominated by rhyolitic volcanism in the central part

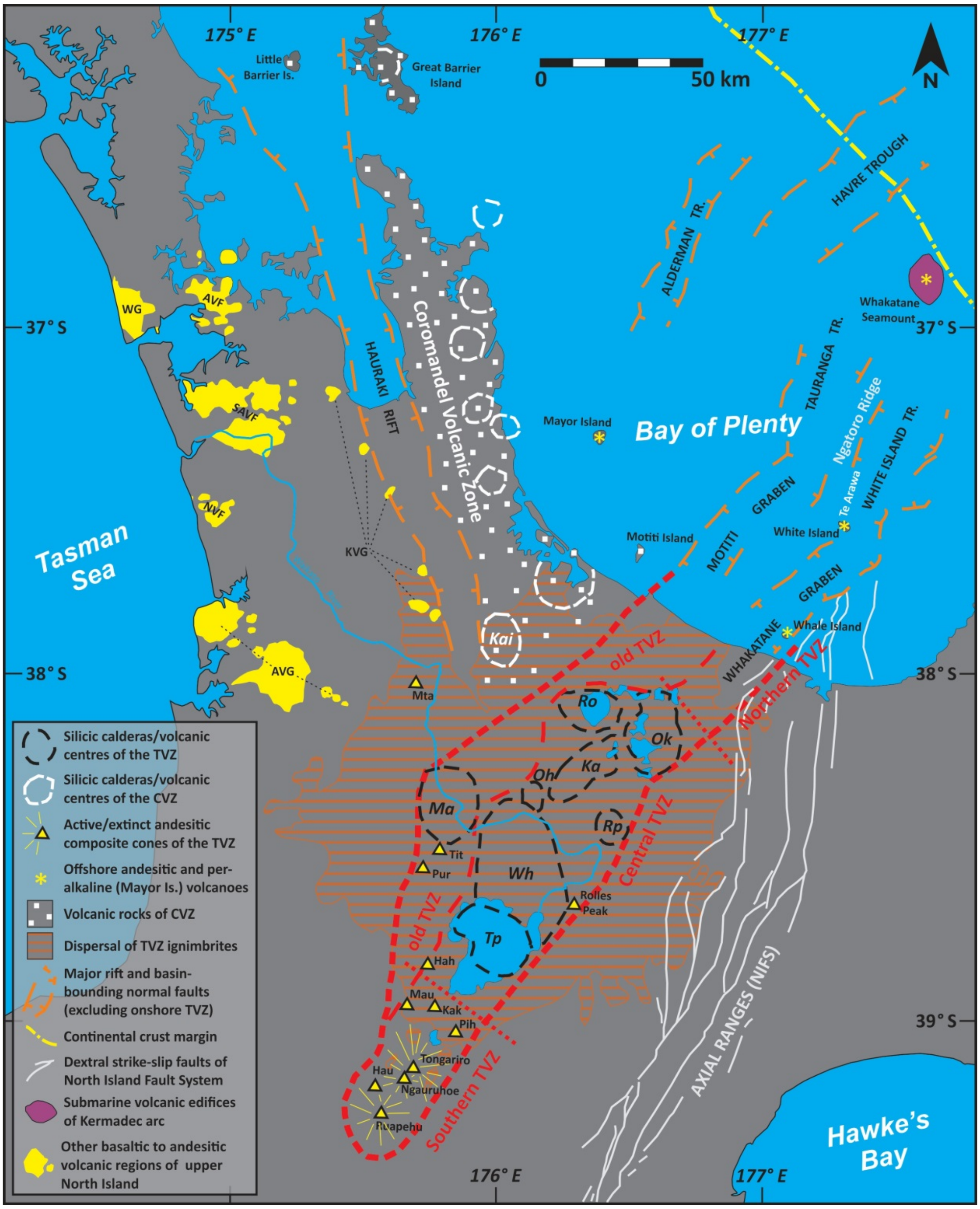
175° E
176° E
177° E
Little Barrier Is.
Great Barrier Island
0
50 km
N
HAVRE TROUGH
ALDERMAN TR.
Whakatane Seamount
37° S
37° S
TAURANGA TR.
Ngatoro Ridge
WHITE ISLAND TR.
Mayor Island
Bay of Plenty
MOTITI
GRABEN
Te Arawa
White Island
Motiti Island
GRABEN
Whale Island
WHAKATANE
Coromandel Volcanic Zone
HAURAKI
RIFT
KVG
WG
AVF
SAVF
NVF
AVG
Tasman Sea
Kai
old TVZ
Northern TVZ
38° S
38° S
Mta
Ro
Ok
Ka
Oh
Ma
Rp
Central TVZ
Tit
Pur
Wh
Rolles Peak
Tp
old TVZ
Hah
Mau
Kak
Pih
Tongariro
Hau
Ngauruhoe
Ruapehu
Southern TVZ
AXIAL RANGES (NIFS)
39° S
Hawke's Bay
176° E
177° E
Silicic calderas/volcanic centres of the TVZ
Silicic calderas/volcanic centres of the CVZ
Active/extinct andesitic composite cones of the TVZ
Offshore andesitic and per-alkaline (Mayor Is.) volcanoes
Volcanic rocks of CVZ
Dispersal of TVZ ignimbrites
Major rift and basin-bounding normal faults (excluding onshore TVZ)
Continental crust margin
Dextral strike-slip faults of North Island Fault System
Submarine volcanic edifices of Kermadec arc
Other basaltic to andesitic volcanic regions of upper North Island

Figure 2.2 Map of the upper North Island of New Zealand indicating the margin and main volcanic structures (calderas: Ma – Mangakino; Ka – Kapenga; Wh – Whakamaru; Oh – Ohakuri; Ro – Rotorua; Rp – Reporoa; Ok – Okataina; Tp – Taupo; and andesitic composite cones: Mta – Maungatautari; Tit – Titiraupenga; Pur – Pureora; Hah – Hauhungaroa; Hau – Hauhungatahi; Mau – Maungakatote; Kak – Kakaramea; Pih - Pihanga) of the old and young TVZ in relation to the CVZ, Kermadec arc, Havre Trough and other Neogene volcanic fields of the North Island; WG – Waitakere Group; AVF – Auckland Volcanic Field; SAVF – South Auckland Volcanic Field; NVF – Ngatatura Volcanic Field; KVG – Kiwitahi Volcanic Group; AVG – Alexandra Volcanic Group; Kai – Kaimai Volcanic Centre (CVZ). Map modified from Briggs et al. (2005) and Rowland et al. (2010), complemented with data from the GNS 1:250000 map series (Edbrooke, 2001; Edbrooke, 2005; Townsend et al., 2008; Leonard et al., 2010; Lee et al., 2011). Offshore Bay of Plenty structures after Wright (1992), TVZ delineation after Wilson et al. (1995).

of the TVZ (Deering et al., 2011). There is another subdivision of the history of the TVZ based on the spatial and temporal distribution of eruptive vents. Here, an 'old' TVZ (2 Ma to 0.35 Ma) is separated from the 'young' TVZ by the initiation of the ignimbrite flare-up at the Whakamaru caldera at 0.35 Ma (Wilson et al., 1995; Gravley et al., 2016). The latter subdivision is somewhat controversial, because there is a large-scale spatial and temporal overlap between the old and the young TVZ activity (Fig. 2.2).

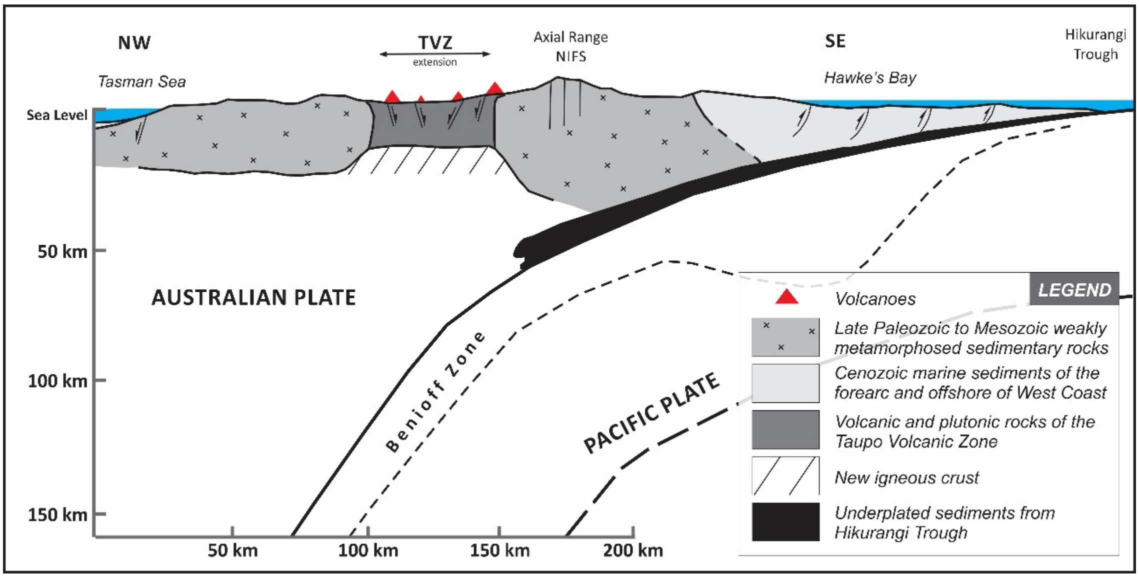
NW
TVZ
extension
Axial Range
NIFS
SE
Hikurangi
Trough
Tasman Sea
Hawke's Bay
Sea Level
50 km
100 km
150 km
AUSTRALIAN PLATE
Benioff Zone
PACIFIC PLATE
50 km
100 km
150 km
200 km
LEGEND
Volcanoes
Late Paleozoic to Mesozoic weakly metamorphosed sedimentary rocks
Cenozoic marine sediments of the forearc and offshore of West Coast
Volcanic and plutonic rocks of the Taupo Volcanic Zone
New igneous crust
Underplated sediments from Hikurangi Trough

Figure 2.3 Schematic SE-NW trending cross-section of the central North Island, with the main structural elements of the crust and upper mantle as determined by seismology modified after Cole and Spinks (2009).

The early andesitic activity of the TVZ is not very well known, and is only represented by two poorly-exposed andesitic stratovolcanoes (Titiraupenga and Pureora, Fig. 2.2) and a few submerged andesite/dacite lava bodies intersected by geothermal drillholes (Graham et al., 1995; Leonard et al., 2010). Recent findings indicate that minor rhyolitic activity was also occurring from 1.9 Ma (Gravley et al., 2016), however the large-volume andesitic-rhyolitic volcanism in the TVZ was initiated by two ignimbrite eruptions at 1.55 and 1.53 Ma (Table 2.1) after a ~0.5 Ma quiescence since the formation of the 2.09 Ma Waiteariki Ignimbrite (Kaimai Volcanic Centre, CVZ) (Briggs et al., 2005; Wilson et al., 2009). The western part of the TVZ, which is mostly buried by younger ignimbrites (e.g. the Whakamaru and Mamaku Plateau Ignimbrites), was identified as the source of these earliest TVZ ignimbrites, where the only recognised caldera structure is the Mangakino Volcanic Centre (Houghton et al., 1995b; Wilson et al., 1995). Besides the several small to moderate-sized (30-100 km^3) ignimbrite eruptions, three large-volume ignimbrite sequences (Ongatiti, Kidnappers and Rocky Hill) were emplaced between 1.2 and 1.0 Ma (Houghton et al., 1995b; Wilson et al., 2009; Deering et al., 2011) (Table 2.1). At this time, the volcanic activity was migrating to the east, which is presumed to be the reason for the progression or acceleration of the rifting of the TVZ (Wilson et al., 1995). By 0.9 Ma, the western TVZ became inactive and the volcanic activity continued at the east side of the Mangakino Volcanic Centre, characterised by predominantly less explosive andesitic volcanism until 0.7 Ma (Cole, 1981; Wilson et al., 1995; Deering et al., 2011). Simultaneously, typical arc-related volcanism had appeared in the south (e.g. Hauhungatahi, Cameron et al., 2010) (Figs. 2.2 and 2.4), which indicates an additional southward development of the rift during this period. The evolved andesitic composite cones lying near the axis of the rift subsided and have been found at 1-2 km depth, except the deeply-eroded Rolles Peak that is located on the eastern margin of the rift (Wilson et al., 1995; Deering et al., 2011) (Figs. 2.2 and 2.6). By the time of the eruption of Waiotapu Ignimbrite (0.71 Ma) (Table 2.1) the caldera volcanism had shifted to the Kapenga Volcanic Centre, indicating the waning conditions for arc-specific andesitic activity within the central part of the TVZ.

The first half of the second period (0.7 Ma to 0.34) is mostly characterised by dome-building episodes, interrupted by the eruption of the Utu Ignimbrite (~90 km^3) at 0.55 Ma (Deering et al., 2010; Deering et al., 2011) (Table 2.1). Large-scale rhyolitic activity initiated at ~0.35 Ma resulted in the eruption of at least 2300 km^3 of ignimbrite (Whakamaru Group) by a series of events within a 10 ky period (Houghton et al., 1995b; Wilson et al., 2009; Gravley et al., 2016). The source of the flare-up was the Whakamaru Volcanic Centre (Fig. 2.2), which indicates the southward advancement of caldera volcanism. In the following 60-80 ky, another six caldera-forming events occurred, producing more than 600 km^3 of ignimbrite erupted from various sources (Gravley et al., 2006; Gravley et al., 2007; Wilson et al., 2009; Gravley et al., 2016) (Table 2.1). This intense explosive episode was followed by mostly effusive volcanism producing a large number of lava domes and associated smaller-volume ignimbrites up to the combined volume of 5-6 km^3 (Wilson et al., 1986; Leonard, 2003; Leonard et al., 2010).

Name	Source caldera	Age (ka)	Age error	Dating method	DRE volume (km^3)	Reference
Taupo Pumice F	Taupo	1.8	0.05	C14	35	1
Oruanui Formation	Taupo	25.4	0.2	C14	530	5
Rotoiti Formation	Okataina	45 or 61	1.4		80	1, 4
Mokai	uncertain	210	6	Ar/Ar	40	1
Kaingaroa Formation	Reporoa	281	21	Ar/Ar	100	1
Ohakuri Formation	Ohakuri	~280-290		Ar/Ar	100	1, 5
Mamaku Plateau F.	Rotorua	~280-290		Ar/Ar	145	1, 5
Pokai Formation	Kapenga	~300		Ar/Ar	100	1, 5
Chimpanzee Formation	Kapenga	uncertain			50	1, 5
Matahina Formation	Okataina	322	7	Ar/Ar	150	1, 5
Whakamaru Group, Paeroa Subgroup	Whakamaru	339	5	Ar/Ar	110	5, 6
Whakamaru Group F.	Whakamaru	349	4	Ar/Ar	2200	5, 6
Utu ignimbrite	Okataina	~549		Ar/Ar	90	3
Waiotapu Formation	Kapenga	710	60	K/Ar	100	1
Rahopaka	?Kapenga	720	30	K/Ar	30	1
Tikorangi	?Kapenga	890	40	K/Ar	30	1
Marshall Formation	?Mangakino	950	30	K/Ar	50	1
Akatarewa ignimbrite	uncertain	950	50	K/Ar		5
Rocky Hill ignimbrite	Mangakino	1000	50	K/Ar	200	1
Kidnappers ignimbrite	Mangakino	1010	10	K/Ar	1200	1
Ahuroa ignimbrite	Mangakino	1180	20	K/Ar	100	1
Unit D	?Mangakino	1200	40	K/Ar	100	1
Ongatiti Formation	Mangakino	1210	40	K/Ar	400	1
Unit C (Pouakani F.)	Mangakino	1400	100	K/Ar	50	1, 2
Unit B (Tolley F.)	?Mangakino	1530	40	K/Ar	100	1, 2
Ngaroma Formation	?Mangakino	1550	50	K/Ar	100	1
Unit F (Link Formation)	uncertain	1600	90	K/Ar	30	1,2
Torlesse Subgroup (metasedimentary basement rocks)		Late Jurassic				5

Table 2.1 Stratigraphic relationship, source and estimated volumes of large-volume, caldera-forming eruptions of the TVZ. DRE volume estimates for most deposits are based on known mapped extents and recorded thicknesses that are converted, assuming that bulk volumes are equivalent to magma volumes when erosion and co-eruptive fall deposits now missing are taken into account (Wilson et al. 2009). The age of eruptions was compiled from: 1 – Wilson et al. (2009); 2 – Leonard et al. (2010); 3 – Deering et al. (2010); 4 – Danišík et al. (2012); 5 – Downs et al. (2014b); 6 – Gravley et al. (2016).

Simultaneously, the southern part of the TVZ was characterised by cyclic cone-building and destructive periods at Tongariro and Ruapehu volcanoes (Gamble et al., 2003; Tost and Cronin, 2015). The geological record of the last ~50 ka evolution of the TVZ (usually referred to as the modern TVZ; Wilson et al., 1995) is more detailed, with about 70 notable eruptions spread throughout the central part of the TVZ (Wilson et al., 2009; Ashwell et al., 2013). Three of these eruptions involved by caldera-forming activity, producing widespread ignimbrites (Rotoiti, Oruanui, Taupo Pumice) with a combined total volume of 645 km^3 (Wilson et al., 2009) (Table 2.1).

Historically, andesitic volcanic activity occurred regularly at White Island (Houghton and Nairn, 1991) and at the stratovolcanoes of the southern TVZ. The last major activity occurred in 1974-1975 at Ngauruhoe (Nairn and Self, 1978), and in 1995-1996 at Ruapehu (Cronin et al., 1998), while the latest, but minor, activity was initiated at the Te Maari craters on the northern slopes of Tongariro in 2012 (Breard et al., 2014; Pardo et al., 2014). The 1886 basaltic fissure eruption of Tarawera (Okataina Volcanic Centre) is the only historical magmatic eruption from the central TVZ, which produced ~1 km^3 of basaltic ejecta (Walker et al., 1984; Nairn, 2002; Leonard et al., 2010) (Fig. 2.2).

2.2 Volcanic architecture of the young TVZ

The TVZ is a rifting arc running across the North Island through 280 km from Ohakune (Rangataua craters) located on the southern ring plain of Ruapehu volcano (Figs. 2.2 and 2.4) to the continental margin north from White Island in the Bay of Plenty (Fig. 2.2). The maximum width of the young TVZ is about 50 km at the central part marked off by the vent locations of the past 0.34 Ma (Wilson et al., 1995). From a geomorphic point of view, the extent of the volcanic region of the TVZ is significantly larger than the area enclosed by vents due to the ignimbrite plateaus extending over the Taupo rift at the eastern (Kaingaroa Plateau) and the western (Mamaku Plateau) sides (Leonard et al., 2010) (Fig. 2.2). Due to the extensive and thick ignimbrite coverage at the NW margin of the TVZ, the volcanic structures of the old TVZ may have been obscured, thus the structural boundary of both the TVZ and CVZ is poorly defined. The tectonic depression of the Taupo rift located at the axis of the TVZ represents the back-arc basin characterised by normal faulting and rhyolitic and minor basaltic volcanism at the central TVZ (Cole, 1990). The activity of the southern TVZ and the eastern margin of the central TVZ more resemble the characteristics of arc volcanism in terms of the chemical composition of rocks and volcanic architecture, while other parts are defined by caldera structures relating to a volcanism more controlled by the intra-arc extension (Spinks et al., 2005; Downs et al., 2014a). Due to this dichotomy, the young TVZ is spatially partitioned into three different parts based on the volcanic architecture and the characteristics of volcanism; the northern and southern TVZ are dominated by long-lived stratovolcanoes with predominantly andesitic volcanism, while the central TVZ is characterised predominantly by the rhyolitic activity of calderas (Fig.2.2) (Wilson et al., 1995). The available data indicates that deposits and edifices have been formed by small-volume eruptions, with basaltic to rhyolitic compositions only in the southern and central TVZ.

2.2.1 Northern TVZ

The physiography of the onshore northern TVZ, dominated by a coastal lowland, overlays the Whakatane Graben (Cole, 1990) (Fig. 2.2). The seaward part is completely infilled by young pyroclastic and fluvial sedimentary rocks, whereas the remaining areas are dominated by the dissected ignimbrite plateau formed by the deposits of the Okataina Volcanic Centre (Fig. 2.3) (Leonard et al., 2010). A few highly-eroded volcanic edifices emerge from the ignimbrite. These are characterised by andesitic to dacitic compositions of pre-Whakamaru ages (e.g. Manawahe) (Kear, 2004; Leonard et al., 2010). The Holocene Putauaki/Edgecumbe lava dome complex located on the border of the northern and central TVZ is described under the the central TVZ, due to the similarities with other lava dome complexes (e.g. Tauhara) of the central TVZ.

Arc and back-arc volcanism is spatially well separated within the offshore northern TVZ. The volcanic arc emerges from the sea level only at Whale (Moutohora) and White (Whakaari) Islands (Burt et al., 1996; Cole et al., 2000), but other basaltic andesitic to dacitic submarine edifices are inferred at Te Arawa High and along the Ngatoro Ridge in the northern continuation of the massif of White Island (Wright, 1992) (Fig. 2.2). The 1000 m high andesitic Whakatane Seamount is located separately from the Ngatoro Ridge at the boundary of the northern TVZ and the Kermadec Arc, and its conical morphology resembles more the other seamounts at the southern end of the Kermadec Arc emerging from the oceanic basement (Gamble et al., 1993b; Wright, 1994; Smith and Price, 2006). The back-arc manifests itself at the actively subsiding Motiti Graben – Tauranga Trough, with several submarine volcanic knolls consisting of basaltic to dacitic rocks (Wright, 1992) (Fig. 2.2).

2.2.2 Southern TVZ

The landscape of the southern TVZ, often referred to as the Tongariro Volcanic Centre (TgVC), comprises two active large stratovolcanoes (Ruapehu and Tongariro) and other extinct composite cones and monogenetic structures of varying sizes (Fig. 2.4). Both large stratovolcanoes have extensive ring plains comprising a low-gradient apron around the volcanic cones composed of the deposits of debris avalanches, pyroclastic flows and fallout, as well as reworked laharic and fluvial sequences (Cole, 1978; Hackett and Houghton, 1989). The Ruapehu and Tongariro ringplains party overlay the structural boundary of the southern TVZ and the adjacent low-lying parts of the dissected Kaimanawa Mountains on the eastern and the Matemateaonga Range on the western side of the TgVC.

The at least 350 ky long volcanic history of the Ruapehu volcano (Tost et al., 2016) has been dominated by activity at its summit craters, where the present western summit crater is occupied by an acidic crater lake (Carrivick et al., 2009). The eruption styles of Ruapehu were strongly influenced by the existence of crater lakes, which occupied one of the summit craters within the past 10 ky (Donoghue et al., 1997; Pardo et al., 2012a). In contrast, the summit region of the Tongariro volcano indicates that numerous vents were active in the past thousands of years and were distributed over a larger area. The vent of the Ngauruhoe volcano is regarded as the most active/productive part of the Tongariro volcano, as this edifice started to develop only about 6.5 ka (Cronin and Neall, 1997; Moebis, 2010). Between the two massifs, along the axis of the TVZ parasitic vents, voluminous lava and significant explosive activity was produced from the Saddle Cone and Tama Lakes from about 10 ka (Nairn et al., 1998; Conway et al., 2016) (loc. 4, Fig. 2.4). The activity of a parasitic vent on the southern slope of Ruapehu produced the 15 km long Rangataua lava flow at about 10-12 ka (Price et al., 2012) (loc. 3, Fig. 2.4).

Two smaller composite cones are located at the northern end of the TgVC: Kakaramea and Pihanga. The edifice of Kakaramea has been considerably dissected by erosion and faulting, while the Pihanga structure is more intact with the exception of the lower flank on the NW side, which is intersected by the 1.5 km wide NNE-trending Rotopounamu Graben. The opening of the graben was associated with volcanic activity which formed scoria cones and lava flows (Cole, 1978) (loc. 7, Fig.2.4). Rocks of Kakaramea have been dated at 170-220 ka, and Pihanga andesite yielded an age of 125 ka. The morphology of cones the Rotopounamu Graben indicates a significantly younger age than the Pihanga volcano. There is a poorly known small edifice on the eastern flank of Kakaramea, which has to be younger than the massif of the Kakaramea and may also relate to the activity of the Rotopounamu Graben (loc. 8, Fig. 2.4).

Maungaku and Maungakatote are small relatively old, poorly-known andesitic cones located at the western margin of the Taupo rift (Fig. 2.4). There is no direct dating of their rocks available, but stratigraphic observations indicate that their activity just post dates the deposition of the Whakamaru Group ignimbrites and related tephra (Cole, 1978).

The earliest known edifice of the TgVC is the andesitic Hauhungatahi volcano formed about 0.9 Ma, whose remnants are exposed on an upfaulted block of Tertiary marine sediments at the western margin of the Taupo rift (Cameron et al., 2010) (Fig. 2.4). The inferred original size of this structure is comparable with the Kakaramea and Pihanga volcanoes (Hackett, 1985).

Monogenetic/small-volume volcanic activity has occurred at four locations outside the area of the axis of the Taupo rift; Rangataua Lakes, Ohakune, Pukeonake and Waimarino. Two of these volcanic centres are located on the southern ring plain of Ruapehu near Ohakune township and are both characterised by phreatomagmatic activity. Rangataua Craters/Lakes (also known as the Rangatau, Rangatauanui and Ohakune Lakes) represent the southernmost volcanic activity of the TVZ (loc. 1, Fig.

2.4), which formed at least two craters associated with phreatomagmatic and Strombolian eruptive styles along an east-west trending fault (Cole, 1978). Due to the lack of outcrops, the evolution and volcanic architecture of this monogenetic volcano remains poorly known. The Ohakune Volcanic Complex (OVC) (also known as the Ohakune Craters and Rochfort Crater) is the other monogenetic cone complex of this area, which is also aligned to an east-west trending fault (for more details of the OVC see Chapter 5) (loc. 2, Fig. 2.4). Pukeonake is located at the west side of the Tongariro massif about 5.5 km from the Ngauruhoe summit that marks the axis of the Taupo rift (loc. 5, Fig. 2.4). Volcanic activity occurred along a north-south trending fissure, forming a 143 m high scoria cone, a few mounds of agglutinated/welded spatter north from the cone, and a series of lava flows covering about 55 km^2 of area (Cole, 1978; Hackett, 1985; Hackett and Houghton, 1989).

In contrast with the basic andesitic composition of the above-mentioned small-volume eruptions, the rock type of the Waimarino volcano displays the most primitive characteristics (tholeiitic basalt with low alumina and high Mg/(Mg+Fe^{2+}) ratio) within the southern TVZ (Hackett, 1985; Gamble et al., 1990). This volcano has an unusually easterly location compared with other vents of the TgVC, with a distance of 15 km from the axis of the TVZ (loc. 6, Fig. 2.4). The Waimarino eruption formed a scoria cone and lava flows that advanced 2-2.5 km to the north from the scoria cone (Hackett, 1985; Lee et al., 2011).

The age of the Waimarino eruption post-dates the 25.4 ka Oruanui eruption, whereas the overlying Tongariro Subgroup tephras indicate an age older than ~14 ka (Hackett, 1985; Donoghue et al., 1995). Stratigraphically, Pukeonake and the two other locations near Ohakune are overlain by the Oruanui tephra, but the absence of paleosoils or a major erosional break suggests that these eruptions occurred not much earlier than the deposition of the Oruanui tephra (Houghton and Hackett, 1984; Hackett, 1985). Additionally, radiometric dating on charred wood from the medial/distal sequence of the OVC implies an age of 31.5 ka (Froggatt and Lowe, 1990).

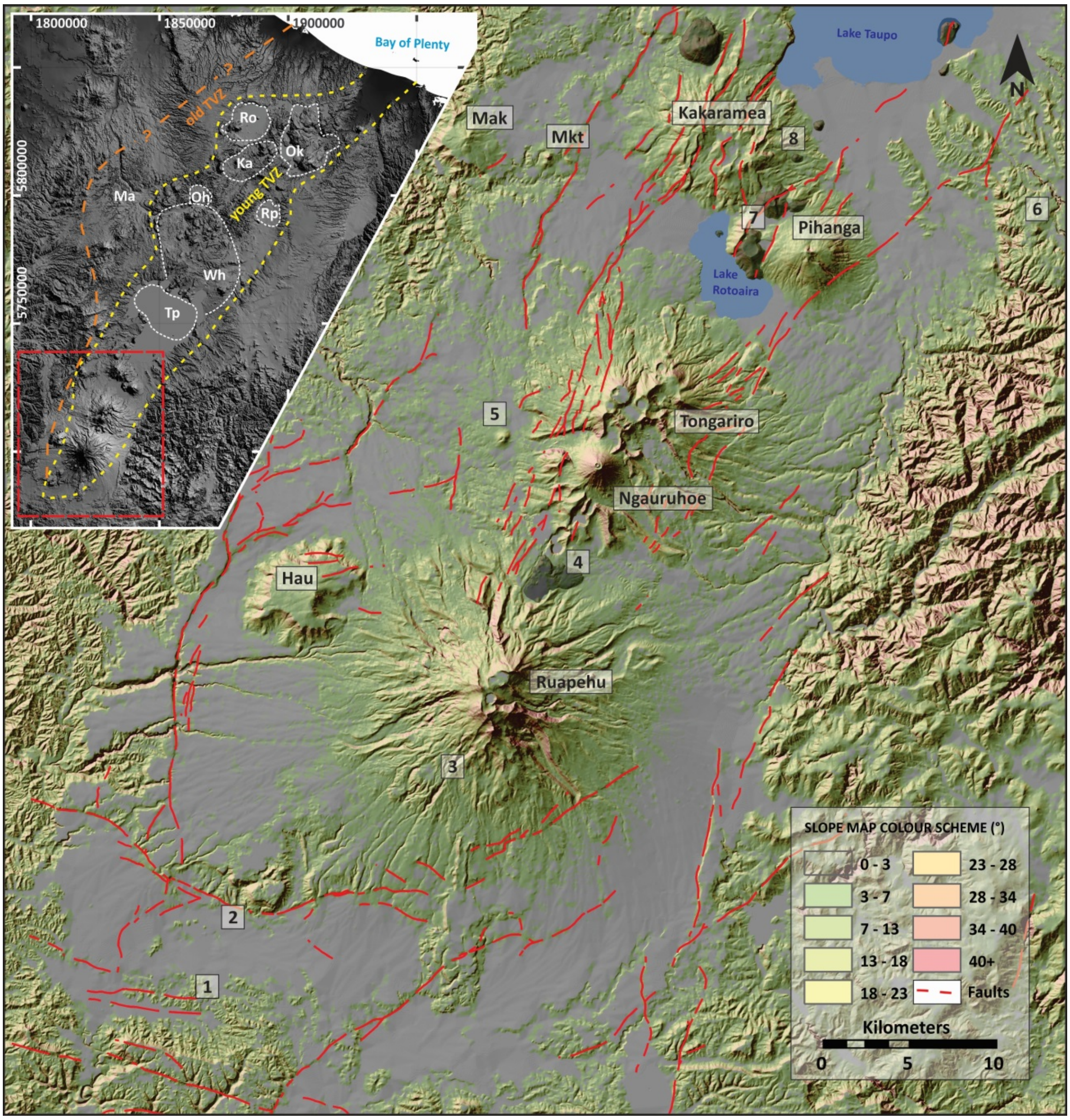
1800000
1850000
1900000
Bay of Plenty
5800000
5750000
old TVZ
?
young TVZ
Ro
Ok
Ka
Ma
Oh
Rp
Wh
Tp
Lake Taupo
N
Mak
Mkt
Kakaramea
8
7
6
Pihanga
Lake Rotoaira
5
Tongariro
Ngauruhoe
4
Hau
Ruapehu
3
2
1
SLOPE MAP COLOUR SCHEME (°)
0 - 3
3 - 7
7 - 13
13 - 18
18 - 23
23 - 28
28 - 34
34 - 40
40+
Faults
Kilometers
0
5
10

Figure 2.4 Topography of the southern TVZ/Tongariro Volcanic Centre as displayed on a shaded slope map derived from an 8 m DEM (LINZ - Land Information New Zealand, 2012). The inset map shows its geographic position and extent within the TVZ, coordinates are in NZTM2000. The vent locations mentioned in the text are labelled: Hau – Hauhungatahi; Mak – Maungaku; Mkt – Maungakatote; 1 – Rangataua Craters; 2 – OVC; 3 – inferred source vent of Rangataua lava flow; 4 – Saddle Cone and Tama Lakes; 5 – Pukeonake; 6 – Waimarino; 7 – vents in the Rotopounamu Graben (from the south: Puketopo, Pukemohono, Lake Rotopounamu and Onepoto); 8 – Te Pohanga.

2.2.3 Central TVZ

The dominantly rhyolitic central TVZ starts from the silicic lava body of Motuopuhi Island (Lake Rotoaira) in the south, and overlaps with the southern TVZ (loc. 9; Fig. 2.5). It extends to the Edgecumbe/Putauaki lava dome complex in the vicinity of

Kawerau township (Cole, 1990) (Figs. 2.2 and 2.7). This ~130 km long section of the young TVZ is defined by a 10-12 km wide NNE trending central rift zone (also called Taupo Fault Belt or Taupo Rift) and seven caldera structures (Taupo, Whakamaru, Ohakuri, Reporoa, Kapenga, Rotorua and Okataina) (Wilson et al., 1995; Spinks et al., 2005; Gravley et al., 2007; Cole and Spinks, 2009; Leonard et al., 2010). Gravity data-based calculations suggest a 2.5-3 km thickness of lava and pyroclastic material has accumulated on the top of the down-faulted greywacke basement, which corresponds to an erupted volume of 15000–20000 km^3 during the entire history of the central part of the TVZ (Houghton et al., 1995b). It is believed that at least 26 large-volume caldera-forming eruptions occurred within the past 1.6 Ma, which comprise DRE volumes of single eruptions from 30-1500 km^3 (Table 2.1) (Houghton et al., 1995b; Wilson et al., 2009; Gravley et al., 2016). The erupted ignimbrites travelled occasionally to the coast of the Tasman Sea in the west and Hawke's Bay in the east, and have formed the Mamaku and Kaingaora Plateaus along the margin of the TVZ (Figs. 2.2 and 2.7). The exceptionally high magma flux of the central TVZ maintains 23 geothermal fields that have an estimated natural heat output of 4200 ± 500MW (Bibby et al., 1995; Kissling and Weir, 2005).

The southern part of the central TVZ is dominated by Lake Taupo, which is the largest lake in New Zealand occupying an area of about 620 km^2 (Manville et al., 1999). Lake Taupo and its neighbourhood together comprise the Taupo Volcanic Centre (Tp). The broad northern part of the lake represents the depression formed by the caldera-forming Oruanui eruption at 25.4 ka (Vandergoes et al., 2013). The deepest point of the lake at 155 m is located at the eastern part of the Oruanui caldera, which points to the second caldera collapse having occurred during the 1.8 ka Taupo Pumice eruption (Irwin, 1972; Wilson and Walker, 1985; Davy and Caldwell, 1998; Wilson, 2001; Lowe et al., 2013). Post-Oruanui volcanic activity mostly occurred within the structure of the Oruanui collapse along a NNE-SSW trending lineament (Fig. 2.5), and produced ~13 km^3 of volcanic material (without the 35 km^3 volume of Taupo Pumice) by mostly rhyolitic sub-Plinian to Plinian eruptions (Wilson et al., 2009). The two mounds of the Horomatangi Reefs and Waitahanui Bank may represent lava domes that post-date the 1.8 ka caldera collapse (loc. 12, Fig. 2.5) (Irwin, 1972; Wilson and Walker, 1985; Wilson et al., 1986; Wilson, 1993; De Ronde et al., 2002; LINZ - Land Information New Zealand, 2013; Barker et al., 2014).

The southern basin of the lake is mostly considered to be a volcanotectonic graben, however it seems that the subsidence characterised by the northward dipping orientation of the pre-Oruanui surface rocks under the lake bed occurred in response to the Oruanui eruption (Davy and Caldwell, 1998), which would qualify the southern basin to be part of the caldera characterised by trapdoor collapse or subsidence (Wilson, 2001; Cole et al., 2005). The high cliffs of the western and northern lake shores are composed of Whakamaru Group ignimbrites and rhyolitic lava domes (Leonard et al., 2010). Magnetic data indicates that there are numerous lava dome edifices sitting on the Whakamaru sequence within the down-sagged southern basin of Lake Taupo (Davy and Caldwell, 1998). The scalloped shape of the northern lake shore is controlled by the locations of the NNE trending 100-200 ka coalesced domes, with positions defined by the fault system of the Taupo rift. Outside of the limit of Lake Taupo, post-Oruanui volcanic activity is limited to a handful of locations. The eruptions of Acacia Bay (unit D) and Ouaha Hills (unit W) produced lava domes with the ages of 11.4 ka and 2.75 ka, respectively (loc. 13 and 14) (Wilson et al., 2009; Leonard et al., 2010), while Wilson et al. (1986) also proposed a young age (~10 ka) for the Kuharua dome (loc. 10, Fig. 2.5), and its minimum age was later modified to 13.8 ka due to new stratigraphic observations (Froggatt and Solloway, 1986). Based on geomorphic observations, a post-Oruanui age for the dacite eruptions around the Motuoapa Peninsula was also proposed (loc. 11, Fig. 2.5, Chapter 8). Additionally, the recently examined phreatomagmatic basaltic succession at the lake shore near Kinloch suggests a maximum age of ~9.5 ky (Matheson, 2010). There are two further locations where activities indicate an age coherent with the post-Oruanui activity of the Taupo Volcanic Centre. Volcanic/hydrothermal explosions around Lake Rotokawa occurred at least eight times between 22.6 ka and 3.4 ka, from which the largest explosion produced 11 m thick breccia deposit dispersed within a 12 km^2 area at ~6 ka (Browne and Lawless, 2001; McNamara et al., 2016) (loc. 16, Fig. 2.5). Despite the lack of juvenile material found, the relatively large-volume deep excavation (~450 m) and widespread distribution of the deposits suggest some contribution by a magmatic process (Browne and Lawless, 2001). The 16.5 ka Puketerata Volcanic Complex (PVC) is located farther north at the southern margin of the Maroa Volcanic Centre (Brooker et al., 1993) (loc. 17, Figs. 2.5 and 2.6) and is characterised by phreatomagmatic activity together with the formation of two lava domes. A newly-discovered basaltic sequence indicates that maar-forming eruptions occurred earlier at the same location (for more details see Chapters 6 and 7).

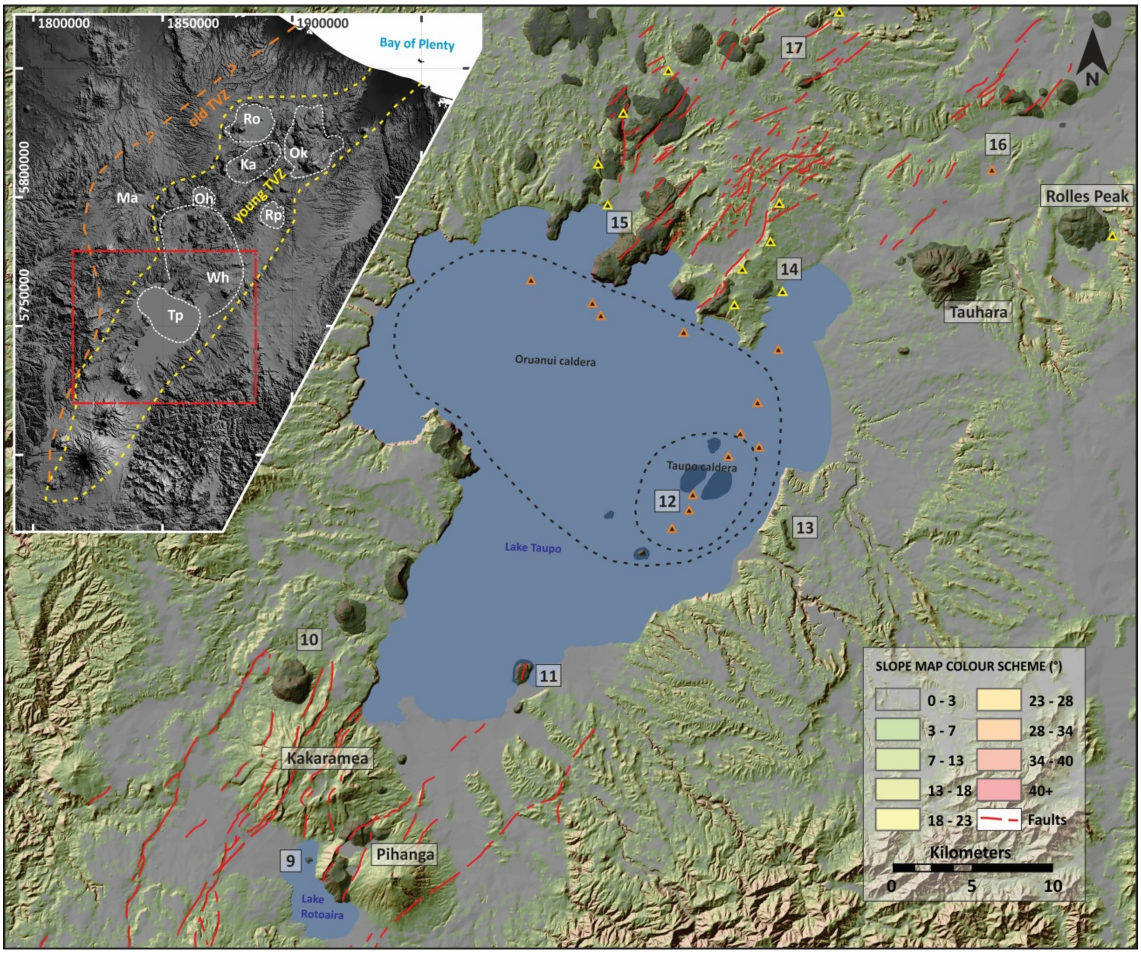
1800000
1850000
1900000
Bay of Plenty
5800000
5750000
old TVZ
young TVZ
Ro
Ok
Ka
Ma
Oh
Rp
Wh
Tp
N
17
16
Rolles Peak
15
14
Tauhara
Oruanui caldera
Taupo caldera
12
13
Lake Taupo
10
11
Kakaramea
9
Pihanga
Lake Rotoaira
SLOPE MAP COLOUR SCHEME (°)
0 - 3
3 - 7
7 - 13
13 - 18
18 - 23
23 - 28
28 - 34
34 - 40
40+
Faults
Kilometers
0
5
10

Figure 2.5 Topography of the Taupo Volcanic Centre as displayed on a shaded slope map derived from an 8 m DEM (LINZ – Land Information New Zealand, 2012). The inset map shows its geographic position and extent within the TVZ, coordinates are in NZTM2000. The vent locations mentioned in the text are labelled: 9 – Motuopuhi Island; 10 – Kuharua; 11 – Motuoapa Peninsula; 12 – inferred post-Oruanui vents related to a NNE-SSW trending lineament; 13 – Ouaha Hills; 14 – Acacia Bay dome; 15 – Kinloch Basalt; 16 – Lake Rotokawa; 17 – PVC and Te Hukui Basalt.

The Whakamaru Volcanic Centre (Wh) is located north of the Oruanui caldera with an inferred overlap. The margin of this caldera complex is defined at the western side by the Western Dome Belt (WDB) (Fig. 2.6), while the other sections are delineated on the basis of geophysical data and the thickness and dispersal of Whakamaru Group ignimbrites (Wilson et al., 1986). The morphology of the faulted "Northwestern Dome Complex" indicates a possible additional extension of the Whakamaru to the north (Fig. 2.6). This area was later overprinted by the ~290 ka caldera forming eruption of the Ohakuri Volcanic Centre (Oh), which produced ~100 km^3 (DRE) of volcanic material (Gravley et al., 2006; Gravley et al., 2007; Wilson et al., 2009; Gravley et al., 2016). The history of the area prior to the Whakamaru eruption is poorly known due to the lack of exposure of older successions. The oldest structures were found at the Whakaahu dome belt 2 km west from the WDB, which at age ~1 Ma suggests a relationship with the activity of the Mangakino Volcanic Centre (Brown, 1994) (loc. 18, Fig. 2.6).

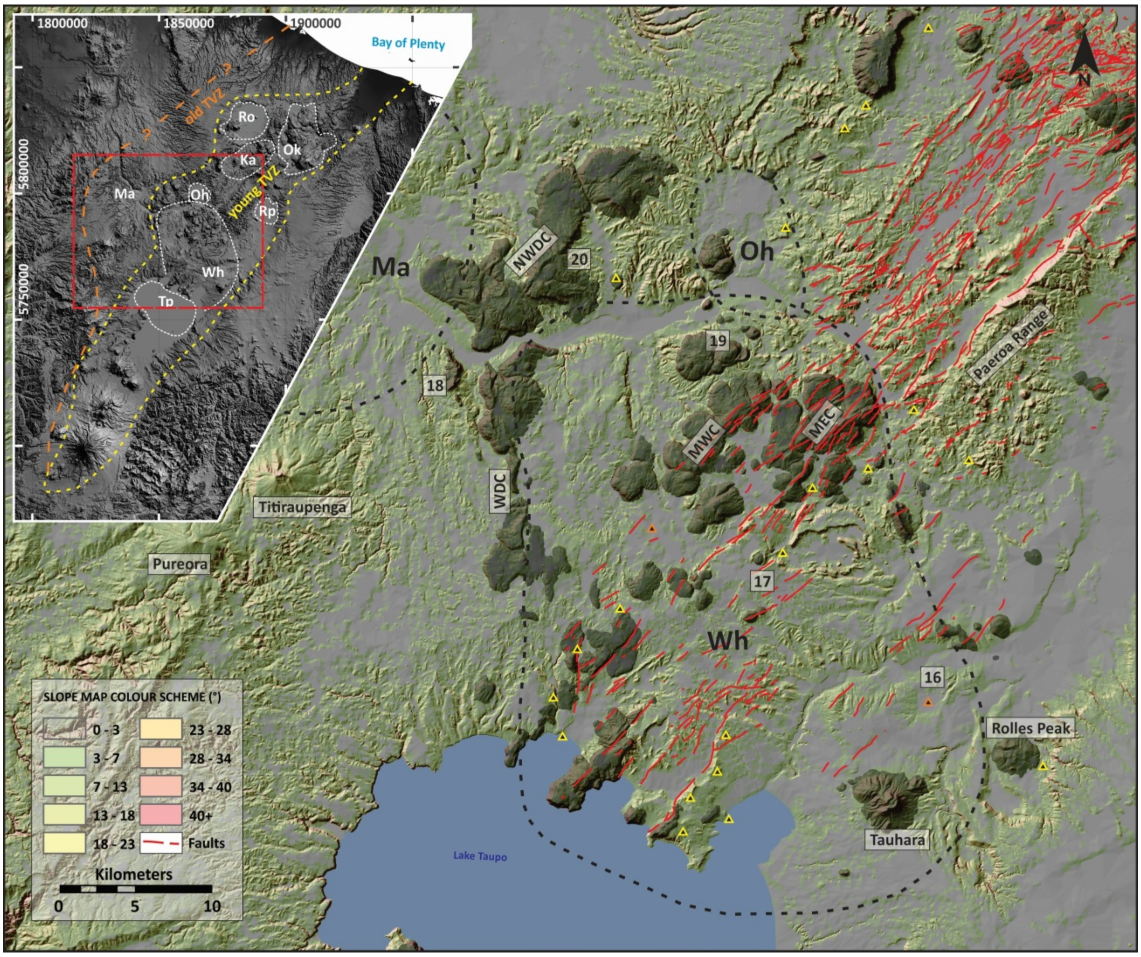
1800000
1850000
1900000
Bay of Plenty
old TVZ
young TVZ
Ro
Ok
Ka
Ma
Oh
Rp
Wh
Tp
5800000
5750000
N
Ma
NWDC
20
Oh
19
18
MWC
MEC
Paeroa Range
WDC
Titiraupenga
Pureora
17
Wh
16
Rolles Peak
Tauhara
Lake Taupo
SLOPE MAP COLOUR SCHEME (°)
0 - 3
3 - 7
7 - 13
13 - 18
18 - 23
23 - 28
28 - 34
34 - 40
40+
Faults
Kilometers
0
5
10

Figure 2.6 Topography of the Whakamaru (Wh) and the Ohakuri (Oh) Volcanic Centres as displayed on a shaded slope map derived from an 8 m DEM (LINZ – Land Information New Zealand, 2012). The inset map shows its geographic position and extent within the TVZ. The vent locations mentioned in the text are labelled: WDC – Western Dome Complex; NWDC – Northwestern Dome Complex; MWC – Maroa West Complex; MEC – Maroa East Complex; 16 – Lake Rotokawa; 17 – PVC and Te Hukui maars; 18 – Whakaahu Dome Belt; 19 – Pukeahua Dome Complex; 20 – Whakamaru Domes and Coulees (part of NWDC).

The age of the series of collapse events at Whakamaru was previously dated at 340-320 ka (Houghton et al., 1995b), but the recent Ar/Ar age determinations slightly modified these ages (Downs et al., 2014b). The earlier eruptions, such as Whakamaru, Manunui, Rangitaiki and Te Whaiti, occurred at ~349 ka, while Paeroa Subgroup ignimbrites are most likely sourced from a fissure vent located along the depression westward from the Paeroa Range at ~339 ka (Downs et al., 2014b) (Fig. 2.6).

Post-caldera volcanism was characterised by extensive dome-building activity along the caldera margins at Northwestern Dome Complex (NWDC) and Western Dome Complex (WDC) between 313 and 141 ka (Houghton et al., 1991) and the internal part between 305 and 80 ka (Leonard, 2003; Downs et al., 2014a). The early activity of the Maroa Volcanic Centre (MVC), located in the NE part of Whakamaru (Fig. 2.6), was characterised by vigorous explosive activity with the eruption of locally distributed ignimbrites (Korotai, Putauaki, Orakonui, Atiamuri), with estimated volumes of 1-4 km^3 per single eruption periods (Leonard, 2003). Volcanism at MVC culminated between 251 and 222 ka with the emplacement of the majority of the domes of the Maroa Western and Eastern Complexes. These two dome lineaments may represent similar structural conditions to the late Pleistocene-Holocene Tarawera and Haroharo Dome Complexes at the Okataina Volcanic Centre. Subsequent activity formed mostly smaller dome complexes and isolated domes. Explosive activity relating to lava dome emplacement is poorly known within Whakamaru, excluding the few moderate volume ignimbrites mentioned earlier. Besides the phreatomagmatic PVC (loc. 17, Figs. 2.5 and 2.6), explosive activity has been preserved only in the vicinity of the Pukeahua Dome Complex and Whakamaru dome (NWDC, loc. 19 and 20, Fig. 2.6). The pyroclastic fans of Pukeahua consist of locally-sourced ignimbrites and extensive block-and-ash flow deposits representing the most explosive dome-forming period in this region (Leonard, 2003).

The Reporoa Volcanic Centre (Rp) is located at the eastern margin of the TVZ with a clear offset to the main axis of the Taupo rift (Beresford and Cole, 2000; Spinks et al., 2005) (Fig. 2.7). The formation of the caldera was accompanied by the eruption of the ~100 km^3 ignimbrite of the Kaingaroa Formation deposited mostly east from the source (Beresford and Cole, 2000; Wilson et al., 2009). Downs et al. (2014a) recently revised the ages of Reporoa-related pyroclastic rocks and dome lavas, which set a new caldera-forming eruption age at ~280 ka, in accordance with the 285 ka age suggested earlier by Manning (1996). As the Kaingaroa ignimbrite overlays the Ohakuri ignimbrite, which interfingers with the Rotorua sourced Mamaku Plateau ignimbrite, the previously determined age of ~240 ka of these two latter caldera formations, as well as the ages of the earlier Pokai, Chimpanzee and Matahina eruptions, had to be redefined (Gravley et al., 2007; Gravley et al., 2016).

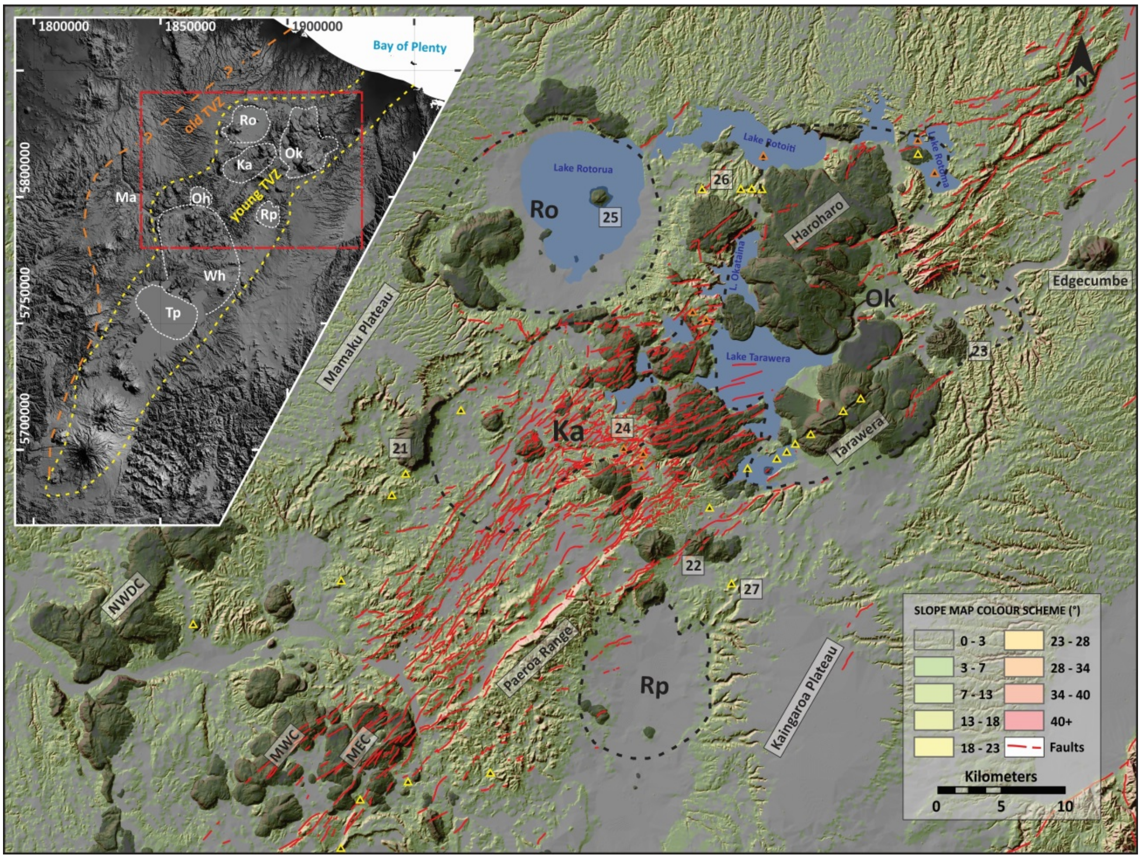
1800000
1850000
1900000
Bay of Plenty
old TVZ
young TVZ
Ro
Ka
Ok
Ma
Oh
Rp
Wh
Tp
5800000
5750000
5700000
N
Lake Rotorua
Ro
25
Lake Rotoiti
Lake Rotoma
26
Haroharo
L. Okataina
Edgecumbe
Ok
23
Lake Tarawera
Tarawera
Mamaku Plateau
Ka
24
21
22
27
NWDC
Paeroa Range
Rp
Kaingaroa Plateau
MWC
MEC
SLOPE MAP COLOUR SCHEME (°)
0 - 3
3 - 7
7 - 13
13 - 18
18 - 23
23 - 28
28 - 34
34 - 40
40+
Faults
Kilometers
0
5
10

Figure 2.7 Topography of the *Kapenga (Ka)-Reporoa (Rp)-Rotorua (Ro)- and Okataina (Ok) Volcanic Centres as displayed on a shaded slope map derived from an 8 m DEM (LINZ – Land Information New Zealand, 2012). The inset map shows its geographic position and extent within the TVZ. The vent locations mentioned in the text are labelled: NWDC – Northwestern Dome Complex; MWC – Maroa West Complex; MEC – Maroa East Complex; 21 – Horohoro Cliffs; 22 – Maungaongaonga and Maungakakaramea/Rainbow Mountain; 23 – Puhipuhi lava dome complex 24 – Earthquake Flat volcano; 25 – Mokoia Island; 26 – Rotokawau-Rotoatua fissure vents; 27 – Terrace Road Basalt.*

Rotorua Volcanic Centre (Ro), similar to Reporoa, is an extra-rift caldera located at the western margin of the young TVZ (Spinks et al., 2005). The climactic eruption of Rotorua most likely occurred between 280-290 ka, forming a 21 km diameter multiblock collapsed structure whose eastern half is currently occupied by a lake (Milner et al., 2002; Ashwell et al., 2013; Downs et al., 2014a; Gravley et al., 2016). The caldera-forming eruption produced a volume of 145-150 km^3 ignimbrite (Mamaku Plateau Formation) mostly deposited westward from the source (Milner et al., 2002; Wilson et al., 2009; Gravley et al., 2016). Exposed structures of post-caldera activity indicate two periods of lava extrusions (Wilson et al., 1984; Ashwell et al., 2013). The SW part of the caldera characterised by the lowest gravity anomaly is occupied by the ~ 200 ka Ngongotaha lava dome complex, Pukehangi, and a few smaller buried or partially-buried domes located on the lake shore (Milner et al., 2002; Ashwell et al., 2013). The second period most likely occurred between 45 and 36 ka, with the formation of Mokoia Island and other mostly buried domes located along the SE shore of Lake Rotorua (Ashwell et al., 2013) (loc. 25, Fig. 2.7).

Kapenga Volcanic Centre (Ka) is the oldest and least known caldera structure of the young TVZ. Early activity pre-dates the formation of the Whakamaru Group ignimbrites, during which it most likely was the source of the Tikorangi (30 km^3), Rahopaka (30 km^3) and Waiotapu (100 km^3) ignimbrites (Houghton et al., 1995b; Wilson et al., 2009). Geophysical data suggests that Kapenga is composed of two distinct structures, comprising one smaller basin at the NE part and another at the central-southern part (Wilson et al., 1984). The ~320-300 ka Chimpanzee (50 km^3) and Pokai (100 km^3) ignimbrites are considered to have originated from the Kapenga Volcanic Centre, however these deposits only crop out as scattered patches within the deep gullies and fragmented edge of the Mamaku Plateau (Leonard et al., 2010). It is believed that the current morphology of the southern part of the Kapenga caldera marking by the scar of the Horohoro Cliffs was formed by a volcano-tectonic event that caused the paired eruption of the Rotorua and Ohakuri Volcanic Centres (Gravley et al., 2007) (loc. 21, Fig. 2.7). Post-caldera volcanism was more dominant at the northern part adjacent to the Okataina Volcanic Centre. The poor age determination of the majority of volcanic deposits does not allow us to classify these eruptions to either volcanic centres, while the few better-studied eruptions clearly relate to the volcanism of the Okataina Volcanic Centre (e.g. Earthquake Flat volcano) (Nairn and Kohn, 1973; Charlier et al., 2003; Shane et al., 2005) (loc. 24, Fig.2.7). The youngest known intra-caldera dome of Kapenga, located in the central-western part of the caldera, yields an age of ~136 ka (Leonard et al., 2010).

The complex outline of the Okataina Volcanic Centre (Ok) is the imprint of overlapping nested caldera collapses and post-caldera subsidence structures and scars of NE trending faults (Spinks et al., 2005; Cole et al., 2010) (Fig. 2.7). Since the Whakamaru activity two large climactic eruptions occurred at Okataina, which produced the ~320 ka Matahina ignimbrite (150 km^3) and the 45 or 61 ka Rotoiti ignimbrite (80 km^3) (Shane et al., 2005; Wilson et al., 2007; Danišík et al., 2012; Downs et al., 2014a). Drill core data suggests that the activity of the Okataina area dates back to 550 ka, and was characterised by extrusive and explosive activity, including the eruption of the Utu Ignimbrite (Deering et al., 2010). The Rotoiti eruption occurred at the northern part of Haroharo Caldera, and its vent area is now completely buried by younger lavas (Nairn, 2002). Subsequent activity was characterised by 14 rhyodacitic to rhyolitic Plinian events (Mangaone Pyroclastics Subgroup), with a total DRE volume of ~22 km^3 that erupted between 45 and 28 ka from inside the Haroharo caldera (Froggatt and Lowe, 1990; Jurado-Chichay and Walker, 2000; Nairn, 2002; Smith et al., 2002). Exposed extrusive rocks within the Haroharo caldera are located along the Haroharo and Tarawera dome complexes, tracing the active two linear vent zones of Okataina. The two dome complexes are characterised by overlapping and coalesced bodies of lava domes and coulees, with associated pyroclastic fans erupted from distinct but closely-spaced vents (Nairn, 2002). The two vent zones became active during the eruptions of the Mangaone Pyroclastics, but surface rocks encompass only nine rhyolitic and one basaltic eruptive episode from 21 ka to the present (Jurado-Chichay and Walker, 2000; Nairn, 2002). Each eruptive period has produced lava domes or coulees and voluminous tephra, except the basaltic Plinian event of Tarawera which occurred at the end of the 19th century (Fig. 2.7). The combined DRE volume of these eruptions is estimated at 85 km^3 (Nairn, 2002). Only one major Holocene volcanic event occurred outside the two vent zones that formed a chain of maar craters along a 4.5 km long east-west trending alignment. This 3.4 ka fissure eruption (Rotokawau-Rotaoatua) produced approximately 0.5 km^3 of basaltic ejecta through phreatomagmatic and Strombolian activity (loc. 26, Fig. 2.7) (Nairn, 2002).

Eruptions with andesitic/dacitic compositions are very rare in the central TVZ and their volcanic structures are mostly restricted to the eastern margin. These composite cones or dome complexes, previously referred to as polygenetic volcanoes, represent the conventional arc magmatism within the central TVZ (Cole, 1990; Wilson et al., 1995). These conical-shaped lava dome complexes, with associated pyroclastic fans (such as Edgecumbe, Puhipuhi, Maungakakaramea/Rainbow Mountains and Tauhara), are most likely characterised by a single eruption period that lasted no longer then a few hundred to several hundreds years (Lewis, 1968; Duncan, 1970; Carroll et al., 1997; Nairn, 2002) (Figs. 2.5-2.7), which brings into question their polygenetic origin and similarities with the long-lived arc-type massifs of the southern TVZ. The usual volume of these largest dome complexes do not exceed 3-4 km^3, which complies with the largest rhyolitic dome eruptions of the TVZ (Chapters 3 and 9).

The volcanism of the central TVZ is generally characterised by two extremes regarding the erupted volumes and the frequency of events. The stratigraphy and the landscape are dominated by the overwhelming volume of products associated with caldera-forming events, however the recurring time of these events is relatively low (Table 2.1). This is in contrast with the small-volume (or monogenetic) activity, which occurs more frequently and usually produces less than 1 km^3 volume of volcanic material. As the location of small-volume events is scattered broadly within the entire area of the central TVZ (Chapter 9), their hazard potential is high in spite of their expected lower eruption volumes.

Chapter

3

Chapter 3 reviews the silicic monogenetic volcanism in terms of the possible eruption styles and the associated volcanic structures. The summary contains some statements from mafic monogenetic volcanoes where the knowledge of the silicic volcanism is void (e.g. root zones of silicic diatremes). The second part of the chapter focuses on the characteristics of lava domes. At the end of the chapter, linked to the existing classification of lava domes, a new morphometry–based lava dome classification is proposed.

Chapter 3 – Review of silicic monogenetic volcanism and a new classification for domes

Monogenetic volcanism involving mafic magmas has been comprehensively studied (e.g. Head and Wilson, 1989; Valentine and Gregg, 2008; Németh, 2010; White and Ross, 2011; Kereszturi and Németh, 2012). In contrast, silicic monogenetic eruptions are less well known, due to their comparatively rarer appearance in monogenetic fields (Abrams and Siebe, 1994; Toprak, 1998; Davies et al., 2008; Zimmer et al., 2010; Austin-Erickson et al., 2011; Németh et al., 2012b; Ross et al., 2017), and their significance is also a bit overlooked in volcanic settings characterised by complex plumbing systems, such as calderas (Sieh and Bursik, 1986; Brooker et al., 1993; Kósik et al., 2017a). In caldera settings the very common silicic lava domes and flows are mostly studied as point sources of individual eruptions, but their broader significance as being possible precursors of larger events or the consequences of their eruptions through variable eruption styles and their relatively high recurrence times is rarely taken into account especially for spatially dispersed events. A volcano monogenetic is characterised by one eruptive period occurring over a relatively limited timespan, during which the eruption produces a small volume (less than 1 km^3) of petrologically homogeneous volcanic material (Wood, 1979; Walker, 2000; Smith and Németh, 2017). The majority of silicic eruptions within caldera settings meet the definition of monogenetic volcanism as they are characterised by short lived or one-off eruptions and usually have less than 1 km^3 of erupted volume (e.g. Sieh and Bursik, 1986; Brooker et al., 1993). Although the sensu-stricto distinction between monogenetic and polygenetic is clear, the transition between the two end members seems now more continuous than it was previously (Németh and Kereszturi, 2015; Smith and Németh, 2017). An important research goal is to understand the spatial and temporal relationship of satellite/parasitic eruptions with associated central volcanoes, as well as the degree of connectivity between their plumbing systems (e.g. Andronico et al., 2005; Geshi et al., 2007). In caldera settings, the validity of naming a vent as “satellite” can be problematic due to the usual absence of a localised main conduit and the large aerial aspect of a caldera depression. Within such a setting, the recognition of compound monogenetic versus polygenetic structures is quite difficult (e.g. Cole, 1970;

Hobden et al., 1996). Due to the great number of variables that may influence the silicic eruptions, the diversity of eruptive processes and the evolving volcanic structures is higher than in basaltic regimes. In many basaltic and silicic cases, in spite of the small eruptive volumes, the nature of eruptions is not clear enough to classify them into monogenetic or polygenetic (e.g. Bradshaw and Smith, 1994; Freda et al., 2006). Due to these uncertainties, White and Ross (2011) recommended changing the name of monogenetic volcanoes to "small volcanoes" as determined by the frequent multiple styles of eruptions of the monogenetic volcanoes (for instance, from initial phreatomagmatic via magmatic eruptions to lava effusion, and see other possible ways of development of basaltic activity and the resulting complex landforms, e.g. Kereszturi et al., 2012) and occasionally longer evolution (e.g. the Paricutin eruption lasted nine years; Pioli et al., 2008). In the silicic realm, besides the requirements of a short timespan and one eruptive period, a more permissive definition including eruptive volumes up to 5 km^3 may be justified. In addition, volcanoes are classified monogenetic if they meet the criteria of the previously outlined and widely accepted definition, complementing it with a "petrogenetic sense" (Smith and Németh, 2017), which requires that there is no direct relationship between the plumbing system of a small-volume volcano and the main conduit of a central volcano (Fig. 3.1).

The classical term "monogenetic volcanism" can be separated into two types by location: (1) the isolated or individual volcanoes of monogenetic volcanic fields; and (2) the parasitic activity of polygenetic central volcanoes (Fig. 3.1) (de la Cruz-Reyna and Yokoyama, 2011). Monogenetic parasitic vents might have a relationship with the plumbing system of their polygenetic counterparts and can appear on the flank and ringplain of composite volcanoes (Miller, 1980; Hackett and Houghton, 1989; Mazzarini and Armienti, 2001; Corazzato and Tibaldi, 2006), composite volcanoes with associated summit calderas (Crandell and Mullineaux, 1978; De Rita et al., 1997; Sottili et al., 2009; Goto and Johmori, 2015), or shield volcanoes (Wolfe et al., 1997; Ablay and Martı, 2000; Brenna et al., 2011).

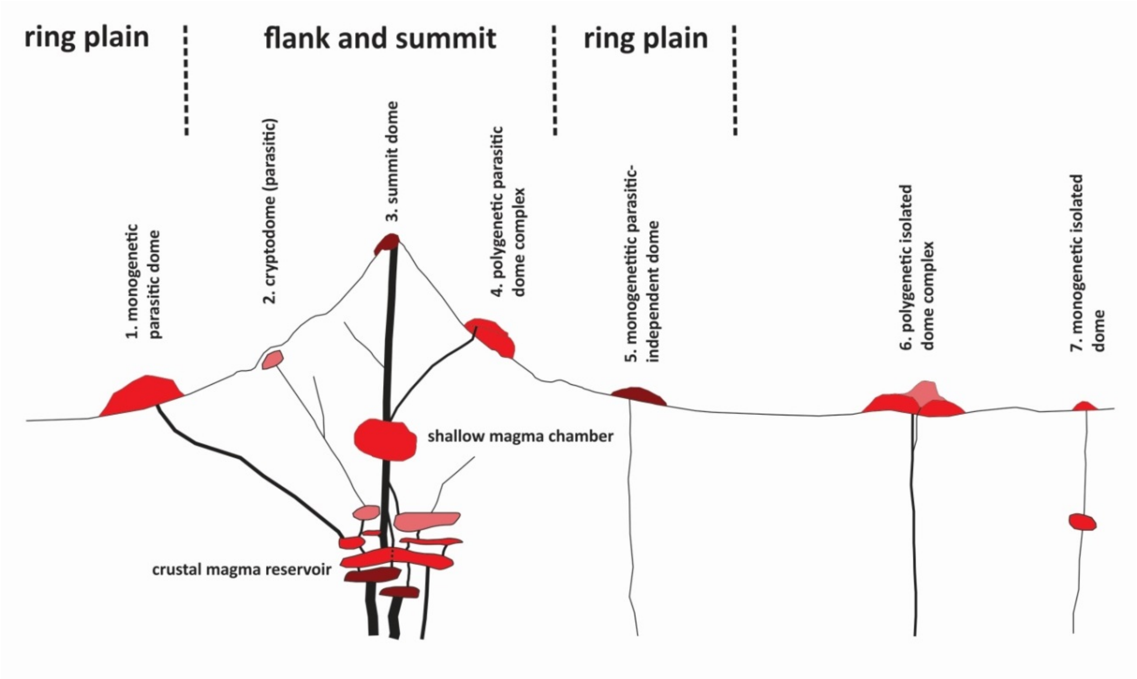
ring plain
flank and summit
ring plain
1. monogenetic parasitic dome
2. cryptodome (parasitic)
3. summit dome
4. polygenetic parasitic dome complex
5. monogenetitic parasitic-independent dome
6. polygenetic isolated dome complex
7. monogenetic isolated dome
shallow magma chamber
crustal magma reservoir

Figure 3.1 Potential relationship of small-volume volcanism (typical erupted volume <1 km^3 DRE) based on their spatial and magma plumbing system relationships to polygenetic central vent volcanism.

3.1 Eruptive styles and processes

In order to understand the processes operating during silicic eruptions, it is important to determine which factors are regulating the eruptions and how these affect the volcanic activity. Fragmentation is the most crucial factor of all, which is strongly influenced by the physical properties of magma, such as viscosity, volatile content and permeability (Cas and Wright, 1988; Dingwell, 1998b; Mueller et al., 2008). The ascending silicic magma can reach the surface with and without fragmentation. Uprising magma that reaches the surface without explosions (without significant fragmentation) mostly results in the creation of lava domes or it forms viscous lava flows. In many cases, the quick vesiculation of uprising magma leads to magma fragmentation that causes volcanic explosions. Other conditions that result in fragmentation are magma interaction with external water, or clogging of the conduit by the cooling melt. The dynamics of fragmentation strongly influences the eruptive behaviour and resulting volcanic products and landforms, therefore it is worth separating the magmatic (dry or internal) and the hydromagmatic (wet or external) explosive processes (Walker, 1973; Kokelaar, 1986; Dingwell, 1998a; Austin-Erickson et al., 2008).

During magmatic fragmentation, explosivity is driven by the exsolution and quick expansion of initially dissolved volatiles (e.g. H_2O and CO_2) of the melt. Effective outgassing takes place in physically open systems and presumes highly permeable magmatic foams. In contrast, ineffective outgassing results in magma remaining in a physically closed system until sudden vesiculation leads to energetic fragmentation and an explosive eruption (Okumura et al., 2013; Castro et al., 2014). Silicic melts can contain up to seven wt % of H_20, which expands some 1600 times in volume as it converts from fluid to gas (Lockwood and Hazlett, 2013). Typically, dry explosive fragmentation of silicic magma may trigger Vulcanian, sub-Plinian and Plinian-style eruptions (Walker, 1973; Wohletz and Heiken, 1992), which usually results in the truncation of the existing edifice. Among them, the most common is the Vulcanian eruption coupled with ballistics and minor pyroclastic density currents, and it may also trigger dome collapses, generating rock falls or block-and-ash flows (e.g. Rodríguez-Elizarrarás et al., 1991; Matthews et al., 1997; Robertson et al., 1998; Carn et al., 2004).

Hydromagmatic/hydrovolcanic explosive fragmentation refers to the interaction of magma and external water-causing explosive eruptions (Sheridan and Wohletz, 1983; Lorenz, 1985; Wohletz, 1986; White, 1996a; Wohletz and Zimanowski, 2000; Lorenz, 2003; Austin-Erickson et al., 2008; Tait et al., 2009; Kereszturi and Németh, 2012). The style of magma and water interaction and the resulting emerging edifice primarily depend on the effective magma to water mass ratio along with other factors, such as the role of sediment-laden coolants and shock waves that triggered by wall collapses or volcanic earthquakes (Sohn, 1996; White, 1996a), determining two types of eruption styles: Taalian/phreatomagmatic and Surtseyan (Kokelaar, 1983).

Sensu stricto phreatomagmatic eruptions are attributed to a subaerial process, in which fragmentation is triggered by a *molten fuel-coolant interaction (MFCI or FCI)*, usually generating crater-type monogenetic volcanoes, such as tuff rings and maars (White, 1996a; Wohletz and Zimanowski, 2000; Büttner et al., 2002; Kereszturi and

Németh, 2012). During the MFCI process, rhyolitic magmas transform heat to mechanical energy in a way different to basaltic systems because the high viscosity of silicic melts hinders the effective mingling of melt and water (Austin-Erickson et al., 2008). The mechanical deformation of the rhyolitic melt during the ascent will cause superficial brittle-type fragmentation, leading to the acceleration of mingling, which ultimately can create the conditions for launching the MFCI process (Austin-Erickson et al., 2008). The following steps are similar to the basaltic systems, where the mixing produces vapour films between the fuel and coolant. These vapour films will collapse, generating the primary phreatomagmatic fragmentation of magma and producing shock waves. Then, the superheated steam expands rapidly, generating a second stage of fragmentation (Wohletz, 1986; Zimanowski et al., 1997a; Büttner and Zimanowski, 1998; Wohletz and Zimanowski, 2000). Commonly, the interaction between magma and groundwater triggers phreatomagmatic eruptions which excavate the basement (Lorenz and Kurszlaukis, 2007; White and Ross, 2011). The tephra accumulates around the crater by dominantly pyroclastic density currents form circular low-elevation tephra rings or cones. However, as demonstrated by the number of subaerial purely effusive lava emplacement events occured in the sea, lakes or swamps (e.g. the 1971-1972 eruption of *Soufriere, St. Vincent*; Aspinall et al., 1973), the ascending silicic magma will not interact with the external water effectively to produce phreatomagmatic fragmentation in the absence of an effective brittle-type fragmentation (Austin-Erickson et al., 2008).

Surtseyan-style eruptions occur when the magma to water ratio is low (e.g. in a shallow subaqueous environment) (Kokelaar, 1983; Kokelaar and Durant, 1983; Mastin and Witter, 2000). The Surtseyan-style explosions are characterised by a sustained mixing of melt and coolant, creating steam from the water, which periodically generates tear-apart fragments from the tip of the ascending magma. This process is less efficient at fragmentation in comparison with phreatomagmatic eruptions, yielding a continuous ejection of tephra, which is the source of early underwater pyroclastic density currents, gravity flows and floating pumice (Thorarinsson, 1965; White, 1996b; Vaughan and Webley, 2010). As the accumulating pyroclastic mound grows into a shallow depth (approximately 20-30 m from the wavebase) the tephra jets become emergent and tephra fall becomes the dominant depositional process (Sohn, 1996; White, 1996b).

3.2 Volcanic products and landforms relating to silicic explosive volcanism

In order to reconstruct past volcanic activity, it is essential to examine the volcanic landforms in conjunction with the erupted volcanic materials. The main types of explosive silicic monogenetic edifices are tuff cones, pumice cones, maars, tuff rings and the rarely occurring silicic spatter cones (Walker, 1993; Walker, 2000; Furukawa and Kamata, 2004; Self et al., 2008; Ross et al., 2017). In spite of the short period of activity of silicic monogenetic volcanoes, the style of activity can vary dramatically during the eruption, forming compound edifices (e.g. a lava dome in a tuff ring) and a range of mingled volcanic materials, as seen in their basaltic counterparts as well (e.g. Brooker et al., 1993; Németh, 2010; Németh et al., 2012; Kereszturi et al., 2014; Kósik et al. 2017a). The emplacement of lava flows and domes is also frequently accompanied by explosive activity (Newhall and Melson, 1983; Heiken and Wohletz, 1987).

Pyroclastic cones are the most abundant of the volcanic structures of the Earth, mostly formed by the eruption of mafic magmas. Subaerial silicic explosive activity is usually formed by extensive sheet-like sequences comprising deposits of fallout and pyroclastic density currents relating to sub-Plinian/Plinian activity (Cas and Wright, 1988). However, in some documented cases low cones were constructed around the vent by the fallout of the jet region of the Plinian column (Fierstein et al., 1997; Riedel et al., 2003; Yasui and Koyaguchi, 2004). These so-called ultraproximal cones are characterised by distinct wide craters and very steep inner slopes (Riedel et al., 2003), such as at *Los Loros volcano, Argentina* (Németh et al., 2012b), or *Earthquake Flat volcano, New Zealand* (Charlier et al., 2003), but are often referred to as tuff cones, pumice cones or tuff rings (e.g. Nairn, 2002; Charlier et al., 2003; Kobayashi et al., 2005; Németh et al., 2012b; Johnston et al., 2014).

Many factors about the formation of pumice cones are unclear. The abundance of pumice fragments comprising these structures indicates a high gas content in the erupting magma, however the limited dispersal of pyroclastic fragments indicates relatively low-energy fragmentation and explosion. The morphology of pumice cones is similar to that of the larger scoria cones, but they typically have a slightly wider crater diameter versus their base diameter with a ratio of 0.42 (Wood, 1980; Favalli et al., 2009; Kereszturi and Németh, 2012; Karátson, 2014). The growth of pumice cones is often accompanied by the extrusion of obsidian lava flows, and sometimes pumice layers of the edifice are interbedded with blocks of obsidian lava (Kobayashi, 1982; Dellino and La Volpe, 1995; Cousens et al., 2003; Jensen et al., 2009; Shea et al., 2017). The fallout, pyroclastic surge and small-scale pyroclastic flow deposits of *Monte Pilato, Lipari (Italy)* suggest that various types of fragmentation are typical during the development of such pyroclastic cones. Based on image analysis of particle morphology, Dellino and La Volpe (1995) observed features of magmatic fragmentation for a generation of pumiceous fallout layers of Monte Pilato, while the ash beds indicate features more typical of hydromagmatic fragmentation. Others suggest underwater eruption for generating pumice cones, with less effective fragmentation than observed in basaltic Surtseyan tuff cones (Jensen et al., 2009). The formation of the *Puʻu Wa awa cone (Hualālai volcano, Hawaii)* was explained by conduit processes triggering eruptions (similar to violent Strombolian to Vulcanian activity) without substantial interaction with external water (Shea et al., 2017)

Tuff cones are believed to be formed by Surtseyan-style eruptions that take place in a shallow subaqueous environment (Kokelaar, 1983; Mastin and Witter, 2000). The documented basal sequences of Surtseyan volcanoes indicate a continuous magma uprush maintained by the closely-spaced ejection of tephra jets that may generate a steam cupola above the vents at the condition of 20-200 m water depth (Mueller, 2003). The growth of the subaqueous mound is mostly facilitated by the generation of eruption-fed pyrocalstic density currents depositing at the bottom of the lake or sea (White, 1996b). The existence of armoured and/or accretional lapilli and ballistically transported fragments relates to water-free conditions that are linked to the formation of steam cupolas (Mueller, 2003). The growing pyroclastic mound can emerge from the water, forming a subaerial pyroclastic cone (Thorarinsson, 1965; Thorarinsson, 1967; White, 1996b). The subaerial part of the tuff cones are built up from various layers of tephra originating from wet pyroclastic density currents and slurries, which can contain reworked fine tephra and coarse fragments of magmatic and lithic material conveyed by tephra jets (Wohletz and Sheridan, 1983; Sohn and Chough, 1992; Abrams and Siebe, 1994; Cole et al., 2001; Solgevik et al., 2007; Zanon et al., 2009; Mattsson, 2010; Sohn et al., 2012). Surseyan-style eruptions continue until the water no longer has access to the vent and gives way to lava effusion (e.g. *Monte Pilato-Rocche Rosse, Lipari, Italy,* Davì et al., 2011*; Surtsey, Iceland,* Thorarinsson, 1965; *Volcán Bárcena, San Benedicto, Revillagigedo Islands, Mexico,* Richards, 1959; and *Nishinoshima, Japan,* Maeno et al. 2016). The morphology of the emerging edifice is affected by the rate of tephra production, as well as the migration and depth of explosion loci (Thorarinsson, 1965; Kokelaar, 1983; Kokelaar and Durant, 1983). The resulting landform usually develops into a conical shape, with 5-20° outward-dipping, and steeper, up to 38° inward-dipping angles of the strata (Wohletz and Sheridan, 1983; Abrams and Siebe, 1994; Solgevik et al., 2007). Silicic tuff cones are quite rare landforms (e.g. *Cerro Xalapaxco, Mexico*; Abrams and Siebe, 1994), yet their shape is similar to pumice cones, thus the distinction between pumice cones and silicic tuff cones can be ambiguous (e.g. Kobayashi et al, 2013). Tuff cone structures are very vulnerable to erosion, especially against sea waves, without capping of the lava (Thorarinsson, 1967; Cole et al., 2001; Sohn et al., 2012).

The maar or maar-diatreme volcanoes originate from phreatomagmatic eruptions, creating deep craters with steep-sided walls (Lorenz, 1986; White and Ross, 2011). Two models are available describing the formation of maar-diatreme structures (Lorenz, 1986; Valentine and White, 2012). Lorenz's model suggests the downward progradation and/or lateral migration of explosion loci, according to the hydrogeological and local substrate settings or following regional faults (e.g. *Ukinrek Maars, Alaska* Kienle et al. 1980; *Tihany maars, Hungary,* Németh et al., 2001; *Tecuitlapa Maar, Mexico,* Ort and Carrasco-Núñez, 2009, *Yangpori Diatreme, SE Korea,* Son et al., 2012). In this model the general evolution of diatremes is based on an incremental growth, during which the locus of explosive activity progressively deepens and the diatreme widens due to the subsidence (Lorenz, 1986).

In contrast, recently developed models support that in many cases MFCI occurs at varying depths during the course of the activity, although it is most effective at shallow depths where the critical pressure is higher than the hydrostatic pressure. Thus, deep-seated explosions are rarely powerful enough to erupt (Valentine and White, 2012; Valentine et al., 2014; Graettinger et al., 2015). As commonly documented, the explosivity is highly influenced by the hydrological conditions (Németh et al, 2001; Carrasco-Nunez et al., 2007), as the longer-lived activity of subaerial volcanoes usually quickly depletes the substrate or blocks the surface sources and they gradually become dry explosive or effusive eruptions (e.g. *Ság-hegy, Western Hungary*, Martin and Németh, 2004; and *Motukorea tuff ring, Auckland Volcanic Field, New Zealand*, Agustín-Flores et al., 2015). The shape of the upper part of the diatreme can be similar to a pipe or a champagne glass, whereas the deeper diatreme structures commonly have steep walls regardless of the litology of the basement (Lorenz, 2003; Lorenz and Kurszlaukis, 2007; Delpit et al., 2014). The champagne glass shape is typical where the rocks of the basement are soft and unconsolidated, resulting in the retreat of the crater rim by slides and slumps or lateral collapses (Németh et al., 2007; Pirrung et al., 2008; White and Ross, 2011). Typical crater diameters are between a few hundred metres to 2-3 kilometres (Wood, 1979; Wohletz and Sheridan, 1983; White and Ross, 2011). Most of the maars with large diameters were formed as a result of the amalgamation of multiple maar basins or the coalescence of closely-spaced vents, such as the *Blue Lake* and *Lake Purrumbete maars, SE Australia* (Jordan et al., 2013; van Otterloo et al., 2013), and the *Espenberg maars, Seward Peninsula, Alaska* (Begét et al., 1996). In contrast, steeper and narrower craters are more typical of spatially-focused eruptions excavating hard country rocks (Wohletz and Sheridan, 1983; Lorenz, 2003; Martin and Németh, 2005; Auer et al., 2007; Lorenz, 2007; Lorenz and Kurszlaukis, 2007; White and Ross, 2011). Evolving pyroclastic density currents and tephra fallout build up an ejecta ring around the crater, which is rarely higher than 50 m (Lorenz, 1986; Lorenz and Kurszlaukis, 2007; White and Ross, 2011; Kereszturi and Németh, 2012). The deposits of diatremes and tephra rings can be distinguished based on the volcanic materials. The deposits filling up a diatreme structure can be subdivided into root zone, lower diatreme and upper diatreme sequences (White and Ross, 2011). The root zone is the lowest and narrowest part of the diatreme, just above the feeder dyke where the deepest phreatomagmatic explosions occur (Lorenz and Kurszlaukis, 2007; White and Ross, 2011). The ususal mafic dyke diameter (1-3 m) (Delaney and Pollard, 1981; Geshi et al., 2010) is considerably slimmer than the observed silicic dykes, with up to a few hundred metres of thickness, which can cause substantial differences in the structure of the deeper zones between the silicic and mafic systems (Ross et al., 2017). The rocks of the root zones are characterised by breccias consisting of coarse-grained angular or subangular clasts originating from the immediately surrounding country rocks along with coherent intrusions, peperites and some pyroclastic material. The country rock region often displays jigsaw-fit textures and these rocks are called contact or explosion breccias at basaltic diatremes (Lorenz and Kurszlaukis, 2007; White and Ross, 2011). Silicic intrusions of diatremes may induce epithermal mineralisations (Sillitoe et al., 1984; Sillitoe et al., 1985; Davies et al., 2008). Above the contact breccias the pyroclatic sequence is mixed and unbedded in comparison to the upper diatreme, where the sequence is characterised by primarily thinly-bedded tephra or alternating primarily thinly-bedded and reworked thickly-bedded tephra with the occasianal presence of the collapsed blocks of the crater walls (White and Ross, 2011). During the syn-eruptive period, intra-diatreme faulting becomes more common due to the subsidence of the crater infill, which can combine with magma intrusion, resulting in dykes, plugs or lava dome emplacement (Lorenz and Kurszlaukis, 2007; Németh and Martin, 2007; Németh et al., 2008; Austin-Erickson et al., 2011; White and Ross, 2011).

The craters or morphological structures excavated by phreatic eruptions are referred to as phreatic explosion craters (Barberi et al., 1992). Phreatic explosions are caused by the sudden release of steam generated as a result of the flashing of water coming in contact with magma. Explosion craters may also form by the sudden release of CO_2 that accompanies the excavation of country rocks with no involvement of any juvenile material (Allard et al., 1989; Browne and Lawless, 2001). The diameter of phreatic explosion craters ranges between tens of metres to over 1 km (Muffler et al., 1971). These craters are usually surrounded by phreatic breccia deposits composed of various-sized ballistically transported lithic fragments immersed into a muddy matrix that is subordinately interbedded with base surge layers (Barberi et al., 1992; Browne and Lawless, 2001). The subsurface part of the structure is also called a diatreme and is characterised by brecciated country rocks having a subvertical upward-flaring arrangement (Browne and Lawless, 2001). Some authors discriminate hydrothermal eruptions as a restricted category for such explosions, whose energy is exclusively derived from heat loss and phase changes in convecting hot water/steam-dominated hydrothermal systems (Browne and Lawless, 2001). The crater diameters created by so-called hydrothermal explosions range between a few metres to up to 200 m, but the inferred focal depths may exceed 450 m (Sigvaldason, 1992; Browne and Lawless, 2001; McNamara et al., 2016). As the proof of the exact triggering mechanism of these explosions with no juvenile components is difficult to determine, and the generated pyroclastic rocks are almost identical. The eruptions that occur in geothermal fields are usually referred to as hydrothermal explosions (e.g. Muffler et al., 1971; Sillitoe et al., 1984; Browne and Lawless, 2001), while eruptions associated with conduits of active volcanoes are mostly expressed as phreatic eruptions/explosions (e.g. Allard et al., 1989; Christenson et al., 2010; Kato et al., 2015; Rouwet et al., 2017).

Tuff rings are also believed to be formed by phreatomagmatic eruptions (e.g. Austin-Erickson et al., 2001; Németh et al. 2012). The distinctive feature of the tuff rings from maars is their crater, which does not cut deeply into the pre-eruptive surface due to the characteristically shallow-seated explosive activity, thus diatremes are embryionic or missing (Wohletz and Sheridan, 1983; Martin and Németh, 2004; Martin and Németh, 2005; Austin-Erickson et al., 2011; White and Ross, 2011). The crater surrounding the ejecta rings build up by surges and fallout from discrete blasts, creating a stratified sequence with dune- and cross-bedding honeycombed by ballistic lithics (Chough and Sohn, 1990; Brooker et al., 1993; Lorenz, 2007; Austin-Erickson et al., 2011; White and Ross, 2011). The late stage deposits of the *Tepexitl tuff ring (Mexico)* are dry and coarse grained without bedding, and can be interpreted as a final vent-clearing event destroying the ascending magma plug (Austin-Erickson et al., 2011), while the *Los Loros tuff ring (Argentina)* exhibits an upper sequence showing that a distinct eruption generated a small-volume welded ignimbrite partly overlain by lava flows and block-and-ash flow deposits (Németh et al., 2012b). The crater formation of these silicic small-volume volcanoes is usually followed by the extrusion of lava domes (e.g. Brooker et al., 1993), otherwise the crater will fill up by sliding, slumping and lake sedimentation (e.g. Németh et al. 2008).

Silicic magmatic explosive eruptions are usually powerful due to their high volatile content, but rarely form spatter deposits or spatter rings through low energy activity. The main identifying features for these volcanic structures are the spatter, agglutinate and welded clastogenetic lavas, which are generated by the silicic counterpart of Strombolian (or Hawaiian) style lava-fountain eruptions and/or associated pyroclastic flows with rheomorphism (Furukawa and Kamata, 2004). In contrast with the mafic magmas, silicic melts are too viscous under usual circumstances to fragment plastically. Thus, the enigmatic silicic spatter eruptions require atypically low magma viscosity in spite of the rhyolitic composition, which may occur with magmas of peralkaline composition (Mahood and Hildreth, 1986), a magmatic temperature as high as ~1000°C (Henry et al., 1988; Henry et al., 1989), a low water content (Creaser and White, 1991), or a high fluorine content (Duffield, 1990)**.** However, chemical analyses of the spatter deposits of the *Yamakogawa Rhyolite (Kyushu, Japan)* show a calc-alkaline composition with the presence of biotite phenocrysts, which supports relatively low magmatic temperatures and high magmatic water content (Furukawa and Kamata, 2004). Self et al. (2008) proposed that degassed silicic magma might have been fragmented by the influence of external water. Others (e.g. Jaupart and Allegre, 1991; Castro et al., 2014) have considered over-pressurising of the conduit owing to the decreasing gas loss as a possible explanation for the formation of silicic spatter deposits. Subaqueous silicic deposits with fluidal silicic fragments from the Archean *Hunter Mine Group (Abitibi greenstone belt, Canada)* indicate that lava-fountaining and spatter generation is possible at a water depth of 200 m (Mueller and White, 1992). Their observations suggest that silicic spatters were formed under a steam cupola that inhibited water ingress to the fountain. The existence of such deposits suggests a high temperature and a degassed nature as preconditions for lava-fountaining of silicic eruptions (Henry et al., 1988; Henry et al., 1989; Mueller and White, 1992).

3.3 Lava domes and coulees

Lava domes and **coulees (viscous lava flows)** are the most common landforms of monogenetic silicic eruptions and their occurrence is frequent at composite volcanoes as well (Fig. 3.1) (Wohletz and Heiken, 1992). The nature of their formation and morphologic features relates with the physical properties of the erupting magma regardless of the settings of emplacement (volcanic fields versus summit crater of composite cones). Due to the limited observed lava dome emplacement at volcanic fields, most of the volcanic processes were defined during dome formation on composite cones or lava dome complexes, such as *Mt. St. Helens, USA; Santiaguito, Guatemala; Unzen, Japan; Soufriere Hills, Montserrat*.

In contrast with lava flows, the lava domes tend to pile up over their vents due to the higher viscosity (Fink and Anderson, 2000). The coulees have aspects of both a lava flow and domes as they have experienced some flow away from the vent (Blake, 1990; Fink and Anderson, 2000). The formation of lava domes may be endogenic (intrusive) or exogenic (extrusive) (Anderson and Fink, 1990; Fink et al., 1990; Kaneko et al., 2002; Hale and Wadge, 2008; Bernstein et al., 2013). Endogenic dome growth means that the enlargement of the dome occurs due to the influx of lava into the interior. In contrast, exogenic dome growth requires new magma to deposit on top of the previous surface, creating discrete lobes or lava spines (Wohletz and Heiken, 1992; Fink and Anderson, 2000). The transition between the two types of dome growth is common and often influenced by the changes in effusion rate, which may lead to enhanced explosive activity and lava dome collapses (Ryan et al., 2010; Husain et al., 2014). The effusion rates of historical dome eruptions vary from less than 0.1 m^3/s to about 300 m^3/s (Siswowidjoyo et al., 1995; Pyle, 2000; Lyman et al., 2004), based on field observations (e.g. Mimatsu diagram, Yokoyama, 2002) and volume calculations using DEMs. Most of the long-term effusion rates fall between 0.2 m^3/s to 20 m^3/s in events observed during the past 100 years (Table 3.1) (Newhall and Melson, 1983; Yokoyama, 2005). Horizontal lava dome dimensions vary from a few metres to several kilometres. Their height rarely surpasses 1 km. The growth of the lava dome by itself is unaccompanied by significant hazard (Fink and Anderson, 2000), but the associated collapses and explosive activity tend to generate hot pyroclastic density currents that may run out several kilometres from the vents (Sieh and Bursik, 1986; Rodríguez-Elizarrarás et al., 1991; Ui et al., 1999; Cole et al., 2002; Kósik et al., 2017a). The emplacement of lava domes (including all kinds of occurrence) caused about 32000 fatalities in the 20th century (Fink and Anderson, 2000), which amounts to more than 40% of the total deaths caused by volcanic eruptions.

Dome eruption	Region	Lava type and SiO_2 content (%)		Volume of dome structure (10^6 m^3)	Average grow rate (m^3/s)
Mt Pelée (1902)	West Indies	A	62	0.03	3.6
Tarumai (1909)	Hokkaido	A	60	15	120
Novarupta (1912)	Alaska	R	73	5	0.3
Santaguito (1922-25)	Guatemala	D	64	200	1.9
Dafni dome, Santorini (1925-26)	Greece	D	65	360	4.2
Showa Iwo-jima (Kikai) (1934-35)	Kyushu	D-R	67-73	6.2	1.2
Mt. Usu/Showashinzan (1944)	Hokkaido	D	69	44	1.3
Rinjani (1944)	Lombok	BA	52	74	127
Ruapehu (1945)	New Zealand	A	60	20	2.3
Mt. Lamington (1951)	Papua N.G.	A	59	60	18.5
Bezymianny (1956)	Kamchatka	A	60	42	16.2
Volcán de Colima (1975-76)	Mexico	A	59	1	0.05
Soufriere S.V. (1979)	West Indies	BA	55	35	6.3
Mt St Helens (1980)	USA	D	63	10	9.7
Shiveluch (1980)	Kamchatka	A	61	10	2.2
Redoubt (1989-90)	Alaska	A	60	20	25.5
Unzen (1990-92)	Kyushu	D	66	50	4.6-6.9
Soufriere Hills (1995-97)	West Indies	A	60	68	2.3
Popocatepetl (1996)	Mexico	A	64	11	2.1
Volcán de Colima (1998)	Mexico	A	59	0.4	4.4
Chaitén (2008-09)	Chile	R	75	500	45.0
Cordón Caulle (2011-12)	Chile	R	70	400	20-60

Table 3.1 Effusion rates of well-documented lava dome extrusions from the 20th and 21st centuries (Newhall and Melson, 1983; Yokoyama, 2005; Pallister et al., 2013; Tuffen et al., 2013).

3.3.1 Factors determining the shape and volcanic hazard of lava domes

The emplacement of the evolving landforms is driven mostly by the physical properties (internal factors) of the erupting magma (Blake, 1990; Fink et al., 1991; de Silva et al., 1994; Fink and Griffiths, 1998; Fink and Anderson, 2000; Gregg and Fink, 2000; Stevenson et al., 2001; Lyman et al., 2004; Yokoyama, 2005; Husain et al., 2014), however the inclination of the pre-eruption surface, environmental conditions, surface processes and tectonics (external factors) also influence their formation (Christiansen and Peterson, 1981; Matthews et al., 2002; Carn et al., 2004; Lara et al., 2004; Herd et al., 2005; Austin-Erickson et al., 2011).

Viscosity is the most important physical feature in the generation, transport and eruption of magmas. Several factors affect magma viscosity, namely, temperature and cooling rates, melt composition, crystallinity, exsolved fluid phases and degassing (Griffiths and Fink, 1993; Stasiuk et al., 1993; Harris et al., 2002; Giordano et al., 2008; Petford, 2009; Tuffen et al., 2013). In terms of the chemical composition of the melt, its dissolved volatiles, such as H_2O and F, might have a strong impact as a small quantitative change can cause large and nonlinear changes in the viscosity of magmas (Hui and Zhang, 2007; Giordano et al., 2008). It is assumed that the rhyolitic melts have a high magmatic gas content (min. 2-3 wt %) (Jaupart and Allègre, 1991), which degasses near the conduit walls and vents as the magma ascends (Fink and Anderson, 2000). Newhall and Melson (1983) claimed that the majority of dome growth associated with any explosive activity is related to the proportion of dissolved H_2O or the crystal content and viscosity in the case of water-poor magmas (Newhall and Melson, 1983; Sparks, 1997).

Furthermore, explosions may have been triggered by the change of physical properties of the magma (e.g. increasing viscosity, crystallisation and decreasing permeability), hindering the effective outgassing and causing the overpressurisation of the conduit (Okumura et al., 2009; Castro et al., 2014). Explosive activity with a wide range of VEI values may occur before, intermittently and after dome growth (Newhall and Melson, 1983). The explosive activity associated with lava domes ranges from milder vent-clearing phreatic/phreatomagmatic eruptions, or Vulcanian eruptions, to Plinian-style sustained pumice eruptions (Heiken and Wohletz, 1987; Wohletz and Heiken, 1992; Sparks, 1997; Moran et al., 2008). The 2008-2009 eruption of Chaitén, Chile and the 2011-2012 eruption of Cordón Caulle, Chile highlighted that effusive rhyolites may display a range of highly explosive behaviours. Sub-Plinian to Plinian-style energetic volcanic blasts with pyroclastic fountains commonly occur not only alternately, but simultaneously with lava effusion, lasting weeks to months from the same vent that also produces metre-sized ballistics and pyroclastic density currents (Lara, 2009; Pallister et al., 2013; Tuffen et al., 2013; Castro et al., 2014). The explosive-effusive transition is mostly controlled by shallow conduit processes, such as permeability changes and degassing of magma (e.g. Adams et al., 2006; Castro and Gardner, 2008; Lavallée et al., 2012; Cabrera et al., 2015; Kennedy et al., 2016). Emplacement of viscous lava accompanied with frequent block-and-ash flow generation is often called as Peléan-style activity after the 1902 eruption of Mt Pelée, Martinique. Besides the magma properties, external factors can increase explosivity or trigger explosions, such as the interaction of magma with external water (Brooker et al., 1993; Austin-Erickson et al., 2011), a sudden reduction of load on the conduit due to a major edifice failure (Christiansen and Peterson, 1981; Herd et al., 2005), regional earthquakes (Lara et al., 2004) or intensive rainfall (Matthews et al., 2002; Carn et al., 2004).

The style of lava dome growth and dome morphology depends on a dimensionless parameter (Ψ_B) predicted from the ratio of the timescale of solidification (time required for the magma surface to cool down to its solidification temperature) to the timescale of advection (time elapsed for the flow to advance a distance equal to its thickness) (Griffiths and Fink, 1997). The effusion rate and the yield strength of the lava are the main factors determining the characteristics of advection of the flow/dome (Griffiths and Fink, 1997; Fink and Griffiths, 1998), which is strongly influenced by the slope angle of the pre-erupting surface (Fink, 1993; Fink and Anderson, 2000; Gregg and Fink, 2000; Lyman et al., 2004). High effusion rates and small yield strength will result in domes with a thin solid crust spreading in all directions, whereas steep-sided domes consisting of distinct lobes or spines occurs in the case of lower effusion rates and high yield strength (Griffiths and Fink, 1997; Fink and Griffiths, 1998).

The final morphology of the lava domes concerns the style(s) of their emplacement and the duration of the eruption (Fink and Anderson, 2000; Husain et al., 2014), as well as any destructive events during the dome growth, which represents the most significant volcanic hazard. Typically, the main reasons for edifice failure are dome instability due to the oversteepening of slopes during dome growth or earthquakes, and the overpressurisation of the interior of the lava dome (Fink and Manley, 1989; Voight and Elsworth, 1997; Voight, 2000; Harris et al., 2003; Husain et al., 2014). In both cases, the activity is accompanied by pyroclastic density current generation and may also produce explosive eruptions.

Commonly, dense pyroclastic density currents (block-and-ash flows) are confined to the valleys, but the pyroclastic surges may affect broader areas (Fisher and Schmincke, 1984; Cas and Wright, 1988; Druitt, 1998). Variations in effusion rate usually increase the frequency of explosions and collapses, thus the observations of effusion rates and developing dome morphology may support the determination of possible hazards of the activity (Griffiths and Fink, 1997). In contrast, the Plinian activity of lava domes mostly does not correlate to the magma of the evolving dome, and instead represents a distinct gas-rich magma batch erupting through the same vent (Pallister et al., 1992; Fink and Anderson, 2000). In this case, the dome morphology is not indicative of the explosive activity, but the change of eruptive behaviour can be forecasted by the monitoring of degassing, ground deformation and seismicity (Harlow et al., 1996; Fink and Anderson, 2000).

Steep-sided or hydrothermally altered edifices pose a threat after or between active emplacement periods through the risk of rockfalls and debris avalanches, as documented at *El Brujo, Santiaguito, Guatemala* (Fink and Anderson, 2000) and *Chaos Crags, Mount Lassen, USA* (Crandell et al., 1974). The dome growth together with the syn- and post-volcanic failures will determine the shape of the evolved domes, which will be further modified by the erosional processes, making the reconstruction of the style of their formation difficult.

3.3.2 Surface and internal structures of lava domes

The surface and internal structures of lava domes and coulees provide a great opportunity to understand the factors of their emplacement and degassing and cooling histories (Christiansen and Lipman, 1966; Fink, 1980b; Fink, 1983; Manley, 1992; Stevenson et al., 1994; Duffield et al., 1995; Fink and Anderson, 2000; Stevenson et al., 2001; Stewart and McPhie, 2003; Maeno and Taniguchi, 2006; Hale, 2008; Závada et al., 2009; Závada et al., 2015). From the surface to the interior there are various structural units and features. The surface of the lava dome may be smooth (crease structures) near the vent area in the case of ductile deformation (Anderson and Fink, 1990; Anderson and Fink, 1992) (Fig. 3.2B-C), but fracturing results in a blocky dome surface, called as a carapace breccia. Its block size can vary from a few centimetres to more than 5 m in diameter. The average block size decreases with higher effusion rates and with distance from the vent area to the flow front (Anderson et al., 1998; Fink and Griffiths, 1998; Bulmer et al., 2005). During the advancement of lava the fracturing blocks are mingled, which results in a diverse mixture of lava blocks with different textures. Explosion pits are common features of lava domes and flows formed by Vulcanian-style eruptions above the vent and they relate to overpressurisation of the dome or flow interior, due to gas released by crystallisation

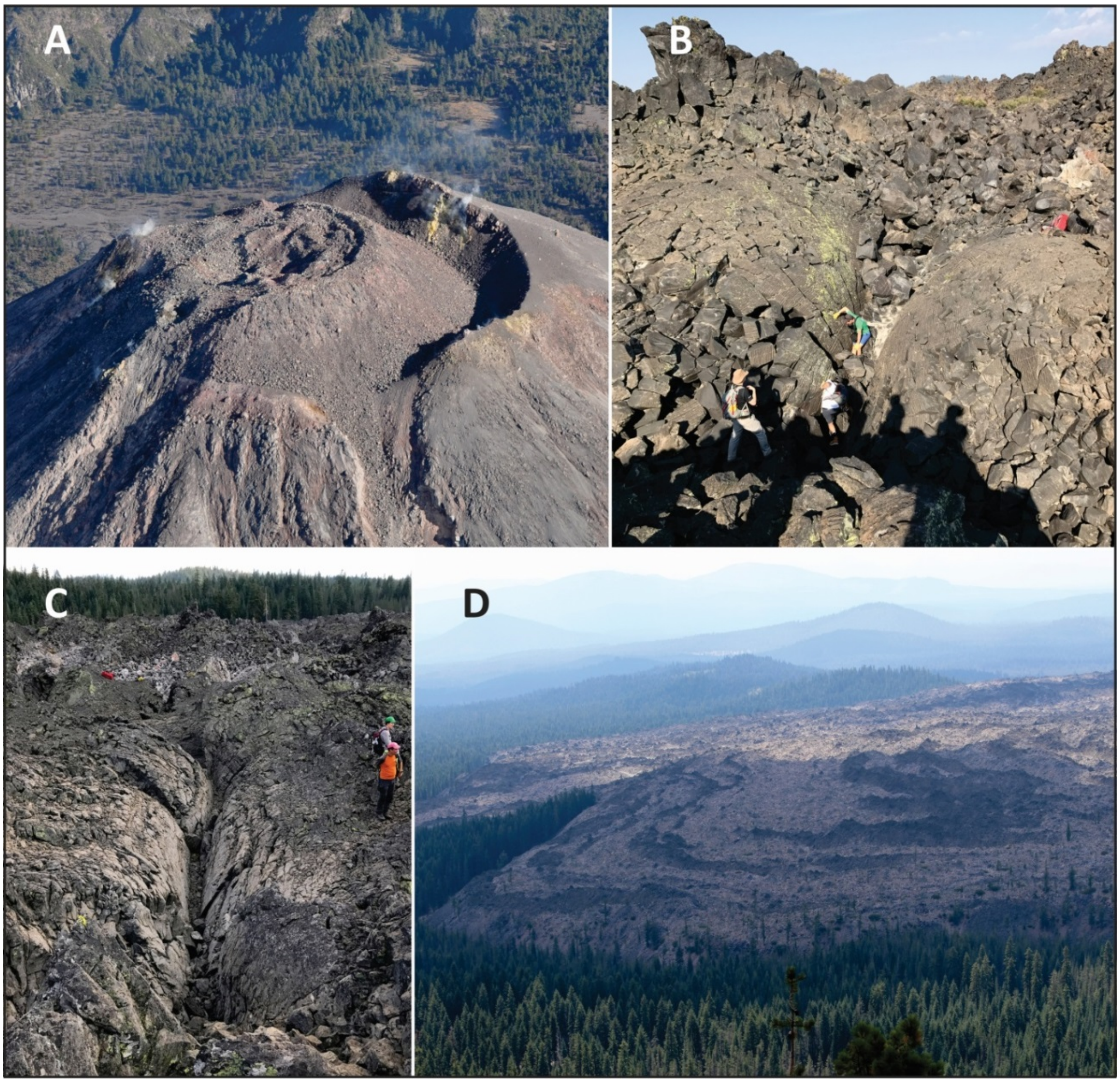

Figure 3.2 Surface textural features of lava domes. A – explosion pits on the surface of the 2011 dome of Volcán de Colima (photo courtesy: J. Farquharson/CIIV, Universidad de Colima), Mexico; B – Crease structure on the Little Glass Mountain flow, Medicine Lake volcano, USA; C – Crease structure on the Medicine Lake Glass Flow, Medicine Lake volcano, USA; D – Ogives/flow ridges of the Little Glass Mountain flow, Medicine Lake volcano, USA. Light-coloured areas represent finely vesicular pumice (FVP) texture, whereas darker areas comprise obsidian and coarsely vesicular pumice (CVP) textures.

(Fig. 3.2A). The depth of the explosion pits can be tens of metres, while the maximal diameter may reach a few hundred metres above the vent, and pits at other parts the dome/flow surface are characterised by smaller depths and diameters (Fink and Anderson, 2000).

Ogives (compressional or flow ridges) are formed by folded structures with their axes perpendicular to the flow direction, and form in response to compression generated by the flow advancement (Fig. 3.2D). Well-developed fold ridges require higher carapace viscosity than the interior of the dome, but must also be able to deform in a ductile manner. The wavelength of the folds depends on the thickness of the carapace and the chemical composition of the lava, and the higher SiO_2 leads to the larger wavelength of the folds. The height of the ogives increases by the higher viscosity difference and typically emerge 10-15 m from the flow surface (Fink, 1980b; Fink and Anderson, 2000; Hughes, 2015).

The sheeted, folded and flow-layered carapace of a rhyolite body consists of three main layers: finely vesicular pumice (FVP) near the surface, a dividing obsidian unit, and coarsely vesicular pumice (CVP) in the inner side. Sometimes a second obsidian unit occurs in the interior of the carapace (Fink and Manley, 1987; Manley and Fink, 1987; Stevenson et al., 1994; Fink and Griffiths, 1998). Two models explain the variations of these lava textures. According to the first model, the lava erupts as a dense obsidian that later degasses, which results in the inflation of the outer vesicular zone (FVP) and the inner vesicular zone (CVP) (Fink and Anderson, 2000). The second model proposes that the rhyolitic melt erupts as inflated magmatic foam. Due to the combined effect of degassing and compression the foam will collapse, forming obsidian layers (Eichelberger et al., 1986; Friedman, 1989; Jaupart and Allègre, 1991; Fink et al., 1992; Fink and Anderson, 2000). The innermost portion of the rhyolitic dome or flow is usually a massive dense rhyolite, but sometimes the crystalline rhyolite is interbedded with obsidian units (Fink and Manley, 1987; Fink and Anderson, 2000). The base of the lava body has an inner obsidian and a basal breccia unit (Christiansen and Lipman, 1966; Manley and Fink, 1987; Stevenson et al., 1994; Duffield et al., 1995; Maeno and Taniguchi, 2006) (Fig. 3.3).

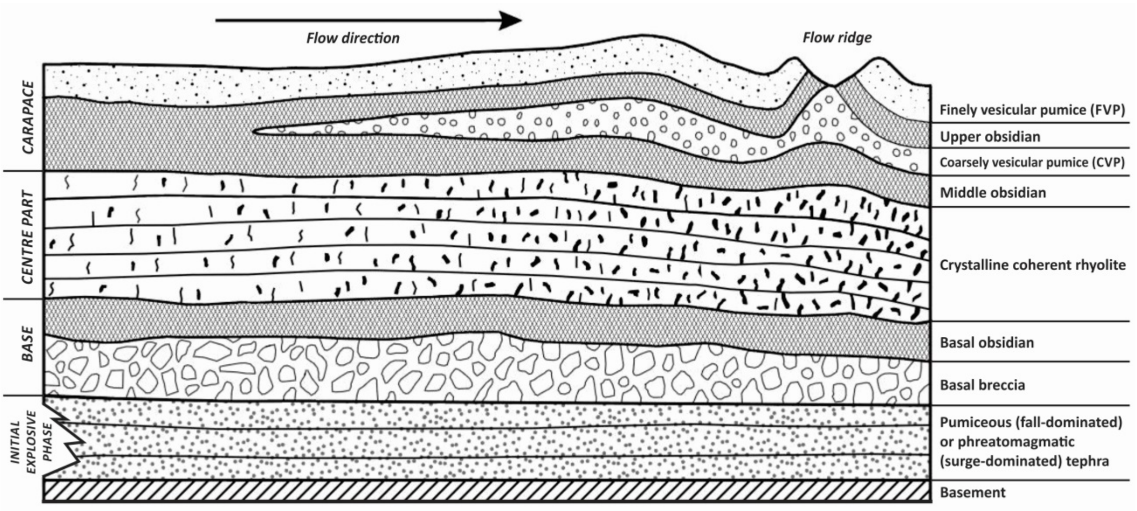
Flow direction
Flow ridge
CARAPACE
CENTRE PART
BASE
INITIAL EXPLOSIVE PHASE
Finely vesicular pumice (FVP)
Upper obsidian
Coarsely vesicular pumice (CVP)
Middle obsidian
Crystalline coherent rhyolite
Basal obsidian
Basal breccia
Pumiceous (fall-dominated) or phreatomagmatic (surge-dominated) tephra
Basement

Figure 3.3 Schematic cross section of a rhyolitic obsidian flow based on drill core observations from Obsidian Dome in the Inyo dome chain, Long Valley caldera, USA, figure modified after Fink and Manley (1987).

The inner part of lava bodies often shows two other types of structural textures with different genesis: flow banding and jointing. Flow banding forms during the extrusion from the vent. The flow banding tends to be vertical near the vent zone and horizontal in the basal sequences due to basal shear. The banding of the flow top usually dips towards the vent area, indicating a lateral stretching of the upper parts of the lava body (Christiansen and Lipman, 1966; Fink, 1983; Fink, 1993; Smith and Houston, 1994; Duffield et al., 1995).

Many kinds of joints can be formed during the emplacement and the cooling of silicic lava bodies (e.g. sheet joints, shrinkage joints, columnar joints, onion skin joints). The sheet joints are parallel to the cooling surface and/or the flow foliation. The formation of the former sheet joints is caused by different cooling and crystallisation rates, while the second type forms in response to flow stresses (Bonnichsen and Kauffman, 1987; Fink and Anderson, 2000). The most frequent and recognisable joint type of the silicic dome interior is columnar jointing, which results from contraction during the cooling of the lava bodies (Spry, 1962; Budkewitsch and Robin, 1994; Grossenbacher and McDuffie, 1995). The diameter and the regularity of the columnar joint polygons relate to the cooling rate, which means the lava bodies show narrower columns near their edge and wider columns in the core region (Grossenbacher and McDuffie, 1995; Goto and McPhie, 1998).

3.3.3 Appearance at different volcanotectonic environments and relationship with polygenetic volcanoes

Lava domes are common volcanic features appearing in various volcanotectonic environments characterised by site-specific features and eruptive behaviours. They most commonly occur at subduction zones with continental (e.g. *Crater Lake, Newberry volcano, Mt. St. Helens (USA), Islas Quemadas, Ilopngo (El Salvador), Taranaki (New Zealand), Sierra la Primavera (Mexico), Tarumae, Mt. Usu (Japan), Cerro Chao (Chile)*) and oceanic crusts such as *Brothers (New Zealand), Mt. Pelee, Soufriere, Soufriere Hills (Lesser Antilles), Niijima (Japan)*, as well as continental rift zones (e.g. *Auvergne (France), Coso Volcanic Field, Inyo Craters, Valles Caldera, Yellowstone (USA), Dama Ali (Ethiopia), Cerro Prieto (Mexico)*). Lava domes are relatively common where intraplate volcanism occurs through a thick continental crust such as at *Harrat Rahat (Saudi Arabia), Acigöl* and *Erciyes Dagi (Turkey), Mt. Halla (Jeju).* Rare occurrences have been reported from oceanic rift zones (e.g. *Bouvet (Antarctica), Furnas (Azores), Geysir (Iceland), San Benedicto and Socorro, Revillagigedo Islands (Mexico)*). Lava domes are almost absent in oceanic intraplate settings because the lavas are usually too fluid, however a few lava domes appear at *Tenerife (Spain)* where there is a relative abundance of lavas characterised by more evolved compositions. Hybrid tectonic settings, rifting and mantle plumes, such as in Iceland (e.g. Gunnarsson et al., 1998), or subduction and rifting such as in the TVZ, New Zealand (Rowland et al., 2010; Deering et al., 2011) and Zacoalco Graben, Mexico (Allan, 1986), greatly promotes lava dome volcanism.

Besides the tectonic settings, the spatial relationship of lava domes with other volcanic structures and their conduits is an important factor to consider when evaluating their formation and possible hazards. Lava domes can occur on the flank/ring plain of composite and shield volcanoes and may occlude the main conduits of these volcanoes. They may also occur in volcanic fields and caldera settings. Having examined the main features of these possible relationships lava domes can be classified into two groups (Fig. 3.1). The first group comprises domes emplaced at the flanks (parasitic dome) or as a summit dome are commonly characterised by intermediate compositions and represent one eruptive cycle/episode during the lifespan of the composite volcano. These domes usually have short lifetime due to the frequent destructive events at the summit. With regard to their relative high potential energy, the dome collapse poses a significant threat to their low-lying surrounds if the dome is overgrown by the rim of the crater, as demonstrated by the activity at *Sinabung, Merapi (Indonesia)* and *Volcán de Colima (Mexico)* (Saucedo et al., 2004; Gomez et al., 2008; Yulianto and Sofan, 2016). The second group of lava domes, mostly relating to faults and caldera structures, are characterised by eruptions occurring from newly-forming vents. Thus, these lava domes are usually emplaced to a levelled or gently-sloping low-lying surface or within a crater (Chapter 7), and only the thickness of the emplaced lava body represents its possible potential energy.

This kind of volcanic activity in most cases meets the diagnostic features of monogenetic/small-volume volcanism (White and Ross, 2011; Németh and Kereszturi, 2015). Occasionally the erupted volumes significantly exceed the 1 km^3 upper limit of monogenetic/small-volume eruptions (e.g. *Cerro Chao* – 22 km^3, *Chile*; de Silva et al., 1994), however the other features (e.g. lifespan) of these eruptions are very similar to monogenetic volcanism. Some of the lava dome complexes represent the borderline between the monogenetic and polygenetic dome growth. The summit regions of lava dome complexes tend to reach a similar height as smaller composite volcanoes and are usually characterised by intermediate chemical compositions. From this perspective, these edifices and related activity are similar to the domes of composite volcanoes (e.g. *Santiaguito, Guatemala*; Harris et al., 2003), however the lifespan of some of the eruptions may not have been significantly longer than a few decades to hundreds of years (e.g. Tauhara; Lewis, 1968, and Mt. Edgecumbe; Carroll et al., 1997, New Zealand), more than the most prolonged monogenetic eruptions (Pioli et al., 2008).

The emplacement of lava domes in caldera environments may be defined by the spatial relationship, such as the small-volume volcanism aligned to the ring structures of the calderas (e.g. *Toya caldera – Mt. Usu, Japan; Whakamaru – Western Dome Belt, New Zealand; Valles-Toledo Caldera Complex, USA*), or appear along fault lines or in clusters within or outside of the boundary of caldera structures (Bacon et al., 1980; Leonard, 2003; Cole et al., 2005) (Fig. 3.4). The influence of strong regional tectonism can be detached easily as the domes are arranged in chains, such as the *Maroa and*

Tarawera dome complexes, New Zealand (Nairn, 2002; Leonard et al., 2010); *Ceboruco–San Pedro volcanic field, Mexico* (Petrone et al., 2003; Frey et al., 2004); *Coso Volcanic Field* and *Inyo domes, USA* (Bacon et al., 1980; Bailey, 1989)*;* and *Chaîne des Puys, Auvergne, France* (Plenier et al., 2007). Besides the spatial relationships, the temporal and geochemical relationships between the emplaced lava domes and the climactic eruption-inducing caldera collapses are very important issues to understand.

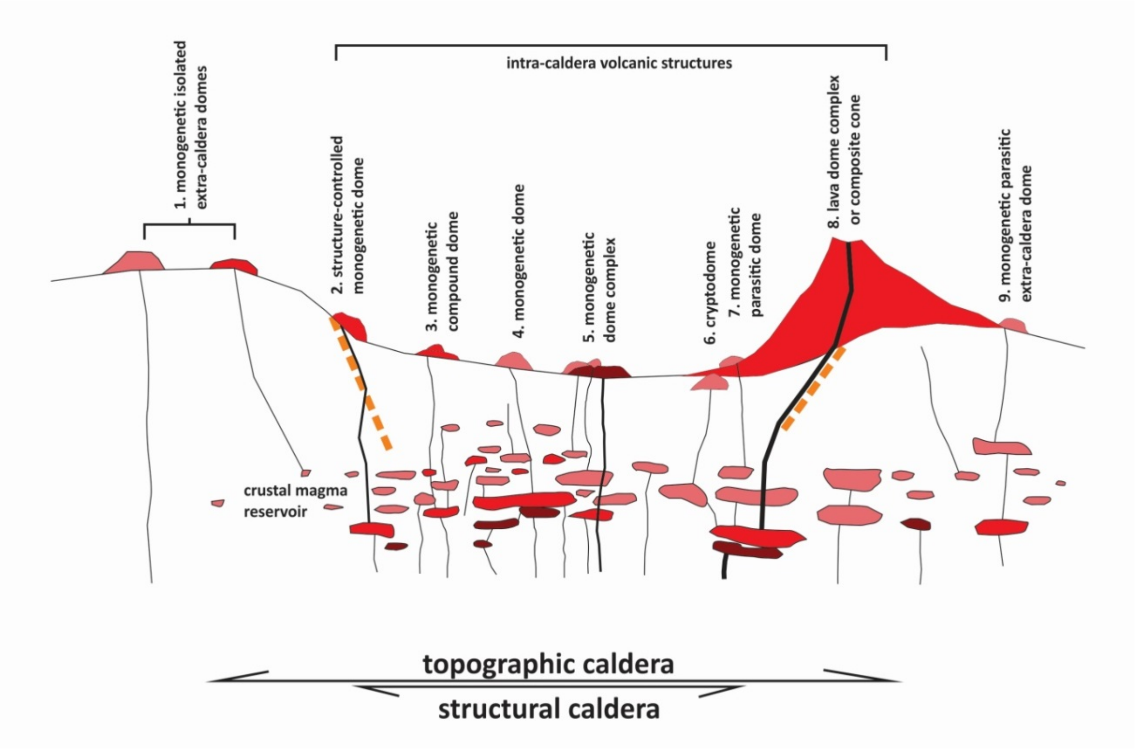
intra-caldera volcanic structures
1. monogenetic isolated extra-caldera domes
2. structure-controlled monogenetic dome
3. monogenetic compound dome
4. monogenetic dome
5. monogenetic dome complex
6. cryptodome
7. monogenetic parasitic dome
8. lava dome complex or composite cone
9. monogenetic parasitic extra-caldera dome
crustal magma reservoir
topographic caldera
structural caldera

Figure 3.4 Potential relationship of small-volume volcanoes (erupted volume <~2-3 km^3 DRE) based on their spatial and magma plumbing system characters to caldera volcanoes. Examples: 1 – Kuharua, SW from Lake Taupo; 2 – Western Dome Complex, Whakamaru; 3 – Rangitukua, SW shore of Lake Taupo; 4 – Puketerata, central Whakamaru; 5 – Motuoapa Peninsula, SE shore of Lake Taupo; 6 cryptodome of Edgecumbe (NE lower flank of the main cone); 7 – Showashinzan, Mt Usu, Japan (there is no New Zealand example); 8 – Tauhara; 9 – Saddle Cone, Ruapehu.

3.3.4 Existing morphometric classifications of lava domes

The first morphological classification of lava domes was carried out by Blake (1990), based on the observations reviewed by Williams (1932) and laboratory experiments using isothermal Bingham slurries of kaolin and water. Blake (1990) distinguished four types of lava domes by the height versus diameter ratio of the edifice, related to the estimated yield strength of the magmas. The four classifications are: (1) Upheaved plugs; (2) Peléan domes; (3) Low lava domes; and (4) Coulees (Fig. 3.5).

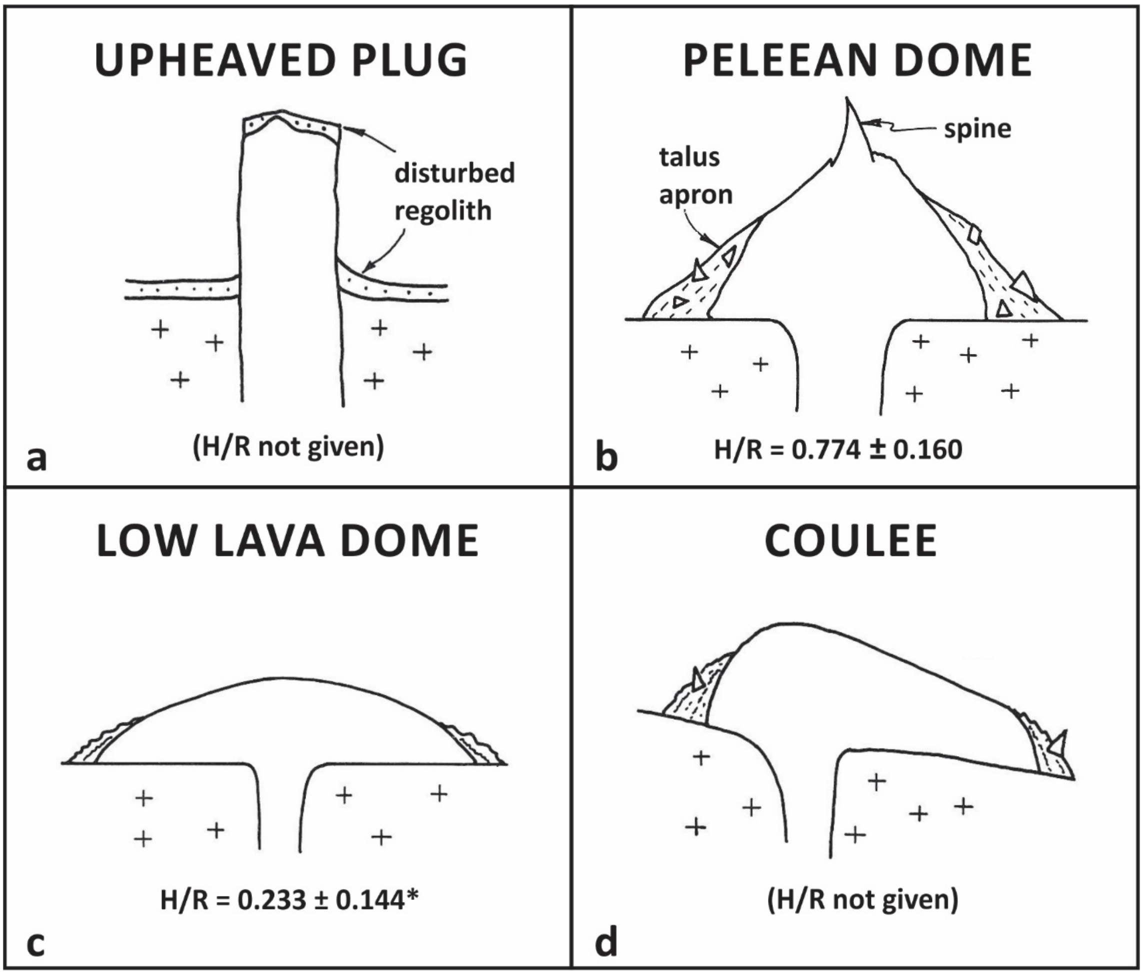
UPHEAVED PLUG
disturbed regolith
a
(H/R not given)
PELEEAN DOME
spine
talus apron
b
H/R = 0.774 ± 0.160
LOW LAVA DOME
H/R = 0.233 ± 0.144*
c
COULEE
(H/R not given)
d

*Figure 3.5 Classification of lava domes by dome height (H) versus radius (R) ratio (Blake, 1990). H/R calculations of Peléan domes were based on nine historically erupted domes of composite volcanoes/lava dome complexes, whereas low lava dome values were achieved from 16 domes of La Primavera (Mexico), eight domes of the Coso Volcanic Field (USA) and five unidentifiable domes of the Maroa Volcanic Centre (New Zealand). *For low lava domes the average H/R value was recalculated from the graphics of Fig. 13. of Blake's paper (1990), as it was expressed differently than for the values of the Peléan domes, figure modified after Blake (1990).*

1. The lava of upheaved plugs is very viscous and strong because it is emerging from the conduit without any deformation (Williams, 1932). The diameter of the plug is equal to that of the vent and sometimes the heights exceed its diameter (e.g. Mt. Pelée, Tanguy, 2004) (Fig. 3.5a).

2. Peléan/Peléean domes grow over many months to years with repeated destruction phases triggered by oversteepening or explosions generating dome collapse, block-

and-ash flows, first described by LaCroix (1904) during the 1902 eruption of Mt. Pelée, Martinique, Lesser Antilles. Lava spines and fins frequently thrust up from the summit area (exogenic growth), or large areas swell up due to the injection of new magma into the interior of the lava dome body (endogenic growth). Sometimes the fluid magma can be squeezed out through cracks, generating small lava flows or hot rock avalanches/rockfalls on the steep sides of the dome. The disintegration of the jagged carapace and spines results in the accumulation of a debris apron called ”crumble breccia”, thickly wrapping the majority of the slopes of the dome. Thus, the edifice shape of the dome looks pyramidal or conical (Blake, 1990) (Fig. 3.5b).

3. The low lava domes have smoothed gently convex profiles in contrast with the steep conical shape of Peléan domes. In contrast with the Peléan dome growth, explosive activity is uncommon during low lava dome growth because of effective degassing that manifests itself through profuse and spectacular steaming (Blake, 1990). The continuous inflation of fresh low viscosity magma forces the dome to spread. The name of this dome type reflects the main morphological difference (smaller height versus radius ratio) in comparison with the Peléan dome (Blake, 1990) (Fig. 3.5c).

4. The coulees are stubby lava bodies elongated to the direction of the aspect and depend on the ground slope angle and the viscous parameters of the lava. They represent a transitional morphotype between roundish low lava domes and long lava flows (Blake, 1990) (Fig. 3.5d).

The experiments undertaken by Blake (1990) were not able to account for the effect of cooling, therefore a new classification scheme was proposed based on laboratory simulations using kaolin powder suspended in liquid polyethylene glycol wax (Griffiths and Fink, 1992a; Fink and Griffiths, 1998). The advantage of polyethylene glycol wax is that, depending on the temperature and the applied stress, it has the ability to deform in either ductile or brittle ways similar to the lavas (Fink and Griffiths, 1990; Griffiths and Fink, 1997; Fink and Griffiths, 1998). Besides the laboratory experiments, they also included field measurements and photographic analyses into the classification schemes, grouping the lava domes into four types – (1) Spiny; (2) Lobate; (3) Platy; and (4) Axisymmetric – that eventually relates to eruption conditions, the morphology and the surface texture of the dome, and the thickness of the forming carapace (Fink and Griffiths, 1998; Fink and Anderson, 2000) (Fig. 3.6). The order of the presentation of the dome categories corresponds to the decreasing yield strength. Yield strength (Ψ_B) is a dimensionless number, incorporating various factors that affect the emplacement of lavas, such as gravity, density, strength, extrusion rate, eruption temperature and glass transition temperature.

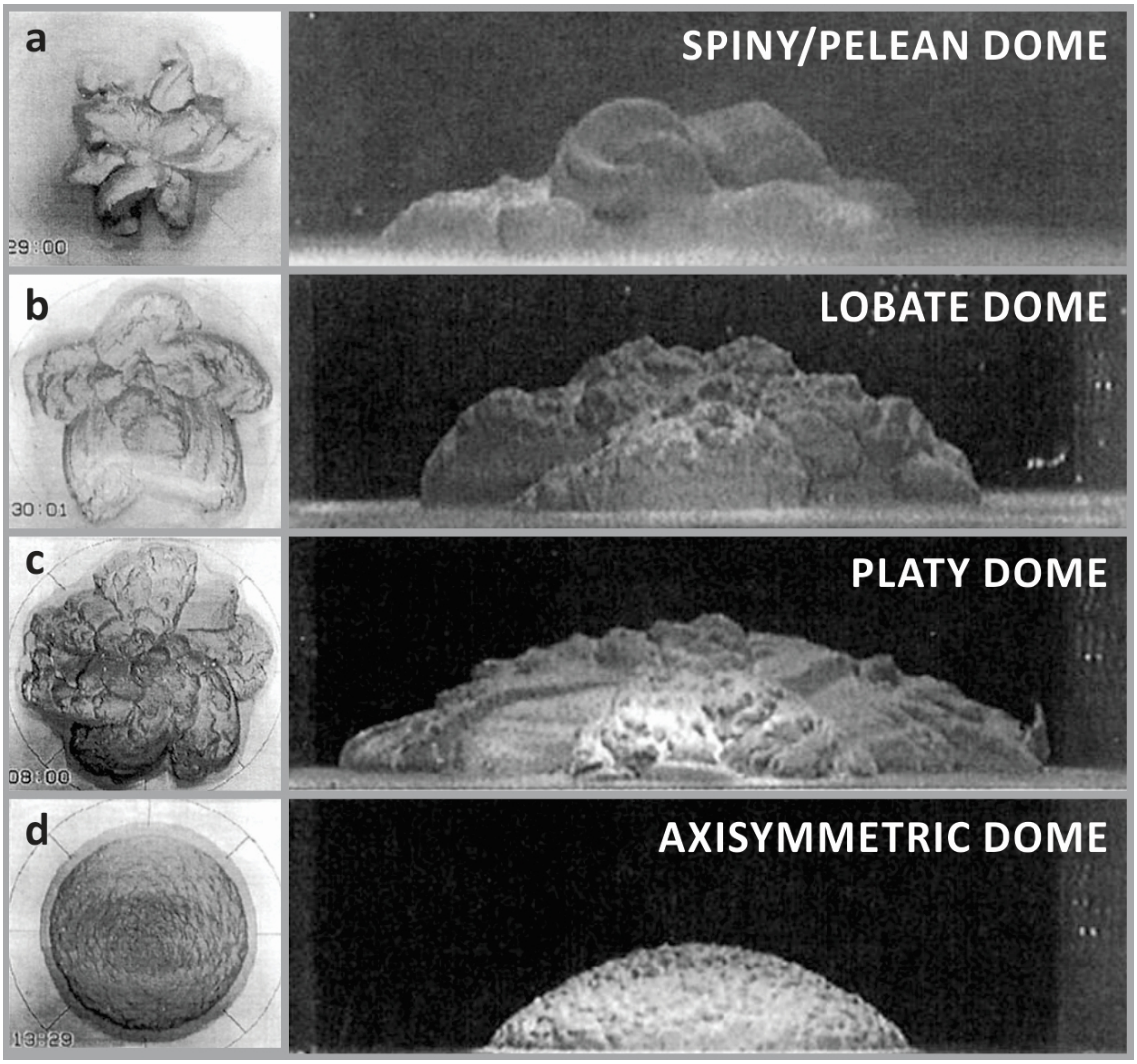

Figure 3.6 The classification of lava domes by morphology and surface textures of lava domes corresponds to the decrease of Ψ_B from spiny to axisymmetric domes (Fink and Griffiths, 1998).

1. Spiny domes, also called Peléan domes, are essentially the same as a Peléan dome in Blake's (1990) classification. The eponymous eruption was the dome building of Mt. Pelée in 1902; the frequently active *Santiaguito (Guatemala)* and the 1993-1994

activity of *Unzen*'s mature phase *(Japan)* may also be classified as spiny/Peléan domes (Rose, 1973; Nakada et al., 1995; Fink and Anderson, 2000).

2. Lobate domes are composed of a series of distinct exogenic lobes that emerge separately from the vent and commonly advance in a single direction, creating an initial outline resembling a clover leaf (Fig. 3.6b). This shape disappears as the growth continues and new lobes advance subhorizontally, creating ridges and grooves parallel with the flow direction. The average slope angle is lower than the sides of the spiny domes, however the collapse of the flow fronts can generate block-and-ash flows and often dome growth is followed by significant Plinian-style explosive activity (e.g. Redoubt, Mt. St. Helens, Pinatubo) (Fink and Griffiths, 1998; Fink and Anderson, 2000). The average widths of the lobes range from 100-500 m, and they are commonly covered with small blocks, although the vent region sometimes displays very smooth surfaces in an area of a few hundred square metres (Fink and Griffiths, 1998). These smooth areas, called crease structures*,* form mainly in response to lateral spreading by repeated fracture processes (Murase et al., 1985; Anderson and Fink, 1990; Anderson and Fink, 1992; Griffiths and Fink, 1997).

3**.** Platy domes are formed by endogenic processes, thus the growing lava body may merge with the central region, making the outline much more circular and more rounded. Platy domes have a lower profile in cross-section than the previous two dome types (Fig. 3.6c). On the surface of the advancing dome, angular ridges are formed oriented parallel and perpendicular to the flow direction due to peripheral stretching and compression. This combination of folding and fracturing causes the lava surface to be broken up into a few hundred square metre flat pieces, divided by shallow crevices or generating surface breccia (Fink and Griffiths, 1998; Fink and Anderson, 2000). Historical examples for this type of dome are *Mt. Merapi (Java, Indonesia)* and *Soufriere (St. Vincent, Lesser Antilles)* (Fink and Anderson, 2000).

4. Axisymmetric domes are the counterpart of the low lava domes and coulees from Blake's (1990) classification (Fink and Griffiths, 1998). These domes have the most circular outlines if the growth occurs in a flat area. In other cases, the outline can be highly irregular (Fig. 3.6d). The initial cross-sectional profile is similar to platy domes with lower relief. The surface of the dome is frequently covered with small blocks

displaying different degrees of vesiculation and crystallisation. Marginal levees and transverse folds form during the advancing flow on steeper slopes, while radial fractures are generated directly over the vent or near the flow front (Fink, 1980a; Duffield et al., 1995; Fink and Griffiths, 1998). The flow front is characterised by a talus apron made up of relatively small blocks. This type of lava dome emplacement is not commonly associated with strong magmatic explosions, but the lava body surfaces often exhibit shallow (depth of a few metres to tens of metres) explosion pits (Fink and Griffiths, 1998; Fink and Anderson, 2000). These pit craters are commonly located above the central vent, but sometimes the degassing and cooling processes of the large rhyolite flows produce rootless pit craters far away from the active vent (Fink and Manley, 1989). A Holocene example of a well-studied axisymmetric dome is the *Big Obsidian Flow at Newberry volcano, Oregon, USA* (Fink and Anderson, 2000).

Blake (1990) and Fink and Griffiths (1998) identify a special type of lava dome, emplaced within the overlying rocks forming a minor visible hump on the surface (Minakami et al., 1951). These structures are called cryptodomes because in many cases they remain hidden. In others, they may produce fumaroles or small eruptions without any molten material reaching the surface, as shown by the early evolution of the Showa-shinzan lava dome in the Usu volcano and Hiyoriyama cryptodome, Kuttara volcano, Japan (Minakami et al., 1951; Goto et al., 2011). Cryptodomes may trigger violent eruptions such as in the case of Mt St. Helens in 1980, where the weight of a satellite cryptodome destabilised the northern flank, causing sector collapse (Donnadieu et al., 2001). The resulting explosion of this cryptodome triggered a high energy debris avalanche and a lateral blast (Christiansen and Peterson, 1981; Fink and Anderson, 2000). Even though the recent cryptodome-forming eruptions occurred in subaerial environments (e.g. Minakami et al., 1951; Christiansen and Peterson, 1981; Siebert et al., 1987), a large number of cryptodomes are known to have been emplaced in a subaqueous environment (e.g. *Momo-iwa, Rebun Island, Japan; Kalogeros cryptodome, Milos, Greece*) (Goto and McPhie, 1998; Stewart and McPhie, 2003; Rosa et al., 2010). In contrast, with domes emplaced to the ground surface, little is known about cryptodomes because only indirect observations (e.g. surface deformation) are available. Thus the examination of the inner structures of cryptodomes is an important area to understand their growth mechanisms.

The shapes of lava domes achieved by laboratory experiments (Blake, 1990; Fink and Griffiths, 1998; Lyman et al., 2004) only partially show similarities with the real lava domes in nature. The main reason is that these experiments cannot effectively model the commonly occurring destructive events during the lava dome emplacement, especially common in the case of lava with higher yield strengths. Another issue is that the yield strength of the lobe fronts can be orders of magnitude higher than the lava during extrusion from the vent. The eruptive behaviour of lava emplacement depends on the conditions within and above the conduit. Thus, the characterisation of lava emplacement based on the surface morphology of advanced parts of edifices may provide misleading information. For this reason, a new classification is necessary to make a comparison between the shape of natural domes and the morphological observations in relation to the yield strength of domes obtained by laboratory experiments.

3.4 New lava dome classification based on macro-morphometry of dome surfaces

The aim of this new morphology-based classification is to be able to detect the characteristic features of lava domes by GIS-based terrain/edifice analysis. Hundreds of natural lava domes morphologies were examined and the most typical lava domes have been chosen to demonstrate the morphological differences between the suggested divisions (Figs 3.7-3.11). The new classification compares the natural lava domes to the classification of Fink and Griffiths (1998) and provides characteristic morphometrical parameters or features for each morphotype (Table 3.2). The basic concept of this classification is the mapping of positions and gradient of the steepest slopes as a function of relative elevation in order to estimate the relative yield strength of the contributing lava. In general, high yield strength results in the steepest slopes in in situ rocks near the vent, while magma is characterised by lower yield strength and tends to flow, resulting in the steepest slopes being located on their talus aprons near to the foot of the structure. The steepest slopes of talus aprons range between 35-

42°corresponding to the angle of repose of the loose rubble (Borgia et al., 1983; Francou and Manté, 1990; Iverson, 1990), whereas in situ lavas have high yield strength and the slope angles are characterised by angles higher than 45-50°, which occasionally reach near 90° at the spines. The decreasing yield strength generally results in a lower aspect ratio for the dome structures as proposed by Blake (1990), however the height value as a function of the diameter of the structure is not sufficient alone for detailed classification. Classification that relies on surface micro-morphology (e.g. Fink and Griffiths, 1998) can be misleading too, as many low aspect ratio domes indicate surface morphology similar to spiny domes (e.g. some of the Devil Hill domes, South Sister, USA). This phenomena can be attributed to the different physical conditions of lava between distal and near vent areas. The correct yield strength estimation of magma/lava during extrusion can contribute to the evaluation of volcanic hazards as higher yield strength may indicate lower temperatures or low ascent/effusion rates, which may facilitate magma quenching and interaction with external water. In contrast whereas fast ascent or rapid decompression usually leads to an explosive eruption caused by the quick expansion of volatile-rich magma (e.g. Alidibirov and Dingwell, 1996; Papale, 1999; Gonnermann and Manga, 2007).

	Emplacement style	Summit morphology	Location of steepest slopes	Extent and volume of debris apron	Aspect ratio
Rockfall-dominated spiny domes	Exogenic	conical	upper third of the dome	major	0.2-1
Flat-topped spiny domes	Exogenic (endogenic)	flat	at the break off of the flat top	major	0.2-0.6
Lobate domes	Exogenic	embrionic: ridged mature: flat	on the foothill	minor	0.2-0.5
Platy domes	Endogenic	convex rounded	on the foothill	minor	0.2-0.5
Axisymmetric domes	Endogenic	flat	on the foothill	minor	0.01-0.2

Table 3.2 Summary of the characteristic morphometric features of domes distinguished in the new classification proposed (preliminary results).

Since lava domes can be formed by different styles of magma emplacement (e.g. spiny to platy at Unzen; Nakada et al., 1995; Nakada et al., 1999), the eventual shape of lava domes may controlled by the emplacement style of the most significant period of dome growth, or it may display structures relating to distinct styles of emplacement in its history, assuming subsequent periods of growth do not cover earlier (e.g. *Rangitukua dome, New Zealand*, Fig. 3.10D).

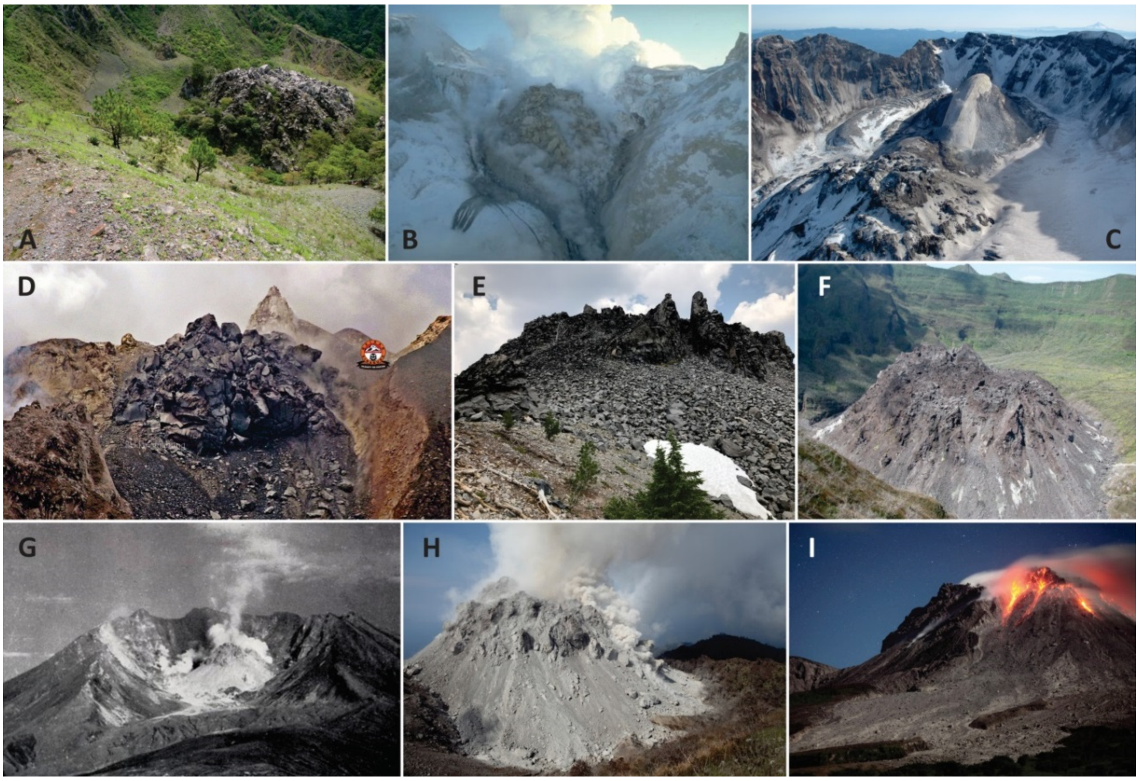

Figure 3.7 Examples for rockfall-dominated spiny domes with characteristic conical shape summits. A – Ceboruco 1870, Mexico (photo courtesy: J. Méndez Harper); B – Mt. Redoubt 1990, Alaska (photo courtesy: Alaska Volcano Observatory); C – Mt. St. Helens 2005, USA (photo courtesy: Cascade Volcano Observatory); D – Sinabung 2016, Indonesia (photo courtesy: Z. Ginting); E – Devil Hill domes ~2 ka, South Sister, USA; F – Kelut 2007, Indonesia (photo courtesy: Smithsonian Institution); G – Bezymianny 1956, Russia (photo courtesy: G.S. Gorshkov); H – Paluweh 2012, Indonesia (photo courtesy: R. Roscoe/Stocktrek Images); I – Soufriere Hills 2010, Montserrat (photo courtesy: photovolcanica.com).

1. Rockfall-dominated spiny (Peléan) domes have steep-sided pyramidal summits whose general shape is influenced by the extrusion and gravitational destruction of lava. After the embryonic stage (e.g. Fig. 3.7D) a debris apron will form due to the passive collapse of lava spines and short viscous lobes. The dome growth is characterised by strong degassing, thus explosions are occasional during the emplacement. Upheaved plugs (Blake, 1990) are considered to represent the initial or restarting phase of lava intrusion, which is characterised by lavas with high viscosity, whereas the glass transition occurs prior to the lava reaching the surface. The lower

part of the dome is blanketed by a 35-42° steep debris apron (Borgia et al., 1983), while the upper part consists of coherent or in situ blocks of lava characterised by steeper slopes up to 70-75°. The outlines of these domes in map view are usually circular, but within open craters, such as Sinabung, Indonesia they are usually characterised by elongated edifices and extensive debris fields in the lower flanks of the parent volcano as a result of frequent deposition from block-and-ash flows and rockfalls. These domes predominantly occur at the summit of composite volcanoes and lava dome complexes as a result of very low (<1 m^3/s) effusion rates (Table 3.2).

2. Flat-topped spiny domes are characterised by flat tops with or without explosion pits, with a variety of sizes as a result of intense explosive activity during or after lava emplacement. The most common Vulcanian-style explosive and lower energy degassing events facilitate the formation of an extensive debris apron surrounding the edifice by the collapse of spines or lobes of uprising lava together with ballistically transported fragments. Presumably, due to gravitation and the pushing of fresh material, the structure slowly spreads preventing protrusion of the central regions of the structure (e.g. *Holocene domes of South Sister volcano*, Fink and Anderson, 2017). The apron's slope values are similar to the rockfall-dominated spiny domes (35-42°) and correspond to the angle of the repose of the fragments comprising the structure (Borgia et al., 1983). Usually above the apron the solid in situ part of the structure is visible with steeper slopes than the apron, however in some cases the apron can reach the level of the flat summit, especially in the case of older domes or strong explosive activity (Fig. 3.8). These flat-topped spiny domes appear more frequently than the rockfall-dominated type in every environment. Rockfalls and block-and-ash flows commonly occur, but are usually less voluminous than the rockfall-dominated spiny domes because the explosive activity or spreading prevents the growth and persistence of large unstable spines on top of the edifice.

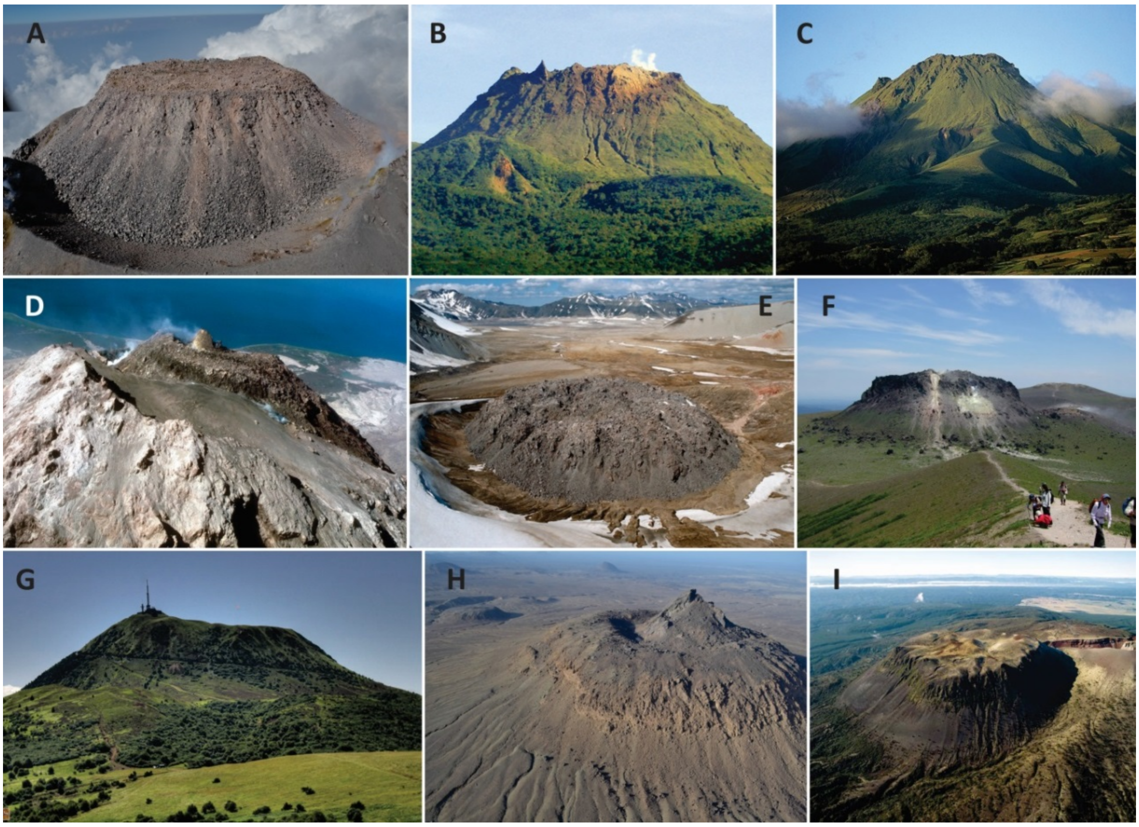

Figure 3.8 Flat-topped spiny domes with characteristic flat tops that change without transition to the steep-sided slopes. A – Volcan de Colima 2010, Mexico (photo courtesy: CIIV, Universidad de Colima); B – Soufriere ~3 ka, Gaudeloupe (photo courtesy: Smithsonian Institution); C – Mt. Pelee 1902, Martinique (photo courtesy: Smithsonian Institution); D – Augustine 1986, Alaska (photo courtesy: Alaska Volcano Observatory); E – Novarupta 1912, Alaska (photo courtesy: Alaska Volcano Observatory); F – Tarumai 1909, Japan (photo courtesy: panoramio.com); G – Puy de Dome ~10 ka, Auvergne, France (photo courtesy: gettyimages); H – Um Raqubah, Saudi Arabia (photo courtesy: K. Németh); I – Wahanga ~1314, Okataina, New Zealand (photo courtesy: teara.govt.nz).

3. Lobate domes are composed of a series of distinct exogenic lobes that emerge separately from the vent and commonly advance in a single direction. However, the initial outline, suggested by Fink and Griffiths (1998), disappears as the growth continues and tends to have a circular outline, and ridges of the former lobes blend to each other (e.g. the dome evolution of Soufriere from 1971-1972, Fig. 3.9F and B). The collapse of the flow fronts often generates rockfalls or small-scale block-and-ash flows, which finally result in a debris apron surrounding the dome in the direction of the advancements. For this reason, the resulting dome shapes of long-lasting eruptions are very similar to flat-topped spiny domes, especially if explosive activity was common during their emplacement. The maximal slope values of the edifice may somewhat

exceed the maximal steepness of the debris apron but remain below the steepest parts of the spiny domes (Fig. 3.9). Matured lobate domes might have been able to be recognised by their slightly lower slope values of the debris apron and the remnant of a spreading centre (or crease structures), which appears as a few metres deep ditch with various lengths at the summit region of the domes. Additionally, the height versus diameter ratio of lobate domes is supposed to indicate smaller values than spiny domes due to their observed lower yield strength (Blake, 1990; Lyman et al., 2004), however there are many factors (e.g. destructive modification of the dome summits, growth in a crater, partial burial of the edifice) that may modify the dome structures or blur the observations.

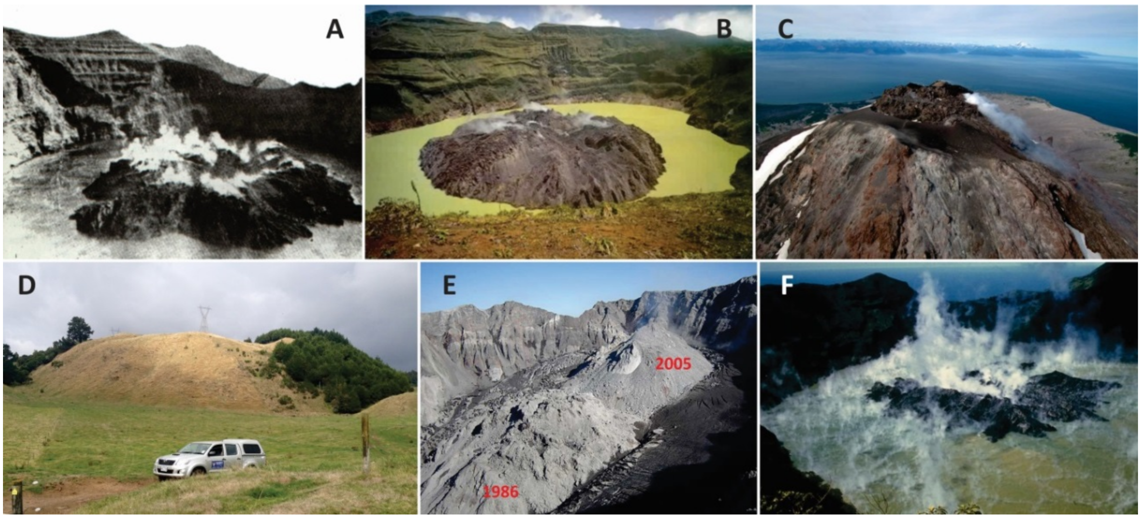

Figure 3.9 Lobate domes with characteristic zigzag-shaped outlines in the early phases. A – Awu 1931, Indonesia (photo courtesy: Smithsonian Institution); B – Soufriere 1972, St. Vincent (photo courtesy: The University of West Indies, Seismic Research Unit); C – Augustine 2011, Alaska (photo courtesy: Alaska Volcano Observatory); D – Puketerata ~16 ka, New Zealand; E – Mt. St. Helens 1986, USA (photo courtesy: Cascade Volcano Observatory); F – Soufriere 1971, St. Vincent (photo courtesy: Smithsonian Institution).

4. Platy domes have a convex summit region in a cross-section with slope values increasing with distance from its summit. By the inflation of the dome interior, the dome advances equally in every direction in the case of a relatively flat pre-eruption surface. Moderate slopes will cause a slightly asymmetric shape of the structure with lower values to downhill and steeper slopes to uphill (e.g. *Pukekaikiore, New Zealand*, Fig. 3.10J). The steepest slopes form near the foothill of the edifices up to 50°, however the lower foothills may be covered by talus breccia characterised by less

steep slope angles. The summit areas occasionally tend to be indented after the inflation force retreats (Fig. 3.10). Explosive activity is uncommon during this kind of lava emplacement, thus only instability triggered rockfalls and block-and-ash flows pose a threat in their neighbourhood. This kind of activity is common at open summit craters of composite volcanoes, such as at *Sinabung and Merapi (Indonesia)* (Fig. 3.10A, C-F).

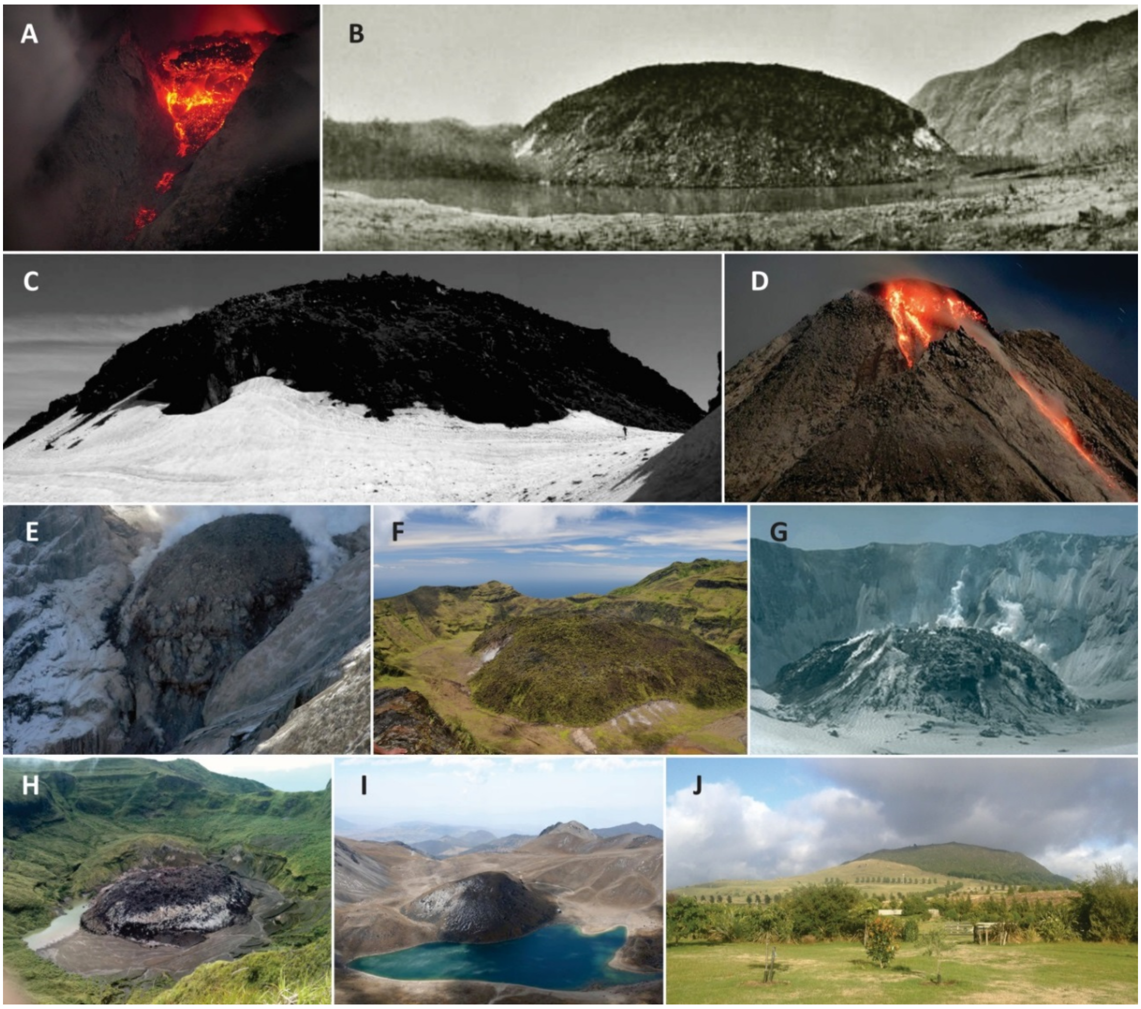

Figure 3.10 Platy domes with characteristic convex summit and increasing slope gradient moving away from the vent. A – Sinabung 2014, Indonesia (photo courtesy: M. Szlegat); B – Galunggung 1918, Indonesia (photo courtesy: Smithsonian Institution); C – Taranaki ~1785, New Zealand (photo courtesy: Platz et al., 2012); D – Merapi 2012, Indonesia (photo courtesy: AP Images); E – Mt. Redoubt 2009, Alaska (photo courtesy: Alaska Volcano Observatory); F – Soufriere 1979, St. Vincent (photo courtesy: D. Pyle); G – Mt. St. Helens 1980, USA (photo courtesy: Smithsonian Institution); H – Awu 2004, Indonesia (photo courtesy: flickr.com); I – El Ombligo, Nevado de Toluca ~1350, Mexico (photo courtesy: hiveminer.com); J – Pukekaikiore, Taupo, New Zealand.

5. Axisymmetric domes represent the emplacement of lavas with the lowest viscosity and yield strength. Circular layout is very rare because even the smallest gradients can influence the direction of their expansion. This type of lava dome is a transitional morphotype between domes and flows and on steeper slopes they behave as lava flows. The edifices can be divided into two areas. Most of their area can be classified as a summit, while the other parts are the foothills, with these lower parts covered by talus breccia. The foothills without talus breccia coverage represent the steepest slopes that may be up to 60-70°, and in other cases the maximal angle of the repose of the talus will indicate the highest gradients. Summits are flat or tabulate at large scale, however the common formation of ogives and crease structures provides uneven smaller-scale morphology on the summit area of the axisymmetric domes (Fig. 3.11).

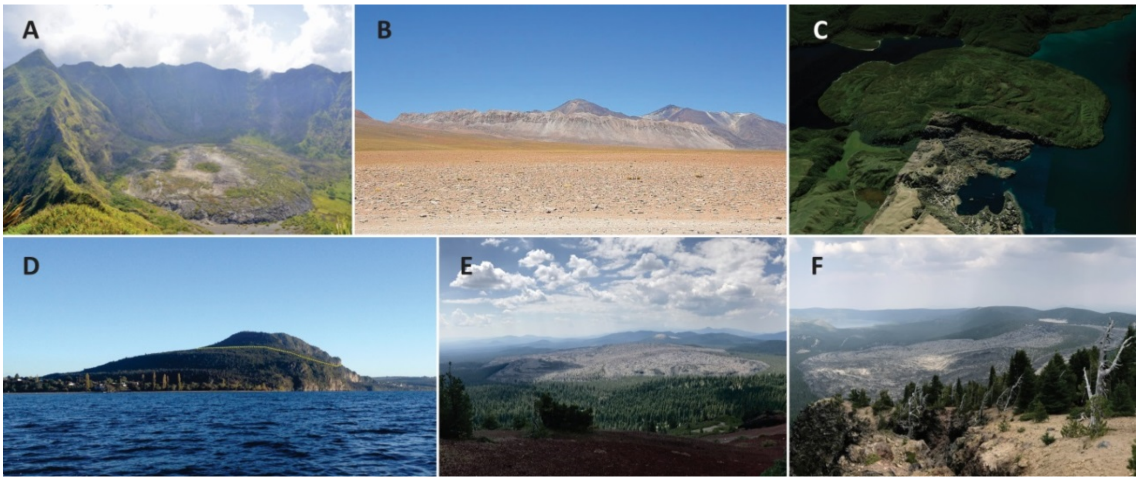

Figure 3.11 Axisymmetric domes with characteristic low aspect ratio and flat tops aside from crease structures, pressure ridges and diapirs. A – Kei Besi/Makian 1988, Indonesia (photo courtesy: W. Piecha); B – Chillahuita ~400 ka Chile (photo courtesy: volcano.oregonstate.edu); C – Te Horoa ~5 ka, Okataina, New Zealand (Google Earth image); D – Rangitukua (lower part) ~130 ka, New Zealand; E – Little Glass Mountain, Medicine Lake volcano ~1ka, USA; F – Big Obsidian Flow, Newberry volcano ~1 ka, USA.

There are further lava dome structures (coulees, complex/compound domes and lava dome complexes), which cannot be classified into the above-mentioned classes because their overall shape does not reflect the physical properties of the erupting lava and neither do they relate to destructive processes. The morphology of these lava domes was strongly influenced by the gradient of the pre-eruptive surface, or they have a complex structure due to multiple eruption episodes characterised by different yield strengths.

Coulees are asymmetric, elongated hybrids of lava domes and viscous flows with a thickness of up to a few hundred metres. The summit area is usually tabulate or concave and fragmented by ogives that can be more than 30 m high. The side/foothill of these flows represents the steepest parts of the structures and they are often covered by talus breccia (Fig. 3.12). Hypothetically, lavas characterised by lower yield strengths (lobate to axisymmetric styles) may emplace as coulees, however only elongated edifices with platy and axisymmetric features have been classified/named as coulees yet. Their surface structures usually indicate higher viscosity and yield strength manifested by more crease and ramp structures than the overall shape of the coulee suggests, which is attributed to (for example) the different lava temperatures near the vent and the advanced lobes.

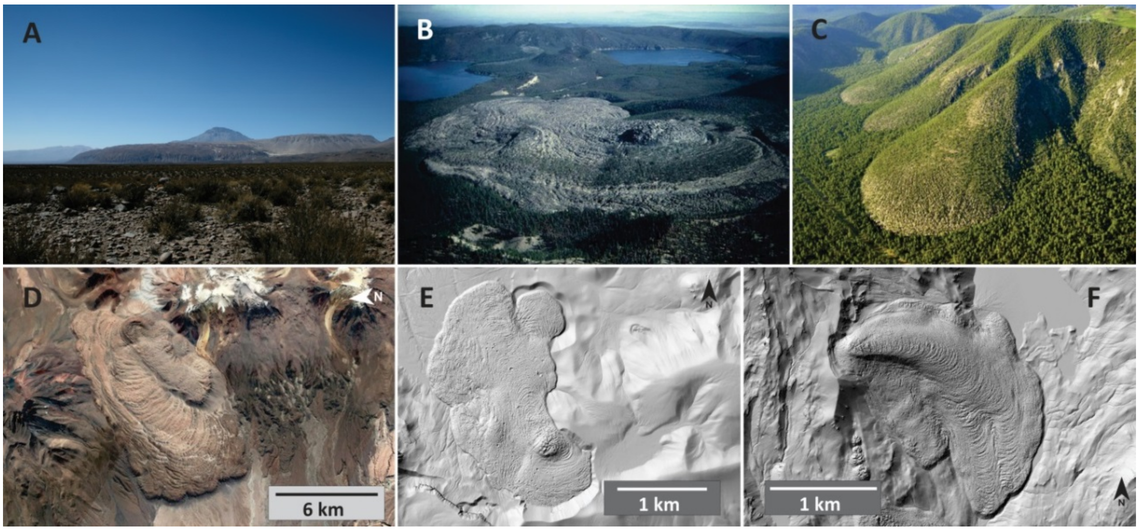

Figure 3.12 Examples of coulees. A – Cerro Chao ~400 ka, Chile (photo courtesy: volcano.oregonstate.edu); B – Big Obsidian Flow, Newberry volcano ~1 ka, USA (photo courtesy: R. A. Jensen); C – Mt. Elden, San Francisco Volcanic Field, USA (photo courtesy: mountainproject.com); D – Satellite image of Cerro Chao, Chile (Google Earth image); E – 1 m resolution LiDAR DEM of Big Obsidian Flow, Newberry volcano, USA; F – 1 m resolution LiDAR DEM of Newberry Flow, South Sister, USA.

Compound domes are characterised by the emplacement of two or more distinct dome lobes with different morphotypes occurring one after another within a limited timeframe. The lavas are sourced from the same vent and the different phases of the eruption may indicate major differences in terms of explosive behaviour and related hazards. Lava domes are classified into compound domes only if the morphology clearly indicates the multi-stage formation and the distinction of the structures relating to the different stages is evident. Most frequently the lower part of this kind of the edifice represents a structure formed by the emplacement of lava with lower yield strength, which is followed by the effusion of more viscous lavas (e.g. *Pukekaikiore and Rangitukua domes, west shore of Lake Taupo*, Figs 3.10J and 3.11D).

Lava dome complexes are predominantly formed by the multiple emplacements of viscous lava flows and domes. Dome complexes can be classified into two different types, Tarawera-type and Putauaki-type, indicating differences in the morphology and timespan of the activity.

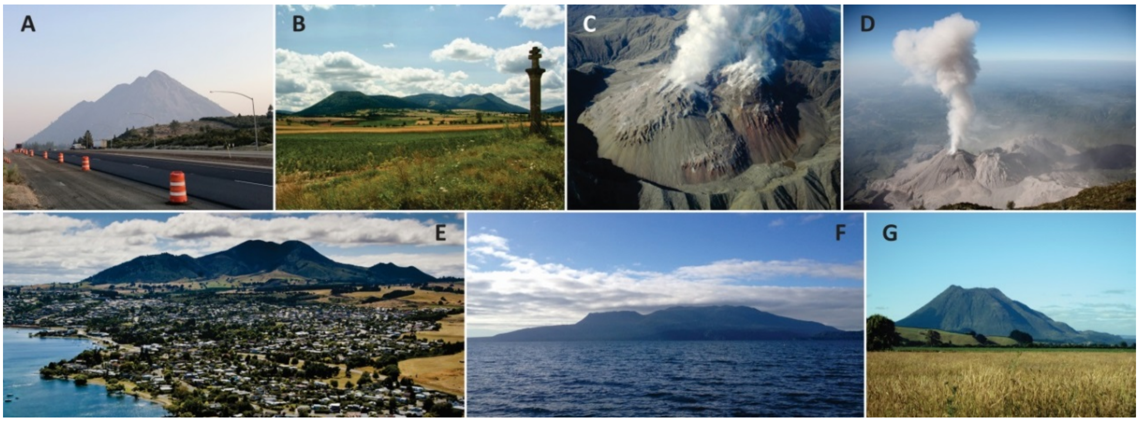

Figure 3.13 Examples of lava dome complexes. A – Black Butte, ~10 ka, Mt. Shasta, USA; B – Ciomadul/Csomád ~28 ka, Romania (photo courtesy: D. Karátson); C – Chaitén 2010, Chile (photo courtesy: D. Schneider); D – Santiaguito 2012, Guatemala (photo courtesy: photovolcanica.com); E – Tauhara, ~190 ka, New Zealand (photo courtesy: greatlaketaupo.com); F – Tarawera Volcanic Complex, 1886, New Zealand, G – Edgecumbe/Putauaki ~2.5 ka, New Zealand (photo courtesy: wikipedia.org).

The dome complexes similar to Tarawera-type structures are characterised by coalesced edifices whose lavas erupted from distinct but closely-spaced vents in a cluster or along a lineament (Fig. 3.13B, F). The activity of single vents is restricted to a relatively limited timeframe (months to years) and the new vent openings occur randomly, controlled by the structural features of the upper crust such as faults and weakness zones. Distinct eruptive episodes may be characterised by different eruption styles due to the possible changes in chemical composition or physical properties of the magma, which is manifested by the diverse architecture of single edifices and related products. The overall lifespan of these dome complexes can last for tens to hundreds of thousands of years (Fig. 3.13B and F). Thus, this type of dome complex is a polygenetic volcano in the broad sense without having a central vent, but consists of numerous independent monogenetic edifices. In contrast, Putauaki-type dome complexes have a conical shape due to the existing central vent, which produces the majority of the volcanic products (Fig. 3.13A, C-E, G). Lava clogs in the conduit may force the central vent to shift, or the opening of parasitic vents modifies the conical shape of the edifice, as well as triggers eruptions and/or sector collapses. The central vent usually terminates in a crater mostly occupied by a summit dome. The dome emplacement is characterised by lavas with higher viscosities, thus mostly spiny or lobate-style structures form, which is accompanied with explosive activity and block-and-ash flow generation. The lifespan of these volcanic complexes may last for years to less than a few hundred years (e.g. *Edgecumbe, New Zealand*). There are examples of polygenetic volcanoes that indicate similar activity to Putauaki-type lava dome complexes (e.g. *Lascar, Stage II, Chile* Gardeweg et al., 1998; *High Börzsöny, Hungary,* Karátson et al., 2000) for hundreds to thousands of years, however this kind of activity represents only a small portion of the total evolution of polygenetic volcanoes. In contrast with the Tarawera-type dome complexes, Putauaki-type structures may appear as stand-alone volcanic structures (Edgecumbe/Putauaki, Tauhara) or as parasitic cones of composite volcanoes (e.g. *Black Butte – Mt. Shasta; Chaos Crags – Lassen Peak; Santiaguito – Santa Maria*) (Fig. 3.13). The overall morphology and size (edifice volume) of Putauaki-type dome complexes may be very similar to small composite cones or larger conical-shaped domes, whereas Tarawera-type dome complexes have a distinct morphology (Fig. 3.14).

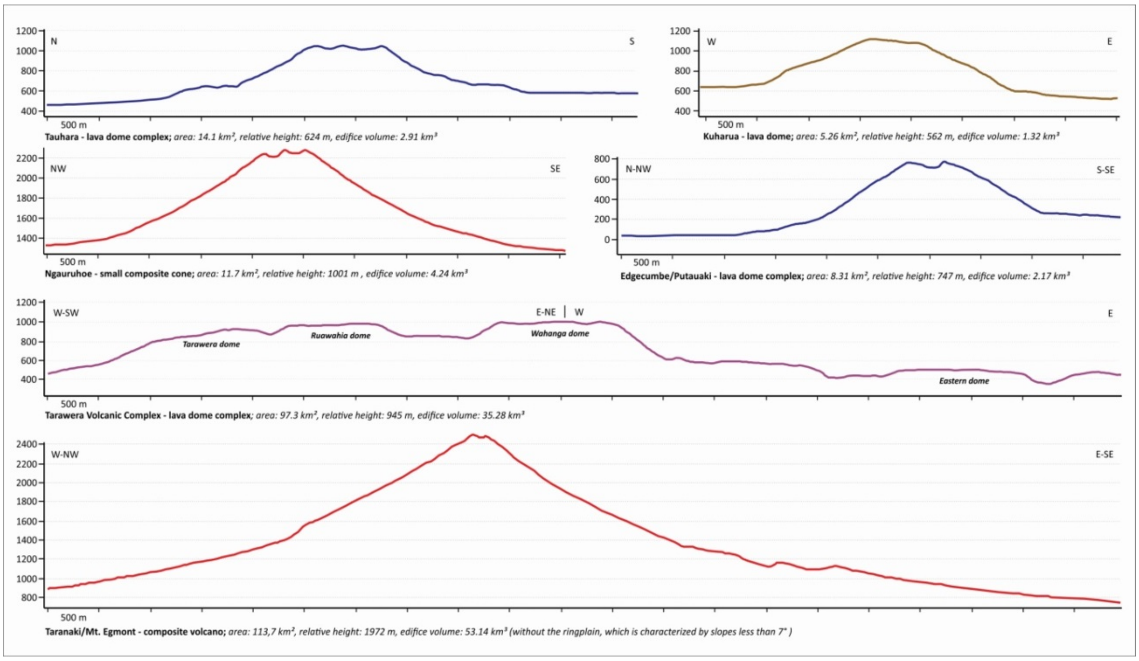

Figure 3.14 Comparison of shape of lava dome complexes with other conical-shaped volcanic structures (lava dome and composite volcanoes) with examples from New Zealand. Cross-sections were derived from an 8 m NZ DEM (LINZ - Land Information New Zealand, 2012).

Chapter

4

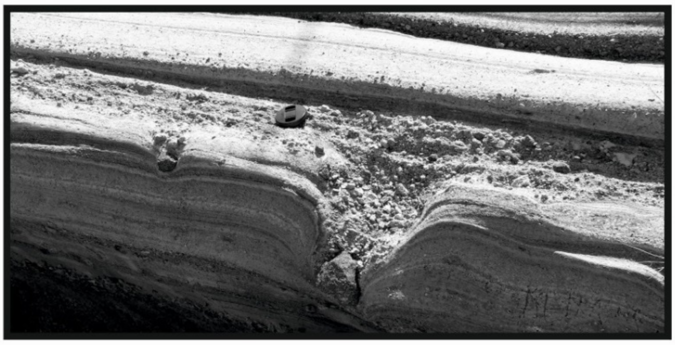

Chapter 4 provides a detailed overview of the field and laboratory techniques, including the characteristics of the source data used for digital terrain analysis.

Chapter 4 – Methodology

This research was carried out at two different scales. Data from the entire TVZ has been acquired by remote sensing methods and used to produce Digital Elevation Models (DEMs) which were than interrogated to extract the spatial distribution of vents, morphometric characteristics of distinct volcanic edifices, and geomorphological and structural properties of the entire TVZ. Based on the preliminary characterisation of the TVZ's small-volume volcanism, three case study localities (Ohakune, Puketerata and Motuoapa) have been selected. These represent the range of possible magma types, eruption styles and environmental conditions within the TVZ, and will be used for the determination of potential hazards for future eruptions. Detailed field work at each of the case study sites was aimed at unfolding the stratigraphic and sedimentological features of the example localities. Lava and pyroclastic samples have been examined for grain size, density and componentry distributions, and thin sections and plugs were created for petrographic and geochemical investigations. The geomorphology of the example localities was surveyed by Real Time Kinematic (RTK) Global Positioning System (GPS) and a Terrestrial Laser Scanner (TLS) to improve DEMs, and TLS was also used for collecting georeferenced stratigraphic data at Ohakune.

4.1 Laboratory techniques

4.1.1 Grain size distribution

The grain sizes of pyroclastic rocks were described in the field after Wentworth (1922) using the terminology of White and Houghton (2006). Depending on the estimated average grain size, approximately 0.5-3 kg of sample was collected from selected units. Samples were dried and weighted, and then were hand-sieved at 0.5 phi intervals between -5.0 and 4.0 phi. The distribution of fragments larger than -5 phi was evaluated by field observations or image analysis of the outcrops (e.g. Capaccioni and Sarocchi, 1996). In the case of the material accumulated in the pan exceeding 10% of the total weight, particles smaller than 3 phi were further analysed by a Laser Scattering Particle Size Analyser (LPA). Grain size parameters, such as mean, sorting, skewness and kurtosis, were calculated using the Gradistat 8.0 software run in Microsoft Excel (Walker, 1971; Blott and Pye, 2001).

4.1.2 Componentry and glass morphometry analyses

The analysis of the componentry of selected size fractions was preceded by the cleaning of fragments, by multiple immersions in distilled water or distilled water and 10% HCl acid inside an ultrasonic bath for 10-30 minutes. Selected fractions of the cleaned sample were randomly scattered to double-sided adhesive tape that had already been stuck to a petrographic micro-slide. Microscopic observations were aided by point counting on stereomicroscopic images using JMicroVision 1.2.7 software with the use of random sampling taking 170-180 grains. Within the two examined fractions of the Ohakune samples (0.5 and 2.0 phi) vesicular and dense glass, cogenetic and accidental lithic fragments, crystals and aggregates were distinguished. Subsamples of the cleaned fractions were also analysed for glass morphometry. Samples were coated in gold and were examined by the FEI Quanta 200 environmental Scanning Electron Microscope (SEM) at the Manawatu Microscopy and Imaging Centre, Massey University.

4.1.3 Density measurements

At least 30, fragments from the -2-5 to -3.5 classes per single pyroclastic beds or subsamples of larger blocks/bombs or lava were measured for envelope, skeletal and solid densities. Envelope or bulk density measurements include all the pores of samples from which the vesicularity can be calculated by known dense rock density. At skeletal density measurements only isolated pores are included, whereas at solid density measurements all the pores are excluded providing the dense rock density of the samples. Prior to the measurements, samples were dried at 45-50°C for at least 24 hours, then their weight was logged to three decimal places. Envelope/bulk density (d_{ENV}) was determined by a Micromeritics Geopyc 1360 Analyser, which applies the Archimedes principle utilising a quasi-fluid displacement medium composed of microspheres having a high degree of flowability. It was set to have five runs per sample to provide average volume and density with standard deviations for each measured sample. Skeletal (d_{SK}) and solid densities (d_{SOL}) were determined using a Quantachrome Ultrapycnometer 1000, using N_2 gas as the flowing medium. For d_{SK} this implies the volume and density of the sample, including the enclosed porosity, and a pulse (nine cycles with pressurisation/depressurisation) was used as purge mode through 10 runs per sample. For d_{SOL} the samples were crushed with an agate mortar to open the enclosed porosity. The pulverised samples were measured over 10 runs per sample using one minute long continuous flow as a purge mode. The obtained average d_{SOL} is supposed to be greater than or equal to d_{SK}. The $1-(d_{ENV}/d_{SOL})$ corresponds to the porosity/vesicularity of the samples.

4.1.4 Vesicularity and rock/clast microtexture analysis

Besides general petrographic and texture observations of thin sections by optical microscopy, the microtexture of volcanic rocks was mapped through 2D Backscattered Electron Imaging (BSE) of thin sections using SEM. Multiple BSE images were taken at different magnifications, striving to meet the requirements of representativeness and to ensure that the resolution was sufficient to capture all the size ranges of textural features with appropriate resolution. BSE images were supplemented with macroscopic images of flat cuts of hand specimens taken by a Canon Pixma MP160 document scanner or Canon 1200D camera. The images were edited in IrfanView to remove image flaws (e.g. objects adhered to the thin sections or scratches) and in ImageJ to filter and transform the images to grayscale. The vesicularity and number density, and shape and size of the vesicles, were captured and calculated by ImageJ and Matlab-based FOAMS (Fast Object Acquisition and Measurement System) software using the method of exponential image nesting (Sahagian and Proussevitch, 1998; Shea et al., 2010). The two methods indicate a major difference within the discrimination of vesicles (Fig. 4.1). The determination of 3D vesicularity of samples using ImageJ was based on 2D vesicularity of images using Delesse's principle (Baddeley and Jensen, 2002), which assumes that the mineral or vesicle area percentage in a plane section is an estimate of its percentage of volume in 3D. This assumption is valid in the case of the homogenous distribution of examined features and the sample is representative of the entire rock (Baddeley and Jensen, 2002). The

FOAMS-based examination may exclude significant bubble areas (Fig. 4.1C), being less suitable for vesicularity calculations. By both methods it was possible to characterise the bubble number density (N_V), mean diameter and mean area of vesicles, as well as their shape parameters (Orsi et al., 1992; Shea et al., 2010).

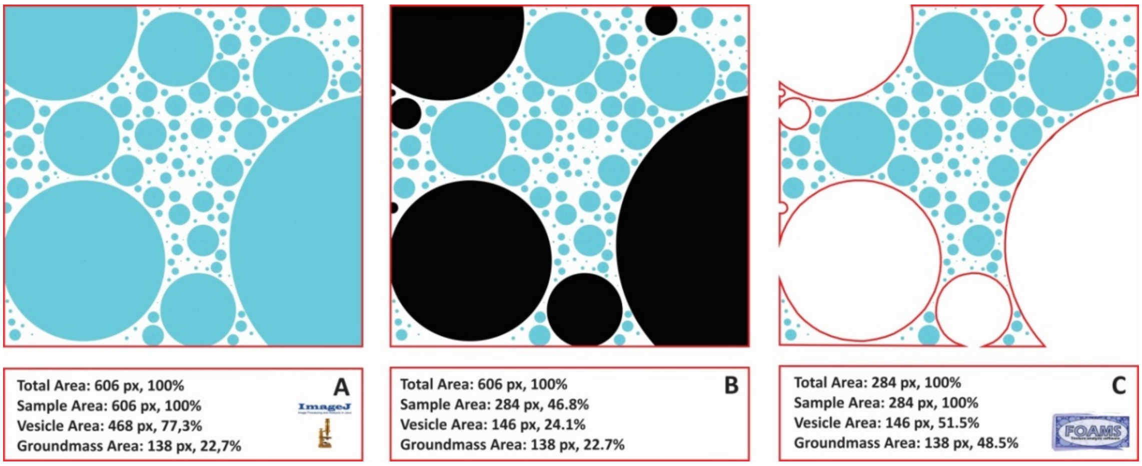
Total Area: 606 px, 100%
Sample Area: 606 px, 100%
Vesicle Area: 468 px, 77,3%
Groundmass Area: 138 px, 22,7%
A
ImageJ
Total Area: 606 px, 100%
Sample Area: 284 px, 46.8%
Vesicle Area: 146 px, 24.1%
Groundmass Area: 138 px, 22.7%
B
Total Area: 284 px, 100%
Sample Area: 284 px, 100%
Vesicle Area: 146 px, 51.5%
Groundmass Area: 138 px, 48.5%
C
FOAMS

Figure 4.1 Comparison of methods in the recognition of vesicles using 2D imagery. Experimental results are indicated. A – ImageJ-based measurement considers all the area of the image, however the incomplete vesicle shapes have to be excluded from the result of shape analyses; B – This hypothetic method includes all the vesicle area in total, but the incomplete vesicles have been excluded from the area of the vesicles; C – FOAMS-based measurements exclude all the incomplete vesicles, thus the measured total vesicularity of the sample will be lower than the actual vesicularity.

4.1.5 Electron Probe Micro-Analysis (EPMA)

Glass compositions and mineral chemistry of samples from Ohakune and Motuoapa were obtained from well-polished thin sections using a JEOL JXA-840 EPMA equipped with a Princeton Gamma Tech Prism 2000 Si (Li) EDS X-ray detector at Massey University. The equipment was employing an accelerating voltage of 15kV, a beam current of 800pA and 100s live count time. Mineral phases were measured by a 2 µm focused beam, and a defocused beam of 10 or 20 µm was used for glass to minimise Na loss. Because the display/imaging quality of the equipment was considered inadequate for mapping the samples, all the areas of the thin sections were captured by a Nikon Eclipse E600W POL polarising optical microscope and the images were merged together by Adobe Photoshop CC 14 software. The high resolution images of the thin sections were allowed to discriminate different textures of glass, as well as textural features of minerals during EPMA.

Puketerata samples were examined by energy dispersive (EDS) and wavelength dispersive (WDS) spectroscopy at the State Geological Institute of Dionýz Štúr, Slovakia using a CAMECA SX-100 electron probe micro-analyser. Silicate phases and Fe-Ti oxides were analysed at standard conditions; acceleration voltage 15 kV, target current 20 nA and beam diameter 1-5 µm. To minimise Na losses in the glass analysis they were measured using a beam diameter of 10 µm, first with target current 3 nA to measure Na and subsequently other elements at standard conditions.

4.1.6 X-ray fluorescence spectrometry (XRF)

Juvenile scoria and dense juvenile fragments from pyroclastic beds from the newly found Te Hukui basalt (located at the vicinity of the Puketerata), as well as juvenile lithic fragments and lava rocks from the Motuoapa Peninsula, have been analysed for whole rock major and trace element geochemistry. The preparation for the determination of major and trace element compositions requires different methods. The dried samples were crushed and milled by Rocklab's ring grinder to get at least 10-12 g of powder. The milled sample was put to the oven at 110°C for 2.5 hours, and then it was kept in a desiccator for one night.

Glass disc for major element compositions: 2 g of the sample was put into a heat resistant crucible and was kept in an oven at 900°C for 30 minutes. The volatile content/loss of ignition (LOI) of the sample was determined by the sample's weight loss after the heating at 900°C. After keeping the ignited sample in the desiccator for one night, 0.8 g of sample was mixed with 8 g of X-Ray Flux (57% lithium tetraborate and 43% of lithium metaborate). The homogenised substance was fused at 1100°C, then solidified as a glass disc.

Pressed pellets for trace element compositions: Before the preparation of pressed pellets a freshly made PVA solution was needed. A PVA solution has organic compounds of polyvinyl alcohol powder, 16% ethanol and distilled H_2O that ensure no contamination from any elements measurable by XRF. For PVA solutions, in a few days the solution starts to decompose, thus it was used as 14 g of PVA powder, 33.3 ml of 16% ethanol and distilled H_2O to make up to 0.2

litres in a beaker. The solution was prepared on a hot plate at 50-75°C using a magnetic stirrer until the perfect dissolution of PVA powder occurred. The dissolution may take 1.5-2 hours. 8 g of samples were used from the leftovers of the sample that was kept in the desiccator for a night after the 2.5 hour long drying for each pressed pellet. In a crucible, 25 droplets of PVA solution was added by a pipette to the sample and was mixed until all the sample textures became unified. This mixture was put into an aluminium cap, which was pressed at 14-15 t for 40-50 seconds by a VANEOX – 25 t manual press.

Samples were measured by a BRUKER S8 TIGER 1 kw wavelength dispersive X-ray fluorescence spectrometer at the University of Waikato in Hamilton, New Zealand. Interference-corrected spectra intensities were converted to oxide concentrations using calibration curves consisting of natural standards closely approximating the matrix of our samples.

4.2 Digital terrain analysis

4.2.1 Introduction

The main sources of digital elevation data originate from photogrammetric surveys based on stereoscopic interpretation of aerial or satellite imagery. Other frequently used sources are the digitised contours of topographic maps. Higher resolution elevation data can be acquired by airborne laser scanning (ALS), or TLS and GPS surveys. Depending on the data acquisition and pre-processing of digital elevation datasets, it is possible to having three types of 3D representation of the terrain's surface: Digital Surface Model (DSM), Digital Elevation Model (DEM), and Digital Terrain Model (DTM). DEMs are a general term for any type of spatially seamless elevation data (Kereszturi and Procter, 2016), but in a strict sense DEMs represent the surface of the bare Earth with ground objects removed. DTMs are modified DEMs that have been augmented by elements, such as breaklines and observations other than the original data to correct for artefacts produced by using only the original data, while DSM represents the surveyed original point cloud including ground objects (e.g. buildings and vegetation) (Pereira and Janssen, 1999; Höhle and Höhle, 2009). In many cases, DEMs are used as a synonym for DTMs for all practical purposes. Elevation data is usually collected as points during the surveys and may be interpolated to a raster, where the elevation data is stored in a regularly spaced array as individual grid cells or vector-based contour lines or a Triangulated Irregular Network (TIN), comprising vertices with a series of edges to form a network of triangles. The edges of TINs form contiguous, non-overlapping triangular facets. In contrast with the unified resolution of grids, nodes of TIN can be placed irregularly, thus the resolution can change depending on the variability of the surface (Fig. 4.2).

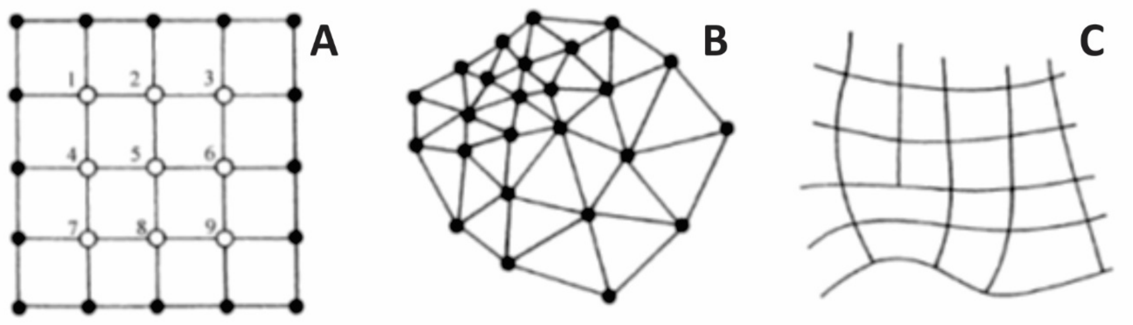

Figure 4.2 The most common types of elevation data networks (Moore et al., 1991). A – Raster-based grid; B – Vector-based TIN; C – Vector-based contours (polylines).

4.2.2 Sources of digital elevation data used for terrain analysis

The entire area of the TVZ is covered by DTMs derived from satellite-sensed imagery (ASTER and SRTM) and contour-based DEMs, whose spatial data was derived from the digitised contours of the New Zealand Topo50 map series having a scale of 1:50000. ASTER (Advanced Spaceborne Thermal Emission and Reflection Radiometer) obtains moderate resolution images of the Earth from the Terra satellite in different wavelengths, ranging from visible to thermal infrared regions of the electromagnetic spectrum. ASTER-recorded stereo imagery has the capability to produce DSMs with a resolution of 30 m (Hirano et al., 2003). SRTM (Shuttle Radar Topography Mission) data was obtained by a Synthetic Aperture Radar (SAR) that was operating for 11 days in February 2000 on-board the space shuttle *Endeavour* (Farr and Kobrick, 2000; Rosen et al., 2000; Farr et al., 2007). Previously, SRTM data for regions outside the USA were available at three arc-seconds (~90 m resolution), and full resolution of one arc-second global data was available from late 2015 between 50° north and 50° south with a resolution of ~30 m.

An 8 m contour-derived DEM is available from LINZ that was created by the interpolation of 20 m contours and shore lines from LINZ Topo50 maps (NZ 8 m Digital Elevation Model, 2012). The 8 m DEM is orthorectified to New Zealand Transverse Mercator 2000 (NZTM2000) projection, while being transformed to New Zealand Geodetic Datum 2000 (NZGD2000). With the aim to be ideal for cartographic visualisation, post-processing and filtering was performed, which modified the elevation values of the pixels of the 8 m DEM. Thus, a DEM with a 4 m grid resolution was created from the contours of the Topo50 map series complemented with the bathymetry of eight lakes (Okataina, Rotoaira, Rotoiti, Rotomahana, Rotoma, Rotorua, Tarawera, Taupo) (Irwin, 1969a; Irwin, 1969b; Irwin, 1972; Irwin, 1982; Garlick et al., 1999; LINZ - Land Information New Zealand, 2013) by natural neighbour interpolation (Bobach and Umlauf, 2006) for the purpose of edifice volume calculations and terrain analysis.

A 5 m spatial resolution photogrammetry-based DTM is available for the region of Waikato projected to NZTM2000 with the vertical datum of NZGD2000, which covers more than two-thirds of the central TVZ (Waikato Regional Aerial Photography Service - WRAPS, 2012). Ninety percent of the points have up to 3 m error, but the rest (10%) is characterised by significantly higher inaccuracies (Waikato Regional Aerial Photography Service - WRAPS, 2012). Thus, this data may be suitable for terrain analysis of restricted areas, such as edifices of selected lava domes. A hybrid contour and photogrammetry-based DTM with 5 m spatial resolution was used for the terrain analysis of Puketerata. A 2 m resolution photogrammetry-based DSM was used at Ohakune after filtering out the vegetation. Motuoapa was examined by a 1 m LiDAR (Light Detection and Ranging) DEM surveyed from an airplane by a Leica ALS50 laser scanner. The data was captured in June and July 2006, having NZTM2000 projection with Moturiki 1953 vertical datum. The dataset has an accuracy of 0.5 m horizontally and 0.15 m vertically (Waikato Regional Council and NZ Aerial Mapping Ltd., 2006).

RTK GPS survey data was collected at Ohakune and Puketerata using a Leica Viva GS14 GNSS (Global Navigation Satellite System) receiver using a Leica S15 Field Controller. Real-time position corrections were carried out using cellular connections to real-time differential correction sources. In the case of a lack of a mobile network the real-time corrections were pushed through using a base station. The points of topography were captured to NZTM2000 projection with WGS84 vertical datum. A **TLS** survey was completed at Ohakune using a Leica Nova MS50 MultiStation. The locations of the survey station were measured by RTK GPS using NZTM2000 projection with WGS84 vertical datum. The quarry walls were surveyed with 15 mm point spacing from a 30 m distance, whereas topographical characterisation was carried out by multiple scans using approximately 20 cm point spacing at 100 m. The surveyed point clouds were processed using Leica Cyclone 8.0 software. Outlier points were removed manually. The point clouds were exported from the Cyclone model space to ASCII files.

4.2.3 Defining topographic/terrain attributes

Land surface is characterised by various geomorphic parameters, or attributes or indices, that can be extracted from DEMs. Primary topographic attributes are mostly calculated from the directional derivates of the topographic surface and describe the variablility of terrain morphology (Wilson and Gallant, 2000). Primary attributes can be categorised on the basis of the way of extraction: (1) The data itself that is directly stored in the DEM (e.g. elevation) and attributes can be extracted by combining the DEM with another DEM or non-terrain information (e.g. area, volume); (2) First-order derivates are vectors that point to the direction of change on the surface, and it has a length (e.g. slope) and a direction component (e.g. aspect); (3) Second-order derivates, such as curvatures, indicate whether or not the first derivative is increasing or decreasing. Secondary topographic attributes can be extracted by the combination of two or more primary attributes, such as regional landform maps (Hammond, 1964; Dikau et al., 1991) or stream power indices (Wilson and Gallant, 2000). The following terrain attributes have been used during this research:

> **Slope** indicates the rate of change of elevation in the direction of the steepest descent. The steepness of the slope is usually given in degrees.

Aspect is strongly related to the slope as it expresses the orientation of the steepest descent. Aspect is given in degrees clockwise from north.

Relief indicates a vertical elevation change in a landscape. Relief is calculated for each pixel based on the maximum and minimum elevation within a specified radius.

Elevation **profile** is a two-dimensional cross-sectional view of the topography along a specified line that can be derived from point, line, raster or TIN sources.

Area describes the space in a horizontal plane enclosed by a feature relating to a geological or geomorphologic object.

Volume is determined by the grid cell-based difference between two surfaces within a specified area. Surfaces can be expressed as an equal-elevated plane, an inclined plane, or an interpolated surface based on the available data.

Plan curvature is the second derivative, expressing the rate of change of aspect along a contour. The main geomorphologic usage is the differentiation of ridges or summits, hillslopes and valleys.

Profile curvature is a second derivative**,** expressing the rate of the change of slope down a flow line. Profile curvature differentiates convex (slope increasing downhill) and concave (slope decreasing downhill) slope profiles, facilitating the recognition of primary volcanic structures and debris aprons.

Hammond-type macro landform classification was performed using one arc second SRTM data characterised by 30 m resolution. The characterisation of the geomorphology is divided into three subdivisions: slope, relief and profile (Hammond, 1964). The combination of these three primary attributes leads to the distinction of 96 possible sub-classes, which were merged into the 24 super-classes as proposed by Dikau et al. (1991).

Chapter

5

Chapter 5 presents the new findings about the volcanic activity of the andesitic Ohakune Volcanic Complex, including the evaluation of eruption styles, the evolution of volcanic architecture, duration of volcanic activity and its relationship to the activity of Ruapehu volcano.

This chapter is based on a published journal paper:

Kósik, S., Németh, K., Kereszturi, G., Procter, J.N., Zellmer, G.F. and Geshi, N. 2016: Phreatomagmatic and water-influenced Strombolian eruptions of a small-volume parasitic cone complex on the southern ringplain of Mt. Ruapehu, New Zealand: Facies architecture and eruption mechanisms of the Ohakune Volcanic Complex controlled by an unstable fissure eruption. Journal of Volcanology and Geothermal Research, 327: 99–115.

Statement of contribution (DRC16 form) is at Appendix D

Chapter 5 – Eruption mechanisms and evolution of the Ohakune Volcanic Complex

5.1 Introduction

Monogenetic (or small-volume) basaltic volcanoes occur within every geodynamic regime of the Earth and their associated volcanism is characterised by a range of eruption styles, eruptive materials and geomorphology (Sheridan and Wohletz, 1983; Lorenz, 1986; Head and Wilson, 1989; Valentine and Gregg, 2008; Németh, 2010; White and Ross, 2011; Kereszturi and Németh, 2012; Németh and Kereszturi, 2015). The determining factor of the eruptive behaviour of a volcano and the resulting volcanic products is the type of magma fragmentation (Lorenz, 1973; Walker, 1973; Kokelaar, 1983; Parfitt, 2004). Magmatic or dry fragmentation is characterised by exsolution and quick expansion of initially dissolved volatiles (e.g. H_2O and CO_2). The ascending bubbles coalesce and collapse near the surface and the exiting gas bursts result in Strombolian or Hawaiian eruptions (Parfitt, 2004; Houghton and Gonnermann, 2008; Valentine and Gregg, 2008). The main differences between these two eruptive styles are the speed of the gas flux with respect to magma rise (Parfitt, 2004) and differences between the ejection mechanisms of fragments during eruptions (e.g. the duration of particles remaining as ballistics is greater in Strombolian eruptions, and particles transported by fallout jets is more common in Strombolian activity) (Riedel et al., 2003; Capaccioni and Cuccoli, 2005). Hawaiian eruptions exhibit higher magma flux that allows limited cooling within the fire-fountain, which results in agglutination or fusing due to the high accumulation rate of the fragments (Head and Wilson, 1989), while the clasts from Strombolian eruptions cool prior to landing (Walker, 1973; Vergniolle and Mangan, 2000). Hydromagmatic or wet fragmentation refers to the interaction of magma and external water resulting in the conversion of magmatic heat to mechanical energy (Sheridan and Wohletz, 1983; Lorenz, 1985; Wohletz, 1986; White, 1996a; Wohletz and Zimanowski, 2000; Lorenz, 2003; Kereszturi and Németh, 2012). The interaction and the resulting volcanic processes in most cases primarily depend on the water/magma ratio, lending to two basic types of fragmentation: phreatomagmatic (Taalian) and Surtseyan (Kokelaar, 1983; Wohletz and Sheridan, 1983; White, 1996a; Kereszturi and Németh, 2012). During Surtseyan-style eruptions the water to magma ratio is high enough (e.g. in a shallow subaqueous environment) to allow continuous bulk mixing and fragmentation. As a result, the Surtseyan-style eruptions are characterised by quickly recurring, short-lived tephra jets, causing the rapid growth of a volcanic pile and the growth of a tuff cone (Thorarinsson, 1965; Kokelaar and Durant, 1983). In contrast, phreatomagmatic eruptions are characterised by lower water/magma ratios in the subaerial environment, in which fragmentation is triggered by a molten fuel-coolant interaction (MFCI) process causing energetic thermohydraulic explosions (Sheridan and Wohletz, 1981; Wohletz, 1986; White, 1996a; Wohletz and Zimanowski, 2000; Büttner et al., 2002). The phreatomagmatic eruptions commonly form two types of volcanoes, depending on the substrate (Lorenz, 2003; Auer et al., 2007) and the depth of excavation: tuff rings and maars. Both types have an ejecta ring around their craters, but in contrast with tuff rings, maar craters cut deeply into the pre-eruptive surface and are underlain by a mixture of volcanic and country rock fragments composed of debris commonly referred to as the diatreme (Wohletz and Sheridan, 1983; Martin and Németh, 2005; White and Ross, 2011; Kereszturi and Németh, 2012; Agustin-Flores et al., 2014). During phreatomagmatic eruptions the explosion loci often exhibit a downward or lateral migration according to the hydrologic and local substrate settings or following regional faults as it documented at *Ukinrek Maars, Alaska* (Kienle et al., 1980), *Cerro Xalapaxco* (Abrams and Siebe, 1994) and *Tecuitlapa Maar* (Ort and Carrasco-Núñez, 2009), *central Mexico*, *Tihany maars, Hungary* (Németh et al., 2001), and *Yangpori diatreme, SE Korea* (Son et al., 2012). Newer models presume that MFCI occurs at varying depths within the diatreme during the course of the activity, although it is most effective at shallow depth, where the hydrostatic pressure is less than the critical pressure. Thus, deep-seated explosions are rarely powerful enough to erupt (Valentine and White, 2012; Graettinger et al., 2015). As commonly documented, longer-lived eruptions of subaerial volcanoes and scoria cones quickly deplete the water from the substrate or surface sources and gradually become dry explosive and/or effusive eruptions, such as *Ság-hegy, western Hungary* (Martin and Németh, 2004), *Crosa de Sant Dalmai maar, NE Spain* (Pedrazzi et al., 2014b), and *Motukorea tuff ring, Auckland Volcanic Field, New Zealand* (Agustín-Flores et al., 2015). An alternating pattern of phreatomagmatic and magmatic activity may also be exhibited due to vertical or lateral migration of eruption loci, providing new influx of water from distinct aquifers (e.g. *Rothenberg volcano, East Eifel; Tihany maars, Hungary; Atexcac maar, eastern Mexico*; Houghton and Schmincke, 1986; Németh et al., 2001; Carrasco-Núñez et al., 2007), or due to change in magma flux as documented at *White Island, New Zealand* (Houghton and Nairn, 1991).

The Ohakune Volcanic Complex (OVC), North Island, New Zealand was previously examined by Houghton and Hackett (1984). Their study was based on the examination of outcrops in quarries that were cut into the scoria cones and the tuff rings. Since their work the extent of the main quarry has increased significantly, exposing a much larger internal portion of this small-volume volcano. The currently exposed volcanic units show evidence for new vent openings and simultaneous activity of distinct vents characterised by different eruption styles resulting in a very complicated volcanic architecture. Due to the continual influence of external water and the relatively small volume of magmatic eruptions in the final phases, volcanic features from the embryonic stage of the activity were not completely covered, making the OVC one of the few known locations that retains vital information on the evolution of monogenetic volcanoes affected by complex changes of vent loci (Houghton and Schmincke, 1989; Pedrazzi et al., 2014b; Agustín-Flores et al., 2015). Previous studies concentrated on the central vent volcanism and related hazards (e.g. Cronin et al., 2003; McClelland and Erwin, 2003; Graettinger et al., 2010; Pardo et al., 2012b), rather than focussing on the hazards produced by such a volcanism within the TVZ in terms of eruption cloud height, eruptive volumes and potential longevity of an eruption. This study is the first step towards assessing the volcanic hazards associated with small-volume volcanism with respect to the relationship between parasitic/satellite volcanoes and their larger polygenetic counterparts of the TVZ. We focus on the understanding of the eruptive conditions including influencing factors of fragmentation, dominant eruptive and depositional mechanisms, the range of the eruptive products created by different eruptive styles and the preserved geochemical characteristics. Furthermore new Geographical Information Systems (GIS) techniques allow utilizing a high resolution Digital Terrain Model (DTM) in order to study the geomorphologic features, providing great support in the understanding of the temporal evolution of this monogenetic volcano and contributing to the identification of the hazards of future small-volume eruptions within the TVZ (Fig. 5.1).

5.2 Regional setting

The late Pleistocene andesitic OVC (also known as Rochfort Crater) is located within the south-southwest ringplain of Ruapehu stratovolcano (Fig. 5.1). Volcanic activity in the southern end of the TVZ dates back to the eruption of *Hauhungatahi volcano* (Fig. 5.1), which has been dated at 921 ± 40 ky by $^{40}Ar/^{39}Ar$ (Cameron et al., 2010). This earliest activity was followed by the construction of primeval edifices of Ruapehu, which are mostly eroded and overlapped by the present Ruapehu volcano about 250 ky ago (Hackett and Houghton, 1989; Tost and Cronin, 2015). The OVC, along with another monogenetic volcano (*Rangataua Craters*), are the southernmost appearance of volcanic activity within the TVZ (Fig. 5.1) (Cole et al., 1986; Hackett and Houghton, 1989). The surrounding county rocks are mostly reworked volcaniclastic sediments of Mt. Ruapehu and andesitic to rhyolitic fallout tephra from various sources (Hackett and Houghton, 1989; Moebis, 2010). Pliocene marine sediments (mostly siltstones and sandstones of the Matemateaonga Formation) underlie the volcanic edifice and volcaniclastic series, and occasionally crop out as uplifted fault-bounded blocks (Townsend et al., 2008). The eruptions of the OVC are most likely linked to the E-W trending Ohakune Fault (Fig. 5.2) (Houghton and Hackett, 1984). The eruptions started in a flat or slightly sloping laharic depositional environment, where the unconsolidated reworked volcaniclastic sediments could have been divided by newly formed river pathways. The youngest sediments of the pre-eruptive surface are sourced from the products of the 60-15 ky old Mangawhero Formation (Hackett and Houghton, 1989), while the OVC deposits disconfomably overlain by the Kawakawa/Oruanui Tephra, which gives a minimum age of 25.4 ka for the activity (Hackett and Houghton, 1989; Vandergoes et al., 2013). Radiocarbon dating on charred wood from an OVC associated coarse lapilli layer from a distal outcrop to the south of the vents (Fig. 5.2) yields a date of 31,500±300 yr BP (Froggatt and Lowe, 1990).

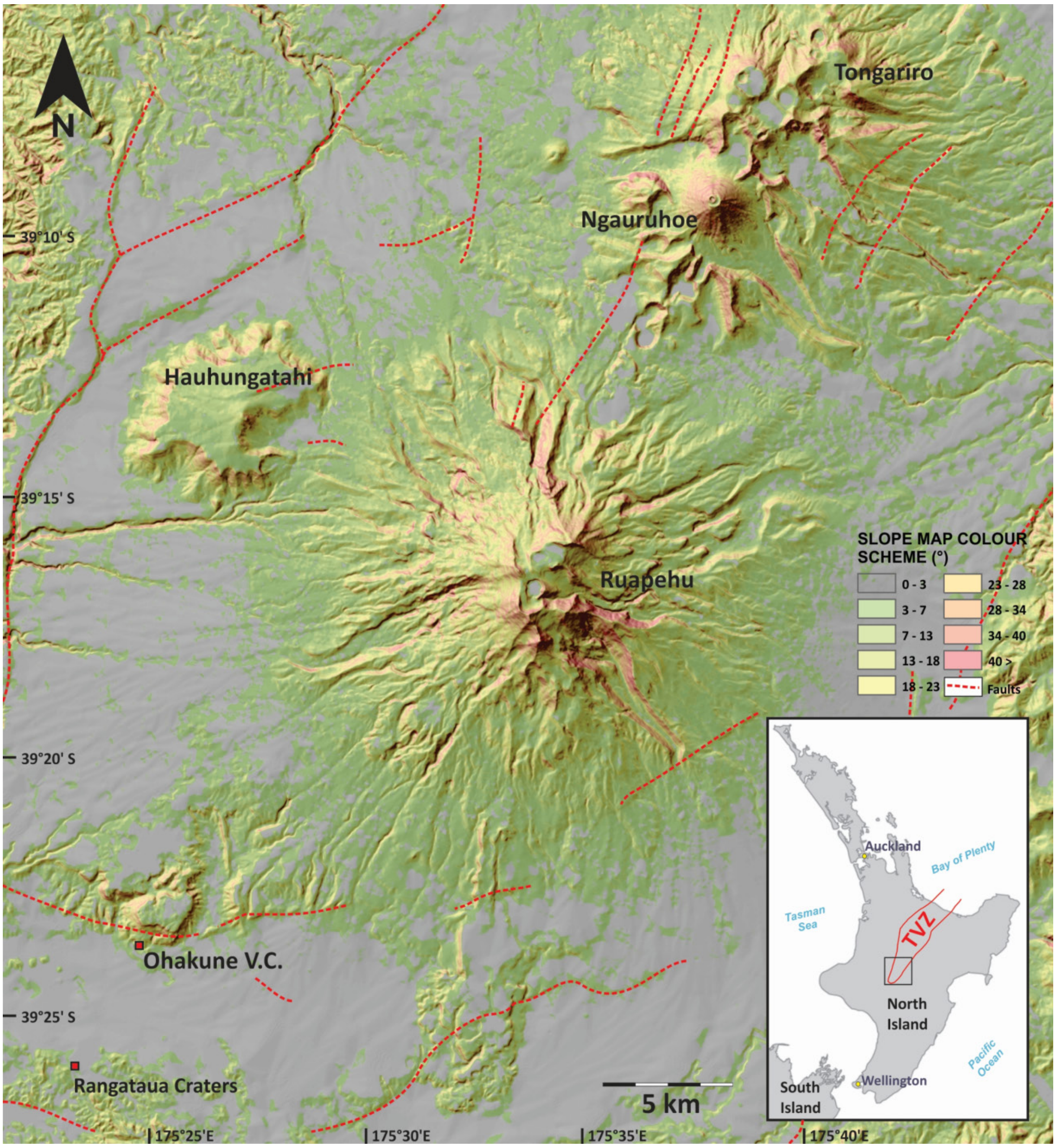
N
Tongariro
Ngauruhoe
Hauhungatahi
Ruapehu
Ohakune V.C.
Rangataua Craters
39°10' S
39°15' S
39°20' S
39°25' S
175°25'E
175°30'E
175°35'E
175°40'E
5 km
SLOPE MAP COLOUR SCHEME (°)
0 - 3
3 - 7
7 - 13
13 - 18
18 - 23
23 - 28
28 - 34
34 - 40
40 >
Faults
Auckland
Bay of Plenty
Tasman Sea
TVZ
North Island
Pacific Ocean
Wellington
South Island

Figure 5.1 Topography of the southern, dominantly andesitic part of the TVZ as shown on shaded slope map derived from a 8 m DEM (LINZ - Land Information New Zealand, 2012). Inset map shows its geographic position within New Zealand.

5.3 Materials and methods

5.3.1 Field observations and sampling

The proximal sequence of the ejecta ring, the outer edifice described as tuff ring by Houghton and Hacket (1984), was examined in terms of thickness, colour, bedding structures and grading, componentry and grain morphology. We also examined the distal sequence in order to correlate the existing units (Fig. 5.2). High resolution georeferenced thickness data of individual eruptive units from within the eastern ejecta ring (Fig. 5.2) were collected by Terrestrial Laser Scanner (TLS). The quarry walls were surveyed using approximately 15 mm point spacing at 30 m distance by TLS, along with high resolution photographs. The units named as A-E, G, H, I, K-M, O-Q and U (Fig. 5.4) were sampled from the proximal facies of the edifice within the quarry. In addition, large juvenile fragments (>10 cm in diameter) were collected from the massive ballistic beds (A, D, H, J, T, X) (Fig. 5.4) for density, petrography and geochemical analysis. The surface morphology of the ejecta ring was mapped using TLS and RTK GPS to upgrade the remotely sensed Digital Terrain Model (DTM) (Gómez-Vasconcelos et al., 2016) for edifice volume and unit volume calculations.

5.3.2 Sample preparation and analytical techniques

The grain size distribution of the matrix supported units were defined using phi sizes from -5 phi (32 mm) to 4 phi (0.63 mm) at half phi intervals. Particles smaller than 4 phi were analysed by a Partica LA-950V2 Laser Scattering Particle Size Distribution Analyser at Massey University. Grain size parameters were calculated using the Gradistat 8.0 program (Folk and Ward, 1957; Walker, 1971; Blott and Pye, 2001). The componentry and the morphological characteristics of the fragments were examined at -3, 0.5 and 2 phi under a stereomicroscope and a FEI Quanta 200 environmental Scanning Electron Microscope (SEM). The majority of samples had to be cleaned in an ultrasonic bath in order to disaggregate the adhering fine material. The microscopic observations were complemented with point counting of stereomicroscopic images using the JMicroVision 1.2.7 software. Five subsamples of blocks and bombs from each of the bomb-bearing units (A, D, H, J, T, X) were examined to determine envelope densities and vesicularities, which was carried out using a Micromeritics GeoPyc 1360 analyser. We also measured the densities for 30 -3 phi clasts from A, D, K, M, P units. Vesicularity and clast microtextures of the blocks/bombs were determined using 2D macroscopic and SEM image analysis for 10 samples from 6 units (Table 5.1). Macroscopic high resolution images have been taken from each sample (with an extent of 40 to 60 cm^2) by a photo and document scanner (Canon Pixma MP160), while the smaller vesicles were mapped through backscattered electron imaging (BSE) of thin sections striving to the requirement of representativeness. Two macroscopic images and nine microscopic images were captured at 25x and 100x magnifications ensuring that the resolution was sufficient to capture all size ranges of bubbles with appropriate resolution. 2D vesicularity was measured using ImageJ and the Matlab™-based FOAMS (Fast Object Acquisition and Measurement System) software by the method of exponential image nesting (Shea et al., 2010). Applying stereological conversion of vesicles by FOAMS provided further details of vesicle textures (e.g. vesicle size and vesicle volume distributions), vesicle size and shape properties which preserve information on the eruptive conditions (e.g. bubble nucleation or degassing) (Shea et al., 2010). Geochemical compositions were determined for single ash particles from matrix-rich (A-E, G-I, L) units (Fig. 5.2) at the size of 0.5 phi with a JEOL JXA-840 Electron Microprobe Analyser (EMPA) equipped with a Princeton Gamma Tech Prism 2000 Si(Li) EDS X-ray detector at Massey University, employing an accelerating voltage of 15 kV and a 10 µm defocused beam. Groundmass glass of spatter bombs were analysed with defocused beam and olivine and pyroxene crystals of the scoriaceous fragments from the bomb beds (D, H, J, T, X units) with a focused beam by EMPA. Elemental analysis and mapping of thin sections was accomplished by energy dispersive x-ray spectroscope (EDAX) of SEM.

5.4 Architecture of Ohakune Volcanic Complex

The OVC has previously been described as a kilometre wide slightly elongated tuff ring with intra-crater scoria cones (Houghton and Hackett, 1984). Based on a DTM (Horizons Regional Council, 2016), aerial photo from 1951 and field observations, the northern section of the tuff ring appears undeveloped due to lack of space between the vents and the Ohakune fault scarp. Only scoriaceous beds are exposed at the eastern section of the edifice that correlates with the pyroclastic successions at higher stratigraphic levels (Figs. 5.2, 5.3). Furthermore dense vegetation makes access difficult, and erosion by the Mangawhero River makes reconstruction difficult in this part of the volcanic complex. It appears that the southern section may also not be a single edifice, but rather consists of coalesced ejecta rings formed by alternating phreatomagmatic and Strombolian eruptions from separate vents (Figs. 5.2, 5.3). For these reasons, the outer complex edifice is not an ordinary tuff ring (Lorenz, 1986; Kereszturi and Németh, 2012), and we will refer to it here as an ejecta ring. There are at least 5 depressions between the ejecta ring structures and the fault plane, which probably reflects the location of the eruptive vents that were active during the final eruptive phases (Fig. 5.2). Most of these pits form a 600 m long fissure zone subparallel with the Ohakune Fault, which may indicate that the area was penetrated by the extruding tips of a blade-like dyke. Three of the depressions host the craters of a large and two small late stage scoria/spatter cones (Fig. 5.2).

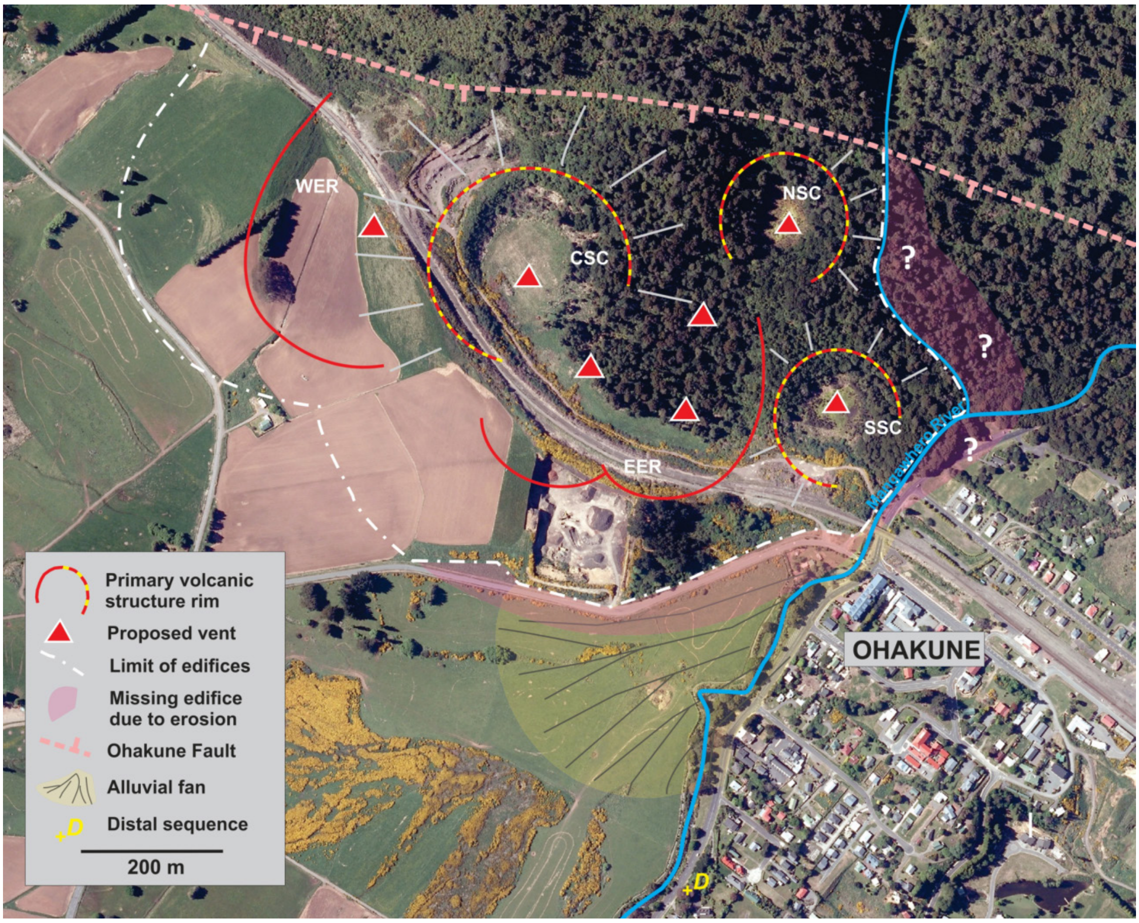
WER
CSC
NSC
SSC
EER
?
?
?
Mangawhero River
OHAKUNE
D
Primary volcanic structure rim
Proposed vent
Limit of edifices
Missing edifice due to erosion
Ohakune Fault
Alluvial fan
D Distal sequence
200 m

Figure 5.2 Aerial photograph of OVC with its proposed architecture. The main edifices are labelled; West ejecta ring (WER), East ejecta ring (EER), Central scoria cone (CSC), South scoria cone (SSC), North scoria cone (NSC).

The proximal sequences of the inner and outer edifices are exposed at several quarries. The largest inner scoria/spatter edifice (CSC) (Figs. 5.2, 5.3) has a bedded structure of coarse scoria and agglutinated scoria units, alternating with clastogenetic lava flow units (Fig. 5.3, Appendix A.5.2). The majority of the edifice of the scoria cone has been quarried away except the north section. The proximal sequence of the ejecta ring is very well exposed in a quarry that is currently active (Figs. 5.3, 5.4); however the contact with the country rock is not visible (Fig. 5.4).

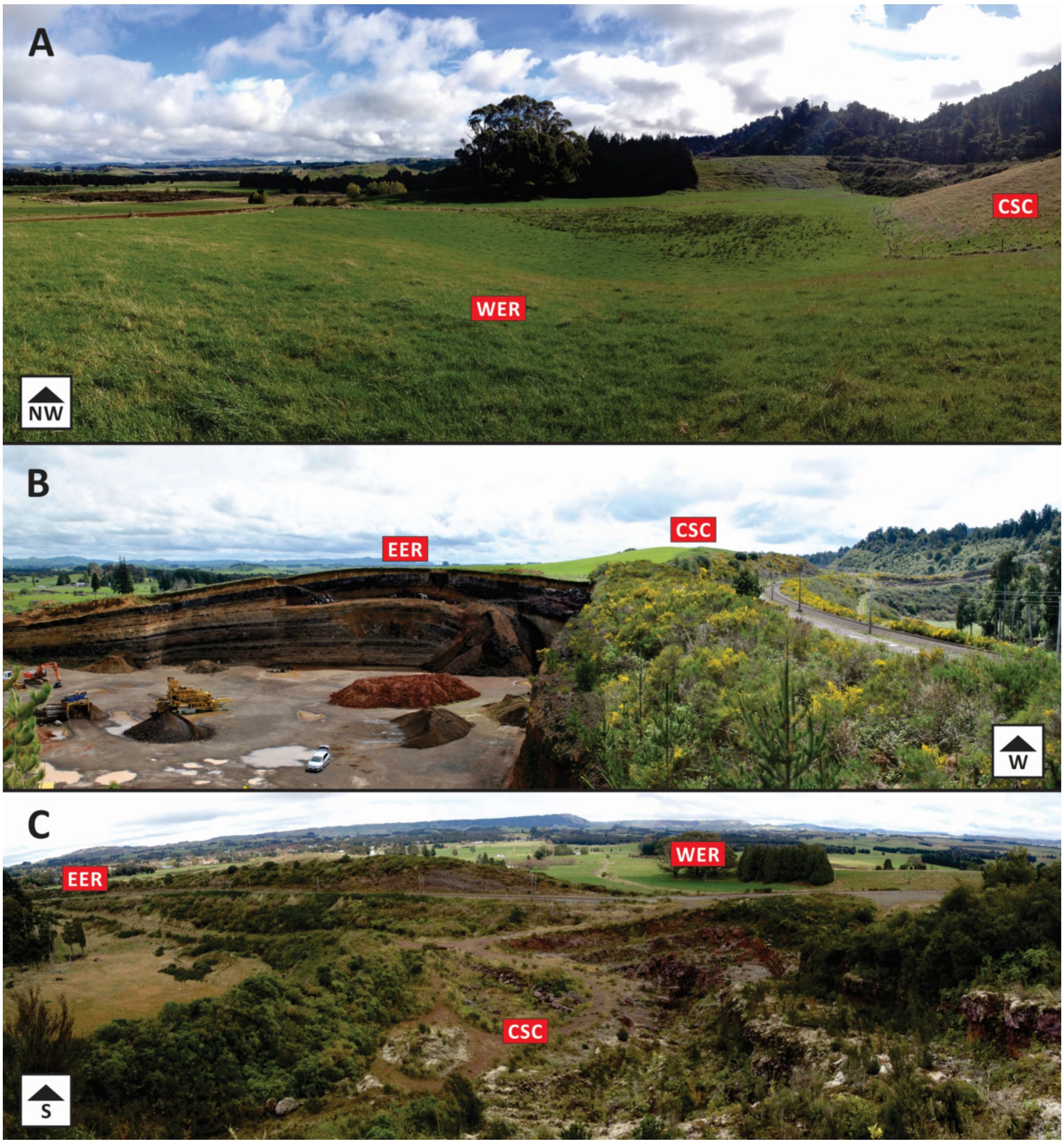

Figure 5.3 Morphological features of OVC. A: View from the rim of WER to its crater floor. On the right edge the foot of the CSC partly fill in the crater. B: The quarried section of the coalesced EER and the rim of CSC. C: View from the highest part of the CSC to its crater floor (grassland) and its quarried interior of alternating welded and unwelded Strombolian (or Hawaiian) units. The railway line is also cut through the scoria cone and EER on the left and WER on the right.

Geomorphologic observations, coupled with Real-Time Kinematic (RTK) GPS measurements, showed that the pre-eruptive country rocks are located at the altitude of 585-590 m above sea level, thus about 10 m of the initial sequence has not yet been exposed. The lowest visible units are light-coloured and matrix-rich, while the upper units appear to be the scoria-dominated units alternating with units of pyroclastic density currents and poorly-sorted units of weathered scoriaceous fragments with denser lava blocks. The distal sequence comprises a 1.8-thick unit that is situated about 600 m south of the OVC on the left side of Mangawhero River (Fig. 5.2). The distal outcrops have been separated from the OVC by fluvial erosion prior to the Oruanui eruption (25.4 ky) and those deeply cut channels have been later occupied by fluvial sediments as part of the formation of an alluvial fan (Fig. 5.2).

5.5 Stratigraphy and sedimentology

The active quarry exposes the coalesced eastern ejecta ring (EER) (Figs. 5.2, 5.3). The walls are north-west radially orientated to the ejecta ring, providing a proximal to distal cross-section of the volcano. At the NW corner of the quarry we identified an unconformity. In relation to the unconformity a small fault is also visible with decreasing offsets from the base to the top (Fig. 5.4). The lowest, barely exposed units are thick-bedded and poorly-sorted with accidental lithics from the laharic basement and dense lava fragments from the OVC eruption alternating with massive ash beds. The upper sequence of the ejecta ring is characterised by dark-coloured bomb beds alternating with light-coloured ash beds and mixed beds through the approximately 22 m thick visible succession. 95% of the fragments are clearly associated with the magma erupted from OVC, the most distinctive feature of which is the high content (10-15%) of pyroxene and olivine phenocrysts up to 0.8 cm in size. The fine tephra deposited at the OVC typically have a high amount of aggregates and dust-adhered fragments with a lack of accretionary lapilli (Fig. 5.5). The ash particles also display heterogeneity in terms of colour (dark to light brown), alteration, vesicularity, and shape (skeletal/irregular to blocky) (Fig. 5.5). The majority of the ash fragments are moderately vesicular (Fig. 5.5c-d). There is an insignificant amount of accidental lithics in the finer grain size. Most of the lapilli and block fragments are dark-coloured dense or vesicular andesitic juveniles up to 25-30 cm. The remaining accessory fragments are mostly well-rounded andesitic boulders of the fluvial-laharic basement originated from Ruapehu and a small percentage of baked sedimentary rocks (Fig. 5.4). The exposed units were labelled (Fig. 5.4) and classified into four lithofacies on the basis of sedimentological characters (e.g. componentry, grain size distribution and sedimentary structures) (Fig. 5.4); 1. Ab: ash beds (C, E, G, L, N, O, Q, S units), 2. Ab_C: ash beds with coarse fragments (A, I, U), 3. Bb_A: bomb beds with ash (B, D, H, K, P, R, X_{Lower}), 4. Bb: spatter-scoria bomb beds (J, M, T, X_{Upper}).

5.5.1 Ash beds (Ab)

5.5.1.1 Description

Ash beds are matrix-supported massive, diffusively stratified or planar bedded with internal low angle unconformities. The beds are poorly-sorted and predominantly composed of fresh and varying amounts of yellowish to brownish coloured palagonitised ash and lapilli fragments from -3 phi to 7 phi in size with a peak at 3.5 phi. Mud-coating is frequent on the surface of fragments (Appendix A.5.2). Some ash beds exhibit stratification by the alternation of finer and coarser layers, where the coarsest layers often show inverse grading (e.g O1 layer). The tephra has a damp, adhesive behaviour. Impact sags are rare within the quarry. The biggest clasts (up to 20 cm) are either altered vesicular or dense, slightly scoriaceous fragments correlated to the Ohakune eruption, and rounded andesite cobbles of Ruapehu origin. The thickness of the units is variable (≤50 cm thick), and visible single layers are in the range of 1 cm to 25 cm thick. Individual beds usually exhibit irregular thickness variations without appreciable thinning trends within the quarry (Fig. 5.4). The distal counterparts are mostly thinly stratified ash (-1 to 7 phi in size) with low angle cross and dune bedding structures. The distal sequence exhibits soft sediment deformation and impact sags with ballistic bombs up to 10 cm in size (Appendix A.5.2).

5.5.1.2 Emplacement interpretation

The high proportion of mud-coated fragments and the wet and massive nature of beds imply an abundance of water during the eruptions and during deposition (Heiken and Wohletz, 1985; Sohn and Chough, 1989; Houghton and Smith, 1993). The clearly visible cross and dune bedding of the distal deposits confirms the dilute pyroclastic density current origin of these deposits. Palagonitised ash fragments and fine dust is probably derived from the slurry of the crater floor. Hence, minor recycling of juvenile fragments from the earlier products of the OVC activity must have occurred (Houghton and Smith, 1993; D'Oriano et al., 2014). The majority of coarser fragments are likely to have been transported by ballistic trajectories or in pyroclastic density currents at the proximal section, while the coarser fragments clearly have a ballistic origin at the distal sequence (Fisher and Schmincke, 1984; Sohn and Chough, 1989). Therefore, Ab units

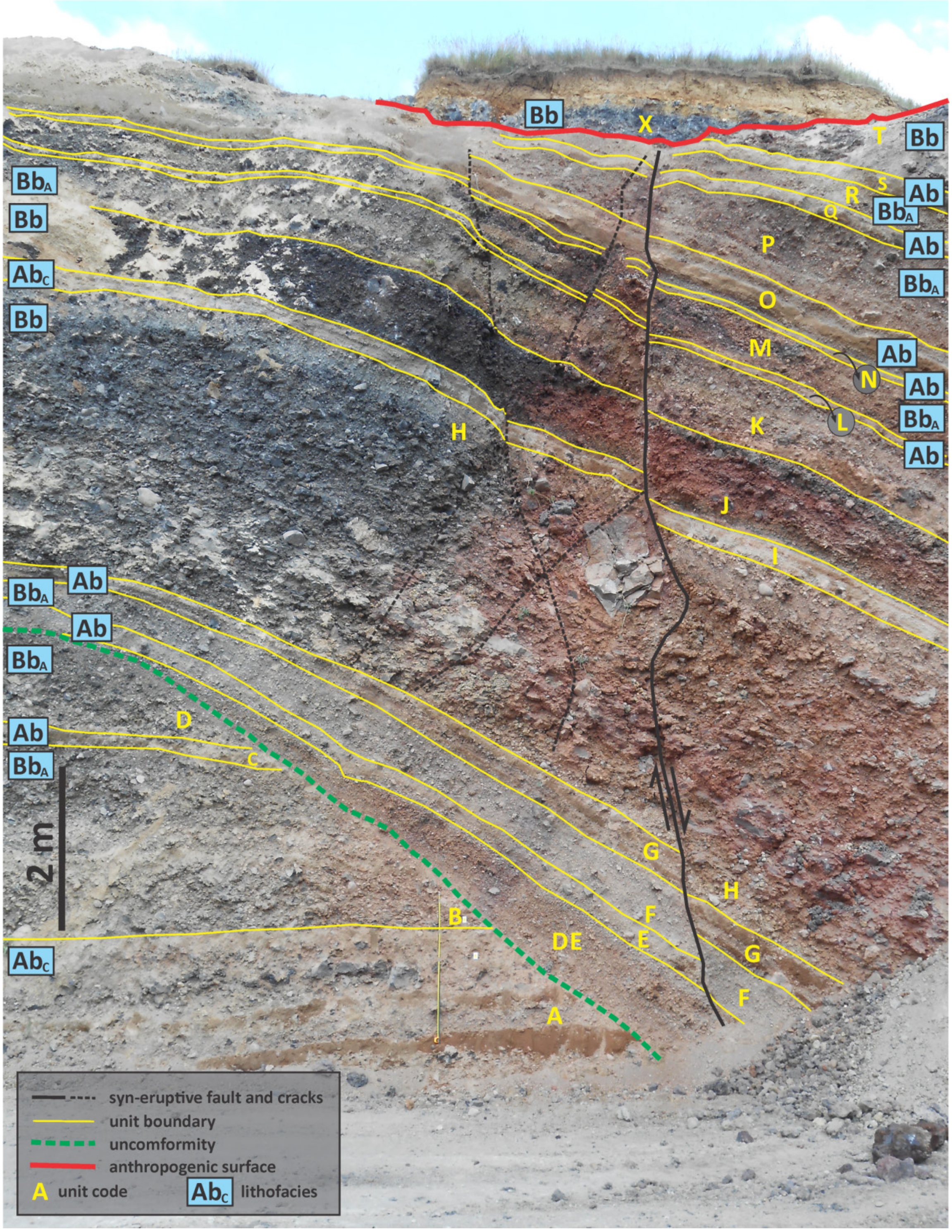
Bb
X
T
Bb
Bb$_A$
Bb
Ab$_C$
Bb
S
R
Q
Ab
Bb$_A$
P
Ab
Bb$_A$
O
M
Ab
N
Ab
L
K
Bb$_A$
Ab
H
J
I
Bb$_A$
Ab
Ab
Bb$_A$
D
Ab
C
Bb$_A$
2 m
G
H
B
F
E
DE
G
F
A
Ab$_C$
syn-eruptive fault and cracks
unit boundary
uncomformity
anthropogenic surface
A unit code
Ab$_C$ lithofacies

Figure 5.4 Stratigraphic sequence of the proximal part of EER at the northwest corner of the quarry. This is one of the locations exhibits the opening of a new vent. Note the oxidation pattern of right hand side of the fault.

were most likely deposited as a result of discrete phreatomagmatic explosions generating wet pyroclastic surges and some tephra fall.

5.5.2 Ash beds with coarse fragments (Ab_C)

5.5.2.1 Description

Ash beds with coarse fragments are matrix-supported, very poorly-sorted units with variable amounts of coarse lapilli and bomb size clasts (Fig. 5.6). The matrix is composed of fresh juvenile, mud-coated and palagonitised ash and medium lapilli fragments between -3 to 7 phi in size with the main peak at -2.5 to -1.5 phi. The larger sized lapilli and bombs are composed of rounded andesite cobbles and fresh olivine/pyroxene-bearing andesitic fragments up to 50 cm in size. Some of the lava fragments are vesicular with a dense core exhibiting conchoidal fractures, others have cauliflower or plastically deformed shapes. None of the clasts have formed visible impact sags. The fraction of these larger clasts is significantly higher than in the Ab units. Ab_C units often have internal bedding without sharp depositional or erosional contacts. These units were typically interstratified with subunits that are analogous to Ab-type lithofacies traverses through the outcrop (Fig. 5.4).

5.5.2.2 Emplacement interpretation

The lack of the sharp internal contacts and impact sags suggest continuous deposition by fallout and debris jets, while the relatively coarse average size as well as the smaller portion of very fine (<3 phi) juvenile fragments imply less energetic fragmentation than in the Ab units. The massive beds of Ab_C interstratified with Ab beds may be the result of a sustained, but varying level of interaction of magma with external water at shallow depth, which enables a near-continuous discharge of tephra and gases coinciding with more energetic discrete explosions. The continuous uprush produced a complex deposition of fresh dry ash, recycled damp ash and aggregates from the contact zone of the dyke edge and conduit wall, similar to the 1976-1982 eruption of White Island, New Zealand (Houghton and Nairn, 1991). However, the fresh, sometimes plastically deformed bombs (in unit A) suggest that the middle part of the dyke could have produced drier Strombolian-type fragments occasionally.

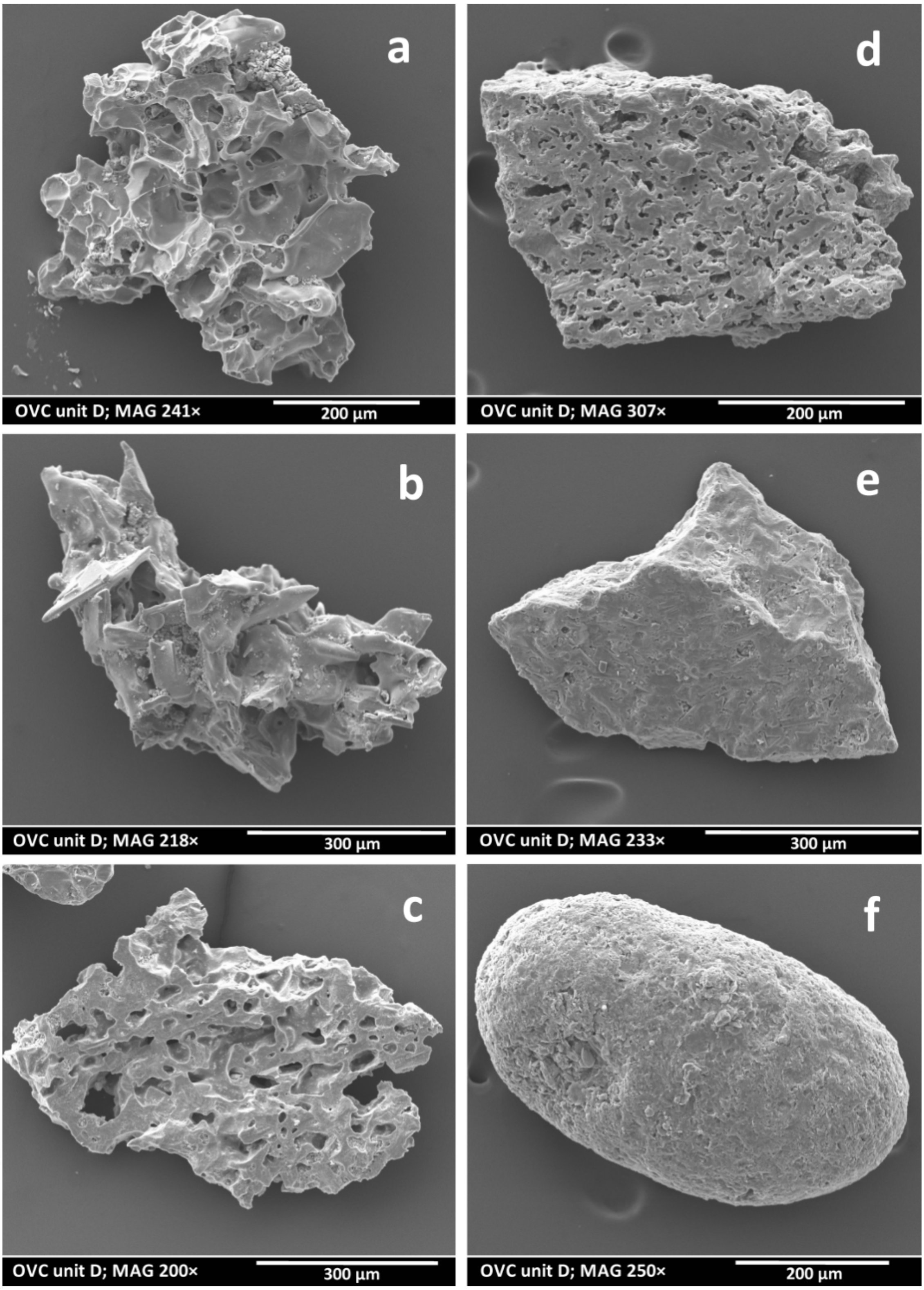
a
OVC unit D; MAG 241×
200 µm
d
OVC unit D; MAG 307×
200 µm
b
OVC unit D; MAG 218×
300 µm
e
OVC unit D; MAG 233×
300 µm
c
OVC unit D; MAG 200×
300 µm
f
OVC unit D; MAG 250×
200 µm

Figure 5.5 SEM images of juvenile ash fragments characterised by high to low vesicularities (A–E) and a typical aggregate (F). Type a with spherical vesicles is extremely rare at OVC would represent Strombolian fragmentation (Heiken and Wohletz, 1985), type b with microlites is the most vesicular of the common fragments and might related to eruptions with minor influence by water/magma interaction, while c–e types might have more phreatomagmatic origin. By comparison, a block was smashed by hammer and the bits were similar to type-c fragments.

Strombolian/Hawaiian and phreatomagmatic eruptions usually represent very different types of magma fragmentation (Wohletz and McQueen, 1984), however there are a few documented eruptions that exhibit both fragmentation processes at the same time (Moore et al., 1966; Kienle et al., 1980; Dzurisin et al., 1995; Valentine et al., 2000). There are some alternative models for magma fragmentation and admixture of tephra from two contrasting eruptions. Depending on variations in vent geometry and hydrological conditions the products could have originated from different parts or depths of the same vent or fissure (Houghton and Schmincke, 1986; Dzurisin et al., 1995; Valentine and White, 2012) or from two or more localised vents along a fissure (Moore et al., 1966; Kienle et al., 1980; Pedrazzi et al., 2014a; Belousov et al., 2015). Alternatively, these units can be interpreted as products of a long-lasting transitional phase between phreatomagmatic and magmatic phases of Strombolian/Hawaiian eruption (Belousov et al., 2015), which might have been emplaced by spatter/scoria-bearing pyroclastic density currents (Valentine et al., 2000). One of the Ab$_C$-type units (U) is interfingering with a bomb bed (unit X), which indicates that the two units did not form by explosions from a single vent. The fragmentation during stronger discrete eruptions produced a higher amount of fine ash deposited by wet pyroclastic surges and tephra fallout. The slightly higher proportion of accidental fragments that originate from the shallow laharic basement demonstrates that the eruption loci were still of shallow depths without notable excavation.

5.5.3 Bomb beds with ash (Bb$_A$)

5.5.3.1 Description

The BbA lithofacies is clast-supported and predominantly made up from mud-coated, weathered (oxidised at very proximal locations) and fresh juvenile lapilli and bomb sized fragments with various amounts of fines, usually without stratification (Fig. 5.4). The ratio of the ash and lapilli/bomb fragments can vary vertically within the same unit. In a few locations the ash rich portions are arranged into hardly distinguishable graded sheets. The majority of coarse juvenile fragments are 3-10 cm in size with a maximum of 25-30 cm in diameter in loosely packed clast-supported beds. The bigger clasts sometimes display shapes generated by plastic deformation. Some of these flattened clasts have experienced agglutination. Other clasts are dense lapilli and blocks with fractured edges exhibiting various degrees of alteration. At the NW corner of the quarry the fragments are oxidised, but in other locations yellowish to brownish alteration of clasts can be observed. The ash componentry is identical to the other ash-rich units. Mud-coating is common to all clasts and at all grain size classes. Ballistic bomb sags are not visible, but the impact of the biggest andesitic boulders can form minor distortions. The thickness of the units can vary between 0.3 and 3.5 meter.

5.5.3.2 Emplacement interpretation

The tephra associated with Bb_A units have most likely originated from two sources. The average grain size, the shape of the coarsest fragments, lack of matrix, and the dominance of moderate to highly vesiculated juvenile fragments suggest that these units have originated from Strombolian-style eruptions (McGetchin et al., 1974; Houghton and Hackett, 1984). The documented clast flattening and agglutination imply occasionally higher retained heat, which might have been caused by the fluctuation of the effusion rate during Strombolian activity. However the varying proportions of fine material, componentry (e.g. mud-coated fragments and aggregates), fractured, altered juvenile blocks and accidental boulders all suggest that fresh juveniles erupted through slurry-filled craters. The altered earlier fragments were mixed with Strombolian products. The adhering dust on the surface of clasts across a wide spectrum of grain sizes suggests a broad recycling and in-situ palagonitization of the glassy rinds of pyroclasts (Houghton and Smith, 1993). The high portion of dust-adhered fragments demonstrates an abundance of water in the eruption plume, thus material comprising the Bb_A unit products did not form by magmatic fragmentation alone. There are two alternative models for the magma fragmentation and mixture of tephra from two contrasting eruption styles. Depending on the variations of vent geometry and hydrological conditions the products could have originated from different parts of the same vent or fissure (Houghton and Schmincke, 1986; Dzurisin et al., 1995) or from two or more localised vents along a fissure (Kienle et al., 1980; Pedrazzi et al., 2014a; Belousov et al., 2015).

5.5.4 Spatter-scoria bomb beds (Bb)

5.5.4.1 Description

Spatter-scoria bomb beds are clast-supported without any internal bedding. The upper boundary is sharp, but the lower can be sharp or grading into AbC-type units. Bb units are made up from oxidised or fresh juvenile fragments of plastically deformed and cauliflower-shaped coarse lapilli and blocks (Appendix A.5.2) or bombs with minor amounts of medium lapilli (0.5-1 cm in size). The grain size distribution of these beds implies better sorting than the other lithofacies. The average clast size ranges between 3 and 10 cm, the maximum clast size is observed up to 30 cm. These units often exhibit agglutination as well as locally confined welding (Fig. 5.4).

5.5.4.2 Emplacement interpretation

The lack of admixed ash, the plastically deformed fragments and the short dispersal range of the rapidly thinning beds suggest that Bb beds originated from vents characterised by low energy Strombolian and/or Hawaiian-style activity. However, the existence of the large number of dense cauliflower-shaped blocks suggests rapid cooling of the magma prior to eruptions (Kienle et al., 1980). In addition, the interfingering ash-dominated lithofacies (Ab, Ab_C) demonstrates that other phreatomagmatic vents could have been active at the same time referring to the abundance of water to other parts of the dyke.

5.6 Density and vesicle microtexture analysis

Clast densities and vesicle textures (e.g. vesicle size and shape, vesicle number densities) provide information on characterizing the conditions of magma ascent and degassing, and may also elucidate the changing conditions within the conduit between consecutive eruptive phases (Houghton and Wilson, 1989; Parfitt, 2004; Moitra et al., 2013). The skeletal (absolute) density determined for blocks/bombs was 2.85-2.90 g/cm^3. The bombs/blocks exhibit different envelope densities than the lapilli size clasts. The lapilli (-3 phi) average densities are between 1.27-1.33 g/cm^3, while the bombs have densities of 1.52-1.54 and 1.72-1.82 g/cm^3. The modes show a similar pattern of 1.0-1.2 g/cm^3 for lapilli size and 1.5-1.7 g/cm^3 for bomb/block size (Fig. 5.6).

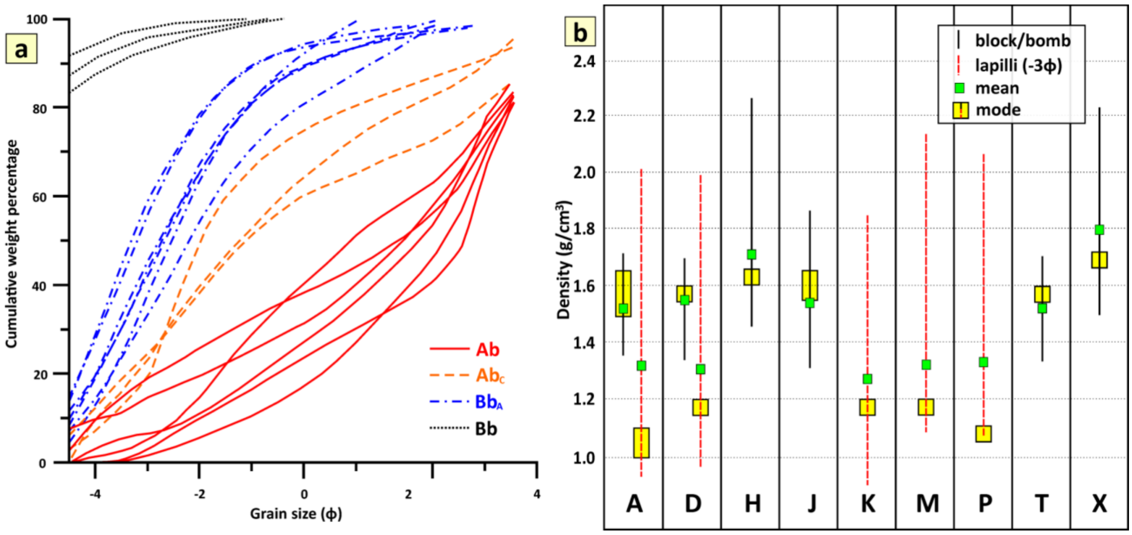

Figure 5.6 a – Cumulative grain size distribution of distinct units from the proximal sequence of EER. Bb unit distributions are only represent estimations based on field observations. b – Density variations of bomb/block and lapilli (−3 phi) sized juvenile fragments from EER proximal sequence.

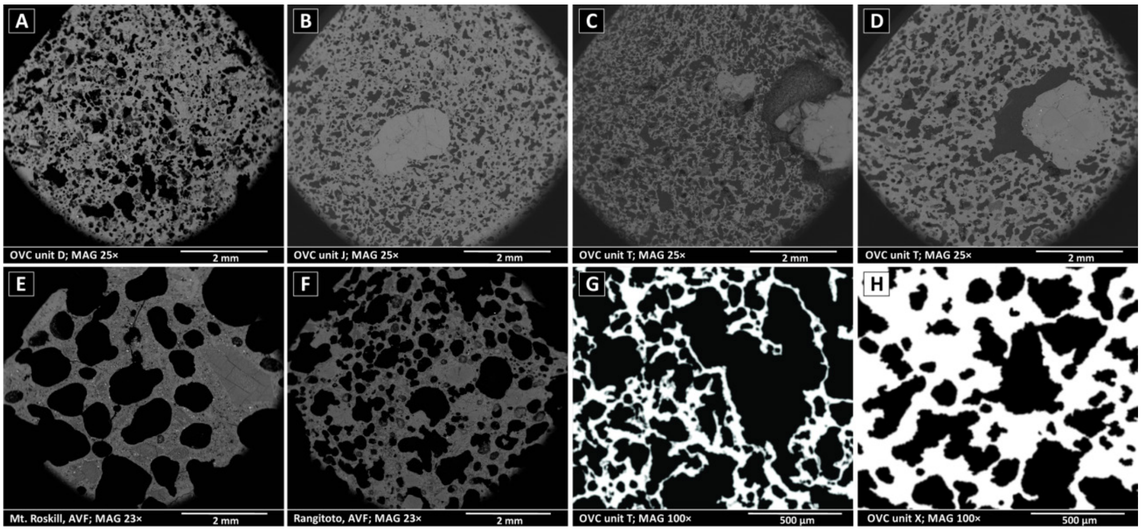
A
OVC unit D; MAG 25×
2 mm
B
OVC unit J; MAG 25×
2 mm
C
OVC unit T; MAG 25×
2 mm
D
OVC unit T; MAG 25×
2 mm
E
Mt. Roskill, AVF; MAG 23×
2 mm
F
Rangitoto, AVF; MAG 23×
2 mm
G
OVC unit T; MAG 100×
500 µm
H
OVC unit X; MAG 100×
500 µm

Figure 5.7 SEM images of bombs/blocks (A–D, G, H) from OVC and SEM images of scoria fragments from Mt. Roskill (E) and Rangitoto (F), Auckland Volcanic Field (AVF) for comparison. The two samples from AVF exhibit a Hawaiian and Strombolian (or Violent Strombolian)-style eruptions (Kereszturi, unpublished data) as the vesicles show mostly spherical or subspherical shapes (Lautze and Houghton, 2007; Moitra et al., 2013). The textures of samples from OVC are completely different from textures forming during these mild types of eruptions, however similar to basaltic Plinian eruptions of Etna 122 BCE and Tarawera 1886 (Moitra et al., 2013).

The 3D vesicularity was calculated applying a 2.85 g/cm^3 solid density, yielding values significantly higher (26.4-51.4%) than the FOAMS-calculated integrated 2D vesicularities (22.1-31.6%). The 2D shape of the bubbles usually exhibits irregularities (polylobate shapes) due to frequent coalescence inducing a large-scale interconnectivity of the vesicles (Fig. 5.7, Table 5.1). Most of the equivalent diameters of vesicles are smaller than 1 mm and range between 0.005 and 14.9 mm with an average of 0.97-0.308 mm. Typically, 50-70% of bubbles are smaller than 0.1 mm, except for unit X where these small bubbles made up only 16-20% (Table 1). Vesicle number density values vary from 6.5×10^2 to 4.69×10^3 mm^{-3} (Fig. 5.9, Table 5.1).

Sample code	Density derived (BV) (%)	2D BV (%) (ImageJ)	2D BV (%) (Foams)	N_V (corr) (mm^{-3})	EqDi range (mm)	Mean EqDi (mm)	Mean Area (mm^2)	Regularity (Shea et al. 2010)	Shape factor (Orsi et al. 1992)
A1	46.6	42	26.5	1.22×10^3	0.015-5.168	0.112	0.034	0.8501	0.6023
D1	44.2	45.1	25.9	1.55×10^3	0.015-4.015	0.136	0.046	0.8302	0.5989
D3	43.3	43.8	31.6	2×10^3	0.012-7.116	0.166	0.114	0.831	0.6144
H2	38.3	47.7	28.8	1.57×10^3	0.005-3.939	0.172	0.061	0.8322	0.6066
H3	39.1	28.4	24.6	1.71×10^3	0.005-2.154	0.143	0.041	0.8807	0.6357
J4	39	31.2	25.5	3.15×10^3	0.005-2.076	0.097	0.025	0.8739	0.6045
T1	51.4	47.9	28.4	4.69×10^3	0.005-5.351	0.189	0.108	0.7948	0.5663
T3	44.5	53.3	28.9	1.7×10^3	0.005-14.895	0.308	0.397	0.8147	0.6050
X2	39.8	38.1	22.1	6.5×10^2	0.005-2.622	0.177	0.070	0.8333	0.5957
X3	26.4	44.1	27.2	1.46×10^3	0.006-1.341	0.172	0.036	0.848	0.4931

Table 5.1 Bubble volume (BV), bubble number density (NV) and typical sizes (equivalent diameter: EqDi) and shapes of vesicles (Regularity, Shape factor) for distinct units and clasts from the proximal sequence of EER.

5.6.1 Interpretation of observed density and vesicle microtextures features

In comparison with the results of previous density measurements from OVC, similarities exist between our lapilli densities and the density measurements of clasts from “S beds” and “Pb beds” from Houghton and Hackett (1984). Minimum values are 1 g/cm^3, but our maximum values are larger by 0.5 g/cm^3 than earlier results. That could be an explanation, why our mean densities are larger by approx. 0.1 g/cm^3. The bomb/block densities of this study are similar to the bomb density values published in Houghton and Hackett (1984) from the unwelded parts of the inner scoria cone. The density differences between the two examined clast sizes suggest that they originated from different parts of the magma and may represent different fragmentation and eruption styles. Furthermore, units H and X are more heterogeneous with clasts also having higher densities. It is clear that the heterogeneous clast assemblage originated from the same eruption phase; hence any conduit process (e.g. intensified degassing from a more fluid melt) could have been responsible for the recorded density diversities.

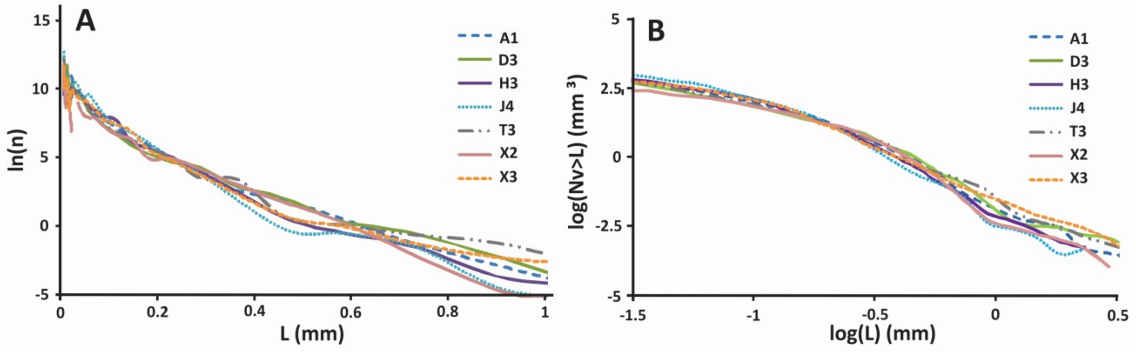

Figure 5.8 A – Vesicle size distributions (VSD) are ln(n) as a function of L plots,with ln(n) the log of the vesicle number densities per size class, and L is the equivalent diameter in mm. The left part of the segment mostly reflects multiple stages of bubble nucleation and growth. The lower part of the VSD slopes often exhibit coalescence (e.g. J4, T3) which may have occurred at multiple stages. B – Cumulative vesicle size distributions (CVSD) are log(N_V > L) as a function of log(L) plots, where N_V is the total vesicle number density. Vesicle density measurements were used based on the objects per cubic mm greater than L. CVSD trends also suggest multiple stage of nucleation and growth with coalescence and bubble collapse events in most of the cases (e.g. A1, D3, J4, T3, X2) (Shea et al., 2010).

Even the vesicle textures and shapes from the most Strombolian-like beds (Bb_A and Bb lithofacies) are completely different to textures originating from other Strombolian (violent Strombolian) and Hawaiian eruptions (Lautze and Houghton, 2007; Gurioli et al., 2008; Cimarelli et al., 2010; Stovall et al., 2011; Moitra et al., 2013; Kereszturi and Németh, 2016) (Fig. 5.7). Vesicle textures from the OVC exhibit similar features to the products of basaltic Plinian eruptions of Etna, 122 BC and Tarawera, 1886 (Sable et al., 2006; Moitra et al., 2013) and the hydromagmatic eruptions of the Ilchulbong tuff cone (Murtagh et al., 2011). Based on tephra properties of distal outcrops and the estimated dispersal it is assumed that the Ohakune eruption does not correspond to basaltic Plinian eruptions, thus it is proposed that the observed vesicle textures may have formed by effects of interaction with external water. Results of quantitative analysis of FOAMS verify coalescence of the vesicles and indicate multiple stages of nucleation and growth (Fig. 5.8). The calculated bubble number density values of the OVC eruption are lower than those from the Ilchulbong tuff cone, but within the range of other small-volume eruptions from Hawaiian and Taalian in style (Fig. 5.9) (Murtagh et al., 2011; Stovall et al., 2011).

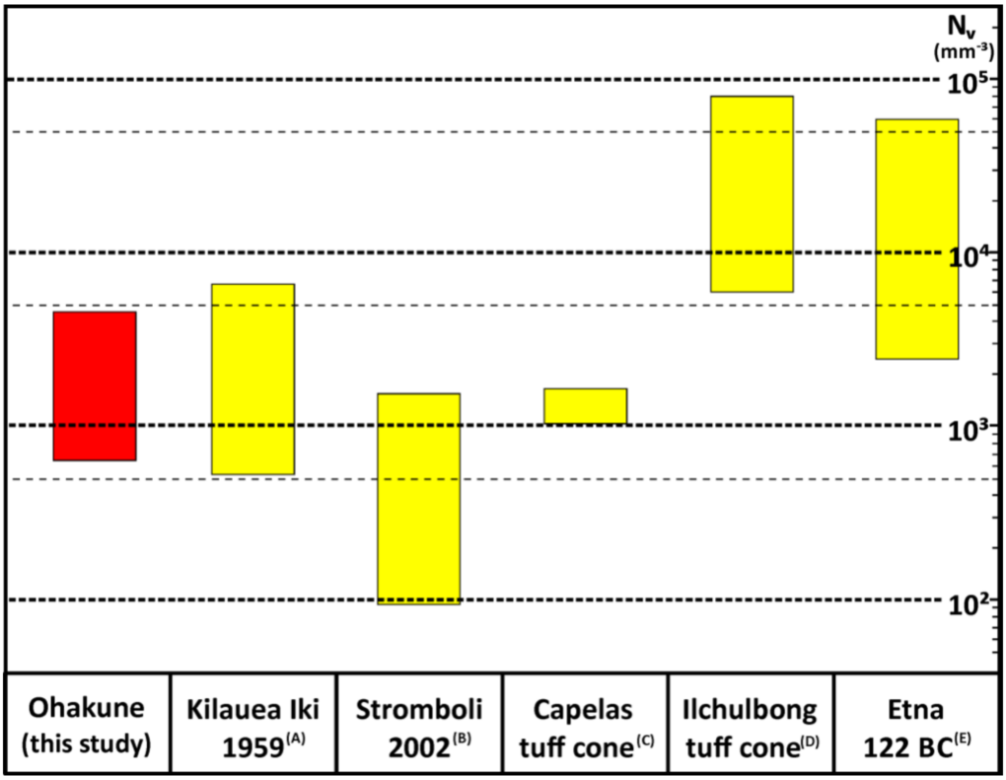

Figure 5.9 Range of OVC bubble number density (N_V) values measured on blocks and bombs from Bb and Bb_A type units in comparison with selected eruptions exhibiting different eruption styles; (A) Stovall et al. (2011);(B) Lautze and Houghton (2007); (C) Mattsson (2010); (D) Murtagh et al. (2011); (E) Sable et al. (2006).

5.7 Petrology, geochemistry and thermobarometry

The fresh block/bomb fragments of the Ohakune andesite are dark grey in colour with inequigranular/hyalopilitic textures, containing 0.1-0.8 cm light green to yellowish, mostly isometric or broken pyroxene and olivine crystals and crystal nodules (Fig. 5.10). Even the densest clasts have visible vesicles with uneven distributions. We determined the major element geochemistry of glass fragments from ash samples as well as of groundmass glass and phenocrysts of bomb/block fragments (Appendix A.5.1). The main observation is that the blocks/bombs groundmass glass results display a restricted compositional range in comparison with ash fragments (Figs. 5.11-13). Harker diagrams of oxide distributions follow trends of depletion in MgO, FeO, and CaO, enrichment of K_2O, and Na_2O, and initial enrichment followed by depletion in Al_2O_3 and Na_2O versus SiO_2 (Fig. 5.11), although there is significant scatter in the low- to intermediate silica range. Glass compositions range from basaltic andesite to rhyolite in the TAS classification, i.e. range to much more evolved compositions than the bulk rock (57% SiO_2) (Hackett and Houghton, 1989). Strikingly, compositions broadly follow an iron enrichment trend in the AFM diagram (Fig. 5.12), atypical for continental arc volcanic products (e.g. Ruapehu compositions, Price et al., 2012) and more characteristic for magmas related to decompression induced melting.

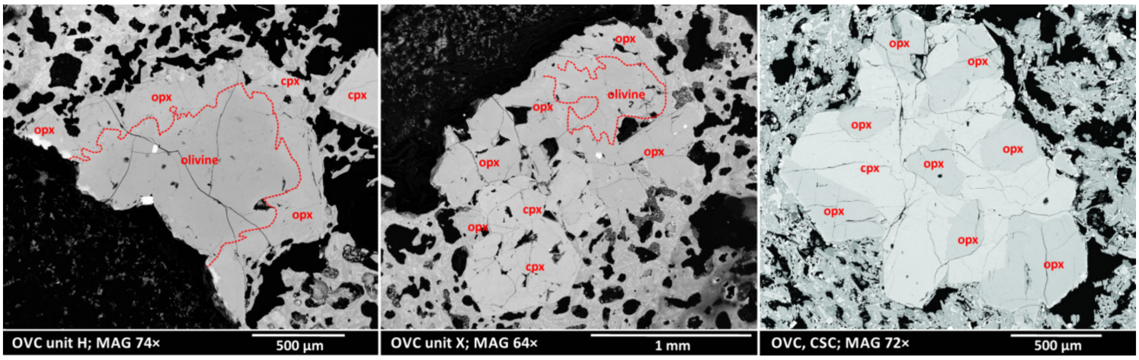

Figure 5.10 SEM images of phenocrysts (antecrysts) from Bb and Bb_A type units showing the hyalopilitic textures and growth relationship between olivine, orthopyroxene and clinopyroxene. Element mapping was executed by EDAX.

We examined compositional variations through time by plotting chemical data from consecutive units (Fig. 5.13). The ash geochemistry exhibits a great compositional variation within all the examined oxides, and its average values show significant fluctuations through time (SiO_2: 62-67 wt %; K_2O: 1.2-2.7 wt %; MgO: 1.5-3.1 wt %). In contrast, the averages of groundmass glass compositions measured from blocks/bombs display comparatively minor variations (Figs. 5.11, 5.13).

Microscopic and SEM imaging indicates that the crystal cargo consists of olivine, clinopyroxene (cpx) and orthopyroxene (opx). The olivine crystals display corona-textured reaction rims due to dissolution followed by opx overgrowth (Zellmer et al., 2016) (Fig. 5.10). Furthermore, touching crystals of cpx and opx are in chemical equilibrium (Fig. 5.10), allowing the calculation of P-T conditions of crystallization (Table 5.2). The groundmass of the rock is usually moderately microlithic with plagioclase laths up to 50-60 µm in size and isometric opx, cpx and olivine microphenocrysts. The groundmass microlite content of the examined samples varies from 15 to 25%.

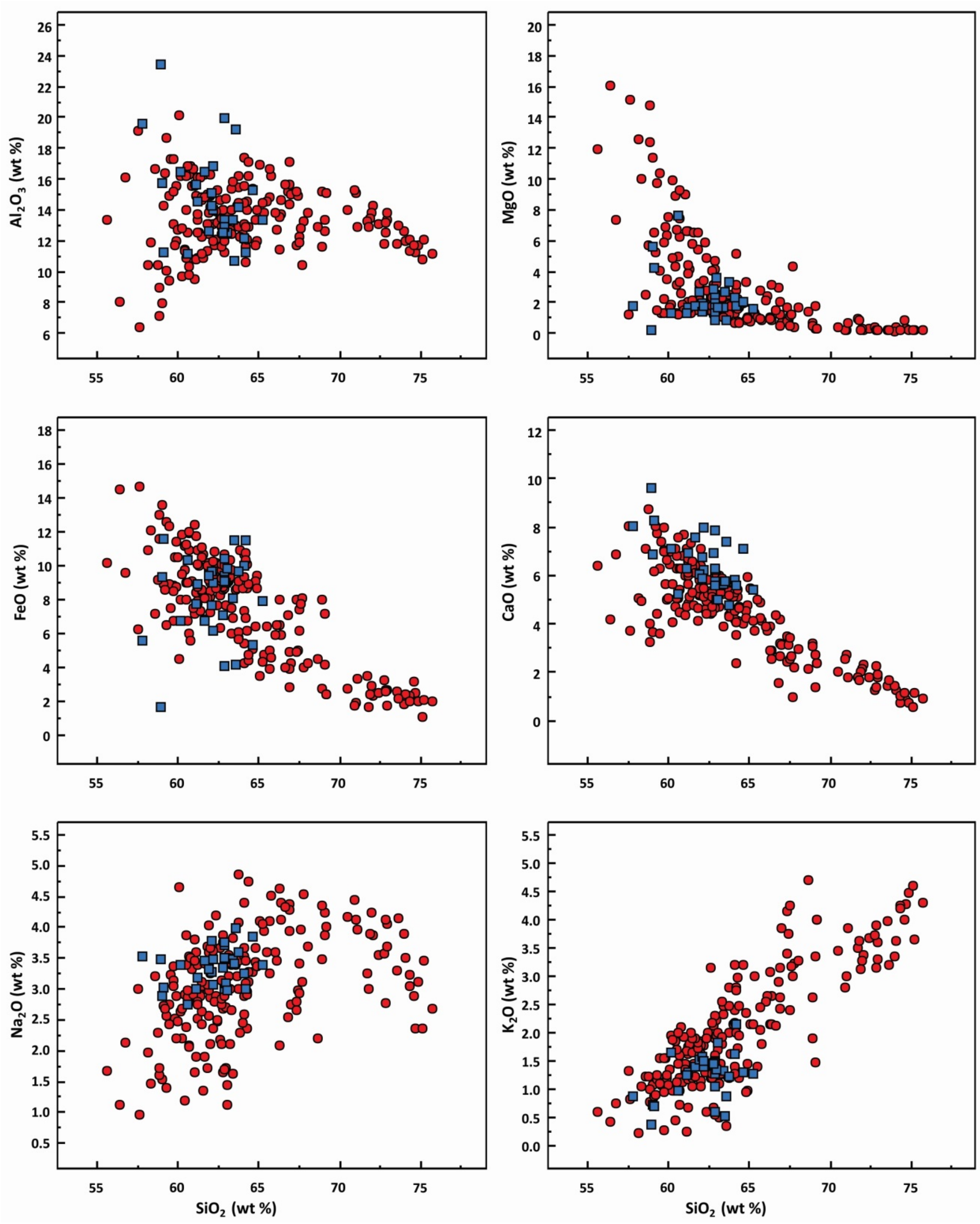

Figure 5.11 Harker diagrams for selected major element oxides normalised to water-free compositions. Red circles represent ash fragments, blue squares represent groundmass glass compositions of blocks and bombs.

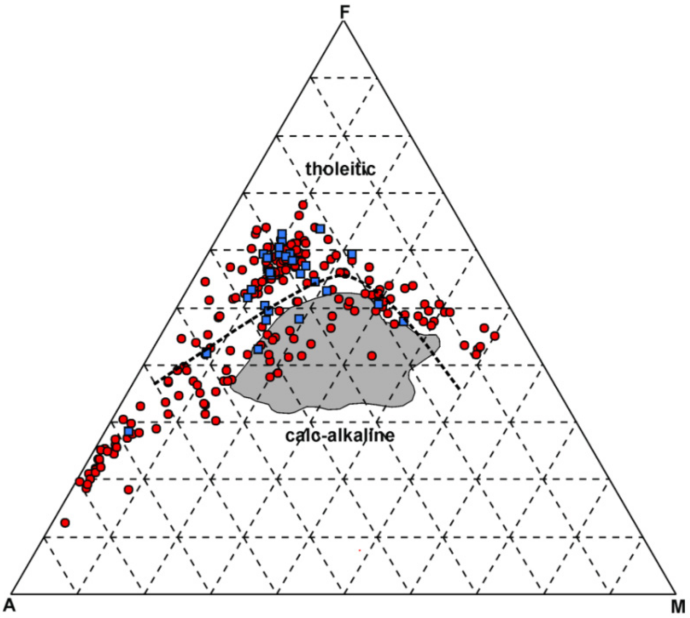

Figure 5.12 AFM diagram shows glass compositions measured on ash fragments (red circles) and groundmass glass of blocks and bombs (blue squares) in comparison with whole rock compositions of Ruapehu volcano (grey field) (Price et al., 2012, e-appendix 10).

Two-pyroxenes geothermobarometry, sampled units	Eqn 36 T (°C)	Eqn 37 T (°C)	Eqn 38 P (kbar)	Observed K_D (Fe-Mg)	Estimated depth (km)
D	1046	1034	5.4	0.981	**18**
D	1041	1052	4.8	0.850	**16**
H	1035	1053	5.3	0.970	**17.8**
X	1043	1036	4.8	0.847	**16**
Cpx-liquid geothermobarometry (Deering et al. 2011)	Eqn 33 T (°C)	Eqn 34 T (°C)	Eqn 31 P (kbar)	Eqn 35 K_D (Fe-Mg)	Calculated depth (km)
Ohakune	1137	1152	6.4	0.281	21.4

Table 5.2 Results of geothermobarometry calculations utilizing Putirka's (2008) two-pyroxene calculations on phenocrysts of bombs and blocks. Earlier calculations (Deering et al., 2011) indicate deeper source region for the erupted magma.

We calculated crystallization temperatures and depth by thermobarometry utilizing Putirka's (2008) two-pyroxene calibrations. Our results yield lower temperatures (1034-1053°C) and pressures (4.8-5.4 kbar) than previous estimates based on cpx-liquid thermobarometry (Table 5.2) (Deering et al., 2011). Using 2.7 g/cm^3 for crustal density (Deering et al., 2011), the two-pyroxene method indicates 16-18 km crystallization depth (Table 5.2).

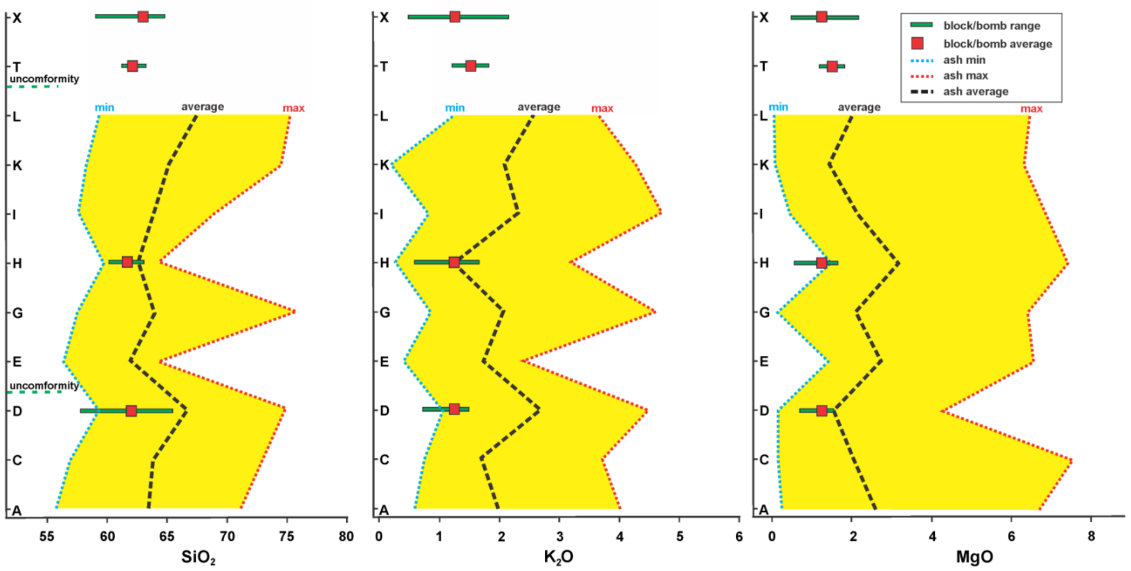

Figure 5.13 Compositional variations of SiO_2, K_2O and MgO of ash (yellow fields) and blocks and bombs through the sequence.

5.7.1 Evaluation of the results of petrology, geochemistry and thermobarometry

The observed iron enrichment trend suggests that magmatism at the OVC is related to decompression-melting with little contribution from the subducting slab. This is consistent with the location of the OVC at the southernmost end of the TVZ at the tip of the southwards propagating extension zone. Further, the relatively minor groundmass glass compositional variations measured from blocks/bombs suggest that the compositional characteristics of the eruptive products are not attributable to multiple magma batches with different chemical compositions. Instead, variations in ash compositions may reflect changes in magma ascent rate accompanied by variations in the degrees of cooling, degassing, decompression rates and resulting microlite crystallization (Cashman and Blundy, 2000). Turning to the phenocryst phases, the OVC andesitic magma may represent a mixture of crystals and melts as a result of polybaric fractional crystallization and magma mixing, similar to other erupted andesitic to dacitic rocks from Tongariro Volcanic Centre (Price et al., 2012). For example, the lack of plagioclase phenocrysts in these intermediate composition eruption products suggests that the nodules and grains of opx, cpx and olivine may represent antecrystic material picked up from a crystal mush of an earlier stalled and cooled magma (e.g. Zellmer et al., 2014). One possible petrogenetic scenario is that this crystal mush is remobilised by intrusion of an andesitic to dacitic melt, which ultimately carries the earlier formed crystals of olivine, opx, and cpx to the surface. Corona textures of the olivines may have formed during mush remobilization at depth. The final crystallization event occurred at shallow (tens to hundreds of meters) depth, forming the microlitic groundmass during the relatively fast magma ascent at the onset of eruption. The calculated crystallization depths are slightly shallower than the previous calculations by Deering et al. (2011) (Table 5.2) yet both results are within the acceptable depth range of a crystal mush zone or magma source (Deering et al., 2011).

5.8 Eruptive volume calculations

The eruptive volumes are essential for understanding the evolution, eruptive styles and related hazards of small-volume volcanoes (Guilbaud et al., 2012; Le Corvec et al., 2013; Kereszturi et al., 2014b; Bebbington, 2015; Németh and Kereszturi, 2015). Monogenetic volcanoes usually have a wide variety of eruptive styles and products as demonstrated by the volcanic sequence of the OVC. To account for this complexity, we employed the eruptive volume scheme used in the Auckland Volcanic Field, New Zealand (Kereszturi et al., 2013). Due to the overall small proportion of lithics in the exposed sequences, we do not expect diatreme structures beneath the edifice, thus we calculate volumes for proximal ejecta rings and scoria cones as well as distal tephra deposits (Fig. 5.14). The edifice volume was calculated from a DTM using a uniformly 585 m asl plane as the pre-eruptive surface, whereas the distal tephra volume was calculated by applying exponential thinning (Pyle, 1989) with the considerations of thinning trends measured within the quarry and thickness and sedimentological observations at distal outcrops. Using our componentry, density, and vesicularity data (Fig. 5.6, Table 5.1) and the earlier density measurement for the central scoria cone (Houghton and Hackett, 1984), we could convert bulk distal tephra and edifice volumes to DRE volumes (Fig. 5.14, Table 5.3), using the method developed by Kereszturi et al. (2013).

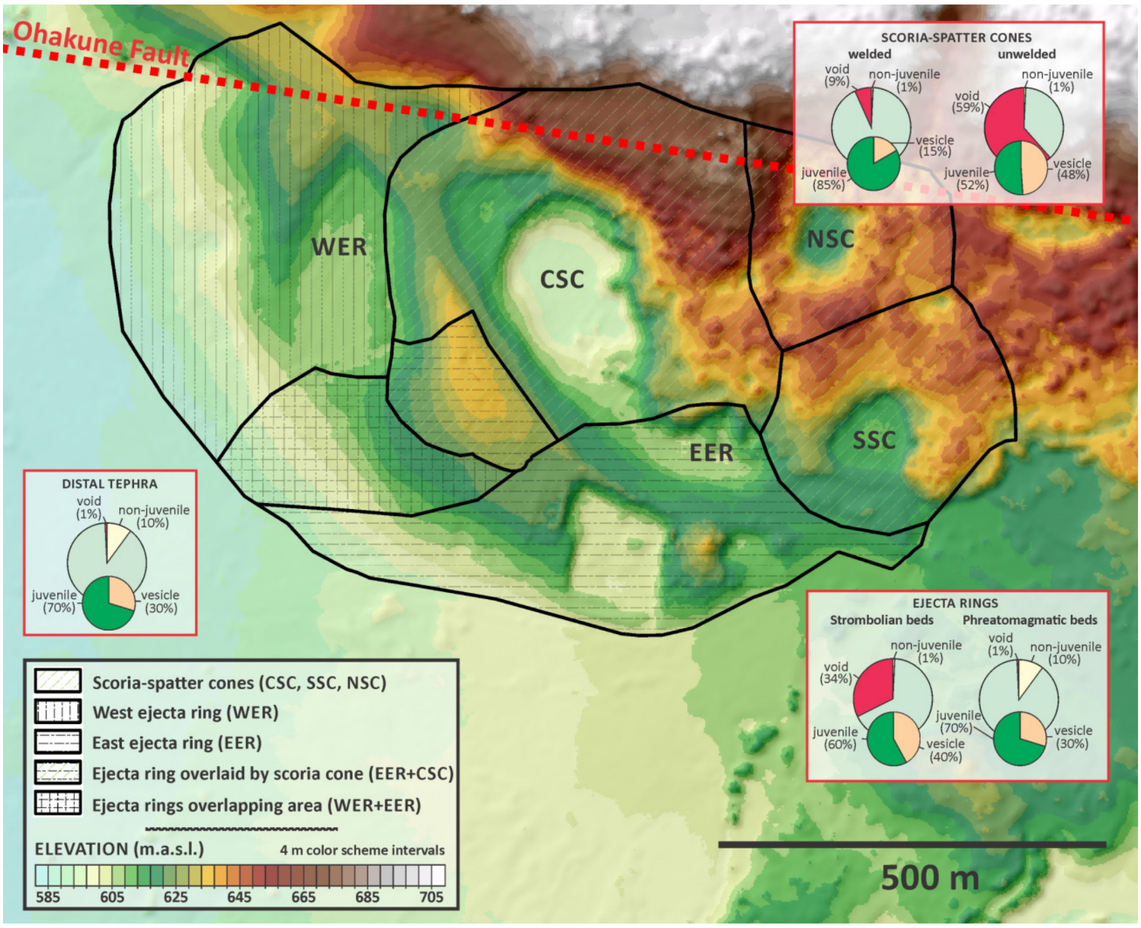
Ohakune Fault
SCORIA-SPATTER CONES
welded
void (9%)
non-juvenile (1%)
vesicle (15%)
juvenile (85%)
unwelded
non-juvenile (1%)
void (59%)
vesicle (48%)
juvenile (52%)
WER
CSC
NSC
EER
SSC
DISTAL TEPHRA
void (1%)
non-juvenile (10%)
juvenile (70%)
vesicle (30%)
EJECTA RINGS
Strombolian beds
void (34%)
non-juvenile (1%)
juvenile (60%)
juvenile (70%)
vesicle (40%)
Phreatomagmatic beds
void (1%)
non-juvenile (10%)
vesicle (30%)
Scoria-spatter cones (CSC, SSC, NSC)
West ejecta ring (WER)
East ejecta ring (EER)
Ejecta ring overlaid by scoria cone (EER+CSC)
Ejecta rings overlapping area (WER+EER)
ELEVATION (m.a.s.l.)
4 m color scheme intervals
585
605
625
645
665
685
705
500 m

Figure 5.14 Delineation of distinct edifices of OVC. The obtained area and thickness values were applied for bulk volume calculations. Pie charts represent the DRE correction scheme applied for volume estimation from the different parts of the volcanic complex (Kereszturi et al., 2013). As the first step of the DRE corrections, the bigger pie charts imply the proportion of juvenile, non-juvenile and interparticle void space. Secondly, the smaller pie charts show the remaining juvenile content was corrected with the available vesicularities.

The obtained 12.36×10^6 m^3 DRE total erupted volume includes 2.99×10^6 m^3 (24.2%) rough DRE distal volume and 9.36×10^6 m^3 (75.8%) edifice DRE volume. It seems that the DRE volume of the phreatomagmatic and magmatic products is broadly equal, but scoriaceous deposits are dominant within the edifices (Fig. 5.4). Due to the morphological differences between the west ejecta ring (WER) and east ejecta ring (EER) (Fig. 5.2), we do not expect significant contribution of Strombolian deposits within the succession of WER. Thus the volume of the WER was only calculated with phreatomagmatic successions. Uncertainties exist surrounding the possible volumes of eroded sequences of the eastern part of the volcanic complex. The calculated distal volume should be considered only as a minimum value due to the small number of distal thickness measurements. The accuracy of topographic data and data availability for pre-eruptive surface determination can also contribute to the uncertainties associated with volume calculations.

	Bulk volume (10^6 m^3)	DRE index	DRE Volume (10^6 m^3)
Central scoria cone (CSC)	8.07	0.487	3.98
South scoria cone (SSC)	3.51	0.208	0.73
North scoria cone (NSC)	3.34	0.208	0.69
West ejecta ring (WER)	3.99	0.45	1.80
East ejecta ring (EER) (Total)	5.12		2.16
EER (magmatic)	*2.38*	*0.39*	*0.93*
EER (phreatomagmatic)	*2.74*	*0.45*	*1.23*
Total Edifice	**24.03**		**9.36**
Distal	4.80	0.623	2.99
Total	**28.83**		**12.36**
Total magmatic	*17.30*		*6.34*
Total phreatomagmatic	*11.53*		*6.02*

Table 5.3 Results of DRE volume estimations for the OVC based on bulk edifice volume calculated from DTM of Ohakune and DRE correction schemes presented at Fig. 5.14.

5.9 Discussion

5.9.1 Fragmentation and eruptive styles

Despite the absence of accretionary lapilli and the rare occurrence of blocky glass fragments, other features of pyroclastic fragments (e.g. glass alteration – palagonitization, aggregates of ash, presence of mud-coating and secondary minerals inside the cavities) is indicative of a hydrovolcanic origin of the ash-rich beds (as evidenced by Ab and Ab_C lithofacies) (Sheridan and Wohletz, 1983; Cioni et al., 1992). Furthermore, sedimentary features such as plastically deformed bomb sags and soft sediment deformations support a water-saturated nature of pyroclastic density currents (Fisher and Schmincke, 1984; Németh et al., 2001). At first glance, the coarser bomb beds (Bb_A and Bb lithofacies) of the ejecta rings show a magmatic (likely Strombolian) origin through their grain size properties (coarse fragments with better sorting) and plastically deformed shapes. However these beds commonly contain cauliflower-shaped bombs (Fig. 5.4), which are usually characteristic of hydrovolcanic fragmentation (Kienle et al., 1980; Fisher and Schmincke, 1984). Moreover the ash fragments of the Bb_A beds show identical features with fragments from the ash beds. The examined vesicle microtexture properties of the largest clasts from the Strombolian beds do not exhibit the typical micro-textural characteristics of Strombolian fragments (Fig. 5.7). The size and shape of vesicles as well as the bubble number density values might reflect an increased degree of cooling and higher viscosities similar to the properties of hydrovolcanic eruptions. It seems that throughout the course of the activity water was abundant, which implies the eruptions were unable to permanently dry out the shallow basement (Lorenz, 1986; Lorenz, 2007). The componentry analyses exhibit small percentages of accidental fragments dominantly from the subsurface laharic deposits, indicating that excavation was minor and the fragmentation likely occurred at very shallow depth. The detected heterogeneities of clast densities in units H and X indicate mingling of degassed dense magma with hotter gas-rich melt within the conduit. This suggests that the ascent rate extensively fluctuated and the stalling degassed upper part was broken through from time to time by fresh magma with varying intensity (Lautze and Houghton, 2007). The higher ascent rates of fresh magma resulted in sustained Strombolian, occasionally Hawaiian eruptions with little influence from water (water to magma ratio around 0.1), while the lower ascent rates dominantly led to phreatomagmatic eruptions with higher water concentrations. The transitions from phreatomagmatic to Strombolian eruptions and vice versa were rapid.

5.9.2 Eruption history

Although the initial craters are highly obscured, the geomorphology, calculated volume and stratigraphy is inconclusive for the existence of a kilometre wide tuff ring (Houghton and Hackett, 1984). In contrast, we envisage an elongated composite ejecta ring around an at least 600 m long eruptive fissure aligned to the Ohakune Fault, similar to several examples such as *Izu-Oshima, Japan* (Sumner, 1998); *Hverfjall eruptive fissure, Iceland* (Mattsson and Höskuldsson, 2011); *Easy Chair, Lunar Crater Volcanic Field, USA* (Valentine and Cortés, 2013); and *Tolbachik, Russia* (Belousov et al., 2015). The activity of the eruptive centre was initiated by hydrovolcanic eruptions characterised by a sustained low eruptive column due to the abundance of surface and groundwater. The resulting ejecta ring was 15-20 m high, 300-400 m wide along the fissure and characterised by dominantly debris jets and fallout deposits interbedded by layers related to wet pyroclastic density currents (Figs. 5.4, 5.15). The subsequent eruptions were localised into widened and disjointed vents usually inducing changes in mass flux within other areas of the vent zone (Valentine and Gregg, 2008). The usual fluctuating pressure conditions and ascent rates (Keating et al., 2008) and the result of alternations of magmatic and phreatomagmatic eruptions may have been facilitated through the increased entry of groundwater into the shallow plumbing system. This, and increasing load on the crater rims could have easily led to the destabilisation of the loose surface deposits and the solidifying dyke margins as well (Gutmann, 2002) as demonstrated by the crater rim subsidence (syn-eruptive faulting) at the quarry (Fig. 5.4). The OVC sequence exhibits the relocation of the active vent(s) within the fissure zone (Fig. 5.4) probably due to the collapse of destabilised areas from time to time. The proximity of the source is clearly implied by the thermal oxidation along the fault (Fig. 5.4) similarly to the welded and agglutinated units of the CSC (Fig. 5.3). The frequent vent-shifting prevented the long term development of a single edifice. Rather, the products were accumulated at the southern margin of the fissure, forming a multisource ejecta ring structure (EER). This was constructed from water-influenced Strombolian bomb beds (Bb, Bb_A lithofacies) alternating with dense and wet pyroclastic surge and fallout deposits (Ab lithofacies). The deposited pyroclasts within the fissure zone were removed by subsequent eruptions leaving a hollow, the smaller pits indicating the area where the dyke intersected the surface (Fig. 5.14). Similar morphological features have been reported from many monogenetic volcanoes within the Auckland Volcanic Field, such as *Crater Hill* (Houghton et al., 1999); and *Three Kings* (Kereszturi et al., 2014b). Because the eastern part of the volcanic complex was eroded by the Mangawhero River, it is difficult to determine if there were any eruptions (possibly small phreatomagmatic blasts) along the eastern extension of the fissure. The late stage evolution was characterised by localization of stable vents producing Strombolian/Hawaiian fountains due to higher ascent rates and decreased water influence, however the axis of the fissure remained unburied indicating the existence of vent-clearing phreatomagmatic blasts along the other part of the fissure (Fig. 5.15).

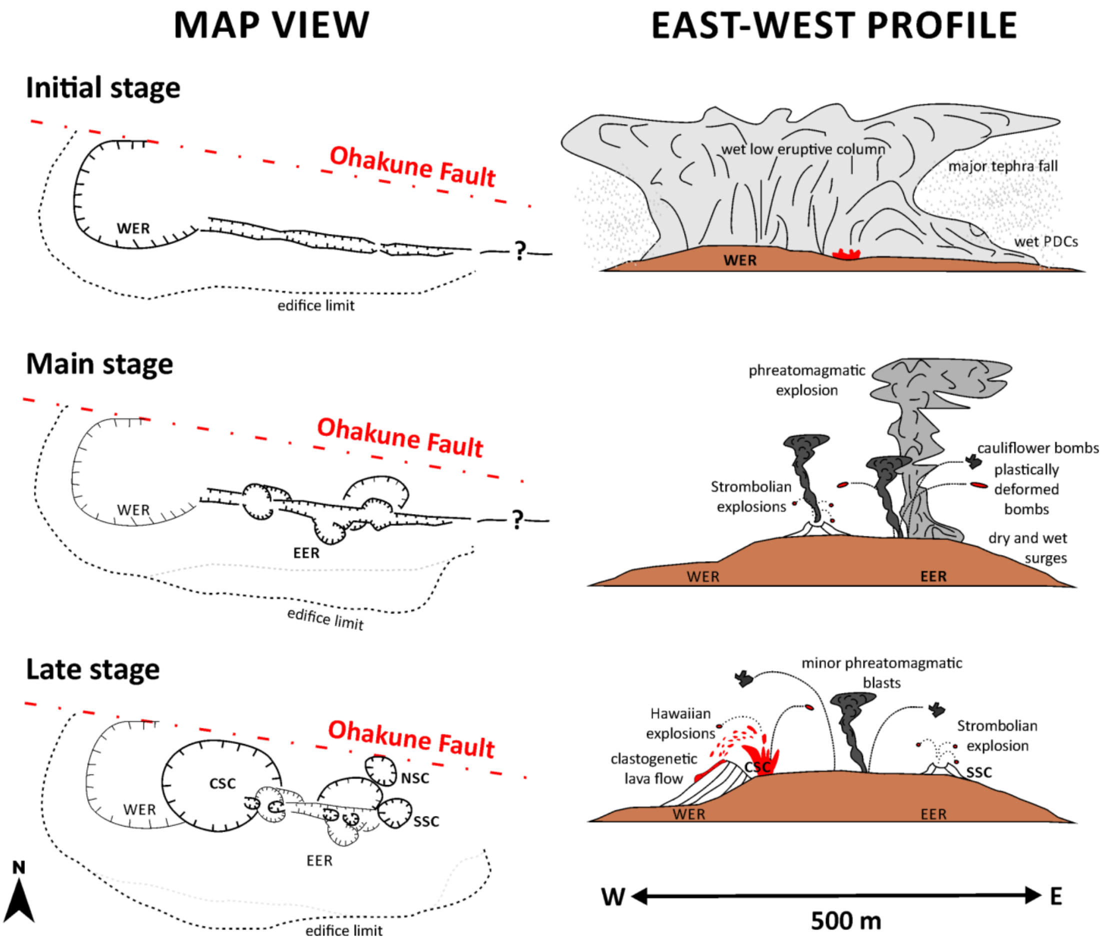
MAP VIEW
EAST-WEST PROFILE
Initial stage
Ohakune Fault
WER
?
edifice limit
wet low eruptive column
major tephra fall
wet PDCs
WER
Main stage
Ohakune Fault
WER
?
EER
edifice limit
phreatomagmatic explosion
cauliflower bombs
Strombolian explosions
plastically deformed bombs
dry and wet surges
WER
EER
Late stage
Ohakune Fault
CSC
NSC
WER
SSC
EER
N
edifice limit
minor phreatomagmatic blasts
Hawaiian explosions
clastogenetic lava flow
CSC
Strombolian explosion
SSC
WER
EER
W
E
500 m

Figure 5.15 Cartoon showing the evolution of facies architecture and eruptive mechanism during the OVC formation (see text for explanation).

5.9.3 Volcanic hazard assessment

The eruptive styles associated with small-volume volcanoes are usually strongly influenced by magma ascent rates (Wilson and Head, 1981; Parfitt, 2004; Valentine and Gregg, 2008) and the availability of external water (Kokelaar, 1986). Despite the lack of direct observations of magma ascent rates, there are various methods for its estimation such as field observations of facies architectures (Houghton et al., 1999), average size of mantle xenoliths (Sparks et al., 1977) and water-content and zonation of olivine crystals (Peslier and Luhr, 2006; Jankovics et al., 2013). The Ohakune sequence exhibits transitions between phreatomagmatic and Strombolian as well as Strombolian and Hawaiian eruptive styles, the latter implying ascent rates varying around 0.1 m/s (Parfitt, 2004) in the case of a point source stabilised vent. The earlier stage fissure or multiple source eruptions could have been characterised by fluctuating high ascent rates coincident with significant water influx and increased water/magma ratios. Near surface ascent rates might have exhibited differences to the lower feeding systems due to guidance of the fault and syn-intrusive extension. We assume an 1 m width for the feeder dyke as an average of observations (Geshi et al., 2010), and note that the facies architecture (Houghton et al., 1999) and possible effects of fault guidance suggest a similar or shorter dyke length for the lower feeding system. Combining, the possible source depth estimated of 18 km obtained by two-pyroxene geothermobarometry with an average ascent rate of approx. 0.1 m/s, we argue that the magma may have reached the surface within 50 hours. Considering the range of ascent rates for the shallow plumbing system (0.01-1 m/s), and the extent of the active vent area, it is possible to calculate effusion rates. This analyses suggests peak effusion rates of 25 m^3/s for the initial hydrovolcanic phase, 8 m^3/s for the late stage Hawaiian fountains and <0.1 m^3/s for the lowest discharge periods. Using the volume calculations and ascent/effusion rates it is possible to estimate the duration of the activity of the OVC. The duration using an inferred discharge rate of 1-2 m^3/s corresponds to a maximum duration of 2.5 to 5 months for the entire event. Even though this duration seems to be rather long for this type of volcanism however the lack of erosional structures throughout the eruptive sequence would suggest a shorter duration. In addition, the OVC erupted from multiple vents, the timing and duration of each vent remains unclear due to scarce outcrops to examine stratigraphic relationships and geochemical characteristics. It is also unclear whether each vent operated simultaneously or were there time gaps between such activities. These features of the OVC have to be studied in more detail in the future.

It is difficult to evaluate if there is any relationship between the OVC’s feeding system and the main conduits of Ruapehu volcano, because the deep structure of southern slope and ringplain of Ruapehu volcano is not known. Magnetotelluric surveys did not propose large scale accumulation of magma shallower than 14 km beneath Ruapehu (Ingham et al., 2009). However, the plumbing system might include the network of small-volume dispersed magma storages in the mid- and shallow crust (Price et al., 2012). Our proposed 16-18 km depth for the accumulation of magma erupted at OVC corresponds to the upper part of mush zones of the heavily intruded lower crust

(Deering et al., 2011). In spite of the analogous petrogenesis of the OVC and some of Ruapehu magmas (Price et al., 2012) we do not expect the OVC to have a closer relationship with the plumbing system of main conduit of Ruapehu than to any of the other three composite volcanoes of the Tongariro Volcanic Centre (Fig. 5.12). On the basis of the available major element oxide data, it appears that the eruptions around Ohakune represent the first precursors of the southward expansion of the andesitic arc of the TVZ, and that the OVC conduit is independent of the main feeder system of Mt. Ruapehu.

5.10 Conclusion

The OVC provides an opportunity to examine an eruptive sequence characterised by alternating eruptive styles. The resulting deposits indicate that the rising magma erupted through multiple vents by fire-fountaining to water-influenced Strombolian explosions alternated with phreatomagmatic blasts. It appears that after the initial vent opening, the most significant controlling factors were the changing vent geometries and variable interaction with external water, while the final phase was characterised by higher effusion rates, which enabled the isolation from the source of external water inducing fire-fountaining eruptions and the generation of short clastogenetic lava flows. This study has revealed that the volcanic architecture of the OVC is much more complex than previously believed, and that the phreatomagmatism was constantly present during its activity. This study indicates that the active vents can be unstable and abrupt changes in eruption location (likely influenced by faults) and eruption styles can occur, significantly increasing the hazard of such small-volume eruptions. The duration of several months of such events is also significant in terms of volcanic hazards and considerably longer than previously considered at OVC. It is believed, there is a very small likelihood of a future volcanic event in the same location yet for future similar eruptions in the southern TVZ (south of Ruapehu) they would have a similar duration under the same tectonic influences. The eruptive behaviour of the OVC is also considered typical for future monogenetic eruptions within the other parts of Taupo Volcanic Zone.

Chapter

6

Chapter 6 presents the first results from a newly discovered high–alumina basalt occurrence in the vicinity of Puketerata Volcanic Complex.

This chapter is based on a published journal paper:

Kósik, S., Németh, K., Procter, J.N. and Zellmer, G. 2017: Maar-diatreme volcanism relating to the pyroclastic sequence of a newly discovered high–alumina basalt in the Maroa Volcanic Centre, Taupo Volcanic Zone, New Zealand. Journal of Volcanology and Geothermal Research, 341: 363–370.

Statement of contribution (DRC16 form) is at Appendix D

Chapter 6 – Maar-diatreme volcanism relating to the Te Hukui Basalt

Preamble

This chapter is published as a short communication because it was aimed to report as quickly as possible the previously unknown basaltic succession of the Te Hukui. Thus, neither its extents nor the details of technical information, description of data collection and supporting photo documentation are comparable to the other three chapters (Chapters 5, 7-8) presented as case studies for eruption scenarios for the small-volume volcanism of the TVZ. In spite of many uncertain aspects of the evolution of the Te Hukui volcano need to be explored, the characteristics of the examined pyroclastic deposits display clearly the most dominant eruptive processes. Along with late stage Strombolian eruptions, the volcanic activity of the Te Hukui was dominated by phreatomagmatic activity characterised by deep-seated explosiove interaction between magma and groundwater resulting the excavation of previously unknown basement rocks. Hence, this eruption contributes greatly to the inventory of possible eruption scenarios of the volcanism of the TVZ. This preamble is aimed to provide supplementary images and desctiptive materials to support the interpretations.

The locality and the characteristics of exposures

So far two outcrops identified at both sides of the Te Hukui stream (Figs. 6.P.1A and 6.1b) exposing the pyroclastic sequences of the Te Hukui eruption. On the left side of the stream the deposits are underlain by a pumice-bearing lapilli tuff. Here the maximum observed thickness of the sequence is 9 m at a 10 m section of the 40 m long exposure (Fig. 6.P. 1B). On the other side of the stream in a roadcut there is a 30 m long and 1-2 m heigh exposure of the Te Hukui sequence. The lowermost exposed layers represent the polymict country rock breccia of unit B (Figs. 6.2 and 6.3) at about 5 meter lower elevation than on the other side of the stream. Due to dip angle of the deposits the overall exposed thickness of the deposits exceeds 10 m (Fig. 6.P. 1C). The major difference between the two localities is that they represent different distance from the inferred crater margins. This is manifested in the dominant reworking processes, such as the epiclastic layers formed by mass movements on the left bank of the stream, whereas the outcrop on the right bank is dominated by fluvial reworking.

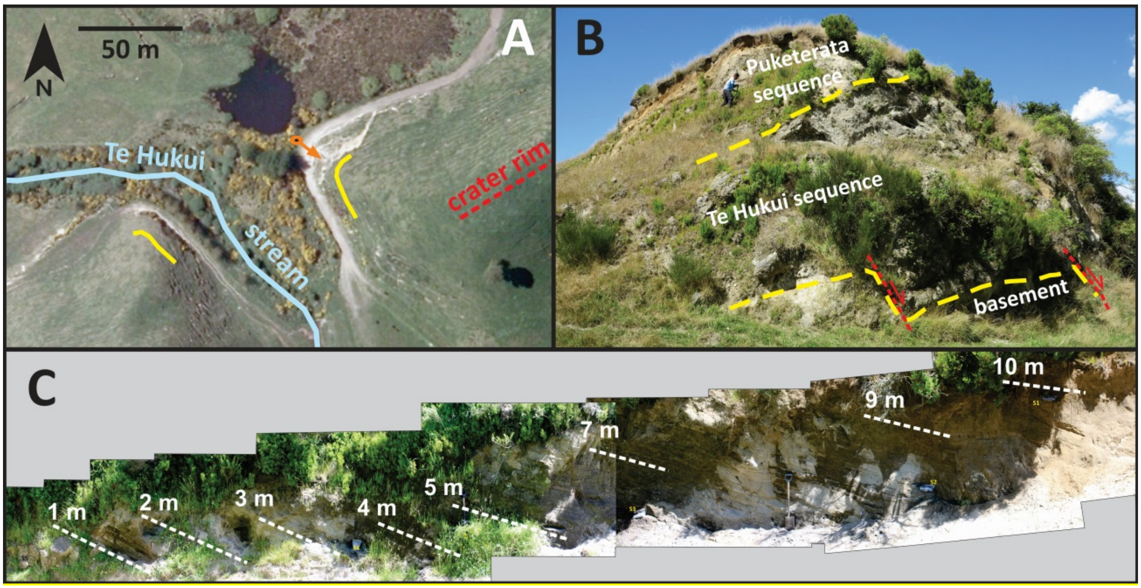

Figure 6.P.1 A – Locations and exposures of the Te Hukui sequence (yellow lines). See Fig. 6.1 for the location in its broader environment. Orange arrow indicates the viewpoint of B. B – Overview of the type locality of the Te Hukui sequence on the left bank of Te Hukui stream. C – Roadcut exposure of the Te Hukui sequence on the right bank of the Te Hukui stream (full size panoramic image along with further supporing pictures are in Appendix A.6.1).

Materials and methods

Besides the field observations, multiple pyroclastic/epiclastic beds were sampled. Uncemented samples were hand-sieved for grain size distribution and componentry analysis. Thin sections were made from two dense juvenile/cogenetic lithic fragments of basalt. The thin sections along with selected ash fractions were examined by light and Scanning Electron Microscopy at Massey University. X-ray elemental mapping of thin sections were conducted using an energy dispersive X-ray spectrometer (EDS; Oxford X-Max 150) installed on the FE-SEM at Hokkaido University in Sapporo, Japan, employing a 15 keV electron beam probe with current of 13 nA. Two whole-rock major and trace element analyses were carried out from both cogenetic lithic and scoriaceous juvenile fragements by XRF at the University of Waikato in Hamilton.

6.1 Introduction

Most of the basalts of the central part of the TVZ are considered high-alumina basalts (HAB) (Kuno, 1960) originating from partial melting of the depleted upper mantle (Cole, 1973; Graham et al., 1995). Basaltic volcanism is considered to be only a small portion of the total volume of volcanic material erupted from the TVZ, but it is ubiquitous across the TVZ (Houghton et al., 1987; Wilson et al., 1995; Hiess et al., 2007). Basaltic volcanism plays an important role in the generation of rhyolites and also in triggering silicic eruptions (Graham et al., 1995; Leonard et al., 2002). The rise of basaltic dykes is most likely controlled by extensional tectonism (Gamble et al., 1990) whereas the eruptive vents are linked to major faults and often indicate fissural activity (Hiess et al., 2007). Eruptive styles range from effusive lava to basaltic Plinian activity (Houghton et al., 1987; Brown et al., 1994; Sable et al., 2009). Basaltic eruptions occurring at locations such as *Kaiapo* and *K-Trig* (Brown et al., 1994), *Acacia Bay* (Wilson and Smith, 1985), and *Kinloch* (Matheson, 2010) (Fig. 6.1) demonstrate the effects of magma/water interaction in or close to lake environments. The available data on other known occurrences of mafic deposits in the TVZ (e.g. *Ben Lomond, Marotiri, Kakuk*i) (Fig. 6.1) also point to phreatomagmatic phases during their evolution, but they are considered to have been dominated by less energetic, predominantly Strombolian-style eruptions (Wilson et al., 1986; Houghton et al., 1987). Detailed field work at the silicic Puketerata Volcanic Complex (Kósik et al., 2016a) has led to the discovery of a previously unknown basaltic rock association characterised by ~50% of SiO_2 (Fig. 6.1). The chaotically dipping contacts of stratified tuff and lapilli tuff, massive lapilli tuff and polymict country rock breccia indicate that various styles of proximal deposition took place on a steep slope. This kind of deposition is distinctive for diatremes, which typically evolve as a result of the excavation of the country rocks by deep-seated phreatomagmatic eruptions, leading to syn- and post-eruptive sedimentation within the crater (White and Ross, 2011; Valentine and White, 2012). The basaltic deposits have been exposed by the excavation of the later rhyolitic eruption of Puketerata, which indicates a long erosional period between the formation of basaltic maar(s) and the Puketerata eruption. Phreatomagmatism also seems to be the dominant process for small-volume eruptions around Puketerata and other parts of the Taupo-Whakamaru area (Fig. 1).

6.2 Geological background

Maroa Volcanic Centre (MVC) is located at the NE quadrant of Whakamaru Volcanic Centre (WVC), which was the source of at least 2200 km^3 DRE ignimbrite at ~350 ka (Downs et al., 2014b; Gravley et al., 2016). In the south, the WVC overlaps with the younger Taupo Volcanic Centre, which sourced two climactic eruptions associated with caldera formations at 25.4 and 1.8 ka (Wilson and Walker, 1985; Vandergoes et al., 2013). Early activity of the MVC was characterised by vigorous explosive activity with the eruption of locally distributed, relatively small-volume ignimbrites (e.g. Putauaki, Orakonui) and isolated lava domes from 305 to ~250 ka (Leonard, 2003). Volcanism at Maroa culminated between 251 and 222 ka with the emplacement of the majority of the domes of the Maroa Western (MWC) and Eastern Complexes (MEC) (Fig. 6.1). Subsequent activity formed mostly smaller silicic dome complexes and isolated lava domes and flows, characterised by decreasing recurrence time and decreased volumes from individual eruptions (Leonard, 2003). The 16.5 ka Puketerata Volcanic Complex is the youngest volcano of the Maroa system and erupted along a 2.5 km long fissure parallel to the Orakeikorako Fault (Brooker et al., 1993; Kósik et al., 2016a). The initial maar-forming phase was followed by emplacement of two lava domes accompanied by phreatomagmatic activity (Kósik et al., 2016a).

Compared with rhyolitic eruptions, basaltic volcanic activity of the Taupo-Whakamaru area is insignificant, representing less than 0.1% volume of the total erupted material (Wilson et al., 1995), however petrological features of rhyolitic rocks indicate that mafic magmas have a vital role in the evolution of silicic magmas (Houghton et al., 1987; Leonard et al., 2002). The available stratigraphic evidence indicates that basaltic eruptions occurred between 200 and 10 ka within the Taupo-Whakamaru area (Wilson et al., 1986; Matheson, 2010).

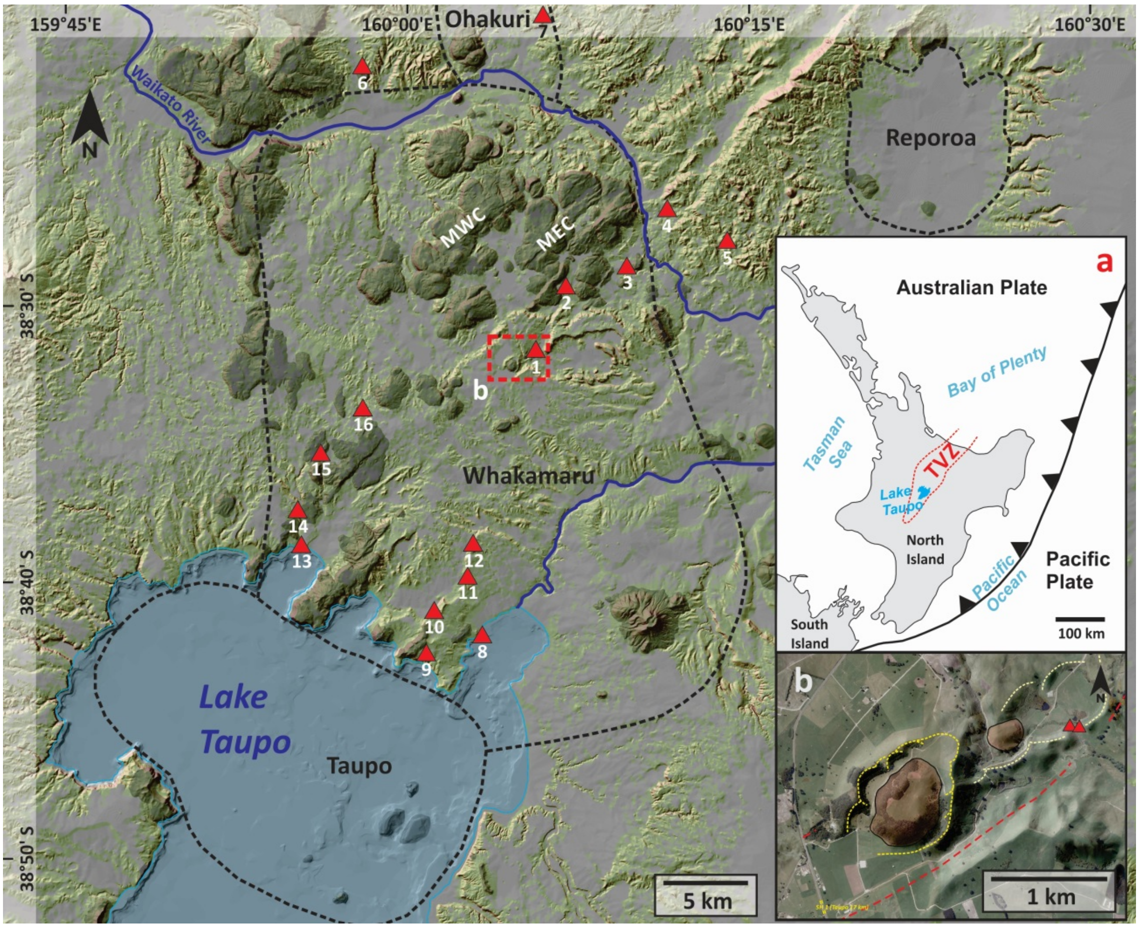
159°45'E
160°00'E
Ohakuri
160°15'E
160°30'E
Waikato River
N
Reporoa
MWC
MEC
38°30' S
38°40' S
38°50' S
b
Whakamaru
Lake Taupo
Taupo
5 km
1
2
3
4
5
6
7
8
9
10
11
12
13
14
15
16
a
Australian Plate
Bay of Plenty
Tasman Sea
TVZ
Lake Taupo
North Island
Pacific Plate
Pacific Ocean
South Island
100 km
b
N
1 km

Figure 6.1 Spatial distribution of the basaltic vents within the Whakamaru-Taupo area as displayed on a shaded slope map derived from an 8 m DEM (LINZ - Land Information New Zealand, 2012). Shaded areas represent the edifices of silicic lava domes. Basaltic vents: 1 – Te Hukui, 2 – Tatua, 3 – Kakuki, 4 – Akatarewa Stream, 5 – Mangamingi Road, 6 – Ongaroto, 7 – Trig 8543/Matapan, 8 – Acacia Bay, 9 – Pekanui, 10 – Kaiapo, 11 – K-Trig, 12 – Punatekahi, 13 – Kinloch, 14 – Otaketake Stream, 15 – Marotiri, 16 – Poihipi/Ben Lomond. Caldera margins with black dashed line after Houghton et al. (1995a). Inset maps: (a) shows the geographic position of TVZ; (b) red triangles indicate the location of Te Hukui basalt exposures in relation with the architecture of the Puketerata Volcanic Complex (shaded structures are lava domes of Puketerata, yellow and white dashed lines show the rim of ejecta ring and maar craters, red dashed line represents the Orakeikorako Fault) (Kósik et al., 2016a).

6.3 Stratigraphy and sedimentology

The newly discovered basalt (Te Hukui Basalt – suggested stratigraphic name) is exposed on both sides of the Te Hukui Stream, where the stream cuts across the southeastern side of the crater wall of Puketerata (Kósik et al., 2016a) (Fig. 6.1b). At the left bank of the stream (38°32'41.15"S; 176° 4'11.73"E) the basaltic deposits are underlain by the ignimbrite of the Orakonui Formation (Brooker et al., 1993). The lowest 10-40 cm of the Te Hukui sequence is a well-sorted strongly cemented and altered lapilli unit (**A**) exhibiting yellowish-brownish discoloration. This is followed by an at least 5 m thick matrix-supported breccia unit with a sharp basal erosional contact (**unit B**). The breccia is characterised by mostly angular variably-altered blocks up to 40 cm across, set within a weathered light grey ash (Figs. 6.2a, d). The lithic fragments of the breccia comprise ignimbrite of the basement (Fig. 6.3b) and at least five different types of silica-rich extrusive rocks (Fig. 6.3a) which are neither similar to the immediate basement nor to the vesiculated basalt lithics found within the upper part of the sequence. Four faults dipping westward are visible within the 25 m long section of the breccia, with throws ranging between 30 and 150 cm. The subsequent unit (**C**) is an approximately 1 m thick, poorly-sorted and strongly-cemented lapilli tuff with lithic clasts up to 2-3 cm in size, including rare basaltic fragments and pumices and lithic clasts of the basement (Fig. 6.4a), which were most likely deposited from dense pyroclastic density currents (PDCs). The pyroclastic flow unit is overlain by a 90 cm thick stratified unit (**D**) with alternating light grey coloured, poorly-sorted PDC beds and better sorted layers dominated by dark grey vesiculated coarse ash and fine lapilli (Fig. 6.2b). The uppermost parts of the sequence have undergone slumping characterised by variably inclined parts of moderately-sorted beds comprising loose dark grey basaltic juvenile fragments and light grey rounded clasts of the basement alternating with finer-grained, more cohesive layers with cross-bedding structures (**unit F**), and lapilli tuff layers with similar textures to unit C without strong cementation (**unit E**) (Figs. 6.2b, e). The average grain size of the well-sorted beds is coarse ash with rare varyingly vesiculated basaltic lithic clast up to 5-6 cm in size. About 90% of the fragments of these beds are basaltic ash and scoria. The larger (-1.5 to -3.5 phi size) scoriaceous fragments have ragged, angular, rarely slightly fluidal shapes with enclosed accidental fragments and crystals (Fig. 6.4b). About 30% of ash indicates spherical vesicles with varying width of vesicle walls (Figs. 6.4c-d). The rest of the particles comprise basaltic ash with low vesicularities, crystals, and rhyolitic ash with pipe vesicles (Figs. 6.4c-d). The Te Hukui sequence is overlain by a paleosol which clearly separates it from the overlying rhyolitic pyroclastic deposits related to Puketerata activity.

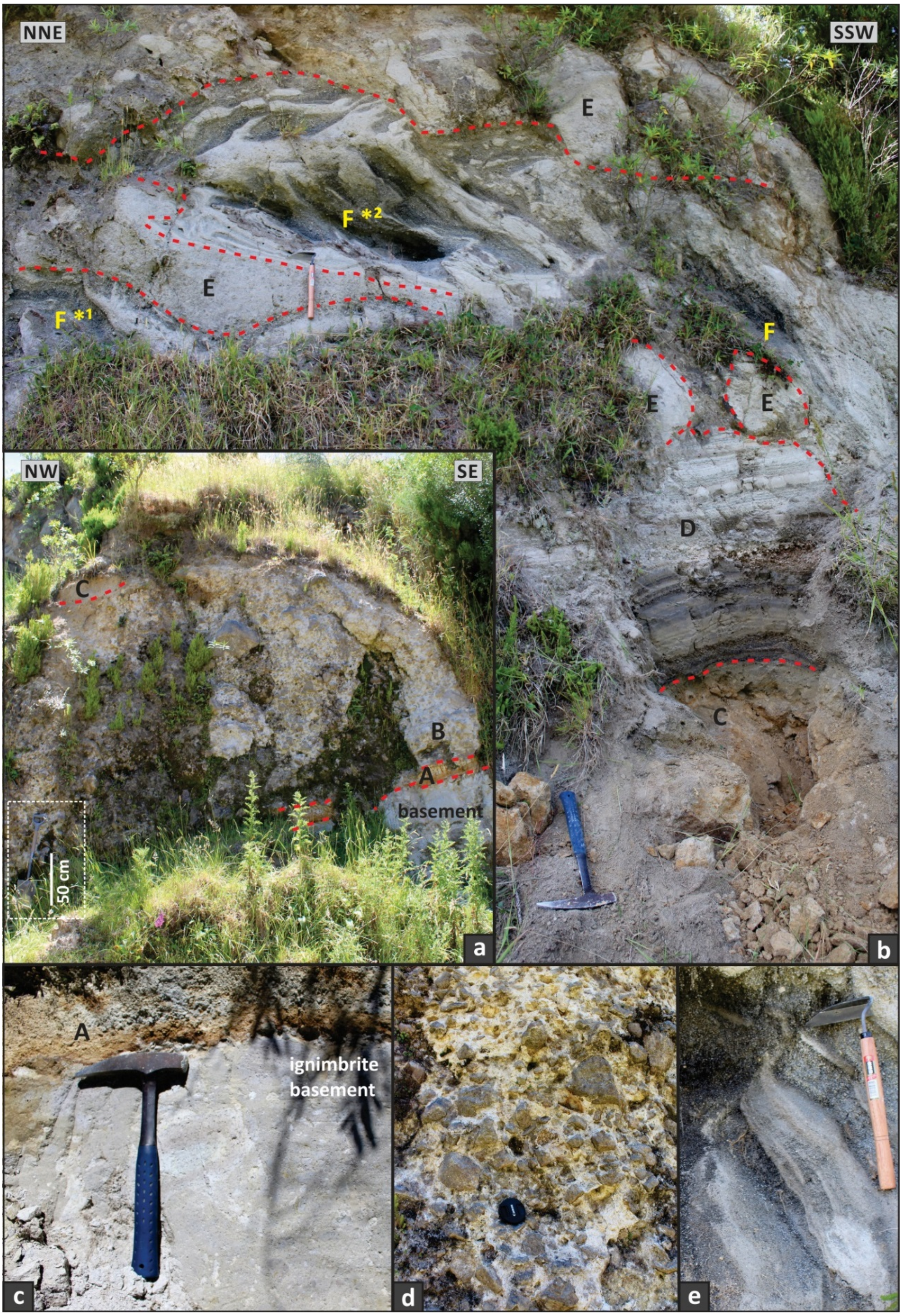
NNE
SSW
E
F *2
E
F *1
F
E
E
D
C
NW
SE
C
B
A
basement
50 cm
a
b
A
ignimbrite basement
c
d
e

Figure 6.2 Lower (a) and upper (b) section of Te Hukui Basalt at the E side of the Te Hukui Stream; (c) indicates unit A and its contact with the basement Orakonui ignimbrite; (d. massive polymict breccia of unit B; (b) and (e) show the topmost part of the sequence with variously inclined units of moderately to well-sorted coarse ash and poorly-sorted fine ash layers (unit F).

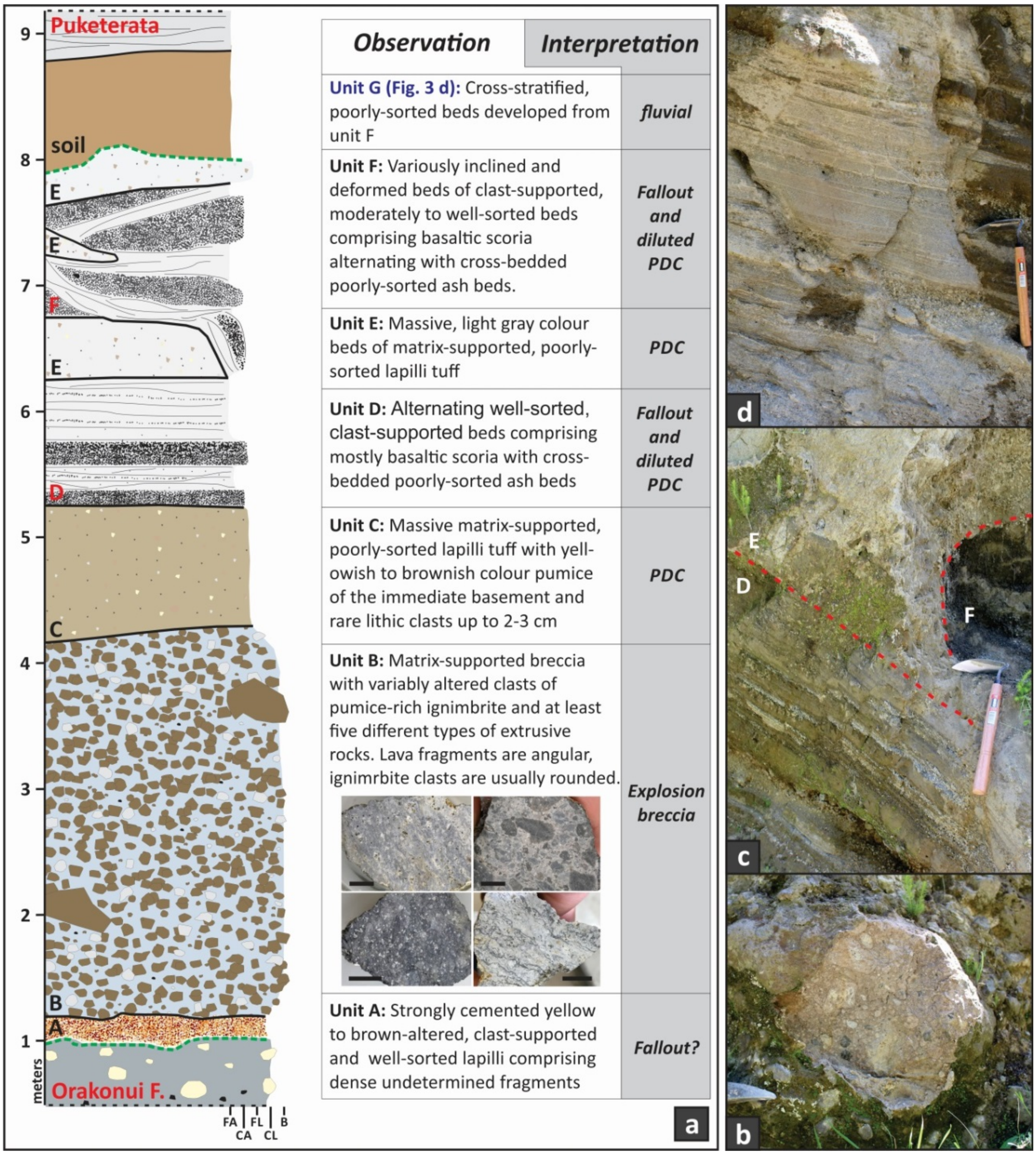

Observation	Interpretation
Unit G (Fig. 3 d): Cross-stratified, poorly-sorted beds developed from unit F	*fluvial*
Unit F: Variously inclined and deformed beds of clast-supported, moderately to well-sorted beds comprising basaltic scoria alternating with cross-bedded poorly-sorted ash beds.	*Fallout and diluted PDC*
Unit E: Massive, light gray colour beds of matrix-supported, poorly-sorted lapilli tuff	*PDC*
Unit D: Alternating well-sorted, clast-supported beds comprising mostly basaltic scoria with cross-bedded poorly-sorted ash beds	*Fallout and diluted PDC*
Unit C: Massive matrix-supported, poorly-sorted lapilli tuff with yellowish to brownish colour pumice of the immediate basement and rare lithic clasts up to 2-3 cm	*PDC*
Unit B: Matrix-supported breccia with variably altered clasts of pumice-rich ignimbrite and at least five different types of extrusive rocks. Lava fragments are angular, ignimrbite clasts are usually rounded.	*Explosion breccia*
Unit A: Strongly cemented yellow to brown-altered, clast-supported and well-sorted lapilli comprising dense undetermined fragments	*Fallout?*

Figure 6.3 Stratigraphic log of the eastern outcrop of Te Hukui sequence (a) with images of accidental lithic fragments of unit B (scales represent 1 cm), and characteristic sections from the western outcrop (b-d); (b) shows a ~50 cm ignimbrite block from unit B, (d) indicates the uppermost part of western outcrop comprising of reworked deposits accumulated near the bottom of the Te Hukui crater, intersected by a listric normal fault.

At the right side of the stream (W outcrop: 38°32'42.43"S; 176° 4'8.94"E) only the uppermost part of the Te Hukui breccia is visible (Fig. 6.3b), and the subsequent 3 m show similarities with the upper sequence of the eastern outcrop (Fig. 3c). The bottom 1 m of the upper sequence (of at least 6 m thickness) is poorly exposed, but the upper part is characterised by cross-stratified lensoidal layers of coarse ash to lapilli and few mm to circa 1 cm thick layers of fine ash dipping to the NW (Fig. 3d). At the SE end of the section (nearer to the breccia), the dip angles are higher than at the NW end of the outcrop, with dip directions to the west. Listric normal faulting was observed at the western part of the outcrop, dipping towards the current depression (Fig. 6.3d).

6.4 Petrography and geochemistry of the Te Hukui Basalt

A 6 cm sized vesicle-rich comagmatic lithic fragment was collected from unit F for petrological investigation, which was complemented by whole rock geochemical characterization of an additional comagmatic lithic clast and hand-picked scoriaceous lapilli fragments (Fig. 6.4b) from two distinct beds of unit F (indicated by asterisks, Fig. 6.2b). The lithic fragments are dark grey in colour with varying vesicular to micro-vesicular textures (Fig. 6.4e). The spherical-shaped vesicles are up to 2 mm in diameter, displaying rare coalescence (Figs. 6.4g-h). The basalt is porphyritic, with 55-60% phenocryst and microphenocryst content (Figs. 6.4g-h). Phenocryst phases mostly consist of euhedral plagioclase, clinopyroxene, olivine, and rare glomerophorphyritic aggregates of mostly subhedral crystals of the same mineral association (Fig. 6.4f). Microphenocrysts are mostly lath-shaped plagioclase feldspars. The groundmass is fully crystallised with plagioclase, clinopyroxene, olivine and opaque phases (Figs. 6.4g-h). Plagioclase phenocrysts have a maximum size of 2 mm ranging down to microphenocryst sizes. The larger grains are tabular in shape, while lath shapes are more common for smaller crystals. Larger plagioclase grains show a wide diversity in zonation patterns: (1) Na-rich resorbed core, Ca-rich rim (Fig. 6.4i); (2) sieve-textured, resorbed Na-rich core, Ca-rich rim (Fig. 6.4j); (3) sieve-textured core without visible resorption and oscillatory zoning outside the core; (4) resorbed Na-rich core and oscillatory zoned rim; (5) Na-rich core with Ca-rich and Na-rich overgrowths and a Ca-rich rim; and (6) Na-rich plagioclase without zoning and characterised by distinctive extinction angles occurs rarely. Clinopyroxenes are usually 0.8 to 0.2 mm in size without any zonation or resorption. Olivine phenocrysts always have a thin resorption rim. Most commonly their size is between 0.3 to 0.1 mm, and oscillatory zoning is sometimes visible by SEM within the smaller grains. Element mapping of larger plagioclases also indicates Ca-rich rims and Na-rich cores, with some crystals having multiple Ca-rich zones overgrown on Na-rich cores and zones (Figs. 6.3k-l).

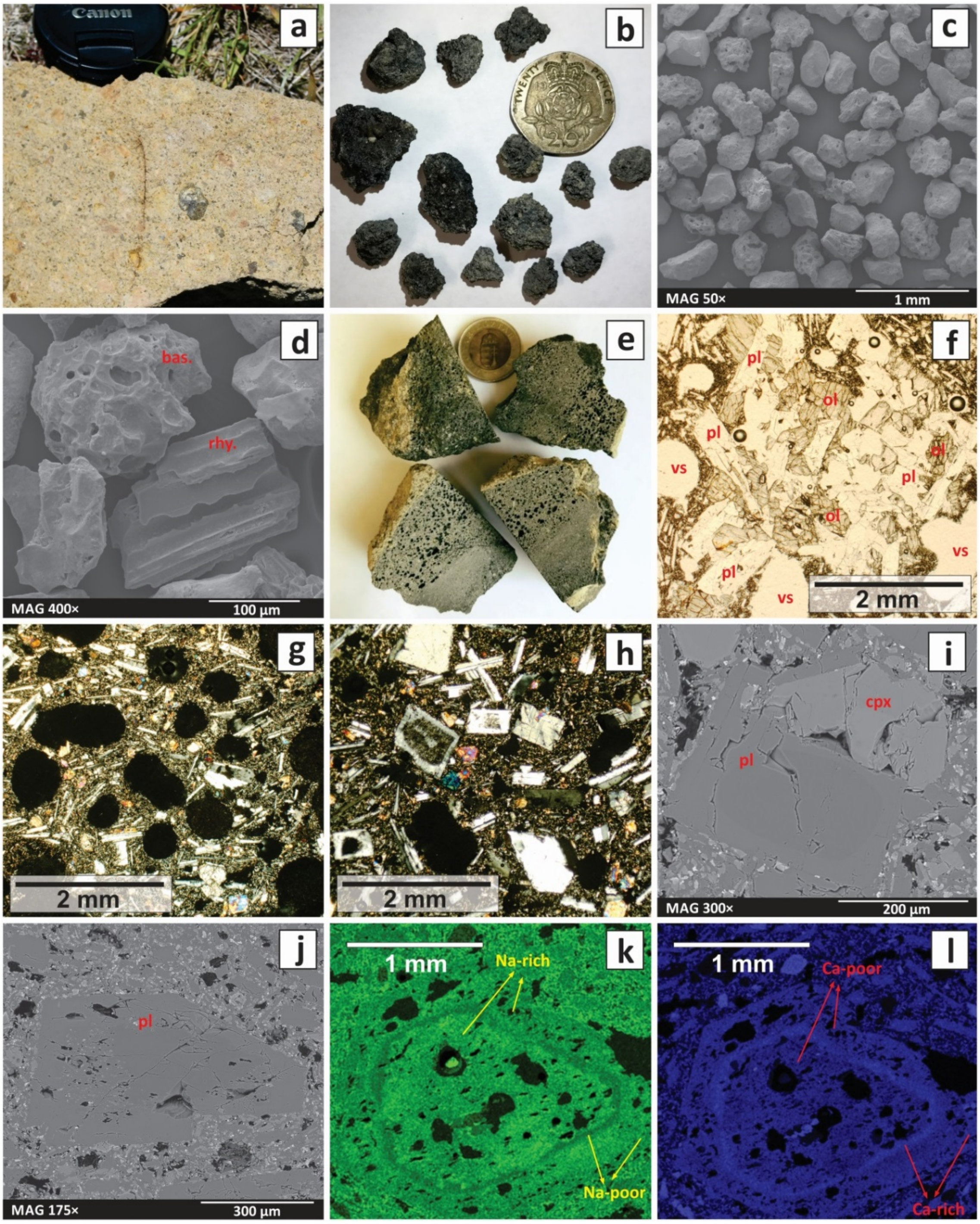
a
b
c
MAG 50×
1 mm
d
bas.
rhy.
MAG 400×
100 µm
e
f
pl
ol
pl
vs
ol
pl
ol
vs
pl
vs
2 mm
g
2 mm
h
2 mm
i
cpx
pl
MAG 300×
200 µm
j
pl
MAG 175×
300 µm
k
1 mm
Na-rich
Na-poor
l
1 mm
Ca-poor
Ca-rich

Figure 6.4 Grain morphology and petrographic characteristics of the Te Hukui Basalt; (a) slightly cemented lapilli tuff of unit C; (b) grain morphology of -2.5 - -3.5 phi size scoriaceous juvenile fragments from unit F; (c) grain morphology of bulk 2 phi fragments from unit F, (SEM image); (d) typical morphology of 3 phi size basaltic juvenile and accidental rhyolitic fragments, (SEM image); (e) vesicle textures of lithic clast with two types of vesicularity; (f) crystal nodule with plagioclase (pl) and olivine (ol) crystals; (g-h) groundmass textures, vesicle shapes with predominantly lath shaped plagioclase crystals, cross polarised light; (i) SEM image of clinopyroxene (cpx) and plagioclase crystal with resorbed Na-rich core; (j) SEM image of plagioclase crystal with Na-rich spongy cellular core; (k-l) Na and Ca element map of zoned plagioclase crystal captured by field emission SEM (Hokkaido University).

		Te Hukui *1 (lithic A)	Te Hukui *1 (lithic B)	Te Hukui *1 (S.1 scoria)	Te Hukui *2 (S.2 scoria)	Tatua (Hiess et al. 2007)	Ben Lomond (Hiess et al. 2007)
SiO_2	(%)	50.25	49.78	51.94	52.08	50.33	49.65
TiO_2	(%)	1.26	1.26	1.22	1.30	1.31	1.14
Al_2O_3	(%)	16.79	16.95	17.07	17.16	17.09	17.95
Fe_2O_3 (T)	(%)	10.24	10.25	9.97	9.97	10.36	10.9
MnO	(%)	0.17	0.17	0.17	0.17	0.17	0.18
MgO	(%)	6.59	6.73	6.14	6.17	6.21	5.78
CaO	(%)	10.69	10.61	9.98	9.86	10.34	9.48
Na_2O	(%)	3.07	3.16	3.06	2.90	3.18	2.64
K_2O	(%)	0.43	0.44	0.59	0.56	0.41	0.32
P_2O_3	(%)	0.23	0.24	0.23	0.22	0.24	0.17
LOI	(%)	0.30	1.84	0.70	1.00	0.44	2.07
Total	(%)	100.02	100.02	101.06	101.38	100.08	100.28
Sc	(ppm)		29		32		
V	(ppm)		239		226	240	266
Cr	(ppm)		81		52	29	38
Co	(ppm)		35		34		
Ni	(ppm)		41		32	27	24
Cu	(ppm)		23		41		
Zn	(ppm)		78		81	82	89
Ga	(ppm)		18		19	18	18
As	(ppm)		5		5		
Rb	(ppm)		12		18	2	4
Sr	(ppm)		307		295	335	296
Y	(ppm)		23		27	29	34
Zr	(ppm)		130		139	147	88
Nb	(ppm)		4		4	8	5
Mo	(ppm)		4		4		
Cs	(ppm)		10		11		
Ba	(ppm)		125		176	143	494
La	(ppm)		1		5	5	5
Ce	(ppm)		24		33	33	31
Nd	(ppm)		20		15	27	16
Pb	(ppm)		3		3		
Th	(ppm)		4		4	3	3
U	(ppm)		3		3	1	3

Table 6.1 Whole rock major and trace element geochemistry of the Te Hukui Basalt and compositions of Tatua and Ben Lomond Basalts (Hiess et al., 2007). The scoriaceous fragments for S.1 and S.2 samples were collected from the outcrop on the eastern side of Te Hukui Stream from unit F as indicated in Fig. 2b by asterisks. Compositions of scoriaceous fragments indicate some contamination with country rocks. Analyses are by XRF at University of Waikato, New Zealand.

The whole rock geochemical characteristics are very similar to other HAB localities with a slightly lower Al_2O_3 content (Table 6.1). TAS classification indicates that the chemical composition is closest to the Tatua Basalt (Fig. 6.5) (Hiess et al., 2007), which is the nearest known HAB occurrence to Te Hukui (Fig. 6.1).

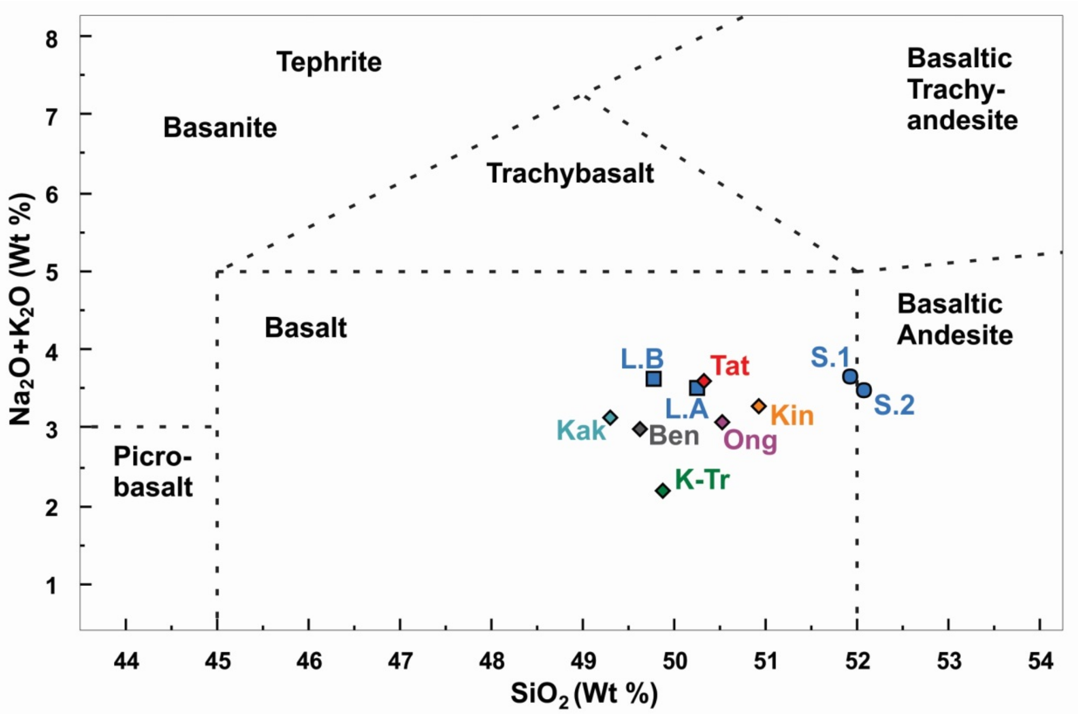

Figure 6.5 TAS classification of Te Hukui basalt (L.A. lithic A; L.B. lithic B; S.1. – scoria; S.2. – scoria) and other basalts of the Taupo-Whakamaru area (Ben. – Ben Lomond; Kak. – Kakuki; Kin. – Kinloch; K-Tr. – K-Trig; Ong. – Ongaroto; Tat. – Tatua) (Brown et al., 1994; Hiess et al., 2007; Matheson, 2010).

6.5 Discussion and conclusions

The topographic position of the newly discovered basaltic association is identical with the neighbouring ridges consisting of the Orakonui Formation. This suggests that both the Te Hukui Basalt and ignimbrite exposures of the basement at the side of the present craters were exposed by excavation relating to Puketerata activity. However, the spatial relationship between the craters of the older Te Hukui and younger Puketerata eruptions is unclear. Thus, we propose two feasible explanations based on the morphological observations (Fig. 6.6) of the sequence; (a) surfical Te Hukui deposits had already eroded prior to the Puketerata eruption, which then exposed the intra-crater deposits, or (b) the Puketerata eruption occurred through the existing crater of Te Hukui, which widened the crater and exposed the older Te Hukui deposits that were deposited in proximity of the crater.

The polymict breccia characterised by andesitic to rhyolitic lithic components, which have not been found on the surface, suggests deep excavation due to magma/water interaction that occurred at least a few hundreds of meters below the surface. The variably inclined layers most likely formed by slumping, on the steep inner wall of the crater. These sedimentological features are indicative for maar-diatreme volcanism, while the existence of stratified pyroclastic beds corresponds to an upper diatreme facies (White and Ross, 2011). The formation of diatremes induced by energetic phreatomagmatic activity (Lorenz, 2007) is indicated by pyroclastic flow and surge beds. The extra-crater deposits of typical maar-forming activity have a maximum thickness of a few tens of meters near the source (Wohletz and Sheridan, 1983), and their typically unconsolidated nature makes them very vulnerable to erosion. The lack of basaltic deposits of the surrounding area suggests high erosion rates, further supporting a model in which the exposed sequence was deposited within the depression of the crater (Fig. 6.6a).

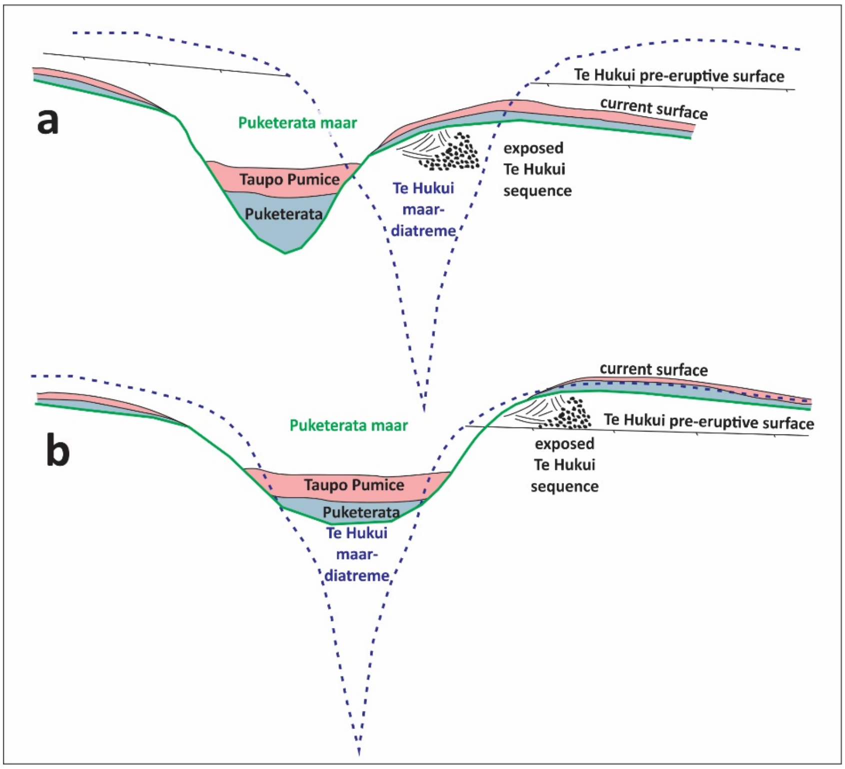
a
Te Hukui pre-eruptive surface
current surface
Puketerata maar
Taupo Pumice
Puketerata
Te Hukui
maar-
diatreme
exposed
Te Hukui
sequence
b
current surface
Puketerata maar
Te Hukui pre-eruptive surface
exposed
Te Hukui
sequence
Taupo Pumice
Puketerata
Te Hukui
maar-
diatreme

Figure 6.6 Possible topographic relationships between the craters of the Te Hukui Basalt and Puketerata subject to the exposure of the Te Hukui sequence, not to scale; (a) Te Hukui sequence represents intra-crater deposits; (b) exposed Te Hukui sequence represents the remnant of ejecta ring. In both cases, the Te Hukui outcrops were exposed by the latter Puketerata activity.

The Te Hukui sequence can be divided into three different divisions by the dominant characteristics of deposits. The formation of the lowest division (units A-C) was dominated by high fragmentation of the erupting magma and admixture with variously fragmented country rocks as a result of deep-seated phreatomagmatic explosions (Lorenz, 1986; Valentine and White, 2012). The middle division (D-F) indicates an alternation of magmatic and phreatomagmatic eruptions. The lapilli sized fragments of fall beds correspond to Strombolian activity (e.g. Houghton and Gonnermann, 2008), while the shapes of juvenile ash indicates either a Strombolian or a phreatomagmatic origin, similar to the activity at Ohakune, TVZ (Chapter 5; Kósik et al., 2016b). The sampled basaltic lithic fragments most likely originated from the margin of the conduit/vent, where the lava solidified as part of a larger body prior to fragmentation and transportation to their locality. The upper division (only found at the western outcrop) is considered to present reworked deposits of the ejecta ring through granular flows and fluvial sedimentation.

The petrological and geochemical investigation revealed that the composition of the Te Hukui basalt is very similar to other HABs within the TVZ. Rare Na-rich plagioclase xenocrysts and complex plagioclase zonation patterns imply some degree of mixing with rhyolitic magma prior to eruption. The mafic chemical composition of the erupted material with signs of minor interaction with rhyolitic magma suggest that the dyke feeding the Te Hukui eruption did not interact with eruptible rhyolitic melt lenses, but instead shot through a crystal mush (Fig. 6.7). Stalling/underplating mafic melts need of the order of 10^3 years to equilibrate with their environment (Annen, 2011), thus at least a few thousands of years are required to increase the amount of eruptible silicic melt by multiple basaltic intrusions and underplating to produce a rhyolitic eruption at the same location.

The stratigraphic age of the Te Hukui Formation is older than the Puketerata activity, while its maximum age corresponds to the age of the ignimbrites of Orakonui Formation (244-268 ka) (Leonard, 2003). The thick soil horizon (most likely correlating to Mokai Sand; Vucetich and Pullar, 1969) on the top of the basalt demonstrates that this basaltic activity was an eruptive event distinct from the activity of Puketerata, and it sets the minimum age of the Te Hukui event before the eruption of the Oruanui Ignimbrite (25.4 ka) (Vandergoes et al., 2013). Considering that this area was characterised by significant erosion before and after the climactic Oruanui eruption, the deeply eroded basaltic sequence is at least a few thousand years older than the Oruanui eruption. Besides high erosional rates, burial was the most important factor that modified the broader landscape. Thus it cannot be ruled out that our knowledge about the locations of all the basaltic vents or deposits is incomplete. It seems that most of the HAB occurrences are arranged to an eastern and a western fault zone (Fig. 6.1), located at the edges of a central extensional area of the TVZ affected by young faulting. This kind of arrangement may have been influenced by the physical conditions of the silicic magma reservoirs, such as the crystal mush/eruptible melt ratio.

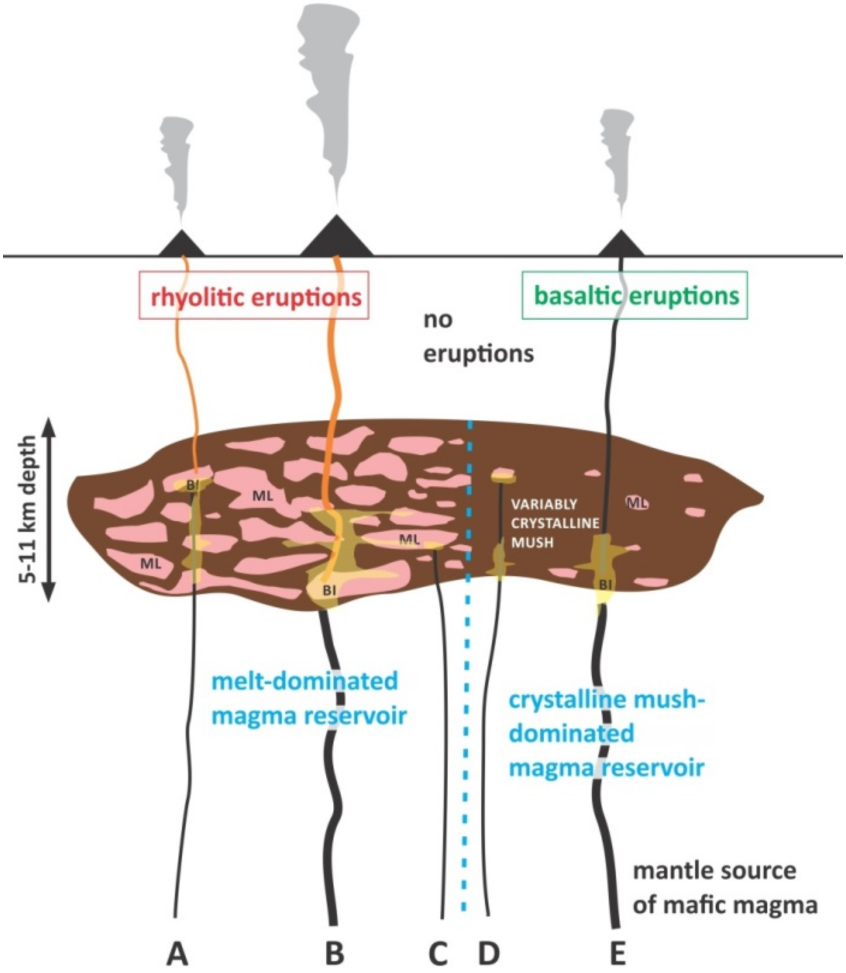
rhyolitic eruptions
basaltic eruptions
no
eruptions
5-11 km depth
BI
ML
ML
ML
BI
ML
VARIABLY
CRYSTALLINE
MUSH
ML
BI
melt-dominated
magma reservoir
crystalline mush-
dominated
magma reservoir
mantle source
of mafic magma
A
B
C
D
E

Figure 6.7 Conceptual model for possible rock types of erupting magma due to the interaction between variable sized basaltic magma intrusions (BI) and rhyolitic melt lenses (ML) in case of a melt-dominated or crystal mush-dominated silicic magma reservoir. Basaltic eruptions are expected only in case of minor interaction with melt lenses (E), while other cases basaltic magma may trigger rhyolitic eruption (A and B) or mixing with rhyolitic magma without eruption (C and D). Magma reservoir model modified after Cashman and Giordano (2014).

Chapter 7

Chapter 7 presents new results on the volcanic and landscape evolution of the silicic phreatomagmatic and lava dome–forming activity of the Puketerata Volcanic Complex.

This chapter is based on a published journal paper:

Kósik, S., Németh, K., Lexa, J and Procter, J.N. 2017: Understanding the evolution of a small-volume silicic fissure eruption: Puketerata Volcanic Complex, Taupo Volcanic Zone, New Zealand. Journal of Volcanology and Geothermal Research, in press, https://doi.org/ 10.1016/j.j volgeores.2017.12.008

Statement of contribution (DRC16 form) is at Appendix D

Chapter 7 – Understanding the evolution of the Puketerata Volcanic Complex

7.1 Introduction

The Taupo Volcanic Zone (TVZ) is the most productive silicic volcanic region in the world with at least 12 caldera forming eruptions producing over 3300 km^3 DRE of magma during the last 350 ka (Houghton et al., 1995b; Wilson et al., 1995; Wilson et al., 2009). From a volcanic hazards perspective, the smaller pre/post-caldera eruptions which occur 2-3 orders of magnitude more frequently (Nairn, 2002; Leonard et al., 2010) need more attention within the TVZ hazardscape. These eruptions are mostly characterised by small eruptive volumes (<1 km^3 DRE) through a single eruptive episode originating from newly formed vents. Such explosive/effusive characteristics of these events meet the diagnostic features of monogenetic/small-volume volcanism (White and Ross, 2011; Németh and Kereszturi, 2015). Within the TVZ, small-volume eruptions usually form viscous lava flows or domes with their magma originating from the same crustal depths as the products of the caldera-forming eruptions (Nairn et al., 2004; Heise et al., 2007; Deering et al., 2011) producing snapshots of the condition of the magma reservoir. Dome-forming eruptions commonly associated with explosive activity occur before, intermittently, and/or after the dome emplacement with varying intensity (Newhall and Melson, 1983; Heiken and Wohletz, 1987; Sparks, 1997; Okumura et al., 2009; Zimmer et al., 2010). Explosive behaviour of silicic magmas largely depends on the dissolved H_2O contents, however explosions may have been triggered by the change of physical properties of magma (e.g. increasing viscosity, crystallization, and decreasing permeability) hindering the effective outgassing and causing the overpressurization of the conduit (Okumura et al., 2009; Castro et al., 2014). The interaction of magma with external water also influences explosivity (Brooker et al., 1993; Austin-Erickson et al., 2011).

The explosive activity associated with lava dome formation ranges from vent clearing phreatomagmatic eruptions through phreatic and Vulcanian eruptions to Plinian-style with sustained eruption columns generating pumiceous deposits (Newhall and Melson, 1983; Heiken and Wohletz, 1987; Sparks, 1997). The physical properties of erupting magma also decisively influence the emplacement style of lava domes implying two end-members; endogenous and exogenous growth (Fink and Anderson, 2000). Endogenous (intrusive) growth is characterised by the expansion of a dome by the influx of fresh lava into the dome interior, while during exogenous (extrusive) growth fresh lava is emplaced as discrete flow lobes or lava spines on top of the earlier formed edifice (Fink and Anderson, 2000). The style of dome growth and the underlying topography will determine the morphology of domes and their internal properties (Christiansen and Lipman, 1966; Fink, 1983; Fink and Manley, 1987; Blake, 1990; Grossenbacher and McDuffie, 1995; Fink and Griffiths, 1998; Fink and Anderson, 2000; Lyman et al., 2004; Hale and Wadge, 2008). The evolving topography and internal structures of lava domes are also influenced by the shape of the feeding vent (Costa et al., 2007), that can be characterised by a point source/circular conduit (Christiansen and Peterson, 1981; Yokoyama et al., 1981; Williams and Self, 1983) or linear source/dyke fed conduits mostly at silicic calderas and rift zones (Fink and Pollard, 1983; Nakada et al., 1999; Aguirre-Díaz and Labarthe-Hernández, 2003; Ashwell et al., 2013). The role of phreatomagmatism in regard to dome evolution is a largely overlooked topic and hence there are only a few sites (Ross et al., 2017), such as at *Cerro Pizzaro, Mexico* (Riggs and Carrasco-Núñez, 2004); *Cerro Pinto, Mexico* (Zimmer et al., 2010); *Tepexitl, Mexico* (Austin-Erickson et al., 2011); *Hoya de Estrada, Mexico* (Cano-Cruz and Carrasco-Núñez, 2008); and *Panum tuff ring-dome complex, Mono Craters, California* (Sieh and Bursik, 1986) where this specific issue has been directly addressed. There are a large number of localities, where the role of this eruption style is evident but has not been linked directly, and the silicic lava domes are commonly associated with ejecta rings especially in mature volcanic fields in intracontinental settings such as those in *Anatolia* (Druitt et al., 1995), *Central Slovakia* (Lexa and Pošteková, 2012), *Saudi Arabia* (Moufti and Németh, 2016), *Northern Sudan* (Franz et al., 1999) and *Northern Patagonia* (Hernando et al., 2012). Despite the at least 300 lava domes forming in the past 0.5 Ma within the TVZ (Leonard et al., 2010) (Fig. 7.1), we only know a few locations, such as Hipaua dome, Tauhara (Rosenberg and Kilgour, 2000), Ngangiho (Leonard, 2003), and Puketerata (Brooker et al., 1993) (Fig. 7.2) where dome-related phreatomagmatic successions were found and documented reasonably well. There are convincing evidences, such as extensive lacustrine sediments (Bignall et al., 2010), lake terraces (Ashwell et al., 2013), and the existence of long-lived hydrothermal systems (Rowland and Sibson, 2004), to infer that the hydrogeological-climatic settings in the time of most of these young lava domes formed in the TVZ were similar to present-day conditions. This study attempts to define the role of phreatomagmatism associated with lava dome emplacement, which has not been addressed yet in detail within the TVZ. The youngest (16.5 ka), best exposed and most well-preserved silicic phreatomagmatic succession of the TVZ is a maar-dome complex called Puketerata (Fig. 7.2) (Brooker et al., 1993). The diversity of evolved volcanic products and edifices within this small volcanic complex highlights the complexity of the evolution of silicic dyke-fed dome eruptions. This study aims to describe the fine scale (eruptive pulse by pulse; Manville et al., 2009a) evolution of the volcanic activity associated with dome emplacement using the available stratigraphic record, geomorphic features of the volcanic structures, and petrological and geochemical characteristics of the eruptive products. We also aim to understand the relative role of the internal (conduit processes) and external controlling parameters in the evolution of the volcanic complex, such as magma-water interaction and edifice growth and ascertain the possible timescales of this small-volume volcanic event. This research is aimed at contributing to the hazard assessment of TVZ's small-volume volcanism.

7.2 Geological setting

The TVZ is a rifting arc located at the southern end of the Tonga-Kermadec Arc and has been forming for the past 2 Ma as a result of the oblique subduction of the Pacific Plate underneath the Australian Plate and the resulting back-arc extension (Wilson et al., 1984; Cole, 1990; Davey et al., 1995; Wilson et al., 1995; Acocella et al., 2003; Wallace et al., 2004; Spinks et al., 2005; Rowland et al., 2010; Reyners, 2013) (Fig. 7.1). The northern (Bay of Plenty) and the southern part (Tongariro Volcanic Centre) of the TVZ is characterised by mostly andesitic volcanism, while the central TVZ includes seven rhyolite calderas/caldera complexes with hundreds of lava domes that have formed over the past 350 ka (Wilson et al., 1995; Spinks et al., 2005) (Fig. 7.1). The Puketerata Volcanic Complex (PVC) is located in the rhyolitic central segment of the TVZ within the ~350 ka Whakamaru caldera (Brown et al., 1998; Downs et al., 2014b)

(Figs. 7.1 and 7.2). Post-caldera volcanism is characterised by lava dome emplacement and associated explosive activity occurring irregularly between 305 to 16.5 ka (Leonard et al., 2010). The most active period was between 251-222 ka producing more than 20 km^3 of DRE volume of pyroclastic material and lava, forming the majority of the domes of the Maroa Volcanic Centre (MVC) (Leonard, 2003) (Fig. 7.2). The PVC represents the youngest dome forming event with well-preserved pyroclastic successions (Froggatt and Lowe, 1990; Brooker et al., 1993; Leonard et al., 2010). The PVC formed on a fault-bounded, gently incised ignimbrite-dominated topography at the southern margin of Maroa Volcanic Centre (MVC) (Fig. 7.2). The faults of the area are considered have been active in the past 128 ka (Leonard et al., 2010). The proximal and medial sequences of PVC are usually underlain by a 1-2 m thick soily sand and loess (Mokai Sand Formation, Vucetich and Pullar, 1969), which is sitting on the erosion surface of the ~256 ka non-welded/sintered ignimbrite of Orakonui Formation (Leonard, 2003) and pyroclastic sequences of maar-forming Te Hukui Basalt (Chapter 6; Kósik et al., 2017b). The eruptive vents of the PVC were formed along a lineament parallel to the nearby located NE-SW trending Orakeikorako Fault (Fig. 7.2). The Puketerata deposits are blanketed by the 1.8 ka Taupo Pumice Formation (Hogg et al., 2011), which veneers the surface, yet is mostly eroded from the highest part of the edifices (summit of the domes and the rim of the tuff ring). The low lying areas and depressions including the crater floors were buried by the valley-fill facies of Taupo Pumice, which thickness usually exceeds here 20-25 m (Froggatt, 1981; Walker and Wilson, 1983; Wilson, 1985).

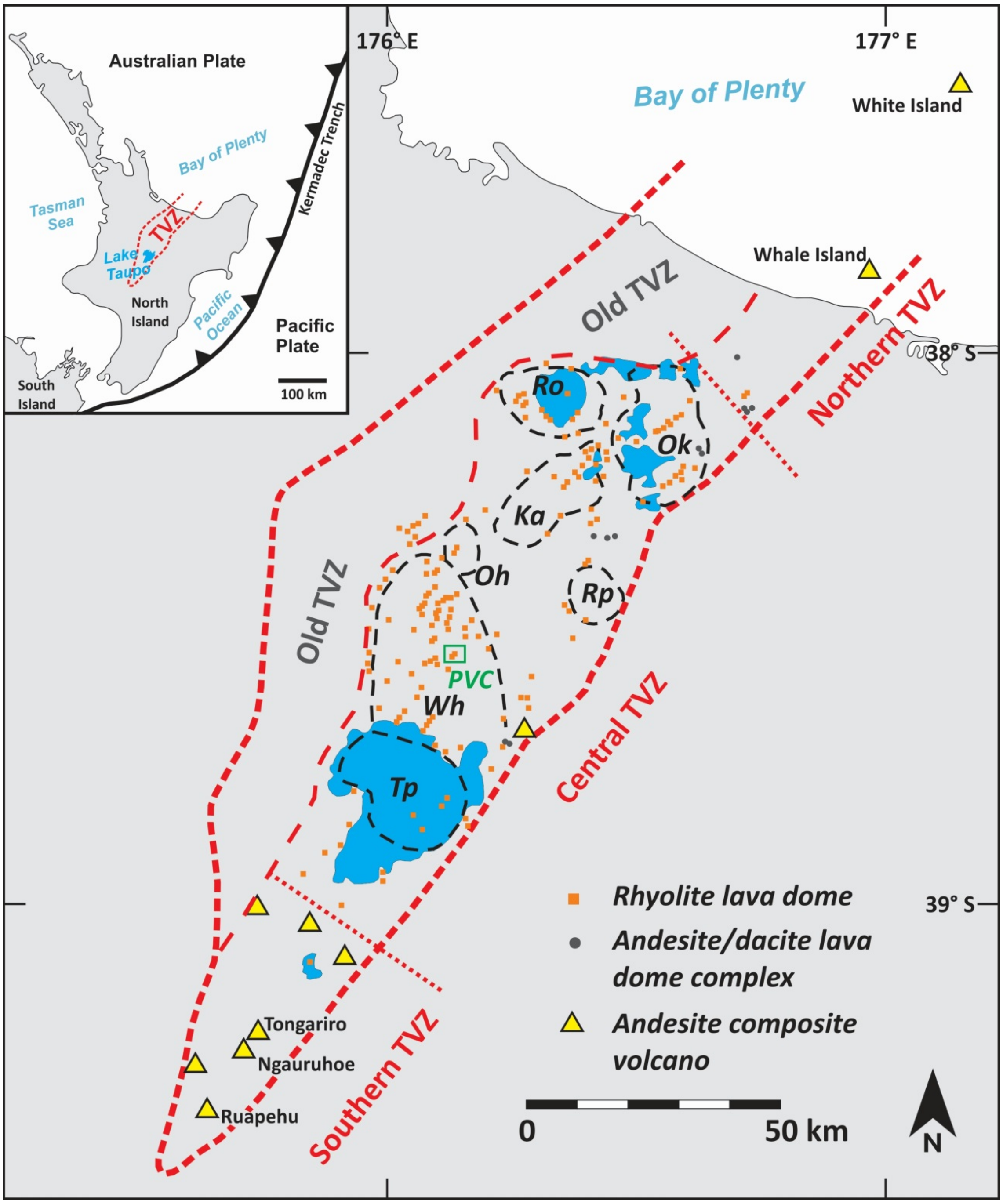
Australian Plate
Bay of Plenty
Tasman Sea
TVZ
Kermadec Trench
Lake Taupo
North Island
Pacific Ocean
Pacific Plate
South Island
100 km
176° E
177° E
Bay of Plenty
White Island
Whale Island
Old TVZ
Northern TVZ
38° S
Ro
Ok
Ka
Oh
Rp
Old TVZ
PVC
Wh
Tp
Central TVZ
39° S
Tongariro
Ngauruhoe
Ruapehu
Southern TVZ
Rhyolite lava dome
Andesite/dacite lava dome complex
Andesite composite volcano
0
50 km
N

Figure 7.1 Regional map showing the geographic location of the Taupo Volcanic Zone (TVZ) and the site of study (PVC) within the North Island and its relative position to the subduction of the Pacific Plate beneath the Australian Plate (inset map). The border (bold red dashed lines) between the Old TVZ and the Young TVZ and the present-day compositional divisions (red dotted lines) between the more andesitic Southern and Northern TVZ and the rhyolitic Central TVZ are from Wilson et al. (1995). Outlines of rhyolitic calderas (black dashed lines) located within the Young TVZ are from Houghton et al.(1995b) Ka – Kapenga; Ro – Rotorua; Rp - Reporoa; Tp – Taupo; Wh – Whakamaru; Ok – Okataina; Oh – Ohakuri. Vent locations of domes, dome complexes and coulees were mapped from 8 m NZ DEM (LINZ - Land Information New Zealand, 2012) using geological maps of Rotorua area (Leonard et al., 2010) and Okataina Volcanic Centre (Nairn, 2002).

7.3 Methods

About 50 outcrops were found (Fig. 7.2) with pyroclastic units related to the activity of the PVC. Six of those outcrops located within an area enclosed by the rim of the tuff ring represent proximal pyroclastic sequences. Medial outcrops preserve fallout and pyroclastic density currents (PDC) beds, while the distal sequences are characterised mostly by fallout deposits (Fig. 7.2). Rhyolite lavas of the dome-forming phases are accessible at the summits of the two domes and on the outer slopes of the ejecta ring as fragments at outcrops with coarse PDC deposits. Besides the detailed stratigraphic and sedimentological characterization of 32 sites, granulometry and componentry of 70 units from 20 sites were examined. Bulk density measurements of lapilli fragments (−3 phi and -2.5 phi) from fallout beds were carried out using Micromeritics GeoPyc 1360 Envelope Density Analyser. The skeletal densities (which do not consider the volume of connected pores through the sample) were determined by Quantachrome Ultrapycnometer 1000 hosted at Massey University, using N_2 gas as the flowing medium. Petrological characterization of the samples were determined through thin sections by light microscopy, Scanning Electron Microscopy (SEM) equipped with energy dispersive x-ray spectroscope (EDAX) at Massey University, New Zealand and backscattered electron imaging (BSE), Energy Dispersive (EDS) and Wavelength Dispersive (WDS) Spectroscopy was carried out for the characterization of mineral phases at the State Geological Institute of Dionýz Štúr, Slovakia, using a CAMECA SX-100 Electron Probe Micro Analyser (EPMA). Silicate phases and Fe-Ti oxides were analysed at standard conditions: acceleration voltage 15 kV, target current 20 nA and beam diameter 1 – 5 µm. To minimise Na losses of glass analyses they were measured using beam diameter 10 µm, firstly with target current 3 nA to measure Na and subsequently other elements at standard conditions. Water content of glasses was estimated by the "volatile by difference" technique (Devine et al., 1995; Blundy and Cashman, 2008), assuming that the difference between the total of the EPMA analysis and 100% is represented by water. The geomorphology of the entire area of the volcanic complex was examined by an 8 m resolution NZ Digital Elevation Model (DEM) from LINZ - Land Information New Zealand (2012). A better quality stereo imagery-based DEM with 5 m resolution was used for the lava dome and the surrounding ejecta ring. Additionally, geomorphic observations coupled with Real-Time Kinematic (RTK) GPS measurements were made at five cross sections of the edifices for improving the DEM-based volume calculations and specifying the elevation of diagnostic volcano-geomorphic features (e.g. summit of lava dome, crater floors) of the volcanic complex.

7.4 Architecture of the Puketerata Volcanic Complex

The PVC was earlier described as a NE-aligned, 4 km alignment of five vents including two lava domes, a tuff ring and three flat-floored explosion pits (Brooker et al., 1993). Using DEMs, RTK GPS for terrain modelling and field observations we measured considerably different values for morphometry of these edifices than the earlier study (Brooker et al., 1993), thus the volcanic features of the complex are reclassified as maars, lava domes and an ejecta ring surrounding the larger dome (Figs. 7.2-7.4).

7.4.1 Maars

At Puketerata, at least four coalesced craters with arched rims and diameters of 400-500 m are located to the NE from the main lava dome (Profile A-B, Figs. 7.2-7.4). The current crater floors are within 470-478 m asl in elevation, 30-35 m deeper than their surrounding rims. Despite there being little information about the depth of these volcanic structures, the morphology of the craters fit to conventional maar descriptions as their crater floors are below the pre-eruptive surface by at least 25 m (Figs. 7.2-7.4) (Lorenz, 1986; White and Ross, 2011). The initial maar-forming products are barely visible possibly due to the erosion and the small scale nature of the events.

7.4.2 Ejecta ring

The larger lava dome is bounded by an ejecta ring that has been referred to as a tuff ring in earlier studies (Brooker et al., 1993) (Fig. 7.2). The thickness of the Puketerata deposits and its topographic position indicate that the evolution of this structure differs from the maar craters. The rim of this elongated structure is scalloped, forming several discrete lobes. The axis of elongation is subparallel to the vents enclosing an ellipse with a rim to rim axis length of 1100 and 850 m (Fig. 7.2). The elevation of the

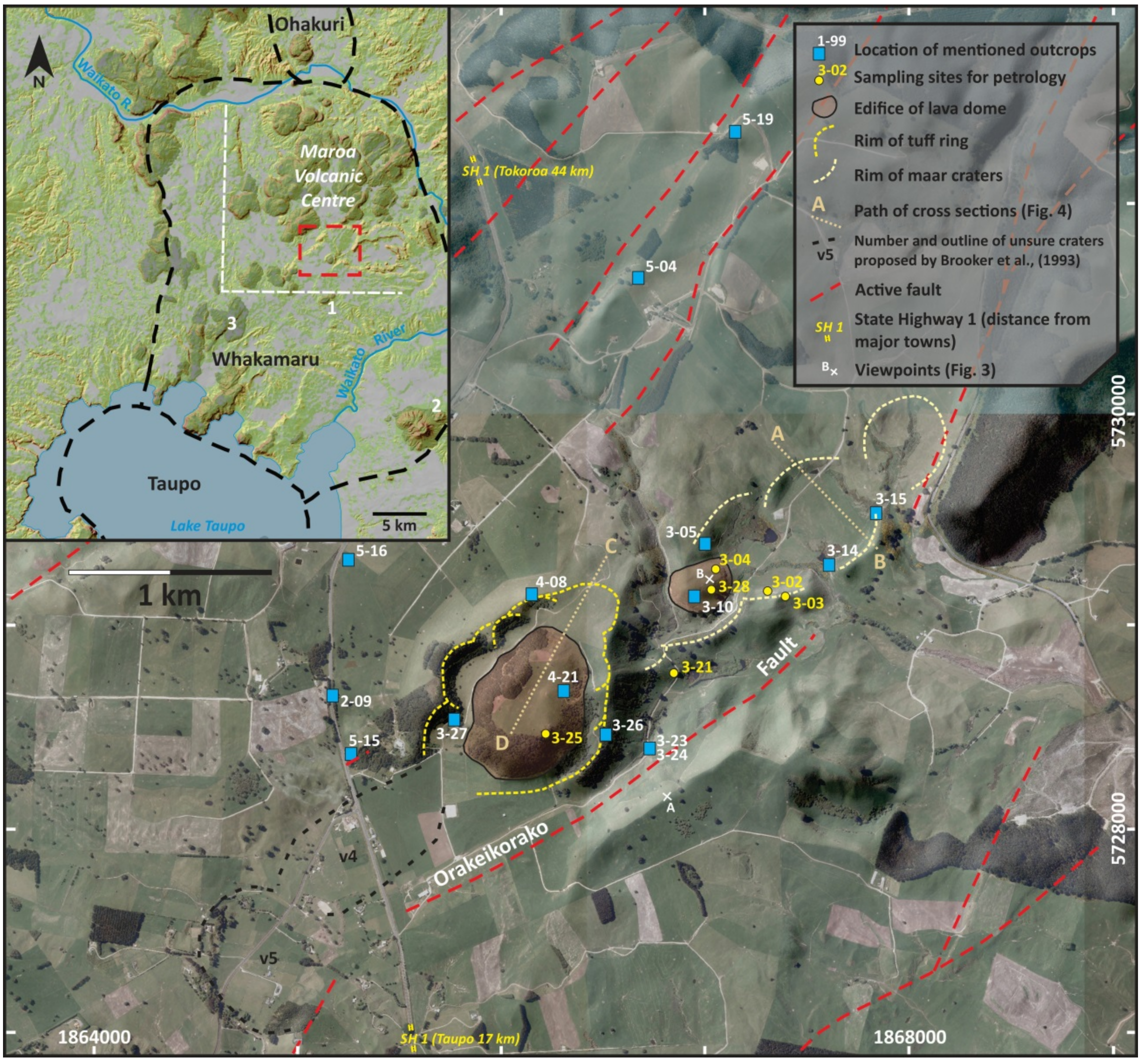
Ohakuri
N
Waikato R
Maroa Volcanic Centre
1
3
Whakamaru
Waikato River
2
Taupo
Lake Taupo
5 km
1 km
1-99 Location of mentioned outcrops
3-02 Sampling sites for petrology
Edifice of lava dome
Rim of tuff ring
Rim of maar craters
A Path of cross sections (Fig. 4)
v5 Number and outline of unsure craters proposed by Brooker et al., (1993)
Active fault
SH 1 State Highway 1 (distance from major towns)
B× Viewpoints (Fig. 3)
SH 1 (Tokoroa 44 km)
5-19
5-04
A
3-15
3-05
3-14
B
3-04
3-28
3-10
3-02
3-03
4-08
C
5-16
3-21
Fault
4-21
2-09
3-27
3-26
3-23
3-24
5-15
D
3-25
A
Orakeikorako
v4
v5
SH 1 (Taupo 17 km)
1864000
1868000
5730000
5728000

Figure 7.2 Location of the PVC (red dashed square) within the Maroa Volcanic Complex with the nearby lava domes (shaded areas), calderas (dashed lines) and mentioned lava domes/flows; 1 Ngangiho, 2 Hipaua, 3 Ben Lomond (inset map) and architecture of the PVC with the active faults (Langridge et al., 2016) and the important exposures of the Puketerata sequence Coordinates are given in New Zealand Transverse Mercator 2000 (NZTM2000) projection. Letters A and B indicate the viewpoints for Fig. 7.3.

western foothills is about 590 m asl, while the other side is an incised valley, characterised by the gradual decrease of the elevation from 575 m to 494 m asl (Fig. 7.5). On the left side of this valley crops out the only contact between the pre-eruptive surface and the initial volcanoclastic unit of this structure at the elevation of 536 m asl (loc. 3-23) (Fig. 7.2). This elevation is roughly comparable with the eastern rim summit elevations of the maar craters. As the area of the western foothill is extraordinary flat in comparison to the gently sloping surface at the western neighbourhood of the maars, it is assumed that the western foothill of the ejecta ring was affected by significant post-Puketerata burial with similar thicknesses (20-25 m) to other low-lying areas. Applying the estimated average basement height and the absolute height of the ejecta ring, the relative height is about 90-100 m of this structure. There is a moat between the rim of the ejecta ring and the dome which widens on the western side at four locations characterised by half-round or circular structures with flatted floors of different elevations (1: 608 m, 2: 624 m, 3: 615, 4: 592 m asl, Fig. 7.5). The moat is less developed on the eastern side due to the lava dome overlying on the lower part of the ejecta ring. The ejecta ring has unusually steep outer slopes. On the eastern side, along the ridge of the incised valley the ejecta ring is characterised by a 31.1° average slope. The western outer slopes have an average slope angle of 22.8° and seem unaffected by significant erosion (Fig. 7.5, Table 7.1). The relative height and the outer slope angles of the Puketerata ejecta ring in comparison with other ejecta rings (Table 7.1) indicates

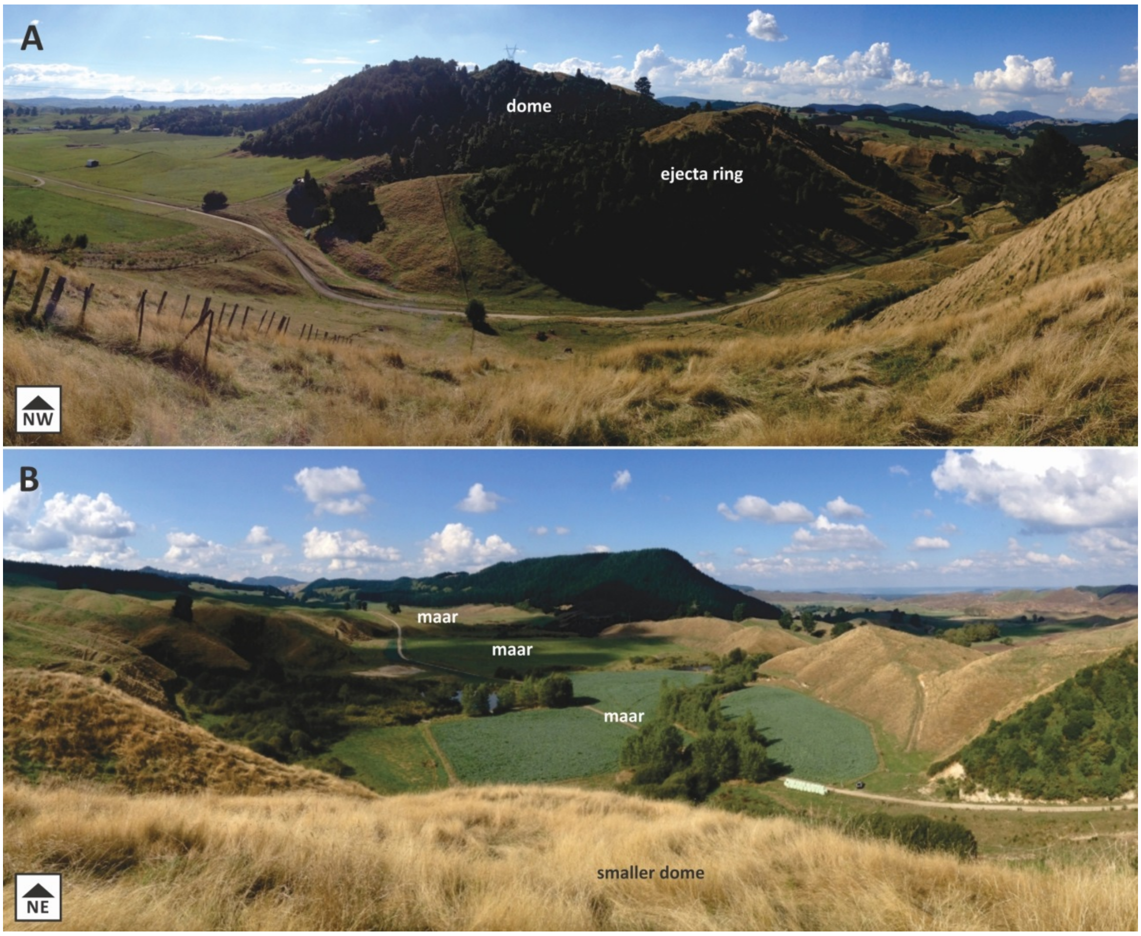

Figure 7.3 Panoramic views of the structures of the Puketerata Volcanic Complex. A: The larger dome and the surrounding ejecta ring from the top of the fault carp of the Orakeikorako Fault. B: View from the summit of the smaller dome to chain of the maar craters (locations of viewpoints are shown at Fig. 7.2).

anomalous values for a conventional ejecta rings of maars and tuff rings (Wohletz and Sheridan, 1983). The elevation of the ejecta ring decreases gradually at the NE and SW sector and it is breached within the axis of the fissure at the SW quadrant.

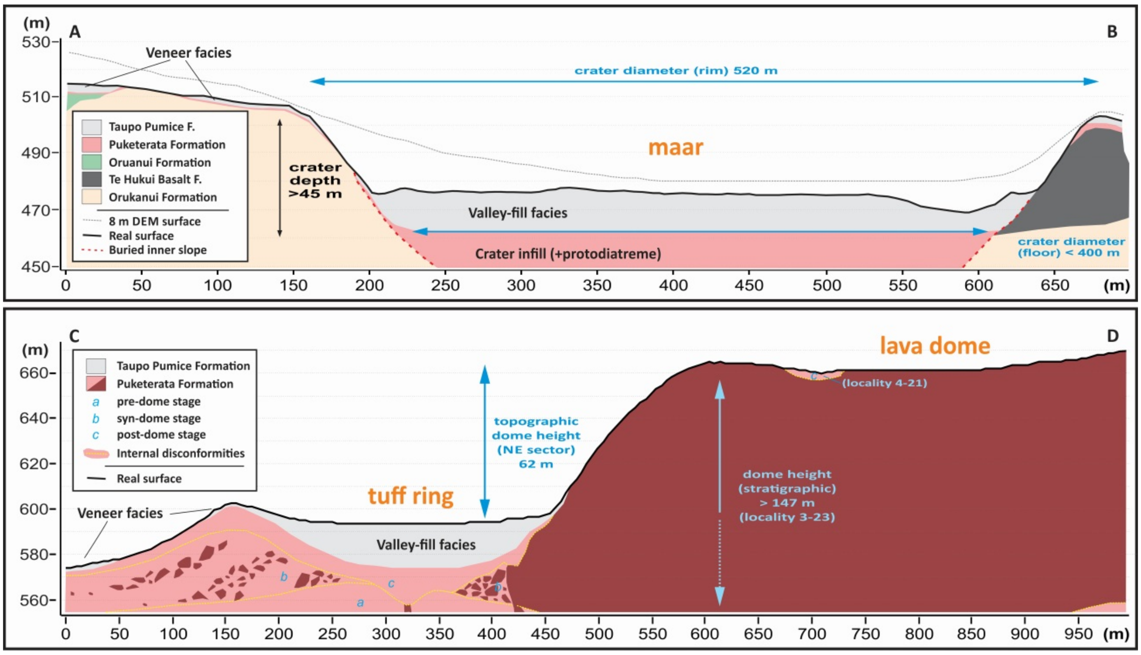
(m)
A
B
Veneer facies
crater diameter (rim) 520 m
maar
Taupo Pumice F.
Puketerata Formation
Oruanui Formation
Te Hukui Basalt F.
Orukanui Formation
8 m DEM surface
Real surface
Buried inner slope
crater depth >45 m
Valley-fill facies
Crater infill (+protodiatreme)
crater diameter (floor) < 400 m
530
510
490
470
450
0
50
100
150
200
250
300
350
400
450
500
550
600
650
(m)
C
D
lava dome
Taupo Pumice Formation
Puketerata Formation
a pre-dome stage
b syn-dome stage
c post-dome stage
Internal disconformities
Real surface
topographic dome height (NE sector) 62 m
(locality 4-21)
dome height (stratigraphic) > 147 m (locality 3-23)
tuff ring
Veneer facies
Valley-fill facies
a
b
c
660
640
620
600
580
560
0
50
100
150
200
250
300
350
400
450
500
550
600
650
700
750
800
850
900
950
(m)

Figure 7.4 Cross sections from the prominent parts of the volcanic complex used 2x vertical exaggeration. The paths of the cross sections are shown at Fig.7.2.

The resolution of the existing DEMs do not allow for the characterization of the vent 4 and 5 (v4, v5, Fig. 7.2) along the SW extension of the volcanic complex as indicated by Brooker et al. (1993). Field observations reveal normal faulting on the northern margin of the elongated depression of vent 4 at locality 5-15 (Figs. 7.2 and 7.8), while the 600 m wide, half-round shape of vent 5 is more recognizable although the rims and the suspected floor were also affected by significant burial by the Taupo Ignimbrite (Fig. 7.2). Despite of this, these depressions may relate to the Puketerata eruption, which evaluation should require geophysical surveys and/or further terrain analysis in the future on the availability of high (1 m or better) resolution DEM.

volcano	location	relative height (m)	max slopes (°)	data source
Crater Hill (B)	AVF	25	6.8	2 m LiDAR DEM
Brown Island (B)	AVF	45	8.5	2 m LiDAR DEM
Pukaki (B)	AVF	18	4.1	2 m LiDAR DEM
Robertson Hill (B)	AVF	10	2.5	2 m LiDAR DEM
Ohakune VC (B)	TVZ	37	11.6	8 m NZ DEM
Lunar Crater (B)	LCVF	34	8.6	1 m LiDAR DEM
Kaleni (RH)	Acigöl C.	25	5.7	30 m ASTER DEM
Panum Crater (RH)	MC	65	18.8	10 m contour DEM
Cerro Pinto (RH)	S-O	210*	13.5	30 m ASTER DEM
Tepexitl (RH)	S-O	43	14.1	30 m ASTER DEM
Puketerata (W_{flank})	TVZ	100	22.8	5 m DEM
Puketerata (E_{flank})			31.1	

*Table 7.1 Morphometrical characteristics of selected basaltic (B) and rhyolitic (RH) ejecta rings of tuff rings and maars from the Acigöl Complex, Central Anatolia; Lunar Crater Volcanic Field (LCVF) and Mono Craters (MC), California; Serdán-Oriental (S-O), Trans-Mexican Volcanic Belt and Auckland Volcanic Field (AVF) and Taupo Volcanic Zone (TVZ), New Zealand). *Cerro Pinto ejecta ring most likely sits on the top of block-and-ash flow fans, which extra height difference is included in the 210 m (Zimmer et al., 2010).*

7.4.3 Lava domes

Two lava domes formed within the PVC (Fig. 7.2). The lower portion of the elongated larger lava dome is overlain by the valley fill deposits of Taupo Pumice at the southern extension of the volcanic fissure. The flat area at the S-SW foothill has an elevation of 568 m, but earlier drill holes had to pass through a 20-30 m thickness of pumice-rich ignimbrite, which is covering the current surface (Fig. 7.4). The summit area of the dome (black dotted line, Fig. 7.5) located above the 662 m contour line has an irregular morphology with four 10-20 m high, slightly elongated hillocks comprising blocks of rhyolite lava. The elevated parts of the summit encompass a 200 m long and 5 m deep trench parallel with the longer axis of the dome with a few concentric pits probably representing the fissure vent (Fig. 7.5) as proposed for the Panum dome, Mono Craters, California (Sieh and Bursik, 1986). The highest point of the lava dome is 684 m asl located on the southeast hillock, thus the topographic height of dome is about 115 m.

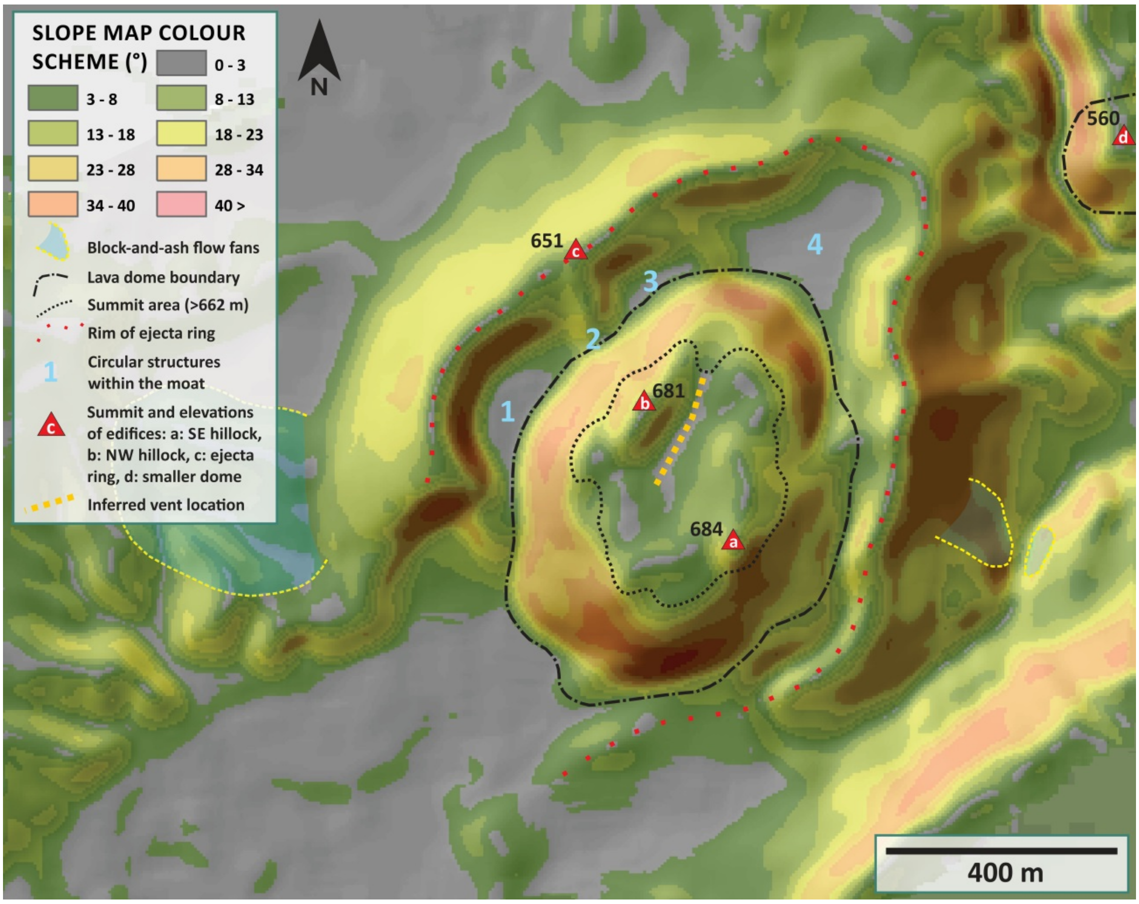
SLOPE MAP COLOUR SCHEME (°)
0 - 3
3 - 8
8 - 13
13 - 18
18 - 23
23 - 28
28 - 34
34 - 40
40 >
Block-and-ash flow fans
Lava dome boundary
Summit area (>662 m)
Rim of ejecta ring
Circular structures within the moat
Summit and elevations of edifices: a: SE hillock, b: NW hillock, c: ejecta ring, d: smaller dome
Inferred vent location
N
651
c
560
d
681
b
684
a
1
2
3
4
400 m

Figure 7.5 Slope map of the dome and surrounded ejecta ring using a 5 m resolution shaded relief DEM layer as a background indicates the main morphologic features of the volcanic edifice.

The steepest slopes are located at the elevation between 610-640 m asl, 20-50 m lower than the level of the dome summit. The maximum slope angles are up to 41° that may represent the gradient of the coherent lava (Karátson et al., 2013), whereas the average is 29.1° for steepest slopes, which corresponds to the angle of repose of loose talus of domes reported elsewhere (Hale, 2008). The smaller dome (Fig. 7.2) has occupied the deep crater next to the NE side of the ejecta ring. This edifice encloses a 200 × 300 m area and its summit elevation is 75 m higher than the current floor of the crater in which it formed (Figs. 7.2 and 7.5).

7.5 Stratigraphy and sedimentology

7.5.1 General features

Puketerata-related deposits are characterised by the heterogeneity of volcanic products due to the variety of volcanic processes. The pyroclastic sequences can be classified into 5 lithofacies on the basis of componentry and sedimentological characteristics (e.g. grain size distribution and sedimentary structures; Sohn and Chough, 1989; Németh et al., 2012a; Pedrazzi et al., 2014b) and some of their appearance are characteristic in specific locations (e.g. only proximal or distal).

Tuff breccia (EXB), Pinkish to grey coloured blocks of the country rocks up to 15 cm in size (ignimbrite of Orakonui Formation) were found in a strongly pedogenesised fine-rich matrix. The tuff breccia is sitting on the fractured surface of Orakonui Formation and is overlain by the Taupo Pumice. The occurrence is limited to two small outcrops located on the steep inner slopes of maar craters (3-04, 3-15, Fig. 7.2). *This lithofacies is interpreted as a vent opening explosion breccia related to the formation of maar craters* (e.g. Wohletz and Sheridan, 1983).

Cross-bedded tuff or lapilli tuff (WS, DS) The most voluminous deposits related to the explosive activity of the PVC are cross/dune-bedded, matrix-supported, poorly-sorted beds with two distinct types. The more common type is characterised by cohesive fine-dominated matrix with accretionary lapilli and bomb sag structures. Interbedding of patchy or continuous horizons of better sorted, slightly coarser layers are common and likely represent minor fallout events. The other type is high in coarse, slightly rounded dense fragments up to 1-2 cm in size. These coarse clasts are likely transported together with the fine fragments. *The deposit of cohesive fine-grained beds is interpreted as products of wet pyroclastic surges (WS) while the coarser beds may represent dry pyroclastic surges or diluted parts of pyroclastic flows (DS)* (e.g. Chough and Sohn, 1990).

Lithic-rich lapilli (F) Lithic-rich lapilli beds are moderately to well-sorted, clast-supported layers from cm to half a meter thick. Normally they do not show any stratification or grading, but sometimes lapilli beds are intercalated with WS or DS units. The majority of the fragments are angular lapilli-sized essential fragments dominated by moderately to non-vesicular clasts originating from a solidified rhyolitic body prior to fragmentation. The occurrence of this lithofacies is widespread and can be recognised at all medial outcrops. *These units represent the fallout deposits from major eruption columns, the larger events were numbered from F1 to F8 (Fig. 7.8).*

Breccia/tuff breccia (BAF) This lithofacies is characterised by variable amount of blocks versus ash whose lapilli and block sized fragments originally formed as part of the larger lava dome, and later transported to the current position. Clast-supported types only occur within the moat and eastern outer slope of the tuff ring (localities 2-09, 3-27, 3-23, Fig. 7.2), while medial locations usually contains less than 10% of those dense coarse fragments (e.g. locality 5-16., Fig. 2). These fragments are moderately to non-vesicular glassy biotite-bearing rhyolite, thus classified as essential clasts. *The occurrence of the distinct breccia/tuff breccia bodies seems horizontally limited and it is concluded to represent the deposits relating to the destruction or collapsing of a lava dome. The majority of these beds are transported by block-and-ash flows (BAF) but the fine-poor units may relate to larger rockfall events that commonly occur during lava dome growth (Calder et al., 2002).*

Distal tephra (DT) Distal outcrops are usually characterised by internal erosional disconformities and strongly pedogenesised upper sequences (e.g. localities 5-04 and 5-19). Except one major coarse, well sorted layer, the majority of these sequences seem very similar without any stratification. *Their grain size distributions confirm the bimodal nature of some of these deposits (fall ± diluted PDC origin)*.

7.5.2 Proximal sequences

Proximal outcrops are located at three distinct parts of the tuff ring-lava dome edifice: near the rim of the ejecta ring (loc. 4-08 and 3-26, Fig. 7.2) or on the summit of lava dome in an elevated position (loc. 4-21, Fig. 7.2), within the moat between the lava dome and the western ridge of the ejecta ring (loc. 3-27, Fig. 7.2), and at the outer slopes of the eastern ridge of the ejecta ring within the valley (Localities 3-23 and 3-24, Fig. 7.2). These localities due to their geographic position represent different stages of the evolution of the volcanic complex, thus exhibit substantial differences (Fig. 7.6).

7.5.2.1 Eastern outer slopes of tuff ring

The initial products are exposed at the bottom of the valley incising into the eastern flank of the ejecta ring (loc. 3-23 and 3-24, Fig. 7.2). The Puketerata units have been deposited on a thick paleosol layer and are characterised by a 5 cm thick WS unit which is followed by a 50 cm thick, predominantly DS unit interbedded with a few cm thick fall (F) unit. In the subsequent 2.5 meter sequence the majority of units are similar to the initial unit, which was interbedded with a few well-sorted, up to 10 cm thick fall (F) layers. The exposures in the right side of the valley (loc. 3-24, Fig. 7.2) represent a sequence higher in stratigraphic position than the basal succession yet is unconformable. From the base to top this outcrop consists of: (1) A 50 cm thick unit composed of a number of WS layers, (2) 60 cm thick matrix to clast-supported, moderately-sorted breccia unit (transitional between fallout and rockfall), (3-4) WS and DS units (loc. 3-24, Fig. 7.6). About 20 meters down slope on the same side of the valley there is exposed a few very well-sorted fall (F) unit interbedded with WS beds and a subsequent 2 m thick BAF deposit. The outcrop on left side of the valley represents the product from the inception of the Puketerata eruption, while the right side of the valley's deposits relate to the growth and occasional destructing of lava dome.

7.5.2.2 Moat successions

These deposits are mostly characterised by coarse (clast size up to 1 m) BAF units formed by the explosive and/or gravitational destruction of domes resulting from rockfalls and collapses. Disconformities, inward dipping and changes of the angle of stratification imply excavation and subsequent deposition of PDCs into the newly formed surface morphology originated from the newly advancing lava lobes (loc. 3-27, Fig. 7.2). Higher stratigraphic sequences (loc. 4-08, 5-07, Fig. 7.2) show beds of fallout and DS or BAF deposits with indefinite stratification including trains of angular blocks besides the massive breccia beds (loc. 4-08, Fig. 7.6).

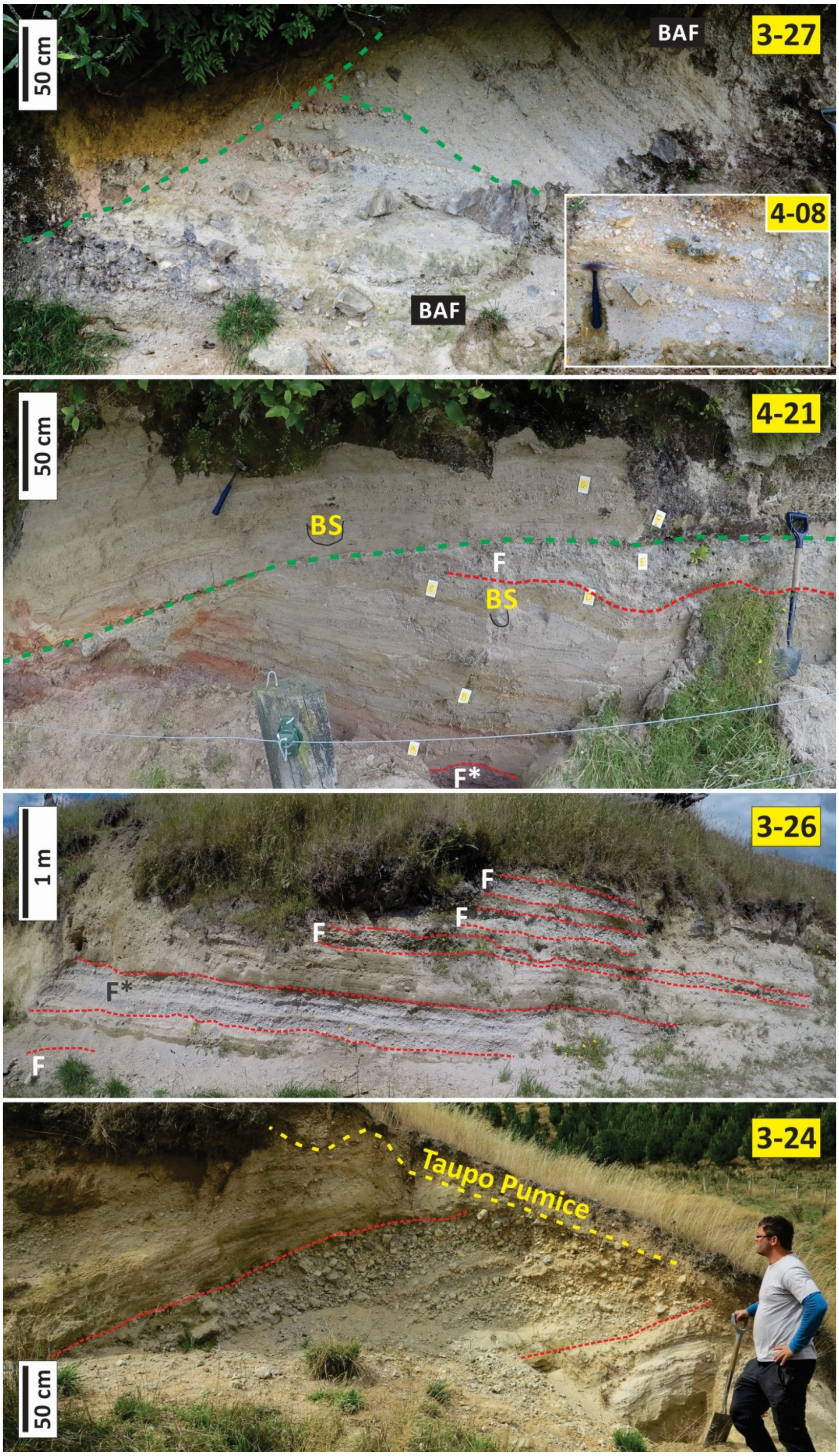
50 cm
BAF
3-27
BAF
4-08
50 cm
4-21
BS
F
BS
F*
1 m
3-26
F
F
F
F*
F
3-24
Taupo Pumice
50 cm

Figure 7.6 Key outcrops at proximal locations. Green dashed lines indicate internal disconformities, yellow dashed lines indicate the boundary between Puketerata and the subsequent Taupo Pumice deposits. Fall beds (F) are delimited by red dashed lines. BS: bomb sags. For accurate geographic positions of the outcrops see Fig. 7.2.

7.5.2.3 Elevated localities on the eastern rim of the tuff ring and the summit of the larger lava dome

At the locality 3-26, five major fall (F) beds are exposed that are interbedded and separated from each other by WS and DS units. Bedding sags are common and formed by angular or subangular fragments with a maximum diameter of 10-15 cm. (loc. 3-26, Fig. 7.6). The lower part of the succession on the lava dome (loc. 4-21, Fig. 7.2) shows similar deposits found on the eastern rim of the tuff ring with two major fall beds and WS units. A disconformity cuts the deposits at an angle and the subsequent deposits are dipping in the opposite direction. The upper succession exhibits the alternation of cohesive very fine beds (WS) with DS units (loc. 4-21, Fig. 7.6). Considering the stratigraphic and topographic position, some of these units may have depositioned due to the eruptions creating the current scalloped morphology of the ejecta ring at the late stage of the Puketerata activity.

7.5.3 Medial sequences

Detailed stratigraphic observations were completed at two different localities exposed at State Highway 1 (SH1) (loc. 2-09, 5-15, Fig. 7.2). These outcrops contain the most complete stratigraphic section preserving the activity of PVC. However, it is not possible to determine the stratigraphic relationship between these medial successions and the units observed at elevated proximal locations. Eight major tephra fallout events (F1-F8) have been distinguished, which were used as dividing markers of the activity (Figs 7.7-7.8). The initial phase produced WS beds interbedded by two major and several minor tephra falls (Figs. 7.7-7.8). Bedding sags are common from angular blocks up to 10-15 cm in size. The deposits change above the F2 event and are characterised by coarse DS beds, a well-sorted fallout unit and further well-sorted discontinuously appearing structures which may have been remnants of further fallout beds.

The cross-bedded nature of these coarse beds is most recognizable above fall event F3, where the grain size is gradually decreasing (loc. 2-09, Fig. 7.2). These units were overlain by a 40-50 cm thick coarse (average clast size is 2-3 cm in diameter) fall unit (F4) characterised with clast densities between 1.35 and 2.1 g/cm^3 (Fig. 7.9). During and after the main fall event WS beds formed again together with several minor and three major fall units (F5, F6, F7) (Figs. 7.7-7.8). The WS beds located just under and above fall bed F7 were hit by a large number of impact bombs. These beds are underlain by a poorly-sorted, matrix-supported unit which cut into the sequence at least down to the fall event F4. This contains angular fragments up to 20 cm in size and exhibits significant incision (Fig. 7.7). This unit is classified as a block-and-ash flow breccia (BAF1). Above this breccia unit the sequence consist of predominantly WS units and a fall event where deposits are interbedded with some WS beds. Finally a second poorly-sorted breccia unit (BAF2) is deposited at the top of the remaining sequence. The larger clasts are of BAF and fallout deposits are dense or moderately vesicular without large vesicles and pumiceous textures.

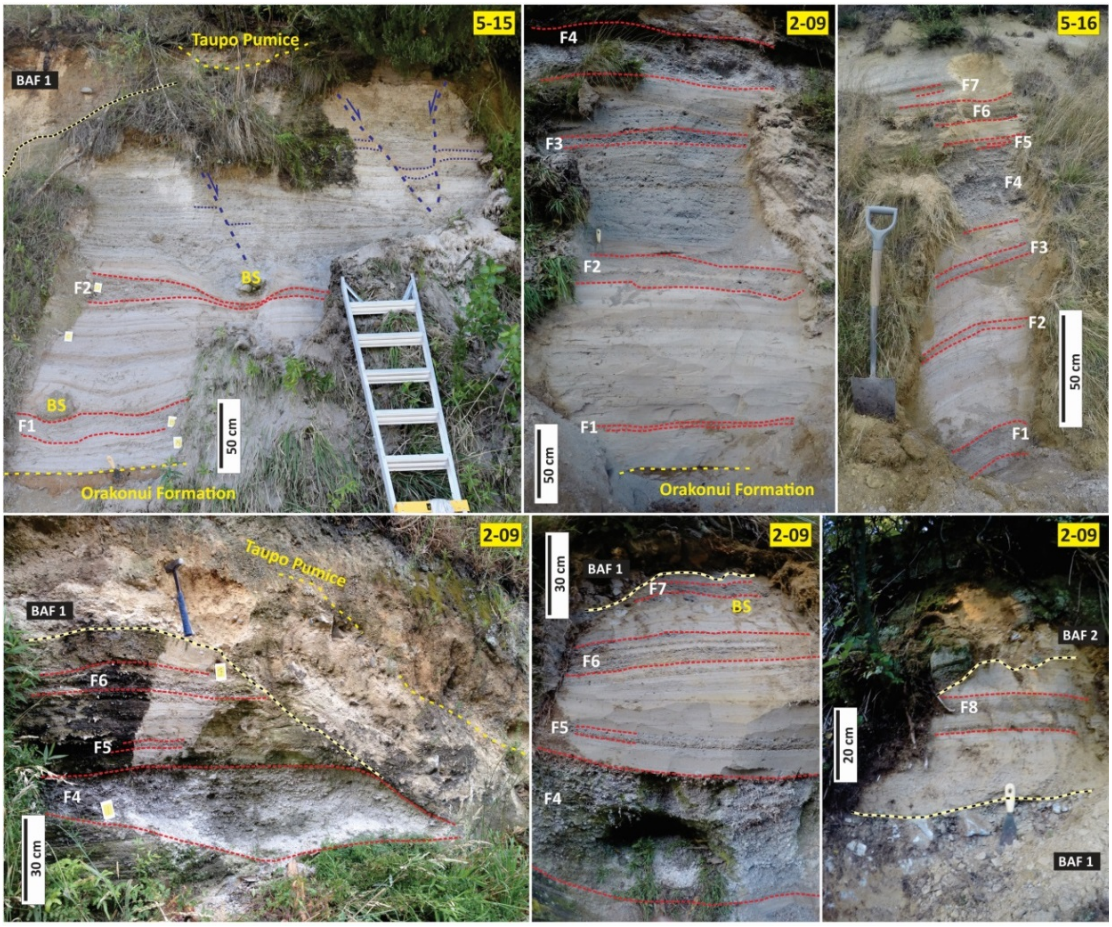
5-15
Taupo Pumice
BAF 1
F2
BS
BS
F1
50 cm
Orakonui Formation
2-09
F4
F3
F2
F1
50 cm
Orakonui Formation
5-16
F7
F6
F5
F4
F3
F2
50 cm
F1
2-09
Taupo Pumice
BAF 1
F6
F5
F4
30 cm
2-09
30 cm
BAF 1
F7
BS
F6
F5
F4
2-09
BAF 2
F8
20 cm
BAF 1

Figure 7.7 Main outcrops at the road cut of State Highway 1. Major fall beds (F1 to F8) are delimited by red dashed line, block-and-ash flow units (BAF) delimited by black dashed line within yellow background. BS: bomb sags. Yellow dashed lines indicate the boundary between the basement, Puketerata and the subsequent Taupo Pumice deposits. Blue dashed and dotted lines indicate faults and related displacements (5-15). For precise locations of the outcrops see Fig.7.2.

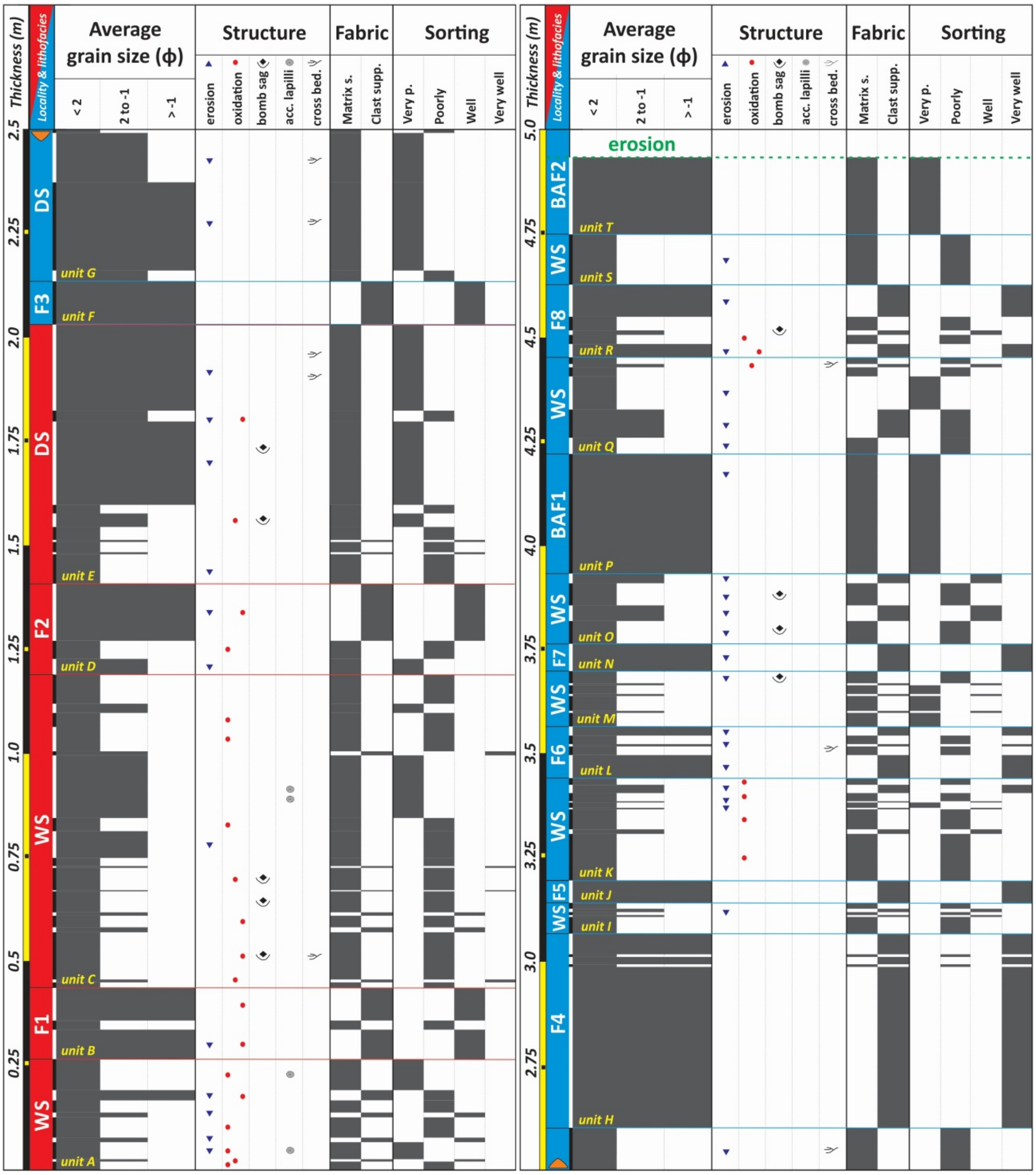

Figure 7.8 Detailed stratigraphic log of the medial deposits of PVC. The lower 2 m (red) observed at locality 5-15, (Figs. 7.2 and 7.7) while the upper part (blue) incorporates the upper sequence from locality 2-09 (Figs. 7.2 and 7.7). The most dominant lithofacies is indicated for each unit using abbreviations of lithofacies.

7.5.4 Density, vesicularity and volume calculations

The skeletal densities of erupted rocks were measured on the samples collected from the summits of the two lava domes (localities 3-04 and 3-25), a block-and-ash flow unit from locality 3-24 and the F4 fall bed from locality 2-09 (Fig. 7.2). Skeletal density values are scattered between 2.34-2.51 g/cm^3. Envelope densities were measured from different fall units from the outcrops located at the road cut of SH1 (F2, F3, F4, F6 beds) and one-one fall bed of localities 4-21 and 3-26). Single clast envelope densities are distributed from 1.35 to 2.63 g/cm^3 (Fig. 7.9). Based on the density measurements, the clasts of the fall beds exhibit about 30% average vesicularity. This value was used for the conversion from bulk volumes to DRE volumes (Table 7.2). The volume calculation of the two domes and the ejecta ring were carried out using DEMs and stratigraphic observations. Medial and distal volumes was determined by georeferencing the isopach map published by Lloyd (1972) and utilizing exponential thinning tephra fall volume calculation scheme from Pyle (1989) to be comparable to the earlier calculation of Brooker et al. (1993). New area calculations revealed that the 1 cm isopach encloses only 235 km^2, 73% of the earlier calculated area (Brooker et al., 1993) (Table 7.2). The medial-distal volumes also exhibit significant differences compared with earlier studies (Brooker et al., 1993), which even cannot explain by the area differences and neither corresponds to bulk nor DRE volumes. The ejecta ring (45.1 × 10^6 m^3) and the lava domes (52.7× 10^6 m^3) combined volume is roughly two-thirds of entire erupted DRE products (142.5× 10^6 m^3) (Table 7.2).

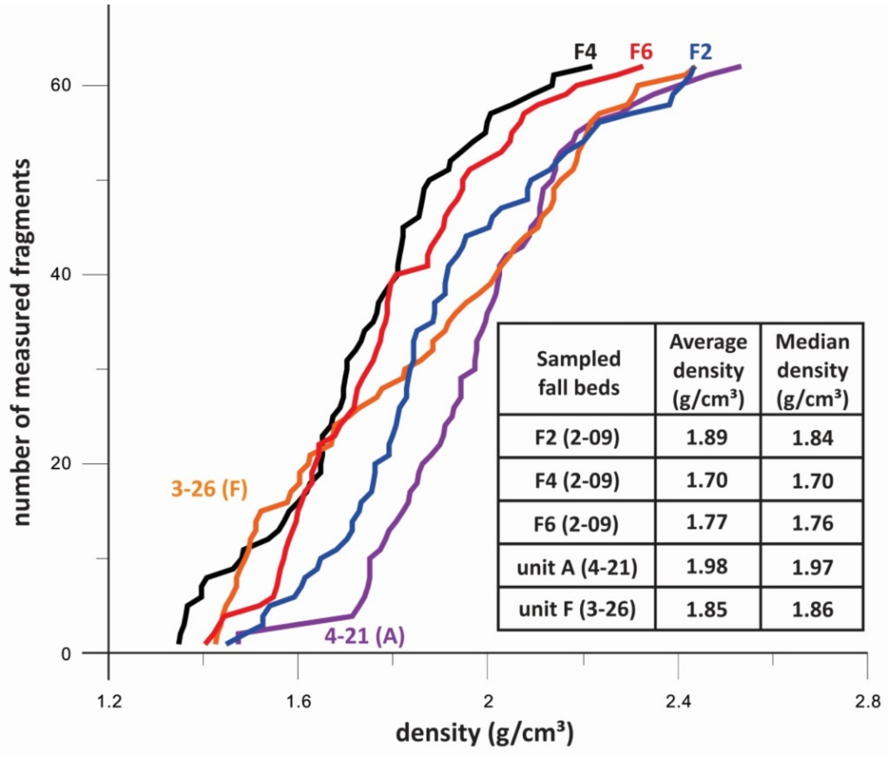

Sampled fall beds	Average density (g/cm³)	Median density (g/cm³)
F2 (2-09)	1.89	1.84
F4 (2-09)	1.70	1.70
F6 (2-09)	1.77	1.76
unit A (4-21)	1.98	1.97
unit F (3-26)	1.85	1.86

Figure 7.9 Density distribution of essential clast from selected major fallout beds. (F2, F4, F6 represents single fall beds sampled from 2-09 (Fig. 7.7), the other two layers marked by asterisks at 4-21 and 3-26 (Fig. 7.6).

	Area km^2	**Bulk volume 10^6 m^3**	**DRE index**	**DRE volume 10^6 m^3**	**% of total products**
Tuff ring - 568 m (8 m DEM)	0.89	31.44	0.85		
Tuff ring - 568 m (5 m DEM)		27.34		23.24	
Tuff ring - 546 m (5 m DEM)		**53.02**		**45.07**	**31.6**
Larger lava dome - 568 m (8 m DEM)	0.36	26.57	0.95		
Larger lava dome -568 m (5 m DEM)		25.47		24.20	
Larger lava dome - 536 m (5 m DEM)		36.91		35.06	
Larger lava dome - 460 m (5 m DEM)		**50.48**		**47.96**	**33.6**
Smaller lava dome - 478 m (8 m DEM)	0.07	3.77	0.95		
Smaller lava dome - 478 m (corrected)		3.61		3.43	
Smaller lava dome - 460 m (corrected)		**4.97**		**4.72**	**3.3**
Total edifices	**0**	**108.47**		**97.74**	**68.6**
medial and distal (Pyle, 1989)	**233.83**	**63.97**	0.7	**44.78**	**31.4**
Total	**233.83**	**172.44**		**142.52**	

Table 7.2 Volume calculation's results of distinct structures of PVC (excluding diatremes) using different resolution DEMs and basement elevations have been identified from cross sections (Fig. 7.4) and field observations. DRE indexes were defined by density measurements of fragments collected from fall beds (Fig. 7.9) and the observed vesicularity of dome rocks.

7.6 Petrology and thermobarometry

7.6.1 Puketerata rhyolites

Six samples have been selected for the investigation of the petrographic and petrological characteristics of the Puketerata rhyolites collected from various stratigraphic levels and different parts of the PVC (Fig. 7.2). The examined samples can be divided into two slightly different groups by their petrography. The rhyolites of samples 3-02 and 3-03 (angular lithic fragments in phreatomagmatic pyroclastic dry surge deposits) and 3-04 and 3-28 (dense lava from the top of the northern small dome) that represent lower stratigraphic levels indicate higher phenocrysts content with larger grains than the rhyolites that were collected from localities 3-21 (impacted bomb) and 3-25 (dense lava from the top of the main dome) (Fig. 7.2). Besides that, both types of rhyolites are porphyritic with 30-35% phenocrysts in glassy groundmass of hyaline to hyalopilitic texture (Fig. 7.10A). Mostly euhedral to subhedral phenocrysts are represented by plagioclase, quartz, biotite, amphibole, Ti-magnetite and ilmenite within the range from 0.2 to 5.0 mm in size. Some samples (e.g. 3-02 and 3-21, Fig. 7.2) show also rare xenocrysts/xenoliths of plagioclase along with attached radially oriented aggregates of plagioclase and quartz that occur also as solitary grains. Apatite and zircon occur as accessory minerals.

Plagioclase phenocrysts (18-22%; max. 5.0 mm, mostly 0.5 – 1.5 mm, min. 0.3 mm) have usually tabular shapes and mostly occur as individual grains or glomerocrysts. They show a characteristic zonality with resorbed cores of variable composition (An_{38-56}) replaced in patchy pattern and surrounded by Ca-rich overgrowth (An_{72-75}) that grades outward into a 50 – 200 µm wide rim showing fine oscillatory zoning and progressive An depletion rimward (An_{36-42} at the edge) without any sign of resorbtion or Ab-rich overgrowth. Resorbed plagioclase cores include or are intergrown with amphibole, biotite and Fe-Ti oxides. ***Quartz phenocrysts*** (6-9%; max. 2.5 mm, mostly 0.5 – 1.0 mm, min. 0.2 mm) are strongly resorbed with extensive embayments, often present as remnants only. Cathodoluminescence examination reveals a zonation usually with a brighter core (relatively enriched in Ti) surrounded by generally darker oscillatory zones, including zones of resorbtion. They do not include other minerals, while microphenocrysts of plagioclase and/or biotite occur in their resorbtion embayments. ***Biotite*** (3-4%; max. 2.5 mm, mostly 0.4 – 0,8 mm, min. 0.2 mm) occurs as euhedral phenocrysts – “books” of small to moderate thickness as well as subhedral grains intergrowth with plagioclase cores, amphibole and/or Fe-Ti oxides. ***Amphibole*** (around 1%; 0.3 –1 mm) occurs as individual euhedral phenocrysts with enclosed grains of Fe-Ti oxides, apatites and rare melt inclusions or as subhedral crystals intergrown with plagioclase cores, biotite and/or Fe-Ti oxides. The cores of amphiboles often include remnants of resorbed orthopyroxene. ***Titanomagnetite*** (0.5-1%; mostly 0.1 – 0.3 mm) occurs as individual euhedral phenocrysts with enclosed minute crystals as well as subhedral intergrown crystals with plagioclase cores, amphibole and/or biotite. Crystals do not exhibit exsolution lamellae or signs of degradation. Their Ti content varies within 8.6-11.5%. ***Ilmenite*** (around 0.1%; mostly < 0.1 mm) occurs as fresh individual grains and/or in association with titanomagnetite, usually in aggregates with or enclosed in plagioclase cores, amphibole and biotite.

The **groundmass** is glassy with rare microlites of pyroxene, biotite and apatite and characterised by diverse appearance of textures. Glass is locally affected by incipient devitrification and/or alteration. Dense glass with no or limited porosity shows a network of cracks, often curved, that disintegrate glass into rectangular to globular fragments 0.1 – 0.8 mm in diameter (Fig. 7.10A-B). The same cracks affect also quartz and plagioclase phenocrysts. The more dominant porous glass shows two stages of vesiculation (Fig. 7.10C, F). The first stage is represented by extremely stretched thin tube-like pores or their traces that define a pronounced fluidal texture deformed around phenocrysts (t1-type, Fig. 7.10F). The second stage is represented by relatively large vesicles, rounded to partially rectangular in shape, generally aligned with the orientation of the fluidal texture (t2-type, Fig. 7.10F). However, they are not deformed or show only insignificant deformation. Some of the vesicles next to phenocrysts indicate an involvement of cavitation as one of the processes of their nucleation and growth. Glass among vesicles is affected by fracturing as in the case of dense glass (Fig. 7.10D). Some of the samples indicate a pronounced preferential orientation and fluidal texture that is expressed especially by flow banding (Fig. 7.10E-F) and vesicularity (Fig. 7.10F). Rare spherulites appear in glassy groundmass of the sample from the top of the main dome. Groundmass glass compositions are homogenous with exception of its apparent water content (Appendix A.7.1). Using the “water by difference” method (Devine et al., 1995) its water content varies in the range 0.29-2.94% with a median of 1.32% and standard deviation of 0.67 that corresponds roughly to the expected error of the method (Blundy and Cashman, 2008) (Table 7.3).

	SiO_2	**TiO_2**	**Al_2O_3**	**FeO**	**MnO**	**MgO**	**CaO**	**Na_2O**	**K_2O**	**P_2O_5**	**SO_3**	**Cl**	**Total**
max	77.47	0.47	12.69	1.22	0.10	0.08	0.77	3.95	4.88	0.06	0.08	0.23	99.71
min	74.78	0.04	11.85	0.71	0.00	0.00	0.57	3.25	4.09	0.00	0.00	0.15	97.06
median	76.65	0.07	12.29	0.82	0.06	0.04	0.67	3.43	4.47	0.00	0.00	0.17	98.68
stdv	0.71	0.07	0.20	0.09	0.03	0.02	0.04	0.17	0.22	0.02	0.02	0.02	0.67

Table 7.3 Compositional range of groundmass glass based on 29 measurements on samples from 3-02, 3-03, 3-04 and 3-21 (Fig. 7.2).

7.6.2 Intensive parameters

Thermobarometers applied to the phenocrysts assemblage (Appendix A.7.2) point to temperature and pressure in magma chamber prior to the eruption around 750 °C and 1 – 1.5 kbar, corresponding to the depth 4.3 – 6.4 km (using mean rock density 2336 kg/m^3; Tenzer et al., 2011). For the estimation of eruption temperature we have used Putirka’s (2008) feldspar-liquid and two-feldspar thermometers (Table 7.4).

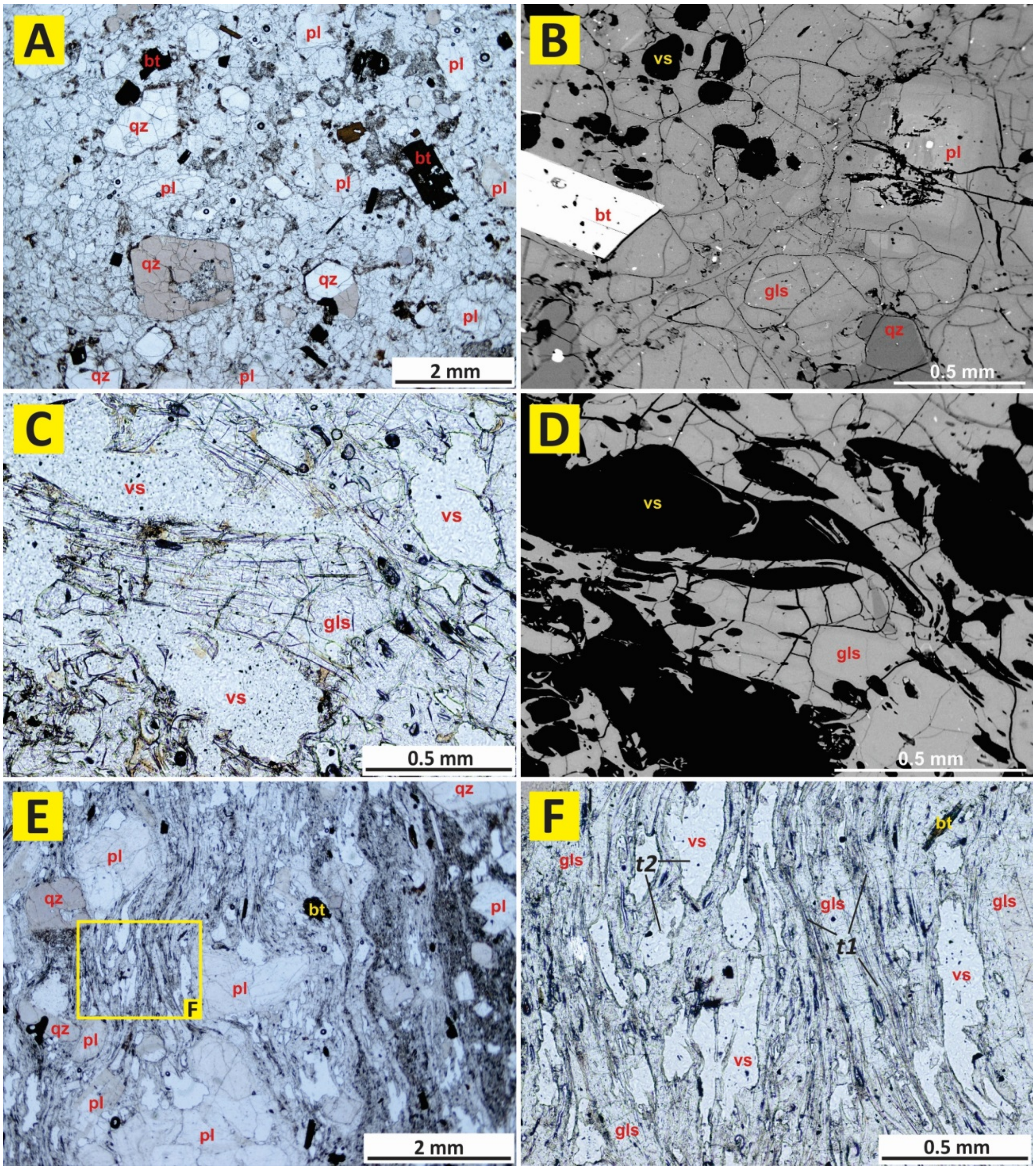
A
pl
bt
pl
qz
pl
bt
pl
pl
qz
qz
pl
qz
pl
2 mm
B
vs
pl
bt
gls
qz
0.5 mm
C
vs
vs
gls
vs
0.5 mm
D
vs
gls
0.5 mm
E
qz
pl
qz
bt
pl
F
pl
qz
pl
pl
pl
2 mm
F
vs
gls
t2
bt
gls
gls
t1
vs
vs
gls
0.5 mm

Figure 7.10 Photomicrographs and BSE images of Puketerata rhyolite. A: Most frequent phenocrysts; plagioclase (pl), biotite (bt) quartz (qz) in glassy fractured groundmass (sample 3-02), B: network of fractures in dense glass (sample 3-02), C: variability of textures of vesicularity (sample 3-03) , D: BSE image of C showing fracturing of glass among vesicles (sample 3-03), E: Deformed flow banding, dark bands are rich in microlites (sample 3-21), F: detail from E showing two types (t1 and t2) of vesicularity in fluidal glassy groundmass (sample 3-21).

While plagioclase-liquid thermometry provided consistent results, thermometers involving alkali feldspar microlites provide lower temperatures. This is probably an effect of deviation from the equilibrium crystallization at the state of undercooling affecting more strongly alkali feldspar microlites. The calculations suggest that the eruption temperature was between 799 and 855 °C (Table 7.4).

If erupting magma is water saturated, as evidenced by the presence of vesicles, water content of groundmass glass reflects the pressure at which cooling melt passed through glass transition. We have used "VolatileCalc" of Newman and Lowenstern (2002) to calculate volatile saturation pressure and thus to establish approximate depth at which phreatomagmatic eruptions could have been initiated. The calculated volatile saturation pressure indicates 145 bar corresponding to 620 m depth using 2336 kg/m^3 as mean rock density (Tenzer et al., 2011).

	T (°C) equation 23	T (°C) equation 24a	T (°C) average
Plagioclase margins / groundmass glass (n = 29)			
max	925	868	897
min	852	809	830
median	878	831	**855**
stdv	17.9	13.7	16
Plagioclase microlites / groundmass glass (n = 15)			
max	882	837	860
min	869	823	846
median	873	830	**851**
stdv	4.8	4.3	4.6
	T (°C) equation 24b	T (°C) equation 24c	T (°C) average
alkali feldspar (anorthite) microlites / groundmass glass (n = 12)			
max	864	804	834
min	783	773	778
median	813	784	**799**
stdv	23.5	13.6	18.6
	T (°C) equation 27b	T (°C) global regression	T (°C) average
Plagioclase microlites / alkali feldspar microlites (n = 15)			
max	820	843	832
min	763	787	775
median	807	830	**819**
stdv	18.7	19.5	19.1

Table 7.4 Thermometry results based on feldspar-liquid and two-feldspar thermometers of Putirka (2008). For groundmass glass and plagioclase major element compositions see Appendix A.7.1.

7.7 Discussion

7.7.1 Eruption conditions and the role of phreatomagmatism

Based on preliminary amphibole and plagioclase-amphibole thermobarometry (Appendix A.7.2) the pre-eruption temperature and pressure of the Puketerata rhyolite is around 750 °C and 1 – 1.5 kbar that corresponds to other crystal-rich, hydrous rhyolitic magmas from the TVZ (e.g. Smith et al., 2005; Shane et al., 2007; Matthews et al., 2012; Allan et al., 2013). While the eruption temperatures of ignimbrites are close to the pre-eruptive conditions, the extrusive domes and related pyroclastics are changing as they become almost dry prior reaching the surface due to continuous degassing (Fink et al., 1992; Eichelberger, 1995). A higher temperature is required to drive lava effusion owing to the simultaneous rise of viscosity as a result of fluid loss (Eichelberger, 1995). We have addressed this issue by applying feldspar-melt and two-feldspar thermometry to plagioclase phenocryst rim – groundmass glass, plagioclase microlite – groundmass glass, alkali feldspar microlite – groundmass glass and plagioclase microlite – alkali feldspar microlite pairs (Table 7.4) with the assumption that these pairs have been equilibrated during upward transport of magma, thus representing the magma temperature immediately prior to its eruption. Lower temperatures in the case of alkali feldspar - microlite pairs can reflect a higher sensitivity of alkali feldspar to decompression driven crystallization in the state of undercooling leading to deviations from equilibrium (e.g. Blundy and Cashman, 2008). This suggests that the eruption temperature of magma was close to 850 °C similar to the nearby located Ben Lomond obsidian flow (Sharp et al., 1996) (Fig. 7.2). In the case of microlite-rich bands of the larger dome, the ~100 °C temperature rise might be explained by decompression/degassing driven crystallization (Blundy and Cashman, 2008), however microlites are almost absent from the northern smaller dome and related pyroclastic deposits. Another possible cause of the temperature increase is the invasion of mafic magma into the stagnant magma reservoir, which is a common eruption triggering mechanism within the TVZ (e.g. Nairn et al., 2004; Shane et al., 2007). This possibility is determined through the recorded overgrowth of resorbed plagioclase cores by calcic plagioclase zone that grades outward into a wider zone characterised by An-depletion rimward. This idea is further supported by the antecedent basaltic eruption (Te Hukui) found at the same location as the PVC which also exhibits signs of mixing of rhyolitic and basaltic magma (Chapter 6; Kósik et al., 2017b). A similar event probably initiated the eruption of Puketerata rhyolites. Crystallization (of phenocrysts) was suddenly interrupted and reappeared (as microlites) at higher temperature only as a result of extensive degassing during transport in the volcanic conduit. The temperature rise was likely caused by intrusion of mafic magma although there was not enough time available for mixing or to influence the phenocrysts chemical stability due to the immediate eruption.

Groundmass glass of Puketerata rhyolites displays three textural properties relating to the magma transport, quenching and explosive fragmentation. The firstly formed extremely elongated tube-like pores that are defining the fluidal texture of the rocks represent an open system degassing with bubble coalescence and shearing during uprise through conduit (e.g. Eichelberger, 1995; Castro et al., 2012). The rounded to rectangular shaped bigger vesicles formed at later stages with limited signs of deformation reflect a decrease of pressure prior to quenching. The glass is highly fractured independently from its vesicularity. The fracturing of dense glass and plagioclase and quartz phenocrysts has created globular fragments, sometimes mimicking the texture of perlitic glass (Fig. 7.10B). The vesiculated glass is fractured, angular shards variably bounded by fractures and former bubble walls (Fig. 7.10D). Fracturing corresponds to poorly vesicular, blocky clasts with curviplanar faces and sharp edges (Brooker et al., 1993). These observations verify that fracturing postdated both stages of vesiculation and most likely was driven by contraction associated with melt quenching, fast cooling and glass transition. The estimated water content of groundmass glass implies the glass transition occurred at a depth of around 620 m. Fracturing and fragmentation could continue at lower temperatures and depth as evidenced in the case of hyaloclastites (Porreca et al., 2014). Fragmentation of quenched rhyolitic magma allows the acceleration of mixing with groundwater, which ultimately can create the conditions for launching the MFCI process leading to phreatomagmatic eruptions (Wohletz and Zimanowski, 2000; Austin-Erickson et al., 2008). The widespread pyroclastic deposits of Puketerata demonstrate the dominance of phreatomagmatic explosive activity within every stages of its evolution. The low permeability and slightly sintered ignimbrite of the basement (Leonard et al., 2010) was cut by the Orakeikorako Fault increasing significantly its hydraulic permeability (Lorenz, 2003). The pre-existing maar structure(s) could have functioned as aquifers complemented by an increased surface water flow linked to the fault, which provides adequate water resupply for both deep-seated and near-surface phreatomagmatic activity similar to examples from the *West Eifel Volcanic Field, Germany* (Lorenz, 2003) and *Garrotxa Volcanic Field, Spain* (e.g. Martí et al., 2011). Deep-seated explosions are rarely powerful enough to erupt to the surface because of the prevailing high hydrostatic pressure (Valentine and White, 2012; Graettinger et al., 2014). Continuing activity enables the admixing of fragmented country rocks with the newly erupting volcanic material by debris -and tephra jets. This causes the subsidence of the crater floor and collapsing of the crater walls which induce the widening of the crater (Lorenz and Kurszlaukis, 2007; Valentine and White, 2012), which is the model envisaged for the PVC. The almost complete absence of country-rock bearing products from the PVC basal sequence most likely relate to the maar-forming phase indicating that either the energy of initial explosions were not high enough to fragment and disperse material (Valentine and White, 2012; Graettinger et al., 2015) or the erosion could have removed the majority of these pyroclastic deposits from the surrounding steep slopes. The lack of accidental fragments of the subsequent pyroclastic beds suggests that explosions were only triggered at shallow depth (Brooker et al., 1993). The fragments of the fall units represent variously degassed internal portions of the domes (Fig. 7.9) whereas the breccia dominated units either associated to the destruction of the lava dome by explosions due to overpressurization of the interior or by pure gravitational collapses (Fink and Manley, 1989; Voight, 2000; Calder et al., 2002).

7.7.2 Emplacement of lava domes in relation to associated ejecta rings

Morphometric parameters and surface structures of lava domes provide a great opportunity to understand the factors of their emplacement (Blake, 1990; Anderson and Fink, 1992; Anderson et al., 1998; Fink and Griffiths, 1998; Fink and Anderson, 2000). Two morphologic classifications of lava domes have been carried out aiming to relate their morphology to the effusive conditions (Blake, 1990; Fink and Griffiths, 1998) and 4 types of lava domes have been distinguished (Fink and Griffiths, 1998).

These models have not been able to cope with the factors modifying the original shape of lava domes, such as edifice failures and post growth burial, thus the shape parameters used (e.g. height/radius ratio) (Blake, 1990) rarely characterise the original shape of original edifices. In contrast, the morphology of the dome summits and slope characteristics of the flanks may imply lesser alteration by time (Karátson et al., 2013). Earlier studies classified the larger Puketerata dome by its height/radius ratio as a low lava dome (Brooker et al., 1993) which roughly corresponds to platy domes in the classification of Fink and Griffith (1998). However, lava domes that have been enclosed by deep craters or tephra rings should have been excluded from this kind of classification (Blake, 1990) because of the obscuration of the lower parts of the domes. Our stratigraphic and geomorphologic observations indicate the burial of the lower 50-100 m of the dome. Moreover, neither its slopes nor the summit region exhibit similarities to platy domes. The lava dome emplacement was accompanied by frequent explosions and generation of block-and-ash flows which are more related to Peléan activity (Blake, 1990) and the final morphology is more consistent with the characteristics of exogenous spiny or lobate domes (Fink and Griffiths, 1998). Using dome shape parameter (Ψ_B: 0.03-0.62) for spiny-lobate domes, density of PVC rhyolites (Δ= 2400 kg/m^3), solidification parameter (t_s = 32 s), and usual yield strength of rhyolite lavas (τ_0: 3.0x10^{-5} Pa) (Griffiths and Fink, 1992b; Fink and Griffiths, 1998), the estimated eruption rate is ranging from 2 to 40 m^3/s (eq. 9; Lyman et al., 2004). This eruption rate is within the range of eruption rates of lava domes erupted in the 20th century (Yokoyama, 2005), however the typical low effusion rates of the majority of eruptive events (median is 4.4 m^3/s) and the high SiO_2 content of Puketerata rocks suggest more realistic values around the lower limit of the calculated range. The inferred volume originated effusively from the vent beneath the larger dome (92.8×10^6 m^3), including the mass of the larger dome and half of the volume of the fall beds and the ejecta ring material, most likely correspond to a duration of activity at least 7-9 months assuming a steady 4-5 m^3/s eruption rate.

Three ejecta ring-dome complexes with different role of explosive activity were selected for the morphologic analysis of the possible interplay of lava dome emplacement and related explosive activity (Fig. 7.11). The size and morphology of these ejecta rings indicate major differences which are attributed to distinct eruptive behaviours. *Kaleni (Acigöl Complex, central Anatolia, Turkey)* represents the simplest and most frequent evolution scenario of activity within the formation of an initial ejecta ring (of a maar) and a subsequent quiescent lava dome emplacement within the crater (Druitt et al., 1995). In contrast, the north ring of *Cerro Pinto, Mexico* (Zimmer et al., 2010) represents an explosive activity dominated evolution in which the role of dome-forming was only inferred by the extensive coarse breccia deposits. The majority of the tephra ring sequence is dominated by pumiceous fallout deposits indicating in this case the importance of magmatic fragmentation (Zimmer et al., 2010), whereas there are examples (e.g. *Tepexitl, Mexico*) for the dominance of phreatomagmatic and increasing internal pressure related explosive activity for the final large scale destruction of lava dome (Austin-Erickson et al., 2011). The activity of Puketerata and *Panum Crater, USA* can be positioned between these two end-members. Initial phases of these events were also considered as a maar-forming eruption producing breccia excavated from notable depth (Sieh and Bursik, 1986) that was followed by phreatomagmatic eruptions forming pyroclastic surge beds. Subsequent activity was characterised by lava dome growth associated with BAF generations and recurring explosive activity causing multiple destruction events within the crater. The total volume of Panum dome BAFs was estimated to be 13 × 10^6 m^3 DRE (Sieh and Bursik, 1986) which is a slightly larger volume than current visible intra-crater domes there (Fig. 7.11). Stratigraphic observations at Puketerata determined that the most voluminous middle succession of the ejecta ring is dominated by chaotic coarse breccia units of rockfall, block-and-ash flow and explosion breccias, whose dispersal would have been mostly limited to the near vent areas. Furthermore, geomorphic surveys have highlighted, that the PVC ejecta ring is higher than other ring structures and its outer slopes are anomalously steep (Vespermann and Schmincke, 2000) (Fig. 7.5). The inward facing slopes cut through outward sloping bedding similarly to at Panum Crater. This feature was considered as a result of crater widening due to explosions or slumping processes (Sieh and Bursik, 1986). These features and the moat formation should have post-dated the deposition of the breccia units within ejecta ring sequence. Thus, this structure embracing the larger dome in comparison with the earlier described fall and surge-dominated ejecta rings (Wohletz and Sheridan, 1983; Zimmer et al., 2010) represents a breccia-dominated structure mostly piled up due to gravitational collapses.

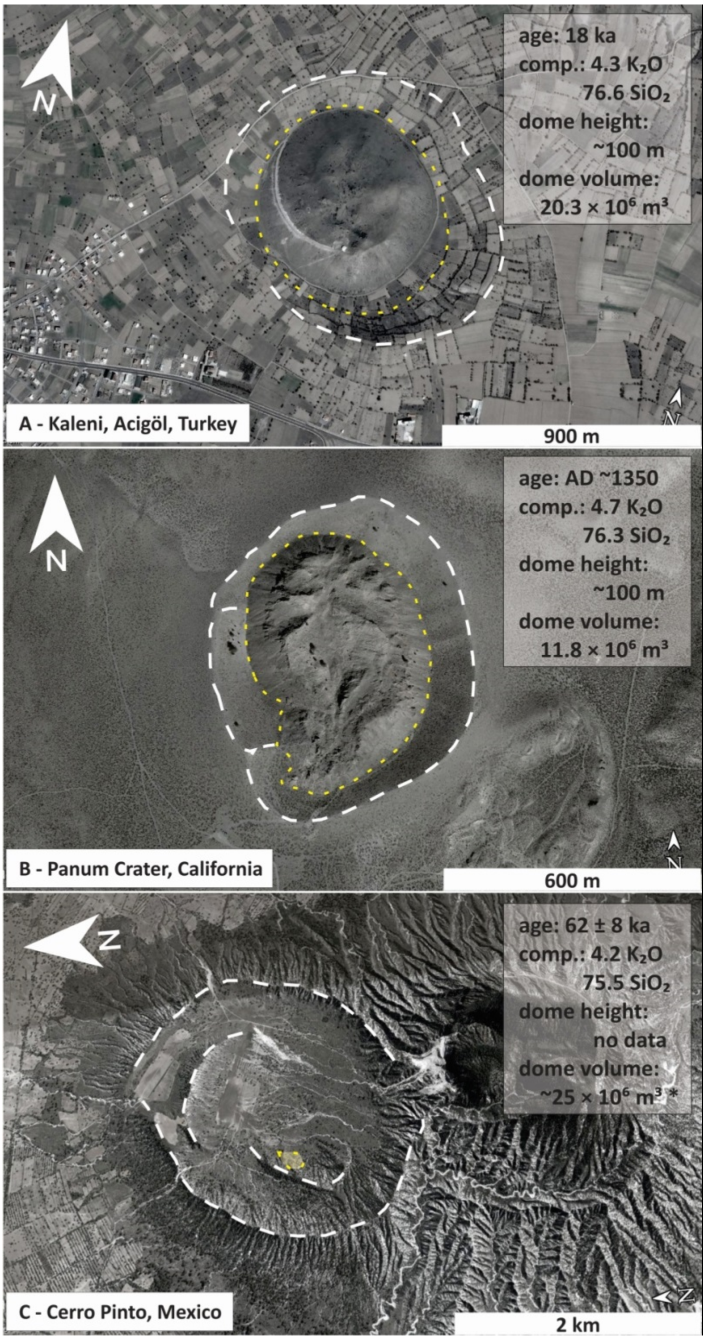
N
age: 18 ka
comp.: 4.3 K_2O
76.6 SiO_2
dome height:
~100 m
dome volume:
20.3 × 10^6 m^3
A - Kaleni, Acigöl, Turkey
900 m
N
age: AD ~1350
comp.: 4.7 K_2O
76.3 SiO_2
dome height:
~100 m
dome volume:
11.8 × 10^6 m^3
B - Panum Crater, California
600 m
N
age: 62 ± 8 ka
comp.: 4.2 K_2O
75.5 SiO_2
dome height:
no data
dome volume:
~25 × 10^6 m^3 *
C - Cerro Pinto, Mexico
2 km

*Figure 7.11 Example for ejecta ring (tuff ring) - lava dome complexes with different evolution. Rims of ejecta rings are marked by white dashed lines, dome margins are marked by yellow dashed lines. Source of data: Kaleni (Druitt et al., 1995); Panum Crater (Sieh and Bursik, 1986; Kelleher and Cameron, 1990); Cerro Pinto (Zimmer et al., 2010).(*Possible dome volume of Cerro Pinto derived from the volume of BAF deposits).*

7.7.3 Evolution of Puketerata Volcanic Complex

The pre-eruptive surface prior to the rhyolitic eruption was characterised by a fault-bounded environment with a watercourse parallel to the Orakeikorako Fault. The left bank of this stream was a gently sloping terrain in contrast with the fault plain and related steep slopes on the right bank (Brooker et al., 1993). The immediate basement rocks indicate powerful basaltic explosive activity prior to the eruption of Puketerata at locality 3-14 (Figs. 7.2, 7.12A) (Kósik et al., 2017b), however the topographic and stratigraphic position of different PVC structures and the glass transitional depth clarifies that the rising magma most likely interacted with groundwater at a reasonable depth inducing some excavation and widening of the earlier formed maar craters along the Orakeikorako Fault (Fig. 7.12B). Besides the four complete circular rim structures of maar craters, an additional nesting rim-like ridge emerges from under the ejecta ring. Therefore it is likely that further maar craters exist towards to southwest, which were overgrown by the larger lava dome and associated debris apron at the middle section of the fissure. Rising magma and explosions occurred gradually in shallower depths generating wet eruption clouds and horizontally moving coherent pyroclastic surges characterised by increasing runout distances. The erosional and oxidation structures indicate that at least shorter (hours to days) breaks may have been common during the deposition of these PDC deposits. The rhyolite textures of the northern small dome and associated pyroclastic sequence in its surroundings are slightly different from the texture of larger dome and related sequences. These minor differences do not change the common origin and evolution of both types of rhyolites, but suggest distinct transport, degassing and cooling processes as a result of the emergence of separate magma batches. The covering thick sequence of fine and coarse surge related beds on the top of the smaller dome demonstrates that this structure must have been constructed earlier than the larger dome and this vent was not active during later times. The coarse-grained angular lapilli rich horizons were formed by intermittent and coeval air fall events, whose clasts are mostly derived from a growing southern lava dome. The transformation to dry pyroclast surges above the event defined by event F2 is probably the sign that the dome expanded beyond the crater terminating the surface ponding of rainwater around the dome. The eruptions produced predominantly dry surges until event F4. This fall unit thickness, grain properties (e.g. higher average grain size and vesicularity up to 45%) and its estimated DRE volume (5-10 × 10^6 m^3) indicate a large scale destruction of that lava dome (Figs. 7.8-7.10). The DRE volumes of fall beds related to the largest explosions, conflict with the features of sub-Plinian activity and correspond to a maximum VEI of 2-3 without reaching the stratosphere. The subsequent activity was mostly characterised by wet diluted PDCs which might be the sign of rainwater accumulation within the newly established depression enclosed by the newly formed ring structure, and fallout beds linked to less destructive internally triggered explosions (Fig. 7.12C). Block-and-ash flow deposition was becoming frequent due to the lava dome growth, but its coarser and dense portion of PDCs were characterised by short runout distances. Several explosions were triggered along the margin of the dome that formed the current morphology of the ejecta ring. The absence of any Puketerata-related beds on the dome summit area and its morphology indicate that some lava effusion and associated weak explosive events represent the final stages of the activity (Fig. 7.12D). The patchy appearance of Puketerata deposits indicates dynamic erosion affecting the area characterised by re-incision of two paleovalleys exposing the sequence between the ejecta ring and a smaller dome and at the eastern side of the tuff ring nearby the Orakeikorako Fault. The last major surface forming event affecting this area was the 1800 AD Taupo eruption, whose products mantled and smoothed the landscape. The depressions and valleys were filled up with thick ignimbrite deposits resetting the landscape.

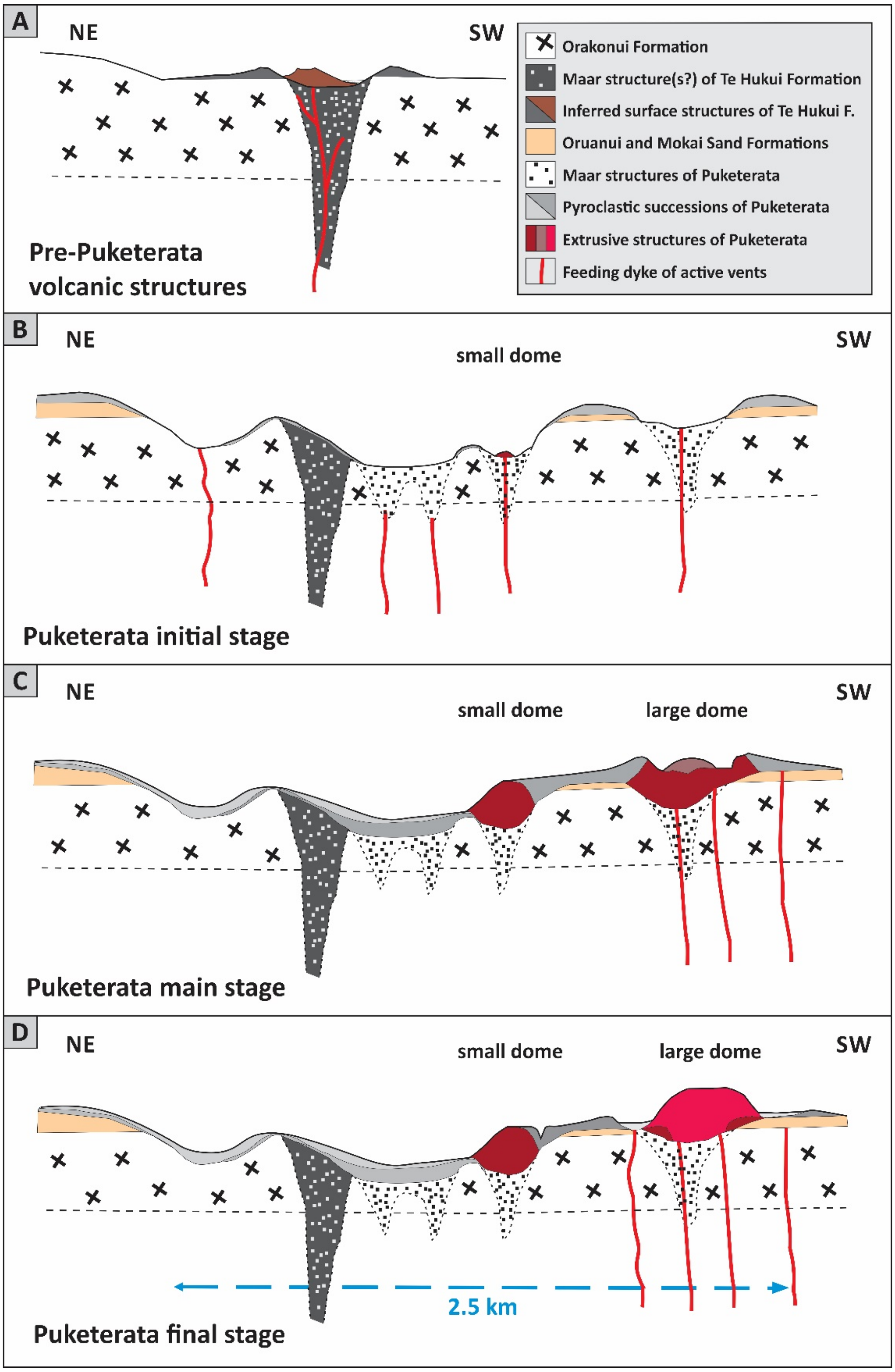
A
NE
SW
Pre-Puketerata volcanic structures
Orakonui Formation
Maar structure(s?) of Te Hukui Formation
Inferred surface structures of Te Hukui F.
Oruanui and Mokai Sand Formations
Maar structures of Puketerata
Pyroclastic successions of Puketerata
Extrusive structures of Puketerata
Feeding dyke of active vents
B
NE
SW
small dome
Puketerata initial stage
C
NE
SW
small dome
large dome
Puketerata main stage
D
NE
SW
small dome
large dome
2.5 km
Puketerata final stage

Figure 7.12 NE-SW trending profiles along the eruptive vents are showing the evolution of the PVC and pre-eruptive volcanic structures (A) at the vicinity of Puketerata (not to scale). Initial phase (B) was characterised by deep to shallow-seated phreatomagmatic activity along the fissure vents. Main stage (C) was dominated by extrusive emplacement of lava domes with associated shallow-seated phreatomagmatic activity and destruction of the larger dome. Excavation of the dome margins created a moat between the dome and the ejecta ring. The late stage of activity was characterised by dome growth with minor explosive activity (D).

7.8 Conclusion

The PVC provides unique eruptive sequences with exposures of varied volcanic facies comprising proximal block-and-ash flow deposits, proximal to medial surge deposits and proximal to distal fall beds. The rhyolite of Puketerata was sourced from a similar depth to the usual silicic eruptions of the TVZ and its ascent was most likely triggered by an intrusion of mafic magma. High temperature microlite crystallization and vesicle textures indicate extensive open system degassing during ascent, whereas secondary vesiculation reflects pressure decrease prior to quenching. The interplay between the degassed and brittle rhyolitic magma and groundwater initiated phreatomagmatic eruptions along a 2.5 km fissure zone. The subsequent activity resulted in the effusive emplacement of two lava domes which was interrupted by phreatomagmatic eruptions resulting in the partial destruction of the larger dome and widespread PDC and fall deposits. The series of destructive events created an apron surrounding the larger dome which separated from its source by late stage explosions excavating the current moat. The 16.5 ka PVC is considered as an example of where phreatomagmatism is a strong controlling factor, however most of the earlier basaltic eruptions and the post-Oruanui sequences also indicate influence of magma/water interaction, thus we assume that phreatomagmatic eruptions can be expected as the main volcanic hazard for the future small-volume eruptions within the TVZ. The evolution of PVC indicates that even the eruption of degassed, very small volume of magma can be associated with a range of volcanic processes from lava dome growth to explosive activity that last for several months to years.

Chapter 8

Chapter 8 presents the findings on a rhyolitic and substantially younger dacitic eruption that contributed to the volcanic activity of Motuoapa Peninsula. On the basis of geomorphic observation there were proposed multiple flood events resulting the decrease of lake level of the 1.8 ka high stand of Lake Taupo.

This chapter is based on a submitted journal paper:

Kósik, S., Németh, K., Procter, J.N., Zellmer, G.F. Stewart, R.B.: Shallow subaqueous to subaerial intra-caldera silicic volcanism of the Motuoapa Peninsula, Taupo Volcanic Zone, New Zealand: Surtseyan and dome-forming eruptions fed by crustal melts. Bulletin of Volcanology

Statement of contribution (DRC16 form) is at Appendix D

Chapter 9

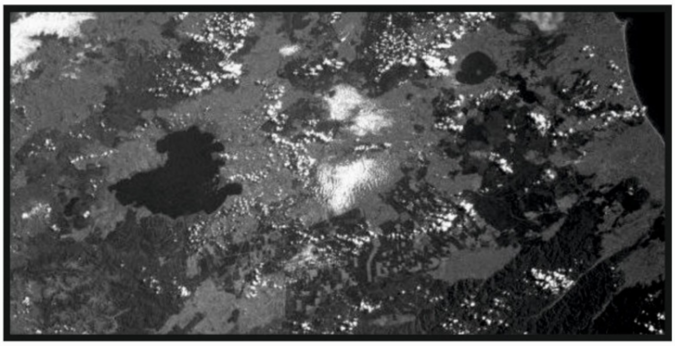

Chapter 9 presents the results of the TVZ–scale spatial, temporal and volumetric analyses of small-volume volcanism based on GIS analysis.

Chapter 9 – Spatial, temporal and volumetric distribution of vents of small-volume eruptions within the TVZ

9.1 Introduction

The landscape of the young TVZ is dominated by seven depressions of calderas and caldera complexes as a result of 12 caldera-forming eruptions in the past 350 ka (Wilson et al., 2009; Gravley et al., 2016). Caldera-formig events are considered to be the most hazardous volcanic activity, due to the eruptive volume and eruption energy that destroy the wildlife and human infrastructure and reset the landscape to a great extent. Besides these large volume (≥35 km^3) eruptions associated with caldera formation, hundreds of smaller-scale volcanic events are known from the TVZ, (Chapters 1, 2 and 5-8) which have produced lava domes or coulees, pyroclastic cones or block-and-ash fans, and pyroclastic sheet-like deposits, such as fallout and small-volume PDC deposits, which often represent fairly energetic volcanic activity and pose immediate hazards in their vicinity.

The existing inventory of these volcanic eruptions is most likely only complete or near complete for the past 45 ka, and only in specific areas, such as at the Okataina and Taupo Volcanic Centres (Wilson et al., 2009). However, a full record of the temporal distribution and erupted volumes of the remaining eruptions would contribute greatly to a better understanding of volcanic evolution and magma production of the entire TVZ (e.g. total magma output volume estimates, total eruption number, total spatio-temporal variations of eruptions etc). To achieve this, a database has been produced, which combines information from the available literature and GIS-based terrain analysis.

For the terrain analyses a DEM with a 4 m grid resolution derived from the contours of topographic maps (New Zealand Topo50) and bathymetric maps of the bigger lakes (Chapter 4) was used. There are limitations and difficulties in the reconstruction of the precise number and locations of past volcanic events. First, the formation of calderas most likely clears away or obscures the structures and deposits that formed in earlier times within the vent/collapse area (e.g. Cole et al., 2005) resulting in an apparent deficit of pre-caldera vents/eruptions. Secondly, the burial by extensive ignimbrite sheets may hide any vents in the vicinity of the calderas, where the pyroclastic deposits may exceed hundreds of metres (e.g. 500-1000 m thickness of Oruanui ignimbrite within the southern basin of Lake Taupo; Davy and Caldwell, 1998). Finally, tectonic movements and erosion are also an important factor that modifies the landscape during which pyroclastic cones/deposits are very vulnerable to erosional processes (Wilson, 1991; Villamor et al., 2017). Besides landscape modification, lakes or seas with a significant water depth may also obscure volcanic structures, such as at Lake Taupo and the larger lakes of the Okataina Volcanic Centre in the TVZ, or at Phlegraean Fields, Italy (Brown et al., 2008; Steinmann et al., 2017) and Kagoshima Bay, Japan (Aramaki, 1984). This problem was addressed by the mapping of lake floors using bathymetry maps. It was also possible to include about 30 subsurface volcanic structures from the Taupo-Reporoa depression (Downs et al., 2014a; Cattell, 2015). These structures are buried under hundreds of metres of lacustrine deposits from ancient Lake Huka, but their locations can be pinpointed as a result of a network of dense boreholes from geothermal exploration (Cattell et al., 2014; Downs et al., 2014a). Vent locations of these subsurface domes may be determined with up to a few kilometres in error.

Most of the DRE volume of distinct explosive eruptions was collected from the literature (Nairn, 2002; Leonard, 2003; Wilson et al., 2009; Leonard et al., 2010; Downs et al., 2014a), whereas the volume of lava extrusions was calculated by their area which was delineated manually from geological maps, and slope and aspect maps, and thickness variations calculated from the surface morphology and base level of volcanic structures using our DEM (Favalli et al., 2009; Grosse et al., 2012; Kereszturi et al., 2013; Di Traglia et al., 2014; Favalli et al., 2014; Favalli and Fornaciai, 2017). Edifice volumes of extrusive bodies (lava domes and coulees) are considered as DRE volumes, with the assumption that the related untraceable pyroclastic deposits and the degree of erosion roughly compensates for the average porosity (5-20%) of lavas (Eichelberger et al., 1986; Fink et al., 1992; Lavallée et al., 2012). Less than 10% of the extrusive bodies were identified from drill holes (Appendix A.9.1; Downs et al., 2014a; Cattell, 2015). The volumes of these subsurface structures were estimated from their drilled maximum thickness using the height-volume correlations (volume = $0.00002h^2$ +

0.002h - 0.1089) of the surficial dome structures of the TVZ. The volume of the pre-caldera structures may be estimated from the accidental lithic content of the pyroclastic product of caldera-forming eruptions by a comprehensive sedimentological and componentry examination, including intra-caldera deposits, such as at *Santorini, Greece* (Karátson et al., 2018). This kind of research exceeds the limit of the present thesis.

The age of single volcanic events (or eruptive period; Manville et al., 2009a) is sourced from the available literature including geological maps (Nairn, 2002; Leonard, 2003; Wilson et al., 2009; Leonard et al., 2010; Ashwell et al., 2013; Downs et al., 2014b). Most of the post-Rotoiti (45 ka) silicic events of the Taupo, Maroa (NE Whakamaru) and Okataina area are well-defined by radiometric dating, however the age of a large number of events within the period 500-128 ka is poorly-constrained and based on mostly stratigraphic observations. In our study we only examined the period between 350 ka and the present because of the limitations of the pre-caldera structures described above. The stratigraphic ages of single eruptions were refined by the age, morphology of the structures located in their neighbourhood and the thickness, or **extent**, of burial by younger deposits.

9.2 Spatial and temporal distribution of eruptive vents

The TVZ comprises approximately 430 vents associated with small-volume volcanism, from which 11 known eruptions occurred prior to the past 500 ka. We distinguished the vents by the chemical composition of their erupted volcanic material (Fig. 9.1). Basaltic or basaltic andesite eruptions are well distributed through the entire TVZ, whereas silicic eruptions occurred only in the central TVZ. Dacites or SiO_2-rich andesites erupted mostly at the eastern margin of the central TVZ, with the three exceptions from the Taupo Volcanic Centre (Fig. 9.1). Rhyodacitic compositions of a few events occurred after the Rotoiti caldera-forming eruption at Okataina (Smith et al., 2005), which are indicated together with rhyolites. The southern TVZ only encompasses four locations (Rangataua Craters, OVC, Pukeonake and Waimarino) that are characterised by mafic magma compositions which erupted between ~15 and 32 ka (Fig. 2.4; Chapter 2).

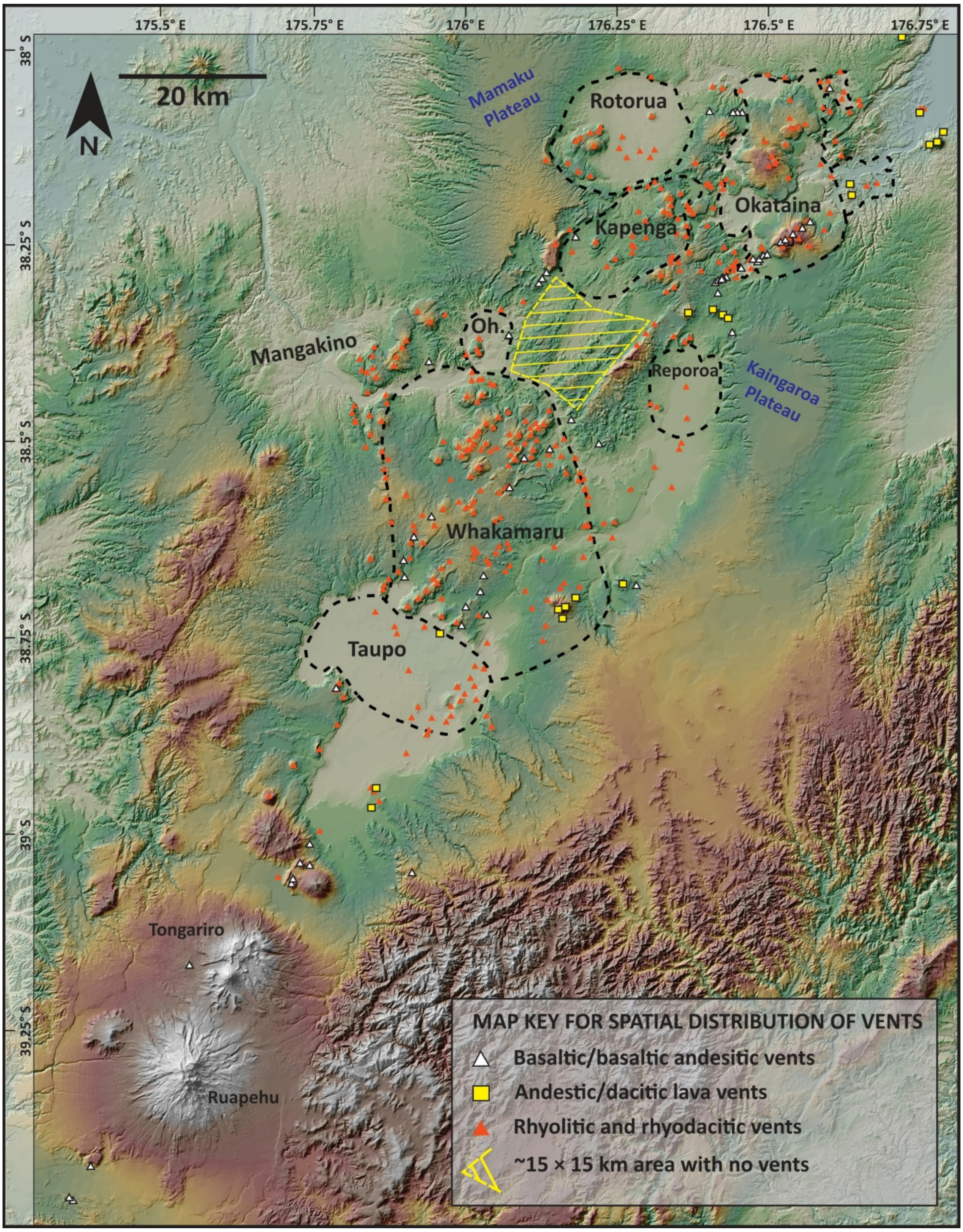
175.5° E
175.75° E
176° E
176.25° E
176.5° E
176.75° E
38° S
38.25° S
38.5° S
38.75° S
39° S
39.25° S
20 km
N
Mamaku Plateau
Rotorua
Okataina
Kapenga
Oh.
Mangakino
Reporoa
Kaingaroa Plateau
Whakamaru
Taupo
Tongariro
Ruapehu
MAP KEY FOR SPATIAL DISTRIBUTION OF VENTS
Basaltic/basaltic andesitic vents
Andestic/dacitic lava vents
Rhyolitic and rhyodacitic vents
~15 × 15 km area with no vents

Figure 9.1 Vent locations of the eruptions of the young TVZ that produced up to 7.5 km^3 DRE volcanic material (Appendix A.9.1). Chemical compositions of the erupted magmas associated with distinct vents are indicated (Nairn, 2002; Leonard et al., 2010). Dashed lines indicate the caldera margins proposed by Wilson et al. (1995). Base map topography was derived from the contour lines of the New Zealand Topo50 map series and the lake bathymetries of the Rotoaira, Taupo, Rotomahana, Tarawera, Okataina, Rotorua, Rotoiti and Rotoma lakes.

Hydrothermal/phreatic eruptions were treated separately, because the known locations probably represent a small proportion of total events due to the fact that the geological maps of TVZ and are not detailed enough to recognise the deposits of such a small event. Most of the known sites of hydrothermal eruptions are concentrated

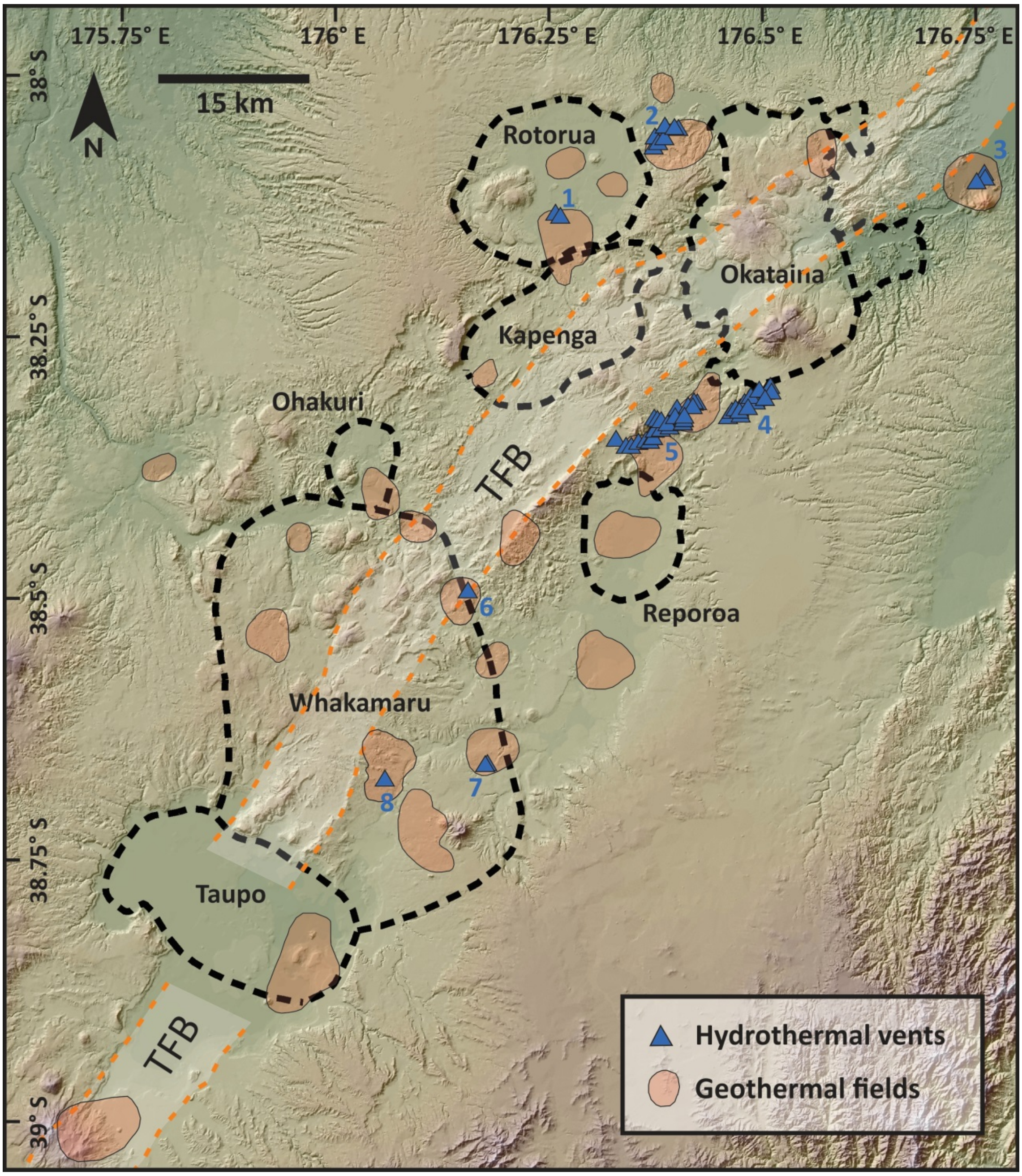
175.75° E
176° E
176.25° E
176.5° E
176.75° E
38° S
38.25° S
38.5° S
38.75° S
39° S
15 km
N
Rotorua
Okataina
Kapenga
Ohakuri
TFB
Reporoa
Whakamaru
Taupo
TFB
1
2
3
4
5
6
7
8
Hydrothermal vents
Geothermal fields

Figure 9.2 Locations of hydrothermal/phreatic eruption craters that have not been associated directly to the activity of polygenetic volcanoes, such as Ruapehu, Tongariro and White Island; 1 – Kairua Park and Te Puia, Rotorua; 2 – Tikitere – Hellsgate Geothermal Park; 3 – Kawerau Geothermal Field; 4 – Rerewhakaaitu fissures; 5 Waimangu-Waiotapu; 6 – Orakeikorako; 7 – Rotokawa; 8 – Craters of the Moon. Geothermal fields are after Rowland and Sibson (2004), caldera margins (black dashed lines) are after Wilson et al. (1995).

around popular tourist sites (e.g. *Craters of the Moon, next to Taupo*) or within areas affected by geothermal exploration where detailed mapping was completed (Fig. 9.2).

9.2.1 Mafic eruptions within the central TVZ

The distribution of mafic eruptions indicates that many occurrences are located at the edges of the Taupo Fault Belt (TFB) at the southern part of central TVZ. Only a few locations, such as Terrace Road Basalt and Waimarino Basalt, are located far away from the TFB at the eastern side of the TVZ (Figs. 2.4 and 2.7; Chapter 2). In the region of Okataina Volcanic Centre four basaltic eruptions are known, from which two significant fissure eruptions occurred in the Holocene age (Tarawera-Rotomahana-Waimangu and Rotokawau- Rotoatua, Fig. 2.7; Chapter 2). The two northern locations are probably located at the edge of the TFB as well, whereas the southern two erupted from the Tarawera Linear Vent Zone, which presumably is also located near to the southern edge of the TFB (Fig. 9.1). The Rerewhakaaitu fissures may represent an extreme east occurrence of basaltic dyking, such as Waimarino (Fig. 9.2). The dyke was arrested only a few tens of metres below the surface, but produced phreatic eruptions along a 5 km long zone. Basaltic eruptions in the TVZ usually produce a very small volume of pyroclastic material, from which distal deposits are very vulnerable to erosion. Thus, there could be many undiscovered basaltic vents. The validity of this assumption is demonstrated by the accidental discovery of the Te Hukui Basalt during this research (Chapter 7).

The temporal distribution of mafic events is poorly constrained. Their mineral compositions and alteration make basaltic rocks unsuitable for accurate radiometric dating. Based on stratigraphic ages, the oldest basalts yield an age of 281 ka (Terrace Road Basalt), whereas the youngest eruption, the 1886 Tarawera-Rotomahana event, is the only historic eruption in New Zealand that occurred in the central TVZ (Fig. 9.4). Petrography of rhyolitic rocks indicates that subsurface basaltic dyking occurs more frequently than dykes reaching the surface (e.g. Chapter 6; Leonard et al., 2002; Shane et al., 2007).

9.2.2 Silicic eruptions within the central TVZ

Silicic vents are distributed roughly evenly, both parallel and perpendicular to the axis of the extension of TVZ, except a 15 × 15 km area north from the margins of the 349 ka Whakamaru caldera where there is no sign of any volcanic activity (Fig. 9.1). The eastern margin of this area is the inferred location of the fissure eruption of the Paeroa Subgroup ignimbrites formed at 339 ka (Downs et al., 2014b). There is an apparent deficit in the vents at the southern basin of Lake Taupo, however geophysical surveys (Davy and Caldwell, 1998) indicate that a number of dome structures covered by 0.5-1 km thick Oruanui deposits lie outside the Oruanui caldera structure. These extrusive structures are emplaced on the top of the ignimbrites that associated to the Whakamaru event (Davy and Caldwell, 1998). The southernmost part of the central TVZ overlaps with the southern TVZ in terms of small-volume eruptions. Within this 8 km long overlapping section, the eruptions are restricted to the Rotopounamu Graben and Lake Rotoaira (Fig. 2.4; Chapter 2). The existing scoria cones and lava flows in the 1.8 km wide graben have an andesitic composition, however Motuopuhi Island in Lake Rotoaira indicates a dacitic/rhyolitic composition and represents the southernmost silicic small-volume eruption in the TVZ (Townsend et al., 2008).

The oldest vents located out of the eastern margin of Whakamaru are characterised by an age of about 1 Ma (Leonard et al., 2010). This age corresponds to the waning activity of the Mangakino Volcanic Centre outside the boundary of the young TVZ (Briggs et al., 1993). Within the young TVZ the oldest structure on the surface is located at the north margin of Reporoa, indicating an age of a little less than 1 Ma. Outside of the structures of Rotorua and Okataina there are many domes with an age between 0.4-0.6 Ma (Fig. 9.1). At the southern half of the central TVZ there are no vents with a pre-Whakamaru (350 ka) age (Leonard et al., 2010). The youngest silicic eruptions have occurred within or relatively close to the Taupo and Okataina Volcanic Centres (Figs. 9.1 and 9.6).

9.2.3 Relationship between vent locations and the structural elements of the TVZ

A statistical approach was applied in an attempt to identify systematic patterns in the spatial distribution of eruptive vents through the correlation with faults (New Zealand Active Faults database; Langridge et al., 2016), and caldera and geothermal field locations/boundaries (Foxall and Baddeley, 2002). Linear objects were converted to points every 10 metres in ArcGIS 10 and the distance was calculated between the vents and nearest point traces of linear objects, such as faults, caldera and geothermal field boundaries. There are limitations and possible error factors from our results: (1) There may be uncertainties in the delineation of structural margins of calderas (Wilson et al., 1995), such as the Puhipuhi basin and Okareka embayment at the Okataina

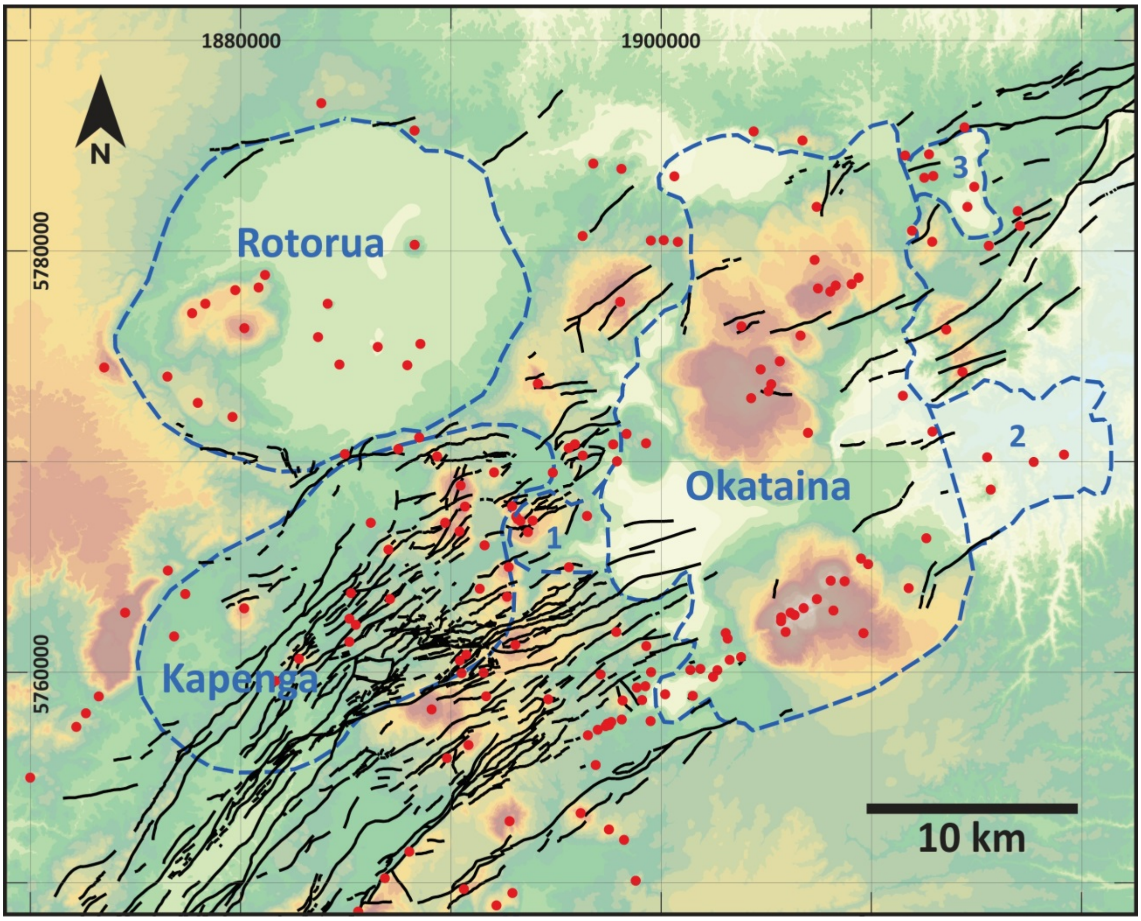

Figure 9.3 Example for the varied awareness of fault locations between relatively old surfaces (area of Kapenga) and areas covered by young volcanic deposits (Okataina) or lakes (Lake Rotorua) based on GNS Active Fault Database. 1 – Okareka embayment; 2 – Puhipuhi basin; 3 – Rotoma caldera. Traces of fault from the 1:250000 active faults database of New Zealand (Langridge et al., 2016), caldera margins are after Wilson et al. (1995). Coordinates are given in NZTM2000 projection.

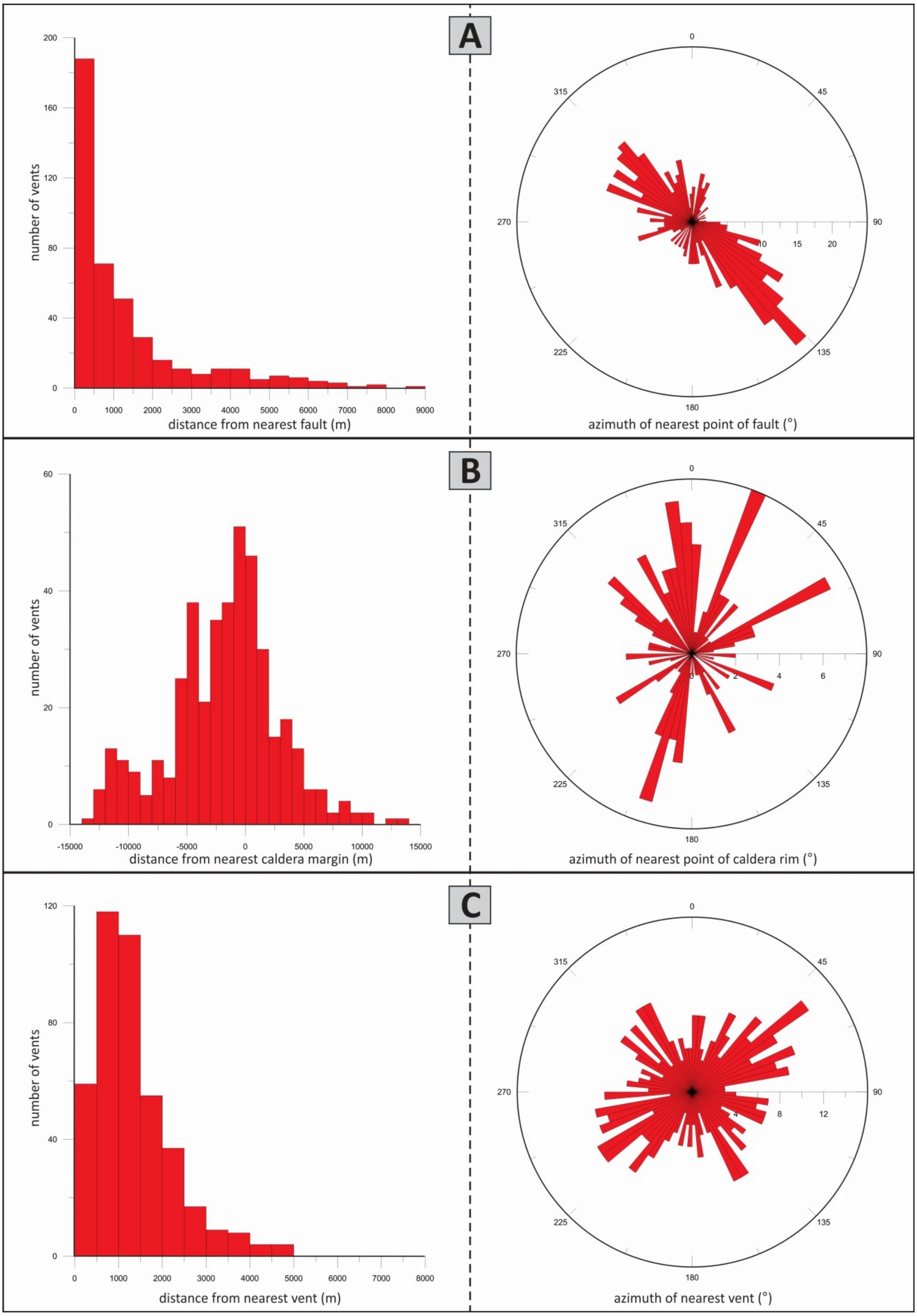

Figure 9.4 Spatial relationships (distance and azimuth) between vents and the nearest structural/volcanic features of the TVZ. A – Vents versus faults; B – Vents versus caldera margins; C – Vents versus vents.

Volcanic Centre (Fig. 9.3) or the margins of older calderas (e.g. Whakamaru); and (2) The completeness of fault mapping is also questionable as the young deposits of calderas obscure the evidence of faulting (Langridge et al., 2016). The TFB crosses the Okataina Volcanic Centre, however the continuity of faults is apparently interrupted inside the caldera (Fig. 9.3). Larger lakes also hide the tectonic lineaments, such as Lake Rotorua and Lake Taupo. In contrast, the older ignimbrite or lava surfaces indicate higher density of faults (e.g. the area of Kapenga), which is expected to be similar at other areas covered by young deposits, lavas and lakes within the TFB (Fig. 9.3). Despite the above mentioned limitations, we found positive correlations with the locations of calderas and fault lines, but there is no correlation with geothermal fields.

The average distance of vents from the nearest faults is about 1300 m, with the values ranging between 0-9 km. About 60% of the vents are located within 1 km of known faults (Fig. 9.4A). If the query area is restricted to specific areas where the majority of the faults are expected to be found (e.g. Kapenga or Maroa), the values indicate only a 200 m average distance between the vents and the nearest trace of faults. This distance is low enough to assume that the vent locations were controlled by the tectonic structures, as indicated by the examples of Ohakune and Puketerata (Chapters 5 and 7). The azimuths of the vents to the nearest fault indicate a deficit in the NE-SW trending directions because of the general orientation of the TFB (Fig. 9.4A).

Based on the spatial relationship of vents of small-volume eruptions and calderas four groups have been established:

> ***A: Vent located well outside of the structural/topographic margin of any caldera:*** the majority of these vents are located either at the south part of the Taupo Volcanic Centre (e.g. Motuoapa, Chapter 8) or south from the Reporoa caldera (Fig. 9.1). Spatially, two of the four dacite lava dome complexes (Edgecumbe and Maungakakaramea/Rainbow Mountain) are also not related to calderas (Fig. 9.1). Structures which appeared prior to the formation of calderas are also classified into this group, such as the dome remnants are located on the margin of Rotorua caldera (Fig. 9.1).

B: Eruption that occurred from an "inactive" caldera: vents were classified into this group if the small-volume eruption is at least 200 ky younger than the date of formation of the caldera. This time is long enough to consider any subsequent volcanic activity in the same place as being associated with a new magmatic cycle. Recent studies of the Toba caldera, Sumatra indicate that post-caldera volcanism occurred within 20 ky after the 74 ka caldera-forming event (Mucek et al., 2017). Residence times of zircons also indicate that magmatic cycles are rarely longer than 100 ky (e.g. Bindeman et al., 2001; Charlier et al., 2004). The relatively young small-volume eruptions of the Whakamaru, Kapenga and Rotorua Volcanic Centres (e.g. *Puketerata*, Chapter 7) were classified into this category.

C: Along the margin of an "active" caldera: there are a large number of events that occurred along the structural margins or ring faults of collapse structures. Most of these vents are located along the east and west margins of Whakamaru, but there are a few examples from Okataina and Taupo as well.

D: Within an "active" caldera, but not relating to any known structure relating to caldera collapse or subsidence: these vents represent the post-caldera activity occurring independently from structural elements of calderas.

Vent locations versus nearest caldera rims indicates that more than 50% of the vents are located within calderas. The highest numbers of vents are located near the caldera rims within a 5 km distance. The highest occurrences of vents are within 1 km of the caldera margins inside or outside of the collapse structure. It is a strong indication that some of the vents of small eruptions are found along the existing caldera margins, such as the western and eastern margins of Whakamaru indicates. The azimuths point to NNE-SSW as the most frequent directions of the nearest caldera margins from the vents (Fig. 9.4B).

The examined vents in relation to one another indicate a range of distance from ~100 m to ~5.5 km, with an average distance of 1370 m. The azimuth to the nearest vents indicates two dominant directions. Most commonly, for a given vent, the nearest vent is located roughly to the direction that is parallel or perpendicular to the orientation of the TVZ (Fig. 9.4C). The parallel arrangement of vents is attributed to the strong influence of the NE-SW trending structural elements of the TVZ in the eruption locations. The perpendicular arrangement may be caused by the effect of extension, which results in the shift of weakness zones perpendicular to the orientation of the TFB.

9.2.4 Temporal distribution of small-volume volcanism and its spatial implications

We examined the overall pattern of temporality of small-volume events and their spatial variation through the TVZ (Fig. 9.5). Only a small number of events were found that occurred before half a million years. Three periods indicate a significantly higher number of events than the average. The earliest indicates that volcanism occurred after the Whakamaru eruption. The second peak comprises regular small events with poorly-constrained ages occurring at the vicinity of the southern Whakamaru area and Lake Taupo around 100 ka. The third peak represents the past 25 ky, in which a relatively high number of events is consistent with the high erupted total volume within the same period. However, small explosive events are very vulnerable to erosion and are easily obscured by the products of subsequent volcanic events. Thus, it is likely that small explosive events are underrepresented in our database by going back in time due to the poor preservation potential of eruptive products.

The Y axis of the spatial distribution as a function of the time chart (Fig. 9.5B) displays the distance of vents from the southernmost vent (Motuopuhi Island, Lake Rotoaira) to the NE, along a hypothetic line that was drawn parallel to the extensional axis of the TVZ. The age variations along the Y axis to the south indicates a younger average age for the volcanism and records notable volcanic activity before and around 0.5 Ma only at the northern part of the central TVZ. Then, the volcanic activity was focused within the Whakamaru area. The data displays the shift after the 350 ka collapse event, but there is no information about the activity prior to the Whakamaru caldera-forming events. The areas of Kapenga and Rotorua only indicate a short period of post-caldera activity that is contrasted with Whakamaru. Around 150 ka, volcanic activity was restarted at Okataina and shifted to the south part of the Taupo area. The gap between the south Taupo and Whakamaru areas represents the collapse features of the Taupo Volcanic Centre, where numerous missing vents/events are expected. Thus, it is hard to determine whether there was quiescence between the ~100-150 ka and the currently active period in the Taupo region. Okataina indicates the same feature relating to the Rotoiti collapse. After 100 ka, the waning activity of Whakamaru was compensated by the massive restart of activity at Okataina and Taupo within the past 50 ky (Fig. 9.5B). At the distance of 85-90 km from the southern starting point (Motuopuhi Island, Lake Rotoaira; Fig. 2.5, Chapter 2), the low incidence of vents is clearly visible on maps (Fig. 9.1 and Fig. 9.5B). This area seems to be functioning as a boundary between the southern and northern regions of the TVZ.

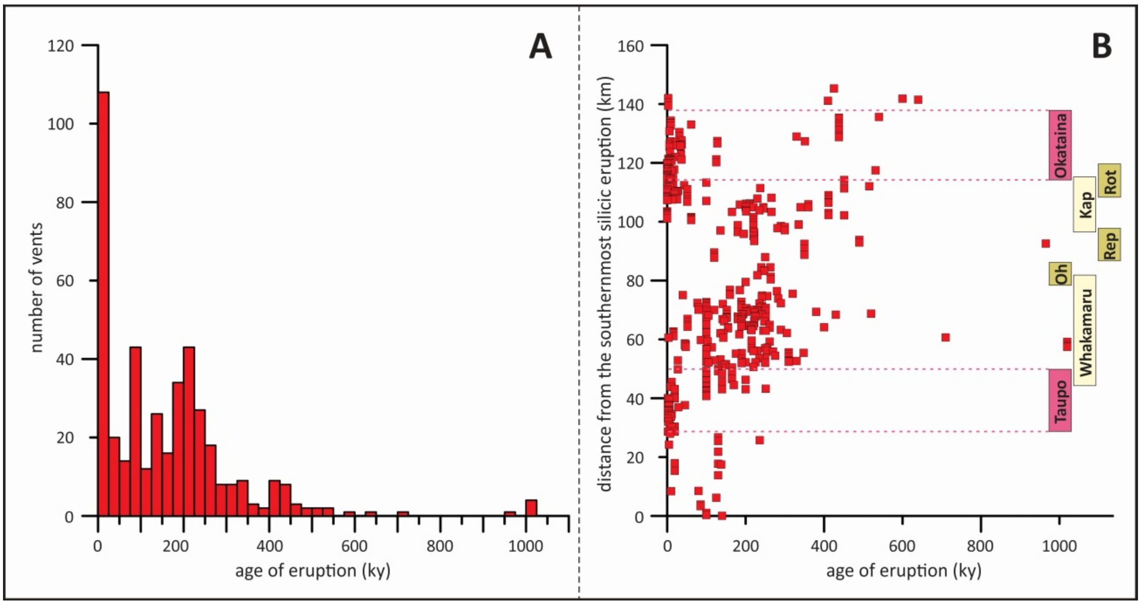

Figure 9.5 Temporal characterisation of the small-volume volcanism of the TVZ. A – Number of vents within a 25 ky intervals. B – Age as a function of distance from the southernmost silicic event (Motuopuhi Island, Lake Rotoaira) to NE along the extensional axis of the TVZ. The NE and SW limits of calderas were indicated by the same way as vent locations.

Spatially, the youngest eruptions (post-Rotoiti) are focused mainly at and in the vicinity of the Okataina and the Taupo Volcanic Centres, however there are five regions outside these calderas where volcanic activity occurred in the past 50-60 ky (Fig. 9.6). The southernmost part of the central TVZ comprises three locations with compositions from basaltic to dacitic and rhyolitic. The expected young age of the rhyolitic eruption (Kuharua) near the SW shore of Lake Taupo needs clarification (Wilson et al., 1986), whereas the Waimarino Basalt and the dacite of Korohe and Motuoapa are emplaced after the Oruanui event (Hackett, 1985; Chapter 8). South Maroa comprises four events between 45 to 16.5 ka (Wilson et al., 2009; Chapter 6), whereas the basaltic event and the cluster of four rhyolitic vents at the eastern margin of Whakamaru yield a bit younger age than the Rotoiti eruption (Leonard et al., 2010). There is a further cluster of post-Rotoiti vents located within the structure of the Rotorua caldera. The age of these vents is also a little bit younger than the Rotoiti event (Ashwell et al., 2013). The only Holocene eruption occurred at Edgecumbe/Putauaki at about 2-3 ka (Carroll et al., 1997). This event produced a conical-shaped lava dome complex with silicic andesitic-dacitic composition (Carroll et al., 1997; Nairn, 2002). The vents of Edgecumbe are located at the NE extension of the Tarawera Linear Vent Zone, thus it might have a strong relationship with the Okataina magmatism. The vents of Earthquake Flat (~45 ka; Wilson et al., 2007; Danišík et al., 2012) are also located outside the boundaries of Okataina (Fig. 9.6), however their identical ages with the Rotoiti event suggest a strong linkage between the two magma reservoirs (Nairn and Kohn, 1973; Shane et al., 2005; Wilson et al., 2007).

Post-caldera activity of the two youngest calderas indicates different spatial and temporal patterns (Fig. 9.6). Most of the Okataina vents are arranged into two linear vent zones (Haroharo and Tarawera) which extend beyond the caldera margins at the west side (Nairn, 2002). A few of the remaining vents were most likely arranged by the structural margin of the Rotoiti collapse. The Taupo Volcanic Centre encompasses two young collapse events. The majority of the Holocene vents were arranged to a linear zone located near the SE margin of the Oruanui collapse, which includes the location of the younger, 232AD collapse structure as well. A number of vents are located parallel to the north margin of the caldera structure, where the faults cross the structural margin of the caldera.

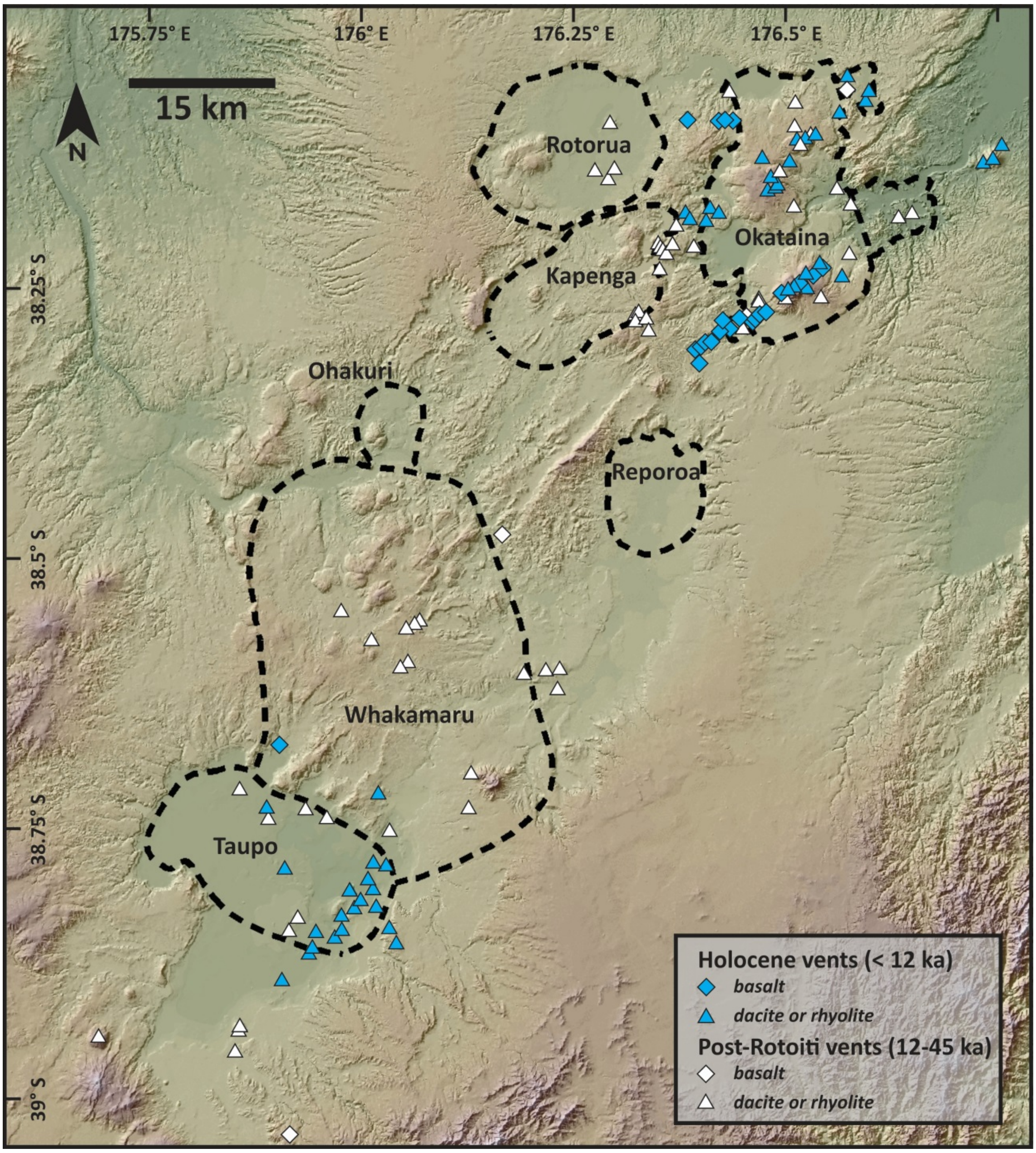
175.75° E
176° E
176.25° E
176.5° E
15 km
N
38.25° S
38.5° S
38.75° S
39° S
Rotorua
Okataina
Kapenga
Ohakuri
Reporoa
Whakamaru
Taupo
Holocene vents (< 12 ka)
basalt
dacite or rhyolite
Post-Rotoiti vents (12-45 ka)
basalt
dacite or rhyolite

Figure 9.6 Spatial distribution of post-Rotoiti basaltic and silicic vents of the central, predominantly silicic part of TVZ. Caldera margins (dashed lines) are indicated after Wilson et al. (1995).

9.3 Eruptive volume distribution in space and time

The examined vents produced DRE volumes between 10^5-10^6 m^3 to 7.5 km^3 as individual eruptive events, however only about 30 eruptive events exceed 2 km^3 (Fig. 9.7A). Many of these larger-volume eruptions occurred along fissure zones during which multiple vents were active. Besides the Taupo-related Unit S eruption (Wilson et al., 2009), just the volume of a few coulees at Okataina, as well as the Edgecumbe and Tauhara lava dome complexes, exceed the volume of 2 km^3 DRE emplaced from a single vent. If we follow the usual sensu stricto volume limitation (up to 1 km^3) of monogenetic/small-volume eruptions (e.g. Németh and Kereszturi, 2015), more than 82% of the events can be defined as small-volume eruptions. However, the 1 km^3 limit is defined by the characteristics of mafic volcanism, which typically produce significantly smaller volumes than the silicic systems. Since the other features of these silicic eruptions meet the requirements of small-volume volcanism (e.g. one-off activity

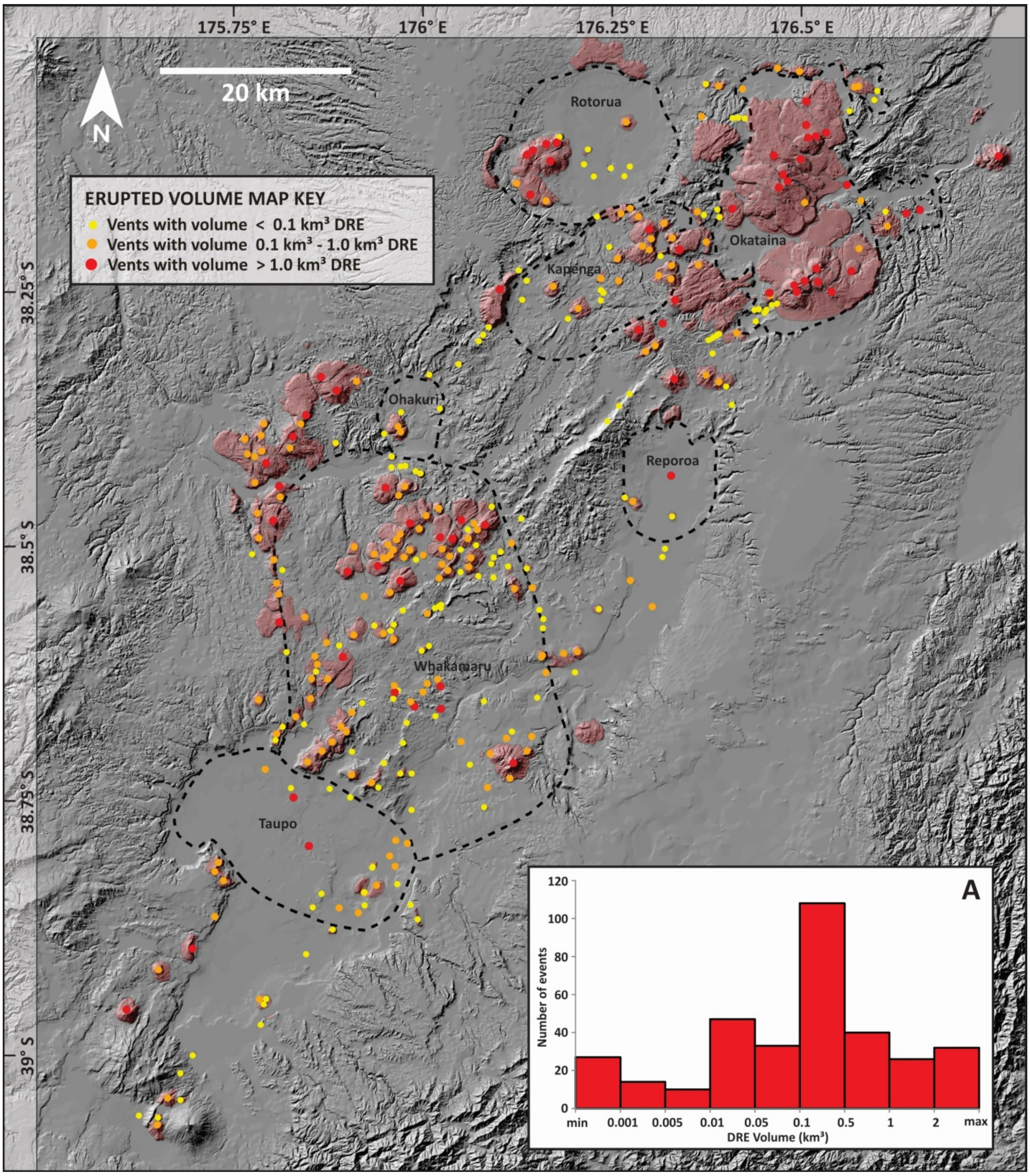
175.75° E
176° E
176.25° E
176.5° E
20 km
N
ERUPTED VOLUME MAP KEY
● Vents with volume < 0.1 km³ DRE
● Vents with volume 0.1 km³ - 1.0 km³ DRE
● Vents with volume > 1.0 km³ DRE
38.25° S
38.5° S
38.75° S
39° S
Rotorua
Okataina
Kapenga
Ohakuri
Reporoa
Whakamaru
Taupo
A
Number of events
0
20
40
60
80
100
120
min
0.001
0.005
0.01
0.05
0.1
0.5
1
2
max
DRE Volume (km³)

Figure 9.7 Spatial distribution of silicic lava domes and coulees (light red shaded areas) and erupted volumes in DRE of effusive and explosive eruptions of TVZ within the past 350 ky. Dashed lines indicate the caldera margins proposed by Wilson et al. (1995). Inset Figure (A) indicates the volume size distribution of distinct volcanic events in the past 350 ky.

and short eruption duration), we propose the increase of acceptable volumes for silicic monogenetic activity up to 5 km^3 DRE for "*one–off*" effusive events. Most frequently, the small-volume eruptions of the TVZ produce a volume of 0.1-0.5 km^3 (Fig. 9.7).

Spatially, only the large events indicate some regularity as the majority of these events that produced more than 1 km^3 DRE volume of volcanic material are located within linear vent zones, such as the Tarawera, Haroharo, Maroa and Ngongotaha dome complexes (Fig. 9.7). At the northern part of the central TVZ events exceeding 2 km^3 are much more frequent than in the south (Fig. 9.8A). Eruptions under 1 km^3 DRE volumes are evenly distributed across the TVZ, except the northern and southern end of TVZ and the area located between 70-90 km from the southernmost end of the examined area, where a notable deficit is found from the size of eruptions above 0.3-0.6 km^3 (Fig. 9.8B).

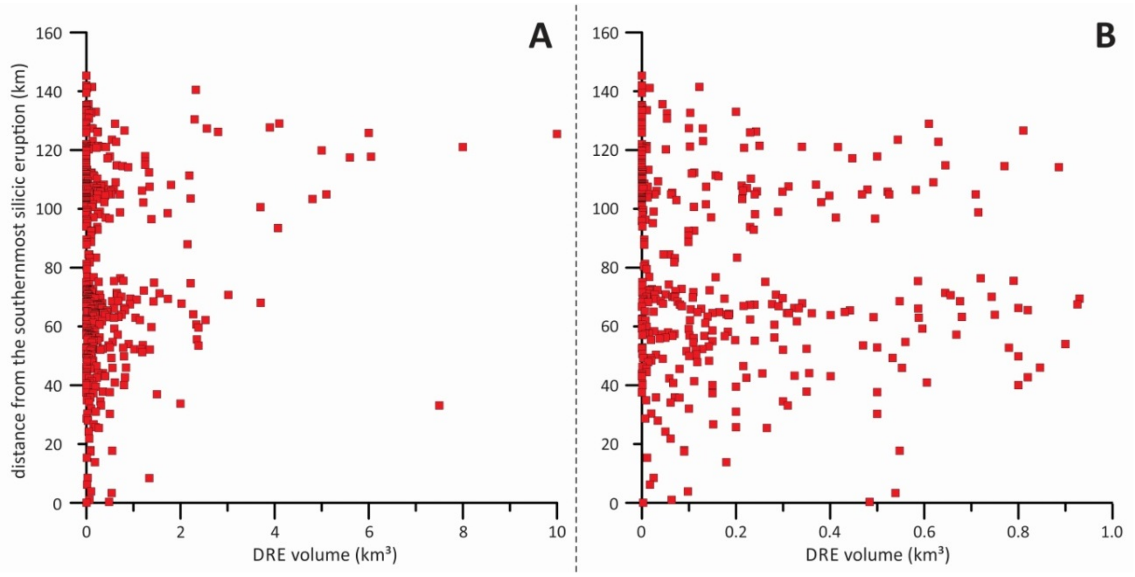

Figure 9.8 DRE volumes as a function of distance from the southernmost silicic event (Motuopuhi Island, Lake Rotoaira) to NE along the extensional axis of TVZ. A indicates erupted volumes under 10 km^3, B is zooming to events under 1 km^3 erupted volumes.

The temporal distribution of the produced volumes may be an indication as to the evolution and overall magma production of the central TVZ. Our data is plotted to a cumulative volume versus time diagram (Fig. 9.9). We found four periods in the past 350 ka characterised by a different volume production of small-volume volcanism. The first period finished around 275 ka when the cumulative graph indicates intensification of magma production. However, since there is limited and presumably deficient data from the 350-275 ka period, we cannot be sure about the data validity of volume production of this period. The second period ends around 180 ka, as indicated by the decrease of magma production from 0.8 km^3 to 0.2 km^3 per 1000 years. The low-production rate period lasted until 45 ka, which is followed by the current period characterised by a very high volcanic material production at the rate of 3 km^3/ky (Fig. 9.9). This production rate corresponds to six times higher than the average of previous 300 ky and 12 times higher than the former 50 ky period. The erupted ~150 km^3 DRE volume of volcanic material is equivalent to the average volume of ignimbrites of caldera-forming eruptions of the TVZ. The spatial distribution is uneven since 24 events of Okataina produced 111.7 km^3, whereas the 38 events of Taupo only produced 18.8 km^3 DRE volume.

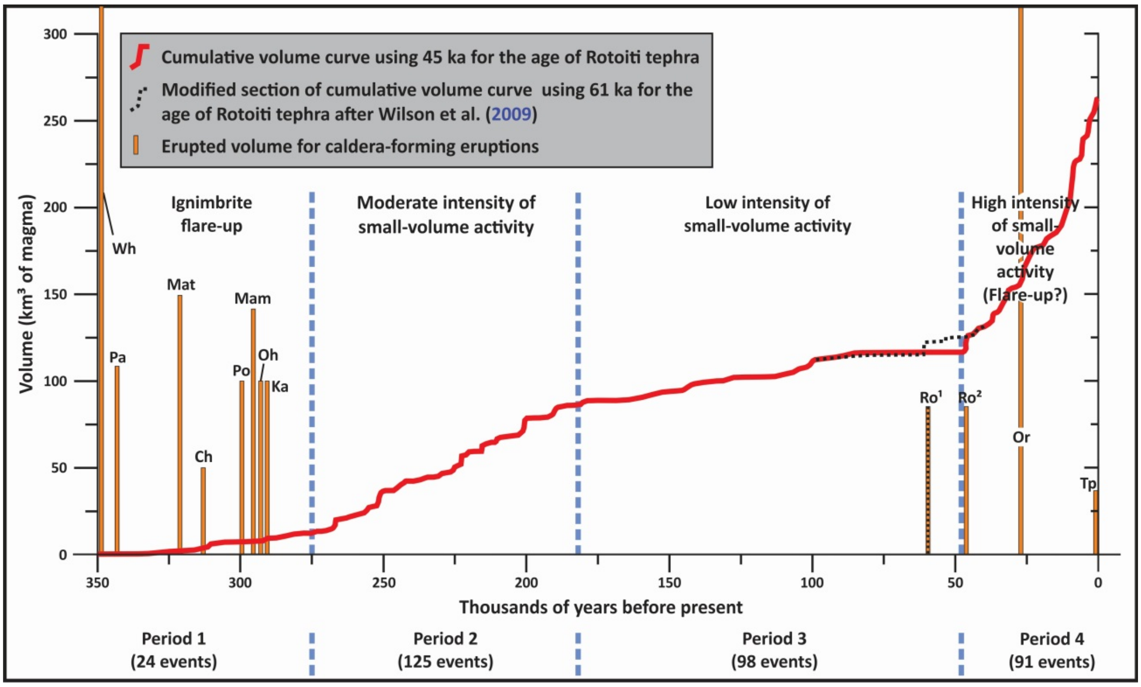

Figure 9.9 Cumulative DRE volumes as a function of time for the central TVZ's 337 small-volume eruptions within the past 350 ka. For comparison, the caldera-forming eruptions' temporal distribution and erupted DRE volumes are indicated after Wilson et al. (2009), Danišík et al. (2012) and Gravley et al. (2016);. Wh – Whakamaru, Pa – Paeroa Subgroup, Mat – Matahina, Ch – Chimpanzee, Po – Pokai, Mam – Mamaku Plateau, Oh – Ohakuri, Ka – Kaingaroa, Mo – Mokai, Ro – Rotoiti, Or – Oruanui, Tp – Taupo.

Chapter 10

Chapter 10 summarises the results from the case studies along with the discussion on the source of erupting magmas, characteristics of eruption styles, and internal and external influencing factors of the small-volume volcanism, as well as their spatio-temporal relationship to caldera-forming eruptions of TVZ. Besides the evaluation of main factors contributing to the hazard of small-volume eruptions, two conceptual models were proposed for eruption location prediction and susceptibility for hydrovolcanic activity within the central TVZ.

Chapter 10 – Discussion and conclusions

10.1 Synthesis of the volcanism of the studied localities

The five eruptions preserved at the three example localities involved various rock types, from basalts to rhyolites and occurred within diverse environmental settings in terms of subsurface and surface hydrology. Chemical composition of magma and environmental conditions primarily influence the eruption conditions and resulting eruption styles that are most dramatically visible in small-volume eruptions (Smith and Németh, 2017). While such interplay between the magma internal physio-chemical conditions and the eruptive environment is most obvious and influential in association with small-volume mafic volcanism, such a relationship likely exists in any type of volcanic systems. However, the recognition of distinct variables might be increasingly complicated in large-volume (polygenetic) systems (e.g. Smith and Nemeth 2017). The studied locations can therefore provide representative examples of volcanism exhibiting the widest possible range of eruption scenarios of relatively small-volume (up to 2-3 km^3) volcanism of the TVZ. Eruptions with volatile-rich silicic magmas that usually induce Plinian/sub-Plinian convective plumes were not included in case studies, as many examples of these were comprehensively studied before from the Taupo and Okataina Volcanic Centres (e.g. Wilson, 1993; Jurado-Chichay and Walker, 2000; Leonard et al., 2002; Kobayashi et al., 2005). Spatially, the location of volcanoes covers the southern half of the TVZ, with one example from the southernmost part of the TVZ (Chapter 5), two eruptions from the southern part of the Taupo Volcanic Centre (Chapter 8) and further two eruptions from the central Whakamaru/southern Maroa area (Chapters 6-7). The calculated erupted volumes of the examined eruptions are based on DEMs matching the most commonly occurring size of eruptions of the TVZ (Chapter 9). The most important features of the volcanic activity of example localities are compiled in Table 10.1.

	Ohakune	***Puketerata***	***Te Hukui***	***Motuoapa rhyolite***	***Korohe and Motuoapa dacite***
Age of eruption	31,5 ka	16,5 ka	> 25,4	138 ± 20 ka	< 25,4
Rock type	Andesite	Rhyolite	Basalt	Rhyolite	Dacite
Bulk SiO_2 content	57%	73%	50%	71,5 - 74,5 %	68.5%
Vent characterictics	Fissure	Fissure	Unknown	Unknown	Fissure
Influence of faults	Yes	Yes	Yes	Yes	Yes
Eruption style(s)	Phreatomagmatic, Strombolian-Hawaiian	Phreatomagmatic, Pelean, Effusive	Phreatomagmatic, Strombolian	Surtseyan, Pelean, Effusive	Effusive, (Pelean)
Evolved volcanic structures	Tuff ring, Cinder cone	Maar - tuff ring, Lava dome	Maar	Tuff cone, Lava dome/coulee	Lava dome
Inferred depth of excavation	Max up to a few tens of meters	Max. up to 600	Significant without known exact depth	Unknown	N/A
Total erupted DRE volume	0.012	0.14	<0,002 (inferred)	0.3	0.045
Volume of pyroclastic deposits	0.012	0.07	<0,002 (inferred)	0.15	None
Length of activity	3-5 months	7-9 months	Hours to days (inferred)	13-26 months	max 1-2 months (inferred)
Dominant stratification	Cross- to plane-parallel-bedded	Cross- to plane-parallel-bedded	Cross- to plane-parallel-bedded	Massive to crudely stratified	N/A
Sedimentary features	Accretionary lapilli, Soft sediment def., Slumping	Accretionary lapilli, Erosive surfaces	Soft sediment def., Slumping	Explosive excavation	N/A
Main transport mode of pyroclastics	Wet base surges, Fallout	Base surges, Block-and-ash-flows, Fallout	Wet base surges, Pyroclastic flows, Fallout	Base surges, Block-and-ash flows, Fallout	N/A
Furthest deposits found from vent(s)	600 m: PDC, fallout, ballistic	8.5 km: fallout 3 km: PDC	Unknown	3 km: lava 1 km: PDC, fallout	lava piled up only above the vent
Dominant juvenile grain size	Coarse lapilli to fine ash	Bomb/block to fine ash	Coarse to fine ash	Bomb/block to coarse ash	N/A
Juvenile content	90-95 %	>95 %	Lower part: 10 % Upper part: 90 %	100%	N/A
Vesicularity of juveniles	Variable	Poor (<30 %)	Variable	Variable	N/A
Dominant accidental lithic phases	Andesitic boulders from the laharic basement	Orukanui Fm.	Orukanui Fm., Variable types of lava	Unknown	N/A
Influence of external water	Yes	Yes	Yes	Yes	Unknown
Substrate type	porous media controlled	fracture controlled	fracture controlled	subaqueous	porous media controlled

Table 10.1 Summary of general eruption-related, petrologic, morphometric, sedimentary and pyroclastic characteristics of studied volcanoes.

10.1.1 Origin, chemical and petrological characteristics of erupted magmas of studied volcanoes

Only the basalt of Te Hukui originated directly from the upper mantle. The volcanic rocks of the other four eruptions comprise crust-sourced more evolved magmas. Various degrees of interaction between different melts, or melts and crystals of the mush zone, have been observed at Te Hukui, Ohakune and Puketerata, whereas Motuoapa and Korohe indicate a high degree of crustal anatexis (Chapter 8) as the main source of magma. Based on petrographic observations, the existence of crystal mush zone is evidenced at Puketerata. The rhyolitic eruption of Puketerata was likely triggered by an intrusion of mafic melt into a stagnant magma reservoir, as documented in many other cases within the TVZ (e.g. Kaharoa eruption, Tarawera; Leonard et al., 2002).

The chemical composition of rocks from other examined localities covers the entire range of TVZ eruptive products (Table 10.1). The Te Hukui basalt is a newly-discovered member of the high-alumina basalt occurrences of the central TVZ. The basalt phenocryst phases consist of plagioclase, clinopyroxene and forsterite-rich olivine. Many of the plagioclase cores are picked up from the silicic crystal mush through which the basaltic dyke reached the surface. In contrast, the low-silica andesite of Ohakune is characterised by a relatively high-silica groundmass glass composition and xeno/antecrystic ferromagnesian mineral assemblage with orthopyroxene, clinopyroxene and olivine. This suggests the remobilisation of a crystal mush of a mafic body by an intrusion of more evolved magma.

The dacite of Motuoapa and Korohe displays an uncommon assemblage of iron-rich ferromagnesian minerals. The nearby Tauhara dacite lava dome complex, as well as other dacite occurrences, display lower iron phenocryst compositions, and the Tauhara magma was predominantly formed by a mixing of silicic and mafic magmas (Graham and Worthington, 1988; Millet et al., 2014), which is in contrast to the suggested anatexis of iron-rich crustal rocks as the main source of Motuoapa dacite.

Two eruptions were examined that are characterised by rhyolitic compositions. The rhyolites of Motuoapa also have an iron-rich ferromagnesian mineral assemblage with amphibole, orthopyroxene and fayalitic olivine. The generation of magma could be very similar to the dacite of Motuoapa, however the plagioclases indicate higher silica content, whereas the ferromagnesian phases indicate higher iron content than the phenocrysts in the dacite. Thus, it was considered that the rhyolite of Motuoapa generated by the anatexis of different crustal rocks with higher iron contents than the dacite protolith. The rhyolites of Puketerata were sourced from the same depth as most of the rhyolites (Chapter 7; Cooper et al., 2012; Allan et al., 2013), representing one of the few post-180 ka central TVZ eruptions containing biotite phenocryst (Chapter 7, Sutton et al., 1995; Deering et al., 2010).

In spite of the small number of examples compared to the total number of small-volume events of TVZ, the magma generation and origin of examined volcanoes displays a great diversity. This suggests that a large number of factors play an important role in magma generation and eruption triggering, which have to be detected for a better understanding of the magmatic processes operating in the TVZ.

10.1.2 Local environmental settings

The importance of environmental settings regarding the eruptive style of volcanic activity was first recognised and well-studied at basaltic volcanic fields, where external factors easily influence the eruptions due to the common low discharge rates (Smith and Németh, 2017), such as at the basaltic *Auckland Volcanic Field* (Kereszturi et al., 2014b) and *Bakony-Balaton Highlands Volcanic Field, Hungary* (Kereszturi et al., 2011), as well as the basaltic-silicic *Serdán-Oriental Basin, Mexico* (Carrasco-Núñez et al., 2007; Zimmer et al., 2010; Austin-Erickson et al., 2011). The volcanic activity of caldera systems is usually characterised by larger discharge rates and silicic compositions, where eruption styles may have substantially been influenced if the depression of the caldera is occupied by lakes or flooded by the sea. Subaqueous explosive eruptions in deep water (>150-200 m) may produce pumice rafts *(e.g. 2012 eruption of Havre caldera, Kermadec arc*; Jutzeler et al., 2014) and eruption-fed pyroclastic density currents (e.g. Allen and McPhie, 2009), such as the origin of the recently recognised *middle unit of the Huka Falls Formation* (Cattell et al., 2014). Phreatoplinian, phreatomagmatic or Surtseyan activity is expected for eruptions occurring in shallow water (e.g. *calderas of southern Kyushu, Japan; Furnas volcano, Azores; Phlegraean Fields, Italy; and Masaya Caldera Complex, Nicaragua*; Nagaoka, 1988; Cole et al., 1995; Orsi et al., 2009; Perez et al., 2009).

The example localities represent essentially distinct environmental conditions in terms of substrate and hydrological properties (Table 10.1). The OVC is located within a distal ring plain setting, where the underlying country rocks are characterised by poorly-sorted, high permeability, unconsolidated laharic sediments and thin fine tephra layers (e.g. Palmer and Neall, 1989; Donoghue and Neall, 2001). The ice-capped Ruapehu volcano provides a constant resupply for groundwater reservoirs and watercourses (McArthur and Shepherd, 1990; Brook, 2009; Tost and Cronin, 2016). The abundance of ground and surface water gives the chance for magma-water interaction in the case of volcanic activity (Salinger, 1980; Hellstrom et al., 1998).

At the present time Motuoapa is located on the shore of Lake Taupo, but it is expected the lake had a larger extent and higher levels at the time of the rhyolite eruption at Motuoapa, based on the geographic position of lacustrine sediments (e.g. Brown et al., 1994). This already supports that the eruption could initiate in a subaqueous environment. The morphology of the Oruanui ignimbrite plateaus surrounding Lake Taupo suggests that dacitic eruptions of Motuoapa and Korohe most likely occurred in similar conditions to the present day. Due to the characteristics of the endogenous dome growth of the dacite, the eruption style does not provide information in relation to the height of the lake level or other environmental conditions due to the subordinate role of magma fracturing during endogenous dome growth, thus preventing effective magma-water interaction (Austin-Erickson et al., 2008).

Puketerata and Te Hukui erupted within an environment characterised by a fault-bounded ignimbrite plateau that was incised by watercourses. Within these settings the abundance of water was most likely limited to the bottom of the deepest valleys. The immediate basement at Puketerata is the slightly sintered Orakonui Formation, which represents a “hard-rock” substrate (Lorenz, 2003).

10.1.3 Eruption styles, type of deposits and morphology of the volcanic structures

The examined deposits were formed by eruptions characterised by various styles from lava effusion to magmatic and hydrovolcanic explosive activity. In general, excluding the dacite eruption of Motuoapa and Korohe, all the eruptions indicate distinct eruption styles operated alternately and/or simultaneously.

10.1.3.1 Mafic to intermediate eruptions

The two eruptions comprising the less evolved magmas (Ohakune, Te Hukui) began with phreatomagmatic phases. Due to the inferred small eruptive volume at Te Hukui (Table 10.1), the eruption most likely finished before the magmatic fragmentation (Strombolian-style activity) became dominant. In contrast, the activity of Ohakune continued for a few months as we inferred from the total erupted volume and characteristic eruption rates, which usually enables the isolation of the vent from the source of external water. However, the entire time of the activity of Ohakune was accompanied by phreatomagmatic activity and only restricted localities of the fissure were characterised by longer-lasting Strombolian-Hawaiian activity. As a result of phreatomagmatic eruptions, the most common transport mechanism was PDCs with additional variable fallout in both cases. Due to the significant depth of fragmentation indicated by the various lithic fragments with no surface exposure elsewhere (Chapter 6), Te Hukui PDC beds contain a high amount of accidental lithic fragments of the country rocks up to 90%, whereas fragmentation of magma at Ohakune occurred at shallow depth or only excavated the shallow basement (e.g. Valentine and White, 2012; Valentine et al., 2014). As a result, Ohakune PDC beds contain only a few percent of accidental lithics, but also contain dense juvenile fragments that were torn apart from the tip of the dyke. Strombolian activity produced coarse ash to lapilli-dominated fallout deposits. The Te Hukui sequence only contains a few of these beds with 10-15 cm thickness. At Ohakune, the contribution of these beds is about 50% of the total erupted volume. At proximal localities Strombolian-Hawaiian activity related fallout beds often exhibit agglutination or welding, and the most welded parts are inferred to be related to short clastogenetic lava flows.

The activity at Ohakune occurred along an at least 600 m long fissure. Due to the variety of Strombolian and phreatomagmatic activity, a hybrid pyroclastic cone evolved around the vent, whose lower sequence was dominated by phreatomagmatic beds, whereas the upper sequence predominantly consists of beds with Strombolian-style origin. This composite structure encompasses a larger and two smaller scoria-spatter cones and further sites of vents along the fissure zone. The edifice of the Te Hukui eruption is eroded and the available deposits were most likely deposited within the crater. Due to the documented deep excavation of country rocks, this volcano is a maar with a steep-sided diatreme which was surrounded by a low ejecta ring at the time of the activity.

Small-volume volcanism with low silica magmas is common at various plate tectonic settings (Smith and Németh, 2017), however comprehensive studies are rarely available from caldera settings. As morphologic features, lava flows and cinder cones are usually recognised (e.g. *Yellowstone caldera, Medicine Lake volcano, and Newberry volcano, USA*; USGS, 1972; MacLeod et al., 1982; Donnelly-Nolan et al., 2008), while small-magnitude phreatomagmatic activity is only reported from a few locations, such as *Alban Hills, Roccamonfina and Phlegraean Fields, Italy* (Cole et al., 1992; Isaia et al., 2004; Giordano et al., 2006); Grímsvötn and Eyjafjallajökull, Iceland (Gudmundsson et al., 2010; Hreinsdóttir et al., 2014); *Aira caldera, Japan* (Moriwaki, 1992); and *Okmok caldera, Alaska* (Wong and Larsen, 2010); *Akademiya Nauk caldera, Kamchatka* (Belousov and Belousova, 2001). A large number of basaltic eruptions of the Medicine Lake volcano produced lava flows, where many of the single eruptive periods produced more than 35 km^3, exceeding the volume of the smallest caldera-forming eruptions of the TVZ (MacLeod et al., 1982). At similar settings to the TVZ, basaltic products represent a minor portion of the total volume. In humid climates phreatomagmatic activity is probably more common than the available records show, however detailed field studies are not available from everywhere to trace their volumetrically insignificant deposits that are vulnerable to erosion. The most striking evidence of phreatomagmatic activity is the large maar craters of the *Colli Albani/Alban Hills* caldera and *Sabatini Volcanic District, Italy* (Giordano et al., 2006; Giaccio et al., 2007; Sottili et al., 2009; Sottili et al., 2012).

10.1.3.2 Silicic eruptions

All three silicic eruptions studied had explosive and effusive phases. Less information is available from the dacite eruptions of Motuoapa and Korohe. The NE-SW alignment of their structures indicates fissural activity (Fig. 8.1; Chapter 8), which was most likely initiated by effusive activity independent of water availability. Explosive activity occurred in the final phase of their evolution, which was most likely related to either the overpressurisation of the conduits or the waning effusion rate causing magma quenching, which often facilitates water-magma interaction (Austin-Erickson et al., 2008). The physical conditions of the magmas of the two rhyolite eruptions, Puketerata and Motuoapa were suitable to quench and interact with external water. As a result, the subaqueous Motuoapa eruption produced Surtseyan activity than continued with a dome emplacement within the crater of the emergent pyroclastic cone. The final phase of the Motuoapa rhyolite eruption was characterised by a lava effusion. Puketerata activity was similar to Motuoapa's, however the ratio of magma and external water was ideal for phreatomagmatic activity. The subsequent lava dome growth was accompanied with explosive activity along the entire evolution of Puketerata. Hydrovolcanic eruptions in both cases were most likely facilitated by the degassed and quenching magma associated with relatively low effusion rates. This kind of activity produced ash-dominated cross-bedded deposits that were transported by pyroclastic surges and travelled at least 3 km from the Puketerata vents. Lava dome emplacement is often interrupted by dome collapses due to explosions or destabilising flanks that trigger the emplacement of block-and-ash flows, creating breccia-dominated fan-shaped units. The largest dome-related explosion of Puketerata caused tephra fall more than 10 km from its vent. Because of the lack of medial or distal facies of pyroclastic succession of Motuoapa, it is hard to evaluate the run-out distances of PDCs and the extent of fallout associated with its subaerial activity. Unlike Puketerata, Motuoapa activity was finished by a long-lasting effusive phase that was most likely characterised by higher effusion rates than its earlier phases (Chapter 8). The lava travelled at least 3 km from the inferred vent location, cropping out at Echo Cliffs.

The arrangement of volcanic structures indicates fissural activity for the dacitic eruptions of Motuoapa-Korohe and the rhyolitic eruptions of Puketerata. Due to the high degree of erosion of the central part of the rhyolite structures of Motuoapa, it is not possible to evaluate whether it was sourced from a single or fissural vent of its activity. The Motuoapa-Korohe eruption formed two similar-sized platy domes caused by endogenic growth. The Motuoapa dacite dome has a crater in the centre of the structure, whereas the Korohe dome's western part is totally missing. The curved scar on the western face of Korohe may relate to explosion or collapse. There is no knowledge of the lower part of the rhyolite edifice of Motuoapa, but the remnant displays a tuff cone sequence that is underlain by pyroclastic tuff breccias originated from collapses of lava dome(s). The eastern flank of the pyroclastic cone is overlain by a ~60 m thick coulee. The Puketerata volcano comprises maar structures along a 2.5 km long fissure with two subsequent lava domes. Later the incidence of eruptions was restricted to the central area of the fissure. The alternating deposition of block-and-ash flows, pyroclastic surges and fallout around the larger dome constructed a pyroclastic structure which was referred as a tuff ring earlier. We suggest that its steep-sided outer slopes indicate its binary origin and represent a hybrid between conventional ejecta rings and block-and-ash flow fans.

The three prolonged eruptions jointly indicate varied eruption styles and resulting multiple types of transport mechanisms operating simultaneously or alternately. As a result, the edifices of these volcanoes exhibit hybrid structures. The eruption conditions usually favour the formation of hybrid volcanic structures only at the initial stages of volcanic activity, such as documented at *Panum Crater, California* (Sieh and Bursik, 1986) and the *Rothenberg cone complex, Germany* (Houghton and Schmincke, 1986), however in the case of an overwhelming subsequent phase the hybrid structures will be hidden.

The formation of silicic lava domes, coulees and flows is very common within caldera settings all over the world, from which the most studied young lava domes are located in the *Long Valley caldera – Coso Volcanic Field, Newberry volcano, Medicine Lake volcano, USA* and *La Primavera volcano, Mexico* (Bacon et al., 1980; Clough et al., 1982; Sieh and Bursik, 1986; Fink and Anderson, 2017). Many of these domes have a Holocene age. Most of these domes are aligned to chains following tectonic structures. In contrast, the lava domes of *Toya caldera, Hokkaido, Japan* form dome clusters by eruptions through closely-spaced vents (Ikeda et al., 1990).

Small-volume cone-forming silicic eruptions are rarely mentioned in the literature at caldera settings, however the phreatomagmatic influence of explosive activity was revealed in many cases, such as *Furnas, Azores* (Cole et al., 1995); *Phlegraean Fields, Italy* (e.g. Brown et al., 2008); the ancient *Scafell caldera, English Lake District* (Brown et al., 2007); *Atitlán caldera, Guatemala* (Rose et al., 1987). Similar structures to Motuoapa are found at the *Newberry volcano* (*Central Pumice Cone*; Jensen et al., 2009) and *Aira caldera, Japan* (*Nabeyama cone*; Kobayashi, 1982), whereas a very similar structure to Puketerata was described from the *Long Valley caldera, USA* (*Panum Crater*; Sieh and Bursik, 1986).

10.2 Factors that controlled the eruption styles and courses of eruptions

Eruption styles are determined by the magma properties (physical and chemical conditions) (Cas and Wright, 1988; Spera, 2000; Wallace and Anderson, 2000) and environmental factors (such as topography, type of substrate, availability of surface and groundwater, climate and actual weather conditions) that characterise the site of the eruptions (e.g. Lorenz, 1984; White, 1990; Sohn, 1996; Németh et al., 2001; Auer et al., 2007; Carrasco-Núñez et al., 2007; Németh et al., 2008; Ort and Carrasco-Núñez, 2009; Kereszturi et al., 2011). The differences in magma properties and environmental settings of the five examined eruptions have resulted in a diversity of eruption styles, transport mechanisms and evolved volcanic structures. The inventory of the main controlling factors of examined eruptions can contribute to the better assessment of volcanic hazards within the TVZ.

10.2.1 Physical properties of magma and eruption rates

The physical properties of magma determine its eruptive behaviour and ascent rate. Primarily, degassing and viscosity are the factors that influence the eruption styles internally. The viscosity is controlled by many factors (e.g. temperature, pressure, volatile content, chemical composition, and crystal and bubble content) from which the chemical composition is known for all the examined eruptions. Viscosity affects the mobility of magma/lava and strongly influences the shape of lava bodies, thus the morphologic and flow properties of examined coherent lava structures are indicative of viscosity. The textural features of coherent lava or pyroclastic fragments may unfold the vesiculation and degassing processes in relation to fragmentation.

The two eruptions are characterised by lower silica magmas (Ohakune and Te Hukui, Chapters 5 and 6), which indicate a difference in viscosity and conduit processes. The

Te Hukui eruption represents a single magma batch with very low viscosity, suggested by the isometric shapes of vesicles. We suggest that at the depth of water-magma interactions the melt conditions were within the volatile solubility. The deep excavation was the result of the contribution of volatile exsolution and expansion due to the interaction between the basaltic magma and coolant. The microlite-rich groundmass of the comagmatic lithic clasts implies near surface lava ponding during the late Strombolian phase with pure outgassing-driven fragmentation. In contrast, Ohakune pyroclastic fragments indicate various degrees of mingling between viscous stagnant magma, with actively vesiculating lower viscosity melt prior to both magmatic and phreatomagmatic fragmentation. The fluctuating eruption rates strongly influenced the course of the Ohakune eruption; the low eruption rate periods were characterised by the stronger influence of external factors, whereas the higher effusion rates imply the lower viscosity/higher temperature of magma, which facilitates the outgassing of melt and lesser influence of external water resulting in milder eruption styles.

Detailed textural data of the silica-rich eruptions is only available from the rocks of the Puketerata eruption, however these observations might also be applicable to the other two eruptions that occurred near the Motuoapa Peninsula. The relationship between the vesicles and fractures that formed during quenching indicates open system degassing prior to the eruption. It suggests that the contribution of magmatic volatiles was minor in the explosive fragmentation of the Puketerata rhyolite. Furthermore, the observed textures relating to magma quenching indicate high viscosity at the time of the extrusion, which allowed the explosive interaction with external water. We expect predominantly similar conditions for the first phases of the rhyolitic eruption at Motuoapa. However, the final phase with the emplacement of coulee indicates significantly lower viscosity, which we attributed to the changing of the ascent/effusion rate. On the basis of morphologies of lava structures, we expect lower effusion rates less than 5 m^3/s for the eruptions of Puketerata and the first phases of Motuoapa rhyolite, whereas the coulee emplacement and the platy dacite domes of Korohe and Motuoapa were emplaced under the conditions of lower viscosities and possibly higher effusion rates.

The examined eruptions were characterised by low to moderate effusion rates between <0.1 and 20 m^3/s that facilitated the outgassing of erupting magmas. These eruption rates are within the range of usual eruption rates of basaltic and silicic small-volume eruptions elsewhere (e.g. Newhall and Melson, 1983; Houghton et al., 1999; Yokoyama, 2005), and only a few large-volume coulee and flow emplacements were attributed to higher effusion rates up to a few hundred m^3/s *(e.g. Crater Glass flow and Dacite Flow in Newberry volcano, USA*; Lyman et al., 2004). Sub-Plinian-Plinian activity usually requires much higher ascent/eruption rates, especially for basaltic Plinian activity, as indicated by the 1886 Tarawera eruption that implies an eruption rate of ~50000 m^3/s (Walker et al., 1984; Sable et al., 2009).

10.2.2 Local substrate properties and availability of external water

Small-volume eruptions may have been strongly controlled by the availability of external water, whose abundance often triggers hydrovolcanic eruptions. The evolution, morphology and pyroclastic deposits of such volcanism are affected by the local substrate properties in which their eruptions occur. Fundamentally, two different end members of substrate can be distinguished in terms of the nature of the aquifer: fracture-controlled (solid rocks); and porous media controlled aquifers that are characteristic of unconsolidated deposits (e.g. Németh et al., 2001; Lorenz, 2003; Ross et al., 2011; White and Ross, 2011).

The Ohakune and Korohe activity erupted through unconsolidated reworked tephras, which were classified as an aquifer that was controlled by porous media. The Korohe eruption was not influenced by the abundance of groundwater due to the physical conditions of its magma. By contrast, the aquifer properties at Ohakune provided a constant supply of groundwater that maintained magma-water interactions during the entire course of the activity. The substrate properties are not only responsible for the water supply and thereby influence the eruption style, they may also control the vent stability as indicated by the shifting of vents at Ohakune.

The two eruptions of Puketerata and Te Hukui, as well as the dacite of Motuoapa, erupted through consolidated low permeability rocks, where the availability of external water may be linked to the occurrence of fractures. As the TFB is tectonically active, consolidated rocks are expected to be fractured, especially in the vicinity of faults. The magma of the Puketerata and Te Hukui eruptions interacted with the confined water of the fracture system relating to the Orakeikorako fault. Besides the differences of the magma properties between the rhyolite and basalt (e.g. dissolved volatile content), other factors such as climate and properties of the fracture system may have played a role in the explosiveness of the eruptions. The preservation of depressions (maar craters) relating to the initial deep-seated eruptions well illustrate the different nature and stability of the basement in comparison to the Ohakune example. The main phase of Puketerata activity may indicate interaction with groundwater and ponding surface water as well, similar to Ohakune.

On the basis of the exposed sequence of Motuoapa, the explosive activity of rhyolite is attributed to magma interaction with the lake water. However, the formation of the coulee in the late stage of activity indicates that the abundance of external water does not necessarily influence the eruption style in the case of low viscosity silicic magmas.

10.3 Relationship between small-volume and caldera-forming eruptions within the TVZ

The possible relationship between calderas and other eruptions that spatially relate to a caldera volcano were summarised in Fig. 3.3 (Chapter 3). However the vent locations of the post-caldera eruptions may not only be determined by the caldera system itself, but the factors that define the formation and location of calderas. According to this, in a narrow sense not all the intra-caldera eruptions necessarily relate to the subsurface processes of the reservoir of the caldera, such as the high-alumina basalts of the TVZ (Graham et al., 1995; Hiess et al., 2007).

Smaller eruptions that are spatially associated with caldera structures may occur before or after the caldera-forming events, however the majority of pre-caldera deposits are destroyed, subsided or blanketed due to the caldera formation, hence the information is inexistent about the pre-caldera volcanism. It is also an issue that eruptions within that timeframe can be classified as associated with caldera activity.

Finally, the relationship with caldera-forming eruptions may be investigated on the basis of chemical compositional and petrological similarities or differences in those eruptions. To unfold this kind of relationship it is important to know the structure of magma reservoirs and the mode of generation of the erupted magmas. The magmas of caldera-forming eruptions of the TVZ are mostly sourced from 4-11 km depth (Matthews et al., 2012; Allan et al., 2013; Shane and Smith, 2013). This region of the crust is stretched due to rifting and is intruded by predominantly evolved magmas (Rowland et al., 2010; Wilson and Rowland, 2016), where the intruded magma is stored as variously interconnected crystal-poor melt lenses and highly-crystallised mush zones (Charlier et al., 2003; Gravley et al., 2007; Wilson and Charlier, 2009; Ellis and Wolff, 2012; Cashman and Giordano, 2014). The erupted magmas of caldera-forming eruptions often indicate that the tapped melt lenses were characterised by very distinct chemical compositions and there was no time for equilibration of melts prior to the eruptions, such as at the eruption of Mamaku Plateau Ignimbrite from the Rotorua and Okataina volcanoes, New Zealand (Storm et al., 2011; Bégué et al., 2014; Storm et al., 2014), and the *Novarupta-Katmai eruption, Alaska* (Hildreth and Fierstein, 2012). Small-volume eruptions may be the manifestations of the evacuation of one or limited numbers of small melt lenses, which chemically may differ from the volcanic products that are sourced from a compositionally equilibrated magma reservoir as well.

The listed uncertainties should call the attention to the fact that some of the events may be independent from the large-scale activity of caldera systems and be controlled by other factors, similar to the volcanism of monogenetic volcanic fields (e.g. Connor, 1990; Lesti et al., 2008; Germa et al., 2013).

10.3.1 Spatial correlations

Taking into account all the known small-volume eruptions of the TVZ (see Chapter 9), about 65% of the vents are located inside one of the post-350 ka calderas. With the assumption that the dimensions of magma reservoirs extend beyond the margins of the collapse structures by at least a few kilometres, only a small number of vents seem spatially independent from the calderas. Most of these eruptions occurred at the southernmost part of the central TVZ. It is important to note that there is a deficit of extra-caldera vents in perpendicular directions from the calderas, which suggests that the magma reservoirs are more confined to the NW or SE relative to the caldera margins. A stronger indication implied for those vent relates to the structural elements of the calderas. From this point of view, about 100 vents are located within 1 km distance from the caldera margins. About half of these vents are parts of vent clusters that are arranged to the eastern and western caldera margins of Whakamaru. Their orientation is characterised by a low angle to the orientation of the TFB, thus we assume a strong relationship between these vent clusters and the post-Whakamaru magmatic processes. The frequency of near margin vents at other TVZ calderas is lower without forming vent clusters. As fault lines parallel to the extensional axis are located nearby to these vents, their strong relationship with the structural elements of calderas is questionable.

There are only a few calderas in continental back-arc/intra-arc rifting settings besides the calderas of the TVZ (e.g. Santorini and Nisyros, Greece; Alban Hills, Italy; Deception Island, Antarctica; Geyer and Marti, 2008), but there is a lack of information about the small number of post-caldera vents. Therefore, the spatial distribution of post-caldera vents was briefly explored in other volcanic systems that are characterised by strong tectonic control with the existence of volcanotectonic graben similar to the TVZ, such as Toba caldera, Sumatra; Newberry volcano, USA; and the calderas of southern Kyushu (e.g. Aira, Ata, and Kikai), Japan. From these examples the structural control is the most apparent at Toba as the elongated outline of the caldera follows the NW-SE trend of tectonic lineaments. The post-caldera eruptions only occurred along these major fault lines within and outside of the limit of the caldera (Mucek et al., 2017). The vent distribution of Newberry volcano displays similarities to the TVZ, with the location of a few of the vents following the outline or the ring structures of the caldera. However, more than 90% of the vents aligned to the faults and are located outside of the caldera boundary (MacLeod et al., 1982). The calderas of southern Kyushu are aligned to a north-south volcanotectonic graben. Post-caldera vents mostly comprise polygenetic volcanoes (e.g. Sakurajima and Kaimondake), whose occurrence is restricted in the rim or inner parts of the caldera structures (Yokoyama and Ohkawa, 1986). The post-caldera activity of the TVZ indicates a striking difference to most of the silicic systems in Japan and Chile, according to the lack of long-lived polygenetic volcanoes having a central vent in the past 350 ka history, and since Edgecumbe and Tauhara are considered to be short-lived lava dome complexes (Chapter 2).

Turning to the case studies, four of the five eruptions are located within the central TVZ. The only exception is the OVC, which is located too far away from the southernmost calderas to assess any relation with caldera volcanism. The spatial relationship between Ohakune and relatively nearby summit vents of Ruapehu is also unlikely because all the vents of Ruapehu are arranged within the extensional axis of the TVZ, whereas the orientation of the Ohakune fissure vent is perpendicular to the extensional axis and located about 6 km east from the path of the axis projected to south.

The rhyolite and dacite eruptions of the Motuoapa Peninsula are located about 10 km from the southern margin of the Oruanui collapse structure. The distance is large enough to envisage that these eruptions were not associated with the magmatism of the Oruanui caldera.

Two eruptions occurred in central Whakamaru (Te Hukui and Puketerata) and are well inside the caldera boundaries of the Whakamaru Volcanic Centre. Due to the young age of Puketerata (16.5 ka), its activity was classified to be part of the evolution of the Taupo Volcanic Centre (Sutton et al., 1995; Barker et al., 2014). The margin of the Oruanui collapse is located 20 km from the nearest Puketerata vent, thus we concluded it as a spatially independent event.

10.3.2 Temporal correlations

Volcanic activity of calderas comprises numerous magmatic cycles that are characterised by inflation and deflation of magma reservoirs within a thousands of years long timeframe as a result of periodic replenishment with hot crystal-poor melts (Christiansen et al., 1977; Pierce et al., 2002; Smith et al., 2005; Kennedy et al., 2012). The temporality of the main recharge periods of magma reservoirs and residence of magma were evaluated by U-Th dating on zircon crystals within the TVZ (Charlier et al., 2003; Charlier et al., 2004; Wilson and Charlier, 2009). Large eruptions usually incorporate zircon populations crystallised for hundreds of thousands of years. However, the older crystals are usually considered as an inherited fraction from earlier magmatic cycles rather than crystallised from long-lived magma bodies (Charlier et al., 2003). As a result, the apparent residence times may exceed 200-300 ky (e.g. at Whakamaru, Brown and Fletcher, 1999), but smaller volume eruption lacks inherited crystals and their zircon ages yield a shorter magma residence ranging from a few thousand years to 50-60 ky (Charlier et al., 2003; Charlier et al., 2004). Based on these inferred residence times, the Oruanui and the current Okataina magmatic system may have been active only since ~100 ka (Charlier et al., 2003; Charlier et al., 2004).

Therefore, the rhyolite eruption of Motuoapa (~138 ka) may represent an earlier magmatic cycle, whereas the dacite eruption can relate to the activity of the Taupo Volcanic Centre based on its age.

The age of Te Hukui basalt is unknown, but the ages of the nearby located basaltic eruptions (e.g. *K-Trig*) was inferred to be similar to the age of Motuoapa (Brown et al., 1994). This weak evidence suggests that the Te Hukui eruption relates neither to the Whakamaru nor the Taupo activity, whereas the 16.5 ka Puketerata eruption fits into the timeframe of the activity of the Taupo Volcanic Centre.

Turning to the inferred magma production of small-volume eruptions for the entire TVZ (Chapter 9), three trend reversals have been observed. The first one is maybe only apparent as a result of the high number of unknown eruptions expected. The second trend reversal at ~180 ka indicates the start of a period that is characterised by lower production. The decrease of volcanic activity coincides with the change of erupted magma type from cold-wet-oxidising to hot-dry reducing magmas (Deering et al., 2010). The youngest trend reversal indicates the intensification of small-volume volcanism at about 45 ka by both the number of events and erupted volumes. It seems that this period is manifested by the Rotoiti caldera-forming event, however the subsurface magmatic processes may have preceded it by some 10,000 years (Charlier et al., 2003; Charlier et al., 2004).

10.3.3 Magma generation and petrological and geochemical aspects

The geochemical and petrological aspect of volcanic products of the TVZ was comprehensively studied on a broad scale in past years (e.g. Sutton et al., 1995; Sutton et al., 2000; Leonard, 2003; Smith et al., 2005; Deering et al., 2010; Deering et al., 2011; Ashwell et al., 2013; Gravley et al., 2016). Here we only focus on the four case studies located in the central TVZ. The magma of the Te Hukui eruption has a composition of high-alumina basalt (Chapter 6). Mafic magmas were originated from the upper mantle (Graham et al., 1995; Hiess et al., 2007), thus this eruption had no relationship to long-lived magma reservoirs. The basalt incorporated some plagioclase phenocrysts that crystallised from more evolved melts, which suggests it passed through silicic mush zones. The rhyolite and dacites in the vicinity of Motuoapa Peninsula indicate distinct iron-rich ferromagnesian phenocryst assemblage from any erupted material sourced from the Taupo Volcanic Centre. Thus, they were also considered to be independent from the Oruanui magma cycles, and may represent the same cycle as the domes at the SW shore of Lake Taupo due to their common iron-rich orthopyroxene contents (Sutton et al., 1995).

The petrography of Puketerata rhyolite is different from the Oruanui products as it contains biotite, while the Oruanui products are characterised by hornblende and orthopyroxene as the main ferromagnesian phases (Sutton et al., 1995). Another three young eruptions contains biotite, whose constructions are classified as the “Northeastern dome type” (Sutton et al., 1995; Barker et al., 2014). Biotite-bearing volcanic material was common at the Whakamaru-related eruptions before 180 ka (Deering et al., 2010). The initial phases of the Oruanui eruption indicate a physical mingling of biotite-bearing and biotite-free magmas (Allan et al., 2012), which suggest that small pockets of biotite-bearing melts either remained eruptible from the earlier magmatic cycle or the increased heat flow of the intrusion of Oruanui magma remobilised the almost frozen Whakamaru-related crystal mush. The rhyolite of Puketerata indicates some interaction with mafic melts, which may have also contributed to the rejuvenation of the Puketerata magma. In spite of the similar source depth of the Puketerata eruption to caldera-forming eruptions of the TVZ (e.g. Shane et al., 2007; Matthews et al., 2012; Allan et al., 2013), the petrological features only indicate a weak relationship with the magmatism of both the Whakamaru and Taupo Volcanic Centres.

10.4 Hazard implications

The hazard posed by these small-volume eruptions consists of two distinct parts. One of them is the eruption style, which mainly controls the transport mechanism of erupted material. The chemical and physical composition of erupting magma strongly determines the way of the fragmentation, which may have been influenced by the specific hydrological or hydrogeological conditions at the site of the eruption. For these reasons, besides the internal parameters of the erupting magma, the eruption site's specific external conditions and their possible impact on the eruption style have to be considered (e.g. Bonadonna et al., 2005; Jenkins et al., 2008; Breard et al., 2014; Kereszturi et al., 2014a; Kereszturi et al., 2014b; Lube et al., 2014). Secondly, the duration of the eruption may strongly affect the vicinity or the broader environment of the eruption site. From an economic point of view, a small to large TVZ eruption may disrupt road and air traffic (Gudmundsson et al., 2010; Wilson et al., 2014) and cause a severe impact on agriculture (Cook et al., 1981; Cronin et al., 1998).

Furthermore, the prediction of the site of further eruptions represents another target in hazard assessment. Earlier studies addressed this issue mostly by the analysis of spatio-temporal distribution of past eruptions (Connor, 1990; Connor et al., 2000; Marti and Felpeto, 2010; Bebbington and Cronin, 2011; Bebbington, 2013; Le Corvec et al., 2013).

Volcanic eruption within the TVZ on any scale would pose multiple risks on the North Island of New Zealand. The main transportation routes (e.g. main railway line and State Higway 1), major townships (Taupo, Rotorua), location of hydroelectric and geothermal power plants and popular tourist destinations are concurrenced with the active/dormant volcanic regions along with extensive farmlands that require personalized risk-management strategies. This research does not aimed to delving into the possible socio-economical impacts of volcanic activity nether to evaluate the capabilities for coping with volcanic perils, however it is believed that will contribute to a better volcanic hazard assessment, which is essential for the assesement of volcanic risk within the entire TVZ (e.g. Wilson et al., 2014)

10.4.1 Vent architecture and eruptive styles

Most of the scattered small-volume eruptions of the TVZ are related to dyke emplacements controlled by the structural features of the TVZ, such as faults and ring structures/margins of calderas similar to many other caldera systems around the world, such as Long Valley caldera, Medicine Lake volcano, USA (Fink and Anderson, 2017; Hildreth and Fierstein, 2017) and Toba caldera, Sumatra (Mucek et al., 2017). As a result, the eruptions are usually characterised by fissural activity. Spatially, fissure vents can be close to contiguous, such as at the 1886 eruption of Tarawera and the 16.5 ka Puketerata (Nairn, 2002, Chapter 7) or interrupted (e.g. Whakatane eruptive episode, Haroharo, Okataina and the dacite eruption of Motuoapa and Korohe; Chapter 8, Nairn, 2002), where the active vents were located several kilometres from each other. Long fissures may intersect areas that are characterised by different environmental conditions, which result in the existence of varied eruption styles at different sections of the fissure vent (e.g. Tarawera; Nairn, 2002). The activity of the fissure eruptions may migrate gradually as documented at the Tarawera fissure (Nairn, 2002) or the active parts shift randomly (e.g. at Ohakune, Chapter 5). As challenging to predict the extent of the vent area(s), even at the eruption initiation, the potential threat of fissural activity is also significant for future eruptions.

The inventory of possible eruption styles of small-volume volcanism was evaluated by the volcanic activity of example localities and the preliminary morphometry-based investigation of extrusive lava structure from the entire TVZ. The chosen example localities only include eruptions with a small influence of magmatic fragmentation, but for covering the full spectrum we are referring to Plinian eruptions from earlier studies from the TVZ.

10.4.1.1 Possible eruptive styles of magmas with low to intermediate silica content

Basaltic and basic andesitic eruptions usually produce Strombolian-Hawaiian explosive activity with or without effusive phases, if there is no involvement of water in the fragmentation process. This kind of mild explosive or effusive activity poses an immediate hazard only at the vicinity of vents, however lava flows of eruptions with larger erupted volume may proceed up to several kilometres from the vent (Chapter 5, Kereszturi et al., 2014a; Kereszturi et al., 2014b). Basaltic Plinian eruptions similar to the 1886 eruption of Tarawera are rare and their high explosivity was most likely facilitated by the high eruption rates, which was orders of magnitude higher in the case of Tarawera (~50000 m^3/s) than the other ordinary basaltic events (Nairn, 2002), assuming the eruption of 1 km^3 DRE dome volcanic material in 5-6 hours. In the case of the availability of external water, low-silica magmas often interact with water and their eruption style turns to hydrovolcanic (Sheridan and Wohletz, 1981; Kokelaar, 1983; Zimanowski, 1998; Wohletz and Zimanowski, 2000). Both Surtseyan and phreatomagmatic eruption styles are associated with the generation of PDCs (most often base surges), which form either from the gas thrust region of overloaded plumes or from the convective thrust region of the eruption cloud by gravitational collapse (Fisher, 1995). Eruption plumes of hydrovolcanic activity may rise up to 20 km (Lorenz, 2007).

In terms of eruption styles, the two examined lower silica eruptions were slightly different. The eruption style and the location of active vents at **Ohakune** were constantly changing and associated with frequently launching tephra jets. As a result, the generation of base surges and the ejection of ballistic bombs were common during the phreatomagmatic phases. Ballistic bombs and surge deposits were found at 600 m from the vent, but the thickness variations of PDC deposits suggest at least 1.5-2 km for the run-out distances of PDCs. Tephra fall and ballistic trajectories of scoria are common only found within the proximal sequence, thus we do not expect the formation of high eruption clouds for the entire activity. Hawaiian-style related clastogenetic lava flows travelled only a few tens of metres downwards on the slope of the cone. In contrast, the deep excavation at **Te Hukui** indicates an energetic initial phase. The high amount of coarse accidental lithic content of PDC deposits suggests that the eruption cloud was overloaded and laterally collapsed immediately after the eruption initiated. The magmatic phase of Te Hukui was minor, and its scoriaceous material may have depositioned only within the maar crater.

Only a few mafic monogenetic eruptions were experienced and documented in the past century (e.g. Ukinrek maars, Alaska and Paricutin, Mexico; Self et al., 1980; Pioli et al., 2008), but the volcanic activity of frequently erupting polygenetic systems are often comparable in terms of eruption styles and the course of an eruption (e.g. Nishinoshima, Japan; Maeno et al., 2016). The shifting of vents that is associated with alternating eruptive styles is reported from many monogenetic eruptions based on their sedimentological records (e.g. Houghton and Schmincke, 1986; Houghton et al., 1999; Martin and Németh, 2004; Ort and Carrasco-Núñez, 2009; van Otterloo et al., 2013; Pedrazzi et al., 2014b; Agustin-Flores et al., 2015), and requires unconsolidated substrate and the abundance of external water similar to at Ohakune.

10.4.1.2 Possible eruptive styles of high-silica magmas

The eruption of silicic magmas is more frequently energetic than the mafic eruptions because of their higher volatile content and the differences in degassing due to their different physical conditions. Magmatic volatile-driven fragmentation during very large eruptions usually induces the rise of high convective plumes that may exceed 30-40 km in height. These sub-Plinian to ultra-Plinian-style eruptions are also characterised by moderate to large eruptive volumes and extensive tephra dispersal, thus their impacts occur on a regional to global scale. The collapse of convective plumes induces PDCs to maybe travel tens of kilometres from the source vent. Volatile-rich magmas occasionally erupt explosively and effusively in the same time (e.g. 2010-2011 eruption of Cordón Caulle volcano, Chile; Schipper et al., 2013). Degassed silicic magmas usually erupt effusively and may be associated with explosive activity as well (e.g. Newhall and Melson, 1983; Heiken and Wohletz, 1987). The viscosity and the yield strength of magma determine the lava emplacement, forming steep-sided lava domes in the case of high viscosity and yield strength, whereas the emplacement of lava flows and coulees indicates the lower viscosity of erupted magma (Fink and Griffiths, 1998). Extrusion of viscous lava may trigger dense PDCs (block-and-ash flows) due to the destabilisation of the side of the edifices, which is particularly hazardous if the collapsing material is characterised by high potential energy (e.g. the lava dome was oversteepened). Future silicic lava dome emplacements at the summit region of Tarawera would pose this kind of threat. Silicic magma’s ability to interact with external water is limited compared to lower silica magmas, as a result of silicic magma-water interaction requiring quenching of magma prior to the interaction with external water. Furthermore the potential maximum energy can be gained by MFCI and is lower than mafic magmas, as the eruption temperature of silicic magmas is generally lower (Spera, 2000). However, the initial volatile content is higher (5-7%) (Wallace and Anderson, 2000), which may contribute to the explosivity. Based on the higher variability of physical properties of silicic magma, their systems are characterised by a more unpredictable nature. The hazard of silicic hydrovolcanic eruptions contrasts significantly with the effusive emplacement of lava, thus the evaluation of susceptible areas for hydrovolcanic eruptive styles is important for hazard assessment and management. The main threat of hydrovolcanic eruptions is diluted PDCs and tephra fall within the broader neighbourhood, whereas the vicinity of the vent may be impacted by the ejection of ballistic bombs.

Two of the three examined silicic eruptions were strongly influenced by magma-water interaction. Cross-bedded deposits of dilute PDCs were recognised 3 km from the vent of **Puketerata**, whereas the 1 cm isopach of tephra fall is situated more than 10 km east from the vent, encompassing an area of ~230 km^2. The dilute portion of block-and-ash flows relating to the collapse of the larger lava dome travelled about 1 km. The rhyolite eruption of **Motuoapa** also produced dilute PDCs relating to the Surtseyan activity and block-and-ash flows, as a result of the collapse of a lava dome that has completely disappeared due to the subsidence and erosion of the western part of the Motuoapa structure. The furthermost pyroclastic deposits are exposed within 1 km from the inferred vent, thus the run-out distances of PDC and the dispersal of tephra fall could be evaluated by the thickness variations of proximal deposits. Based on these observations base surges had to reach at least 2-3 km from the vent, whereas the coarse material of block-and-ash flows was deposited only within 500 m of the vent. There is not enough data available to evaluate the dispersal of fall deposits. The coulee that most likely emplaced purely effusively at the final stage of eruption has travelled at least 3 km from the vent, and the most distal parts are exposed at Echo Cliffs. The dacite of **Korohe and Motuoapa** piled up above their vents. Due to their relatively fluid physical properties and the resulting endogenous growth, the lava did not interact explosively with external water during the dome formation. As a result of the final explosive phase, the rise of a few kilometres high eruption plume and ballistically emplaced blocks is expected to be the main features that were posing a threat.

There are many records of andesitic to dacitic eruptions of lava domes with associated explosive activity from all over the world (e.g. Rose, 1973; Nakada et al., 1999; Saucedo et al., 2002; Yokoyama, 2002; Carn et al., 2004; Bull et al., 2012; Komorowski et al., 2013; Gunawan et al., 2017), however these eruptions are mostly associated with composite volcanoes or lava dome complexes instead of large silicic calderas, except the 1912 Katmai-Novarupta eruption (Hildreth and Fierstein, 2012) and the 1944 eruption of the Showashinzan dome in the vicinity of Usu volcano, Toya caldera, Japan (Yokoyama, 2002). The documented activity of the two recent silicic eruptions of Cordón Caulle and Chaitén, Chile (Pallister et al., 2013; Tuffen et al., 2013) may have well represented what volcanic processes can be expected for the energetic end members of future small-volume eruptions of the TVZ. Eruptions occurring in subaqueous environment may trigger tsunamis, during which the energy of the eruption partially transfers to waves. Tsunamis may affect areas on the shore which would be too far to be reached by PDCs (Latter, 1981; Freundt et al., 2007).

10.4.2 Volume, eruption rates and duration of small-volume eruptions

The impact of eruptions with larger erupted volumes is usually more significant than the smaller eruptions, especially in the case of explosive activity with involvement of silicic magma. In the case of phreatomagmatic activity, even an eruption of small-magma volume can cause havoc in a short-lasting event (e.g. 2010 eruption of Eyjafjallajökull; Weinzierl et al., 2012), while larger magma eruptive rates can produce a sustained eruption with high-rising columns triggering multiple collapses with associated PDCs. The sizes of the examined eruptions are under or around the average in terms of erupted volumes of the total eruptions of the TVZ (Chapter 9) and indicate a broad range of eruptive styles. As explosive activity of silicic volcanoes is most common in the initial phases (Newhall and Melson, 1983), the later, effusively-formed extensive volcanic structures may perfectly overlay or overflow the early pyroclastic constructions. According to this, the apparent dominance of the effusive activity of the

TVZ's small-volume activity can be misleading. The number and volume of small explosive events since the Rotoiti caldera formation seems roughly complete, however the previous periods lack similar events in the geological records due to the low preservation potential of such small events. These inferred eruptions probably do not contribute a lot volumetrically to the total erupted volcanic material of the TVZ, but they would modify the established temporal and spatial distribution of volcanic events.

Regarding volcanic hazards, the duration of eruption is one of the most important factors that needs to be considered. The longevity of explosive eruptions may have been inferred by sedimentological observations and using observations of historical eruptions (e.g. Newhall and Melson, 1983; Nairn, 2002; Yokoyama, 2002; Harris et al., 2003; Parfitt, 2004; Yokoyama, 2005; Pallister et al., 2013; Tuffen et al., 2013; Wolpert et al., 2016). Recent studies suggest that dome-forming eruptions rarely last longer than five years (Wolpert et al., 2016). Eruption/extrusion rates of prehistoric silicic effusive eruptions can be estimated by the morphology of their lava domes based on the correlation between dome morphology and yield strength (Fink and Griffiths, 1998; Lyman et al., 2004). If both the extrusion rates and edifice volumes are available, the eruption duration can be calculated. This method works relatively well if the morphology indicates steady growth, as it was inferred for the Puketerata activity (Chapter 7). The TVZ-specific range of erupted volumes, eruption rates and inferred eruption durations for different type of volcanism is summarised in Table 10.2. The most prolonged small-volume eruptions of the TVZ that are expected to represent the largest impact by their duration relate to the formation of dacite lava dome complexes (e.g. Edgecumbe, Tauhara), and large-volume silicic eruptions dominated by effusive activity, such as the Kaharoa event (Table 10.2). The activity of Edgecumbe and Tauhara may have lasted for tens or hundreds of years, similar to the still active Santiaguito dome complex, Guatemala (Harris et al., 2003)

	erupted volume (km^3)		inferred eruption rates (m^3/s)		inferred range of eruption duration
	min	max	min	max	
basalts and basic andesites	Te Hukui	Tarawera	e.g. Ohakune	Tarawera	hours or days to a few months
	<0.0001	1	<0.01	~50000	
effusively emplaced silicic andesites or dacites of lava dome complexes	Waikeramoana, Rainbow Mts.	Edgecumbe	inferred from Santiaguito (1)		tens of years to hundreds of years
	0.28	2.5	0.01	10	
effusively emplaced dacites or rhyolites	Quarry dome (Maroa)	Kaipara Coulee	infrerred from e.g. Newberry volcano (2)		weeks to years
	<0.001	>2.5	0.01	~300	

Table 10.2 Typical eruption rates and eruption durations of TVZ volcanism derived from eruptive volumes of distinct volcanic events. (1) (Harris et al., 2003), (2) (Lyman et al., 2004).

10.4.3 Towards forecasting volcanic hazard

Similar to monogenetic volcanic fields, the forecasting of the spatial, temporal and eruption-style characteristics of future eruptions of the TVZ is the most challenging problem. The sites of future eruptions may be identified only hours to days prior to the initiation of the eruption by the seismic or ground deformation observations (Manville and Wilson, 2003; Lindsay et al., 2010; Chiodini et al., 2012; Albert et al., 2016). The available probabilistic models for positioning the forthcoming volcanic activity used for other volcanic areas are based on a field-scale analysis of the spatio-temporal pattern of past eruptions using non-parametric density estimation (e.g. kernel density) (Connor, 1990; Connor et al., 2000; Martin et al., 2004a; Kiyosugi et al., 2010; Bebbington and Cronin, 2011; Cappello et al., 2012; Bebbington, 2013). The eruption style and related hazards of mafic and degassed silicic magmas may differ significantly whether interacting or not with external water, as is documented by the volcanism of example localities (Chapters 5-8). The mapping of spatial variations of different environmental factors that contribute to the triggering of hydrovolcanic eruptions provides input for creating conceptual models (e.g. Kereszturi et al., 2014b).

10.4.3.1 Probability model for eruption location prediction

The framework of our conceptual model for the prediction of the site of forthcoming eruptions is based on the spatial and temporal distribution of known vent locations, as well as the observed correlations between vent locations and structural alignments of the TVZ (Chapter 9). This conceptual model represents the first approach to determine eruption location susceptibility within the TVZ using overlaying methods of distinct spatial information. Four different components of the TVZ were considered in this assessment for a first-order conceptual eruption prediction model: (1) post-Whakamaru vent locations derived into a kernel density with a 10 km search radius; (2) active faults with a 500 m buffer (Langridge et al., 2016); (3) post-100 ka intra-caldera areas; and (4) their margins with a 500 m buffer (Wilson et al., 1995; Gravley et al., 2007). The resulting prediction map indices are running from 0-7, where the higher value indicates the greater probability for a future eruption (Fig. 10.1). There are a large number of uncertainties and deficiencies in the structural input parameters, such as the accuracy of the paths of caldera margins and the deficiencies of active faults crossing young volcanoclastic deposits or lakes. The latter has caused an underestimation of probability in broad areas of the TVZ, especially within the limit of the Taupo and Okataina calderas. This model may be improved by introducing other structural data such as geophysical data or stress field measurements (Marti and Felpeto, 2010).

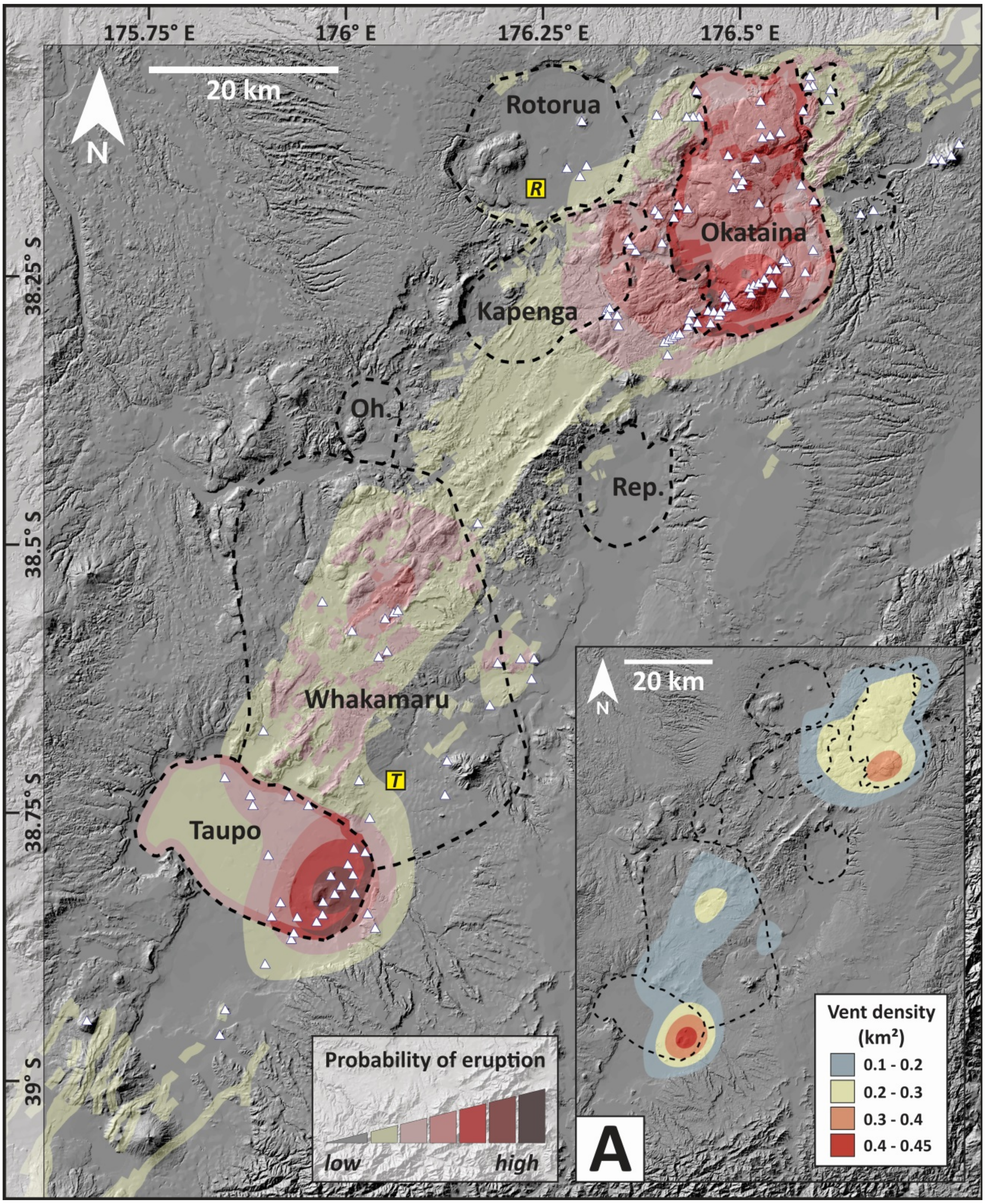
175.75° E
176° E
176.25° E
176.5° E
20 km
N
Rotorua
R
Okataina
Kapenga
Oh.
Rep.
Whakamaru
T
Taupo
38.25° S
38.5° S
38.75° S
39° S
Probability of eruption
low
high
20 km
N
Vent density
(km²)
0.1 - 0.2
0.2 - 0.3
0.3 - 0.4
0.4 - 0.45
A

Figure 10.1 First approach eruption prediction map for small-volume eruptions of the central TVZ prepared by a combined overlay of the 10 km kernel density map of post-Whakamaru eruptions (Inset A) and structural alignments (faults and calderas) of the TVZ from Langridge et al. (2016) and Wilson et al., (1995). Post-Rotoiti eruptions are indicated by white triangles, letters in yellow square indicate the location of major towns (T: Taupo and R: Rotorua).

10.4.3.2 Susceptibility mapping for hydrovolcanic activity of the central TVZ

Hydrovolcanic activity including phreatomagmatic, Surtseyan-style and phreatic eruptions represent an elevated hazard compared to the eruption of the same magma with unabated properties without the involvement of external water. The identification of high and low probability areas for hydrovolcanic activity would be an important contribution to the volcanic hazardscape of TVZ. Our conceptual model based on the TVZ-wide evaluation of environmental factors may influence the eruptions, such as topography, substrate properties and structural elements, that can modify the original substrate properties. Five different environmental factors were selected for building the first approach model by using the overlaying technique: (1) surface waters including lakes and major rivers with a 500 m and 250 m buffer, respectively; (2) geothermal fields (Simpson and Bignall, 2016; WRP Geothermal System, 2016); (3) surficial deposits of unconsolidated fluvial and lacustrine sediments based on the corresponding sheets of QMAP 1:250000 geological maps series (Townsend et al., 2008; Leonard et al., 2010; Lee et al., 2011); (4) morphologic depressions derived from a 4 m grid contour-based DEM by Hammond landform classification (Chapter 4); and (5) active faults of TVZ with a 500 m buffer (Langridge et al., 2016). The surface waters were weighted by three because they provide unlimited water supply to maintain the magma-water interaction, and other factors were weighted for 1. Surface waters are spatially exclusive for the land coverage of unconsolidated sediments and local morphologic depressions in this model. The resulting preliminary susceptibility map indices are running from 0-6, where the higher value indicates the greater probability for hydrovolcanic eruptions or phases (Fig. 10.2). Similar to the eruption location prediction, this model is also affected by the quality of input data, such as the resolution of geological mapping or the extent of unmapped but existing sections of active faults. Uncertainties are also affected by the geothermal field data as there are no agreed boundaries of geothermal fields, and they are often modified due to different purposes. Eruption-style susceptibility models can be improved by more detailed geological data (e.g. thickness of unconsolidated sediments, rock porosity) and the evaluation of distance-based effects on distinct environmental factors (e.g. Kereszturi et al. 2014).

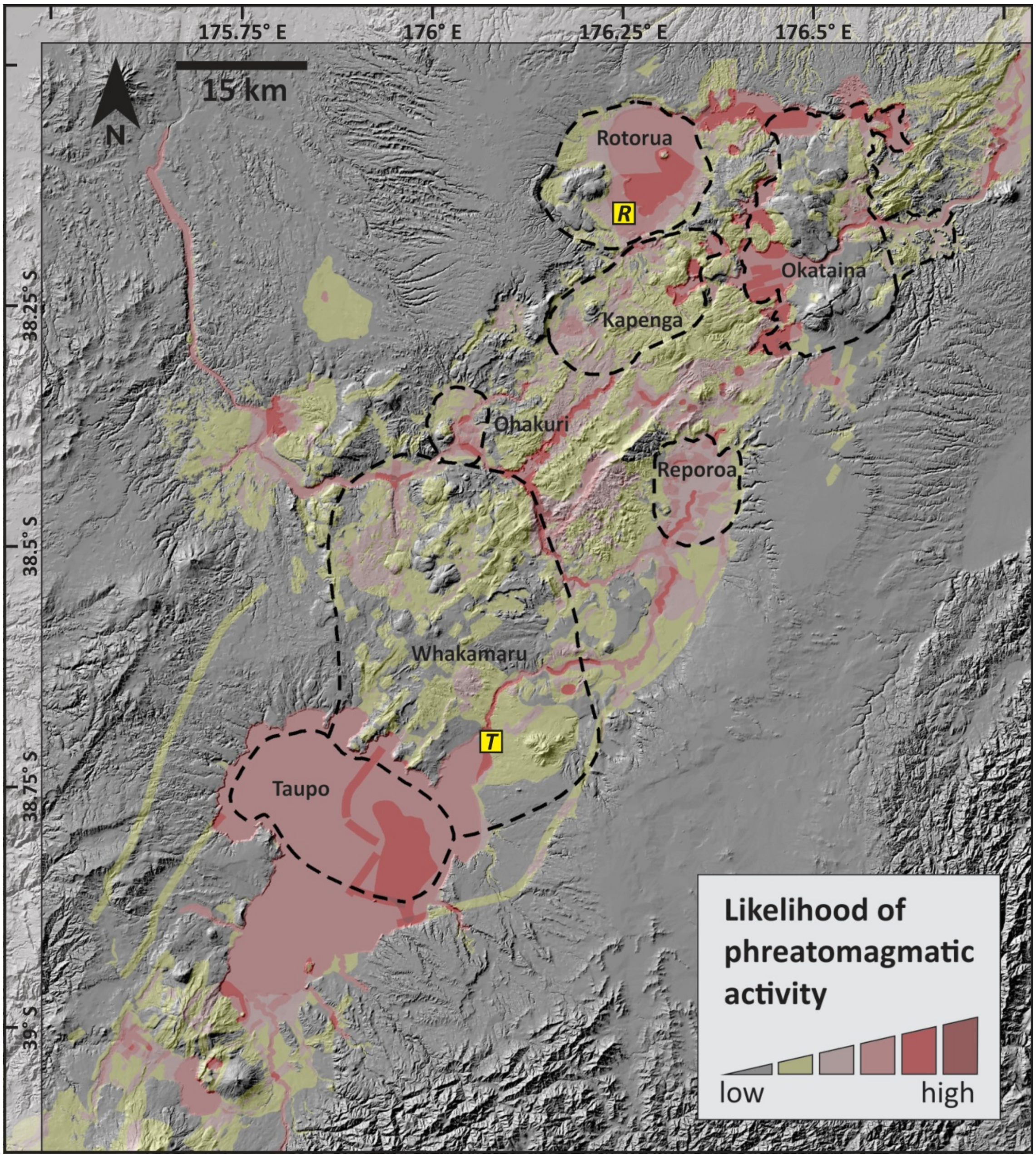
175.75° E
176° E
176.25° E
176.5° E
15 km
N
38.25° S
38.5° S
38.75° S
39° S
Rotorua
R
Okataina
Kapenga
Ohakuri
Reporoa
Whakamaru
T
Taupo
Likelihood of phreatomagmatic activity
low
high

Figure 10.2 Preliminary susceptibility map for hydrovolcanic eruptions within the central TVZ prepared by a combined overlay of spatially-identified environmental factors may contribute to inducing hydrovolcanic activity. Caldera margins after Wilson et al. (1995), letters in yellow square indicate the location of major towns (T:Taupo and R: Rotorua).

10.5 Conclusions

The overall aim of this research was to understand the hazards posed by small-volume eruptions of the TVZ through the volcanic activity of three example localities that are characterised by different chemical compositions and eruptive styles, as well as by exploring the spatial, temporal and volumetric patterns of the small-volume eruptions along the entire TVZ. The study sites were chosen to represent a wide variety of environmental settings, such as unconsolidated reworked volcaniclastic and fluvial deposits, ignimbrite plateaus, subaqueous and near water environments. These sites are considered to be representative of the geoenvironment of the TVZ in its past 350 ky evolution and are suspected to play an important but distinct role in influencing the volcanic activity. Besides the original objectives, a new basaltic rock association was identified and described in the vicinity of the PVC, while it was also revealed that Motuoapa Peninsula and its neighbourhood comprise two temporally distinct eruptions. The identification of eruptive styles, and the longevity of eruptions regarding various internal parameters of magma and external parameters of five low to average volume eruptions, greatly contribute to reveal the possible eruption scenarios of small-volume volcanism across the TVZ.

10.5.1 Main findings in relation to the research objectives

10.5.1.1 Volcanic architecture and evolution of the volcanoes of example localities

- The volcanic activity of the OVC was initiated as an unstable fissure eruption, with common vent shifting that is associated with alternating Strombolian/Hawaiian and phreatomagmatic eruptive styles. As a result, a coalesced hybrid volcanic structure was formed with a morphology resembling a tuff ring, while its pyroclastic succession is dominated by pyroclasts more typical of Strombolian-style explosive activity. This ejecta ring embraces three smaller scoria-spatter cones and a few more depressions of vents related to phreatomagmatic activity. In contrast with the most common course of such a low-silica eruption, the external water was available and influenced the activity for the entire duration. The Ohakune eruption is expected to have lasted in the range of 3-5 months.

- The Te Hukui sequence relates to a newly-discovered basaltic maar-forming eruption occurring in the vicinity of the later silicic Puketerata activity. The energetic explosive activity was demonstrated by the various types of extrusive rocks without preserved surficial expressions and widespread exposures. The exposed section provides a record of an eruption produced relatively thick deposits from moist to dry pyroclastic density currents. The significance of this location is that it demonstrates the chance of strong phreatomagmatic eruptions in the settings of the ignimbrite plateau located far away from large bodies of surface water and that is facilitated by good drainage and potentially good hydrology along faults.
- The activity of the PVC encompassed initial maar-forming eruptions for the emplacement of lava domes, which was most likely triggered by an intrusion of mafic magma to the magma reservoir. Pyroclast density and vesicle shapes of fragments from fallout beds indicate extensive degassing and quenching prior to the eruptions, indicating the important role of magma-water interaction on explosive activity. The ejecta ring around the larger lava dome is morphologically distinct from the ordinary tuff rings due to its composite structure, with beds of diluted PDCs and breccias with block-and-ash flow, rockfall and fallout origin.
- Motuoapa Peninsula and its neighbourhood comprise the cluster of three extrusive bodies, which represent two temporally distinct eruptive periods. The older rhyolitic event was initiated in a subaqueous environment, forming a pyroclastic cone with deposits of Surtseyan activity interbedded with dome collapse related coarse breccias. The second phase was a pure effusive event during which an at least 3 km long low viscosity coulee emplaced in the E-SE sector of the cone. Echo Cliffs represents the distal part of this flow. The younger eruptive event occurred after the Oruanui collapse along a 3 km long fissure forming two dacitic endogenous domes. Both domes experienced some destruction because of explosive activity at the late stage of activity. LiDAR-based digital terrain analysis indicates that about 100 m subsidence of the Motuoapa Peninsula occurred after the rhyolitic activity compared to the east shore of Lake Taupo, while the lake level of ancient Lake Huka could be about

100 m higher than the current level of Lake Taupo. Lake terraces formed during the 1.8 ka high stand of Lake Taupo, suggesting the drainage of the lake by multiple flood events.

10.5.1.2 Spatio-temporal and eruptive style pattern of small-volume volcanism of the central TVZ

- The spatial distribution of post-350 ka vents indicates a weak overall correlation with active calderas and a strong correlation with the tectonic structures of the TVZ. The only exception is the Whakamaru Volcanic Centre, with vents along the caldera margins at the the western, NW and eastern side of the caldera structure.
- In the past 350 ka, about 260 km^3 DRE volume of volcanic material has erupted by small-volume activity within the TVZ. Most commonly the erupted volume was around 0.2 km^3. The cumulative DRE volume of small-volume eruptions as a function of time suggests the significant increase of magma production about 50 ka, roughly coinciding with the Rotoiti caldera-forming eruption. Since then, the Okataina Volcanic Centre is characterised by relatively larger-volume events, with the combined production of about 110 km^3 DRE, whereas the Taupo Volcanic Centre produced only 20 km^3 DRE (by one-and-a-half times as many small-volume eruptions that occurred at the Okataina Volcanic Centre).
- Based on an overlay of various geological, morphometric and land cover data, two types of hazard map were created for the central TVZ. The eruption location prediction map indicates the highest likelihood for future eruptions, whereas the susceptibility map for phreatomagmatic eruptions is mostly useful for the mafic and initial phases of silicic activity, during which the environment often strongly influence the eruption style.

10.5.1.3 Globally relevant general findings

- Initial phases of small-volume eruptions often tend to be unstable with frequently changing eruption styles resulting in hybrid volcanic structures. Initial activity may represent significantly more hazardous activity than the latter phases, thus the evaluation of volcanic hazard should include the detailed sedimentological survey of initial deposits wherever possible. Larger-volume eruptions may hide the evidence in the proximity of the vents, therefore the preserved medial and distal facies are the key for the identification of eruptive behaviours.

- Observed morphometry of natural lava domes does not fit perfectly for existing dome classifications, because these models cannot incorporate all the processes (e.g. destructive events) in relation to the emplacement of lava domes. A new morphology-based classification was suggested, which was linked to the inferred physical properties of emplacing magma/lava. The new classification is aimed at supporting the hazard assessment of lava dome fields with short field-based observations.

10.5.2 Future directions of research

- The morphology of volcanic structures is usually representative of the volcanic evolution of a particular volcano. Many aspects of their volcanic activity would be extractable by digital terrain analysis using high resolution DEMs. As the morphology of extrusive lava structures corresponds to the magma viscosity and yield strength at the time of the emplacement, dome morphology may indicate the likelihood of explosivity. According to the gained experience at example localities, GIS-based investigation of morphology is the key to a quick evaluation of past volcanic activity, helping to highlight the interesting features that require field-based detailed studies.
- The existing knowledge of pyroclastic deposits relating to dome-forming eruptions is twofold. The young Okataina dome-forming eruptions were associated with significant explosive activity independent from the yield strength and viscosity inferred from their morphology. On the other hand, only five to 10 of the rest of the domes have associated pyroclastic deposits or detected morphologic features relating to explosive activity. From this, it is inferred that the role and frequency of explosive activity associated with dome-forming eruptions is larger than is currently apparent. To verify this this role, it

is suggested to initiate field campaigns to detect and characterise the pyroclastic deposits that are associated with extrusive eruptions.

- Hazard mapping and assessment of the TVZ's small-volume volcanism can be improved in many ways, such as using more reliable input parameters, expanding the types of applied input data and integrating probabilistic methods.

10.5.3 Epilogue – personal view

Caldera volcanism is generally considered to be polygenetic volcanism. From the point of view of a magmatic plumbing system, neither the small-volume eruptions nor the caldera-forming eruptions of large silicic systems, such as the existing large calderas of the TVZ, match perfectly to the "polygenetic" criteria (Cas and Wright, 1988; Walker, 2000; Smith and Németh, 2017). There are no long-lived settled magma chambers envisioned in association with many of TVZ's volcanoes of any size, and instead there are rather newly-formed separate melt packages forming lenses in the upper crust which slowly freeze or are evacuated in a short geological time. Almost every small-volume eruption establishes a new eruptive vent similar to basaltic monogenetic fields, which rarely function as the path of subsequent eruptions due to the infill with solidified magma. Caldera-forming eruptions broadly speaking also need to create new vents and re-establish the structure of magma reservoirs. Effusive activity associated with the caldera formation and a small portion of temporally distinct post-caldera eruptions may follow the routes that were established during the evacuation of the magma reservoir. For these reasons, large silicic caldera systems can be interpreted as high-flux volcanic fields with frequent small-volume eruptions that are characterised by larger than average volumes than the usual size of eruptions at monogenetic fields (typically in basaltic systems) and large-volume caldera-forming eruptions. The activity of "real" polygenetic volcanoes may be associated with these volcanic fields.

References

Ablay, G. and Martı, J., 2000. Stratigraphy, structure, and volcanic evolution of the Pico Teide–Pico Viejo formation, Tenerife, Canary Islands. Journal of Volcanology and Geothermal Research, 103(1): 175-208.

Abrams, M.J. and Siebe, C., 1994. Cerro Xalapaxco: an unusual tuff cone with multiple explosion craters, in central Mexico (Puebla). Journal of Volcanology and Geothermal Research, 63(3-4): 183-199.

Acocella, V., Spinks, K.D., Cole, J.W. and Nicol, A., 2003. Oblique back arc rifting of Taupo Volcanic zone, New Zealand. Tectonics, 22(4).

Adams, N.K., Houghton, B.F., Fagents, S.A. and Hildreth, W., 2006. The transition from explosive to effusive eruptive regime: the example of the 1912 Novarupta eruption, Alaska. Geological Society of America Bulletin, 118(5-6): 620-634.

Aguirre-Díaz, G.J. and Labarthe-Hernández, G., 2003. Fissure ignimbrites: Fissure-source origin for voluminous ignimbrites of the Sierra Madre Occidental and its relationship with Basin and Range faulting. Geology, 31(9): 773-776.

Agustin-Flores, J., Németh, K., Cronin, S.J., Lindsay, J.M. and Kereszturi, G., 2015. Construction of the North Head (Maungauika) tuff cone: a product of Surtseyan volcanism, rare in the Auckland Volcanic Field, New Zealand. Bulletin of Volcanology, 77(2): 17.

Agustín-Flores, J., Németh, K., Cronin, S.J., Lindsay, J.M. and Kereszturi, G., 2015. Shallow-seated explosions in the construction of the Motukorea tuff ring (Auckland, New Zealand): evidence from lithic and sedimentary characteristics. Journal of Volcanology and Geothermal Research, 304: 272-286.

Agustin-Flores, J., Németh, K., Cronin, S.J., Lindsay, J.M., Kereszturi, G., Brand, B.D. and Smith, I.E.M., 2014. Phreatomagmatic eruptions through unconsolidated coastal plain sequences, Maungataketake, Auckland Volcanic Field (New Zealand). Journal of Volcanology and Geothermal Research, 276: 46-63.

Albert, H., Costa, F. and Martí, J., 2016. Years to weeks of seismic unrest and magmatic intrusions precede monogenetic eruptions. Geology, 44(3): 211-214.

Alidibirov, M. and Dingwell, D.B., 1996. Magma fragmentation by rapid decompression. Nature, 380(6570): 146-148.

Allan, A.S., Morgan, D.J., Wilson, C.J. and Millet, M.-A., 2013. From mush to eruption in centuries: assembly of the super-sized Oruanui magma body. Contributions to Mineralogy and Petrology, 166(1): 143-164.

Allan, A.S., Wilson, C.J., Millet, M.-A. and Wysoczanski, R.J., 2012. The invisible hand: Tectonic triggering and modulation of a rhyolitic supereruption. Geology, 40(6): 563-566.

Allan, J.F., 1986. Geology of the northern Colima and Zacoalco grabens, southwest Mexico: Late Cenozoic rifting in the Mexican volcanic belt. Geological Society of America Bulletin, 97(4): 473-485.

Allard, P., Dajlevic, D. and Delarue, C., 1989. Origin of carbon dioxide emanation from the 1979 Dieng eruption, Indonesia: Implications for the origin of the 1986 Nyos catastrophe. Journal of Volcanology and Geothermal Research, 39(2-3): 195-206.

Allen, S.R. and McPhie, J., 2009. Products of neptunian eruptions. Geology, 37(7): 639-642.

Anderson, S. and Fink, J., 1990. The development and distribution of surface textures at the Mount St. Helens dome, Lava flows and domes. Springer, pp. 25-46.

Anderson, S.W. and Fink, J.H., 1992. Crease structures: Indicators of emplacement rates and surface stress regimes of lava flows. Geological Society of America Bulletin, 104(5): 615-625.

Anderson, S.W., Stofan, E.R., Plaut, J.J. and Crown, D.A., 1998. Block size distributions on silicic lava flow surfaces: implications for emplacement conditions. Geological Society of America Bulletin, 110(10): 1258-1267.

Andronico, D., Branca, S., Calvari, S., Burton, M., Caltabiano, T., Corsaro, R.A., Del Carlo, P., Garfì, G., Lodato, L. and Miraglia, L., 2005. A multi-disciplinary study of the 2002–03 Etna eruption: insights into a complex plumbing system. Bulletin of Volcanology, 67(4): 314-330.

Annen, C., 2011. Implications of incremental emplacement of magma bodies for magma differentiation, thermal aureole dimensions and plutonism–volcanism relationships. Tectonophysics, 500(1): 3-10.

Aramaki, S., 1984. Formation of the Aira caldera, southern Kyushu,∼ 22,000 years ago. Journal of Geophysical Research: Solid Earth, 89(B10): 8485-8501.

Ashwell, P.A., Kennedy, B.M., Gravley, D.M., von Aulock, F.W. and Cole, J.W., 2013. Insights into caldera and regional structures and magma body distribution from lava domes at Rotorua Caldera, New Zealand. Journal of Volcanology and Geothermal Research, 258: 187-202.

Aspinall, W., Sigurdsson, H. and Shepherd, J., 1973. Eruption of Soufriere Volcano on St. Vincent Island, 1971-1972. Science, 181(4095): 117-124.

Auer, A., Martin, U. and Németh, K., 2007. The Fekete-hegy (Balaton Highland Hungary) "soft-substrate" and "hard-substrate" maar volcanoes in an aligned volcanic complex - Implications for vent geometry, subsurface stratigraphy and the palaeoenvironmental setting. Journal of Volcanology and Geothermal Research, 159(1-3): 225-245.

Austin-Erickson, A., Buettner, R., Dellino, P., Ort, M.H. and Zimanowski, B., 2008. Phreatomagmatic explosions of rhyolitic magma: Experimental and field evidence. Journal of Geophysical Research-Solid Earth, 113(B11).

Austin-Erickson, A., Ort, M.H. and Carrasco-Núñez, G., 2011. Rhyolitic phreatomagmatism explored: Tepexitl tuff ring (Eastern Mexican Volcanic Belt). Journal of Volcanology and Geothermal Research, 201(1-4): 325-341.

Bacon, C.R., Duffield, W.A. and Nakamura, K., 1980. Distribution of Quaternary rhyolite domes of the Coso Range, California: Implications for extent of the geothermal anomaly. Journal of Geophysical Research: Solid Earth, 85(B5): 2425-2433.

Baddeley, A.J. and Jensen, E.B.V., 2002. Stereology: sampling in three dimensions. University of Western Australia. Department of Mathematics and Statistics.

Bailey, R.A., 1989. Geologic map of Long Valley caldera. Mono-Inyo Craters volcanic chain, and vicinity, eastern California: US Geological Survey Miscellaneous Investigations Map I-1933, scale, 1(62,500): 11.

Ballance, P.F., 1976. Evolution of the upper Cenozoic magmatic arc and plate boundary in northern New Zealand. Earth and planetary science letters, 28(3): 356-370.

Ballance, P.F., Ablaev, A.G., Pushchin, I.K., Pletnev, S.P., Birylina, M.G., Itaya, T., Follas, H.A. and Gibson, G.W., 1999. Morphology and history of the Kermadec trench–arc–backarc basin–remnant arc system at 30 to 32 S: geophysical profile, microfossil and K–Ar data. Marine Geology, 159(1): 35-62.

Barberi, F., Bertagnini, A., Landi, P. and Principe, C., 1992. A review on phreatic eruptions and their precursors. Journal of volcanology and geothermal research, 52(4): 231-246.

Barker, S., Wilson, C., Smith, E.G., Charlier, B., Wooden, J.L., Hiess, J. and Ireland, T., 2014. Post-supereruption magmatic reconstruction of Taupo volcano (New Zealand), as reflected in zircon ages and trace elements. Journal of Petrology, 55(8): 1511-1533.

Barnes, P.M. and Lépinay, B.M., 1997. Rates and mechanics of rapid frontal accretion along the very obliquely convergent southern Hikurangi margin, New Zealand. Journal of Geophysical Research: Solid Earth, 102(B11): 24931-24952.

Beanland, S. and Haines, J., 1998. The kinematics of active deformation in the North Island, New Zealand, determined from geological strain rates. New Zealand Journal of Geology and Geophysics, 41(4): 311-323.

Bebbington, M.S., 2013. Assessing spatio-temporal eruption forecasts in a monogenetic volcanic field. Journal of Volcanology and Geothermal Research, 252: 14-28.

Bebbington, M.S., 2015. Spatio-volumetric hazard estimation in the Auckland volcanic field. Bulletin of Volcanology, 77(5): 1-15.

Bebbington, M.S. and Cronin, S.J., 2011. Spatio-temporal hazard estimation in the Auckland Volcanic Field, New Zealand, with a new event-order model. Bulletin of Volcanology, 73(1): 55-72.

Begét, J.E., Hopkins, D.M. and Charron, S.D., 1996. The largest known maars on Earth, Seward Peninsula, northwest Alaska. Arctic: 62-69.

Bégué, F., Deering, C., Gravley, D., Kennedy, B., Chambefort, I., Gualda, G. and Bachmann, O., 2014. Extraction, storage and eruption of multiple isolated magma batches in the paired Mamaku and Ohakuri eruption, Taupo Volcanic Zone, New Zealand. Journal of Petrology, 55(8): 1653-1684.

Belousov, A. and Belousova, M., 2001. Eruptive process, effects and deposits of the 1996 and the ancient basaltic phreatomagmatic eruptions in Karymskoye lake, Kamchatka, Russia. Volcanogenic sedimentation in lacustrine settings. International Association of Sedimentologists Special Publication, 30: 35-60.

Belousov, A., Belousova, M., Edwards, B., Volynets, A. and Melnikov, D., 2015. Overview of the precursors and dynamics of the 2012–13 basaltic fissure eruption of Tolbachik Volcano, Kamchatka, Russia. Journal of Volcanology and Geothermal Research, 299: 19-34.

Beresford, S. and Cole, J., 2000. Kaingaroa Ignimbrite, Taupo volcanic zone, New Zealand: evidence for asymmetric caldera subsidence of the Reporoa caldera. New Zealand Journal of Geology and Geophysics, 43(3): 471-481.

Bernstein, M., Pavez, A., Varley, N., Whelley, P. and Calder, E.S., 2013. Rhyolite lava dome growth styles at Chaitén Volcano, Chile (2008-2009): Interpretation of thermal imagery.

Bibby, H., Caldwell, T., Davey, F. and Webb, T., 1995. Geophysical evidence on the structure of the Taupo Volcanic Zone and its hydrothermal circulation. Journal of volcanology and geothermal research, 68(1-3): 29-58.

Bignall, G., Milicich, S., Ramirez, L., Rosenberg, M., Kilgour, G. and Rae, A., 2010. Geology of the wairakei-Tauhara geothermal system, New Zealand, Proceedings Worlds Geothermal Congress, pp. 25-30.

Bindeman, I.N., Valley, J.W., Wooden, J. and Persing, H.M., 2001. Post-caldera volcanism: in situ measurement of U–Pb age and oxygen isotope ratio in Pleistocene zircons from Yellowstone caldera. Earth and Planetary Science Letters, 189(3): 197-206.

Blake, S., 1990. Viscoplastic models of lava domes, Lava flows and domes. Springer, pp. 88-126.

Blake, S., Wilson, C., Smith, I. and Walker, G., 1992. Petrology and dynamics of the Waimihia mixed magma eruption, Taupo Volcano, New Zealand. Journal of the Geological Society, 149(2): 193-207.

Blott, S.J. and Pye, K., 2001. GRADISTAT: A grain size distribution and statistics package for the analysis of unconsolidated sediments. Earth Surface Processes and Landforms, 26(11): 1237-1248.

Blundy, J. and Cashman, K., 2008. Petrologic reconstruction of magmatic system variables and processes. Reviews in Mineralogy and Geochemistry, 69(1): 179-239.

Bobach, T. and Umlauf, G., 2006. Natural neighbor interpolation and order of continuity. GI Lecture Notes in Informatics, Visualization of Large and Unstructured Data Sets: 68-86.

Bonadonna, C., Connor, C.B., Houghton, B., Connor, L., Byrne, M., Laing, A. and Hincks, T., 2005. Probabilistic modeling of tephra dispersal: Hazard assessment of a multiphase rhyolitic eruption at Tarawera, New Zealand. Journal of Geophysical Research: Solid Earth, 110(B3).

Bonnichsen, B. and Kauffman, D.F., 1987. Physical features of rhyolite lava flows in the Snake River Plain volcanic province, southwestern Idaho. Geological Society of America Special Papers, 212: 119-145.

Booden, M.A., Smith, I.E., Mauk, J.L. and Black, P.M., 2012. Geochemical and isotopic development of the Coromandel Volcanic Zone, northern New Zealand, since 18Ma. Journal of Volcanology and Geothermal Research, 219: 15-32.

Borgia, A., Linneman, S., Spencer, D., Morales, L.D. and Andre, J.B., 1983. Dynamics of lava flow fronts, Arenal volcano, Costa Rica. Journal of volcanology and geothermal research, 19(3-4): 303-329.

Bowman, D., 1971. Geomorphology of the shore terraces of the late Pleistocene Lisan lake (Israel). Palaeogeography, Palaeoclimatology, Palaeoecology, 9(3): 183-209.

Bradshaw, T. and Smith, E.I., 1994. Polygenetic Quaternary volcanism at Crater Flat, Nevada. Journal of Volcanology and Geothermal Research, 63(3-4): 165-182.

Breard, E., Lube, G., Cronin, S., Fitzgerald, R., Kennedy, B., Scheu, B., Montanaro, C., White, J., Tost, M. and Procter, J., 2014. Using the spatial distribution and lithology of ballistic blocks to interpret eruption sequence and dynamics: August 6 2012 Upper Te Maari eruption, New Zealand. Journal of Volcanology and Geothermal Research, 286: 373-386.

Brenna, M., Cronin, S.J., Nemeth, K., Smith, I.E. and Sohn, Y.K., 2011. The influence of magma plumbing complexity on monogenetic eruptions, Jeju Island, Korea. Terra Nova, 23(2): 70-75.

Briggs, R., Gifford, M., Moyle, A., Taylor, S., Norman, M., Houghton, B. and Wilson, C., 1993. Geochemical zoning and eruptive mixing in ignimbrites from Mangakino volcano, Taupo Volcanic Zone, New Zealand. Journal of volcanology and geothermal research, 56(3): 175-203.

Briggs, R., Houghton, B., McWilliams, M. and Wilson, C., 2005. 40Ar/39Ar ages of silicic volcanic rocks in the Tauranga-Kaimai area, New Zealand: Dating the transition between volcanism in the Coromandel Arc and the Taupo Volcanic Zone. New Zealand Journal of Geology and Geophysics, 48(3): 459-469.

Brook, M.S., 2009. Lateral moraine age in Park Valley, Tararua Range, New Zealand. Journal of the Royal Society of New Zealand, 39(2-3): 63-69.

Brooker, M.R., Houghton, B.F., Wilson, C.J.N. and Gamble, J.A., 1993. Pyroclastic phases of a rhyolitic dome-building eruption: Puketarata Tuff Ring, Taupo Volcanic Zone, New Zealand. Bulletin of Volcanology, 55(6): 395-406.

Brown, R., Kokelaar, B. and Branney, M., 2007. Widespread transport of pyroclastic density currents from a large silicic tuff ring: the Glaramara tuff, Scafell caldera, English Lake District, UK. Sedimentology, 54(5): 1163-1190.

Brown, R.J., Orsi, G. and de Vita, S., 2008. New insights into Late Pleistocene explosive volcanic activity and caldera formation on Ischia (southern Italy). Bulletin of Volcanology, 70(5): 583-603.

Brown, S., Smith, R., Cole, J. and Houghton, B., 1994. Compositional and textural characteristics of the strombolian and surtseyan K-Trig basalts, Taupo Volcanic Centre, New Zealand: Implications for eruption dynamics. New Zealand Journal of Geology and Geophysics, 37(1): 113-126.

Brown, S., Wilson, C., Cole, J. and Wooden, J., 1998. The Whakamaru group ignimbrites, Taupo Volcanic Zone, New Zealand: evidence for reverse tapping of a zoned silicic magmatic system. Journal of Volcanology and Geothermal Research, 84(1): 1-37.

Brown, S.J. and Fletcher, I.R., 1999. SHRIMP U-Pb dating of the preeruption growth history of zircons from the 340 ka Whakamaru Ignimbrite, New Zealand: Evidence for> 250 ky magma residence times. Geology, 27(11): 1035-1038.

Brown, S.J.A., 1994. Geology and geochemistry of the Whakamaru Group ignimbrites, and associated rhyolite domes, Taupo Volcanic Zone, New Zealand, Unpublished PhD thesis, University of Canterbury, Christchurch, 288 pp.

Browne, P. and Lawless, J., 2001. Characteristics of hydrothermal eruptions, with examples from New Zealand and elsewhere. Earth-Science Reviews, 52(4): 299-331.

Budkewitsch, P. and Robin, P.-Y., 1994. Modelling the evolution of columnar joints. Journal of Volcanology and Geothermal Research, 59(3): 219-239.

Bull, K.F., Cameron, C., Coombs, M.L., Diefenbach, A., Lopez, T., McNutt, S., Neal, C., Payne, A., Power, J.A. and Schneider, D.J., 2012. The 2009 eruption of Redoubt Volcano, Alaska, State of Alaska, Department of Natural Resources.

Bulmer, M., Glaze, L., Anderson, S. and Shockey, K., 2005. Distinguishing between primary and secondary emplacement events of blocky volcanic deposits using rock size distributions. Journal of Geophysical Research: Solid Earth, 110(B1).

Burt, R., Cole, J. and Vroon, P., 1996. Volcanic geology and geochemistry of Motuhora (Whale Island), Bay of Plenty, New Zealand. New Zealand Journal of Geology and Geophysics, 39(4): 565-580.

Büttner, R., Dellino, P., La Volpe, L., Lorenz, V. and Zimanowski, B., 2002. Thermohydraulic explosions in phreatomagmatic eruptions as evidenced by the comparison between pyroclasts and products from Molten Fuel Coolant Interaction experiments. Journal of Geophysical Research: Solid Earth (1978–2012), 107(B11): ECV 5-1-ECV 5-14.

Büttner, R. and Zimanowski, B., 1998. Physics of thermohydraulic explosions. Physical Review E, 57(5): 5726-5729.

Cabrera, A., Weinberg, R.F. and Wright, H.M., 2015. Magma fracturing and degassing associated with obsidian formation: The explosive–effusive transition. Journal of Volcanology and Geothermal Research, 298: 71-84.

Calder, E., Luckett, R., Sparks, R. and Voight, B., 2002. Mechanisms of lava dome instability and generation of rockfalls and pyroclastic flows at Soufriere Hills Volcano, Montserrat. Geological Society, London, Memoirs, 21(1): 173-190.

Cameron, E., Gamble, J., Price, R., Smith, I., McIntosh, W. and Gardner, M., 2010. The petrology, geochronology and geochemistry of Hauhungatahi volcano, SW Taupo Volcanic Zone. Journal of Volcanology and Geothermal Research, 190(1-2): 179-191.

Cano-Cruz, M. and Carrasco-Núñez, G., 2008. Evolution of a rhyolitic explosion crater (maar): Hoya de Estrada, Valle de Santiago volcanic field Guanajuato, Mexico. Revista Mexicana De Ciencias Geologicas, 25(3): 549-564.

Capaccioni, B. and Cuccoli, F., 2005. Spatter and welded air fall deposits generated by fire-fountaining eruptions: cooling of pyroclasts during transport and deposition. Journal of volcanology and geothermal research, 145(3): 263-280.

Capaccioni, B. and Sarocchi, D., 1996. Computer-assisted image analysis on clast shape fabric from the Orvieto-Bagnoregio ignimbrite (Vulsini District, central Italy): implications on the emplacement mechanisms. Journal of Volcanology and Geothermal Research, 70(1-2): 75-90.

Cappello, A., Neri, M., Acocella, V., Gallo, G., Vicari, A. and Del Negro, C., 2012. Spatial vent opening probability map of Etna volcano (Sicily, Italy). Bulletin of volcanology, 74(9): 2083-2094.

Carey, S., Sigurdsson, H., Mandeville, C. and Bronto, S., 1996. Pyroclastic flows and surges over water: an example from the 1883 Krakatau eruption. Bulletin of Volcanology, 57(7): 493-511.

Carn, S., Watts, R., Thompson, G. and Norton, G., 2004. Anatomy of a lava dome collapse: the 20 March 2000 event at Soufrière Hills Volcano, Montserrat. Journal of Volcanology and Geothermal Research, 131(3): 241-264.

Carrasco-Núñez, G., Ort, M.H. and Romero, C., 2007. Evolution and hydrological conditions of a maar volcano (Atexcac crater, Eastern Mexico). Journal of Volcanology and Geothermal Research, 159(1): 179-197.

Carrivick, J.L., Manville, V. and Cronin, S.J., 2009. A fluid dynamics approach to modelling the 18th March 2007 lahar at Mt. Ruapehu, New Zealand. Bulletin of Volcanology, 71(2): 153-169.

Carroll, L., Gamble, J., Houghton, B., Thordarson, T. and Higham, T., 1997. A radiocarbon age determination for Mount Edgecumbe (Putauaki) volcano, Bay of Plenty, New Zealand.

Cas, R. and Wright, J.V., 1988. Volcanic successions modern and ancient: A geological approach to processes, products and successions. Chapman & Hall, London.

Cashman, K. and Blundy, J., 2000. Degassing and crystallization of ascending andesite and dacite. Philosophical Transactions of the Royal Society of London A: Mathematical, Physical and Engineering Sciences, 358(1770): 1487-1513.

Cashman, K.V. and Giordano, G., 2014. Calderas and magma reservoirs. Journal of Volcanology and Geothermal Research, 288: 28-45.

Cashman, S.M., Kelsey, H.M., Erdman, C.F., Cutten, H.N. and Berryman, K.R., 1992. Strain partitioning between structural domains in the forearc of the Hikurangi subduction zone, New Zealand. Tectonics, 11(2): 242-257.

Castro, J.M., Bindeman, I.N., Tuffen, H. and Schipper, C.I., 2014. Explosive origin of silicic lava: textural and δD–H 2 O evidence for pyroclastic degassing during rhyolite effusion. Earth and Planetary Science Letters, 405: 52-61.

Castro, J.M., Cordonnier, B., Tuffen, H., Tobin, M.J., Puskar, L., Martin, M.C. and Bechtel, H.A., 2012. The role of melt-fracture degassing in defusing explosive rhyolite eruptions at volcan Chaiten. Earth and Planetary Science Letters, 333: 63-69.

Castro, J.M. and Gardner, J.E., 2008. Did magma ascent rate control the explosive-effusive transition at the Inyo volcanic chain, California? Geology, 36(4): 279-282.

Cattell, H., 2015. Volcanic evolution of the Huka Group at Wairakei-Tauhara Geothermal Field, Taupo Volcanic Zone, New Zealand, Unpublished PhD thesis, University of Canterbury, Christchurch, 171 pp.

Cattell, H., Cole, J., Oze, C. and Allen, S., 2014. Eruptive origins of a lacustrine pyroclastic succession: insights from the middle Huka Falls Formation, Taupo Volcanic Zone, New Zealand. New Zealand Journal of Geology and Geophysics, 57(3): 331-343.

Charlier, B., Wilson, C., Lowenstern, J., Blake, S., Van Calsteren, P. and Davidson, J., 2004. Magma generation at a large, hyperactive silicic volcano (Taupo, New Zealand) revealed by U–Th and U–Pb systematics in zircons. Journal of Petrology, 46(1): 3-32.

Charlier, B.L., Wilson, C.J. and Davidson, J.P., 2008. Rapid open-system assembly of a large silicic magma body: time-resolved evidence from cored plagioclase crystals in the Oruanui eruption deposits, New Zealand. Contributions to Mineralogy and Petrology, 156(6): 799-813.

Charlier, B.L.A., Peate, D.W., Wilson, C.J.N., Lowenstern, J.B., Storey, M. and Brown, S.J.A., 2003. Crystallisation ages in coeval silicic magma bodies: U-238-Th-230 disequilibrium evidence from the Rotoiti and Earthquake Flat eruption deposits, Taupo Volcanic Zone, New Zealand. Earth and Planetary Science Letters, 206(3-4): 441-457.

Chiodini, G., Caliro, S., De Martino, P., Avino, R. and Gherardi, F., 2012. Early signals of new volcanic unrest at Campi Flegrei caldera? Insights from geochemical data and physical simulations. Geology, 40(10): 943-946.

Chough, S. and Sohn, Y., 1990. Depositional mechanics and sequences of base surges, Songaksan tuff ring, Cheju Island, Korea. Sedimentology, 37(6): 1115-1135.

Christenson, B., Reyes, A., Young, R., Moebis, A., Sherburn, S., Cole-Baker, J. and Britten, K., 2010. Cyclic processes and factors leading to phreatic eruption events: Insights from the 25 September 2007 eruption through Ruapehu Crater Lake, New Zealand. Journal of Volcanology and Geothermal Research, 191(1): 15-32.

Christiansen, R.L. and Lipman, P.W., 1966. Emplacement and thermal history of a rhyolite lava flow near Fortymile Canyon, southern Nevada. Geological Society of America Bulletin, 77(7): 671-684.

Christiansen, R.L., Lipman, P.W., Carr, W., Byers, F., Orkild, P.P. and Sargent, K., 1977. Timber Mountain–Oasis Valley caldera complex of southern Nevada. Geological Society of America Bulletin, 88(7): 943-959.

Christiansen, R.L. and Peterson, D.W., 1981. Chronology of the 1980 eruptive activity. In: P.W. Lipman and D.R. Mullineaux (Editors), The 1980 eruptions of Mount St. Helens, Washington. U.S. Geological Survey Professional Paper 1250, Washington, pp. 17-30.

Cimarelli, C., Di Traglia, F. and Taddeucci, J., 2010. Basaltic scoria textures from a zoned conduit as precursors to violent Strombolian activity. Geology, 38(5): 439-442.

Cioni, R., Sbrana, A. and Vecci, R., 1992. Morphologic features of juvenile pyroclasts from magmatic and phreatomagmatic deposits of Vesuvius. Journal of Volcanology and Geothermal Research, 51(1-2): 61-78.

Clough, B.J., Wright, J.V. and Walker, G.P.L., 1982. Morphology and dimensions of the young comendite lavas of La Primavera volcano, Mexico. Geological Magazine, 119(5): 477-485.

Cole, J., 1970. Structure and eruptive history of the Tarawera Volcanic Complex. New Zealand journal of geology and geophysics, 13(4): 879-902.

Cole, J., 1973. High-alumina basalts of Taupo volcanic zone, New Zealand. Lithos, 6(1): 53-64.

Cole, J., 1978. Andesites of the Tongariro Volcanic Centre, North Island, New Zealand. Journal of volcanology and geothermal research, 3(1-2): 121-153.

Cole, J., 1981. Genesis of lavas of the Taupo volcanic zone, North Island, New Zealand. Journal of Volcanology and Geothermal Research, 10(4): 317-337.

Cole, J. and Lewis, K., 1981. Evolution of the Taupo-Hikurangi subduction system. Tectonophysics, 72(1-2): 1-21.

Cole, J., Milner, D. and Spinks, K., 2005. Calderas and caldera structures: a review. Earth-Science Reviews, 69(1): 1-26.

Cole, J. and Spinks, K., 2009. Caldera volcanism and rift structure in the Taupo Volcanic Zone, New Zealand. Geological Society, London, Special Publications, 327(1): 9-29.

Cole, J., Thordarson, T. and Burt, R., 2000. Magma origin and evolution of White Island (Whakaari) volcano, Bay of Plenty, New Zealand. Journal of Petrology, 41(6): 867-895.

Cole, J.W., 1990. Structural control and origin of volcanism in the Taupo volcanic zone, New Zealand. Bulletin of volcanology, 52(6): 445-459.

Cole, J.W., Graham, I.J., Hackett, W.R. and Houghton, B.F., 1986. Volcanology and petrology of the Quaternary composite volcanoes of Tongariro volcanic centre, Taupo volcanic zone, Late Cenozoic Volcanism in New Zealand. Royal Society of NZ Bulletin 23, pp. 224-250.

Cole, J.W., Spinks, K.D., Deering, C.D., Nairn, I.A. and Leonard, G.S., 2010. Volcanic and structural evolution of the Okataina Volcanic Centre; dominantly silicic volcanism associated with the Taupo Rift, New Zealand. Journal of Volcanology and Geothermal Research, 190(1-2): 123-135.

Cole, P., Calder, E., Sparks, R., Clarke, A., Druitt, T., Young, S., Herd, R., Harford, C. and Norton, G., 2002. Deposits from dome-collapse and fountain-collapse pyroclastic flows at Soufrière Hills Volcano, Montserrat. Geological Society, London, Memoirs, 21(1): 231-262.

Cole, P., Guest, J., Duncan, A., Chester, D. and Bianchi, R., 1992. Post-collapse volcanic history of calderas on a composite volcano: an example from Roccamonfina, southern Italy. Bulletin of volcanology, 54(4): 253-266.

Cole, P., Guest, J., Duncan, A. and Pacheco, J.-M., 2001. Capelinhos 1957–1958, Faial, Azores: deposits formed by an emergent surtseyan eruption. Bulletin of Volcanology, 63(2): 204-220.

Cole, P., Queiroz, G., Wallenstein, N., Gaspar, J., Duncan, A. and Guest, J., 1995. An historic subplinian/phreatomagmatic eruption: the 1630 AD eruption of Furnas volcano, Sa˜ o Miguel, Azores. Journal of Volcanology and Geothermal Research, 69(1): 117-135.

Connor, C.B., 1990. Cinder cone clustering in the TransMexican Volcanic Belt: implications for structural and petrologic models. Journal of Geophysical Research: Solid Earth, 95(B12): 19395-19405.

Connor, C.B. and Conway, F.M., 2000. Basaltic volcanic fields. Encyclopedia of volcanoes: 331-343.

Connor, C.B., Stamatakos, J.A., Ferrill, D.A., Hill, B.E., Ofoegbu, G.I., Conway, F.M., Sagar, B. and Trapp, J., 2000. Geologic factors controlling patterns of small-volume basaltic volcanism: Application to a volcanic hazards assessment at Yucca Mountain, Nevada. Journal of Geophysical Research: Solid Earth, 105(B1): 417-432.

Conway, C.E., Leonard, G.S., Townsend, D.B., Calvert, A.T., Wilson, C.J., Gamble, J.A. and Eaves, S.R., 2016. A high-resolution 40 Ar/39 Ar lava chronology and edifice construction history for Ruapehu volcano, New Zealand. Journal of Volcanology and Geothermal Research, 327: 152-179.

Cook, R.J., Barron, J., Papendick, R.I. and Williams, G., 1981. Impact on agriculture of the Mount St. Helens eruptions. Science, 211(4477): 16-22.

Cooper, G.F., Wilson, C.J., Millet, M.-A., Baker, J.A. and Smith, E.G., 2012. Systematic tapping of independent magma chambers during the 1Ma Kidnappers supereruption. Earth and Planetary Science Letters, 313: 23-33.

Corazzato, C. and Tibaldi, A., 2006. Fracture control on type, morphology and distribution of parasitic volcanic cones: an example from Mt. Etna, Italy. Journal of Volcanology and Geothermal Research, 158(1): 177-194.

Costa, A., Melnik, O. and Sparks, R., 2007. Controls of conduit geometry and wallrock elasticity on lava dome eruptions. Earth and Planetary Science Letters, 260(1): 137-151.

Cousens, B.L., Clague, D.A. and Sharp, W.D., 2003. Chronology, chemistry, and origin of trachytes from Hualalai Volcano, Hawaii. Geochemistry Geophysics Geosystems, 4.

Crandell, D.R. and Mullineaux, D.R., 1978. Potential hazards from future eruptions of Mount St. Helens volcano, Washington. US Department of the Interior, Geological Survey; Washington, DC.

Crandell, D.R., Mullineaux, D.R., Sigafoos, R.S. and Rubin, M., 1974. Chaos Crags eruptions and rockfall-avalanches, Lassen Volcanic National Park, California. US Geol Surv J Res, 2: 49-59.

Creaser, R.A. and White, A.J., 1991. Yardea Dacite—large-volume, high-temperature felsic volcanism from the Middle Proterozoic of South Australia. Geology, 19(1): 48-51.

Cronin, S., Hedley, M., Neall, V. and Smith, R., 1998. Agronomic impact of tephra fallout from the 1995 and 1996 Ruapehu Volcano eruptions, New Zealand. Environmental Geology, 34(1): 21-30.

Cronin, S.J., Neall, V., Lecointre, J., Hedley, M. and Loganathan, P., 2003. Environmental hazards of fluoride in volcanic ash: a case study from Ruapehu volcano, New Zealand. Journal of Volcanology and Geothermal Research, 121(3): 271-291.

Cronin, S.J. and Neall, V.E., 1997. A late Quaternary stratigraphic framework for the northeastern Ruapehu and eastern Tongariro ring plains, New Zealand. New Zealand journal of geology and geophysics, 40(2): 185-197.

D'Oriano, C., Bertagnini, A., Cioni, R. and Pompilio, M., 2014. Identifying recycled ash in basaltic eruptions. Scientific reports, 4.

Danišík, M., Shane, P., Schmitt, A.K., Hogg, A., Santos, G.M., Storm, S., Evans, N.J., Fifield, L.K. and Lindsay, J.M., 2012. Re-anchoring the late Pleistocene tephrochronology of New Zealand based on concordant radiocarbon ages and combined 238 U/230 Th disequilibrium and (U–Th)/He zircon ages. Earth and Planetary Science Letters, 349: 240-250.

Davey, F., 2010. Crustal seismic reflection measurements across the northern extension of the Taupo Volcanic Zone, North Island, New Zealand. Journal of Volcanology and Geothermal Research, 190(1): 75-81.

Davey, F., Hampton, M., Childs, J., Fisher, M., Lewis, K. and Pettinga, J., 1986. Structure of a growing accretionary prism, Hikurangi margin, New Zealand. Geology, 14(8): 663-666.

Davey, F., Henrys, S. and Lodolo, E., 1995. Asymmetric rifting in a continental back-arc environment, North Island, New Zealand. Journal of Volcanology and Geothermal Research, 68(1): 209-238.

Davì, M., De Rosa, R., Donato, P. and Sulpizio, R., 2011. The Lami pyroclastic succession (Lipari, Aeolian Islands): a clue for unravelling the eruptive dynamics of the Monte Pilato rhyolitic pumice cone. Journal of Volcanology and Geothermal Research, 201(1): 285-300.

Davidson, L. and Mathison, C., 1973. Manganiferous orthopyroxenes and garnets from metamorphosed iron formation of the Quairading district, Western Australia. Neues Jahrb. Mineral. Monatsh, 2: 47-57.

Davies, A.G., Cooke, D.R., Gemmell, J.B. and Simpson, K.A., 2008. Diatreme breccias at the Kelian gold mine, Kalimantan, Indonesia: Precursors to epithermal gold mineralization. Economic Geology, 103(4): 689-716.

Davy, B. and Caldwell, T., 1998. Gravity, magnetic and seismic surveys of the caldera complex, Lake Taupo, North Island, New Zealand. Journal of volcanology and geothermal research, 81(1): 69-89.

de la Cruz-Reyna, S. and Yokoyama, I., 2011. A geophysical characterization of monogenetic volcanism. Geofísica internacional, 50(4): 465-484.

De Rita, D., Giordano, G. and Milli, S., 1997. Forestepping-backstepping stacking pattern of volcaniclastic successions: Roccamonfina volcano, Italy. Journal of Volcanology and Geothermal Research, 78(3): 267-288.

De Ronde, C., Stoffers, P., Garbe-Schönberg, D., Christenson, B., Jones, B., Manconi, R., Browne, P., Hissmann, K., Botz, R. and Davy, B., 2002. Discovery of active hydrothermal venting in Lake Taupo, New Zealand. Journal of Volcanology and Geothermal Research, 115(3): 257-275.

de Silva, S.L., Self, S., Francis, P., Drake, R. and Carlos, R.R., 1994. Effusive silicic volcanism in the Central Andes: The Chao dacite and other young lavas of the Altiplano-Puna Volcanic Complex. Journal of Geophysical Research: Solid Earth, 99(B9): 17805-17825.

Deer, W., Howie, R. and Zussman, J., 1967. Rock-forming minerals: Framework Silicates, Volume 4. Longmans, London.

Deer, W., Howie, R. and Zussman, J., 1982. Rock-forming minerals, Orthosilicates, Volume 1A. Longman, New York.

Deer, W.A., Howie, R.A. and Zussman, J., 1997. Rock-forming minerals: Single-chain Silicates, Volume 2A. Geological Society of London.

Deering, C., Bachmann, O., Dufek, J. and Gravley, D., 2011. Rift-related transition from andesite to rhyolite volcanism in the Taupo Volcanic Zone (New Zealand) controlled by crystal–melt dynamics in mush zones with variable mineral assemblages. Journal of Petrology, 52(11): 2243-2263.

Deering, C.D., Gravley, D.M., Vogel, T.A., Cole, J.W. and Leonard, G.S., 2010. Origins of cold-wet-oxidizing to hot-dry-reducing rhyolite magma cycles and distribution in the Taupo Volcanic Zone, New Zealand. Contributions to Mineralogy and Petrology, 160(4): 609-629.

Delaney, P.T. and Pollard, D.D., 1981. Deformation of host rocks and flow of magma during growth of minette dikes and breccia-bearing intrusions near Ship Rock, New Mexico. 2330-7102, USGPO.

Dellino, P. and La Volpe, L., 1995. Fragmentation versus transportation mechanisms in the pyroclastic sequence of Monte Pilato-Rocche Rosse (Lipari, Italy). Journal of Volcanology and Geothermal Research, 64(3-4): 211-231.

Delpit, S., Ross, P.-S. and Hearn, B.C., 2014. Deep-bedded ultramafic diatremes in the Missouri River Breaks volcanic field, Montana, USA: 1 km of syn-eruptive subsidence. Bulletin of Volcanology, 76(7): 832.

Denton, J.S., Tuffen, H., Gilbert, J.S. and Odling, N., 2009. The hydration and alteration of perlite and rhyolite. Journal of the Geological Society, 166(5): 895-904.

Devine, J.D., Gardner, J.E., Brack, H.P., Laynet, G.D. and Rutherford, M.J., 1995. Comparison of microanalytical methods for estimating H20 contents of silicic volcanic glasses. American Mineralogist, 80(3-4): 319-328.

Di Traglia, F., Morelli, S., Casagli, N. and Monroy, V.H.G., 2014. Semi-automatic delimitation of volcanic edifice boundaries: Validation and application to the cinder cones of the Tancitaro–Nueva Italia region (Michoacán–Guanajuato Volcanic Field, Mexico). Geomorphology, 219: 152-160.

Dikau, R., Brabb, E.E. and Mark, R.M., 1991. Landform classification of New Mexico by computer. 2331-1258, US Dept. of the Interior, US Geological Survey.

Dingwell, D.B., 1998a. Magma degassing and fragmentation: recent experimental advances. From Magma to Tephra-Modelling physical processes of explosive volcanic eruptions.

Dingwell, D.B., 1998b. Recent experimental progress in the physical description of silicic magma relevant to explosive volcanism. Geological Society, London, Special Publications, 145(1): 9-26.

Donnadieu, F., Merle, O. and Besson, J.-C., 2001. Volcanic edifice stability during cryptodome intrusion. Bulletin of Volcanology, 63(1): 61-72.

Donnelly-Nolan, J.M., Grove, T.L., Lanphere, M.A., Champion, D.E. and Ramsey, D.W., 2008. Eruptive history and tectonic setting of Medicine Lake Volcano, a large rear-arc volcano in the southern Cascades. Journal of Volcanology and Geothermal Research, 177(2): 313-328.

Donoghue, S., Neall, V. and Palmer, A., 1995. Stratigraphy and chronology of late Quaternary andesitic tephra deposits, Tongariro Volcanic Centre, New Zealand. Journal of the Royal Society of New Zealand, 25(2): 115-206.

Donoghue, S., Neall, V., Palmer, A. and Stewart, R., 1997. The volcanic history of Ruapehu during the past 2 millennia based on the record of Tufa Trig tephras. Bulletin of Volcanology, 59(2): 136-146.

Donoghue, S.L. and Neall, V.E., 2001. Late Quaternary constructional history of the southeastern Ruapehu ring plain, New Zealand. New Zealand Journal of Geology and Geophysics, 44(3): 439-466.

Downs, D.T., Rowland, J.V., Wilson, C.J.N., Rosenberg, M.D., Leonard, G.S. and Calvert, A.T., 2014a. Evolution of the intra-arc Taupo-Reporoa Basin within the Taupo Volcanic Zone of New Zealand. Geosphere, 10(1): 185-206.

Downs, D.T., Wilson, C.J.N., Cole, J.W., Rowland, J.V., Calvert, A.T., Leonard, G.S. and Keall, J.M., 2014b. Age and eruptive center of the Paeroa Subgroup ignimbrites (Whakamaru Group) within the Taupo Volcanic Zone of New Zealand. Geological Society of America Bulletin, 126(9-10): 1131-1144.

Druitt, T., 1998. Pyroclastic density currents. Geological Society, London, Special Publications, 145(1): 145-182.

Druitt, T., Brenchley, P., Gökten, Y. and Francaviglia, V., 1995. Late Quaternary rhyolitic eruptions from the Acigöl Complex, central Turkey. Journal of the Geological Society, 152(4): 655-667.

Duchesne, J.-C., 1972. Pyroxènes et olivines dans le massif de Bjerkreim-Sogndal (Norvège méridionale). Contribution à l'étude de ls série anorthosite-mangérite. 24th IGC, Section 2: 320-328.

Duffield, W.A., 1990. Eruptive fountains of silicic magma and their possible effects on the tin content of fountain-fed lavas, Taylor Creek Rhyolite, New Mexico. Geological Society of America Special Papers, 246: 251-262.

Duffield, W.A., Richter, D.H. and Priest, S.S., 1995. Physical volcanology of silicic lava domes as exemplified by the Taylor Creek Rhyolite, Catron and Sierra Counties, New Mexico. US Geol Surv Map I-2399, 1(50,000).

Duncan, A.R., 1970. The petrology and petrochemistry of andesite and dacite volcanoes in eastern Bay of Plenty, New Zealand, Unpublished PhD Thesis, Victoria Univeristy of Wellington, Wellington 316 pp.

Dzurisin, D., Lockwood, J.P., Casadevall, T.J. and Rubin, M., 1995. The Uwekahuna Ash Member of the Puna Basalt: product of violent phreatomagmatic eruptions at Kilauea volcano, Hawaii, between 2800 and 2100 14 C years ago. Journal of Volcanology and Geothermal Research, 66(1): 163-184.

Edbrooke, S., 2001. Geology of the Auckland Area: Scale 1: 250 000. Institute of Geological & Nuclear Sciences.

Edbrooke, S., 2005. 1: 250 000 Geological Map. Waikato. Institute of Geological & Nuclear Sciences.

Eichelberger, J., 1995. Silicic volcanism: ascent of viscous magmas from crustal reservoirs. Annual Review of Earth and Planetary Sciences, 23: 41-64.

Eichelberger, J., Carrigan, C., Westrich, H. and Price, R., 1986. Non-explosive silicic volcanism. Nature, 323(6089): 598-602.

Ellis, B.S. and Wolff, J.A., 2012. Complex storage of rhyolite in the central Snake River Plain. Journal of Volcanology and Geothermal Research, 211: 1-11.

Engel, A., Engel, C.G. and Havens, R., 1964. Mineralogy of amphibolite interlayers in the gneiss complex, northwest Adirondack Mountains, New York. The Journal of Geology, 72(2): 131-156.

Ewart, A., Bryan, W. and Gill, J., 1973. Mineralogy and geochemistry of the younger volcanic islands of Tonga, SW Pacific. Journal of Petrology, 14(3): 429-465.

Ewart, A., Hildreth, W. and Carmichael, I.S., 1975. Quaternary acid magma in New Zealand. Contributions to mineralogy and petrology, 51(1): 1-27.

Farr, T.G. and Kobrick, M., 2000. Shuttle Radar Topography Mission produces a wealth of data. Eos, Transactions American Geophysical Union, 81(48): 583-585.

Farr, T.G., Rosen, P.A., Caro, E., Crippen, R., Duren, R., Hensley, S., Kobrick, M., Paller, M., Rodriguez, E. and Roth, L., 2007. The shuttle radar topography mission. Reviews of geophysics, 45(2).

Favalli, M. and Fornaciai, A., 2017. Visualization and comparison of DEM-derived parameters. Application to volcanic areas. Geomorphology, 290: 69-84.

Favalli, M., Karátson, D., Mazzarini, F., Pareschi, M.T. and Boschi, E., 2009. Morphometry of scoria cones located on a volcano flank: a case study from Mt. Etna (Italy), based on high-resolution LiDAR data. Journal of Volcanology and Geothermal Research, 186(3): 320-330.

Favalli, M., Karátson, D., Yepes, J. and Nannipieri, L., 2014. Surface fitting in geomorphology - Examples for regular-shaped volcanic landforms. Geomorphology, 221: 139-149.

Fierstein, J., Houghton, B., Wilson, C. and Hildreth, W., 1997. Complexities of plinian fall deposition at vent: an example from the 1912 Novarupta eruption (Alaska). Journal of Volcanology and Geothermal Research, 76(3-4): 215-227.

Fink, J., 1980a. Gravity instability in the Holocene Big and Little Glass Mountain rhyolitic obsidian flows, northern California. Tectonophysics, 66(1): 147-166.

Fink, J., 1980b. Surface folding and viscosity of rhyolite flows. Geology, 8(5): 250-254.

Fink, J., Bridges, N. and Griffiths, R., 1991. Factors controlling lava dome morphology.

Fink, J. and Manley, C., 1989. Explosive volcanic activity generated from within advancing silicic lava flows, Volcanic Hazards. Springer, pp. 169-179.

Fink, J.H., 1983. Structure and emplacement of a rhyolitic obsidian flow: Little Glass Mountain, Medicine Lake Highland, northern California. GSA Bulletin, 94(3): 362-380.

Fink, J.H., 1993. The emplacement of silicic lava flows and associated hazards. Active lavas. UCL Press, London: 5-24.

Fink, J.H. and Anderson, S.W., 2000. Lava domes and coulees. In: H. Sigurdsson, B.F. Houghton, S.R. McNutt, H. Rymer and J. Stix (Editors), Encyclopedia of volcanoes, pp. 307-319.

Fink, J.H. and Anderson, S.W., 2017. Emplacement of Holocene silicic lava flows and domes at Newberry, South Sister, and Medicine Lake volcanoes, California and Oregon. 2328-0328, US Geological Survey.

Fink, J.H., Anderson, S.W. and Manley, C.R., 1992. Textural constraints on effusive silicic volcanism: Beyond the permeable foam model. Journal of Geophysical Research: Solid Earth, 97(B6): 9073-9083.

Fink, J.H. and Griffiths, R.W., 1990. Radial spreading of viscous-gravity currents with solidifying crust. Journal of Fluid Mechanics, 221: 485-509.

Fink, J.H. and Griffiths, R.W., 1998. Morphology, eruption rates, and rheology of lava domes: Insights from laboratory models. Journal of Geophysical Research: Solid Earth, 103(B1): 527-545.

Fink, J.H., Malin, M.C. and Anderson, S.W., 1990. Intrusive and extrusive growth of the Mount St Helens lava dome. Nature, 348.

Fink, J.H. and Manley, C.R., 1987. Origin of pumiceous and glassy textures in rhyolite flows and domes. Geological Society of America Special Papers, 212: 77-88.

Fink, J.H. and Pollard, D.D., 1983. Structural evidence for dikes beneath silicic domes, Medicine Lake Highland Volcano, California. Geology, 11(8): 458-461.

Fisher, R.V., 1995. Decoupling of pyroclastic currents: hazards assessments. Journal of Volcanology and Geothermal Research, 66(1): 257-263.

Fisher, R.V. and Schmincke, H.-U., 1984. Pyroclastic rocks. Springer Berlin.

Folk, R.L. and Ward, W.C., 1957. Brazos River bar: a study in the significance of grain size parameters. Journal of Sedimentary Research, 27(1).

Foxall, R. and Baddeley, A., 2002. Nonparametric measures of association between a spatial point process and a random set, with geological applications. Journal of the Royal Statistical Society: Series C (Applied Statistics), 51(2): 165-182.

Francou, B. and Manté, C., 1990. Analysis of the segmentation in the profile of Alpine talus slopes. Permafrost and Periglacial Processes, 1(1): 53-60.

Franz, G., Steiner, G., Volker, F., Pudlo, D. and Hammerschmidt, K., 1999. Plume related alkaline magmatism in central Africa—the Meidob Hills (W Sudan). Chemical Geology, 157(1): 27-47.

Freda, C., Gaeta, M., Karner, D.B., Marra, F., Renne, P.R., Taddeucci, J., Scarlato, P., Christensen, J.N. and Dallai, L., 2006. Eruptive history and petrologic evolution of the Albano multiple maar (Alban Hills, Central Italy). Bulletin of Volcanology, 68(6): 567-591.

Freundt, A., 2003. Entrance of hot pyroclastic flows into the sea: experimental observations. Bulletin of Volcanology, 65(2-3): 144-164.

Freundt, A., Strauch, W., Kutterolf, S. and Schmincke, H.-U., 2007. Volcanogenic tsunamis in lakes: examples from Nicaragua and general implications. Pure and Applied Geophysics, 164(2): 527-545.

Frey, H.M., Lange, R.A., Hall, C.M. and Delgado-Granados, H., 2004. Magma eruption rates constrained by 40Ar/39Ar chronology and GIS for the Ceboruco–San Pedro volcanic field, western Mexico. Geological Society of America Bulletin, 116(3-4): 259-276.

Friedman, I., 1989. Are extrusive rhyolites produced from permeable foam eruptions? Bulletin of volcanology, 51(1): 69-71.

Froggatt, P., 1981. Stratigraphy and nature of Taupo pumice formation. New Zealand journal of geology and geophysics, 24(2): 231-248.

Froggatt, P.C. and Lowe, D.J., 1990. A review of late Quaternary silicic and some other tephra formations from New Zealand: their stratigraphy, nomenclature, distribution, volume, and age. New Zealand journal of geology and geophysics, 33(1): 89-109.

Froggatt, P.C. and Solloway, G.J., 1986. Correlation of Papanetu Tephra to Karapiti Tephra, central North Island, New Zealand. New Zealand journal of geology and geophysics, 29(3): 303-313.

Furukawa, K. and Kamata, H., 2004. Eruption and emplacement of the Yamakogawa Rhyolite in central Kyushu, Japan: A model for emplacement of rhyolitic spatter. Earth Planets and Space, 56(5): 517-524.

Gamble, J., Smith, I., McCulloch, M., Graham, I. and Kokelaar, B., 1993a. The geochemistry and petrogenesis of basalts from the Taupo Volcanic Zone and Kermadec Island Arc, SW Pacific. Journal of volcanology and geothermal research, 54(3-4): 265-290.

Gamble, J., Wright, I. and Baker, J., 1993b. Seafloor geology and petrology in the oceanic to continental transition zone of the Kermadec-Havre-Taupo Volcanic Zone arc system, New Zealand. New Zealand Journal of Geology and Geophysics, 36(4): 417-435.

Gamble, J.A., Price, R.C., Smith, I.E., McIntosh, W.C. and Dunbar, N.W., 2003. 40 Ar/39 Ar geochronology of magmatic activity, magma flux and hazards at Ruapehu Volcano, Taupo volcanic zone, New Zealand. Journal of Volcanology and Geothermal Research, 120(3): 271-287.

Gamble, J.A., Smith, I.E., Graham, I.J., Kokelaar, B.P., Cole, J.W., Houghton, B.F. and Wilson, C.J., 1990. The petrology, phase relations and tectonic setting of basalts from the Taupo Volcanic Zone, New Zealand and the Kermadec Island Arc-Havre Trough, SW Pacific. Journal of volcanology and geothermal research, 43(1-4): 253-270.

Gardeweg, M., Sparks, R. and Matthews, S., 1998. Evolution of Lascar volcano, northern Chile. Journal of the Geological Society, 155(1): 89-104.

Gardner, J.E., Befus, K.S., Watkins, J., Hesse, M. and Miller, N., 2012. Compositional gradients surrounding spherulites in obsidian and their relationship to spherulite growth and lava cooling. Bulletin of Volcanology, 74(8): 1865-1879.

Garlick, R.D., Hill, A. and Mitchell, J.S., 1999. Lake Rotoaira 1 : 10 000, LAke Chart Series. NIWA.

Germa, A., Connor, L.J., Cañon-Tapia, E. and Le Corvec, N., 2013. Tectonic and magmatic controls on the location of post-subduction monogenetic volcanoes in Baja California, Mexico, revealed through spatial analysis of eruptive vents. Bulletin of volcanology, 75(12): 782.

Geshi, N., Kusumoto, S. and Gudmundsson, A., 2010. Geometric difference between non-feeder and feeder dikes. Geology, 38(3): 195-198.

Geshi, N., Umino, S., Kumagai, H., Sinton, J.M., White, S.M., Kisimoto, K. and Hilde, T.W., 2007. Discrete plumbing systems and heterogeneous magma sources of a 24 km 3 off-axis lava field on the western flank of East Pacific Rise, 14 S. Earth and Planetary Science Letters, 258(1): 61-72.

Geyer, A. and Marti, J., 2008. The new worldwide collapse caldera database (CCDB): A tool for studying and understanding caldera processes. Journal of Volcanology and Geothermal Research, 175(3): 334-354.

Giaccio, B., Sposato, A., Gaeta, M., Marra, F., Palladino, D.M., Taddeucci, J., Barbieri, M., Messina, P. and Rolfo, M.F., 2007. Mid-distal occurrences of the Albano Maar pyroclastic deposits and their relevance for reassessing the eruptive scenarios of the most recent activity at the Colli Albani Volcanic District, Central Italy. Quaternary International, 171: 160-178.

Giordano, D., Russell, J.K. and Dingwell, D.B., 2008. Viscosity of magmatic liquids: a model. Earth and Planetary Science Letters, 271(1): 123-134.

Giordano, G., De Benedetti, A., Diana, A., Diano, G., Gaudioso, F., Marasco, F., Miceli, M., Mollo, S., Cas, R. and Funiciello, R., 2006. The Colli Albani mafic caldera (Roma, Italy): stratigraphy, structure and petrology. Journal of Volcanology and Geothermal Research, 155(1): 49-80.

Gómez-Vasconcelos, M.G., Villamor, P., Cronin, S.J., Procter, J., Kereszturi, G., Palmer, A., Townsend, D., Leonard, G., Berryman, K. and Ashraf, S., 2016. Earthquake history at the eastern boundary of the South Taupo Volcanic Zone, New Zealand. New Zealand Journal of Geology and Geophysics: 1-22.

Gomez, C., Lavigne, F., Lespinasse, N., Hadmoko, D. and Wassmer, P., 2008. Longitudinal structure of pyroclastic-flow deposits, revealed by GPR survey, at Merapi Volcano, Java, Indonesia. Journal of Volcanology and Geothermal Research, 176(4): 439-447.

Gonnermann, H.M. and Manga, M., 2007. The fluid mechanics inside a volcano. Annu. Rev. Fluid Mech., 39: 321-356.

Goto, Y. and Johmori, A., 2015. Internal Structure of Kuttara Caldera, Hokkaido, Japan. Bull. Volcanol. Soc. Japan, 60(1): 35-46.

Goto, Y. and McPhie, J., 1998. Endogenous growth of a Miocene submarine dacite cryptodome, Rebun Island, Hokkaido, Japan. Journal of volcanology and geothermal research, 84(3): 273-286.

Goto, Y., Sasaki, H., Toriguchi, Y. and Hatakeyama, A., 2011. A phreatic explosion after AD 1663 at the Hiyoriyama cryptodome, Kuttara volcano, southwestern Hokkaido, Japan. Bulletin of the Volcanological Society of Japan, 56(4-5): 147-152.

Graettinger, A.H., Manville, V. and Briggs, R.M., 2010. Depositional record of historic lahars in the upper Whangaehu Valley, Mt. Ruapehu, New Zealand: implications for trigger mechanisms, flow dynamics and lahar hazards. Bulletin of volcanology, 72(3): 279-296.

Graettinger, A.H., Valentine, G.A., Sonder, I., Ross, P.S. and White, J.D.L., 2015. Facies distribution of ejecta in analog tephra rings from experiments with single and multiple subsurface explosions. Bulletin of Volcanology, 77(8).

Graettinger, A.H., Valentine, G.A., Sonder, I., Ross, P.S., White, J.D.L. and Taddeucci, J., 2014. Maar-diatreme geometry and deposits: Subsurface blast experiments with variable explosion depth. Geochemistry Geophysics Geosystems, 15(3): 740-764.

Graham, I., Cole, J., Briggs, R., Gamble, J. and Smith, I., 1995. Petrology and petrogenesis of volcanic rocks from the Taupo Volcanic Zone: a review. Journal of volcanology and geothermal research, 68(1): 59-87.

Graham, I.J. and Worthington, T., 1988. Petrogenesis of Tauhara Dacite (Taupo Volcanic Zone, New Zealand)-Evidence for magma mixing between high-alumina andesite and rhyolite. Journal of volcanology and geothermal research, 35(4): 279-294.

Gravley, D., Deering, C., Leonard, G. and Rowland, J., 2016. Ignimbrite flare-ups and their drivers: A New Zealand perspective. Earth-Science Reviews, 162: 65-82.

Gravley, D.M., Wilson, C.J.N., Leonard, G.S. and Cole, J.W., 2007. Double trouble: Paired ignimbrite eruptions and collateral subsidence in the Taupo Volcanic Zone, New Zealand. Geological Society of America Bulletin, 119(1-2): 18-30.

Gravley, D.M., Wilson, C.J.N., Rosenberg, M.D. and Leonard, G.S., 2006. The nature and age of Ohakuri Formation and Ohakuri Group rocks in surface exposures and geothermal drillhole sequences in the central Taupo Volcanic Zone, New Zealand. New Zealand Journal of Geology and Geophysics, 49(3): 305-308.

Gregg, T.K. and Fink, J.H., 2000. A laboratory investigation into the effects of slope on lava flow morphology. Journal of Volcanology and Geothermal Research, 96(3): 145-159.

Griffin, W., Heier, K., Taylor, P. and Weigand, P., 1974. General geology, age and chemistry of the Raftsund mangerite intrusion, Lofoten-Vesterålen. Nor. geol. unders, 312: 1-30.

Griffiths, R.W. and Fink, J.H., 1992a. The morphology of lava flows in planetary environments: Predictions from analog experiments. Journal of Geophysical Research.

Griffiths, R.W. and Fink, J.H., 1992b. Solidification and morphology of submarine lavas: A dependence on extrusion rate. Journal of Geophysical Research.

Griffiths, R.W. and Fink, J.H., 1993. Effects of surface cooling on the spreading of lava flows and domes. Journal of Fluid Mechanics, 252: 667-702.

Griffiths, R.W. and Fink, J.H., 1997. Solidifying Bingham extrusions: a model for the growth of silicic lava domes. Journal of Fluid Mechanics, 347: 13-36.

Grindley, G., 1965. The geology, structure and exploitation of the Wairakei geothermal field, New Zealand, Geological Survey Bulletin 75. Wellington, New Zealand, Department of Scientific and Industrial Research, 131 p.

Grosse, P., de Vries, B.v.W., Euillades, P.A., Kervyn, M. and Petrinovic, I.A., 2012. Systematic morphometric characterization of volcanic edifices using digital elevation models. Geomorphology, 136(1): 114-131.

Grossenbacher, K.A. and McDuffie, S.M., 1995. Conductive cooling of lava: columnar joint diameter and stria width as functions of cooling rate and thermal gradient. Journal of volcanology and geothermal research, 69(1): 95-103.

Gudmundsson, M.T., Pedersen, R., Vogfjörd, K., Thorbjarnardóttir, B., Jakobsdóttir, S. and Roberts, M.J., 2010. Eruptions of Eyjafjallajökull Volcano, Iceland. Eos, Transactions American Geophysical Union, 91(21): 190-191.

Guilbaud, M.-N., Siebe, C., Layer, P. and Salinas, S., 2012. Reconstruction of the volcanic history of the Tacámbaro-Puruarán area (Michoacán, México) reveals high frequency of Holocene monogenetic eruptions. Bulletin of volcanology, 74(5): 1187-1211.

Gunawan, H., Budianto, A., Prambada, O., McCausland, W., Pallister, J. and Iguchi, M., 2017. Overview of the eruptions of Sinabung eruption, 2010 and 2013–present and details of the 2013 phreatomagmatic phase. Journal of Volcanology and Geothermal Research.

Gunnarsson, B., Marsh, B.D. and Taylor, H.P., 1998. Generation of Icelandic rhyolites: silicic lavas from the Torfajökull central volcano. Journal of Volcanology and Geothermal Research, 83(1): 1-45.

Gurioli, L., Harris, A.J.L., Houghton, B.F., Polacci, M. and Ripepe, M., 2008. Textural and geophysical characterization of explosive basaltic activity at Villarrica volcano. Journal of Geophysical Research-Solid Earth, 113(B8).

Gutmann, J.T., 2002. Strombolian and effusive activity as precursors to phreatomagmatism: eruptive sequence at maars of the Pinacate volcanic field, Sonora, Mexico. Journal of Volcanology and Geothermal Research, 113(1): 345-356.

Hackett, W.R., 1985. Geology and petrology of Ruapehu volcano and related vents, Unpublished PhD thesis, Victoria University of Wellington, Wellington, 312 pp.

Hackett, W.R. and Houghton, B.F., 1989. A facies model for a Quaternary andesitic composite volcano: Ruapehu, New Zealand. Bulletin of volcanology, 51(1): 51-68.

Hale, A., 2008. Lava dome growth and evolution with an independently deformable talus. Geophysical Journal International, 174(1): 391-417.

Hale, A.J. and Wadge, G., 2008. The transition from endogenous to exogenous growth of lava domes with the development of shear bands. Journal of Volcanology and Geothermal Research, 171(3): 237-257.

Hammond, E.H., 1964. Analysis of properties in land form geography: an application to broad-scale land form mapping. Annals of the Association of American Geographers, 54(1): 11-19.

Harlow, D.H., Power, J.A., Laguerta, E.P., Ambubuyog, G., White, R.A. and Hoblitt, R.P., 1996. Precursory seismicity and forecasting of the June 15, 1991, eruption of Mount Pinatubo. Fire and Mud: eruptions and lahars of Mount Pinatubo, Philippines: 223-247.

Harris, A., Flynn, L., Matías, O. and Rose, W., 2002. The thermal stealth flows of Santiaguito dome, Guatemala: Implications for the cooling and emplacement of dacitic block-lava flows. Geological Society of America Bulletin, 114(5): 533-546.

Harris, A.J., Rose, W.I. and Flynn, L.P., 2003. Temporal trends in lava dome extrusion at Santiaguito 1922–2000. Bulletin of Volcanology, 65(2-3): 77-89.

Harrison, A. and White, R., 2004. Crustal structure of the Taupo Volcanic Zone, New Zealand: stretching and igneous intrusion. Geophysical Research Letters, 31(13).

Head, J.W. and Wilson, L., 1989. Basaltic pyroclastic eruptions: Influence of gas-release patterns and volume fluxes on fountain structure, and the formation of cinder cones, spatter cones, rootless flows, lava ponds and lava flows. Journal of Volcanology and Geothermal Research, 37(3-4): 261-271.

Heiken, G. and Wohletz, K., 1985. Volcanic ash. University of California Press, Berkeley.

Heiken, G. and Wohletz, K., 1987. Tephra deposits associated with silicic domes and lava flows. Geological Society of America Special Papers, 212: 55-76.

Heise, W., Bibby, H.M., Caldwell, T.G., Bannister, S.C., Ogawa, Y., Takakura, S. and Uchida, T., 2007. Melt distribution beneath a young continental rift: the Taupo Volcanic Zone, New Zealand. Geophysical Research Letters, 34(14).

Hellstrom, J., McCulloch, M. and Stone, J., 1998. A detailed 31,000-year record of climate and vegetation change, from the isotope geochemistry of two New Zealand speleothems. Quaternary research, 50(2): 167-178.

Henry, C., Price, J., Parker, D. and Wolff, J., 1989. Mid-Tertiary silicic alkalic magmatism of Trans-Pecos Texas: rheomorphic tuffs and extensive silicic lavas. Field excursions to volcanic terranes in the western United States, 1: 231-274.

Henry, C.D., Price, J.G., Rubin, J.N., Parker, D.F., Wolff, J.A., Self, S., Franklin, R. and Barker, D.S., 1988. Widespread, lavalike silicic volcanic rocks of Trans-Pecos Texas. Geology, 16(6): 509-512.

Henrys, S., Reyners, M. and Bibby, H., 2003. Exploring the plate boundary structure of the North Island, New Zealand. Eos, Transactions American Geophysical Union, 84(31): 289-295.

Herd, R.A., Edmonds, M. and Bass, V.A., 2005. Catastrophic lava dome failure at Soufrière Hills volcano, Montserrat, 12–13 July 2003. Journal of Volcanology and Geothermal Research, 148(3): 234-252.

Hernando, I.R., Llambias, E.J., Gonzalez, P.D. and Sato, K., 2012. Volcanic stratigraphy and evidence of magma mixing in the Quaternary Payun Matru volcano, andean backarc in western Argentina. Andean Geology, 39(1): 158-179.

Herzer, R.H., 1995. Seismic stratigraphy of a buried volcanic arc, Northland, New Zealand and implications for Neogene subduction. Marine and petroleum geology, 12(5): 511-531.

Hiess, J., Cole, J.W. and Spinks, K.D., 2007. Influence of the crust and crustal structure on the location and composition of high-alumina basalts of the Taupo Volcanic Zone, New Zealand. New Zealand Journal of Geology and Geophysics, 50(4): 327-342.

Hildreth, W. and Fierstein, J., 2012. The Novarupta-Katmai Eruption of 1912: Largest Eruption of the Twentieth Century: Centennial Perspectives. Geological Survey (USGS).

Hildreth, W. and Fierstein, J., 2017. Geologic field-trip guide to Long Valley Caldera, California. 2328-0328, US Geological Survey.

Hirano, A., Welch, R. and Lang, H., 2003. Mapping from ASTER stereo image data: DEM validation and accuracy assessment. ISPRS Journal of Photogrammetry and Remote Sensing, 57(5): 356-370.

Hobden, B., Houghton, B., Lanphere, M. and Nairn, I., 1996. Growth of the Tongariro volcanic complex: new evidence from K-Ar age determinations.

Hochmuth, K. and Gohl, K., 2017. Collision of Manihiki Plateau fragments to accretional margins of northern Andes and Antarctic Peninsula. Tectonics, 36(2): 229-240.

Hodgson, K.A. and Nairn, I.A., 2005. The c. AD 1315 syn-eruption and AD 1904 post-eruption breakout floods from Lake Tarawera, Haroharo caldera, North Island, New Zealand. New Zealand Journal of Geology and Geophysics, 48(3): 491-506.

Hogg, A., Lowe, D.J., Palmer, J., Boswijk, G. and Ramsey, C.B., 2011. Revised calendar date for the Taupo eruption derived by 14C wiggle-matching using a New Zealand kauri 14C calibration data set. The Holocene: 0959683611425551.

Höhle, J. and Höhle, M., 2009. Accuracy assessment of digital elevation models by means of robust statistical methods. ISPRS Journal of Photogrammetry and Remote Sensing, 64(4): 398-406.

Horizons Regional Council, 2016. Elevation model supplied by Horizons Regional Council, New Zealand.

Houghton, B., Wilson, C., Lloyd, E., Gamble, J. and Kokelaar, B., 1987. A catalogue of basaltic deposits within the Central Taupo Volcanic Zone. NZ Geologic Survey Record, 18: 95-101.

Houghton, B., Wilson, C., McWilliams, M., Lanphere, M., Weaver, S., Briggs, R. and Pringle, M., 1995a. Chronology and dynamics of a large silicic magmatic system: central Taupo Volcanic Zone, New Zealand. Geology, 23(1): 13-16.

Houghton, B.F. and Gonnermann, H.M., 2008. Basaltic explosive volcanism: Constraints from deposits and models. Chemie Der Erde-Geochemistry, 68(2): 117-140.

Houghton, B.F. and Hackett, W.R., 1984. Strombolian and phreatomagmatic deposits of Ohakune Craters, Ruapehu, New Zealand: a complex interaction between external water and rising basaltic magma. Journal of Volcanology and Geothermal Research, 21(3-4): 207-231.

Houghton, B.F., Lloyd, E.F., Wilson, C.J.N. and Lanphere, M.A., 1991. K-Ar ages from the Western Dome Belt and associated rhyolitic lavas in the Maroa-Taupo srea, Taupo Volcanic Zone, New-Zealand. New Zealand Journal of Geology and Geophysics, 34(1): 99-101.

Houghton, B.F. and Nairn, I.A., 1991. The 1976-1982 strombolian and phreatomagmatic eruptions of White Island, New Zealand: eruptive and depositional mechanisms at a "wet" volcano. Bulletin of Volcanology, 54(1): 25-49.

Houghton, B.F. and Schmincke, H.-U., 1986. Mixed deposits of simultaneous strombolian and phreatomagmatic volcanism: Rothenberg volcano, East Eifel volcanic field. Journal of volcanology and geothermal research, 30(1): 117-130.

Houghton, B.F. and Schmincke, H.U., 1989. Rothenberg scoria cone, East Eifel: a complex Strombolian and phreatomagmatic volcano. Bulletin of Volcanology, 52(1): 28-48.

Houghton, B.F. and Smith, R.T., 1993. Recycling of magmatic clasts during explosive eruptions - estimating the true juvenile content of phreatomagmatic volcanic deposits. Bulletin of Volcanology, 55(6): 414-420.

Houghton, B.F. and Wilson, C.J.N., 1989. A vesicularity index for pyroclastic deposits. Bulletin of Volcanology, 51(6): 451-462.

Houghton, B.F., Wilson, C.J.N., McWilliams, M.O., Lanphere, M.A., Weaver, S.D., Briggs, R.M. and Pringle, M.S., 1995b. Chronology and dynamics of a large silicic magmatic system: Central Taupo Volcanic Zone, New-Zealand. Geology, 23(1): 13-16.

Houghton, B.F., Wilson, C.J.N. and Smith, I.E.M., 1999. Shallow-seated controls on styles of explosive basaltic volcanism: a case study from New Zealand. Journal of Volcanology and Geothermal Research, 91(1): 97-120.

Howie, R.A., 1955. XVIII. - The geochemistry of the charnockite series of Madras, India. Earth and Environmental Science Transactions of The Royal Society of Edinburgh, 62(3): 725-768.

Hreinsdóttir, S., Sigmundsson, F., Roberts, M.J., Björnsson, H., Grapenthin, R., Arason, P., Árnadóttir, T., Hólmjárn, J., Geirsson, H. and Bennett, R.A., 2014. Volcanic plume height correlated with magma-pressure change at Grimsvotn Volcano, Iceland. Nature geoscience, 7(3): 214-218.

Hughes, S.S., 2015. Ogive (Volcanic), Encyclopedia of Planetary Landforms. Springer, pp. 1484-1487.

Hui, H. and Zhang, Y., 2007. Toward a general viscosity equation for natural anhydrous and hydrous silicate melts. Geochimica et Cosmochimica Acta, 71(2): 403-416.

Husain, T., Elsworth, D., Voight, B., Mattioli, G. and Jansma, P., 2014. Influence of extrusion rate and magma rheology on the growth of lava domes: insights from particle-dynamics modeling. Journal of Volcanology and Geothermal Research, 285: 100-117.

Ikeda, Y., Ikeda, T. and Kagami, H., 1990. Caldera-formation from geochemical aspects: A case study of the Toya caldera, southwestern Hokkaido, Japan. Journal of Mineralogy, Petrology and Economic Geology, 85(12): 569-577.

Immega, I.P. and Klein, C., 1976. Mineralogy and petrology of some metamorphic Precambrian iron-formations in southwestern Montana. American Mineralogist, 61(11-12): 1117-1144.

Ingham, M., Bibby, H., Heise, W., Jones, K., Cairns, P., Dravitzki, S., Bennie, S., Caldwell, T. and Ogawa, Y., 2009. A magnetotelluric study of Mount Ruapehu volcano, New Zealand. Geophysical Journal International, 179(2): 887-904.

Irwin, J., 1969a. Lake Rotorua, Provisional Bathymetry 1 : 15 840, Fish. Res. Div. Lake Series. New Zealand Marine Department, Wellington.

Irwin, J., 1969b. Lake Tarawera, Provisional Bathymetry 1 : 25 000, Lake Cahert Series. New Zealand Oceanographic Institute, pp. 1:25,000.

Irwin, J., 1972. Lake Taupo bathymetry, 1 : 50 000, Lake Chart Series. New Zealand Oceanographic Institute.

Irwin, J., 1982. Lake Rotomahana 1 : 9700, Lake Chart Series. New Zealand Oceanographic Institute.

Isaia, R., D'Antonio, M., Dell'Erba, F., Di Vito, M. and Orsi, G., 2004. The Astroni volcano: the only example of closely spaced eruptions in the same vent area during the recent history of the Campi Flegrei caldera (Italy). Journal of Volcanology and Geothermal Research, 133(1): 171-192.

Iverson, R., 1990. Lava domes modeled as brittle shells that enclose pressurized magma, with application to Mount St. Helens, Lava Flows and Domes. Springer, pp. 47-69.

Jankovics, M.É., Dobosi, G., Embey-Isztin, A., Kiss, B., Sági, T., Harangi, S. and Ntaflos, T., 2013. Origin and ascent history of unusually crystal-rich alkaline basaltic magmas from the western Pannonian Basin. Bulletin of volcanology, 75(9): 749.

Jaupart, C. and Allègre, C.J., 1991. Gas content, eruption rate and instabilities of eruption regime in silicic volcanoes. Earth and Planetary Science Letters, 102(3): 413-429.

Jenkins, S., Magill, C., McAneney, J. and Hurst, T., 2008. Multistage volcanic events: tephra hazard simulations for the Okataina Volcanic Center, New Zealand. Journal of Geophysical Research: Earth Surface, 113(F4).

Jensen, R.A., Donnelly-Nolan, J.M. and Mckay, D., 2009. A field guide to Newberry Volcano, Oregon. Field Guides, 15: 53-79.

Johnston, E., Sparks, R., Phillips, J. and Carey, S., 2014. Revised estimates for the volume of the Late Bronze Age Minoan eruption, Santorini, Greece. Journal of the Geological Society, 171(4): 583-590.

Jordan, S., Cas, R. and Hayman, P., 2013. The origin of a large (> 3km) maar volcano by coalescence of multiple shallow craters: Lake Purrumbete maar, southeastern Australia. Journal of Volcanology and Geothermal Research, 254: 5-22.

Jurado-Chichay, Z. and Walker, G., 2000. Stratigraphy and dispersal of the Mangaone Subgroup pyroclastic deposits, Okataina volcanic centre, New Zealand. Journal of Volcanology and Geothermal Research, 104(1): 319-380.

Jutzeler, M., Marsh, R., Carey, R.J., White, J.D., Talling, P.J. and Karlstrom, L., 2014. On the fate of pumice rafts formed during the 2012 Havre submarine eruption. Nature communications, 5.

Jutzeler, M., McPhie, J. and Allen, S.R., 2015. Explosive destruction of a Pliocene hot lava dome underwater: Dogashima (Japan). Journal of Volcanology and Geothermal Research, 304: 75-81.

Kaneko, T., Wooster, M.J. and Nakada, S., 2002. Exogenous and endogenous growth of the Unzen lava dome examined by satellite infrared image analysis. Journal of Volcanology and Geothermal Research, 116(1): 151-160.

Karátson, D., 2014. Vulkanológia II. ELTE Eötvös Kiadó, Budapest.

Karátson, D., Gertisser, R., Telbisz, T., Vereb, V., Quidelleur, X., Druitt, T., Nomikou, P. and Kósik, S., 2018. Towards reconstruction of the lost Late Bronze Age intra-caldera island of Santorini, Greece. Scientific Reports, 8(1): 7026.

Karátson, D., Márton, E., Harangi, S., Józsa, S., Balogh, K., Pécskay, Z., Kovácsvölgyi, S., Szakmány, G. and Dulai, A., 2000. Volcanic evolution and stratigraphy of the Miocene Börzsöny Mountains, Hungary: an integrated study. Geologica Carpathica, 51(1): 325-343.

Karátson, D., Telbisz, T., Harangi, S., Magyari, E., Dunkl, I., Kiss, B., Janosi, C., Veres, D., Braun, M., Fodor, E., Biro, T., Kósik, S., von Eynatten, H. and Lin, D., 2013. Morphometrical and geochronological constraints on the youngest eruptive activity in East-Central Europe at the Ciomadul (Csomad) lava dome complex, East Carpathians. Journal of Volcanology and Geothermal Research, 255: 43-56.

Kato, A., Terakawa, T., Yamanaka, Y., Maeda, Y., Horikawa, S., Matsuhiro, K. and Okuda, T., 2015. Preparatory and precursory processes leading up to the 2014 phreatic eruption of Mount Ontake, Japan. Earth, Planets and Space, 67(1): 111.

Kear, D., 2004. Reassessment of Neogene tectonism and volcanism in North Island, New Zealand. New Zealand Journal of Geology and Geophysics, 47(3): 361-374.

Keating, G.N., Valentine, G.A., Krier, D.J. and Perry, F.V., 2008. Shallow plumbing systems for small-volume basaltic volcanoes. Bulletin of Volcanology, 70(5): 563-582.

Kelleher, P.C. and Cameron, K.L., 1990. The Geochemistry of the Mono Craters-Mono Lake Islands Volcanic Complex, eastern California. Journal of Geophysical Research: Solid Earth, 95(B11): 17643-17659.

Kennedy, B., Wilcock, J. and Stix, J., 2012. Caldera resurgence during magma replenishment and rejuvenation at Valles and Lake City calderas. Bulletin of volcanology, 74(8): 1833-1847.

Kennedy, B.M., Wadsworth, F.B., Vasseur, J., Schipper, C.I., Jellinek, A.M., von Aulock, F.W., Hess, K.-U., Russell, J.K., Lavallée, Y. and Nichols, A.R., 2016. Surface tension driven processes densify and retain permeability in magma and lava. Earth and Planetary Science Letters, 433: 116-124.

Kereszturi, G., Cappello, A., Ganci, G., Procter, J., Németh, K., Del Negro, C. and Cronin, S.J., 2014a. Numerical simulation of basaltic lava flows in the Auckland Volcanic Field, New Zealand—implication for volcanic hazard assessment. Bulletin of volcanology, 76(11): 879.

Kereszturi, G. and Németh, K., 2012. Monogenetic basaltic volcanoes: genetic classification, growth, geomorphology and degradation. INTECH Open Access Publisher.

Kereszturi, G. and Németh, K., 2016. Sedimentology, eruptive mechanism and facies architecture of basaltic scoria cones from the Auckland Volcanic Field (New Zealand). Journal of Volcanology and Geothermal Research, 324: 41-56.

Kereszturi, G., Németh, K., Cronin, S.J., Agustin-Flores, J., Smith, I.E.M. and Lindsay, J., 2013. A model for calculating eruptive volumes for monogenetic volcanoes - Implication for the Quaternary Auckland Volcanic Field, New Zealand. Journal of Volcanology and Geothermal Research, 266: 16-33.

Kereszturi, G., Németh, K., Cronin, S.J., Procter, J. and Agustín-Flores, J., 2014b. Influences on the variability of eruption sequences and style transitions in the Auckland Volcanic Field, New Zealand. Journal of Volcanology and Geothermal Research, 286: 101-115.

Kereszturi, G., Németh, K., Csillag, G., Balogh, K. and Kovacs, J., 2011. The role of external environmental factors in changing eruption styles of monogenetic volcanoes in a Mio/Pleistocene continental volcanic field in western Hungary. Journal of Volcanology and Geothermal Research, 201(1-4): 227-240.

Kereszturi, G. and Procter, J., 2016. Error in topographic attributes for volcanic hazard assessment of the Auckland Volcanic Field (New Zealand). New Zealand Journal of Geology and Geophysics, 59(2): 286-301.

Kereszturi G. unpublished data.

Kienle, J., Kyle, P.R., Self, S., Motyka, R.J. and Lorenz, V., 1980. Ukinrek Maars, Alaska, I. April 1977 eruption sequence, petrology and tectonic setting. Journal of Volcanology and Geothermal Research, 7(1-2): 11-37.

Kilgour, G. and Smith, R., 2008. Stratigraphy, dynamics, and eruption impacts of the dual magma Rotorua eruptive episode, Okataina Volcanic Centre, New Zealand. New Zealand Journal of Geology and Geophysics, 51(4): 367-378.

King, P.R., 2000. Tectonic reconstructions of New Zealand: 40 Ma to the present. New Zealand Journal of Geology and Geophysics, 43(4): 611-638.

Kissling, W. and Weir, G., 2005. The spatial distribution of the geothermal fields in the Taupo Volcanic Zone, New Zealand. Journal of Volcanology and Geothermal Research, 145(1): 136-150.

Kiyosugi, K., Connor, C.B., Zhao, D., Connor, L.J. and Tanaka, K., 2010. Relationships between volcano distribution, crustal structure, and P-wave tomography: an example from the Abu Monogenetic Volcano Group, SW Japan. Bulletin of volcanology, 72(3): 331-340.

Kobayashi, T., 1982. Geology of Sakurajima Volcano: a review. Bulletin of the Volcanological Society of Japan, 27: 277-292.

Kobayashi, T., Imura, R. and Okuno, M., 2013. A Guide for Mid-Conference Field Trip, IAVCEI 2013 Scientific Assembly, Kagoshima, Japan.

Kobayashi, T., Nairn, I., Smith, V. and Shane, P., 2005. Proximal stratigraphy and event sequence of the c. 5600 cal. yr BP Whakatane rhyolite eruption episode from Haroharo volcano, Okataina Volcanic Centre, New Zealand. New Zealand Journal of Geology and Geophysics, 48(3): 471-490.

Kokelaar, B.P., 1983. The mechanism of Surtseyan volcanism. Journal of the Geological Society, 140(6): 939-944.

Kokelaar, B.P., 1986. Magma-water interactions in subaqueous and emergent basaltic volcanism. Bulletin of Volcanology, 48(5): 275-289.

Kokelaar, B.P. and Durant, G.P., 1983. The submarine eruption and erosion of Surtla (Surtsey), Iceland. Journal of Volcanology and Geothermal Research, 19(3-4): 239-246.

Komorowski, J.-C., Jenkins, S., Baxter, P.J., Picquout, A., Lavigne, F., Charbonnier, S., Gertisser, R., Preece, K., Cholik, N. and Budi-Santoso, A., 2013. Paroxysmal dome explosion during the Merapi 2010 eruption: Processes and facies relationships of associated high-energy pyroclastic density currents. Journal of Volcanology and Geothermal Research, 261: 260-294.

Kósik, S., Németh, K., Kereszturi, G., Procter, J. and Lexa, J., 2016a. Understanding the evolution and resulting hazard of a small-volume silicic fissure eruption: Puketerata Volcanic Complex, Taupo Volcanic Zone, New Zealand [abstract], IV International Workshop on Collapse Calderas. IAVCEI Commission on Collapse Caldera, Kitayuzawa, Date City, Hokkaido, Japan, pp. 52.

Kósik, S., Németh, K., Kereszturi, G., Procter, J., Zellmer, G. and Geshi, N., 2016b. Phreatomagmatic and water-influenced Strombolian eruptions of a small-volume parasitic cone complex on the southern ringplain of Mt. Ruapehu, New Zealand: Facies architecture and eruption mechanisms of the Ohakune Volcanic Complex controlled by an unstable fissure eruption. Journal of Volcanology and Geothermal Research, 327: 99-115.

Kósik, S., Németh, K., Lexa, J. and Procter, J.N., 2017a. Understanding the evolution of a small-volume silicic fissure eruption: Puketerata Volcanic Complex, Taupo Volcanic Zone, New Zealand. Journal of Volcanology and Geothermal Research.

Kósik, S., Németh, K., Procter, J. and Zellmer, G., 2017b. Maar-diatreme volcanism relating to the pyroclastic sequence of a newly discovered high-alumina basalt in the Maroa Volcanic Centre, Taupo Volcanic Zone, New Zealand. Journal of Volcanology and Geothermal Research, 341: 363-370.

Kósik, S., Németh, K., Procter, J.N. and Bebbington, M.S., 2017c. Hazard implications of silicic small-volume volcanism within the Taupo Volcanic Zone, New Zealand: spatial, temporal, volumetric and eruptive style distribution of the eruptive vents, IAVCEI 2017 Scientific Assembly - Fostering Integrative Studies of Volcanism, Portland, Oregon, USA.

Kuno, H., 1959. Origin of Cenozoic petrographic provinces of Japan and surrounding areas. Bulletin of Volcanology, 20(1): 37-76.

Kuno, H., 1960. High-alumina basalt. Journal of petrology, 1(1): 121-145.

Kuntz, M.A., Champion, D.E., Spiker, E.C. and Lefebvre, R.H., 1986. Contrasting magma types and steady-state, volume-predictable, basaltic volcanism along the Great Rift, Idaho. Geological Society of America Bulletin, 97(5): 579-594.

Lacroix, A., 1904. La Montagne Pelée et ses éruptions. Masson.

Langridge, R., Ries, W., Litchfield, N., Villamor, P., Van Dissen, R., Barrell, D., Rattenbury, M., Heron, D., Haubrock, S. and Townsend, D., 2016. The New Zealand active faults database. New Zealand Journal of Geology and Geophysics, 59(1): 86-96.

Lara, L., Naranjo, J. and Moreno, H., 2004. Rhyodacitic fissure eruption in Southern Andes (Cordón Caulle; 40.5 S) after the 1960 (Mw: 9.5) Chilean earthquake: a structural interpretation. Journal of Volcanology and Geothermal Research, 138(1): 127-138.

Lara, L.E., 2009. The 2008 eruption of the Chaitén Volcano, Chile: a preliminary report. Andean geology, 36(1): 125-130.

Latter, J., 1981. Tsunamis of volcanic origin: summary of causes, with particular reference to Krakatoa, 1883. Bulletin of Volcanology, 44(3): 467-490.

Lautze, N.C. and Houghton, B.F., 2007. Linking variable explosion style and magma textures during 2002 at Stromboli volcano, Italy. Bulletin of Volcanology, 69(4): 445-460.

Lavallée, Y., Varley, N., Alatorre-Ibargüengoitia, M., Hess, K.-U., Kueppers, U., Mueller, S., Richard, D., Scheu, B., Spieler, O. and Dingwell, D., 2012. Magmatic architecture of dome-building eruptions at Volcán de Colima, Mexico. Bulletin of Volcanology, 74(1): 249-260.

Le Corvec, N., Bebbington, M.S., Lindsay, J.M. and McGee, L.E., 2013. Age, distance, and geochemical evolution within a monogenetic volcanic field: Analyzing patterns in the Auckland Volcanic Field eruption sequence. Geochemistry, Geophysics, Geosystems, 14(9): 3648-3665.

Leake, B.E., Woolley, A.R., Arps, C.E., Birch, W.D., Gilbert, M.C., Grice, J.D., Hawthorne, F.C., Kato, A., Kisch, H.J. and Krivovichev, V.G., 1997. Report. Nomenclature of Amphiboles: Report of the Subcommittee on Amphiboles of the International Mineralogical Association Commission on New Minerals and Mineral Names. Mineralogical Magazine, 61(2): 295-321.

Lee, J., Bland, K., Townsend, D. and Kamp, P., 2011. Geology of the Hawke's Bay area, Institute of Geological and Nuclear Sciences 1:250 000 geological map 8. 1 sheet + 93 p. Lower Hutt, New Zealand. GNS Scinece.

Leonard, G., Cole, J., Nairn, I. and Self, S., 2002. Basalt triggering of the c. AD 1305 Kaharoa rhyolite eruption, Tarawera volcanic complex, New Zealand. Journal of Volcanology and Geothermal Research, 115(3): 461-486.

Leonard, G.S., 2003. The evolution of Maroa Volcanic Centre, Taupo Volcanic Zone, New Zealand, Unpublished PhD thesis, University of Canterbury, Christchurch, 322 pp.

Leonard, G.S., Begg, J.G. and Wilson, C.J.N., 2010. Geology of the Rotorua area. Institute of Geological and Nuclear Sciences 1:250,000 geological map 5. sheet + 102 p. Lower Hutt, New Zealand. GNS Science.

Lesti, C., Giordano, G., Salvini, F. and Cas, R., 2008. Volcano tectonic setting of the intraplate, Pliocene-Holocene, Newer Volcanic Province (southeast Australia): Role of crustal fracture zones. Journal of Geophysical Research: Solid Earth, 113(B7).

Lewis, J.F., 1968. Tauhara Volcano, Taupo Zone: Part I—Geology and Structure. New Zealand Journal of Geology and Geophysics, 11(1): 212-224.

Lexa, J. and Pošteková, K., 2012. Eruptive styles of rhyolite volcanoes in the sedimentary basin setting: the case of the Jastrabá Formation in Central Slovakia. Geoscience Society of New Zealand Miscellaneous Publication 131A: 124.

Lindsay, J., Marzocchi, W., Jolly, G., Constantinescu, R., Selva, J. and Sandri, L., 2010. Towards real-time eruption forecasting in the Auckland Volcanic Field: application of BET_EF during the New Zealand National Disaster Exercise 'Ruaumoko'. Bulletin of Volcanology, 72(2): 185-204.

LINZ - Land Information New Zealand, 2012. NZ 8 m Digital Elevation Model.

LINZ - Land Information New Zealand, 2013. NZ 232 Lake Taupo (Taupomoana). Land Information New Zealand (LINZ).

Lloyd, E.F., 1972. Geology and hot springs of Orakeikorako. New Zealand, Dept. of Scientific and Industrial Research.

Lockwood, J.P. and Hazlett, R.W., 2013. Volcanoes: global perspectives. John Wiley & Sons.

Locock, A.J., 2014. An Excel spreadsheet to classify chemical analyses of amphiboles following the IMA 2012 recommendations. Computers & Geosciences, 62: 1-11.

Lorenz, V., 1973. On the formation of maars. Bull Volcanol, 37(2): 183-204.

Lorenz, V., 1985. Maars and diatremes of phreatomagmatic origin; a review. South African Journal of Geology, 88(2): 459-470.

Lorenz, V., 1986. On the growth of maar and diatremes and its relevance to the formation of tuff rings. Bulletin of Volcanology, 48(5): 265-274.

Lorenz, V., 2003. Maar-diatreme volcanoes, their formation, and their setting in hard-rock or soft-rock environments. Geolines, 15: 72-83.

Lorenz, V., 2007. Syn- and posteruptive hazards of maar-diatreme volcanoes. Journal of Volcanology and Geothermal Research, 159(1-3): 285-312.

Lorenz, V. and Kurszlaukis, S., 2007. Root zone processes in the phreatomagmatic pipe emplacement model and consequences for the evolution of maar-diatreme volcanoes. Journal of Volcanology and Geothermal Research, 159(1-3): 4-32.

Lowe, D.J., Blaauw, M., Hogg, A.G. and Newnham, R.M., 2013. Ages of 24 widespread tephras erupted since 30,000 years ago in New Zealand, with re-evaluation of the timing and palaeoclimatic implications of the Lateglacial cool episode recorded at Kaipo bog. Quaternary Science Reviews, 74: 170-194.

Lube, G., Breard, E.C., Cronin, S.J., Procter, J.N., Brenna, M., Moebis, A., Pardo, N., Stewart, R.B., Jolly, A. and Fournier, N., 2014. Dynamics of surges generated by hydrothermal blasts during the 6 August 2012 Te Maari eruption, Mt. Tongariro, New Zealand. Journal of Volcanology and Geothermal Research, 286: 348-366.

Lyman, A.W., Koenig, E. and Fink, J.H., 2004. Predicting yield strengths and effusion rates of lava domes from morphology and underlying topography. Journal of Volcanology and Geothermal Research, 129(1): 125-138.

MacLeod, N.S., Sherrod, D.R. and Chitwood, L.A., 1982. Geologic map of Newberry Volcano, Deschutes, Klamath, and Lake Counties, Oregon. 2331-1258.

Maeno, F., Nakada, S. and Kaneko, T., 2016. Morphological evolution of a new volcanic islet sustained by compound lava flows. Geology, 44(4): 259-262.

Maeno, F. and Taniguchi, H., 2006. Silicic lava dome growth in the 1934–1935 Showa Iwo-jima eruption, Kikai caldera, south of Kyushu, Japan. Bulletin of volcanology, 68(7-8): 673-688.

Mahood, G.A. and Hildreth, W., 1986. Geology of the peralkaline volcano at Pantelleria, Strait of Sicily. Bulletin of Volcanology, 48(2): 143-172.

Manley, C.R., 1992. Extended cooling and viscous flow of large, hot rhyolite lavas: implications of numerical modeling results. Journal of volcanology and geothermal research, 53(1-4): 27-46.

Manley, C.R. and Fink, J.H., 1987. Internal textures of rhyolite flows as revealed by research drilling. Geology, 15(6): 549-552.

Manning, D., 1996. Middle-late Pleistocene tephrostratigraphy of the eastern Bay of Plenty, New Zealand. Quaternary International, 34: 3-12.

Manville, V., 2010. An overview of break-out floods from intracaldera lakes. Global and Planetary Change, 70(1): 14-23.

Manville, V., Hodgson, K.A. and Nairn, I.A., 2007. A review of break-out floods from volcanogenic lakes in New Zealand. New Zealand Journal of Geology and Geophysics, 50(2): 131-150.

Manville, V., Németh, K. and Kano, K., 2009a. Source to sink: a review of three decades of progress in the understanding of volcaniclastic processes, deposits, and hazards. Sedimentary Geology, 220(3): 136-161.

Manville, V., Segschneider, B., Newton, E., White, J.D.L., Houghton, B.F. and Wilson, C.J.N., 2009b. Environmental impact of the 1.8 ka Taupo eruption, New Zealand: Landscape responses to a large-scale explosive rhyolite eruption. Sedimentary Geology, 220(3-4): 318-336.

Manville, V., White, J., Houghton, B. and Wilson, C., 1999. Paleohydrology and sedimentology of a post–1.8 ka breakout flood from intracaldera Lake Taupo, North Island, New Zealand. Geological Society of America Bulletin, 111(10): 1435-1447.

Manville, V. and Wilson, C.J.N., 2003. Interactions between volcanism, rifting and subsidence: implications of intracaldera palaeoshorelines at Taupo volcano, New Zealand. Journal of the Geological Society, 160: 3-6.

Manville, V. and Wilson, C.J.N., 2004. The 26.5 ka Oruanui eruption, New Zealand: a review of the roles of volcanism and climate in the post-eruptive sedimentary response. New Zealand Journal of Geology and Geophysics, 47(3): 525-547.

Marti, J. and Felpeto, A., 2010. Methodology for the computation of volcanic susceptibility: an example for mafic and felsic eruptions on Tenerife (Canary Islands). Journal of Volcanology and Geothermal Research, 195(1): 69-77.

Martí, J., Planagumà, L., Geyer, A., Canal, E. and Pedrazzi, D., 2011. Complex interaction between Strombolian and phreatomagmatic eruptions in the Quaternary monogenetic volcanism of the Catalan Volcanic Zone (NE of Spain). Journal of Volcanology and Geothermal Research, 201(1): 178-193.

Martin, A.J., Umeda, K., Connor, C.B., Weller, J.N., Zhao, D. and Takahashi, M., 2004a. Modeling long-term volcanic hazards through Bayesian inference: An example from the Tohoku volcanic arc, Japan. Journal of Geophysical Research: Solid Earth, 109(B10).

Martin, U., Breitkreuz, C., Egenhoff, S., Enos, P. and Jansa, L., 2004b. Shallow-marine phreatomagmatic eruptions through a semi-solidified carbonate platform (ODP Leg 144, Site 878, Early Cretaceous, MIT Guyot, West Pacific). Marine Geology, 204(3): 251-272.

Martin, U. and Németh, K., 2004. Peperitic lava lake-fed sills at Sag-hegy, western Hungary: A complex interaction of a wet tephra ring and lava. In: C. Breitkreuz and N. Petford (Editors), Physical Geology of High-Level Magmatic Systems. Geological Society Special Publication, pp. 33-50.

Martin, U. and Németh, K., 2005. Eruptive and depositional history of a Pliocene tuff ring that developed in a fluvio-lacustrine basin: Kissomlyó volcano (western Hungary). Journal of Volcanology and Geothermal Research, 147(3): 342-356.

Martin, U. and White, J., 2001. Depositional and eruptive mechanisms of density current deposits from a submarine vent at the Otago Peninsula, New Zealand. Particulate gravity currents: 245-259.

Mastin, L. and Witter, J., 2000. The hazards of eruptions through lakes and seawater. Journal of Volcanology and Geothermal Research, 97(1): 195-214.

Matheson, M.A., 2010. Eruption dynamics and hydrological implications of basaltic volcanic centres at Lake Taupo, Unpublished MSc thesis, The University of Waikato.

Matthews, A.J., Barclay, J., Carn, S., Thompson, G., Alexander, J., Herd, R. and Williams, C., 2002. Rainfall-induced volcanic activity on Montserrat. Geophysical Research Letters, 29(13).

Matthews, N., Pyle, D., Smith, V., Wilson, C., Huber, C. and Van Hinsberg, V., 2012. Quartz zoning and the pre-eruptive evolution of the~ 340-ka Whakamaru magma systems, New Zealand. Contributions to Mineralogy and Petrology, 163(1): 87-107.

Matthews, S.J., Gardeweg, M.C. and Sparks, R.S.J., 1997. The 1984 to 1996 cyclic activity of Lascar Volcano, northern Chile: cycles of dome growth, dome subsidence, degassing and explosive eruptions. Bulletin of Volcanology, 59(1): 72-82.

Mattsson, H.B., 2010. Textural variation in juvenile pyroclasts from an emergent, Surtseyan-type, volcanic eruption: The Capelas tuff cone, São Miguel (Azores). Journal of Volcanology and Geothermal Research, 189(1): 81-91.

Mattsson, H.B. and Höskuldsson, Á., 2011. Contemporaneous phreatomagmatic and effusive activity along the Hverfjall eruptive fissure, north Iceland: Eruption chronology and resulting deposits. Journal of Volcanology and Geothermal Research, 201(1): 241-252.

Mazzarini, F. and Armienti, P., 2001. Flank Cones at Mount Etna Volcano: Do they have a power-law distribution? Bulletin of Volcanology, 62(6): 420-430.

McArthur, J. and Shepherd, M., 1990. Late Quaternary glaciation of Mt Ruapehu, North Island, New Zealand. Journal of the Royal Society of New Zealand, 20(3): 287-296.

McClelland, E. and Erwin, P.S., 2003. Was a dacite dome implicated in the 9,500 BP collapse of Mt Ruapehu? A palaeomagnetic investigation. Bulletin of volcanology, 65(4): 294-305.

McGetchin, T.R., Settle, M. and Chouet, B.A., 1974. Cinder cone growth modeled after northeast crater, Mount Etna, Sicily. Journal of Geophysical Research, 79(23): 3257-3272.

McNamara, D.D., Sewell, S., Buscarlet, E. and Wallis, I.C., 2016. A review of the Rotokawa geothermal field, New Zealand. Geothermics, 59: 281-293.

Miller, C.D., 1980. Potential hazards from future eruptions in the vicinity of Mount Shasta volcano, northern California. US Department of the Interior, Geological Survey.

Millet, M.A., Tutt, C.M., Handler, M.R. and Baker, J.A., 2014. Processes and time scales of dacite magma assembly and eruption at Tauhara volcano, Taupo Volcanic Zone, New Zealand. Geochemistry, Geophysics, Geosystems, 15(1): 213-237.

Milner, D., Cole, J. and Wood, C., 2002. Asymmetric, multiple-block collapse at Rotorua Caldera, Taupo volcanic zone, New Zealand. Bulletin of Volcanology, 64(2): 134-149.

Minakami, T., Ishikawa, T. and Yagi, K., 1951. The 1944 eruption of volcano Usu in Hokkaido, Japan. Bulletin of Volcanology, 11(1): 45-157.

Mitchell, R.H. and Platt, R.G., 1978. Mafic mineralogy of ferroaugite syenite from the Coldwell alkaline complex, Ontario, Canada. Journal of Petrology, 19(4): 627-651.

Moebis, A., 2010. Understanding the Holocene explosive eruption record of the Tongariro Volcanic Centre, New Zealand, Unpublished PhD thesis, Massey University, Palmerston North, 381 pp.

Moitra, P., Gonnermann, H.M., Houghton, B.F. and Giachetti, T., 2013. Relating vesicle shapes in pyroclasts to eruption styles. Bulletin of Volcanology, 75(2).

Moody, J.B., 1976. Serpentinization: a review. Lithos, 9(2): 125-138.

Moore, I.D., Grayson, R. and Ladson, A., 1991. Digital terrain modelling: a review of hydrological, geomorphological, and biological applications. Hydrological processes, 5(1): 3-30.

Moore, J.G., Nakamura, K. and Alcaraz, A., 1966. The 1965 eruption of Taal volcano. Science, 151(3713): 955-960.

Moran, S.C., Malone, S.D., Qamar, A.I., Thelen, W.A., Wright, A.K. and Caplan-Auerbach, J., 2008. Seismicity associated with renewed dome building at Mount St. Helens, 2004-

2005, A Volcano Rekindled: The Renewed Eruption of Mount St. Helens, 2004–2006. U.S. Geological Survey Professional Paper 1750, pp. 27-60.

Morey, G., Papike, J., Smith, R. and Weiblen, P., 1972. Observations on the contact metamorphism of the Biwabik iron-formation, east Mesabi district, Minnesota. Geological Society of America Memoirs, 135: 225-264.

Morimoto, N., 1988. Nomenclature of pyroxenes. Mineralogy and Petrology, 39(1): 55-76.

Moriwaki, H., 1992. Late Quaternary phreatomagmatic tephra layers and their relation to paleo-sea levels in the area of Aira caldera, southern Kyushu, Japan. Quaternary International, 13: 195-200.

Mortimer, N., 1994. Origin of the Torlesse terrane and coeval rocks, North Island, New Zealand. International geology review, 36(10): 891-910.

Mortimer, N., Campbell, H.J., Stagpoole, M., Wood, R.A., Rattenbury, M.S., Sutherland, R. and Seton, M., 2017. Zealandia: Earth's Hidden Continent. GSA Today, 27(3).

Mortimer, N., Gans, P., Palin, J., Meffre, S., Herzer, R. and Skinner, D., 2010. Location and migration of Miocene–Quaternary volcanic arcs in the SW Pacific region. Journal of Volcanology and Geothermal Research, 190(1): 1-10.

Mortimer, N., Herzer, R., Gans, P., Laporte-Magoni, C., Calvert, A. and Bosch, D., 2007. Oligocene–Miocene tectonic evolution of the South Fiji Basin and Northland Plateau, SW Pacific Ocean: Evidence from petrology and dating of dredged rocks. Marine Geology, 237(1): 1-24.

Moufti, M.R.H. and Németh, K., 2016. Geoheritage of Volcanic Harrats in Saudi Arabia. Springer, Switzerland, 194 pp.

Mucek, A.E., Danišík, M., de Silva, S.L., Schmitt, A.K., Pratomo, I. and Coble, M.A., 2017. Post-supereruption recovery at Toba Caldera. Nature Communications, 8.

Mueller, S., Scheu, B., Spieler, O. and Dingwell, D.B., 2008. Permeability control on magma fragmentation. Geology, 36(5): 399-402.

Mueller, W. and White, J.D., 1992. Felsic fire-fountaining beneath Archean seas: pyroclastic deposits of the 2730 Ma Hunter Mine Group, Quebec, Canada. Journal of Volcanology and Geothermal Research, 54(1-2): 117-134.

Mueller, W.U., 2003. A Subaqueous Eruption Model for Shallow-Water, Small Volume Eruptions: Evidence from Two Precambrian Examples. Explosive subaqueous volcanism: 189-203.

Muffler, L.J.P., White, D. and Truesdell, A., 1971. Hydrothermal explosion craters in Yellowstone National Park. Geological Society of America Bulletin, 82(3): 723-740.

Murase, T., McBirney, A.R. and Melson, W.G., 1985. Viscosity of the dome of Mount St. Helens. Journal of Volcanology and Geothermal Research, 24(1-2): 193-204.

Murtagh, R.M., White, J.D. and Sohn, Y.K., 2011. Pyroclast textures of the Ilchulbong 'wet'tuff cone, Jeju Island, South Korea. Journal of Volcanology and Geothermal Research, 201(1): 385-396.

Nagaoka, S., 1988. The late Quaternary tephra layers from the caldera volcanoes in and around Kagoshima Bay, southern Kyushu, Japan. Geographical Reports of Tokyo Metropolitan University, 23: 49-122.

Nairn, I., 1992. The Te Rere and Okareka eruptive episodes—Okataina Volcanic Centre, Taupo Volcanic Zone, New Zealand. New Zealand journal of geology and geophysics, 35(1): 93-108.

Nairn, I. and Cole, J., 1981. Basalt dikes in the 1886 Tarawera Rift. New Zealand Journal of Geology and Geophysics, 24(5-6): 585-592.

Nairn, I. and Kohn, B., 1973. Relation of the Earthquake Flat Breccia to the Rotoiti Breccia, central North Island, New Zealand. New Zealand journal of geology and geophysics, 16(2): 269-279.

Nairn, I., Shane, P., Cole, J., Leonard, G., Self, S. and Pearson, N., 2004. Rhyolite magma processes of the~ AD 1315 Kaharoa eruption episode, Tarawera volcano, New Zealand. Journal of Volcanology and Geothermal Research, 131(3): 265-294.

Nairn, I.A., 2002. Geology of the Okataina Volcanic Centre, scale 1: 50 000. Institute of Geological and Nuclear Sciences geological map 25. 1 sheet+ 156 p. Institute of Geological and Nuclear Sciences, Lower Hutt, New Zealand.

Nairn, I.A., Kobayashi, T. and Nakagawa, M., 1998. The~ 10 ka multiple vent pyroclastic eruption sequence at Tongariro Volcanic Centre, Taupo Volcanic Zone, New Zealand:: Part 1. Eruptive processes during regional extension. Journal of Volcanology and Geothermal Research, 86(1): 19-44.

Nakada, S., Miyake, Y., Sato, H., Oshima, O. and Fujinawa, A., 1995. Endogenous growth of dacite dome at Unzen volcano (Japan), 1993–1994. Geology, 23(2): 157-160.

Nakada, S., Shimizu, H. and Ohta, K., 1999. Overview of the 1990–1995 eruption at Unzen Volcano. Journal of Volcanology and Geothermal Research, 89(1): 1-22.

Németh, K., 2010. Monogenetic volcanic fields: Origin, sedimentary record, and relationship with polygenetic volcanism. Geological Society of America Special Papers, 470: 43-66.

Németh, K., Cronin, S.J., Smith, I.E.M. and Agustin-Flores, J., 2012a. Amplified hazard of small-volume monogenetic eruptions due to environmental controls, Orakei Basin, Auckland Volcanic Field, New Zealand. Bulletin of Volcanology, 74(9): 2121-2137.

Németh, K., Goth, K., Martin, U., Csillag, G. and Suhr, P., 2008. Reconstructing paleoenvironment, eruption mechanism and paleomorphology of the Pliocene Pula maar, (Hungary). Journal of Volcanology and Geothermal Research, 177(2): 441-456.

Németh, K. and Kereszturi, G., 2015. Monogenetic volcanism: personal views and discussion. International Journal of Earth Sciences, 104(8): 2131-2146.

Németh, K. and Martin, U., 2007. Shallow sill and dyke complex in western Hungary as a possible feeding system of phreatomagmatic volcanoes in "soft-rock" environment. Journal of Volcanology and Geothermal Research, 159(1-3): 138-152.

Németh, K., Martin, U. and Csillag, G., 2007. Pitfalls in erosion level calculation based on remnants of maar and diatreme volcanoes. Geomorphologie-Relief Processus Environnement(3): 225-235.

Németh, K., Martin, U. and Harangi, S., 2001. Miocene phreatomagmatic volcanism at Tihany (Pannonian Basin, Hungary). Journal of Volcanology and Geothermal Research, 111(1-4): 111-135.

Németh, K., Risso, C., Nullo, F., Smith, I.E.M. and Pecskay, Z., 2012b. Facies architecture of an isolated long-lived, nested polygenetic silicic tuff ring erupted in a braided river system: The Los Loros volcano, Mendoza, Argentina. Journal of Volcanology and Geothermal Research, 239: 33-48.

Newhall, C.G. and Melson, W.G., 1983. Explosive activity associated with the growth of volcanic domes. Journal of Volcanology and Geothermal Research, 17(1-4): 111-131.

Newman, S. and Lowenstern, J.B., 2002. VolatileCalc: a silicate melt–H 2 O–CO 2 solution model written in Visual Basic for Excel. Computers & Geosciences, 28(5): 597-604.

Okumura, S., Nakamura, M., Takeuchi, S., Tsuchiyama, A., Nakano, T. and Uesugi, K., 2009. Magma deformation may induce non-explosive volcanism via degassing through bubble networks. Earth and Planetary Science Letters, 281(3): 267-274.

Okumura, S., Nakamura, M., Uesugi, K., Nakano, T. and Fujioka, T., 2013. Coupled effect of magma degassing and rheology on silicic volcanism. Earth and Planetary Science Letters, 362: 163-170.

Orsi, G., Di Vito, M.A., Selva, J. and Marzocchi, W., 2009. Long-term forecast of eruption style and size at Campi Flegrei caldera (Italy). Earth and Planetary Science Letters, 287(1): 265-276.

Orsi, G., Gallo, G., Heiken, G., Wohletz, K., Yu, E. and Bonani, G., 1992. A comprehensive study of pumice formation and dispersal: the Cretaio Tephra of Ischia (Italy). Journal of Volcanology and Geothermal Research, 53(1): 329-354.

Ort, M.H. and Carrasco-Núñez, G., 2009. Lateral vent migration during phreatomagmatic and magmatic eruptions at Tecuitlapa Maar, east-central Mexico. Journal of Volcanology and Geothermal Research, 181(1-2): 67-77.

Pallister, J.S., Diefenbach, A.K., Burton, W.C., Muñoz, J., Griswold, J.P., Lara, L.E., Lowenstern, J.B. and Valenzuela, C.E., 2013. The Chaitén rhyolite lava dome: Eruption sequence, lava dome volumes, rapid effusion rates and source of the rhyolite magma. Andean Geology, 40(2): 277-294.

Pallister, J.S., Hoblitt, R.P. and Reyes, A.G., 1992. A basalt trigger for the 1991 eruptions of Pinatubo Volcano? Nature, 356(6368): 426.

Palmer, B.A. and Neall, V.E., 1989. The Murimotu Formation—9500 year old deposits of a debris avalanche and associated lahars, Mount Ruapehu, North Island, New Zealand. New Zealand journal of geology and geophysics, 32(4): 477-486.

Papale, P., 1999. Strain-induced magma fragmentation in explosive eruptions. Nature, 397(6718): 425-428.

Pardo, N., Cronin, S., Palmer, A., Procter, J. and Smith, I., 2012a. Andesitic Plinian eruptions at Mt. Ruapehu: quantifying the uppermost limits of eruptive parameters. Bulletin of volcanology, 74(5): 1161-1185.

Pardo, N., Cronin, S.J., Palmer, A.S. and Németh, K., 2012b. Reconstructing the largest explosive eruptions of Mt. Ruapehu, New Zealand: lithostratigraphic tools to understand subplinian-plinian eruptions at andesitic volcanoes. Bulletin of Volcanology, 74(3): 617-640.

Parfitt, E.A., 2004. A discussion of the mechanisms of explosive basaltic eruptions. Journal of Volcanology and Geothermal Research, 134(1-2): 77-107.

Pedrazzi, D., Aguire-Diaz, G., Bartolini, S., Marti, J. and Geyer, A., 2014a. The 1970 eruption on Deception Island (Antarctica): eruptive dynamics and implications for volcanic hazards. Journal of the Geological Society, 171(6): 765-778.

Pedrazzi, D., Bolós, X. and Martí, J., 2014b. Phreatomagmatic volcanism in complex hydrogeological environments: la Crosa de Sant Dalmai maar (Catalan Volcanic Zone, NE Spain). Geosphere, 10(1): 170-184.

Pereira, L.G. and Janssen, L., 1999. Suitability of laser data for DTM generation: a case study in the context of road planning and design. ISPRS Journal of Photogrammetry and Remote Sensing, 54(4): 244-253.

Perez, W., Freundt, A., Kutterolf, S. and Schmincke, H.-U., 2009. The Masaya Triple Layer: a 2100 year old basaltic multi-episodic Plinian eruption from the Masaya Caldera Complex (Nicaragua). Journal of Volcanology and Geothermal Research, 179(3): 191-205.

Peslier, A.H. and Luhr, J.F., 2006. Hydrogen loss from olivines in mantle xenoliths from Simcoe (USA) and Mexico: Mafic alkalic magma ascent rates and water budget of the sub-continental lithosphere. Earth and Planetary Science Letters, 242(3): 302-319.

Petford, N., 2009. Which effective viscosity? Mineralogical Magazine, 73(2): 167-191.

Petrone, C.M., Francalanci, L., Carlson, R.W., Ferrari, L. and Conticelli, S., 2003. Unusual coexistence of subduction-related and intraplate-type magmatism: Sr, Nd and Pb isotope and trace element data from the magmatism of the San Pedro–Ceboruco graben (Nayarit, Mexico). Chemical Geology, 193(1): 1-24.

Pierce, K.L., Cannon, K.P., Meyer, G.A., Trebesch, M.J. and Watts, R.D., 2002. Post-glacial inflation-deflation cycles, tilting, and faulting in the Yellowstone caldera based on Yellowstone Lake shorelines. 2331-1258, US Geological Survey.

Pioli, L., Erlund, E., Johnson, E., Cashman, K., Wallace, P., Rosi, M. and Granados, H.D., 2008. Explosive dynamics of violent Strombolian eruptions: the eruption of Parícutin Volcano 1943–1952 (Mexico). Earth and Planetary Science Letters, 271(1): 359-368.

Pirrung, M., Buechel, G., Lorenz, V. and Treutler, H.-C., 2008. Post-eruptive development of the Ukinrek East Maar since its eruption in 1977 AD in the periglacial area of south-west Alaska. Sedimentology, 55(2): 305-334.

Platz, T., Cronin, S.J., Procter, J.N., Neall, V.E. and Foley, S.F., 2012. Non-explosive, dome-forming eruptions at Mt. Taranaki, New Zealand. Geomorphology, 136(1): 15-30.

Plenier, G., Valet, J.-P., Guérin, G., Lefèvre, J.-C., LeGoff, M. and Carter-Stiglitz, B., 2007. Origin and age of the directions recorded during the Laschamp event in the Chaîne des Puys (France). Earth and Planetary Science Letters, 259(3): 414-431.

Porreca, M., Cifelli, F., Soriano, C., Giordano, G., Romano, C., Conticelli, S. and Mattei, M., 2014. Hyaloclastite fragmentation below the glass transition: An example from El Barronal submarine volcanic complex (Spain). Geology, 42(1): 87-90.

Price, R. and Chappell, B., 1975. Fractional crystallisation and the petrology of Dunedin volcano. Contributions to mineralogy and petrology, 53(3): 157-182.

Price, R., McCulloch, M., Smith, I. and Stewart, R., 1992. Pb-Nd-Sr isotopic compositions and trace element characteristics of young volcanic rocks from Egmont Volcano and comparisons with basalts and andesites from the Taupo Volcanic Zone, New Zealand. Geochimica et cosmochimica acta, 56(3): 941-953.

Price, R.C., Gamble, J.A., Smith, I.E., Maas, R., Waight, T., Stewart, R.B. and Woodhead, J., 2012. The anatomy of an Andesite volcano: a time–stratigraphic study of andesite petrogenesis and crustal evolution at Ruapehu Volcano, New Zealand. Journal of Petrology: egs050.

Putirka, K.D., 2008. Thermometers and barometers for volcanic systems. In: K.D. Putirka and F. Tepley (Editors), Minerals, Inclusions and Volcanic Processes, Reviews in Mineralogy and Geochemistry, pp. 61-120.

Pyle, D., 2000. Sizes of volcanic eruptions. Encyclopedia of volcanoes, 1: 263-269.

Pyle, D.M., 1989. The thickness, volume and grainsize of tephra fall deposits. Bulletin of Volcanology, 51(1): 1-15.

Reyners, M., 1998. Plate coupling and the hazard of large subduction thrust earthquakes at the Hikurangi subduction zone, New Zealand. New Zealand Journal of Geology and Geophysics, 41(4): 343-354.

Reyners, M., 2013. The central role of the Hikurangi Plateau in the Cenozoic tectonics of New Zealand and the Southwest Pacific. Earth and Planetary Science Letters, 361: 460-468.

Reyners, M., Eberhart-Phillips, D. and Stuart, G., 2007. The role of fluids in lower-crustal earthquakes near continental rifts. Nature, 446(7139): 1075-1078.

Richards, A.F., 1959. Geology of the islas revillagigedo, mexico. Bull Volcanol, 22(1): 73.

Riedel, C., Ernst, G. and Riley, M., 2003. Controls on the growth and geometry of pyroclastic constructs. Journal of Volcanology and Geothermal Research, 127(1): 121-152.

Riggs, N. and Carrasco-Núñez, G., 2004. Evolution of a complex isolated dome system, Cerro Pizarro, central Mexico. Bulletin of Volcanology, 66(4): 322-335.

Robertson, R., Cole, P., Sparks, R., Harford, C., Lejeune, A., McGuire, W., Miller, A., Murphy, M., Norton, G. and Stevens, N., 1998. The explosive eruption of Soufriere Hills Volcano, Montserrat, West Indies, 17 September, 1996. Geophysical Research Letters, 25(18): 3429-3432.

Rodríguez-Elizarrarás, S., Siebe, C., Komorowski, J.-C., Espíndola, J.M. and Saucedo, R., 1991. Field observations of pristine block-and ash-flow deposits emplaced April 16–17, 1991 at Volcan de Colima, Mexico. Journal of volcanology and geothermal research, 48(3-4): 399-412.

Rosa, C.J., McPhie, J. and Relvas, J.M., 2010. Type of volcanoes hosting the massive sulfide deposits of the Iberian Pyrite Belt. Journal of Volcanology and Geothermal Research, 194(4): 107-126.

Rose, W., 1973. Pattern and mechanism of volcanic activity at the Santiaguito volcanic dome, Guatemala. Bull Volcanol, 37(1): 73.

Rose, W.I., Newhall, C.G., Bornhorst, T.J. and Self, S., 1987. Quaternary silicic pyroclastic deposits of Atitlán Caldera, Guatemala. Journal of volcanology and geothermal research, 33(1-3): 57-80.

Rosen, P.A., Hensley, S., Joughin, I.R., Li, F.K., Madsen, S.N., Rodriguez, E. and Goldstein, R.M., 2000. Synthetic aperture radar interferometry. Proceedings of the IEEE, 88(3): 333-382.

Rosenberg, M.D. and Kilgour, G., 2000. Field trip 1 Taupo Volcano, Geological Society of New Zealand Miscellaneous Publication 117B, pp. 1-10.

Ross, P.-S., Delpit, S., Haller, M.J., Németh, K. and Corbella, H., 2011. Influence of the substrate on maar-diatreme volcanoes - An example of a mixed setting from the Pali Aike volcanic field, Argentina. Journal of Volcanology and Geothermal Research, 201(1-4): 253-271.

Ross, P.-S., Núñez, G.C. and Hayman, P., 2017. Felsic maar-diatreme volcanoes: a review. Bulletin of Volcanology, 79(2): 20.

Rouwet, D., Mora-Amador, R., Ramírez-Umaña, C.J., González, G. and Inguaggiato, S., 2017. Dynamic fluid recycling at Laguna Caliente (Poás, Costa Rica) before and during the 2006–ongoing phreatic eruption cycle (2005–10). Geological Society, London, Special Publications, 437(1): 73-96.

Rowland, J. and Sibson, R., 2001. Extensional fault kinematics within the Taupo Volcanic Zone, New Zealand: soft-linked segmentation of a continental rift system. New Zealand Journal of Geology and Geophysics, 44(2): 271-283.

Rowland, J.V. and Sibson, R.H., 2004. Structural controls on hydrothermal flow in a segmented rift system, Taupo Volcanic Zone, New Zealand. Geofluids, 4(4): 259-283.

Rowland, J.V., Wilson, C.J.N. and Gravley, D.M., 2010. Spatial and temporal variations in magma-assisted rifting, Taupo Volcanic Zone, New Zealand. Journal of Volcanology and Geothermal Research, 190(1-2): 89-108.

Ryan, G., Loughlin, S., James, M., Jones, L., Calder, E., Christopher, T., Strutt, M. and Wadge, G., 2010. Growth of the lava dome and extrusion rates at Soufrière Hills Volcano, Montserrat, West Indies: 2005–2008. Geophysical Research Letters, 37(19).

Sable, J., Houghton, B., Wilson, C. and Carey, R., 2009. Eruption mechanisms during the climax of the Tarawera 1886 basaltic Plinian eruption inferred from microtextural characteristics of the deposits. Studies in volcanology. The legacy of George Walker. Geological Society, London: 129-154.

Sable, J.E., Houghton, B.F., Del Carlo, P. and Coltelli, M., 2006. Changing conditions of magma ascent and fragmentation during the Etna 122 BC basaltic Plinian eruption: evidence from clast microtextures. Journal of Volcanology and Geothermal Research, 158(3): 333-354.

Sahagian, D.L. and Proussevitch, A.A., 1998. 3D particle size distributions from 2D observations: stereology for natural applications. Journal of Volcanology and Geothermal Research, 84(3): 173-196.

Salinger, M., 1980. New Zealand climate: I. precipitation patterns. Monthly weather review, 108(11): 1892-1904.

Saucedo, R., Macías, J. and Bursik, M., 2004. Pyroclastic flow deposits of the 1991 eruption of Volcán de Colima, Mexico. Bulletin of Volcanology, 66(4): 291-306.

Saucedo, R., Macıas, J., Bursik, M., Mora, J., Gavilanes, J. and Cortes, A., 2002. Emplacement of pyroclastic flows during the 1998–1999 eruption of Volcan de Colima, Mexico. Journal of Volcanology and Geothermal Research, 117(1): 129-153.

Schipper, C.I., Castro, J.M., Tuffen, H., James, M.R. and How, P., 2013. Shallow vent architecture during hybrid explosive–effusive activity at Cordón Caulle (Chile, 2011–12): evidence from direct observations and pyroclast textures. Journal of Volcanology and Geothermal Research, 262: 25-37.

Self, S., de Silva, S.L. and Cortes, J.A., 2008. Enigmatic clastogenic rhyolitic volcanism: The Corral de Coquena spatter ring, North Chile. Journal of Volcanology and Geothermal Research, 177(4): 812-821.

Self, S., Kienle, J. and Huot, J.P., 1980. Ukinrek Maars, Alaska, II. Deposits and formation of the 1977 craters. Journal of Volcanology and Geothermal Research, 7(1-2): 39-65.

Shane, P., Martin, S.B., Smith, V.C., Beggs, K.F., Darragh, M.B., Cole, J.W. and Nairn, I.A., 2007. Multiple rhyolite magmas and basalt injection in the 17.7 ka Rerewhakaaitu eruption episode from Tarawera volcanic complex, New Zealand. Journal of Volcanology and Geothermal Research, 164(1-2): 1-26.

Shane, P., Nairn, I.A. and Smith, V.C., 2005. Magma mingling in the~ 50 ka Rotoiti eruption from Okataina Volcanic Centre: implications for geochemical diversity and chronology of large volume rhyolites. Journal of Volcanology and Geothermal Research, 139(3): 295-313.

Shane, P. and Smith, V.C., 2013. Using amphibole crystals to reconstruct magma storage temperatures and pressures for the post-caldera collapse volcanism at Okataina volcano. Lithos, 156: 159-170.

Sharp, T.G., Stevenson, R.J. and Dingwell, D.B., 1996. Microlites and" nanolites" in rhyolitic glass: Microstructural and chemical characterization. Bulletin of volcanology, 57(8): 631-640.

Shea, T., Houghton, B.F., Gurioli, L., Cashman, K.V., Hammer, J.E. and Hobden, B.J., 2010. Textural studies of vesicles in volcanic rocks: An integrated methodology. Journal of Volcanology and Geothermal Research, 190(3-4): 271-289.

Shea, T., Leonhardi, T., Giachetti, T., Lindoo, A., Larsen, J., Sinton, J. and Parsons, E., 2017. Dynamics of an unusual cone-building trachyte eruption at Pu ʻu Wa ʻawa ʻa, Hualālai volcano, Hawai ʻi. Bulletin of Volcanology, 79(4): 26.

Sheridan, M.F. and Wohletz, K.H., 1981. Hydrovolcanic explosions: The systematics of water-pyroclast equilibration. Science, 212(4501): 1387-1389.

Sheridan, M.F. and Wohletz, K.H., 1983. Hydrovolcanism: basic considerations and review. Journal of Volcanology and Geothermal Research, 17(1-4): 1-29.

Siebert, L., Glicken, H. and Ui, T., 1987. Volcanic hazards from Bezymianny-and Bandai-type eruptions. Bulletin of Volcanology, 49(1): 435-459.

Sieh, K. and Bursik, M., 1986. Most recent eruption of the Mono Craters, eastern central California. Journal of Geophysical Research: Solid Earth, 91(B12): 12539-12571.

Sigvaldason, G.E., 1992. Recent hydrothermal explosion craters in an old hyaloclastite flow, central Iceland. Journal of volcanology and geothermal research, 54(1-2): 53-63.

Sillitoe, R.H., Baker, E.M. and Brook, W.A., 1984. Gold deposits and hydrothermal eruption breccias associated with a maar volcano at Wau, Papua New Guinea. Economic Geology, 79(4): 638-655.

Sillitoe, R.H., Grauberger, G.L. and Elliott, J.E., 1985. A diatreme-hosted gold deposit at Montana Tunnels, Montana. Economic Geology, 80(6): 1707-1721.

Simpson, M.P. and Bignall, G., 2016. Undeveloped high-enthalpy geothermal fields of the Taupo Volcanic Zone, New Zealand. Geothermics, 59: 325-346.

Siswowidjoyo, S., Suryo, I. and Yokoyama, I., 1995. Magma eruption rates of Merapi volcano, Central Java, Indonesia during one century (1890–1992). Bulletin of volcanology, 57(2): 111-116.

Smith, D., 1974. Pyroxene-olivine-quartz assemblages in rocks associated with the Nain Anorthosite Massif, Labrador. Journal of Petrology, 15(1): 58-78.

Smith, I., Ruddock, R. and Day, R., 1989. Miocene arc-type volcanic/plutonic complexes of the Northland Peninsula, New Zealand. Royal Society of New Zealand Bulletin, 26: 205-213.

Smith, I.E.M. and Németh, K., 2017. Source to surface model of monogenetic volcanism: a critical review. Geological Society, London, Special Publications, 446(1): 1-28.

Smith, I.E.M. and Price, R.C., 2006. The Tonga–Kermadec arc and Havre–Lau back-arc system: their role in the development of tectonic and magmatic models for the western Pacific. Journal of volcanology and geothermal research, 156(3): 315-331.

Smith, J.V. and Houston, E.C., 1994. Folds produced by gravity spreading of a banded rhyolite lava flow. Journal of volcanology and geothermal research, 63(1-2): 89-94.

Smith, V.C., Shane, P. and Nairn, I.A., 2005. Trends in rhyolite geochemistry, mineralogy, and magma storage during the last 50 kyr at Okataina and Taupo volcanic centres, Taupo Volcanic Zone, New Zealand. Journal of Volcanology and Geothermal Research, 148(3): 372-406.

Smith, V.C., Shane, P. and Smith, I., 2002. Tephrostratigraphy and geochemical fingerprinting of the Mangaone Subgroup tephra beds, Okataina volcanic centre, New Zealand. New Zealand Journal of Geology and Geophysics, 45(2): 207-219.

Sohn, Y. and Chough, S., 1992. The Ilchulbong tuff cone, Cheju Island, South Korea. Sedimentology, 39(4): 523-544.

Sohn, Y.K., 1996. Hydrovolcanic processes forming basaltic tuff rings and cones on Cheju Island, Korea. Geological Society of America Bulletin, 108(10): 1199-1211.

Sohn, Y.K. and Chough, S.K., 1989. Depositional processes of the Suwolbong tuff ring, Cheju Island (Korea). Sedimentology, 36(5): 837-855.

Sohn, Y.K., Cronin, S.J., Brenna, M., Smith, I.E.M., Németh, K., White, J.D.L., Murtagh, R.M., Jeon, Y.M. and Kwon, C.W., 2012. Ilchulbong tuff cone, Jeju Island, Korea, revisited: A compound monogenetic volcano involving multiple magma pulses, shifting vents, and discrete eruptive phases. Geological Society of America Bulletin, 124(3-4): 259-274.

Solgevik, H., Mattsson, H.B. and Hermelin, O., 2007. Growth of an emergent tuff cone: fragmentation and depositional processes recorded in the Capelas tuff cone, São Miguel, Azores. Journal of Volcanology and Geothermal Research, 159(1): 246-266.

Son, M., Kim, J.S., Jung, S., Ki, J.S., Kim, M.-C. and Sohn, Y.K., 2012. Tectonically controlled vent migration during maar–diatreme formation: An example from a Miocene half-graben basin in SE Korea. Journal of Volcanology and Geothermal Research, 223: 29-46.

Sottili, G., Palladino, D.M., Gaeta, M. and Masotta, M., 2012. Origins and energetics of maar volcanoes: examples from the ultrapotassic Sabatini Volcanic District (Roman Province, Central Italy). Bulletin of Volcanology, 74(1): 163-186.

Sottili, G., Taddeucci, J., Palladino, D., Gaeta, M., Scarlato, P. and Ventura, G., 2009. Sub-surface dynamics and eruptive styles of maars in the Colli Albani Volcanic District, Central Italy. Journal of Volcanology and Geothermal Research, 180(2): 189-202.

Sparks, R., Pinkerton, H. and Macdonald, R., 1977. The transport of xenoliths in magmas. Earth and Planetary Science Letters, 35(2): 234-238.

Sparks, R.S.J., 1997. Causes and consequences of pressurisation in lava dome eruptions. Earth and Planetary Science Letters, 150(3): 177-189.

Spera, F.J., 2000. Physical properties of magmas. In: H. Sigurdsson, B.F. Houghton, S.R. McNutt, H. Rymel and J. Stix (Editors), Encyclopedia of volcanoes pp. 171-190.

Spinks, K.D., Acocella, V., Cole, J.W. and Bassett, K.N., 2005. Structural control of volcanism and caldera development in the transtensional Taupo Volcanic Zone, New Zealand. Journal of Volcanology and Geothermal Research, 144(1): 7-22.

Spry, A., 1962. The origin of columnar jointing, particularly in basalt flows. Journal of the Geological Society of Australia, 8(2): 191-216.

Stasiuk, M.V., Jaupart, C., Stephen, R. and Sparks, J., 1993. Influence of cooling on lava-flow dynamics. Geology, 21(4): 335-338.

Steinmann, L., Spiess, V. and Sacchi, M., 2017. Post-collapse evolution of a coastal caldera system: Insights from a 3D multichannel seismic survey from the Campi Flegrei caldera (Italy). Journal of Volcanology and Geothermal Research.

Stephenson, N. and Hensel, H., 1978. A Precambrian fayalite granite from the south coast of Western Australia. Lithos, 11(3): 209-218.

Stevenson, R., Briggs, R. and Hodder, A., 1994. Physical volcanology and emplacement history of the Ben Lomond rhyolite lava flow, Taupo Volcanic Centre, New Zealand. New Zealand Journal of Geology and Geophysics, 37(3): 345-358.

Stevenson, R.J., Dingwell, D.B., Bagdassarov, N.S. and Manley, C.R., 2001. Measurement and implication of" effective" viscosity for rhyolite flow emplacement. Bulletin of volcanology, 63(4): 227-237.

Stewart, A.L. and McPhie, J., 2003. Internal structure and emplacement of an Upper Pliocene dacite cryptodome, Milos Island, Greece. Journal of Volcanology and Geothermal Research, 124(1): 129-148.

Storm, S., Schmitt, A.K., Shane, P. and Lindsay, J.M., 2014. Zircon trace element chemistry at sub-micrometer resolution for Tarawera volcano, New Zealand, and implications for rhyolite magma evolution. Contributions to Mineralogy and Petrology, 167(4): 1000.

Storm, S., Shane, P., Schmitt, A.K. and Lindsay, J.M., 2011. Contrasting punctuated zircon growth in two syn-erupted rhyolite magmas from Tarawera volcano: Insights to crystal diversity in magmatic systems. Earth and Planetary Science Letters, 301(3-4): 511-520.

Stovall, W.K., Houghton, B., Gonnermann, H., Fagents, S. and Swanson, D., 2011. Eruption dynamics of Hawaiian-style fountains: the case study of episode 1 of the Kīlauea Iki 1959 eruption. Bulletin of volcanology, 73(5): 511-529.

Stratford, W. and Stern, T., 2006. Crust and upper mantle structure of a continental backarc: central North Island, New Zealand. Geophysical Journal International, 166(1): 469-484.

Sumner, J.M., 1998. Formation of clastogenic lava flows during fissure eruption and scoria cone collapse: the 1986 eruption of Izu-Oshima Volcano, eastern Japan. Bulletin of Volcanology, 60(3): 195-212.

Sutton, A.N., 1995. Evolution of a large silicic magma system: Taupo volcanic centre, New Zealand. Unpublished PhD Thesis, The Open University, Milton Keynes, United Kingdom, 416 pp.

Sutton, A.N., Blake, S. and Wilson, C.J.N., 1995. An outline geochemistry of rhyolite eruptives from Taupo volcanic centre, New Zealand. Journal of Volcanology and Geothermal Research, 68(1-3): 153-175.

Sutton, A.N., Blake, S., Wilson, C.J.N. and Charlier, B.L.A., 2000. Late Quaternary evolution of a hyperactive rhyolite magmatic system: Taupo volcanic centre, New Zealand. Journal of the Geological Society, 157: 537-552.

Tait, M., Cas, R. and Viramonte, J., 2009. The origin of an unusual tuff ring of perlitic rhyolite pyroclasts: The last explosive phase of the Ramadas Volcanic Centre, Andean Puna, Salta, NW Argentina. Journal of Volcanology and Geothermal Research, 183(1): 1-16.

Tanguy, J.-C., 2004. Rapid dome growth at Montagne Pelée during the early stages of the 1902–1905 eruption: a reconstruction from Lacroix's data. Bulletin of Volcanology, 66(7): 615-621.

Tenzer, R., Sirguey, P., Rattenbury, M. and Nicolson, J., 2011. A digital rock density map of New Zealand. Computers & geosciences, 37(8): 1181-1191.

Thorarinsson, S., 1965. Surtsey eruption course of events and the development of the new island.

Thorarinsson, S., 1967. The Surtsey eruption: Course of events during the year 1966. Surtsey Res Prog Rep, 3: 84-92.

Timm, C., Davy, B., Haase, K., Hoernle, K.A., Graham, I.J., De Ronde, C.E., Woodhead, J., Bassett, D., Hauff, F. and Mortimer, N., 2014. Subduction of the oceanic Hikurangi Plateau and its impact on the Kermadec arc. Nature communications, 5: 4923.

Toprak, V., 1998. Vent distribution and its relation to regional tectonics, Cappadocian Volcanics, Turkey. Journal of Volcanology and Geothermal Research, 85(1): 55-67.

Tost, M. and Cronin, S., 2015. Linking distal volcaniclastic sedimentation and stratigraphy with the development of Ruapehu volcano, New Zealand. Bulletin of Volcanology, 77(11): 1-17.

Tost, M. and Cronin, S., 2016. Climate influence on volcano edifice stability and fluvial landscape evolution surrounding Mount Ruapehu, New Zealand. Geomorphology, 262: 77-90.

Tost, M., Price, R., Cronin, S. and Smith, I., 2016. New insights into the evolution of the magmatic system of a composite andesite volcano revealed by clasts from distal mass-flow deposits: Ruapehu volcano, New Zealand. Bulletin of Volcanology, 78(5): 38.

Townsend, D.B., Vonk, A. and Kamp, P.J.J., 2008. Geology of the Taranaki area. Institute of Geological and Nuclear Sciences 1:250 000 geological map 7. 1 sheet + 77 p. Lower Hutt, New Zealand, GNS Science.

Tsuru, K. and Henry, N., 1937. An iron rich optically positive hypersthene from Manchuria. Min. Mag, 24: 527-528.

Tuffen, H., James, M.R., Castro, J.M. and Schipper, C.I., 2013. Exceptional mobility of an advancing rhyolitic obsidian flow at Cordón Caulle volcano in Chile. Nature communications, 4.

Ui, T., Matsuwo, N., Sumita, M. and Fujinawa, A., 1999. Generation of block and ash flows during the 1990–1995 eruption of Unzen Volcano, Japan. Journal of Volcanology and Geothermal Research, 89(1): 123-137.

USGS, 1972. Geologic map of Yellowstone National Park. 711.

Valentine, G. and Perry, F., 2006. Decreasing magmatic footprints of individual volcanoes in a waning basaltic field. Geophysical Research Letters, 33(14).

Valentine, G., Perry, F. and WoldeGabriel, G., 2000. Field characteristics of deposits from spatter-rich pyroclastic density currents at Summer Coon volcano, Colorado. Journal of volcanology and geothermal research, 104(1): 187-199.

Valentine, G.A. and Cortés, J.A., 2013. Time and space variations in magmatic and phreatomagmatic eruptive processes at Easy Chair (Lunar Crater Volcanic Field, Nevada, USA). Bulletin of Volcanology, 75(9): 752.

Valentine, G.A., Graettinger, A.H. and Sonder, I., 2014. Explosion depths for phreatomagmatic eruptions. Geophysical Research Letters, 41(9): 3045-3051.

Valentine, G.A. and Gregg, T.K.P., 2008. Continental basaltic volcanoes - Processes and problems. Journal of Volcanology and Geothermal Research, 177(4): 857-873.

Valentine, G.A. and White, J.D.L., 2012. Revised conceptual model for maar-diatremes: Subsurface processes, energetics, and eruptive products. Geology, 40(12): 1111-1114.

van Otterloo, J., Cas, R.A. and Sheard, M.J., 2013. Eruption processes and deposit characteristics at the monogenetic Mt. Gambier Volcanic Complex, SE Australia: implications for alternating magmatic and phreatomagmatic activity. Bulletin of Volcanology, 75(8): 737.

Vandergoes, M.J., Hogg, A.G., Lowe, D.J., Newnham, R.M., Denton, G.H., Southon, J., Barrell, D.J.A., Wilson, C.J.N., McGlone, M.S., Allan, A.S.R., Almond, P.C., Petchey, F., Dabell, K., Dieffenbacher-Krall, A.C. and Blaauw, M., 2013. A revised age for the Kawakawa/Oruanui tephra, a key marker for the Last Glacial Maximum in New Zealand. Quaternary Science Reviews, 74: 195-201.

Vaughan, R.G. and Webley, P.W., 2010. Satellite observations of a surtseyan eruption: Hunga Ha'apai, Tonga. Journal of Volcanology and Geothermal Research, 198(1): 177-186.

Vergniolle, S. and Mangan, M.T., 2000. Hawaiian and Strombolian eruptions. In: H. Sigurdsson, B.F. Houghton, S.R. McNutt, H. Rymel and J. Stix (Editors), Encyclopedia of volcanoes, pp. 447-461.

Verwoerd, W. and Chevallier, L., 1987. Contrasting types of surtseyan tuff cones on Marion and Prince Edward islands, southwest Indian Ocean. Bulletin of Volcanology, 49(1): 399-413.

Vespermann, D. and Schmincke, H.-U., 2000. Scoria cones and tuff rings. In: H. Sigurdsson, B.F. Houghton, S.R. McNutt, H. Rymel and J. Stix (Editors), Encyclopedia of Volcanoes, pp. 683-694.

Villamor, P. and Berryman, K., 2001. A late Quaternary extension rate in the Taupo Volcanic Zone, New Zealand, derived from fault slip data. New Zealand Journal of Geology and Geophysics, 44(2): 243-269.

Villamor, P., Berryman, K., Ellis, S., Schreurs, G., Wallace, L., Leonard, G., Langridge, R. and Ries, W., 2017. Rapid Evolution of Subduction-Related Continental Intraarc Rifts: The Taupo Rift, New Zealand. Tectonics.

Voight, B., 2000. Structural stability of andesite volcanoes and lava domes. Philosophical Transactions of the Royal Society of London A: Mathematical, Physical and Engineering Sciences, 358(1770): 1663-1703.

Voight, B. and Elsworth, D., 1997. Failure of volcano slopes. Geotechnique, 47(1): 1-31.

von Lichtan, I., White, J., Manville, V. and Ohneiser, C., 2016. Giant rafted pumice blocks from the most recent eruption of Taupo volcano, New Zealand: Insights from palaeomagnetic and textural data. Journal of Volcanology and Geothermal Research, 318: 73-88.

Vucetich, C.t. and Pullar, W., 1969. Stratigraphy and chronology of late Pleistocene volcanic ash beds in central North Island, New Zealand. New Zealand Journal of Geology and Geophysics, 12(4): 784-837.

Waikato Regional Aerial Photography Service - WRAPS, 2012. Waikato 0.5m Rural Aerial Photos (2012-2013).

Waikato Regional Council and NZ Aerial Mapping Ltd., 2006. 1 m LiDAR DEM.

Walker, G.P., 1993. Basaltic-volcano systems. Geological Society, London, Special Publications, 76(1): 3-38.

Walker, G.P., 2000. Basaltic volcanoes and volcanic systems. Encyclopedia of volcanoes: 283-289.

Walker, G.P.L., 1971. Grain-size characteristics of pyroclastic deposits. The Journal of Geology: 696-714.

Walker, G.P.L., 1973. Explosive volcanic eruptions—a new classification scheme. Geol Rundsch, 62(2): 431-446.

Walker, G.P.L., Self, S. and Wilson, L., 1984. Tarawera 1886, New Zealand - a basaltic Plinian fissure eruption. Journal of Volcanology and Geothermal Research, 21(1-2): 61-78.

Walker, G.P.L. and Wilson, C.J.N., 1983. Lateral variations in the Taupo Ignimbrite. Journal of Volcanology and Geothermal Research, 18(1-4): 117-133.

Wallace, L.M., Beavan, J., McCaffrey, R. and Darby, D., 2004. Subduction zone coupling and tectonic block rotations in the North Island, New Zealand. Journal of Geophysical Research: Solid Earth, 109(B12).

Wallace, P. and Anderson, A.T., 2000. Volatiles in magmas. In: H. Sigurdsson, B.F. Houghton, S.R. McNutt, H. Rymel and J. Stix (Editors), Encyclopedia of volcanoes, pp. 149-170.

Watkins, J., Manga, M., Huber, C. and Martin, M., 2009. Diffusion-controlled spherulite growth in obsidian inferred from H2O concentration profiles. Contributions to Mineralogy and Petrology, 157(2): 163-172.

Weinzierl, B., Sailer, T., Sauer, D., Minikin, A., Reitebuch, O., Mayer, B. and Schumann, U., 2012. The Eyjafjalla eruption in 2010 and the volcanic impact on aviation, Atmospheric Physics. Springer, pp. 625-644.

Wentworth, C.K., 1922. A scale of grade and class terms for clastic sediments. The Journal of Geology, 30(5): 377-392.

White, J.D. and Valentine, G.A., 2016. Magmatic versus phreatomagmatic fragmentation: Absence of evidence is not evidence of absence. Geosphere, 12(5): 1478-1488.

White, J.D.L., 1996a. Impure coolants and interaction dynamics of phreatomagmatic eruptions. Journal of Volcanology and Geothermal Research, 74(3): 155-170.

White, J.D.L., 1996b. Pre-emergent construction of a lacustrine basaltic volcano, Pahvant Butte, Utah (USA). Bulletin of Volcanology, 58(4): 249-262.

White, J.D.L. and Houghton, B.F., 2006. Primary volcaniclastic rocks. Geology, 34(8): 677-680.

White, J.D.L. and Ross, P.-S., 2011. Maar-diatreme volcanoes: A review. Journal of Volcanology and Geothermal Research, 201(1-4): 1-29.

Williams, H., 1932. The history and character of volcanic domes. University of California Press.

Williams, S.N. and Self, S., 1983. The October 1902 plinian eruption of Santa Maria volcano, Guatemala. Journal of Volcanology and Geothermal Research, 16(1-2): 33-56.

Wilson, C., 1993. Stratigraphy, chronology, styles and dynamics of late Quaternary eruptions from Taupo volcano, New Zealand. Philosophical Transactions of the Royal Society of London A: Mathematical, Physical and Engineering Sciences, 343(1668): 205-306.

Wilson, C. and Charlier, B., 2009. Rapid rates of magma generation at contemporaneous magma systems, Taupo Volcano, New Zealand: insights from U–Th model-age spectra in zircons. Journal of Petrology, 50(5): 875-907.

Wilson, C., Houghton, B. and Lloyd, E., 1986. Volcanic history and evolution of the Maroa-Taupo area, central North Island, Late Cenozoic Volcanism in New Zealand. Royal Society of New Zealand, Bulletin, pp. 194-223.

Wilson, C. and Walker, G.P., 1985. The Taupo eruption, New Zealand I. General aspects. Philosophical Transactions of the Royal Society of London A: Mathematical, Physical and Engineering Sciences, 314(1529): 199-228.

Wilson, C.J. and Rowland, J.V., 2016. The volcanic, magmatic and tectonic setting of the Taupo Volcanic Zone, New Zealand, reviewed from a geothermal perspective. Geothermics, 59: 168-187.

Wilson, C.J.N., 1985. The Taupo eruption, New Zealand II. The Taupo Ignimbrite. Philosophical Transactions of the Royal Society of London A: Mathematical, Physical and Engineering Sciences, 314(1529): 229-310.

Wilson, C.J.N., 1991. Ignimbrite morphology and the effects of erosion: a New Zealand case study. Bulletin of Volcanology, 53(8): 635-644.

Wilson, C.J.N., 2001. The 26.5 ka Oruanui eruption, New Zealand: an introduction and overview. Journal of Volcanology and Geothermal Research, 112(1-4): 133-174.

Wilson, C.J.N., Gravley, D.M., Leonard, G.S. and Rowland, J.V., 2009. Volcanism in the central Taupo Volcanic Zone, New Zealand: tempo, styles and controls. Studies in Volcanology: The Legacy of George Walker. Special Publications of IAVCEI, 2: 225-247.

Wilson, C.J.N., Houghton, B.F., McWilliams, M.O., Lanphere, M.A., Weaver, S.D. and Briggs, R.M., 1995. Volcanic and structural evolution of Taupo Volcanic Zone, New Zealand: a review. Journal of Volcanology and Geothermal Research, 68(1-3): 1-28.

Wilson, C.J.N., Rhoades, D.A., Lanphere, M.A., Calvert, A.T., Houghton, B.F., Weaver, S.D. and Cole, J.W., 2007. A multiple-approach radiometric age estimate for the Rotoiti and Earthquake Flat eruptions, New Zealand, with implications for the MIS 4/3 boundary. Quaternary Science Reviews, 26(13-14): 1861-1870.

Wilson, C.J.N., Rogan, A.M., Smith, I.E.M., Northey, D.J., Nairn, I.A. and Houghton, B.F., 1984. Caldera volcanos of the Taupo Volcanic Zone, New Zealand. Journal of Geophysical Research, 89(NB10): 8463-8484.

Wilson, C.J.N. and Smith, I.E.M., 1985. A basaltic phreatomagmatic eruptive centre at Acacia Bay, Taupo volcanic centre. Journal of the Royal Society of New Zealand, 15(3): 329-337.

Wilson, G., Wilson, T., Deligne, N. and Cole, J., 2014. Volcanic hazard impacts to critical infrastructure: A review. Journal of Volcanology and Geothermal Research, 286: 148-182.

Wilson, J.P. and Gallant, J.C., 2000. Terrain analysis: principles and applications.

Wilson, L. and Head, J.W., 1981. Ascent and eruption of basaltic magma on the Earth and Moon. Journal of Geophysical Research, 86(NB4): 2971-3001.

Wohletz, K. and Heiken, G., 1992. Volcanology and geothermal energy. University of California Press Berkeley.

Wohletz, K.H., 1986. Explosive magma-water interactions: Thermodynamics, explosion mechanisms, and field studies. Bulletin of Volcanology, 48(5): 245-264.

Wohletz, K.H. and McQueen, R.G., 1984. Experimental studies of hydromagmatic volcanism, Explosive volcanism: inception, evolution, and hazards - Studies in Geophysics. National Academy Press, Washington, D.C., pp. 158-169.

Wohletz, K.H. and Sheridan, M.F., 1983. Hydrovolcanic explosions II. Evolution of basaltic tuff rings and tuff cones. American Journal of Science, 283(5): 385-413.

Wohletz, K.H. and Zimanowski, B., 2000. Physics of phreatomagmatism; I: Explosion physics. Terra Nostra, 6: 515-523.

Wolfe, E.W., Wise, W.S. and Dalrymple, G.B., 1997. The geology and petrology of Mauna Kea Volcano, Hawaii; a study of postshield volcanism. 2330-7102, USGPO.

Wolpert, R.L., Ogburn, S.E. and Calder, E.S., 2016. The longevity of lava dome eruptions. Journal of Geophysical Research: Solid Earth, 121(2): 676-686.

Wong, L.J. and Larsen, J.F., 2010. The Middle Scoria sequence: A Holocene violent strombolian, subplinian and phreatomagmatic eruption of Okmok volcano, Alaska. Bulletin of volcanology, 72(1): 17.

Wood, C.A., 1979. Monogenetic volcanoes of the terrestrial planets, Lunar and Planetary Science Conference Proceedings, pp. 2815-2840.

Wood, C.A., 1980. Morphometric evolution of cinder cones. Journal of Volcanology and Geothermal Research, 7(3-4): 387-413.

Wright, I., 1994. Nature and tectonic setting of the southern Kermadec submarine arc volcanoes: An overview. Marine Geology, 118(3-4): 217-236.

Wright, I.C., 1992. Shallow structure and active tectonism of an offshore continental back-arc spreading system: the Taupo Volcanic Zone, New Zealand. Marine geology, 103(1-3): 287-309.

WRP Geothermal System, 2016. Geothermal Field Boundaries supplied by Waikato Regional Council.

Yasui, M. and Koyaguchi, T., 2004. Sequence and eruptive style of the 1783 eruption of Asama Volcano, central Japan: a case study of an andesitic explosive eruption generating fountain-fed lava flow, pumice fall, scoria flow and forming a cone. Bulletin of volcanology, 66(3): 243-262.

Yokoyama, I., 2002. Growth mechanism of the 1944 lava dome of Usu volcano in Hokkaido, Japan. Proceedings of the Japan Academy, Series B, 78(1): 6-11.

Yokoyama, I., 2005. Growth rates of lava domes with respect to viscosity of magmas. Annals of Geophysics, 48/6: 957-971.

Yokoyama, I. and Ohkawa, S., 1986. The subsurface structure of the Aira caldera and its vicinity in southern Kyushu, Japan. Journal of volcanology and geothermal research, 30(3-4): 253-282.

Yokoyama, I., Yamashita, H., Watanabe, H. and Okada, H.M., 1981. Geophysical characteristics of dacite volcanism—The 1977–1978 eruption of Usu volcano. Journal of Volcanology and Geothermal Research, 9(4): 335-358.

Yulianto, F. and Sofan, P., 2016. The Utilization of Remotely Sensed Data to Analyze the Estimated Volume of Pyroclastic Deposits and Morphological Changes Caused by the

2010–2015 Eruption of Sinabung Volcano, North Sumatra, Indonesia. Pure and Applied Geophysics, 173(8): 2711-2725.

Zanon, V., Pacheco, J. and Pimentel, A., 2009. Growth and evolution of an emergent tuff cone: Considerations from structural geology, geomorphology and facies analysis of Sao Roque volcano, Sao Miguel (Azores). Journal of Volcanology and Geothermal Research, 180(2-4): 277-291.

Závada, P., Dědeček, P., Lexa, J. and Keller, G., 2015. Devils Tower (Wyoming, USA): A lava coulée emplaced into a maar-diatreme volcano? Geosphere, 11(2): 354-375.

Závada, P., Kratinová, Z., Kusbach, V. and Schulmann, K., 2009. Internal fabric development in complex lava domes. Tectonophysics, 466(1): 101-113.

Zellmer, G.F., Sakamoto, N., Iizuka, Y., Miyoshi, M., Tamura, Y., Hsieh, H.-H. and Yurimoto, H., 2014. Crystal uptake into aphyric arc melts: insights from two-pyroxene pseudo-decompression paths, plagioclase hygrometry, and measurement of hydrogen in olivines from mafic volcanics of SW Japan. Geological Society, London, Special Publications, 385(1): 161-184.

Zellmer, G.F., Sakamoto, N., Matsuda, N., Iizuka, Y., Moebis, A. and Yurimoto, H., 2016. On progress and rate of the peritectic reaction Fo+ SiO 2→ En in natural andesitic arc magmas. Geochimica et Cosmochimica Acta, 185: 383-393.

Zhang, G.-L. and Li, C., 2016. Interactions of the Greater Ontong Java mantle plume component with the Osbourn Trough. Scientific reports, 6: 37561.

Zimanowski, B., 1998. Phreatomagmatic explosions. From Magma to Tephra, 4: 25-53.

Zimanowski, B., Büttner, R. and Lorenz, V., 1997a. Premixing of magma and water in MFCI experiments. Bulletin of Volcanology, 58(6): 491-495.

Zimanowski, B., Büttner, R., Lorenz, V. and Hafele, H.G., 1997b. Fragmentation of basaltic melt in the course of explosive volcanism. Journal of Geophysical Research-Solid Earth, 102(B1): 803-814.

Zimmer, B.W., Riggs, N.R. and Carrasco-Núñez, G., 2010. Evolution of tuff ring-dome complex: the case study of Cerro Pinto, eastern Trans-Mexican Volcanic Belt. Bulletin of Volcanology, 72(10): 1223-1240.

Appendices

Appendix A – Supplementary materials for published papers and papers in preparation

Compiled to a digital data medium:

- **Appendix A.5.1** Supplementary data for geochemical analysis (Ohakune Volcanic Complex)
- **Appendix A.5.2** Supplementary photo evidences (Ohakune Volcanic Complex)
- **Appendix A.6.1** Supplementary photo evidences (Te Hukui)
- **Appendix A.7.1** Supplementary data for geochemical analysis (Puketerata Volcanic Complex)
- **Appendix A.7.2** Preliminary amphibole-plagioclase thermobarometry
- **Appendix A.8.1** Supplementary data for geochemical analysis (Motuoapa Peninsula)
- **Appendix A.9.1** Age, volume and geochemistry of eruptive vents of the TVZ within the past 350 ky

Appendix B – Grain size distribution and envelope density analyses

Compiled to a digital data medium:

- **Appendix B.5.1** Grain size distribution of samples from the Ohakune Volcanic Complex
- **Appendix B.5.2** Results of envelope density analysis (Ohakune Volcanic Complex)
- **Appendix B.6.1** Grain size distribution of samples of the Te Hukui Basalt
- **Appendix B.7.1** Grain size distribution of samples from the Puketerata Volcanic Complex
- **Appendix B.7.2** Results of envelope density analysis (Puketerata Volcanic Complex)

- **Appendix B.8.1** Grain size distribution of samples from the Motuoapa Peninsula

- **Appendix B.8.2** Results of envelope density analysis (Motuoapa Peninsula)

Appendix C – Raster and vector datasets used for the evaluation of the spatial, temporal and volumetric distribution of vents of small-volume eruptions of the Taupo Volcanic Zone

Compiled to a digital data medium:

- **TVZ_bathy_4m.tif** – 4 m grid resolution DEM interpolated and itegrated from contours of New Zealand Topo50 map series and bathymetry contours of larger lakes located within the TVZ (Okataina, Rotoaira, Rotoiti, Rotomahana, Rotoma, Rotorua, Tarawera, Taupo)

- **TVZ_4m_TIN** – Vectorised surface of the extents of the edifices of small-volume volcanoes (Triangulated Irregular Network (TIN) dataset interpolated from TVZ_bathy_4m.tif)

- **dome_poly.shp** – Mapped extents (polygons) of the edifices of small-volume volcanoes with attributes of the area, perimeter, base surface elevation, highest elevation, relative elevation and edifice volume

- **mafic_vents.shp** – Mapped locations of vents of mafic (basaltic and basic andesitic) small-volume volcanoes with attributes of the age, rock geochemistry and NZTM2000 coordinates

- **central_TVZ_vents.shp** – Mapped locations of vents of small-volume eruptions of the central TVZ with attributes of rock geochemistry and NZTM2000 coordinates. Known maximum thickness is given for inferred 34 vents identified from drill core observations

Appendix D – Statement of contribution

Compiled to a digital data medium:

This thesis contains three published (Chapters 5-7) and one submitted (Chapter 8) articles of international peer-reviewed scientific journals as chapters. This appendix contains the corresponding four "Statement of contribution to doctoral thesis containing publications" forms (DRC16) of Massey University.